FLOW AND COMBUSTION IN AXISYMMETRIC FURNACES

by

Essam Eldin Khalil Hassan Khalil

B.Sc.(Eng),M.Sc.

Thesis submitted for the degree of

Doctor of Philosophy

in the Faculty of Engineering

University of London

and

for the Diploma of Membership

of Imperial College

Mechanical Engineering Department
Imperial College of Science and Technology
London SW7,2AZ.

1976

ABSTRACT

The experimental and computational work reported here is intended to improve understanding of the properties of axisymmetric,gas-fired furnaces. To this end measurements of three components of velocity and the rms of the corresponding fluctuations,of local mean temperature and wall-heat flux were obtained in a model furnace for a range of burner arrangements and initial flow conditions.The measurements were also intended to facilitate the evaluation of combustion models and so to allow the development and quantitative assessment of a design method, based on the solution of finite-difference representations of conservation equations.

A laser-Doppler anemometer,incorporating light frequency shifting by a rotating disc grating,was used to determine the velocity characteristics of the combusting model furnace flows.The same instrumentation was used to determine the characteristics of related isothermal flows:these measurements allowed the chosen two-equation turbulence model to be tested without the complication brought about by combustion.A prespex version of the model furnace was used for the isothermal measurements since it allowed more detailed measurements to be obtained with comparative ease.Mean gas temperature was determined from a calibrated suction pyrometer and wall heat flux from the flow rate of cooling water,and the corresponding inlet and outlet temperatures,which passed through the seperate sections of the furnace wall.

The ability of the solution procedure to represent isothermal flows was tested by comparing results with the measurements in the isothermal flow in the prespex furnace geometry.In addition, comparisons were made with measurements previously reported in a range of elliptic flows.The calculated results were, in general in close agreement with the measurements and certainly sufficiently clear such that the turbulence model was unlikely to be the limiting component

of the solution procedure. It was noted, however, that the properties of blunt-body stabilised flows were less well represented than those of corner recirculations and that the closeness of the agreement tended to deteriorate with increasing swirl.

A preliminary examination of combustion models suggested that diffusion flames would be well represented by single-step fast reaction and a probability of scalar fluctuations based on a clipped Gaussian distribution; Arrhenius and eddy-break up assumptions were considered adequate for premixed arrangements although the turbulence control was later found to be better expressed by the solution of scalar correlations equations along the lines suggested by Borghi. A radiation model based on the use of simplifying assumptions for the angular variation of the radiant intensity, was preferred on the grounds that the flux equations can be easily coupled with the numerical solution of the flow equations. Density fluctuation correlation equations were found to be necessary in the calculation of NO_x and resulted , for example, in significantly different calculated values of mean temperature.

The solution procedure was compared with the previously reported velocity, energy and pollution based properties of many authors and with the measurements obtained in the present furnace. In general, the velocities were represented to within 10%; the mean temperature to better than ±150K; and the wall heat flux to 15%. Intermediate species can also be determined and the results for NO_x, for example, suggested that with a super equilibrium constant of 2.4, measurements could be represented to within ±20% with similar trends.

ACKNOWLEDGEMENTS

This work has been carried out with the financial support of the United Kingdom Atomic Energy Research Establishment,Harwell under the supervision of Prof.J.H.Whitelaw.

The author is pleased to acknowledge the guidance,encouragement and inspiration provided by his supervisor,Prof.J.H.Whitelaw,in the research programme of this thesis.Prof.Whitelaw also generously fostered the author's professional intrests by promoting connections with academic and research communities outside Imperial College.

I am grateful to members of the A.E.R.E.,Dr.P.Hutchinson who monitored the project and continued help and interest.The various aspects of the work have benefitted from valuable comment and critisism by Drs.R.J.Baker, A.D.Gosman,J.Truelove and G.Wigley to whom I owe my thanks.

Finally I should like to thank the technical staff of the combustion laboratory at Imperial College and A.E.R.E. for their assistance during the experiments.Thanks are also due to Ms.S.J.Chambers for performing the arduous task of typing this and other work.

A last but not least,thanks and gratitude are due to my parants and my wife for their encouragement and help.

CONTENTS.

	Page
ABSTRACT	2
ACKNOWLEDGEMENTS	4
CONTENTS	5
NOMENCLATURE	8
1. INTRODUCTION	
1.1 Aims of present investigation	12
1.2 Previous investigations	14
2. CALCULATION PROCEDURE	
Introduction	25
2.1 Differential equations and boundary conditions	26
2.2 Numerical solution procedure	34
2.2.1 Grid arrangement	35
2.2.2 Finite difference equations	36
2.2.3 Solution algorithm	38
2.2.4 Miscelleneous details	38
2.3 Turbulence models	43
2.3.1 Turbulence model of the present work	45
2.3.2 Wall functions	49
2.4 Combustion models	51
2.4.1 Introductory remarks	51
2.4.2 Fast chemical reaction models	54
2.4.3 Finite chemical reaction models	64
2.4.4 Effect of turbulence fluctuation correlations on reaction rates	70
2.4.5 Summary	79

		Page
2.5	Radiation models	82
	2.5.1 General	82
	2.5.2 Radiation model used in present investigation	85
2.6	Pollutant formation models	87
	2.6.1 Models for calculating nitric oxides	88
	2.6.2 Models for calculating unburned hydrocarbons	90
2.7	Closure	92
3.	EXPERIMENTAL INVESTIGATION	
3.1	Description of equipments and instrumentation	95
3.2	Experimental procedure	106
3.3	Results	107
3.4	Error analysis and precision	113
3.5	Summary	117
4.	ISOTHERMAL FLOW CALCULATIONS	
4.1	Introduction	120
4.2	Flow properties in turbulent recirculating flows	121
4.3	Flow properties in present flow configurations	138
4.4	Discussion and implications of the present calculations	142
4.5	Concluding remarks	144
5.	CALCULATED PROPERTIES IN TURBULENT REACTING FLOWS	
5.1	Comparison between calculated flame properties and the corresponding measurements of previous investigations	147
5.2	Comparison between calculated flame properties and the corresponding measurements of the present investigations	169
5.3	Assessment of combustion models	175
5.4	Calculation outside range of measurements	180
5.5	Concluding remarks	188

Page

6. SUMMARY OF CONCLUSIONS AND RECOMMENDATIONS

6.1 Summary of conclusions 191

6.2 Recommendations for future work 194

REFERENCES 198

APPENDICES

Appendix A1 209

Appendix A2 211

Appendix A3 218

Appendix A4 257

Appendix A5 265

Appendix A6 272

Appendix A7 289

Appendix A8 295

FIGURES 317

NOMENCLATURE

A	area
A_o	preexponential coefficient
a	absorption coefficient in radiation model
a_o, a_1, a_2, a_3	constants in specific heat expression
C	mole fraction
C_p	specific heat at constant pressure
C_1, C_2, C_μ	constants of the two-equation turbulence model
C_{g_1}, C_{g_2}	constants of the combustion model
C_R	eddy break up constant
D, d	diameter
D_ℓ	laminar diffusion coefficient
E	activation energy
$\bar{f}$	mean mixture fraction
f'	fluctuating mixture fraction = $f-\bar{f}$
g	square of concentration fluctuation, $g = \overline{(f - \bar{f})^2}$
g_i	gravitational acceleration
H	mean stagnation enthalpy
h	fluctuating stagnation enthalpy
H_{fu}	heat of reaction of fuel
I	intensity
i	stoichiometric mass of oxygen per unit mass of fuel
k	kinetic energy of turbulence = $\frac{1}{2}(\bar{u}^2 + \bar{v}^2 + \bar{w}^2)$
K	constant of log law.
ℓ	length
M_a	mean mass fraction of species a
m_a	fluctuating mass fraction of species a
P	pressure

$P(\Phi)$	probability distribution of Φ
Q	heat flux
R	universal gas constant
R_{fu}	rate of fuel consumption
R_x, R_y	net radiation fluxes in the x and y directions
r	radial distance from the centreline
s	scattering coefficient in the radiation model
S	swirl number , defined in Appendix A1
S_Φ	mean source term in the Φ equation
St	Stanton number
t	time
$\bar{T}$	mean temperature
T'	fluctuating temperature
$\bar{U}$	mean axial velocity component
u	fluctuating component of axial velocity
$\bar{U}_j$	mean velocity component in the x_j direction
u_j	fluctuating velocity component in the x_j direction
$\bar{V}$	mean radial velocity component
v	fluctuating component of radial velocity
$\bar{W}$	mean tangential velocity component
w	fluctuating component of tangential velocity
$\overset{o}{W}$	molecular weight
x	axial distance from the burner exit
x_j	distance along the j coordinate direction
y	radial distances from the burner centreline
y_a	width of burner annulus

Greek Symbols

Γ_Φ	turbulent exchange coefficient in the Φ equation

δ	Dirac Delta function
δ_{ij}	Kronecker Delta
ε	dissipation of turbulent kinetic energy
θ	beam intersecting angle
λ	laser source wave length
μ	molecular viscosity
$\bar{\rho}$	mean density
ρ'	density fluctuation
ν	frequency
σ	Stefan-Boltzmann constant
σ_{Φ}	Schmidt and Prandtl number for any variable Φ
τ	time scale
Φ	mean component of a scalar quantity Φ
ϕ	fluctuating component of a scalar quantity Φ

Subscripts

a	species
b	bulk
c	central recirculation zone
c.w	cooling water
D	Doppler
eff	effective(including the effects of turbulence)
f	furnace
fu	fuel
j	jet
max	maximum
min	minimum
Ox	oxidant
Pr	product
r	recirculation

st	stoichiometric
t	turbulent
w	wall
o	at the centre

CHAPTER 1

INTRODUCTION

1.1 Aim of Present Investigation

1.1.1 Flow Considered

The thesis is concerned with turbulent flow in axisymmetric furnaces; reacting and non-reacting flows with and without swirl are considered. The flow downstream of a confined, axisymmetric jet arrangement, which is typical of the type of flows considered, is illustrated in figure 1.1 where regions of forward and reverse velocities are indicated. In the initial region, where the mixing of the coaxial jets occurs, the flow pattern is similar in terms of centreline velocity decay and spreading rate to that of a coaxial jet issuing into stagnant surroundings. The sudden enlargement creates reverse flow regions, of size governed by the expansion ratio, at the corners of the confining cylinder and these influence the entrainment to the developing coaxial jet. The introduction of swirl in the annular stream shortens the developing region and may create a central recirculation zone whose size depends on the ratio of the tangential to axial momentum at the jet exit. The influence of combustion was not quantitatively appreciated although, in general, it tends to accelerate the flow; its quantification is one of the contributions of the present contribution.

The flow configuration of the previous paragraph, with a central jet flow of fuel and an annulus flow of air, ignites when the temperature is high enough for reaction to occur. The unpremixed flame can be stabilized on the wall between the two jets. The introduction of swirl and the consequent region of recirculation along the centreline causes hot gases to recirculate and raises the temperature of the reactants entering this stabilization region.

In general, a well designed furnace has a stabilized flame with maximum combustion efficiency; the mean flow and turbulence fields have a major influence on the flame structure and the formation of pollutant is strongly temperature dependent. The present investigation provides data which is intended to assist the furnace designer and which allows the assessment and quantification of a calculation procedure developed to allow the calculation of furnace-flow properties. The calculation method is compared with present and previous experimental results and is shown to allow a valuable contribution to design.

1.1.2 Practical relevance and purposes

The flow described briefly in the previous subsection is relevant to several practical applications including furnaces which form the main motivation for the present work. In furnaces, and particularly in fire tube arrangements, the burner may consist of coaxial jets, and the heat released from the resulting flame is transferred to the containing walls by convection and radiation. The flame stabilization is governed by many factors such as, for example, furnace dimensions, burner dimensions and air and fuel stream velocities. In order to stabilize the flame, a disc (baffle) may be used to create a recirculation zone or swirl is imparted to the air stream to create a central recirculation zone. The first method of flame stabilization is more suitable for premixed flames, where premixed reactants flow through the annular space to the combustion chamber as shown in figure 1.2; in this arrangement, chemical reaction rate may have a strong influence on the reaction and resulting flame properties. In diffusion flames, separate streams of air and fuel enter the furnace and the flame is controlled mainly by the mixing of the reactants; in particular, the swirl generated in the air stream causes the hot gases to recirculate and preheat the fresh reactants, hence preventing blow off. A

typical flow pattern in the vicinity of the central recirculation zone is shown in figure 1.2.

In addition to fire tube boilers, the present investigation is relevant to the flow in rotary cement kilns where the cement ore is poured in at one end of the slowly rotating axisymmetric enclosure with the burner located at the other end. The heat released from the flame is transferred to the molten cement which is discharged from the flame end as shown in figure 1.3.

The objectives of the present work are directly related to the applications discussed above and may be stated as:

to provide experimental information which helps to quantify the influence of swirl and combustion on aerodynamic and heat transfer properties of two-dimensional, axisymmetric, furnace type flows.

to develop and test the ability of turbulence and combustion models to represent the present and previous measurements.

and to provide a method for the calculation of the flow, heat transfer and pollutant characteristics of two-dimensional, axisymmetric furnaces and, by comparison with experiment, to assess its range of applicability and precision.

The measured properties include, mean and fluctuating velocity components, mean temperature and wall heat flux. The influence of flow and geometrical parameters are determined by a combination of numerical solutions and measurements. The numerical method solves appropriate conservation equations in finite difference form and embodies the turbulence and combustion models.

1.2 Previous Investigations

In this section, previous experimental and computational investigations of furnace flows are reported to provide an indication of the knowledge

available at the start of the present work, i.e. 1973. This historical record is complemented by comments on the precision of the various measurement techniques and an assessment of the available information. The relative merits of previous computational investigations of furnace flows are also assessed.

1.2.1 Experimental Investigations

Previous experimental investigations of direct relevance to the present work are listed in Table 1.1, where measured properties, measuring techniques and flow configurations are displayed. The combusting-flow investigations relate only to furnace geometries. Chedaille et al. (1966) provided a review of earlier measurements of mean velocities and concentrations in coaxial jets and furnaces and these are not reconsidered here. The investigations summarised in table 1.1 encompass a comparatively narrow range of flows and often provide insufficient detail and precision: they demonstrate the need for improved measurements and, at least in terms of $\bar{U}$, $\tilde{u}$ and $\bar{T}$, these are provided in the present work. These data are, however, useful in that they can aid the testing and assessing of the validity of the calculation procedure developed here and do encompass a wider range of flow configurations, akin to furnace flows than could readily be obtained in a single investigation. Table 1.2 illustrates the geometrical configurations of these previous measurements.

Previous velocity measurements, apart from those of Owen (1975) and Baker et al. (1974a), were carried out with pitot probes which can intefere with the flow, particularly in regions of recirculation, and can result in erroneous velocity information. Moreover, pitot probes and hot-wires are unable to resolve the flow directions and their use near recirculation zones can lead to large errors. The technique of laser Doppler anemometry, in contrast, does not interfere with the flow and allows the direction of

Table 1.1

Reference	Velocities		Concentration	Temperature	Wall Heat Flux	NO	Flow Type
	mean	rms					
Afrosimova (1967)	pitot probe	-	-	suction pyrom.	-	-	isothermal combustion
Ijmuiden (1970, 1971, 1974)	pitot sphere	-	Sampling Probe	Suction Pyrom. thermocouples	radiation flux meters	chemi-luministic	isothermal combustion
Wu et al (1971)	pitot probe	-	Sampling Probe	thermocouples	radiation flux meters	-	isothermal combustion
Bilger et al (1972a)	pitot probe	-	Sampling Probe	thermocouples	-	chemi-luministic	combustion
Steward et al (1972)	pitot probe	-	Sampling Probe	thermocouples	radiation flux meters	-	combustion
Gunther et al (1972)	-	-	Sampling Probe	thermocouples	-	-	combustion
Baker et al (1974a)	laser anemometry		-	-	-	-	combustion
El Mahallawy et al (1973) Lockwood et al (1974)	-	-	Sampling Probe	-	-	-	combustion
Beltagui et al (1974, 1975)	pitot probe	-	Sampling Probe	thermocouples	-	-	isothermal combustion
Owen (1975)	laser anemometry		-	-	-	-	isothermal combustion
Lenze et al (1974,1975)	-	-	Sampling Probe	thermocouples	-	-	combustion
El Ghobashi (1974)	-	-	Sampling Ionization Probe	-	-	-	combustion
Khalil et al (1974)	pitot probe	-	Sampling Probe	thermocouples	-	-	hot mixing
Paauw (1974)	pitot probe	-	Sampling Probe	thermocouples	-	chemi-luministic	combustion
Bowman et al (1975)	pitot probe	-	Sampling Probe	double sonic orifice	-	chemi-luministic	combustion
Cernansky et al (1974)	-	-	-	thermocouples	-	chemi-luministic	combustion

Table 1.2

Reference	Length mm	Diameter mm	Expansion ratio	Fuel Supply	Comments
Afrosimova (1967)	1600	800	1:3	Town Gas	With combustion
Ijmuiden (1970, 1971, 1974)	6250	2000	1:11.4	Nat. gas with quarl	Sq. section with and without swirl
Wu et al (1971)	5000	900	1:6.87	Nat. gas conentrations jets with quarl	With and without swirl combustion
Bilger et al (1972a)	1800	305	Co-flowing	Hydrogen	Sq. section without swirl
Steward et al (1972)	720	254	Co-flowing	Propane	Partially premixed
Gunther et al (1972)	2500	450	Co-flowing	Town gas	Without swirl
Baker et al (1974a)	6250	2000	1:11.4	Nat. Gas with quarl	
El Mahallawy et al (1973) Lockwood et al (1974)	1900	210	1:2.69	Town gas	With & without swirl
Beltagui et al (1974, 1975)	1400 900	450 225	1:5 1:2.5	Town gas Single jet	Isothermal and pre-mixed flame
Owen (1975)	1220	125	1:1.43	Air	Without swirl Isothermal flow
Lenze et al (1974, 1975)	2500	450	Co-flowing	Nat. gas Town gas	Without swirl
El Ghobashi (1974)	1900	210	1:2.69	Town gas	Without swirl combustion
Khalil et al (1974)	2100	210	1:2.69	Air	With and without swirl non reacting
Paauw (1974)	1400	outlet 300,660	Conical furnace	Nat. gas	Cone angle 22°
Bowman et al (1975)	1210	122.3	1:1.3	Methane concentric jets	
Cernansky et al (1974)	356	58.0	Co-flowing	Propane	With swirl

flow to be resolved; as a result, precise measurements can be obtained in regions of recirculation. The early work of Baker et al. (1974b) was concerned with demonstrating the use of laser Doppler anemometry in flames and in related regions of flow recirculation.

Measurements of local gas concentrations have been obtained with isokinetic sampling techniques which are discussed in detail in Bilger (1972b). Mean gas temperatures have been measured with thermocouples and suction pyrometers with a likely precision of ± 5%. The related uncertainties depend on the probe size, coating material, number of shields and detailed studies of uncertainties have been reported by Odidi (1974) for thermocouples and Khalil (1975) for suction pyrometers. In general, the measurements are likely to be more reliable in regions of small gradients, in non-reacting flows and where the fluctuations are smaller. Measured radiative heat fluxes have been determined by ellipsoidal radiometers which were inserted in the furnace and an overall balance on the furnace cooling sections carried out to obtain the convective portion of the total load. The likely precision of heat flux measurements were reported by Braud et al. (1972).

Most previous velocity measurements in furnaces were obtained with pitot probes and hence more reliable experimental data particularly in recirculation zones, were needed and together with turbulence intensity distributions could be obtained with a laser Doppler anemometer . In the context of the present calculations, previous experimental investigations are deficient in that values of measured properties were not provided at inlet and exit. The solution of differential equations requires boundary conditions and comparisons between experiments and calculations are imperfect unless the boundary values are known. Thus, in carrying out the present experimental program it was required to measure the velocity and

temperature distributions around the physical boundary corresponding to the solution domain.

1.2.2 Calculation Methods

Significant theoretical advances have been made since the late 1960's and stem from the utilization of digital computers to allow the solution of simultaneous partial differential equations which represent the conservation of mass, momentum, energy and species. The solution of the unsteady, three-dimensional equations appropriate to a turbulent flow cannot be obtained due to limitations of storage and computing time and, as a consequence, equations based on time averaged values of velocity, density, temperature and chemical species concentrations have been solved. The exact equations for time averaged properties contain unknowns such as $\overline{u_i u_j}$ and $\overline{u_i \rho'}$ in the momentum equation and $\overline{\phi u_i}$ and $\overline{\phi \rho'}$ in the conservation equation for any scalar $\bar{\Phi}$ ($\bar{M}_{fu}$, $\bar{T}$, $\bar{M}_{ox}$, $\bar{f}$, $\bar{H}$, ...) as shown below.

The conservation equations which relate to the present flow configuration may be expressed as;

mass
$$\frac{\partial}{\partial x_j}\left(\bar{\rho}\ \bar{U}_j + \overline{\rho' u_j}\right) = 0 \qquad 1.1$$

momentum
$$\left(\bar{\rho}\ \bar{U}_i + \overline{\rho' u_i}\right)\frac{\partial}{\partial x_i}\ \bar{U}_j = -\frac{\partial \bar{P}}{\partial x_i} + \frac{\partial}{\partial x_i}\left(\mu \frac{\partial \bar{U}_j}{\partial x_i}\right) - \frac{\partial}{\partial x_i}\ \bar{\rho}\ \overline{u_i u_j}$$

$$- \bar{U}_i \frac{\partial}{\partial x_i}\ \overline{u_j \rho'} - \overline{\rho' u_j}\ \frac{\partial \bar{U}_i}{\partial x_i} \qquad 1.2$$

scalar transport,
$$\left(\bar{\rho}\ \bar{U}_i + \overline{\rho' u_i}\right)\frac{\partial}{\partial x_i}\ \bar{\Phi} = S_\Phi + \frac{\partial}{\partial x_i}\left(\bar{\rho}\ \Gamma_\Phi \frac{\partial \Phi}{\partial x_i}\right) - \frac{\partial}{\partial x_i}\ \bar{\rho}\ \overline{u_i \phi}$$

$$- \bar{U}_i \frac{\partial}{\partial x_i}\ \overline{\phi \rho'} - \overline{\rho' \Phi}\ \frac{\partial \bar{U}_i}{\partial x_i} \qquad 1.3$$

The Reynolds stress term $\overline{u_i u_j}$ which appears in equation 1.2 has been the subject of many theoretical investigations of turbulent shear flows. Various models of turbulence have been suggested to replace the early work of Prandtl (1925) which introduced the mixing length but which was found to be inadequate for recirculating flows, Roberts (1972). These turbulence models required the solution of transport equations for turbulence quantities such as kinetic energy of turbulence and its dissipation rate, Rotta (1951), Harlow and Nakayama (1967) and Rodi (1972) or alternatively solves transport equations for the Reynolds stresses themselves in addition to turbulent kinetic energy and its dissipation rate, Launder et al. (1975). The turbulence model which solves for the kinetic energy and its dissipation rate was tested for free shear flows by Launder et at. (1972) and for boundary layers, Jones and Launder (1973) and Launder et al. (1973) and showed reasonable agreement with experimental information.

Previous computational investigations of turbulent furnace flows have been carried out with the aid of equations for conservation of mass, momentum and scalar entities, as shown in table 1.3. In these papers, calculated and measured results were compared to illustrate the agreement which can be obtained from procedures of this type with simple forms of equations 1.1, 1.2 and 1.3. No detailed comparisons were reported in the swirling turbulent flames, with large recirculation zones; which are found in real furnaces.

In addition to the turbulence model, a combustion model is required in reacting flows, to provide information of the correlation terms, i.e. $\overline{u_i \phi}$, $\overline{\rho' u_i}$, $\overline{\rho' \phi}$ and S_ϕ, which appear in the conservation equations. The combustion model should account for the effect of the temperature and species concentration fluctuations on the local density and the time averaged rate of fuel consumption and, consequently, the flame structure. Most of the

Table 1.3

Reference	Flow Type			Turbulence Model	Combustion Model	Radiation Model	Comparisons
	State	Configuration	Swirl				
Pun and Spalding (1967)	flame	2-D axi-sym.	zero and finite	mixing length	fast chemical reaction	-	no comparisons with expt.
Gosman et al (1969)	jet/ flame	2-D axi-sym.	zero and finite	mixing length	fast chemical reaction	-	no comparisons with expt.
Spalding (1970)	flame	2-D	zero	k-w	eddy break up model	-	comparisons with expt.
Patankar et al (1972)	flame	2-D	zero	k-ε	fast chemical reaction	flux model	no comparison with expt.
Pai et al (1972)	flame	3-D	zero and finite	mixing length	fast chemical reaction	-	comparisons with expt.
Evans et al (1973)	jet/ flame	2-D axi-sym.	zero and finite	mixing length	fast chemical reaction	-	no comparison with expt.
Anasoulis et al (1973)	flame	2-D axi-sym.	zero and finite	mixing length	fast chemical reaction	-	comparison with expt.
Gosman et al (1973)	flame	3-D	zero	k- ε	fast chemical reaction with fluctuations	flux model	comparison with expt.
El Ghobashi et al (1974)	flame	2-D axi-sym.	zero	k- ε	fast chemistry with fluctuations	-	comparison with expt.
Gosman et al (1974)	jet	2-D axi-sym.	zero	k- ε	-	-	comparison with expt.

previous investigations, shown in table 1.3, neglected the effect of turbulence fluctuations on the time averaged properties, e.g. Patankar and Spalding (1970) and McGuirk (1971). The effect of density fluctuations was not considered at all while for premixed flames, the effect of turbulence on the reaction rate was represented through an eddy break up sink term in the fuel conservation equation as suggested by Spalding (1970). For diffusion flames, the assumptions of fast chemical reaction can result in a reduction of the number of equations to be solved, and the effect of turbulence on the flame structure was introduced by considering the flame sheet fluctuating around its mean location producing a flame brush as reported by Spalding (1971) Gosman et al (1973) and El-Ghobashi et al. (1974).

Attempts to predict furnace flow performance have been reported by Pun and Spalding (1967), Pai and Lowes (1972) and Evans et al. (1973) for axisymmetric flames. Adiabatic walls were considered and radiative transfer to and from the furnace walls was therefore neglected although in real furnace flows, radiative fluxes cannot be neglected. The consideration of radiation can result in equations which are of an integro-differential nature but simplified models have been suggested, for example, by Lockwood et al. (1971) and Gosman et al. (1973). These models are based on the solution of transport equations for the net radiative fluxes in the coordinate directions and the evaluation of the corresponding source/sink term in the energy equation due to the radiation from gases.

The calculation of pollutant characteristics is also relevant to the present investigations and can be achieved by the solution of appropriate species-concentration equations and a knowledge of the related reaction kinetic equations and constants. The rate of formation of (NO), for example, has been discussed in detail by Caretto (1975) and shown to be very sensitive to the calculated gas temperature. Previous calculations

have been reported, for example, by Anasoulis et al. (1973) and indicated large discrepancies with measured values.

The measurements reported in the references of table I.1 and the calculations of table I.3 are deficient in several respects which have been discussed briefly in the previous paragraphs. Perhaps the greatest deficiency is that previous investigations have not combined experimental and computational work and, as a consequence, the experimental investigations are insufficiently complete to allow the calculation methods to be satisfactorily tested. The present investigation to a significant extent, removes this deficiency.

In the following chapters, the work required to fulfill the objectives of section 1.1.2 is reported under the headings 'Calculation Procedure', 'Experimental investigation', 'Isothermal flow calculations' and 'Calculated properties in turbulent reacting flows'. The order of presentation has been chosen to allow the calculation procedure to be described prior to the description of the experimental techniques and the comparison of the calculated results with measurements.

In chapter 2, the conservation equations appropriate to steady, two-dimensional, confined, turbulent, recirculating, reacting and non-reacting flows are discussed with appropriate boundary conditions. The numerical procedure is described next together with the computational algorithm used in the present work. The turbulence model embodied in the computational scheme is also described with appropriate modifications for the present flow situations. This is followed by a description of the various modelling approaches to reacting flows which are discussed with respect to their physical significance, formulation and limitations. The radiation and pollution formation models are also discussed; no attempt was made to improve the radiation model but pollution models were developed to take account of the temperature fluctuations and detailed chemistry effects.

The experimental investigations are described in chapter 3, where the combustor rig and the velocity and temperature measuring techniques are reported in detail together with the experimental procedure and measuring conditions. The chapter ends with an assessment of the likely precision of the measurements.

The calculated results for the isothermal flows in confined configurations are compared with the corresponding previous and present experimental measurements in chapter 4 and allows an assessment of the validity of the turbulence model and the computational procedure of chapter 2.

The calculated and measured flow properties obtained in reacting furnace type flows are presented, compared and discussed in Chapter 5. Calculations, appropriate to the flow and geometry boundary conditions of the present measurements, are presented for a number of combustion models of different complexity and comparison with experiment facilitates a choice. Comparison with the experiments of previous authors are made on the basis of the appropriate combustion model. In all cases, the precision and the possibility of its improvement is discussed.

The main findings of the thesis are summarised in a final chapter; the achievements are compared with the objectives and suggestions made as to the most profitable areas for future work.

CHAPTER 2

CALCULATION PROCEDURE

Introduction

The present chapter has been prepared to describe and discuss the problems associated with the formulation of the equations appropriate to furnace type flows, in terms of the governing conservation equations, turbulence and combustion modelling assumptions and the computational procedure required to solve the equations with boundary and inlet conditions. The elliptic partial differential equations which govern the transport of mass, momentum, energy and scalar properties, are presented in the first section; they are restricted to steady, gaseous phase, two-dimensional and axisymmetric flow situations where recirculation may occur, such as in furnace type flows. These time-averaged equations contain, for turbulent flows, second order correlations of fluctuating properties and models to determine these correlations are necessary to make the equations soluble.

The governing differential equations, expressed in finite difference form, are solved numerically by an iterative procedure which is described in section two of this chapter. The various assumptions, limitations and required convergence criteria to satisfy the conservation equations are also discussed in the section. In the third section, the turbulence models embodied in the present scheme to represent the unknown correlations, are discussed and the appropriate modifications for reacting flows suggested. The chosen turbulence model, in the form of a set of steady partial differential equations, allows the predictions of the aerodynamic properties of the flow.

In reacting flows, various combustion-model assumptions are necessary to allow the calculation of the rate of fuel consumption and energy release. These assumptions are described in section four and include the effects of turbulence-chemistry interactions, chemical kinetics and density fluctuations. The radiation heat fluxes appear in the energy conservation equation and

the governing transport equations of these fluxes, embodied in a four flux radiation model, are described in section five. The pollutant formation in reacting flows is represented by the solution of the appropriate species conservation equations which include the effects of temperature and concentration fluctuations and are discussed in section six of this chapter.

2.1 Differential Equations and Boundary conditions.

The partial differential equations which govern the motion of fluids can be expressed in tensor form as follows,

Continuity equation

$$\frac{\partial}{\partial x_j} (\rho U_j) = - \frac{\partial \rho}{\partial t} \qquad 2.1.1$$

and the momentum equations,

$$\frac{\partial}{\partial x_j} (\rho U_i U_j) = S_{U_i} - \frac{\partial \sigma_{ij}}{\partial x_j} - \frac{\partial \rho U_i}{\partial t} \qquad 2.1.2$$

where

$$\sigma_{ij} = P\delta_{ij} - \mu \left(\frac{\partial U_i}{\partial x_j} + \frac{\partial U_j}{\partial x_i}\right) + \frac{2}{3} \mu \frac{\partial U_i}{\partial x_j} \delta_{ij}$$

δ_{ij} is the kronecker-delta function $= \begin{matrix} 0 & i \neq j \\ 1 & i = j \end{matrix}$

The instantaneous velocities and densities in equations 2.1.1 and 2.1.2 can be decomposed into mean and fluctuating components as;

$$U_j = \overline{U_j} + u_j$$
$$\rho = \bar{\rho} + \rho' \qquad 2.1.3$$

Introducing the definitions of equation 2.1.3 into the continuity equation, and then time averaging and assuming steady state, results in the equation:

$$\frac{\partial}{\partial x_j} (\bar{\rho}\, \bar{U}_j + \overline{\rho' u_j}) = 0 \qquad 2.1.4$$

Similarly, for the momentum equations,

$$(\bar{\rho}\bar{U}_j + \overline{\rho' u_j}) \frac{\partial \bar{U}_i}{\partial x_j} = \bar{S}_{U_i} - \frac{\partial \bar{\sigma}_{ij}}{\partial x_j} - \frac{\partial}{\partial x_j} (\bar{\rho}\, \overline{u_i u_j} + \overline{\rho' u_i u_j} + \bar{U}_j\, \overline{\rho' u_i})$$

where

$$\bar{\sigma}_{ij} = \bar{P}\delta_{ij} - \bar{\mu} \left(\frac{\partial \bar{U}_i}{\partial x_j} + \frac{\partial \bar{U}_j}{\partial x_i} \right) + \frac{2}{3} \bar{\mu} \frac{\partial \bar{U}_i}{\partial x_j} \delta_{ij} + \frac{2}{3} \overline{\mu' \frac{\partial u_i}{\partial x_j}} \delta_{ij} \qquad 2.1.5$$

$$- \overline{\mu' \left(\frac{\partial u_i}{\partial x_j} + \frac{\partial u_j}{\partial x_i} \right)}$$

Neglecting the fluctuations in laminar viscosity in equation 2.1.5, the expression for $\bar{\sigma}_{ij}$ takes the same form as σ_{ij} but with all variables time averaged. The equations describing the transport of a scalar fluid property $\bar{\Phi}$ can, in a similar manner, be expressed as;

$$(\bar{\rho}\, \bar{U}_j + \overline{\rho' u_j}) \frac{\partial \bar{\Phi}}{\partial x_j} = \bar{S}_\Phi - \frac{\partial \bar{J}_{\Phi,j}}{\partial x_j} - \frac{\partial}{\partial x_j} (\bar{\rho}\, \overline{u_j \phi} + \overline{\rho' u_j \phi} + \bar{U}_j\, \overline{\rho' \phi}) \qquad 2.1.6$$

where $-\bar{J}_{\Phi,j}$ is the flux of Φ along the j^{th} direction and can be expressed by Fick's law as;

$$\bar{J}_{\Phi,j} = - \Gamma_{\Phi_{,\ell}} \frac{\partial \bar{\Phi}}{\partial x_j} \qquad 2.1.7$$

with $\Gamma_{\Phi_{,\ell}}$ equals to μ/σ_Φ.

σ_Φ is the Prandtl/Schmidt number appropriate to the transport of Φ;

$\bar{S}_\Phi$ is the source/sink of the property $\bar{\Phi}$;

and ϕ is the fluctuating component of the property, Φ, $\phi = \Phi - \bar{\Phi}$.

The number of the time averaged conservation equations is less than the number of the unknown terms contained in these equations. Thus the correlations $\overline{\rho' u_j}$, $\overline{u_i u_j}$, $\overline{u_i \phi}$ and $\overline{\rho' \phi}$ must be predetermined, modelled or neglected. For non reacting flows, the equations of interest are those governing the mass and momentum and, hence, modelling of the entity $\overline{u_i u_j}$

is needed in order to solve the set of differential equations. In reacting flows, density fluctuation correlation specifications are also required. Different approaches to estimate these correlation terms, which appear in equations 2.1.4, 2.1.5 and 2.1.6, are considered as follows;

1. All terms involving density fluctuations may be ignored and hence the only correlation to be modelled is $\overline{u_i u_j}$. This approach is appropriate to non reacting flows where densities are uniform or vary by a small amount.

2. For situations where combustion and density gradients are involved, equations for all correlations involving density fluctuations should be solved. This implies transport equations for each correlation and involves further modelling.

3. It is possible to write equations (2.1.4, 2.1.5 and 2.1.6) in a form such that density fluctuation correlations do not appear and hence the equations have a form similar to that of the non-reactive equation. This involves Favre averaging (1969) according to the equation:

$$\tilde{U}_j = \bar{U}_j + \overline{\rho' u_j'}/\bar{\rho} \qquad 2.1.8$$

where

$\bar{U}_j$ is the average velocity

$\tilde{U}_j$ is the mass weighted velocity or Favre averaged velocity.

The Favre averaged form of the conservation equations 2.1.4, 2.1.5 and 2.1.6 is obtained by substituting equation 2.1.8 into the conservation equations, and the result is;

1. Continuity equation,

$$\frac{\partial}{\partial x_j} \bar{\rho}\, \tilde{U}_j = 0 \qquad 2.1.9$$

2. Momentum conservation equation,

$$(\bar{\rho}\,\tilde{U}_j)\,\frac{\partial}{\partial x_j}\,\tilde{U}_i = \bar{S}_{U_i} - \frac{\partial \tilde{\sigma}_{ij}}{\partial x_j} - \frac{\partial}{\partial x_j}\,\bar{\rho}\,\widetilde{u_i u_j} \qquad 2.1.10$$

where

$$\tilde{\sigma}_{ij} = \bar{P}\delta_{ij} - \tilde{\mu}\left(\frac{\partial \tilde{U}_i}{\partial x_j} + \frac{\partial \tilde{U}_j}{\partial x_i}\right) + \frac{2}{3}\tilde{\mu}\,\frac{\partial \tilde{U}_i}{\partial x_j}\,\delta_{ij}$$

3. Scalar property conservation equation,

$$(\bar{\rho}\,\tilde{U}_j)\,\frac{\partial \tilde{\Phi}}{\partial x_j} = \bar{S}_\Phi - \frac{\partial}{\partial x_j}\,\bar{\rho}\,\widetilde{u_i \phi} + \frac{\partial}{\partial x_j}\,\frac{\tilde{\mu}}{\sigma_\Phi}\,\frac{\partial \tilde{\Phi}}{\partial x_j} \qquad 2.1.11$$

One of the problems associated with this method of averaging is the comparison with experimental data since most of the measurements record time-averaged properties and not the Favre averaged ones. The time or ensemble averaged variables are undoubtedly different from the Favre-averaged ones but the magnitude of the difference is unknown for reacting flows. An attempt to quantify the difference, by solving equations for the various correlation terms, is described later in thischapter. Unfortunately various terms in the correlation equations have themselves to be modelled and, as will be discussed, the absolute accuracy of the result is difficult to quantify.

The conservation equations are non-linear partial differential and elliptic in form in flows where flow reversal occurs, i.e. in situations similar to those of present interest. The closure of the aerodynamic equations requires the solution of supplementary equations for the shear stresses $\overline{u_i u_j}$. The present turbulence model provides the required relationship through the eddy or turbulent viscosity concept as described later in the chapter. The term $\overline{u_i u_j}$ is generally expressed as:

$$-\bar{\rho}\,\overline{u_i u_j} = \Gamma_{U,t}\left(\frac{\partial \bar{U}_i}{\partial x_j} + \frac{\partial \bar{U}_j}{\partial x_i}\right)$$

Turbulence models of this type have not been evaluated for a wide range of recirculating flows and, prior to this work, their appropriateness to confined sudden expansion flows was unknown. The term $\overline{u_i\phi}$ which appears in equation 2.1.6 was generally replaced by an exchange coefficient $\Gamma_{\Phi,t}$ and mean gradient of Φ as;

$$-\overline{u_i\phi} = \Gamma_{\Phi,t} \frac{\partial\bar{\Phi}}{\partial x_j}$$

The conservation equations of mass, momentum, chemical species and energy have been discussed in general time-dependent, three-dimensional form in many references, e.g. Favre (1969), Bray (1973) and Bilger (1975). In these papers, attempts were made to model the effects of turbulence in terms of mean quantities, but the analysis was restricted to boundary layer and shear flow assumptions which are not appropriate in the present flow configurations. In the present investigation, the turbulent fluctuation correlation terms which appear in the conservation equations for confined elliptic flows are modelled, in terms of mean properties, as discussed in the rest of this chapter.

Most of the flows considered in the present investigation are akin to axisymmetric furnace configurations, and hence the conservation equations are expressed in axisymmetric cylindrical polar coordinates as follows;

$$\frac{1}{\bar{\rho}} \left\{\frac{\partial}{\partial x} (\bar{\rho}\,\tilde{U}\,\bar{\Phi}) + \frac{1}{r}\frac{\partial}{\partial r} (\bar{\rho}\, r\, \tilde{V}\, \bar{\Phi})\right\} \qquad 2.1.12$$

$$= \frac{\bar{S}_\Phi}{\bar{\rho}} + \frac{1}{\bar{\rho}}\frac{\partial}{\partial x} \left(\Gamma_{\Phi_{eff}} \frac{\partial\bar{\Phi}}{\partial x}\right) + \frac{1}{\bar{\rho} r}\frac{\partial}{\partial r} \left(r\, \Gamma_{\Phi_{eff}} \frac{\partial\bar{\Phi}}{\partial r}\right)$$

where

$$\Gamma_{\Phi_{eff}} = \Gamma_{\Phi,t} + \Gamma_{\Phi,\ell}$$

and $\Gamma_{\Phi,t} = \mu_t/\sigma_{\Phi,t}$ where $\sigma_{\Phi,t}$ is the turbulent equivalent of the Prandtl

or Schmidt number. The properties represented by $\bar{\Phi}$, $\bar{S}_{\Phi}$ and $\Gamma_{\Phi_{eff}}$ are indicated in table 2.1.1. As will be demonstrated, the dependent variables representing scalar properties in the table are not all required for all calculations.

Boundary Conditions

The conservation equations represented by equation 2.1.12 and table 2.1.1 are solved numerically in finite difference form. The solution domain is identified by boundaries which characterise the geometrical boundaries of the flow. In the present work, confined flows are considered and hence it is necessary to include the effect of walls on the momentum, energy and species balance. Solid boundaries do not allow mass transfer, but allow heat transfer across the walls, as in furnaces. The wall treatment is described later in section 2.3. The four boundaries of the solution domain are discussed in the following paragraphs in the context of the boundary conditions which correspond to each. Since the equations are elliptic in form, boundary conditions must be specified for each dependent variable at each of the four boundaries.

Inlet Plane

The geometry of the coaxial jet and the sudden expansion imply zero values of velocity except where the air and fuel flow enter through the annulus and central jet. The velocity distributions and turbulence properties corresponding to the equations of the turbulence model must be specified and, where possible these correspond to experimental information. The same is true of other dependent variables, such as temperature and species concentration.

Symmetry axis

Along the axis of symmetry the gradients in the radial direction of all variables are equal to zero, i.e. $\partial\bar{\Phi}/\partial y$ = zero.

Table 2.1.1

Variable ϕ	$\Gamma_{\phi_{eff}}$	S_ϕ
$\bar{U}$	μ_{eff}	$\frac{\partial}{\partial x}\mu_{eff}\frac{\partial \bar{U}}{\partial x}+\frac{1}{r}\frac{\partial}{\partial r}\mu_{eff}r\frac{\partial \bar{V}}{\partial x}-\frac{\partial \bar{P}}{\partial x}-\frac{\partial}{\partial x}\bar{U}\overline{\rho' u}-\frac{1}{r}\frac{\partial}{\partial r}r\bar{V}\overline{\rho' u}$
$\bar{V}$	μ_{eff}	$\frac{\partial}{\partial x}\mu_{eff}\frac{\partial \bar{U}}{\partial r}+\frac{1}{r}\frac{\partial}{\partial r}\mu_{eff}r\frac{\partial \bar{V}}{\partial r}-\frac{\partial \bar{P}}{\partial r}-2\frac{\mu_{eff}\bar{V}}{r^2}+\frac{\bar{\rho}\bar{W}^2}{r}-\frac{\partial}{\partial x}\bar{U}\overline{\rho' v}-\frac{1}{r}\frac{\partial}{\partial r}r\bar{V}\overline{\rho' v}$
$\bar{W}$	μ_{eff}	$-\left(\frac{\mu_{eff}}{r^2}+\frac{\bar{\rho}\bar{V}}{r}+\frac{\partial \mu_{eff}}{r\partial r}\right)\bar{W}$
$\bar{k}$	$\frac{\mu_{eff}}{\sigma_k}$	$G_{k_1}-\bar{\rho}\epsilon-\bar{\rho}\bar{k}\left(\frac{\partial \bar{U}}{\partial x}+\frac{1}{r}\frac{\partial}{\partial r}r\bar{V}\right)+\frac{\mu_{eff}}{\sigma_\rho}\frac{\partial \bar{k}}{\partial x}\frac{\partial \bar{\rho}}{\partial x}+\frac{1}{r}\frac{\mu_{eff}}{\sigma_\rho}\frac{\partial}{\partial r}\bar{k}\,r\frac{\partial \bar{\rho}}{\partial r}$
ϵ	$\frac{\mu_{eff}}{\sigma_\epsilon}$	$\frac{\epsilon}{\bar{k}}\left(C_1 G_{k_1}-C_2\bar{\rho}\epsilon\right)$
$\bar{H}$	$\frac{\mu_{eff}}{\sigma_h}$	$2a(R_x+R_y-2\sigma\bar{T}^4)-\frac{\partial}{\partial x}\bar{U}\overline{\rho' h}-\frac{1}{r}\frac{\partial}{\partial r}r\bar{V}\overline{\rho' h}$
$\bar{f}$	$\frac{\mu_{eff}}{\sigma_f}$	0
$\bar{M}_{fu}$	$\frac{\mu_{eff}}{\sigma_{fu}}$	$-A\bar{\rho}^2\bar{M}_{fu}\bar{M}_{ox}\exp(-E/R\bar{T})-\frac{\partial}{\partial x}\bar{U}\overline{\rho' m_{fu}}-\frac{1}{r}\frac{\partial}{\partial r}r\bar{V}\overline{\rho' m_{fu}}$
$\overline{m_{fu}^2}$	$\frac{\mu_{eff}}{\sigma_{fu}}$	$C_{g_1}G_{g_1}-C_{g_2}\bar{\rho}\frac{\epsilon}{\bar{k}}m_{fu}^2-2\bar{\rho}^2 A\bar{M}_{ox}\bar{M}_{fu}\exp(-E/R\bar{T})\left(\frac{\overline{m_{fu}^2}}{\bar{M}_{fu}}+\frac{\overline{m_{ox}m_{fu}}}{\bar{M}_{ox}}\right)$
$\overline{m_{fu}m_{ox}}$	$\frac{\mu_{eff}}{\sigma_{fu}}$	$C_{g_1}G_{g_2}-C_{g_2}\bar{\rho}\frac{\epsilon}{\bar{k}}\overline{m_{ox}m_{fu}}-\bar{\rho}^2 A\bar{M}_{ox}\bar{M}_{fu}\exp(-E/RT)\left(\frac{\overline{m_{ox}^2}}{\bar{M}_{ox}}+\frac{\overline{m_{fu}^2}}{\bar{M}_{fu}}+\left(\frac{1}{\bar{M}_{fu}}+\frac{i}{\bar{M}_{ox}}\right)\overline{m_{ox}m_{fu}}\right)$
$\overline{\rho' u}$	$\frac{\mu_{eff}}{\sigma_\phi}$	$\left[-\overline{uu}\frac{\partial \bar{\rho}}{\partial x}-\overline{uv}\frac{\partial \bar{\rho}}{\partial r}-0.4\,\overline{\rho' u}\left(\frac{\partial \bar{U}}{\partial x}\right)-0.2\,\overline{\rho' v}\left(\frac{\partial \bar{U}}{\partial r}+\frac{\partial \bar{V}}{\partial x}\right)-2.5\frac{\epsilon}{\bar{k}}\overline{\rho' u}\right]$
$\overline{\rho' v}$	$\frac{\mu_{eff}}{\sigma_\phi}$	$\left[-\overline{uv}\frac{\partial \bar{\rho}}{\partial x}-\overline{vv}\frac{\partial \bar{\rho}}{\partial r}-0.4\,\overline{\rho' v}\left(\frac{\partial \bar{V}}{\partial r}\right)-0.2\,\overline{\rho' u}\left(\frac{\partial \bar{V}}{\partial x}+\frac{\partial \bar{U}}{\partial r}\right)-2.5\frac{\epsilon}{\bar{k}}\overline{\rho' v}\right]$
$\overline{\rho' \varphi}$	$\frac{\mu_{eff}}{\sigma_\phi}$	$\left[-\overline{u\varphi}\frac{\partial \bar{\rho}}{\partial x}-\overline{\varphi v}\frac{\partial \bar{\rho}}{\partial r}-\left(\frac{\partial \bar{U}}{\partial x}+\frac{\partial r\bar{V}}{r\partial r}\right)\overline{\rho'\varphi}-\overline{\rho' u}\frac{\partial \bar{\varphi}}{\partial x}-\frac{\overline{\rho' v}}{r}\frac{\partial r\bar{\varphi}}{\partial r}+\overline{\rho' S_\phi}\right]\bar{\rho}$

$$G_{k_1}=\mu_{eff}\left(2\left(\left(\frac{\partial \bar{U}}{\partial x}\right)^2+\left(\frac{\partial \bar{V}}{\partial r}\right)^2+\left(\frac{\bar{V}}{r}\right)^2\right)+\left(\frac{\partial \bar{W}}{\partial x}\right)^2+\left(r\frac{\partial}{\partial r}\left(\frac{\bar{W}}{r}\right)\right)^2+\left(\frac{\partial \bar{U}}{\partial r}+\frac{\partial \bar{V}}{\partial x}\right)^2\right)$$

$$G_{g_1}=\mu_{eff}\left(\left(\frac{\partial \bar{f}}{\partial x}\right)^2+\left(\frac{\partial \bar{f}}{\partial r}\right)^2\right)$$

$$G_{g_1}=\mu_{eff}\left(\left(\frac{\partial \bar{M}_{fu}}{\partial x}\right)^2+\left(\frac{\partial \bar{M}_{fu}}{\partial r}\right)^2\right)$$

$$G_{g_2}=\mu_{eff}\left(\left(\frac{\partial \bar{M}_{fu}}{\partial x}\cdot\frac{\partial \bar{M}_{ox}}{\partial x}\right)+\left(\frac{\partial \bar{M}_{fu}}{\partial r}\cdot\frac{\partial \bar{M}_{ox}}{\partial r}\right)\right)$$

Exit Plane

The exit conditions are difficult to specify but are usually of little importance. In the practice of Gosman et al. (1969), i.e. the axial gradients, $\partial\bar{\Phi}/\partial x$ were assumed zero and that the overall conservation of mass and species was satisfied. The exit plane location was taken far downstream, so as not to influence the upstream properties.

Enclosure Wall

This wall is usually the cylindrical, outer boundaries of the flow domain. The wall is impermeable and the boundary conditions are specified through wall functions as described later in the chapter. In general, the velocities are zero and the temperature or heat flux distribution is known.

Thermodynamic Properties

The density of mixtures of air, the combusting gases and the combustion products can be represented with adequate precision for the present purposes, by the equation of state for a perfect gas,

$$\rho = P/(R\ T/\overset{o}{W}_{mix}) \qquad 2.1.13$$

with $\overset{o}{W}_{mix}$ and P determined from the appropriate mass fractions and Dalton's law of partial pressures. The gas molecular weight is obtained from;

$$1/\overset{o}{W}_{mix} = \Sigma\, M_a/\overset{o}{W}_a \qquad 2.1.14$$

and the heat of reaction of the fuel is represented by;

$$H_{fu} = \Sigma\, M_a\, H_a \qquad 2.1.15$$

with the values of H_a, determined from JANAF chemical tables (1971).

The specific heat of the mixture was obtained from the equation;

$$\bar{C}_p = \Sigma\, \bar{M}_a\, \bar{C}_{p_a}$$

where

$$\bar{C}_{p_a} = a_o + a_1\,\bar{T} + a_2\,\bar{T}^2 + a_3\,\bar{T}^3 \qquad 2.1.16$$

with the values of the coefficients provided, for each species by Tribus (1961). The use of lower order polynomials has been found to be significantly less satisfactory than the third order polynomials used here. The definition of the total enthalpy of the mixture $\bar{H}$ is expressed as;

$$\bar{H} = \bar{M}_{fu} H_{fu} + \bar{M}_a \overline{C_{p_a}} \bar{T} + (\bar{U}^2 + \bar{V}^2 + \bar{W}^2) / 2 \qquad 2.1.17$$

2.2 Numerical Solution Procedures

The conservation equations governing the flow field are difficult to solve analytically due to their complexity. With the advent of digital computers however, it has been possible to solve them numerically.

The first steps in the development of a numerical procedure for solving the governing differential equations are to superimpose a grid distribution on the flow domain to discretize the differential equations on all the grid points of the flow field; and to obtain "equivalent" algebraic expressions called finite-difference equations. The accuracy of the set of the finite-difference equations which approximate the partial differential equations is dependent on the formulation of the difference equations and on the number of the grid nodes which represent the flow field.

Three main approaches have been followed to obtain the finite difference equations from the differential equations;

(i) Taylor series expansions of the differentials with truncation of higher order terms of the series;

(ii) integration over finite elements employing some vibrational principle;

(iii) integration of the differential equations over small control volumes surrounding each grid node.

Critical examination of the resulting finite difference equations using the methods (ii) and (iii) was reported by Antonopoulos (1975) and showed

that in most cases, the resultant equations are the same. As regards the method of expansion in Taylor series, the method is less general than (ii) and (iii) because apart from offering less physical insight in the derivation of the finite difference equations, the reciprocity requirement for the fluxes at locations midway between grid nodes usually leads to the central difference formulation which is inaccurate representation of the fluxes at high Peclet numbers; therefore this method was not used. The second method (ii) is associated with the finite element technique and was discarded in the present work because of the difficulty of describing the boundary conditions. Thus, in the present work, method (iii) was used to obtain the finite difference equations for the conservation of mass, momentum, total enthalpy and species concentration.

In this section, details are provided for the numerical procedure used to solve the set of difference equations representing the conservation of mass, momentum, energy and scalar entities. The main feature of the procedure is the use of the SIMPLE numerical scheme of the Semi Implicit Method for Pressure-Linked Equations, proposed by Carreto et al. (1972) and Patankar et al. (1972). In the following subsections, details of grid arrangement, location of variables, near wall regions, the difference equations and the SIMPLE algorithm are given. The section ends with comments on stability, accuracy and convergence of the numerical procedure.

2.2.1 Grid arrangement

The numerical grid system consisted of a set of orthogonal intersecting grid lines in the x-y plane, with no restrictions on the distribution of grid lines in the solution domain. The intersections of these grid lines formed the grid nodes at which all flow properties except the velocities U and V were stored. The axial velocity U was located midway between grid nodes in the axial direction, while the radial velocity V

was located midway between grid nodes in the radial direction. Figure 2.2.1 shows the grid arrangement in the x-y plane. Since the flows reported here were mainly two dimensional and axisymmetric, there was no need to specify any information for the θ plane.

2.2.2 Finite difference equations

The finite difference counterpart of the general partial differential equation 2.1.12 is derived by supposing that each variable is enclosed in its own control volume or "cell" as shown in figure 2.2.1. The grid node P was surrounded by two x-direction neighbouring points W and E in the west and east directions and two nodes N and S in the north and south y-directions. The partial differential equation is integrated over the control volume with the aid of assumptions about the relations between the nodal values of Φ and the rates of generation/destruction of this entity Φ within the cell and its transport by convection and diffusion across the cell boundaries. The former is represented in linearised form as

$$S_\Phi = \int_v S_\Phi \, dV = S_u + S_P \, \Phi_P \qquad 2.2.1$$

and the latter by expressions of the form :

$$\rho U_w \frac{(\Phi_P + \Phi_W)}{2} A - \Gamma_{\Phi_w} \frac{(\Phi_P - \Phi_W)}{\delta x_{PW}} A \qquad 2.2.2$$

where the quantity $Pe_W \equiv \rho U_w \, \delta x_{pW} / \Gamma_{\Phi_W}$ is small and by:

$$\begin{aligned} &\rho U_w \, \Phi_W \quad , \quad U_w > 0 \\ &\rho U_w \, \Phi_P \quad , \quad U_w < 0 \end{aligned} \qquad 2.2.3$$

when Pe_w is large. Here the subscripts P and W refer to the central and west nodes respectively, and w denotes the intervening cell boundary. Assembly of the above, and similar expressions for the remaining boundaries

yields the finite difference equation as;

$$(A_P - S_P)\ \Phi_P = \sum_n A_n \Phi_n + S_u \qquad 2.2.4$$

where

$\sum_n$ denotes summation over the neighbouring nodes, N, S, E and W,

$A_P \equiv \sum_n A_n$.

The coefficient A_n is the net convection diffusion flux and is expressed as;

$$A_n = D_n^* - C_n$$

where

$$D_n^* = 0.5\ (D_n + |C_n| + |D_n - |C_n|\ |),$$

$$D_n = \Gamma_{\Phi,n}\ A/\delta x \qquad 2.2.5$$

$$C_n = \rho U_n\ A/2$$

Equations of this kind are written for each of the variables U, V, W, Φ at every cell, with appropriate modifications being made to the total flux expressions 2.2.2 and 2.2.3 at cells adjoining the boundaries of the solution domain to account for the conditions imposed there.

An equation for the remaining unknown, pressure, is obtained by combining the continuity and momentum equations in the manner explained in references by Caretto et al. (1972) and Patankar et al. (1972): this entails connecting changes in pressure, denoted P' with changes in the velocities U and V by approximate formulae derived from the momentum finite difference equations as;

$$U_e = U_e^* + D_E^u\ (P_P' - P_E')$$

and

$$U_w = U_w^* + D_W^u\ (P_W' - P_P') \qquad 2.2.6$$

and similarly for V_n and V_s. The starred values are guessed values and D_E^u, D_W^u are the pressure difference coefficients. Substitution of these formulae into the continuity equation yields a partial differential equation for p' similar to 2.2.4, with S_u now representing the local continuity imbalance in the prevailing velocity field.

2.2.3 Solution algorithm

The finite difference equations are solved by iteration, employing inner and outer sequences. The outer iteration sequence involves the cyclic application of the following steps: firstly, a field of intermediate axial and radial velocities, denoted by U^* and V^* is obtained by solving the associated momentum equations using the prevailing pressures P^*. Then continuity is enforced, by solving the equations for p' and thereby determining the required adjustments to the velocities and pressures. The equations for the remaining variables are then solved in turn, and the whole process is repeated until a satisfactory solution is obtained as the residuals (inbalance) in any of the finite difference equations is less than 10^{-4} of a specified inlet value of the entity in question.

The inner iteration sequence is employed to solve the equation sets for the individual variables. Solution is by a form of block iteration, in which a simple recurrance formula described by Gosman et al. (1974) among others, is used to solve simultaneously for the Φ's along each grid line, in the line by line counterpart of point GaussSeidel iteration. Complete convergence of the inner sequence is not necessary, and usually one to three applications of the block procedure suffices.

2.2.4 Miscellaneous details

The numerical solution is required to pass two acceptance tests; firstly, it must satisfy the finite difference equations when substituted into them (typically, the imbalance must be 0.1% or less); and secondly, it must be invariant with further increase in the number of grid nodes. These two tests

are discussed as follows.

2.2.4.1 Convergence and stability

The simultaneous and non-linear character of the finite difference equations necessitates that special measures be employed to procure numerical stability (convergence): these include under relaxation of the solution of the momentum and turbulence equations by under relaxation factors which relate the old and the new values of Φ as follows;

$$\Phi = \beta \Phi_{new} + (1-\beta) \Phi_{old} \qquad 2.2.7$$

where β is the under relaxation factor which was varied between 0.3 and 0.7 for the three velocity components as the number of iterations increases. For the turbulence quantities, β was taken as 0.8 and for other variables as 0.9.

In swirling flows, a practice of gradual introduction of swirl was adopted, by increasing the value of swirl number gradually with iteration to the specified value. Convergence problems associated with reacting flows were observed and the local mixture density was heavily under-relaxed to prevent divergence; the corresponding value of β was 0.2. The residuals decreased monotonically after around 50 iterations and satisfied the convergence criteria of all residuals less than 10^{-4} at 200 to 400 iterations, depending on the flow configuration.

The flow chart of the computer program (TEACH-T)*, which solves the finite difference equations 2.2.4, is shown in figure 2.2.2 and its core memory requirement when running on a CDC 6600 machine is expressed as;

---

*At an early stage of this work, a similar computer program (EASI) was used, but the results shown within the thesis were obtained with the TEACH program, developed and tested for elliptic reacting flows.

C.M. = (16000 + 4 x number of grid nodes x number of equations)

words and the CDC 6600 C.P.U. time is;

C.P.U. = 0.0005 S/iteration/grid node/equation solved.

Examples of the variation of the residuals in U, V and W momentum equations and the continuity equation, with the number of iterations are shown in figures 2.2.3 to 2.2.5 for various flow situations. In figure, 2.2.3, the variation of the normalised residuals with iterations is shown for the case of sudden axisymmetric expansion for grids of 16 x 16 and 20 x 20; the monotonic convergence was slower for the 20 x 20 grid. The distribution of the residuals for non reacting coaxial jets in a sudden expansion is shown in figure 2.2.4 and was obtained for the flow of case 1 of table 3.2 shown later in chapter 3. The influence of swirl on the convergence rate is shown in figure 2.2.5 for the swirling flame situation of Cernansky et al. (1974) (S = 0.31), at higher swirl numbers, the converged solution was obtained after 340 iterations for S = 0.52.

2.2.4.2 Influence of grid size and arrangement

It is important to test the grid dependence of a solution and to use the minimum number of nodes which can give a grid independent solution. In the present investigation, a series of tests were performed for each flow configuration to determine the influence of the number and distribution of grid nodes. Various grid distribution functions can be used, for example, a linear progression where the ratio between any successive locations was less than 1.2; it is also possible to specify the grid nodes individually. An analysis of the errors resulting from the use of non-uniform grids, without the application of proper correction, showed that the errors in $\partial^2\Phi/\partial x^2$, for example, is given by

$$\text{Error } \alpha \; 1/6 \; \frac{\partial^3 \Phi}{\partial x^3} \; \left(\frac{\delta x_+^3 - \delta x_-^3}{\delta x^2}\right) \qquad 2.2.8$$

where δx_+ and δx_- are the distances between the nodes E and P and P and W respectively and δx the uniform spacing. If $\delta x_+ \neq \delta x_-$, the error is finite and increases as the non uniformity increases. From figure 2.2.1, it can be seen that U_E lies midway between E and P nodes while U_P lies midway between W and P nodes. For the U-momentum equation, the control volume is shown by the hatched area in figure 2.2.1. The velocity U_e does not equal 1/2 $(U_E + U_P)$ as would be the case for uniform grid spacing, but is a weighted average of U_E and U_P; i.e.

$$U_e = U_E \left(1 - \frac{\delta x_+}{\delta x_+ + \delta x_-}\right) + U_P \left(\frac{\delta x_+}{\delta x_+ + \delta x_-}\right) \qquad 2.2.9$$

and reduces to $(U_E + U_P)/2$ when δx_+ equals δx_-.

Various computational tests were performed to determine the influence of grid distributions and size. The centreline distributions of mean axial velocity are shown on figure 2.2.6, for a sudden expansion axi-symmetric flow at a Reynolds number of 6000 and expansion ratio d/D of 0.388. Grid sizes of 16 x 16, 20 x 20 and 25 x 25 are presented in the figure for two different initial velocity profiles. The distributions obtained with the 20 x 20 and 25 x 25 grid nodes were sensibly the same and the obtained local flow properties were found to be grid independent. The wall shear stress τ_w distributions are shown in figure 2.2.7 for grid 16 x 16, 20 x 20 and 25 x 25 grid node arrangements. The distributions obtained with the aid of the two largest grid sizes, were the same and differed from that obtained with the 16 x 16 grid arrangement.

These results may be regarded as typical of the computational investigations of Khalil (1976) where the effect of grid size and arrangement, among others, on the obtained calculations, was discussed.

2.2.4.3 Numerical accuracy and false diffusion

To represent the convective and diffusive flux expressions in the finite difference equations, three different schemes can be used. These

are the central, upwind and hybrid difference formulae. The central difference expressions give unrealistic results for $|Pe|>2.0$. At large $|Pe|$, the upwind difference is preferable as reported by Gosman et al. (1974). A combincation of the two expressions, namely the hybrid formula, gives better representation of the combined fluxes for all values of the $|Pe|$, therefore it was used in the present calculation procedure.

One of the numerical errors associated with the finite difference representation of the conservation equations is the false diffusion. It occurs because, all the finite difference schemes evaluate Φ_P as weighted mean of the surrounding Φ's. The errors due to false diffusion diminish when the streamlines are parallel to the mesh and for small values of Pe; the false exchange coefficient Γ_{false} was given by; Gosman et al. (1969) as;

$$\frac{\Gamma_{false}}{\Gamma_{\Phi_{eff}}} = 0.36 \; R_{loc} \; \sigma_{\Phi} \; \left(\frac{\mu}{\mu_{eff}}\right) \; \left(\frac{\Delta x}{L}\right) \sin(2\alpha) \qquad 2.2.10$$

where

$R_{loc} \equiv \bar{\rho} \; \bar{U} \; L/\mu$ is a Reynolds number based in typical length L of the problem considered.

α is the angle that the velocity vectors make with the coordinate system.

Δx is the grid node spacing (mesh size).

The effect of false diffusion is important in laminar flows, but at high Reynolds number, i.e. in turbulent flows, the effective viscosity μ_{eff} is much larger than the laminar one and the influence of flase diffusion diminishes.

2.2.4.4 Calculation of exponential source terms

In the calculation of the exponential term, which appears in the source term of species conservation equation and is strongly temperature dependent,

an average value over the cell replaces that estimated at the nodal point, and is given by the expression;

$$\exp(-E/R\bar{T}) = \int_y \int_x \exp(-E/R\bar{T})\, dxdy \Big/ \int_y \int_x dxdy$$

$$= \frac{\exp(-B)}{a\, b\, B^2} \{\exp(Ba\eta_b) - \exp(Ba\eta_a)\} \{\exp(Bb\zeta_b) - \exp(Bb\zeta_a)\}$$

where

$$a = \frac{\Delta x}{\bar{T}_p} \left(\frac{\partial \bar{T}}{\partial x}\right)_p \qquad \eta = \frac{x - x_p}{x_b - x_a}$$

$$b = \frac{\Delta y}{\bar{T}_p} \left(\frac{\partial \bar{T}}{\partial y}\right)_p \qquad \zeta = \frac{y - y_p}{y_b - y_a}$$

$$B = \frac{E}{R\bar{T}}$$

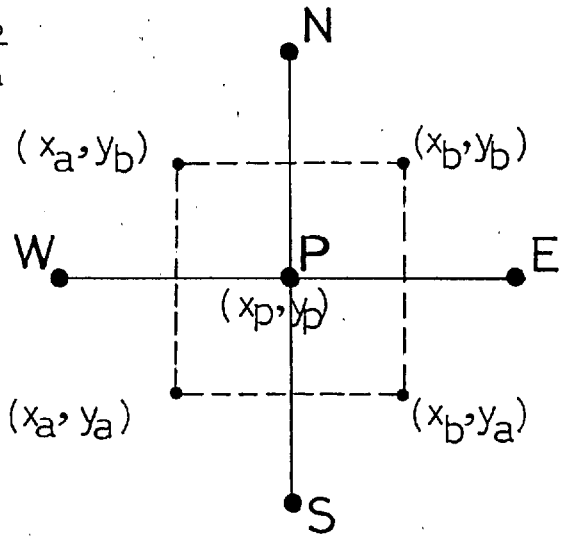

Previous calculations of NO concentrations, Hutchinson et al (1976), were obtained with this expression and the obtained concentrations did not depend on the grid arrangements.

The influence of the improper specification of inlet profiles on local flow pattern was also investigated, Khalil (1976).

2.3 Turbulence Models

The mean momentum equations described in section 2.1 contain unknown Reynolds stress elements, $\overline{u_i u_j}$. In order to solve the set of momentum

equations, these Reynolds stresses have to be related to the mean hydrodynamic properties of the flow field. There are many ways of relating these stresses to the mean hydrodynamic quantities, either by algebraic expressions or by more complicated partial differential equations.

The eddy or turbulent viscosity concept was introduced by Boussinesq (1877) who suggested that the effective turbulent shear stress, $-\bar{\rho}\,\overline{uv}$, could be replaced by $\mu_t\ \partial\bar{U}/\partial r$. The task of evaluating μ_t, the turbulent viscosity, has been the concern of many workers. A simple algebraic expression for μ_t has been proposed, for example, by Prandtl (1925) with μ_t proportional to ℓ^2 and $(\partial\bar{U}_i/\partial x_j)$ where ℓ is defined as the mixing length appropriate to each flow of the boundary layer type. Alternative expressions have been noted, for example, by Launder et al. (1972).

Further advent in the evaluation of μ_t was the solution of a partial differential equation for the kinetic energy of turbulence as reported by Prandtl (1945) and Bradshaw et al. (1967). The proposals of Kolmogorov (1942), Chou (1945) and Harlow et al (1967) assumed that the local state of the fluid depends on one or more turbulence quantities determined from the solution of the corresponding transport equations. In many flows this allows the turbulent flows to be characterized by two turbulence quantities, for example, the kinetic energy of turbulence k and a characteristic length scale. The solution of differential equations for these two properties was proposed by Harlow et al. (1967) and Jones and Launder (1973).

A second approach to the evaluation of the Reynolds stresses $\overline{u_i u_j}$ is to solve transport equations for the stresses themselves as proposed, for example, by Daly and Harlow (1970) and Launder, Reece and Rodi (1975). These equations represent the turbulent transport, generation, dissipation and redistribution of the Reynolds stresses. For axisymmetric recirculating flows, as in the present investigations, the Reynolds stress model requires at least five partial differential equations in addition to the ones for the

mean flow. The computer time and storage required for solving these equations become prohibitively large when considering the details of the turbulent reacting flows.

2.3.1 The turbulence model of the present work

In the present work, a two equation turbulence model was used. This two equation model is represented by equations for the kinetic energy of turbulence k and its dissipation rate ε. The turbulent viscosity μ_t is calculated from the expression;

$$\mu_t = C_\mu \bar{\rho} k^2/\varepsilon \qquad 2.3.1$$

and the effective viscosity μ_{eff} is expressed as

$$\mu_{eff} = \mu_t + \mu \qquad 2.3.2$$

the kinetic energy k is defined as;

$$k \equiv \frac{1}{2} \overline{u_i u_i} \qquad 2.3.3$$

$$\varepsilon \equiv \frac{\mu}{\bar{\rho}} \overline{\left(\frac{\partial u_i}{\partial x_j} \frac{\partial u_i}{\partial x_j}\right)} \qquad 2.3.4$$

and C_μ is a constant.

The modelled conservation equation for k, deduced by Rodi (1972), was represented by equation 2.1.12 and neglecting the density fluctuations and their correlation;

$$\Gamma_k = \mu_{eff}/\sigma_k$$

$$\bar{S}_k = G - \bar{\rho}\varepsilon \qquad 2.3.5$$

where ,

G = Generation of turbulent energy due to mean velocity gradients

$$= -\bar{\rho}\,\overline{u_i u_j}\;\partial\bar{U}_i/\partial x_j \qquad 2.3.6$$

$$\text{and } \bar{\rho}\,\overline{u_i u_j} = -\left\{\mu_t\left(\frac{\partial \bar{U}_i}{\partial x_j} + \frac{\partial \bar{U}_j}{\partial x_i}\right) - \frac{2}{3}\left(\bar{\rho}\,k - \frac{\mu_t}{\bar{\rho}}\,\bar{U}_\ell\,\frac{\partial \bar{\rho}}{\partial x_\ell}\right)\delta_{ij}\right\} \qquad 2.3.7$$

The corresponding modelled equation for the transport of ε is expressed in the form 2.1.12 and,

$$\Phi = \varepsilon$$

$$\Gamma_\varepsilon = \mu_{eff}/\sigma_\varepsilon$$

and 2.3.8

$$\bar{S}_\varepsilon = C_1\,G\,\frac{\varepsilon}{k} - C_2\,\bar{\rho}\,\frac{\varepsilon^2}{k}$$

C_μ, C_1 and C_2 are the constants of the turbulence model and were obtained from equilibrium flows, turbulence decay behind grids and computer optimization respectively. According to the recommendations of Launder et al. (1972), made after extensive examination of free turbulent flows, the constants appearing in equations 2.3.1 and 2.3.8 take the values of table 2.1.2. These constants were found appropriate for plane jets and mixing layers and modifications were made for free round jets by Rodi (1972).

Various predictions were obtained with the k-ε model for free shear flows and were reported to be in good agreement with the corresponding measurements; e.g. Launder et al. (1972 and 1973). Table 2.3.1 shows some of the flows which had been tested and reasonable agreement was obtained. The values of constants of the two equation turbulence model shown in table 2.1.2 were not appropriate for strongly swirling jets; Morse (1976) found that the constant C_1 should be modified to predict the rate of spread of the coaxial swirling jet of his investigation. The value of C_1 is given as,

$$C_1 = 1.44 + 0.8\,R_i\,\frac{\bar{\rho}\varepsilon}{G} \qquad 2.3.9$$

where

$$R_i = \left(\overline{vw}\,r\,\frac{\partial}{\partial r}\left(\frac{\bar{W}}{r}\right)\right)/\varepsilon$$

Table 2.3.1

Reference	Flow	k-ε constants				
		C_1	C_2	C_μ	σ_k	σ_ε
Launder et al (1972)	Plane jet in a moving stream	1.44	1.92	0.09	1.0	1.3
Launder et al (1973)	Flow in a pipe	1.44	1.92	0.09	1.0	1.3
Launder et al (1973)	Wall jets on cones	1.44	1.92	0.09	1.0	1.3
Matthews et al (1971)	Wall jets	1.44	1.92	0.09	1.0	1.3
Launder et al (1973)	Co flowing jets	1.44	1.92	0.09	1.0	1.3
Launder et al (1973)	Flow along a twisted tape	1.44	1.92	0.09	1.0	1.3
El Ghobashi et al (1975)	Coaxial jets with conen-tration fluctuation	1.45	2.0	0.09	1.0	1.3

which gives the ratio between additional production due to the stress $\overline{vw}$ and the dissipation rate ε. As regards to recirculating confined axisymmetric flows, extensive comparisons have not been reported for non-reacting flows. In table 2.3.1, two examples of axisymmetric flows with recirculations are indicated for coflowing jets and reasonable agreements were obtained; El Ghobashi et al. (1975).

The exact solution for transport of k in a turbulent reacting flow is different from that for the non reacting flow due to the heat release and the density fluctuations correlations. However, for simplicity, the previous turbulent combustion modelling, e.g. El Ghobashi (1974) used the form of equation 2.3.5 appropriate to a non-reacting incompressible flow, Rodi (1972). The exact equation in turbulent reacting flows was described by Bray (1973 and 1974) for boundary layer flows and was extended to elliptic flows by Hutchinson et al. (1976).

Additional terms in the conservation equation of the kinetic energy of turbulence, equation 2.3.5 emerged due to the effect of density changes and are included in the source term of k as follows;

$$\bar{S}_k = G - \bar{\rho}\varepsilon + \frac{\mu_{eff}}{\sigma_\rho}\left(\frac{\partial k}{\partial x}\frac{\partial \bar{\rho}}{\partial x} + \frac{\partial k}{\partial y}\frac{\partial \bar{\rho}}{\partial y}\right) \qquad 2.3.10$$

and σ_ρ equals 0.9. In a typical flame, where the density of the hot products is nearly 20% of that of the fresh air/fuel mixture, the additional terms shown in equation 2.3.10, resulted in less than 20% difference in the local values of k and 2% in mean velocities, concentrations and gas temperatures. These figures stem from the calculation of the flow in a confined coaxial jet configuration and coflowing flow, with and without these additional terms.

In some applications of industrial flames, the influence of buoyancy forces can be significant and can result in asymmetric behaviour of the

flame. The buoyancy force appears in the momentum equations as a source term and preliminary calculations in the furnace of the present investigations showed that these forces had a negligible effect on the flow pattern and heat transfer in the present flow configuration and hence, was neglected.

2.3.2 Wall functions

The form of the k-ε model represented by equations 2.3.5 and 2.3.8 is appropriate to turbulent flows with high turbulence Reynolds number, i.e. for values of

$$Re_w = k^{\frac{1}{2}} \ell_o / \nu \qquad 2.3.11$$

where ν is the kinematic viscosity and $\ell_o = k^{3/2}/\varepsilon$

greater than 5000.

In regions of flow near to a wall the velocities tend to zero at the wall and hence there are zones where the local values of Re_w is so small and the viscous effect is dominant. A large number of grid nodes is needed if the momentum equations are to be solved at each node. This would be costly and, hence, the use of a wall function was introduced.

Near a wall, at point p shown in figure 2.3.1, the flow is predominantly parallel to the wall and the shear stress is assumed constant, as reported by Launder et al. (1972). Thus,

$$\tau_w = (\bar{U}_p \; y_+) \; / \; (y_1 \; u_+) \qquad 2.3.12$$

where $u_+ = \frac{1}{K} \; \ell n \; E \, y_+$

E and K are constants

y_+ is $y_1 \; \bar{\rho} \; k_p^{1/2} \; C_\mu^{1/4} / \mu$

k_p is the value of the kinetic energy of turbulence at p

and y_1 is the distance normal to the wall.

These assumptions led to an equation linking the wall shear stress τ_w to

the velocity parallel to the wall;

$$\frac{\bar{U}_P}{\frac{\tau_w}{\bar{\rho}}} C_\mu^{1/4} k_p^{1/2} = \frac{1}{K} \ln (E y_+) \qquad 2.3.13$$

The constants of the logarithmic law of the wall, K and E, depend on the wall roughness and are given in table 2.1.2. This wall function represents the dependence of the flux of momentum to the wall on the turbulence characteristics at a point p remote from it.

The value of k_p is calculated from the transport equation of k with the diffusion of energy to the solid wall set to zero. The value of ε used to obtain k_p was assumed (Launder et al. 1973) to take the form;

$$\int_0^{y_1} \varepsilon \, dr = C_\mu^{3/4} \frac{k_p^{3/2}}{K} \ln (E y_1 C_\mu^{1/4} k_p^{1/2} \bar{\rho}/\mu) \qquad 2.3.14$$

and can also be written as;

$$\varepsilon y_1 = C_\mu^{3/4} \frac{k_p^{3/2}}{K} \qquad 2.3.15$$

The heat flux to the wall can be represented in a similar manner, denoting the wall temperature and heat flux per unit area as T_w, q_w'', one can write,

$$\frac{\bar{C}_p \{\bar{T}_p - \bar{T}_w\}}{\frac{q_w''}{(\frac{\bar{\rho}}{\bar{\rho}})}} C_\mu^{1/4} k_p^{1/2} = \frac{\sigma_{h,t}}{K} \{E C_\mu^{1/4} k_p^{1/2} y_1 \bar{\rho}/\mu\} + P_j \qquad 2.3.16$$

where

P_j is defined as;

$$P_j = \sigma_{h,t} \frac{\pi/4}{\sin \frac{\pi}{4}} \{\frac{A}{K}\}^{1/2} \{\frac{\sigma_h}{\sigma_{h,t}} - 1\}\{\frac{\sigma_{h,t}}{\sigma_h}\}^{1/4} \qquad 2.3.17$$

A = Van Driest's constant = 26 for smooth walls

$\sigma_{h,t}$ = effective Prandtl number for fully turbulent flows

σ_h = laminar Prandtl number.

The treatment of irregular boundaries and obstacles of various geometries was carried out with the appropriate wall functions. The various grid nodes near an inclined wall are shown in figure 2.3.2 and the resultant velocity U_R is expressed as,

$$U_R = \{((U_P + U_E) / 2)^2 + ((V_P + V_N) / 2)^2 \}^{\frac{1}{2}}$$

The local velocity gradients near the wall were calculated accounting for the wall angle $\theta = \tan^{-1} (\Delta Y/\Delta X)$ and the flow angle $\theta_o = \tan^{-1}\{(V_P + V_N)/(U_P + U_E)\}$. The resultant velocity parallel to the wall is $U_R \cos (\theta_o - \theta)$ and is used in the wall function to obtain the resultant shear stress. In the presence of swirl, the resultant velocity U_{R_θ} is,

$$U_{R_\theta} = \{(U_R \cos (\theta_o - \theta))^2 + W_P^2 \}^{\frac{1}{2}}$$

2.4 Combustion Models

2.4.1 Introductory Remarks

In the present section, the averaged values of chemical and thermodynamic quantities which characterise turbulent flames are the main concern. The determination of the average temperature $\bar{T}$, density $\bar{\rho}$, and mass fraction of chemical species, $\bar{M}_a$, forms the principal objective of the combustion modelling. Two effects are considered in this section; these are the effect of turbulence on reaction rates and of the reaction on the local turbulence.

The local time average value of chemical species mass fraction M_a may be represented as,

$$\bar{M}_a = \int_{M_a} M_a P(M_a) \, d M_a \qquad 2.4.1$$

where $P(M_a)$ is the probability density function of M_a and the corresponding variance of M_a is,

$$\overline{m_a^2} = \int_{M_a} (M_a - \bar{M}_a)^2 P(M_a) \, d M_a \qquad 2.4.2$$

where

$$M_a \equiv \bar{M}_a + m_a$$

The conservation equation of fuel mass fraction $\bar{M}_{fu}$ can be expressed in the form 2.1.6 where the source term $\bar{S}_{fu}$ equals to $\bar{R}_{fu}$, the time average rate of disappearance of fuel due to chemical reaction. The various terms in the fuel conservation equation, expressed in the form 2.1.6, may be calculated at the individual grid nodes of the solution domain. Triple correlation and the laminar diffusion terms are neglected in the present work. The turbulent diffusion term is modelled, after Monin et al. (1971), as

$$-\frac{\partial}{\partial x_j}\left(\bar{\rho}\,\overline{u_i m_{fu}}\right) = \frac{\partial}{\partial x_j}\left(\frac{\mu_{eff}}{\sigma_{fu}}\,\frac{\partial \bar{M}_{fu}}{\partial x_j}\right) \qquad 2.4.3$$

with the value of σ_{fu} taken as 0.9. The term $\overline{\rho' m_{fu}}$ is usually neglected but can be obtained from the corresponding conservation equation as discussed later in the section.

The chemical reaction rate in homogeneous reactions is defined as the rate at which one of the reactants disappears to form products, or the rate at which the products are formed. If the reaction is an oxidation, the fuel concentrations decrease and the rate of formation of the products of combustion is positive. The reaction rate can be expressed (Kondratiev 1964) as;

$$R_{fu} = f^{n}\ (T,\ P,\ \text{composition}) \qquad 2.4.4$$

and the mechanism expressed as;

$$\text{Fuel} + \text{oxidant} \rightarrow \text{Products}\ . \qquad 2.4.5$$

If it is postulated that the rate controlling mechanism involves the collision or interaction of a single molecule of fuel with a single molecule of oxygen, then the rate of reaction is proportional to the collisions of fuel and oxygen since, at a given temperature, the number of collisions

is proportional to the local concentrations of reactants in the mixture;

$$\text{i.e.} \qquad R_{fu} = K_f M_{fu} M_{ox} \qquad 2.4.6$$

The influence of temperature on the rate of reaction may be expressed in terms of the exponential of (-E/RT), suggested by Arrhenius (1889) as,

$$K_f = A_o \exp(-E/RT) \qquad 2.4.7$$

values of A_o and E/R are determined from experiments and have been reported for many elementary reactions by Baulch et al. (1970) and Weldman et al. (1974).

The instantaneous rate of reaction can generally be expressed, see Borghi (1974), as;

$$R_{fu} = (\bar{M}_{fu} + m_{fu})\ (\bar{M}_{ox} + m_{ox})\ (\bar{K}_f + K_f') \qquad 2.4.8$$

If $\exp(T'/T)$ and $(1 + T'/T)^{-\frac{1}{2}}$ are expressed in terms of series expansions, the following equality is obtained;

$$\overline{(\bar{K}_f + K_f')} = A_o \exp(-E/R\bar{T}) \left\{ 1 + \sum_{n=2}^{\infty} P_n \left(\frac{\overline{T'^n}}{\bar{T}^n}\right) \right\}$$

where

$$P_n = \sum_{z=1}^{n} (-1)^{n-z} \frac{n-1\,!}{(n-z)!\ ((z-1)!)^2} \frac{1}{z} \left(\frac{E}{R\bar{T}}\right)^z$$

and

$$\bar{R}_{fu} = A_o \bar{\rho}^2 \bar{M}_{fu} \bar{M}_{ox} \exp(-E/R\bar{T}) \left\{1 + a_o \frac{\overline{m_{fu} m_{ox}}}{\bar{M}_{fu} \bar{M}_{ox}} + a_1 \left(\frac{\sqrt{\overline{T'^2}}}{\bar{T}}\right)^2 \right.$$

$$\left. + a_2 \left(\frac{\overline{T' m_{ox}}}{\bar{T}\,\bar{M}_{ox}} + \frac{\overline{T' m_{fu}}}{\bar{T}\,\bar{M}_{fu}} \right) \right\}, \qquad 2.4.9$$

with the constants a_o, a_1 and a_2 given as;

$$a_o = 1$$

$$a_1 = \tfrac{1}{2} (E/R\bar{T})^2 - E/R\bar{T}$$

$$a_2 = E/R\bar{T}$$

There are two limitations to the above series; the expansion of R_{fu} is valid only for $T'/\bar{T}<1.0$; and the series expansion of an exponential converges slowly, hence the method is applied only to low temperature fluctuations. Borghi (1974) indicated that the approximation becomes poorer as $E/R\bar{T}$ increases, i.e. for high activation energy or low temperature. For convenience, equation 2.4.9 may be rewritten as;

$$\bar{R}_{fu} = A_o \bar{\rho}^2 \bar{M}_{fu} \bar{M}_{ox} \exp(-E/R\bar{T}) \{1+F\} \qquad 2.4.10$$

where the term F includes the influence of turbulence on the time averaged reaction rate and is given by,

$$F = a_o \left\{\frac{\overline{m_{fu} m_{ox}}}{\bar{M}_{fu} \bar{M}_{ox}}\right\} + a_1 \left\{\frac{\sqrt{\overline{T'^2}}}{\bar{T}}\right\}^2 + a_2 \left\{\frac{\overline{T'm_{fu}}}{\bar{T}\bar{M}_{fu}} + \frac{\overline{T'm_{ox}}}{\bar{T}\bar{M}_{ox}}\right\}$$

In the remaining part of this section, various models of combustion, used in the calculations of furnace flames are discussed in view of the assumptions imposed, the models formulation, their physical implications and their validity to the various flame flow configurations. The models considered in this work include models assuming infinitely fast chemical reactions, appropriate to diffusion flames, and others which assume finite reaction rate suitable for premixed flame situations. Models appropriate to arbitrary fuelled systems are also considered. The various equations solved in each model and the basic assumptions involved are shown in table 2.4.1 which also indicates the type of flame to which a particular model is applicable. The validity of each of these models, in turbulent furnace flows, is assessed by comparisons between measurements and calculations as discussed later in chapter 5.

2.4.2 Fast chemical reaction models

These models are based on the assumption that, whenever fuel and oxidant both exist at a point in the flow domain, chemical reaction proceeds

Table 2.4.1

Flame Type	Basic Assumptions	Model	Equations Solved	Remarks
Diffusion	Infinitely fast chemical reaction	1	$U,V,W,k,\varepsilon,P,f,H$	Diffusion flames
	Infinitely fast chemical with concentration fluctuations	2	$U,V,W,k,\varepsilon,P,f,g,H$	Square wave species distribution with time
		3	$U,V,W,k,\varepsilon,P,f,g,H$	Random distribution with time
Premixed	Finite reaction rate — single step	4	$U,V,W,k,\varepsilon,P,\bar{M}_{fu},g_{fu},\overline{m_{fu}m_{ox}},\overline{m_{ox}^2},H,f$	Premixed flames
	Finite reaction rate — multi step (eddy break up formulation)	5	$U,V,W,k,\varepsilon,P,\bar{M}_a,H,f$	Premixed flames, g_a's are obtained from algebraic expressions
Arbitrary fuelled	Finite reaction rate with concentration fluctuations	6	$U,V,W,k,\varepsilon,P,\bar{M}_{fu},\overline{m_{fu}^2},\overline{m_{fu}m_{ox}},\overline{m_{ox}^2},H,f$	Arbitrary fuelled system
	Finite reaction rate with concentration and temperature fluctuations	7	$U,V,W,k,\varepsilon,P,\bar{M}_{fu},\overline{m_{fu}^2},\overline{m_{ox}m_{fu}},\overline{m_{fu}T'},\overline{m_{ox}T'},\overline{\rho'\phi},\overline{T'^2},H,f$	Higher order correlations were obtained from algebraic expressions

Two additional equations for R_x and R_y, are solved.

instantaneously to completion in a single step, producing combustion products. The assumption of instantaneous chemical equilibrium is not far from reality in turbulent unpremixed flames, since the time of recombination of non equilibrium radicals will be smaller than the smallest time scale of turbulence, Gunther et al. (1969).

From the above assumption and the work of Shvab (1948), Zeldovich (1949) and Williams (1965), it can be concluded that a linear combination of the species conservation equations for the unpremixed-reactants, fuel and oxidant, yields an equation whose form is identical to that describing the conservation of chemically inert species, i.e. neither equation has a source term provided that the following assumptions are made;

(a) equal turbulent transport coefficients for the two reactants and products at each point in the field.

(b) fuel and oxygen combine always in a stoichiometric ratio i to produce (1+i) kg of products.

The resultant variable from the combination is the mixture fraction $\bar{f}$ which is defined as;

$$\bar{f} = \frac{\bar{\xi} - \bar{\xi}_A}{\xi_F - \xi_A} \qquad 2.4.11$$

where

$$\bar{\xi} = \bar{M}_{fu} - \bar{M}_{ox}/i \qquad 2.4.12$$

or

$$\bar{\xi} = \bar{M}_{fu} + \bar{M}_{pr}/(1+i) \qquad 2.4.13$$

The subscripts A and F denote air and fuel stream conditions at inlet. The conservation equation for $\bar{f}$ can be expressed in the general form 2.1.12 with;

$$\bar{S}_f = 0$$

$$\Gamma_f = \mu_{eff}/\sigma_f \qquad 2.4.14$$

and σ_f taken as 0.9.

Three of the models used here are based on the above assumptions but differ in the way in which the turbulence fluctuations are introduced: they are described below.

Model 1

This model assumes that fuel and oxidant cannot exist at the same place at any time and that the reaction is infinitely fast and equilibrium is attained. The following useful relations are obtained;

1. In regions of flame where oxidant and products exist, i.e.

$$0 < \bar{f} < \bar{f}_{st}$$

$$\bar{M}_{fu} = 0 \qquad 2.4.15$$

$$\bar{M}_{ox} = \bar{M}_{ox_A}\,(1-\bar{f}/f_{st}) \leqslant \bar{M}_{ox_A}$$

2. In regions of flame where fuel and products exist, i.e.

$$1 > \bar{f} > \bar{f}_{st}$$

$$\bar{M}_{fu} = \bar{M}_{fu_F}\{(\bar{f} - \bar{f}_{st})/(1 - \bar{f}_{st})\} \qquad 2.4.16$$

$$\bar{M}_{ox} = 0$$

$\bar{f}_{st}$ is the stoichiometric value of mixture fraction and is given by,

$$\bar{f}_{st} = \{(i\,\bar{M}_{fu_F}/\bar{M}_{ox_A}) + 1\}^{-1} \qquad 2.4.17$$

and $$\bar{M}_{pr} = 1 - \bar{M}_{ox} - \bar{M}_{fu} \qquad 2.4.18$$

The linear relationship between the instantaneous mass fractions of fuel and oxidant and $\bar{f}$ is shown in figure 2.4.1.

The enthalpy at each point in the flame is obtained in similar manner by solving an equation for $\bar{H}$ where,

$$\bar{H} = \int_o^T \bar{M}_j\,\bar{C}_{p_j}\,d\bar{T} + H_{fu}\,\bar{M}_{fu} + \frac{1}{2}(\bar{U}^2 + \bar{V}^2 + \bar{W}^2) \qquad 2.4.19$$

and $$\bar{C}_{p_j} = \sum_{n=0}^{m} a_n\,\bar{T}^n \quad \text{with } m = 3 \qquad 2.4.20$$

For adiabatic systems and with unity Lewis number, the mixture fraction can be written as,

$$\bar{f} = (\bar{H}-\bar{H}_A)/(\bar{H}_F-\bar{H}_A) \qquad 2.4.21$$

and the values of $\bar{H}_F$ and $\bar{H}_A$ are known boundary conditions,

$$\text{i.e. } \bar{H}_f = \int_o^{\bar{T}_{in}} \bar{C}_{p_F}\, d\bar{T} + H_{fu}\, \bar{M}_{fu_F} \qquad 2.4.22$$

$$\text{and } \bar{H}_A = \int_o^{\bar{T}_{in}} C_{p_A}\, d\bar{T} \qquad 2.4.23$$

The mean gas temperature and density are obtained from,

$$\bar{T} = (\bar{H}-H_{fu}\, \bar{M}_{fu})/\sum_j \bar{M}_j\, \bar{C}_{p_j} \qquad 2.4.24$$

$$\sum_j \bar{M}_j\, \bar{C}_{p_j} = \bar{M}_{ox}\, \bar{C}_{p_{ox}} + \bar{M}_{fu}\, \bar{C}_{p_{fu}} + \bar{M}_{pr}\, \bar{C}_{p_{pr}} \qquad 2.4.25$$

$$\bar{\rho} = \bar{P}/(R\bar{T} \sum_j (\frac{M_j}{W_j})) \qquad 2.4.26$$

In model 1, described above, the fluctuations of f and H are neglected and allowed solutions to be obtained with fast convergence but also, as discussed later, with results which were not always realistic. This model has previously been discussed by Williams (1965), Spalding (1971) and Bilger (1975) and its assumptions were found appropriate to diffusion flames and where excessive air is used. It is an over-simplification to real flame situations and experimental evidence since, for example, Bilger et al. (1972b) showed that in mixing zones of diffusion flames, oxygen and fuel concentrations have finite values.

Effect of Concentration Fluctuations

In contrast to model 1, models 2 and 3 consider the fluctuations of the scalar property ϕ with the assumption of infinitely fast, single step chemical reaction. Due to these fluctuations, fuel and oxidant may exist

at the same location, although at different times. The probability density function $P(\Phi)$ of a scalar entity (Φ) is defined as;

$$P(\Phi)\delta\Phi = \lim_{t\to\infty} \frac{1}{t} \Sigma\, \delta t \qquad 2.4.27$$

which is shown in figure 2.4.2. From the definition, it is implied that $P(\Phi)\delta\Phi$ is the fraction of time that $\Phi(t)$ spends between Φ and $(\Phi + \delta\Phi)$ and that, over a long time interval, the sum of the values of $P(\Phi)\,\delta\Phi$ must be equal to unity,

$$\text{i.e. } \int_{-\infty}^{\infty} P(\Phi)d\Phi = 1 \qquad 2.4.28$$

and hence the time average value of $\bar{\Phi}$ can be expressed as,

$$\bar{\Phi} = \int_{-\infty}^{\infty} \Phi\, p(\Phi)\, d\Phi \qquad 2.4.29$$

which is the first moment of $P(\Phi)$ about the origin $\Phi = 0$; for any other scalar variable $\gamma(\Phi)$, its time average value is expressed as;

$$\bar{\gamma} = \int_{-\infty}^{\infty} \gamma\,(\Phi)\, P(\Phi)\, d\Phi \qquad 2.4.30$$

The effect of turbulence fluctuations on the local flow properties is introduced through the consideration of the concentration fluctuation g; where g is defined as;

$$g \equiv \{\overline{(f-\bar{f})^2}\} \qquad 2.4.31$$

The time average value of any scalar $\Phi(f)$ can be obtained from the knowledge of $P(f)$ which can be readily determined from $\bar{f}$, g and the assumed temporal distribution of f. The local values of $\bar{f}$ are obtained from equation 2.4.14 and the conservation equation, which governs the transport of g, was reported by Spalding (1971) and Bray (1974). The transport equation of g was modelled and used by Spalding (1971) and Naguib (1975) for free diffusion flames and by El Ghobashi (1974) for confined diffusion flames. The validity of the modelled equation was assessed by Naguib (1975), in turbulent diffusion flames

and the agreement with experiments was satisfactory.

In the present model, the modelled form of the g equation, given by El Ghobashi is used and can be used in the form 2.1.12 with;

$$\Gamma_g = \mu_{eff}/\sigma_g$$

$$\bar{S}_g = C_{g_1} \mu_{eff} \left(\left(\frac{\partial \bar{f}}{\partial x}\right)^2 + \left(\frac{\partial \bar{f}}{\partial y}\right)^2 \right) - C_{g_2} \bar{\rho} \frac{\varepsilon}{k} g \qquad 2.4.32$$

and the constants C_{g_1} and C_{g_2} of table 2.1.2.

The time averaged values of any property $\bar{\Phi}$ are obtained from equation 2.4.29 with provision for the characteristics of the probability density function $P(\Phi)$. Many forms of the Pdfs have been proposed for reacting flow calculations. The first was a Gaussian distribution, extending from $-\infty$ to ∞, as was reported by Hawthorne et al (1949) and Thring et al (1953). This assumption is unrealistic when Φ represents the mixture fraction f, mass fraction of fuel, temperature, density etc. as it allows the passive scalars to attain negative or excessively large values. An alternative distribution, a beta function in the physical limits between 0 and 1, was proposed by Richardson et al (1953): limited work was carried out using this proposal as no experimental evidence supporting the assumption that the temporal distribution of passive scalars corresponds to beta function, was available. Spalding (1971) proposed a square wave form of species-time variation, which corresponded to two delta functions representing fuel and oxidant streams. The previous distributions together with other temporal distributions, for example, those reported by Rhodes et al (1972) were reviewed and assessed by El-Ghobashi et al (1974) who indicated that the square wave form can be used as a simple representation of the temporal species distribution.

The Gaussian distribution with limits of $-\infty$ and ∞ was rejected on the basis of the impossibility of having negative f or f greater than unity but

was developed and modified by Naguib (1975) by clipping the distribution at the physical limits of f = 0 and f = 1.0, corresponding to air and fuel streams respectively. The resultant distribution consists of a Gaussian distribution between f = 0 and 1 and two delta functions located at f = 0 and f = 1.

In the present work, two probability density functions, Pdfs, were used; these correspond to;

1. Delta functions at f = 0 and f = 1.0, i.e. a square wave distribution of f with time.
2. Gaussian distribution between f = 0 and 1.0 together with two delta functions at f = 0 and 1.0. This distribution corresponds to a random variation of f with time.

The above distributions were embodied in models 2 and 3 respectively as summarised in the following paragraphs.

Model 2

In model 2, the probability density function of f was represented by double delta functions at f = 0 and 1 with the corresponding square wave temporal distribution divided into four separate regions, as shown in figure 2.4.3 and indicated below;

1. Regions where $1.0>\bar{f}>0$

$$P(f) = A_1 \{\delta(f_+) + \delta(f_-)\} \quad \text{and} \quad A_1 = \tfrac{1}{2}$$

$$f_+ = \bar{f} + g^{\frac{1}{2}} \quad \text{and} \quad f_- = \bar{f} - g^{\frac{1}{2}} \qquad 2.4.33$$

2a. Regions where $\bar{f}<0.5$, and $\bar{f} - g^{\frac{1}{2}}<0.0$

$$P(f) = A_2\, \delta(0) + A_3\, \delta(f_+)$$

$$A_2 = g/(\bar{f}\ (\bar{f} + g/\bar{f})) \qquad 2.4.34$$

$$A_3 = \bar{f}/(\bar{f} + g/\bar{f})$$

2b. Regions where $\bar{f}>0.5$ and $\bar{f} + g^{\frac{1}{2}}>1.0$

$$P(f) = A_2\, \delta(f_-) + A_3\, \delta(1)$$

$$A_2 = (1 - \bar{f})/ (1 - \bar{f} + g/ (1 - \bar{f})) \qquad 2.4.35$$

and

$$A_3 = g / ((1 - \bar{f})^2 + g)$$

3. In regions where large oscillations of f are imposed, such that either fuel or oxidant is present, the probability density function is given by;

$$P(f) = (1 - \bar{f})\ \delta(0) + \bar{f}\ \delta(1)$$

$$g_{max} = (1 - \bar{f})\ \bar{f} \qquad 2.4.36$$

The local values of $\bar{T}$, $\bar{\rho}$, $\bar{M}_{fu}$, $\bar{M}_{ox}$ were obtained from equation 2.4.29 and the probability distributions of equations 2.4.32 to 2.4.36 which express the instataneous values of T, ρ, M_{fu} and M_{ox} in terms of the mixture fraction f. This model was previously used by Spalding (1971), El Ghobashi et al (1974), Khalil et al (1974,1975) and Richter (1976) for diffusion flames and it was concluded that it provides better agreement with experiment than model 1 because it accounts for the effect of turbulent concentration fluctuation.

Model 3

Model 3 differs from model 2 in that the clipped Gaussian probability distribution of mixture fraction is used instead of the double delta function. As the instantaneous value of f must satisfy the constraint, $0<f<1$, the unwanted tails of the conventional Gaussian distribution at $f<0$ and $f>1$, which are physically unrealistic, are accounted for by two Dirac delta functions at f=0 and f=1. The resultant clipped probability distribution is expressed, as given by Naguib (1975), in the form;

$$P(f) = \frac{1}{\sigma\sqrt{2\pi}}\ \exp\ (-\frac{1}{2}\ (\frac{f-\mu}{\sigma})^2)\ *\ \{D(f)\ -D(f-1)\} \qquad 2.4.37$$

$$+ A\ \delta(0) + B\ \delta(1)$$

where

μ is the value of f giving maximum probability.

σ is the variance

D(f) is the Heaviside step function defined as,

$D(\zeta) = 0$, $\zeta < 0$ and $D(\zeta) = 1$, $\zeta > 0$

$\delta(f)$ is the Dirac delta function.

This probability distribution is shown in figure 2.4.4.

The time averaged mixture fraction $\bar{f}$, obtained from equation 2.4.14, is expressed in the form 2.4.29 as;

$$\bar{f} = B + \int_0^1 \frac{f}{\sigma\sqrt{2\pi}} \exp\left(-\frac{1}{2}\left(\frac{f-\mu}{\sigma}\right)^2\right) df \qquad 2.4.38$$

and

$$B = \int_1^\infty P_o(f)\, df, \quad A = \int_{-\infty}^0 P_o(f)\, df \qquad 2.4.39$$

$$P_o(f) = \frac{1}{\sigma\sqrt{2\pi}} \exp\left(-\frac{1}{2}\left(\frac{f-\mu}{\sigma}\right)^2\right)$$

The value of g, the square of concentration fluctuations, obtained from equation 2.4.32 is given as;

$$g = B + \int_0^1 \frac{f^2}{\sigma\sqrt{2\pi}} \exp\left(-\frac{1}{2}\left(\frac{f-\mu}{\sigma}\right)^2\right) df - \bar{f}^2 \qquad 2.4.40$$

Values of $\bar{f}$ and g were calculated from their conservation equations 2.4.14 and 2.4.32 and μ and σ determined from a table in terms of $\bar{f}$ and g. The time averaged value of any property Φ and the variance can be obtained through the equations;

$$\bar{\Phi} = A\,\bar{\Phi}_A + B\bar{\Phi}_F + \int_0^1 \frac{\Phi(f)}{\sigma\sqrt{2\pi}} \exp\left(-\frac{1}{2}\left(\frac{f-\mu}{\sigma}\right)^2\right) df \qquad 2.4.41$$

and

$$\bar{\phi}^2 = B\,\bar{\phi}_F^2 + \int_0^1 \frac{(\Phi(f))^2}{\sigma\sqrt{2\pi}} \exp\left(-\frac{1}{2}\left(\frac{f-\mu}{\sigma}\right)^2\right) df - \bar{\Phi}^2 \qquad 2.4.42$$

The instantaneous values of T, ρ, M_{fu} and M_{ox} were assumed to be functions of f; the corresponding time averaged values can be obtained from

equations 2.4.41 and the square of the fluctuations was obtained from equation 2.4.42.

As for model 2, model 3 requires the solution of aerodynamic equations as well as the f and g conservation equations and consults, in addition, tabulated values of μ and σ for given f and g. The application of this model is limited to diffusion flames as it assumes infinitely fast reactions and does not explicitly include chemical kinetics. Previous investigations of El Ghobashi et al (1974), El Ghobashi (1974), Naguib (1975) and Hutchinson et al (1976) incorporated model 3 and suggested that this model is preferable in free and confined diffusion flames. The basic assumption of fast chemical reaction, incorporated in the models 1 to 3, implies that fuel and oxygen do not coexist and this assumption becomes less appropriate as the reactants are more premixed and the effect of chemistry requires consideration as discussed in the next subsections.

2.4.3 Finite chemical reaction models

In situations where fuel and oxidant are mixed prior to the combustion chamber, the assumption of infinitely fast chemical reaction is invalid and provision for finite rate of reaction is required. Premixed flame situations are found in Gas turbine after burners and baffle stabilized burners. A source term is required in the equation of conservation of species to account for the disappearance of species at finite rate.

The reaction mechanism between fuel and oxygen can take place with intermediate steps, producing radicals in the initiation reactions, which are oxidized in the termination reactions to yield carbon dioxide and water vapour for hydrocarbon fuels. The oxidation of hydrogen and hydrocarbons takes place in multistep reactions; each of these steps is governed by a reaction rate which appears in the corresponding species equation to account for the rate of formation or disappearance of the species. This rate,

expressed in the form 2.4.10, is strongly temperature dependent as indicated by the exponential term and is also dependent to a lesser degree on the local concentrations of reactants.

In the present work, a finite reaction rate of a single step mechanism is obtained with the aid of the eddy break up assumptions of Spalding (1970). The fuel conservation equation is then solved with the appropriate sink term, thus yielding the fuel mass fraction which, together with the values of $\overline{m_{fu}^2}$ obtained from their conservation equation, are used to obtain P(fu). Consequently other properties such as $\bar{T}$, $\bar{\rho}$, $\bar{M}_{ox}$ etc., are obtained in a similar manner to that of model 3 using equations 2.4.41 and 2.4.42 with M_{fu} replacing f. In situations where intermediate steps are incorporated, the same solution procedure is used for each species, as described later in connection with model 5.

Model 4

In the mixing zone of fuel and oxidant, the rate of a single step chemical reaction can be expressed as;

$$R_{fu} = A_o \rho^2 M_{fu} M_{ox} \exp(-E/RT) \qquad 2.4.43$$

Time averaging this Arrhenius expression and neglecting turbulent fluctuations yields;

$$\bar{R}_{fu} = A_o \bar{\rho}^2 \bar{M}_{fu} \bar{M}_{ox} \exp(-E/R\bar{T}) \qquad 2.4.44$$

which is similar to expression 2.4.10 when F equals zero, i.e. when the influence of turbulence on the reaction rate is neglected.

To evaluate the reaction rate, as expressed in 2.4.10, it is necessary to solve additional equations for the conservation of $\overline{m_{ox}^2}$, $\overline{m_{ox} m_{fu}}$, $\overline{T'^2}$, $\overline{m_{ox} T'}$ and $\overline{m_{fu} T'}$. Thus large computer storage is required because the rate expression 2.4.10 includes the effect of turbulence on the reaction rate. To avoid solving these additional equations Spalding (1970) proposed a reaction

rate based on the species concentration fluctuations and the rate of break up of eddies. The eddy break up reaction rate may be expressed as;

$$\bar{R}_{E.BU} = C_R \bar{\rho} \frac{\varepsilon}{k} g_{fu}^{\frac{1}{2}}$$

where

$$g_{fu} = \overline{(M_{fu} - \bar{M}_{fu})^2} \equiv \overline{m_{fu}^2} \qquad 2.4.45$$

and C_R is a constant of the model. The term ε/k has the dimensions of s^{-1} and the diffusion time scale is $\tau_{s_o} \equiv k/\varepsilon$ which should be compared to the chemical kinetic time scale τ_K given by Borghi (1973) as;

$$\tau_K = \{A_o \bar{\rho} (\bar{M}_{ox} + i \bar{M}_{fu}) \exp(-E/R\bar{T})\}^{-1} \qquad 2.4.46$$

The two rates of reaction given by equation 2.4.44 and 2.4.45 are compared together in the computational solution procedure and the smaller of them is taken to represent the effective controlling rate.

In regions where τ_{s_o} is larger than τ_K, the mixing of the reactants is slow and the reactants are at a suitable temperature and concentrations to react as soon as they intimately mix, therefore, the reaction is diffusion controlled, i.e. it is controlled by the smaller rate given by equation 2.4.45. On the other hand, when τ_{s_o} is very small, which corresponds to large dissipation rate of eddies and rapid mixing, the reaction is kinetically influenced; the reactants are in intimate contact but their temperature and concentrations are not suitable for the reaction to proceed; the smaller rate is given in this case by equation 2.4.44.

To determine the eddy break up rate of reaction, it is necessary to evaluate $\overline{m_{fu}^2}$. The conservation equation for $\overline{m_{fu}^2}$, reported by Borghi (1973), Bray (1973), Bilger (1975) and Hutchinson et al (1976) was expressed in the form 2.1.12 and was solved together with the relations;

$$\Gamma_{g_{fu}} = \mu_{eff}/\sigma_g$$

$$\bar{S}_{g_{fu}} = C_{g_1} G_{g_{fu}} - C_{g_2} \bar{\rho} \frac{\varepsilon}{K} \overline{m_{fu}^2} - 2 A_o \bar{\rho}^2 \bar{M}_{fu} \bar{M}_{ox} \exp(-E/R\bar{T})$$

$$\times \left\{ \frac{\overline{m_{fu}^2}}{\bar{M}_{fu}} + \frac{\overline{m_{ox} m_{fu}}}{\bar{M}_{ox}} \right\} \qquad 2.4.47$$

$$\text{and } G_{g_{fu}} = \mu_{eff} \left\{ \left(\frac{\partial \bar{M}_{fu}}{\partial x}\right)^2 + \left(\frac{\partial \bar{M}_{fu}}{\partial y}\right)^2 \right\}$$

The last component of the source term, $\bar{S}_{g_{fu}}$, appears due to the finite source term in the conservation equation $\bar{M}_{fu}$ in contrast to the sourceless mixture fraction conservation equation. Previous investigations using a similar model, e.g. Pope (1976), indicated that the third component of the source term $\bar{S}_{g_{fu}}$ is influential and should be included in the calculations. The term $\overline{m_{fu} m_{ox}}$ which appears in equation 2.4.47 is obtained from the solution of the corresponding conservation equation as discussed later in connection with model 6.

Previous investigations, Mason et al (1973) and Pope (1976) neglected the term $\overline{m_{fu} m_{ox}}$ but it is included in the present work. The value of the eddy break up constant C_R was originally proposed by Spalding (1970) to be 0.53. The value of C_R obtained in the present work, through computer optimisation, was taken as 1.0 which is in reasonable agreement with the value of 1.1 reported by Pope (1976) for turbulent confined flames.

The present model requires the solution of conservation equations for $\bar{M}_{fu}$, $\overline{m_{fu}^2}$ and $\overline{m_{ox} m_{fu}}$. The temporal distribution of M_{fu} corresponded to a clipped Gaussian probability function whose characteristics were obtained from local values of $\bar{M}_{fu}$ and $\overline{m_{fu}^2}$, in a similar manner to model 3. Model 4 is suitable for premixed flames where fuel and oxidant can coexist and was successfully used by Mason et al (1973) and Pope (1976) to calculate

local flame properties. The assumption of single step reaction is not appropriate for many gaseous flames, especially when radical concentrations are required and model 5, discussed in the following paragraphs, is more appropriate to such situations.

Model 5

This model is similar to model 4 with the differance that the chemical reaction takes place in intermediate steps. The net reaction rate is evaluated from the forward and backward reaction rates. Similar to model 4, the influence of turbulence was included, through an eddy break up rate. A clipped Gaussian probability distribution was assumed to represent the temporal distribution of the various species. Simple reaction mechanisms for the oxidation of gaseous fuels were suggested for methane by, for example, Waldman et al (1974). Similar mechanisms are also available for other gaseous fuels but only the methane oxidation mechanism is considered here as the natural gas used in the present investigations was composed mainly of methane. The reaction mechanism of Waldman et al (1974) is shown in figure 2.4.5 with only eight major reaction steps of this mechanism considered here. These were selected on the basis of their major contribution to the formation of the intermediate radicals. The selected reaction steps are;

$$
\begin{aligned}
CH_4 + OH &\rightleftharpoons CH_3 + H_2O \\
CH_3 + O_2 &\rightleftharpoons CH_2O + OH \\
CH_2O + OH &\rightleftharpoons CHO + H_2O \\
CHO + OH &\rightleftharpoons CO + H_2O \\
CO + OH &\rightleftharpoons CO_2 + H \\
H + O_2 &\rightleftharpoons OH + O \\
H_2O + O &\rightleftharpoons OH + OH \\
O_2 + M &\rightleftharpoons O + O + M
\end{aligned}
\qquad 2.4.48
$$

These reaction steps are concerned only with the oxidation path of CH_4; the NO formation path is considered separately in section 2.6, as the concentration of NO is always too small to affect the main reaction mechanism of 2.4.48 or to influence the energy based properties. The rate constants of each of the forward and backward reactions were calculated according to the data of Waldman et al (1974).

For each of the reaction steps, a conservation equation of the chemical species is expressed in the general form 2.1.12 with the rate of formation or disappearance of the species as source or sink term. The forward reaction rate coefficient K_f is expressed as;

$$K_f = \beta \bar{T}^n \exp(-E/R\bar{T}) \qquad 2.4.49$$

where β is the pre-exponential coefficient. The backward reaction rate coefficient K_b can be obtained from the equilibrium constant K_c as;

$$K_b = K_f/K_c \qquad 2.4.50$$

This equilibrium constant, K_c at atmospheric conditions is expressed as;

$$K_c = \exp(-\Delta\overset{\circ}{G}/R\bar{T}) \qquad 2.4.51$$

where,

$$\Delta\overset{\circ}{G} = \sum_{j=1}^{N} (\nu_j'' - \nu_j') \overset{\circ}{g}_j$$

$$\overset{\circ}{g}_j = \bar{H}_j - \bar{T}\bar{S}_j = \text{Gibbs free energy}$$

$$\bar{S}_j = \int_T \overline{C_{P,j}} \frac{d\bar{T}}{\bar{T}} + C_{s,j} = \text{species entropy} \qquad 2.4.52$$

$$\bar{H}_j = \int_T \overline{C_{P,j}}\, d\bar{T} + (C_H - a_{-1})_j$$

$$\text{and} \sum_{j=1}^{N} \nu_j' \overset{\circ}{W}_j \rightleftharpoons \sum_{j=1}^{N} \nu_j'' \overset{\circ}{W}_j \qquad 2.4.53$$

where ν'_j and ν''_j are the stoichiometric coefficients of the reactants and products. $(C_H - a_{-1})_j$ and $C_{s,j}$ are constants related to the heat of formation and entropy of the species.

In the present model, the partial differential conservation equations for all the various species considered, are solved in addition to the aerodynamic conservation equations, which rendered the present model its complexity. In the species conservation equations, the square of the concentration fluctuation g_j is obtained from an algebraic form of equation 2.4.47 be equating the generation of g_j to its dissipation as reported by Hutchinson et al (1976).

Combustion models of the present type, which solves conservation equations for the individual reactions steps, were reported by, among others, Borghi (1974) for carbon monoxide oxidation in a mixing layer. Similar computations were also performed by Leuchter (1974) for hydrogen-oxygen reactions in mixing region of two adjacent streams separated by a thin plate. Both investigations assumed boundary layer flow and were not applied to flow situations where substantial recirculation zones occur. In the present work, model 5 is employed to calculate the intermediate radical concentrations for CH_4 and C_3H_8 flames in confined axisymmetric furnace configurations with large recirculation zones.

2.4.4 Effect of turbulence fluctuation correlations on reaction rates

The effect of turbulence fluctuation correlations on the rate of chemical reaction is determined by decomposing the instantaneous reaction rate, given by equation 2.4.6, into mean and fluctuating components and evaluating them through relations with mean flow properties. Many previous attempts to formulate a statistical theory for turbulent reacting flows were concerned with isothermal reactions; e.g. Donaldson et al (1972 and 1976). Other investigations neglected the effect of density changes on the velocity field , Dopazo et al (1973). When chemical reactions take

place in the mixing zone, the time averaged reaction rate depends on the mixing pattern and chemical kinetics. This rate differs from those calculated from time averaged properties, equation 2.4.44 as explained later.

The types of model assumptions indicated in the previous subsection are appropriate to particular flow situations; for example, models 1 to 3 are appropriate to diffusion flames, where the rate of chemical reaction is infinitely fast; as fuel and oxidant come in intimate contact with each other, they burn. These models, 1 to 3 applied to unpremixed flames, do not require explicit formulation of the rate of reaction. On the other hand, where fuel and oxidant are intimately premixed prior to the combustion chamber, the assumptions of models 1 to 3 are not appropriate and an explicit finite rate of reaction is required. The finite reaction rate models incorporated a single step reaction mechanism, model 4 and multi step reaction mechanism of model 5 and were found appropriate to premixed flames.

The present subsection, however, incorporates general models which can be applied to arbitrary fuelled systems where none of the above models is appropriate by itself. The models described below are intended to represent the types of flames considered in the present work which includes those with complicated burner geometries.

Model 6

The rate of chemical reaction given by equation 2.4.6 and 2.4.7 was decomposed to mean and fluctuating quantities. Time averaging the rate of reaction and neglecting the variation of the rate constant with time due to turbulence, the time averaged reaction rate is expressed as;

$$\bar{R}_{fu} = \bar{K}_f \left(\bar{M}_{fu} \bar{M}_{ox} + \overline{m_{fu} m_{ox}}\right) \qquad 2.4.54$$

The term $\bar{K}_f \equiv A_o \exp(-E/R\bar{T})$ and the term $\overline{m_{fu}\, m_{ox}}$ are intimately related to the turbulent mixing of the two reactants. The magnitude and sign of entity $\overline{m_{fu}\, m_{ox}}$ depends entirely on the manner in which the reactants are introduced into the reaction domain. For non-premixed flames, the correlation $\overline{m_{fu}\, m_{ox}}$ is always negative or zero, since fuel and oxygen concentrations diminish towards each other. In order to calculate $\bar{R}_{fu}$, a conservation equation for $\overline{m_{fu}\, m_{ox}}$ is solved. Several expressions for the conservation equation of this correlation were suggested by Bray (1973) and Borghi (1974). The transport equation for the correlation $\overline{m_{fu}\, m_{ox}}$ is expressed as;

$$\underset{\text{I}}{\frac{\partial}{\partial x}\bar{\rho}\bar{U}\,\overline{m_{fu}\, m_{ox}}} + \underset{\text{II}}{\frac{1}{r}\frac{\partial}{\partial r}\bar{\rho}\bar{V}\, r\,\overline{m_{fu}\, m_{ox}}} = \underset{\text{III}}{D_\ell \operatorname{grad}\overline{m_{fu}\, m_{ox}}}$$

$$\underset{\text{III}}{- 2D_\ell \overline{\operatorname{grad} m_{ox} \cdot \operatorname{grad} m_{fu}}}$$

$$\underset{\text{IV}}{+ 2D_t \operatorname{grad}\bar{M}_{fu} \cdot \operatorname{grad}\bar{M}_{ox}}$$

$$\underset{\text{V}}{- \operatorname{grad}\overline{u\, m_{fu}\, m_{ox}} - \operatorname{grad}\overline{v\, m_{fu}\, m_{ox}}}$$

$$\underset{\text{VI}}{- k_f (\bar{M}_{ox} + i\,\bar{M}_{fu}) \{\overline{m_{fu}\, m_{ox}}\}}$$

$$- k_f \{i\,\bar{M}_{ox}\,\overline{m_{fu}^2} + \bar{M}_{fu}\,\overline{m_{ox}^2}$$

$$+ \overline{(m_{ox} + i m_{fu})\, m_{fu}\, m_{ox}}\} \qquad 2.4.55$$

where D_ℓ is the laminar exchange coefficient.

Term I represents the net rate of convection; term II denotes the laminar diffusion of $\overline{m_{fu}\ m_{ox}}$; and term III, represents the dissipation of the fluctuations due to molecular diffusion. The net generation rate due to the non uniform distribution of local mean mass fractions is expressed in term IV. Terms V and VI contribute to the turbulent diffusion of the entity $\overline{m_{fu}\ m_{ox}}$ and its generation due chemical reaction respectively.

The value of the turbulent diffusion coefficient D_t was given by Monin et al (1971) as

$$D_t = \mu_t/\sigma_f \qquad 2.4.56$$

The dissipation term of the entity $\overline{m_{fu}\ m_{ox}}$, term III, is proportional to the quantity that is being destroyed by viscous action, i.e. $\overline{m_{fu}\ m_{ox}}$, times the local density time ε/k. The latter has the dimensions of $(\text{time})^{-1}$. The term ε/k can be regarded as the rate of decay multiplier for the turbulence energy k; so that the dissipation of mean square velocity fluctuations (i.e. of k) and the dissipation of the entity $\overline{m_{fu}\ m_{ox}}$ proceed at proportional rates, see, for example, Spalding (1975). Term III is expressed as;

$$2\ D_\ell\ \overline{\frac{\partial m_{fu}}{\partial x_j}\frac{\partial m_{ox}}{\partial x_j}} = 2\ \bar{\rho}\ \frac{\varepsilon}{k}\ \overline{m_{fu}\ m_{ox}} \qquad 2.4.57$$

This modelled form of the dissipation term does not explicitly include the laminar schmidt number (i.e. the ratio of kinematic viscosity to diffusivity) which limits its use to schmidt numbers with values close to unity, and consequently could be applied in the present gaseous flame configuration. The turbulent diffusion term V is modelled, Borghi (1974) in the form;

$$\frac{\partial}{\partial x_j}\ \overline{u_i\ m_{fu}\ m_{ox}} \equiv -\frac{\partial}{\partial x_j}\ \frac{\mu_t}{\sigma_f}\frac{\partial}{\partial x_j}\ (\overline{m_{fu}\ m_{ox}}) \qquad 2.4.58$$

and was considered by, for example, Bray (1974) and Bilger (1975). The generation term of the entity $\overline{m_{ox} m_{fu}}$, due to the non-uniform spatial distribution of the entities $\bar{M}_{ox}$ and $\bar{M}_{fu}$, can be either +ve or -ve according to the distribution of the reactants and is expressed as;

$$2 D_t \text{ grad } \bar{M}_{ox} \cdot \text{grad } \bar{M}_{fu} \equiv C_{g_1} G_{g_2} \qquad 2.4.59$$

where C_{g_1} and G_{g_2} are given in table 2.1.1 and 2.1.2. The triple correlations such as $\overline{m_{fu} m_{ox}^2}$ and $\overline{m_{ox} m_{fu}^2}$ were generally neglected on the grounds that their influence was negligibly small at low activation energy as for most of the hydrocarbon oxidation reactions used in this work. The modelled form of the conservation equation of $\overline{m_{fu} m_{ox}}$ can be represented by the form 2.1.12 with the values of Γ_Φ and S_Φ expressed as follows;

$$\Gamma_\Phi = \mu_{eff}/\sigma_f$$

$$S_{Af} = C_{g_1} G_{g_2} - 2 \bar{\rho} \frac{\varepsilon}{k} \overline{m_{fu} m_{ox}} - k_f \bar{M}_{fu} \bar{M}_{ox} \qquad 2.4.60$$

$$x \left\{ \frac{\overline{m_{ox}^2}}{\bar{M}_{ox}} + i \frac{\overline{m_{fu}^2}}{\bar{M}_{fu}} + \left(\frac{1}{\bar{M}_{fu}} + \frac{i}{\bar{M}_{ox}} \right) \overline{m_{fu} m_{ox}} \right\}$$

It can be seen from equation 2.4.54 and 2.4.60 that the entity $\overline{m_{fu} m_{ox}}$ represents the source/sink of the fuel conservation equation due to turbulent fluctuations. The generation of $\overline{m_{fu} m_{ox}}$, due to the effect of turbulence, can be represented in terms of the various time scale of turbulence and chemical kinetics as discussed in the following paragraph.

The Damkohler number N_D defined, Damkohler (1947), as the ratio of a mixing distance (or time) to a reaction distance (or time) equals unity when the reaction distance (or time) and the mixing distance (or time) are equal. An expression of this number N_D is given as;

$$N_D = \tau_s/\tau_k \qquad 2.4.61$$

where τ_k is the time scale of chemical kinetics given by equation 2.4.46 and τ_s is defined as the stretching time of the flame eddies and equals;

$$\tau_s = \{(|\frac{\partial U}{\partial y} + \frac{\partial V}{\partial x}|) + \frac{\varepsilon}{k}\}^{-1} \qquad 2.4.62$$

which accounts for the mixing time in connection with the mean motion and the random turbulence, Spalding (1976). Introducing these definitions in the source term of equation 2.4.60, enables the estimation of the contributions of chemical kinetics and turbulent mixing to the generation of $\overline{m_{fu} m_{ox}}$. In flame situations where reactants are in intimate contact, due to rapid mixing, characterised by large values of ε/k, the reaction is kinetically influenced if $N_D << 1.0$. The influence of chemical kinetics on the formation of $\overline{m_{fu} m_{ox}}$ is hence negligible and only the first two components in the expression of $\bar{S}_{AF}$ are retained. In the flame situations where the temperature is high enough for the reaction to proceed, but the reactant are not in intimate contact, the reaction is controlled by mixing; the chemical kinetic time τ_k is very small relative to τ_s i.e. $N_D >> 1.0$.

The variation of the time scales τ_s, τ_{so} and τ_k and the Damkohler number along a mixing zone of a co-flowing flame is shown in figure 2.4.6 and 2.4.7 respectively. In figure 2.4.8, the variation of N_D with temperature is shown; as the temperature increases, N_D increases and the reaction is more dependent on mixing. Regions where $N_D >> 1.0$ and $N_D << 0.1$ are shown in figure 2.4.9 and corresponds to diffusion controlled and kinetically influenced flames respectively.

The present model requires the solution of the same equations as model 4 in addition to two conservation equations for $\overline{m_{fu} m_{ox}}$ and $\overline{m_{ox}^2}$; the latter is similar to that of 2.4.47 with the appropriate source terms.

The local flow properties were also obtained in a similar manner to model 4 through the specification of $P(M_{fu})$ and the total number of solved equations was twelve for a swirling flame without the consideration of radiation. An approximate form of the conservation equations of $\overline{m_{fu}^2}$, $\overline{m_{ox}m_{fu}}$ and $\overline{m_{ox}^2}$ was obtained by neglecting convection and diffusion fluxes in the conservation equations and hence obtaining algebraic form of the balance of production and dissipation of the scalar entity. This approximation, when applied to scalar fluctuations, gave similar results to those obtained from the corresponding differential equations with differences of the order of 3-8%.

Model 6 includes the effects of turbulence fluctuations on the rate of reactions and the reaction rate dependence on turbulent mixing or chemical kinetics is embodied in the model, in contrast to models 1 to 3 which include the effect of turbulent mixing and models 4 and 5 which use the eddy break up model and neglect the turbulent fluctuation correlations. A final remark, is that model 6 does not include the effect of temperature fluctuations on the reaction rate and in some flow situations, this neglection can lead to serious errors at large activation energies and the next model 7 accounts for this influence.

Model 7

In model 6, the influence of temperature fluctuations on the rate of reaction was neglected, assuming that the activation energy of most of the common gaseous fuels is of the order of 1.59×10^{8} J/k mol^{o}k, i.e. E/R≈18000K In many situations, the activation energy is very high and temperature dependent, for example, the pollutant formation reactions. The time mean rate of reaction $\bar{R}_{fu}$ is expressed by equation 2.4.9 and higher order correlations $\overline{T'^2 m_{fu}}$, $\overline{T'^2 m_{ox}}$ and $\overline{T'^3}$ were neglected.

The truncation errors due to the series expansion, in equation 2.4.9, to the second term only, i.e. model 6, were reported by Borghi (1974). A comparison between the rates obtained from equation 2.4.54 and that obtained

from the exact solution for $E/R\bar{T}$ of 10 and $T'/\bar{T}$ of 0.1 showed an error of 1.5% in the rate of reaction; in flow situations where $E/R\bar{T}$ equals 20, this truncation error was 15% for the same temperature fluctuation level. The analysis of Borghi (1974b) indicated that the approximation of the rate of reaction by a series expansion, equation 2.4.54, became poor as $E/R\bar{T}$ increased; for high activation energy and low mean gas temperature for the same level of temperature fluctuation.

In chemical reactions where the activation energy is large, similar to those of pollution formation, the second order correlations, $\overline{m_{fu}^2}$, $\overline{m_{ox}^2}$, $\overline{m_{fu}T'}$, $\overline{m_{ox}T'}$ and $\overline{T'^2}$ are incorporated in the rate of reaction expression as shown in equation 2.4.9. The series expansion of the rate expression of equation 2.4.8 requires the provision of higher order correlations than those considered by equation 2.4.9. The third order terms, $\overline{T'^3}$, $\overline{T'm_{fu}m_{ox}}$, $\overline{T'^2m_{fu}}$, $\overline{T'^2m_{ox}}$, $\overline{m_{fu}m_{ox}^2}$ and $\overline{m_{fu}^2m_{ox}}$ were neglected in equation 2.4.9; however these terms were evaluated using algebraic expressions, Borghi (1974a) and Donaldson et al (1976), but their magnitudes were found to be negligibly small. The truncation errors in the rate of chemical reaction at $E/R\bar{T}$ of 20 and T'/T of 0.15 were less than 0.5%.

Model 7 incorporated equation 2.4.9, to calculate the rate of fuel consumption, which requires the solution of the conservation equation for entities $\overline{m_{fu}^2}$, $\overline{m_{ox}^2}$, $\overline{m_{fu}m_{ox}}$, $\overline{m_{fu}T'}$, $\overline{m_{ox}T'}$ and $\overline{T'^2}$. From the values of $\bar{M}_{fu}$ and $\overline{m_{fu}^2}$, the characteristics of the clipped Gaussian distribution of M_{fu} were obtained in the same way as in model 4 and the local values of $\bar{T}$, $\bar{\rho}$, $\bar{M}_{ox}$ were consequently obtained from equation 2.4.41 and 2.4.42 with M_{fu} replacing f. This model includes the effects of temperature and concentration fluctuations and their correlations on the time averaged reaction rate. It also requires large computing storage and time requirements and its use was limited to pollutant formation mechanism as the influence of temperature

fluctuations is considerably large. The model can be extended to include higher order correlations and multistep reactions but due to the limited computer capacities is restricted to its present form.

The effect of density fluctuation

The influence of density fluctuation correlations on the convective flux of mass and any other scalar was found to be significant near the reaction zone edge, Bilger (1975). Figure 2.4.10, was obtained for hydrogen diffusion flame and illustrates the effects of including the various terms which appear in the conservation equation; these terms are of the form $\overline{\rho'\phi}$ and $\overline{\rho' u_j}$ when third order density fluctuation correlations were neglected. When the conservation equations are expressed in terms of Favre averaged properties $\tilde{\Phi}$ instead of time averaged $\bar{\Phi}$, these terms disappear but when comparison with experiments is required, the density correlation terms should be calculated.

Additional conservation equations for $\overline{\rho' u_j}$ and $\overline{\rho'\phi}$ were solved with those for mass, momentum, energy and species in models 6 and 7. In figure 2.4.10, curve (3) shows radial profiles of mean temperature when the terms $\overline{\rho' u_j}$ and $\overline{\rho'\phi}$ were neglected, while curve (1) shows the same distributions when these correlations were taken into account. Figure 2.4.11 shows radial profiles of nitric oxide concentrations for different approaches and curves (1) and (2) represent the situations when the additional source of any entity Φ due to the density fluctuation was significant, i.e. $\overline{\rho' u_j} / \bar{\rho}\,\bar{U}_j$ was not small.

The entities $\overline{\rho' u_j}$ and $\overline{\rho'\phi}$ were calculated from differential equations for the transport of these entities expressed in the form 2.1.12 and were described by Hutchinson et al (1976) but can also be obtained from an approximate form, given by Bilger (1975) as;

$$\overline{u_j\rho'} = - \frac{\mu_{eff}}{\sigma_\rho} \frac{\partial \bar{\rho}}{\partial x_j}$$

and

$$\overline{\phi\rho'} = - \frac{\mu_{eff}}{\sigma_\rho} \frac{\partial \bar{\Phi}}{\partial x_j} \qquad 2.4.63$$

In model 6, the assumption of equation 2.4.63 was considered and the correlations were algebraically calculated in terms of density gradients. In model 7, where conservation equations for $\overline{m_a m_b}$, $\overline{T'm_a}$, $\overline{T'm_b}$ and $\overline{T'^2}$ were calculated from the corresponding conservation equations, $\overline{\rho'\phi}$ and $\overline{\rho'u_j}$ were obtained from equation 2.1.12 with appropriate Γ_ϕ and S_ϕ as indicated in table 2.1.1.

The effect of the entities $\overline{\rho'\phi}$ and $\overline{\rho'u_j}$ embodied in models 6 and 7, was found to result in negligible changes in mean velocity and turbulence field. In temperature and pollutant species calculations, the entities $\overline{\rho'\phi}$ and $\overline{\rho'u_j}$ have a significant influence as indicated in figure 2.4.10 and 2.4.11 respectively, but it is concluded that these entities have an insignificant influence when energy based properties are considered. The influence of density-velocity and density-scalar fluctuation correlations and the correlations $\overline{m_a m_b}$ on the rate of pollutant formation was significant; this is because of the high activation energy in the exponential term of equation 2.4.10. As a consequence, these correlations were considered in pollutant formation models as described later in section 2.6.

2.4.5 Summary

This section has been concerned with the modelling of the time averaged conservation equations of scalar entities in turbulent reacting flows. Various modelling assumptions were described in the section and can be mainly classified in accordance to their appropriateness to diffusion, premixed and arbitrary fuelled flames. In turbulent diffusion flames, the assumption of infinitely fast chemical reaction was incorporated in the computational scheme, and this oversimplified assumption enables the calculations of local

flame properties through the solution of one conservation equation for the mixture fraction $\bar{f}$. The effect of concentration fluctuation was also considered in this section in conjunction with the mixture fraction and additional modelled equation for the square of the concentration fluctuation was solved. The time averaged and variance of any scalar entity Φ was obtained from the knowledge of $\bar{f}$, g and the temporal distribution of f. Two temporal distributions of f; the square wave form and the random distribution were considered and corresponded to two delta functions and a clipped Gaussian distribution respectively. Models including the concentration fluctuation effects were found to yield better results than the first model which ignored the concentration fluctuation.

For premixed flames, the above assumptions are not appropriate and finite reaction rate models should be included as a source or sink in the fuel mass fraction conservation equation. The eddy break up assumption was incorporated to account for the effect of turbulence on the single step reaction rate; the fuel concentration fluctuations were required for the rate expression and were obtained from the solution of the corresponding conservation equation. The probability density function of fuel mass fraction was assumed to be represented by clipped Gaussian distribution which is obtained from local values of mean and fluctuating component of fuel mass fraction. The effect of multistep reaction mechanism was also considered and was found appropriate to premixed flames where intermediate radical concentrations are required.

The application of equation 2.4.10 to turbulent reacting flows with arbitrary fuelled systems was reported in two models; the first neglected the effect of temperature fluctuations on the reaction rate and the second accounted for that effect. These two models involved the solution of many additional conservation equations for the second order correlations, but were more general than previous models as the influence of turbulent mixing and chemical kinetics were included and their contributions depend on mean

flow properties.

A closed set of conservation equations for mass averaged quantities can be obtained without modelling velocity density fluctuation correlations;i.e. in Favre average form.These correlations must be then modelled in order to calculate time averaged quantities,which can be compared to the measurements. More work is required on the modelling of the velocity-density fluctuation correlation to investigate their influence on the local flow properties.

The various combustion models discussed in the section are appropriate to different flame configurations.The fast chemical reaction models 1 to 3 embody the assumptions of diffusion or mixing controlled single step reactions,i.e the time scale of mixing τ_s is larger than that of chemical kinetics, τ_k and therefore N_D is>>1.0. The use of these models should be restricted to unpremixed flames where the reactants burn as they mix.The finite chemical reaction models 4 and 5 should be applied to premixed flames where the reactants are in intimate contact but may exist at a low temperature for the initiation of the reaction,i.e the time required for mixing τ_s is much smaller than the chemical reaction time τ_k. This situation corresponds to very small values of the Damkohler number N_D<<1.0 and the reaction is kinetically influenced.

In many practical furnace applications, the flame situation is neither diffusion controlled nor kinetically influenced due to the existance of a burner quarl , where mixing can occur prior to the combustion chamber.In these situations, the time scale of mixing τ_s and that of chemical kinetics, τ_k are of the same order of magnitude and hence none of the previous five models is appropriate. Models 6 and 7 ,are more general than models 1 to 5 as they include the effects of turbulent fluctuations and chemical kinetics in the reaction rate expression. They are expensive to run as they require the solution of many conservation equations, and hence are only most appropriate to arbitrary fuelled flames,i.e $N_D \approx 1.0$, where models 1 to 5 would yield unsatisfactory results

As a result of the above analysis, the reacting flow calculations presented in sections 5.1 and 5.2 make use of the combustion models 3, 4,5, 6 and 7 as follows;

Model 3 for diffusion flames, $N_D >> 1.0$
Models 4&5 for premixed flames, $N_D << 1.0$
Models 6&7 for arbitrary fuelled flames, $N_D \simeq 1.0$

The discrepancies resulting from the use of a non-optimum combustion model are described in section 5.3 , where various models are compared.

2.5 Radiation Models

2.5.1 General

The mathematical investigation of combustion in furnace flows requires adequate treatment of the thermal radiation represented by the source term of the energy conservation equation. Several techniques have been developed for the solution of the radiant heat transfer equation. Of these, the zone method of Hottel et al (1967) has been applied extensively and successfully but requires the solution of an integro-differential equation in finite-difference form; the computational task is considerable because each zone of the furnace space influences each other zone and the computation of the influence coefficients demands large computer storage and running time. As a result, the zone method is not suited to the simultaneous computation of flow and heat transfer field.

Flux methods provide an alternative which is computationally more economical and still reasonably accurate, see for example, Lockwood et al (1971) and Gosman et al (1973). They are based on the use of simplifying assumptions for the angular variation of the radiant intensity which allows the exact integro-differential radiation transport equations to be reduced to a system of approximate ordinary differential equations. This differential form makes the equations ideally suited to numerical solution simultaneously with the flow equations. The accuracy of the method depends

on the assumed form of the angular distribution of intensity. In the Schuster (1905) type of flux model, the intensity was assumed to be independent of direction in each of a number of solid angles spanning the whole range of 4π and has been used for one dimensional planar radiation transfer and extended to two dimensional transfer in curved geometries by Lockwood et al (1971). The radiation intensity distribution, assumed to be dependent on direction, was expressed in a Taylor series expansion, Demarco et al (1975); these expressions when integrated over solid angles of 2π and $4\pi/6$, gave the transport equations of radiative fluxes. The spherical harmonic approach, Siddall (1976), and the discrete ordinate approach, Truelove (1975) can be also considered as flux methods. In the spherical harmonic method, the radiant intensity was formally expanded in a complete set of angle eigen functions, which was truncated at some upper limit. The discrete ordinate approach solved the exact radiation transport equation for a set of discrete directions spanning the range of 4π; angle integrals of intensity are evaluated from the discrete values by numerical quadrature. Comparisons between the various radiation models, as applied to furnace flows, were reported by Whitacre et al (1975), these comparisons indicated that the spherical harmonic approximation is more appropriate to furnace flows as it includes the actual absorption coefficients in contrast to the four flux model of Lockwood et al (1971), and solves a single transport equation for axisymmetric furnace flows.

The radiative heat transfer in practical furnace combustors involves non-grey gases and particulates which can absorb, emit and scatter radiation. The equation for radiative transfer in a medium which emits, absorbs and scatters radiation may be expressed, Hottel et al (1967) as;

$$\nabla (I.\hat{n}) = - (a+s)\ I + \frac{S}{4\pi} \int_{\Omega=4\pi} I\ d\ \Omega' + a\ I_b \qquad 2.5.1$$

Ω' is the solid angle

$\hat{n}$ is a unit vector through the point to which the intensity I is referred.

I_b is the black body emission.

The first term on the right hand side of equation 2.5.1 is the absorption and outscattering flux, while the second term represents the inscattering flux. The third term denotes the black body emission. The intensity vector I is shown in figure 2.5.1 and is dependent on (r, θ, x and Ω). Equation 2.5.1 can be simplified, to remove the integral form by considering a gray non scattering medium;

$$\nabla (I.\hat{n}) = - k_a I + k_a \frac{\sigma T^4}{\pi} \qquad 2.5.2$$

where k_a is the gray gas attenuation coefficient. The radiation intensity vector I can be generally expressed in a Taylor series expansion, Demarco (1975), as;

$$I = A_1.(\hat{r}.\Omega) + A_2.(\hat{\theta}.\Omega) + A_3.(\hat{x}.\Omega) + B_1.(\hat{r}.\Omega)^2 + B_2.(\hat{\theta}.\Omega)^2 + B_3.(\hat{x}.\Omega)^2 \qquad 2.5.3$$

where

A_1, A_2, A_3, B_1, B_2 and B_3 are coefficient of the series and are connected to the intensity in the coordinate directions.

$\hat{r}$, $\hat{\theta}$, $\hat{x}$ are unit vectors of the three polar coordinates r, θ, x.

Ω is unit vector representing a direction.

The soot formation due to the mixture characteristics and the type of flow contributes to the radiative transfer through scattering especially in heavy oils and solid fuels. In gas mixtures, the emittence is a function of the local partial pressure of the different gases;

$$\varepsilon_{gas} = \sum_n a_{g,n}(T) \{1 - \exp(-k_{g,n} (P_{H_2O} + P_{CO_2}) L\} \qquad 2.5.4$$

where

$k_{g,n}$ is the absorption coefficient

P is the partial pressure of the gas.

$a_{g,n}(T)$ is the weighting factor which is a fraction of the black body energy.

L is the optical path length.

In the present work, the radiation from solid particles was neglected as the fuel was burned at near stoichiometry and the flames were non-luminous, and, gas to gas and gas to wall radiation were significant in the flames considered in the present investigations. The accuracy of the radiation flux model of the type described by Demarco et al (1975) can be greatly improved by retaining more terms in the series expansion of the intensity distribution, and consequently solving more equations. In the present flow configurations, at least eight equations were used to obtain the thermal characteristics of the flame and the additional flux equations were kept as simple as was possible to allow reasonable physical representation with low cost.

2.5.2 Radiation model used in present investigation

In the present work a modified version of the four flux model proposed by Gosman and Lockwood (1973) was primarily used, later comparisons with the four flux model of Demarco et al (1975), applied for two dimensional axi-symmetric flows, were carried out. The transport equations of net radial and axial radiative fluxes were solved with local values of absorption and scattering coefficient varying according to local composition, Lockwood et al (1971). The two equations for R_x and R_y incorporated in the model of Gosman et al (1973) were,

$$\frac{\partial}{\partial x}\left(\frac{1}{a}\frac{\partial}{\partial x}R_x\right) = a\,(R_x - \sigma\bar{T}^4) + \frac{s}{2}(R_x - R_y) \qquad 2.5.5$$

and

$$\frac{1}{r}\frac{\partial}{\partial r}\left(\frac{r^2}{ar+1}\right)\frac{\partial R_y}{\partial r} = a\,(R_y - \sigma\bar{T}^4) + \frac{s}{2}(R_y - R_x) \qquad 2.5.6$$

The source term in the enthalpy equation, S_h was expressed as,

$$S_h = 2\,a\,(R_x + R_y - 2\,\sigma\,\bar{T}^4) \qquad 2.5.7$$

Integrating the intensity distribution, equation 2.5.3, in the general expression 2.5.1 over a solid angle 2π, and in the absence of scattering, the flux equations for axisymmetric furnace flows were obtained by Shah (1976) as;

$$\frac{\partial}{\partial x}\,\frac{1}{a}\,\frac{\partial}{\partial x}\,R_x = \frac{4}{3}\,a\,(2\,R_x - R_y - \sigma\,\bar{T}^4) \qquad 2.5.8$$

and $$\frac{\partial}{\partial r}\,\frac{1}{a}\,\frac{\partial}{\partial r}\,R_y = \frac{4}{3}\,a\,(2\,R_y - R_x - \sigma\,\bar{T}^4) \qquad 2.5.9$$

The source term in the enthalpy equation, S_h was expressed as

$$S_h = \frac{16}{9}\,a\,(R_x + R_y - 2\,\sigma\,\bar{T}^4) \qquad 2.5.10$$

The two radiation models, R-I, represented by equations 2.5.5 to 2.5.7 and R-II, represented by equations 2.5.8 to 2.5.10, are compared for the furnace flows of the present configuration.

The predicted distributions of wall heat flux and near wall temperatures, obtained for a swirl number of 0.8 in the straight burner of figure 3.1.1.a, are shown in figure 2.5.2 and the near wall temperature and emission power for the two models are shown in figures 2.5.3 and 2.5.4. In figure 2.5.2, the total wall heat flux obtained by model R-II is larger than that obtained with the aid of model R-I which does not couple the fluxes R_x and R_y, and consequently does not allow the variation of radiation intensity in space. Model R-I leads to lower radiative heat fluxes than those measured. As shown in figure 2.5.3 and 2.5.4, the corresponding predicted near-wall-gas-temperature and emission power obtained with model R-II differ from those of model R-I; the difference can be attributed to the fact that model R-II allows for more gas to wall radiation. In the calculations of figures 2.5.2 to 2.5.4, the radiative heat flux through the wall contributed to nearly 40% of the total wall heat flux and using model R-II rather than R-I did not

give widely different results. In contrast, at the flow situations where the furnace thermal input to surface area is such that the radiative contribution to the wall heat flux is higher than observed in the case of figures 2.5.2 to 2.5.4; for example, Delft furnace, Wu et al (1971) and Ijmuiden furnace, Michelfelder et al (1974), the radiative heat flux contributes to more than 70% of the total wall heat flux and model R-II predicts significantly better wall heat transfer rate which is in reasonable agreement with the measurements.

The use of the view factors was recently suggested by Lockwood and Shah (1976), where rather than increasing the number of the solved equations; (by increasing the terms in the Taylor expansion of the intensity distribution), the relative areas of the integration surface were varied through the specification of free parameters. In this way, the areas were adjusted to give the best representation of the intensity distribution. At the present time, model R-II is the best representation of the four flux model as it accounts for the coupled flux intensities in the coordinate directions, and much further testing is required to establish the optimal functional relationship between the areas and the intensity distribution in the model of Lockwood and Shah.

2.6 Pollutant Formation Models

In the present section, the formation of nitric oxides and carbon monoxide in turbulent reacting furnace flows are considered in turn. The various modelling approximations which had been found useful by previous modelling of combustion are discussed and extended in the present section to incorporate the various effects of temperature and species concentration fluctuations. The two major pollutants, NO and CO are treated separately in the two following subsections. The formation of NO in flames occurs at very small concentrations relative to the reactants and hence does not influence the fuel kinetics described earlier in section 2.4. In contrast, the carbon monoxide formation mechanism is related to the fuel kinetics.

2.6.1 Models for calculating nitric oxides

Combustion generated oxides of nitrogen are presently recognised as major pollutant which react in the surrounding atmosphere to form photochemical smog. The most predominant oxides of nitrogen associated with combustion products is NO, which is later oxidized in the atmosphere to form NO_2. Previous investigations of NO emission have been reported for both premixed and diffusion flames and support the proposed Zeldovich mechanism for NO formation, see for example Iverach et al (1972). This mechanism can be expressed generally as;

$$N_2 + O \rightleftharpoons NO + N \qquad 2.6.1$$

$$O_2 + N \rightleftharpoons NO + O \qquad 2.6.2$$

$$N + OH \rightleftharpoons NO + H \qquad 2.6.3$$

and the O-atom was calculated under equilibrium from the equation.

$$O_2 + M \rightleftharpoons O + O + M \qquad 2.6.4$$

Equation 2.6.3 has been shown, Barrere (1973) to have a significant influence in the situations where the fuel is rich. The reaction rate constants of the individual elementary step reactions may be found in many references on chemical kinetics such as Waldman et al (1974). The simplified NO formation mechanism is shown in figure 2.6.1. Methods of calculation of NO, have been reviewed by Barrere (1973) and Caretto (1975).

The reaction rate of equation 2.6.1 in the simple Zeldovich mechanism, is much slower than that of reaction 2.6.2, which indicates that the formation of {NO} molecule from equation 2.6.1 is accompanied by a release of a N atom, which rapidly forms{NO} according to reaction 2.6.2. Consequently, equation 2.6.1 controls the formation rate as equation 2.6.3 plays a small role in stoichiometric flames. The equilibrium {O} atom concentration can be obtained from equation 2.6.4 and is used together with equation 2.6.7 when superequilibrium is assumed.

The rate of NO formation was found to depend strongly on mean and fluctuating temperatures, see for example, Jones (1975), who numerically integrated the temporal rate of {NO} formation for various temperature fluctuation intensities. At temperature of around 2000°k, and for $\sqrt{\overline{T'^2}}/\bar{T}$ of 0.1, the rate of {NO} formation, when the temperature fluctuations were considered was nearly five times the rate when the fluctuations were neglected. This ratio increased as the mean temperature decreased and the fluctuation intensity increased. Similar investigations were reported by Thompson et al (1975). These illustrated the influence of temperature fluctuations on {NO} formation rate and indicated the need to incorporate it in the pollutant formation rate used in the numerical calculations.

In the present work, the calculated {NO} concentrations are obtained from the corresponding conservation equation which can be expressed in the general form 2.1.12 and the corresponding Γ_{NO} and $\bar{S}_{NO}$ are specified as;

$$\Gamma_{NO} = \mu_{eff}/\sigma_f \qquad 2.6.5$$

and

$$\bar{S}_{NO} = 8.39 \times 10^{16}\, \bar{T}^{-\frac{1}{2}}\, \bar{M}_{N_2}\, \bar{M}_{O_2}^{\frac{1}{2}}\, \exp(-134900/R\bar{T})\, (1 + F) \qquad 2.6.6$$

where

$$F = \frac{\overline{m_{N_2} m_{O_2}}}{\bar{M}_{N_2} \bar{M}_{O_2}} + \frac{E}{R\bar{T}} \left\{ \left(\frac{1}{2}\frac{E}{R\bar{T}} - 1\right) \left(\frac{\sqrt{\overline{T'^2}}}{\bar{T}}\right)^2 + \frac{\overline{T'm_{O_2}}}{\bar{T}\,\bar{M}_{O_2}} + \frac{\overline{T'm_{N_2}}}{\bar{T}\,\bar{M}_{N_2}} \right\}$$

In obtaining $\bar{S}_{NO}$, equation 2.6.6, the {O} atom concentrations were obtained from equation 2.6.4 and were substituted in equation 2.6.1

In situations where concentrations of O-atoms are higher than equilibrium values, the concept of super equilibrium was suggested by Fenimore (1970) and was quantified by Ghazzi et al (1975). Iverach et al (1972) observed that, for hydrocarbon fuel, the simple Zeldovich mechanism was applicable for

equivalence ratios less than 1.5 with O-atom determined for equilibrated conditions, equation 2.6.4: for highly rich flames, the rate calculated for equations 2.6.1 and 2.6.4 required an improbably high O-atom concentration. A mechanism to involve generation of N-atom via the reaction of nitrogen with hydrogen fragments, and their subsequent reaction with OH, was proposed by Fenimore (1970) and appears plausible for highly rich fuel flames.

Thompson et al (1972) calculated O-atom concentration for methane flames by considering the hydrogen-oxygen fast locally equilibrated reaction with;

$$O/(O)_{equilibrium} \equiv H_2/(H_2)_{equilib.} = (OH/(OH)_{equilib})^2 \qquad 2.6.7$$

and recorded this ratio to be of the order of 2.4 at high gas temperature (>1800K). At lower temperature, the measured NO values were found to be in excess of those obtained from the Zeldovich mechanism and showed that the reaction rate temperature dependency did not explain the relative increase in NO. The reason for this increase in NO concentration was the overshoot of O-atom which was governed by the mixing with fresh reactants. Excess NO concentration formed due to the reaction of hydrocarbon fragments with nitrogen molecules is usually known as prompt NO, Fenimore (1970).

In rich fuel flame situations, the superequilibrium O-atom was used and the source term of NO, equation 2.6.6 was multiplied by the super-equilibrium constant which was of the order of 2.4. The present pollutant formation model does not account for any prompt NO as this is appropriate only to very rich flames and particularly in the flame front.

2.6.2 Models for calculating unburned hydrocarbons

The local concentrations of unburnt fuel can be determined from the solution of an appropriate conservation equation but, since the chemical reactions involved in the branch reactions of hydrocarbons to CO_2 and water vapour are numerous and complicated, more complex approaches can be necessary.

It is well known for example, that intermediate reactions involving CO have significant effect on local temperature, Singh (1976).

Previous calculations of unburnt hydrocarbon have been reported, for example, by Borghi (1973) and Singh (1976), and relate to diffusion and premixed flames in mixing layers. They were obtained by considering the reaction equations

$$CO + OH \rightleftharpoons CO_2 + H \qquad 2.6.8$$

$$CO + O \rightleftharpoons CO_2 \qquad 2.6.9$$

The reaction of 2.6.8 is very fast under normal conditions both in the flame region and in the post flame gases. It was indicated, for example, by Palmer (1974), that reaction 2.6.8 controlled the rate of disappearance of CO which is expressed as;

$$\bar{R}_{CO} = - 8.14 \times 10^{8} \bar{\rho}^{2} \bar{M}_{CO} \bar{M}_{OH} \exp(-540/\bar{T}) \qquad 2.6.10$$

A complete model of CO kinetics must include the initial fuel kinetics which form CO as shown by equation 2.4.48 in model 5. It is however possible to compute the local concentrations of products of combustion by using a global reaction rate expression for a hydrocarbon/air reaction. The application of such expressions is usually limited to a narrow range of temperature, pressure and air/fuel ratio in which the original data used to determine the empirical constants were obtained and results in lower gas temperature. A quasi-global scheme has been proposed by Edelman et al (1969) where the initial hydrocarbon fuel was assumed to undergo an overall reaction of the following type;

$$C_n H_m + (\frac{n}{2} + \frac{a}{2}) O_2 \longrightarrow n\ CO + a\ H_2O + (\frac{m}{2} - a)\ H_2 \qquad 2.6.11$$

The rate parameters and the stoichiometric coefficients, a in this reaction are determined empirically. The quasi global mechanism solves equations 2.6.10 and 2.6.11 to determine the carbon monoxide concentrations. Examples

of quasi global reactions have been quoted by Becker (1974).

The local equilibrium concentrations of intermediate species in the CH_4 reaction with air can be obtained by the minimisation of Gibbs free energy, hence the local equilibrium composition can be obtained by means of Newton-Raphson iteration procedure as described by Gordon et al (1971) and used by Hutchinson et al (1976).

In the present investigations, the concentrations of CO were obtained from the solution of the system of equations given in 2.4.48 as detailed previously in model 5. Alternatively, the computer program given by Gordon et al (1971) was used in the present calculations of CO concentrations.

2.7 Closure

The set of partial differential conservation equations governing the flows examined in this thesis are represented by equation 2.1.12 and table 2.1.1, which lists the dependent variables and associated definitions of Γ_Φ and S_Φ. In non reacting flows, the first five conservation equations were solved with the mass conservation. On the other hand, when reacting flows were considered, all the equations of table 2.1.1 were solved simultaneously. The task of the solution procedure of section 2.2 is to solve the conservation equations shown in table 2.1.1, and expressed in finite difference form, with appropriate boundary conditions which, due to the elliptic nature of the conservation equation, take the form of prescriptions of Φ or its normal gradients at all boundaries of the solution domain.

The present investigations incorporated an eddy viscosity concept where the local Reynolds stresses were obtained from algebraic expressions of an effective viscosity and mean velocity gradients. The effective viscosity obtained from a two-equation turbulence model was expressed in terms of kinetic energy of turbulence k and its dissipation rate ε and was modified to suit reacting flows. The turbulence model constants used in the present work were obtained from Launder et al (1972).

Different closure model assumptions are discussed in section 2.4 for reacting flows and include those appropriate to diffusion, premixed and arbitrary fuelled flames. These models vary in complexity from simple ones assuming infinite fast chemical reactions and solving a sourceless equation for mixture fraction, which are appropriate to diffusion flames; to those considering a finite reaction rate and various concentration fluctuation correlations and are suitable for premixed and arbitrary fuelled flames. The constants which appear in the modelled conservation equations embodied in the combustion model are shown in table 2.1.2 and were obtained from Hutchinson et al (1976). Multistep chemical reaction mechanisms are considered only in situations where pollutant emission and intermediate radical concentrations are of interest, such as for nitrogen oxide pollutant formation models. That was because the concentrations of the pollutants are insignificantly small to influence the main reaction. In these situations, the influence of the correlations $\overline{\rho'\phi}$ on the local pollutant concentrations is significant and models accounting for these correlations are used.

The energy conservation equation embodies radiative source term which can be obtained from the radiation flux model described in section 2.5 and thus the wall heat flux distribution can be readily obtained. In section 2.6, the local concentrations of the pollutants nitric oxide and carbon monoxide are obtained from the solution of the corresponding conservation equations of each species. The effect of temperature and concentration fluctuations on the rate of pollutant formation are also considered in section 2.6.

The validity of the turbulence, combustion, radiation and pollutant model assumptions for nonreacting and reacting flows is assessed in Chapters 4 and 5 respectively by comparison with relevant measurements available in the literature and those of the present investigations.

Table 2.1.2

Constant	Value
C_1	1.44
C_2	1.92
C_μ	0.09
σ_k	0.90
σ_ε	1.22
E	8.80
κ	0.4175
C_{g_1}	2.8
C_{g_2}	2.0
σ_h	0.9
σ_ϕ	0.9
σ_f	0.9
C_R	1.0
σ_{fu}	0.9
σ_ρ	0.9

CHAPTER 3

EXPERIMENTAL INVESTIGATION

The experimental investigations of aerodynamic and energy properties in an axisymmetric model furnace, similar to those used in package boilers, are described in this chapter. These investigations include the measurements of mean velocity components and the corresponding normal stresses, obtained for non-reacting and reacting flows, with the aid of a laser Doppler anemometer. In reacting flows, mean gas temperature and wall heat flux distributions were also obtained for various degrees of swirl, with the aid of a suction pyrometer and thermocouples respectively.

The axisymmetric furnace configuration and the experimental facilities are described in detail in the first section of this chapter together with the various measuring techniques and associated instrumentation used to obtain the local velocity and temperature distributions. This is followed, in section 3.2, by a description of the experimental procedure and, in the third section, the measured flow properties and the corresponding flow and boundary conditions, obtained in the axisymmetric model furnace, are described for different flow rates and swirl intensities. Details of the experimental results are given in appendices A2, A3, A4 and A5 while chapters 4 and 5 discuss comparisons between these experimental results and the corresponding results obtained with the calculation procedure of chapter 2. The errors associated with the measurements are considered in the fourth section which assesses the likely precision of the experimental results. The chapter ends with a summary of its content.

3.1 Description of Equipment and Instrumentation

The experimental flow configuration, measuring techniques and associated instrumentation are described in the following subsections.

3.1.1 Experimental flow configuration

The flow configuration was arranged to model the essential features of

practical continuous flow combustion devices such as the flame tube of package boilers. A versatile design was sought to permit independent variation of the various flow parameters, such as air to fuel mass velocity ratio, degree of air swirl, overall equivalence ratio, inlet air flow rate, wall temperatures, heat flux and burner geometry. It permits the measurement of the inlet profiles of mean velocities, turbulence intensities and temperatures which are necessary as inlet conditions for the calculation procedure discussed in the previous chapter.

The experimental configuration comprises an axisymmetric combustor in which a central gaseous fuel stream is mixed with a coaxial annular air stream. The resulting flame is stabilized by a quarl geometry which creates, together with the swirl imported in the air, a zone of hot recirculating combustion gases. This swirl stabilization technique is extensively used in boilers, furnaces and gas turbines. The swirling air flow was generated with the aid of vanes which were interchangable to allow swirl numbers from 0.0 to 0.52.

The burner and furnace arrangements are shown schematically in figure 3.1.1 and the layout of the rig is shown in figure 3.1.2. Two burner arrangements were used in the present experimental investigation and consisted of two coaxial pipes; the inner and outer diameters of the central pipe were 12 and 27 mm respectively and the pipe length to diameter ratio was 40 and ensured developed turbulent flow at the pipe exit. The diameter of the outer pipe was 55 mm and the two flows were kept concentric with the aid of 120^{o} spaced, 2 mm thick supports as shown in figure 3.1.1a. The second burner arrangement had the same central pipe, and a divergent outer pipe whose throat and exit diameters were 55 and 90 mm respectively as shown in figure 3.1.1b.

In order to impart swirl to the air flow, straight swirl vanes were inserted into the annulus air passage as shown in figure 3.1.1; two different

swirlers were used and the corresponding swirl numbers were 0.3 and 0.52, these were calculated from measured inlet velocity profiles as discussed in Appendix A1. The same burner was used for both non-reacting and reacting flows and was supported coaxially at the bottom of an axisymmetric enclosure as shown by the dotted lines in figure 3.1.1. The axisymmetric enclosure used for non-reacting (isothermal) flow experiments was made from 5 mm thick plexiglass and, in common with that used for combusting flows, was 300 mm in diameter and 900 mm in length. The end plate provided a furnace exit diameter of 90 mm. For reacting flows, the plexiglass enclosure was replaced by a double skinned water jacketed steel furnace; it consisted of five sections, separately water cooled and one of the sections was fitted with quartz windows of 100 mm diameter and 5 mm thickness to allow the transmission of the light beams as shown in figure 3.1.3.

The furnace was mounted vertically, in the test rig, on a three dimensional traversing mechanism to allow flow property measurements at various locations. For non-reacting flows, the plexiglass enclosure and burner arrangement moved relative to the optical arrangement. In reacting flow runs, the furnace walls were fixed to the traversing table and the bottom and exit plates moved vertically inside the enclosure with constant spacing of three furnace diameters. The furnace arrangement was installed on a rigid frame to which optical components were also fixed. An extractor fan was installed on the exhaust hood to remove the exhaust gases but did not influence the furnace flow. The three dimensional traversing mechanism was used to move the furnace in three orthogonal directions; the horizontal movement ($r, r\theta$) was accurate to 0.5 mm over 250 mm and the vertical movement (along the enclosureaxis) was accurate to 0.25 mm over a distance of 500 mm.

For the measurements in non-reacting flows, compressed air was supplied through pressure regulators to the central and annular jets at rates which were measured and adjusted with rotometers. In reacting flows, the central

air stream was replaced by British north sea natural gas, whose composition and properties were obtained from Kemp's data book (1975) and are given in table 3.1 of this chapter. The gas was supplied to the furnace from a continuous source and its flow rate regulated and measured with pressure regulators and rotometers respectively.

The cooling water to the furnace was supplied individually to each of the furnace sections and the burner bottom plate by centrifugal pumps and the flow rate in each section was measured by flowmeters. The inlet and outlet cooling water temperatures from the various furnace sections were measured using thermocouples located in the water streams as shown in figure 3.1.4. Figure 3.1.5 illustrates a typical flame in a divergent burner arrangement with swirl number of 0.52, as viewed through the quartz windows.

3.1.2 Instrumentation

Measurements of the components of mean and fluctuating velocity and of temperature were obtained in the present flow configuration with the aid of a laser Doppler anemometer and suction pyrameters respectively. The distribution of wall heat flux, by convection and radiation, was obtained from the local measurements of the cooling water flow rate and the temperature rise at various sections of the furnace.

The principle of the laser anemometry is embodied in the following linear relationship between the particle velocity U_p and the Doppler frequency, ν_D,

$$\text{i.e.} \quad U_p = \frac{\nu_D \quad \lambda}{2 \sin \theta/2} \qquad 3.1.1$$

where λ is the wavelength of transmitted light and θ is the angle between the two intersecting light beams. The proportionality constant in this linear equation is readily determined with high precision and the expression may be compared with the more complex expressions used to evaluate the signals from hot-wire anemometers. Further details of laser anemometry and the practical

Table 3.1

Natural Gas Properties

Property	Value	
Volumetric Composition	CH_4	94.4%
	C_2H_6	3.14%
	N_2	1.40%
	C_3H_8	0.60%
	C_4H_{10}	0.19%
	CO_2	0.04%
Molecular weight	17.03	
Heat of reaction H_{fu}	4.97×10^4	KJ/Kg
Density (at 1 atm & 20°C)	0.703	Kg/m^3
Dynamic viscosity	1.81×10^{-5}	Kg/ms
Stoichiometric coefficient	3.65	

realisation of its principles are given by Durst, Melling and Whitelaw (1976) and, in the context of the present thesis, in subsection 3.1.2a.

The measurements of mean gas temperatures were obtained with the aid of a miniature suction pyrometer and is described in subsection 3.1.2b with the techniques used to measure the wall heat transfer in the various furnace sections.

3.1.2a Laser Anemometry

The laser Doppler anemometer is a non-disturbing fluid velocity-meter where the output signal from a photomultiplier, corresponding to an input of light scattered from fluid particles, is modulated at a frequency proportional to the particle velocity. The fundamental optical components of a typical anemometer are shown in figure 3.2.1 and can be divided into two systems relating respectively to the transmission and collection of light. The transmitting system divides a laser beam into two beams of equal intensity and focuses these to intersect at the position of their waist diameters. At the intersection region, the light intensity varies due to phase differences between the wave fronts of the crossed beams, so that the intensity of the scattered light by particles crossing these fringes rises and falls with time at a rate proportional to their velocity.

The receiving system collects the scattered light from the measuring control volume and focuses it onto a photomultiplier tube which produces a voltage signal proportional to the Doppler frequency. This signal can be processed with instrumentations of the following types;

1. spectrum analyser.
2. frequency tracker.
3. period timer or burst counter.
4. filterbank.
5. Fabry-perot interferometer.
6. photon correlator.

The choice of signal processing systems depends on the properties to be measured, the required precision and the flow configuration. In the present case, the filterbank was selected because of its availability and because, as indicated later in the chapter, it is appropriate to furnace flows.

(a) Optical arrangements

The transmitting system corresponds an argon ion laser operating at wavelength of 488 nm and about 200 mW power, a radial diffraction grating which acted as a beam splitter, and a focussing lens. The diffraction grating was bleached on a circular glass disc with parallel faces to within ±0.006 mm and a diameter of 160 mm; it had 21600 line pairs drawn readily and was described by Wigley (1974). The diffraction grating arrangement is shown in figure 3.2.2.

In conventional fringe anemometry, the fringes formed at the beam crossing are stationary and hence the velocity measurements have an attendant directional ambiguity in regions where negative velocities exist. The fixed grating acts as a beam splitter, giving first order diffracted beams of equal intensity. In recirculating flows, the conventional fringe anemometer fails to sense the velocity direction but when the diffraction grating is rotated, each diffracted beam is shifted in frequency by an amount proportional to the rotational speed and the number of line pairs. The frequency shift ν_s between the two diffracted beams of any order can be written as;

$$\nu_s = 2 N P \omega \qquad 3.1.2$$

where

N is the number of line pairs per revolution,

ω is the frequency of the disc rotation,

P is the order of the diffracted beams.

The frequency difference ν_s in the two beams causes a moving fringe pattern in the control volume, in a direction which depends on the rotation

of the grating. The rotational speed of the motor driving the grating could be varied between 5 and 5500 rpm with 0.2% short term stability for each chosen speed. Eight different rotational speeds were used in the present work and corresponded to frequency shifts of; ±0.28, 0.56, 1.12, 1.68, 2.24, 2.80, 3.35 and 3.85 MHz. A beam expander was used to spread the beam separation and allow the two beams to fall parallel on the focussing lens as shown in figure 3.2.1. The focussing lens had a focal length of 300 mm.

The forward scattered light from the control volume was collected by a lens of diameter 25 mm and focal length of 200 mm and was passed through a 0.75 mm pin hole to the photomultiplier (EMI 9635 QB) cathode. The signal from the photomultiplier was passed through a high pass filter and amplifier before the filterbank signal processor.

Figure 3.2.3 shows the two beams incident on the lens which focuses them to a waist at the focal point. The resulting control volume had an ellipsoidal shape, as shown in figure 3.2.4. The fringe spacing is obtained from the expression;

$$\lambda_* = \frac{\lambda}{2 \sin \theta/2} \qquad 3.1.3$$

and had a value of 3.9 μm when using the first order beams and 1.95 μm when using second order beams. The waist diameter d_m and the control volume length l_m were calculated from the following expressions given by Durst et al (1976);

$$d_m = \frac{5}{\pi} F_\ell \frac{\lambda}{d \cos \theta/2} \qquad 3.1.4$$

where F_ℓ is the focal length of focussing lens, d is the incident beam diameter and

$$l_m = d_m/\sin \theta/2 \qquad 3.1.5$$

The resulting control volume dimensions, using the first order beams, were 3.738 mm long and 0.233 mm in diameter. The intensity distribution of the beams is Gaussian and the beam edges were taken at the $1/e^2$ locations.

(b) Signal processing system

The signal from the photomultiplier is characterized by frequency modulation, amplitude modulation and wide band noise. The frequency modulation contains information about the velocity of particles. A typical intensity modulation, due to particles passing through light and dark fringes, is shown in figure 3.2.5. The operation of the anemometer is dependent on the light scattered from the particles and on the light intensity distribution in the control volume, the shape, size and spatial concentration of the scattering particles. At high scattering particle concentrations, the signal can be continuous, but still strongly amplitude modulated due to the particles moving into and out of the scattering control volume at random times. At low concentrations, particles cross the control volume individually with long intervals between them, relative to the transit time.

In the present work, a filterbank signal processor was used to obtain the velocity information from the photomultiplier signals. The filterbank was designed and manufactured by E. Sayle of the A.E.R.E. (Harwell). The filterbank produces a frequency spectrum of the Doppler signals similar to that from a conventional spectrum analyser but employs the available information from the photomultiplier much more efficiently. The selection of the filterbank was guided by the fact that the Doppler signals are generally more noisy in combusting flow but also by its availability.

The filterbank signal processing system is described in detail by Baker (1974) and Baker and Wigley (1975). It consists of a series of seventy filters within the frequency range from 0.398 MHz to 9.551 MHz. Each of these filters has a constant band width to centre frequency ratio of 5%. The values of the centre frequencies increase logarithmically in a ratio of 1.047129/1, thus producing overlap of adjacent filters at approximately the 3db points. The centre frequencies were preset to ±0.5% and the bandwidth ±1.0% of the true value. The filterbank block diagram is shown in figure 3.2.6.

The signal from the photomultiplier was supplied to the bandpass filters set to admit only signals greater than 300 kHz and less than 10 MHz. The

signals were then amplified and the gain adjusted to limit the output signals to 1 volt peak to peak. The resulting signals were introduced to the seventy individual filters and a threshold level set to reduce the system noise. The outputs of all the filters were simultaneously and continuously compared to determine the most resonant filter. A signal corresponding to the resonant filter was produced and its voltage analogue was used in the following ways;

1. as an input to a time domain analyser which gave an online tracking facility for both mean and rms frequencies.
2. to provide a measure of the signal duty cycle of the processor, i.e. the proportion of time in which signals were present.
3. as an input to one of the seventy separate integrators corresponding to each filter. These integrators had variable time constants and sensitivity which can be adjusted to prevent the output from exceeding the saturation voltage. The voltage analogue was used to trigger a current to charge a capacitor associated with the resonant filter, for the time of the Doppler burst. By scanning and logging the accumulated changes in the seventy individual capacitor stores, the histogram display produced is related to the probability distribution of the Doppler frequencies.

Since the band widths of the filters increase linearly with the centre frequencies, the amplitude output (A_{ν_o}), of the integrator corresponding to any particular filter (ν_o) is related to the probability density function $P(\nu_o)$ as follows;

$$A_{\nu_o} = C.\ P(\nu_o)\ .\ \nu_o$$

where C is an arbitrary constant such that,

$$\int_{-\infty}^{\infty} P(\nu_o)\ d\nu_o = 1$$

and hence;

$$c = \int_{-\infty}^{\infty} \frac{A_{\nu_o}}{\nu_o}\ d\nu_o$$

Statistical analysis of the obtained histogram yielded the mean and rms frequencies. The skewness and flatness factors were readily obtained for each of the measuring points.

A statistical analysis of the effect of the sampled number of bursts on the obtained mean and rms velocity measurements was proposed by Yanta (1973) and extended to high levels of fluctuations by Durao (1976). The percentage error in rms velocities is independent of the rms value and is dependent only on the number of bursts, while the percentage error on the mean velocity increases with the rms value and with the decrease of the number of bursts. In the present work, each probability distribution was made up of 10^4 to 5×10^5 values of instantaneous velocity (depending on the turbulence intensity) and for a 95% confidence level, the corresponding error in the rms velocity, due to the number of samples, was less than 1%. The corresponding error in the mean velocity was less than 0.5% for 100% turbulence intensity. The probability distribution $P(\nu_o)$ obtained from the filterbank is not subject to the bias error discussed by McLaughlin and Tiederman (1972) because each measurement is weighted with the signal duration. A sample of the resulting histogram, at a point in the flow, with the values of $\bar{U}$, $\sqrt{\bar{u}^2}$, skewness and flatness is shown in figure 3.2.7.

3.1.2b Temperature and wall heat flux measurements

In the furnace enclosure and in the presence of combustion, the mean gas temperature had to be measured with simple and robust instrumentation and a suction pyrometer was used. The miniature suction pyrometer consisted of a 5 mm twin holed alumina tube surrounding the thermocouple wires which were made from platinum - 13% rhodium/platinum wires. At the measuring point, gases were sucked, at the calibration rate of 80×10^{-6} m^3/s, past the thermocouple bead to increase the heat transfer rate between the hot gases and the thermocouple bead. The thermocouple terminals were connected to a time domain analyser which displayed the measured thermal emfs in volts.

The suction pyrometer was calibrated by Rhines (1975).

The wall temperatures were measured with standard chromel alumel thermocouples embodied in the furnace wall at the locations shown in figure 3.1.4. The cooling water temperature at inlet and outlet of the various furnace sections were also measured with chromol-alumel thermocouples. These thermocouples were calibrated and connected to a chart recorder which recorded the wall and water temperatures throughout the experiments. The errors associated with temperature measurements are discussed later in the chapter.

The water cooled sections of the furnace were fixed to the traversing table and the burner adjusted inside the furnace to maintain a constant distance between the burner bottom and top plates. The difference between the inlet and outlet cooling water temperatures across the furnace section "D" (figure 3.1.4) were recorded at various burner locations inside the furnace. The rate of heat transfer to the cooling water was estimated from the water flow rate, temperature difference and properties at various axial distances from the bottom plate as;

$$Q_w = m_{c.w}\, C_{p_{c.w}}\, (T_{c.w_o} - T_{c.w_i})/A \qquad 3.1.6$$

where $m_{c.w}$ is the mass flow rate of cooling water

A is the surface area across which the heat is transferred.

3.2 Experimental procedure

The optical arrangement used for velocity measurements was aligned in its fixed position and the axes of the burner and the enclosure were aligned with the three dimensional traverse arrangement in the vertical position. The air and gas supplies were adjusted, with the aid of rotometers, to give the required velocity ratio between the central jet and the annulus flow. The air passed through a fluidized bed of titanium dioxide particles. The signal from the photomultiplier was monitored on an oscilloscope and processed

by the filterbank.

The measuring control volume was located in the desired position and the frequency distribution accumulated. After a total of approximately 10^4 - 5×10^5 signal bursts (depending on the local level of turbulence), the amplitude corresponding to each filter was punched in turn, on paper tape. The results were subsequently fed to the computer for further analysis. The burner and end plates were traversed to allow measurements at different locations in the flow field. Each probability distribution was evaluated to provide the values of mean velocity and normal stress. Values of skewness and flatness factors were also obtained but are not presented.

In reacting flows, the furnace cooling water flow rate in the various furnace sections was adjusted with the aid of rotometers and was maintained constant throughout the experiments. The suction pyrometer, used for mean gas temperature measurements was introduced radially through the furnace wall and adjusted at the location where temperature measurements were desired. The suction rate of the pyrometer was kept constant at 80×10^{-6} m^3/s throughout the experiment. The recorded wall and cooling water temperatures, at each position of the burner plate inside the steel enclosure, were constant within $\pm$ 0.2°C throughout each individual measurement.

Before making the detailed velocity measurements reported in this work, the symmetry of the axial velocity was tested on two orthogonal diameters at values of x/D_f of 0.1 and 1.0 for swirl numbers of 0.0, 0.3 and 0.52; the maximum deviation in mean velocity between any set of four radial traverses at the same value of x/D_f was less than 0.3%. The symmetry of the temperature profiles was tested at values of x/D_f of 0.1 and 1.0 for flames with swirl numbers 0.3 and 0.52; the corresponding maximum deviation in mean gas temperature at the same value of x/D_f was less than 10°K.

3.3 Results

This section describes the various experimental results obtained in the flow configuration of section 3.1.1 with the aid of the techniques of

section 3.1.2. They were obtained for non reacting and reacting flows at annulus Reynolds numbers of 1.75×10^4 and 4.7×10^4 and for various inlet, boundary and flow conditions and are summarised in table 3.2 and 3.3. The lower Reynolds number measurements may be regarded as preliminary and were carried out to allow an examination of the merits of the present laser Doppler anemometer and to assess its ability to measure local flow properties in complex flow situations with recirculation. The selection of the flow rate was governed by the frequency range of the filterbank, which consisted of fifty filters ranging from 0.631 to 6.32 MHz. For the subsequent high Reynolds number measurements, twenty additional filters extended the filterbank range indicated in section 3.2. The higher annulus Reynolds number allowed an increase in the furnace loading, i.e. in the heat transfer to the walls and placed greater emphasis on the radiation heat transfer.

The central jet mass flow rate was zero for the non-swirling, non reacting flows in most measurements: a few non reacting flow measurements were carried out with a finite central jet velocity to investigate its influence on the mixing pattern and recirculation. In reacting flows, the central air jet was replaced by natural gas flowing at a rate corresponding to stoichiometry. The fuel jet Reynolds numbers were 0.41×10^4 and 1.1×10^4 and the corresponding annulus air Reynolds numbers were 1.75×10^4 and 4.7×10^4 respectively. In the low flow rate flame measurements, and in the absence of swirl in the air stream, the resulting flame was not properly stabilised on the burner rim and flame lifts of the order of 20 mm were observed. However, the introduction of a vane swirler in the air stream corresponding to swirl number of 0.52 resulted in a central recirculation zone which stabilised the flame.

The low flow rate flame measurements, (flame 1 and 2) were obtained without cooling water in the furnace jackets and the wall temperatures were of the order of 600 K. No gas temperature measurements were obtained since the object of these experiments was to investigate the feasibility and

Table 3.2

Case	Inlet conditions	Flow conditions			S	Measurements									Inlet profiles
		U_{Fu}	U_{Air}	Re_{x10^4}		$\bar{U}$	$\sqrt{\bar{u}^2}$	$\bar{V}$	$\sqrt{\bar{v}^2}$	$\bar{W}$	$\sqrt{\bar{w}^2}$	$\bar{T}$	Q_w	P(U)	
		m/s	m/s												
1	No quarl	0.0	4.78	1.75	0.0	×	×	×	×	—	×	—	—	×	×
2	No quarl	1.8	4.78	1.75	0.52	×	×	×	×	×	×	—	—	×	×
3	No quarl	1.8	4.78	1.75	0.30	×	×	—	—	—	—	—	—	×	—
4	No quarl	0.0	12.85	4.70	0.0	×	×	×	×	—	—	—	—	×	×
5	No quarl	0.0	12.85	4.70	0.52	×	×	×	×	×	×	—	—	×	×
6	With quarl	0.0	12.85	4.70	0.0	×	×	—	—	—	—	—	—	×	×
7	With quarl	0.0	12.85	4.70	0.30	×	×	×	×	×	×	—	—	×	×
8	With quarl	0.0	12.85	4.70	0.52	×	×	×	×	×	×	—	—	×	×

Table 3.3

Flame	Inlet conditions	Flow conditions			S	flow rate of cooling water	Measurements										Inlet profiles
		U_{Fu}	U_{Air}	Re_{x10^4}			$\bar{U}$	$\sqrt{\overline{u^2}}$	$\bar{V}$	$\sqrt{\overline{v^2}}$	$\bar{W}$	$\sqrt{\overline{w^2}}$	$\bar{T}$	$\bar{T}_w$	Q_w	P(U)	
		m/s	m/s														
1	No quarl	6.7	4.78	1.75	0.0	——	×	×	×	×	—	×	—	—	—	×	×
2	No quarl	6.7	4.78	1.75	0.52	——	×	×	×	×	×	×	—	—	—	×	×
3	No quarl	18.0	12.85	4.70	0.52	1.45Kg/m²s	×	×	×	×	×	×	×	×	×	×	×
4	With quarl	18.0	12.85	4.70	0.30	1.45Kg/m²s	×	×	—	—	×	×	×	×	×	×	×
5	With quarl	18.0	12.85	4.70	0.52	1.45 Kg/m²s	×	×	×	×	×	×	×	×	×	×	×
6	With quarl	18.0	12.85	4.70	0.52	0.66Kg/m²s	×	×	×	×	×	×	×	×	×	×	×

limitations of laser velocimetry in the furnace enclosure. In contrast, for the higher flow rate flame measurements, (flames 3 to 6), the furnace sections were water cooled with flow rates of 1.45 and 0.66 kg/s/m^2 to investigate its effect on the local flow properties and heat transfer. The cooling of the furnace walls was necessary at the higher flow rate to prevent overheating the walls. As a result, the maximum wall temperature was 423 K at the lower cooling rate and 383 K at the higher cooling rate; the corresponding wall temperature distributions are shown in Appendix A3. The burner bottom plate was also water cooled at the same rate as the furnace sections and the corresponding average temperatures were 313 K and 343 K for the high and low cooling rates respectively.

In addition to the measured local flow properties indicated in table 3.2 for non-reacting flows, radial profiles of the local shear stress $\overline{uv}$ were also obtained at low annulus flow rate and for swirl numbers of 0.0 and 0.52. These local shear stress measurements together with the mean velocity and normal stress profiles aided in understanding the turbulence structure of the flow and hence in assessing the validity of the turbulence modelling concepts of Chapter 2 as discussed later in chapter 4. Measured profiles of mean velocity components, the corresponding normal stresses and mean gas temperature were obtained in the vicinity of the burner exit, i.e. at x/D_f less than 0.01, and were used as initial conditions to the numerical solution procedure of chapter 2.

The detailed measurements of mean velocity components, turbulence intensities, mean gas temperature and wall heat flux distributions indicated in table 3.2 and 3.3, are presented in Appendix A3, A4, A5 and are compared with the corresponding calculations in chapters 4 and 5. The measured inlet flow properties are also given in Appendix A3 for various flow and geometrical conditions.

The local flow property measurements obtained with the aid of the present experimental technique and listed in tables 3.2 and 3.3, cover a wide range of inlet conditions, burner geometries and furnace wall conditions. The present mean velocity and turbulence intensity measurements allow an assessment of the validity and capability of the laser Doppler anemometer, described earlier, to measure the three orthogonal velocity components and the corresponding normal stresses in complex flow geometries where flow reversal may occur.

The present experimental investigations provided more detailed velocity information in reacting and non reacting flows under various conditions of flow rate, swirl and burner quarl angle. In contrast to the previous measurements shown in table 1.1, the present measurements, obtained with a laser anemometer, allow more accurate and reliable mean velocity information in recirculation zones. The likely precision of the measurements of wall and central recirculation zones, obtained by pitot probes, is difficult to quantify as the probes interfere with the flow. The present measurements included the regions of flow reversal and define the boundaries of these regions within the precision of the anemometer. In general, however, the present measurements and those of table 1.1 indicate similar trends; as the swirl number increases, the size of the central recirculation zone increases and that at the corner decreases. The present investigations allow the measurements of the turbulence intensity in non reacting and reacting confined flows without disturbing the flow pattern. These measurements assist the understanding of the turbulent reacting flows and are used to improve the numerical schemes, by assessing their validity by comparison of computational results with measured data.

Temperature and total wall heat flux measurements were reported in more detail in the present work and included the effects of swirl, quarl and flow rates on the flame behaviour and stability. These measurements provided

useful guide lines to assist the furnace designer to improve combustion efficiency by selecting the optimum burner design. They allow the assessment of the validity of the combustion models of section 2.4.

3.4 Error analysis and precision

This section has been prepared to indicate the source of error associated with the present measurements; to outline procedures to account for these errors; and to assess the likely precision of the measurements.

3.4.1 Velocity measurements

The error sources associated with velocity and normal stress measurements obtained with the laser anemometer may be summarised as; optically, flow and electronic dependent.

The transmitted beams were focussed to intersect at their waist diameters and the optical arrangement of figure 3.2.1 shows that they intersect at an angle θ. The value of θ was found by measuring the beam separation at a known distance from the crossing and its value was precise to within ±0.3%. The consequent uncertainty in the measured velocity was ±0.35% at an angle θ of 7.19 degrees.

Due to the curvature of the plexiglass enclosure, used in the non reacting flow measurements and its finite thickness (5mm), significant refraction occurred as the cylindrical enclosure was traversed horizontally and radially through the laser beams. This refraction resulted in off-axis deviation of the transmitted beam in the plane of the collection lens and was calculated from the geometry of the optical arrangement to be less than 0.15mm; the results were, therefore, adjusted by a small position correction. In reacting flows, the windows were optically flat, 5mm thick and no variation in the beam angle θ with the furnace position was expected. Furthermore, insignificant variation of the point of intersection, due to small changes in the refractive index of the gases, were obtained.

Measurements of low and negative velocities were made possible by the frequency shifting device. To avoid the neglect of any part of the spectrum,

due to the probability of negative velocities, the value of the frequency shift ν_s should ensure that the minimum frequency $(\nu_s + \nu_D)$ is greater than zero. The important requirement is that the size and direction of the frequency shift are compatible with the flow direction and frequency range of the signal processor. The influence of the selection of the frequency shift on the number of cycles in a Doppler burst was investigated in detail by Khalil and Wigley (1976). The optimum values of the frequency shift were used at each location in the low or negative velocity zones in the flow domain; and satisfy the condition that;

$$(\nu_s + \nu_{min}) > \nu_s/2$$ as found by Khalil and Wigley (1976).

The above mentioned relation was found appropriate to the present flow situations and the number of cycles in any Doppler burst were more than 20.

The flow dependent errors associated with laser velocity measurements are due to the finite size of the control volume which results in velocity gradient broadening. Errors can also result from changes in the local refractive index caused by local temperature gradients, particle size and concentration effects. Melling (1973) discussed the problem of gradient broadening due to measuring spatially-averaged velocity rather than the true time mean velocity at the centre of the control volume. The formulae resulting from Melling's analysis were used to correct the results of the present investigation. The magnitude of the correction associated with the mean velocity due to the finite size of the control volume were of the order of 0.1%. The corresponding corrections associated with the normal stress measurements were generally less than 1% but increased to 4.5% in the vicinity of the furnace wall. These errors decreased far downstream the burner exit as the mean velocity gradients decreased.

In reacting flows, the temperature variation throughout the furnace, results in variations of the refractive index. The gas refractive index

variation with temperature, see for example Weinberg (1963) was small; the subsequent deviation in a single beam through the furnace was calculated by dividing the furnace volume to concentric cylinders of gases of various temperatures, densities and refractive indices. The mean position of the beams intersection in the present flames was shifted by, less than 40 μm, in the radial direction and 4μm in the axial direction, from the corresponding position in isothermal flows. These deviations hardly cause a variation of the half angle θ but worsens the spatial resolution of the signals. In some of the present flow measurements, for example, cases 1, 2 and flames 1 and 2, the intensity of the scattered light was very small and titanium dioxide particles were supplied to the air flow from a fluidized bed and its volumetric flow rate monitored by a bypass system. The rate of seeding was kept to the minimum. Errors can result from gradients in particle concentration due to changes in the volume of fluid caused by temperature gradients or chemical reaction but have been estimated by Asalor and Whitelaw (1975) to be negligible except in the immediate vicinity of a reaction zone. The various effects of seeding particle concentration and size on velocity measurements were discussed by Durst et al. (1976) and Self and Whitelaw (1976).

Signals from the photomultiplier were passed through the bandpass filter and amplifier before entering the filterbank, the frequency response of the input amplifier was non linear. The gain, for small signals, was greater at low frequencies whereas the gain for large signals was greater at high frequencies. Since a signal amplitude threshold level has to be chosen to reduce the system response to noise, the non linearity in the frequency response of the amplifier caused biased frequency measurements. However, it was possible to choose a certain level of amplification for a preset threshold level to counteract the non linearity in the input amplifier. At this threshold level, the frequency response of the amplifier was flat over the whole frequency range to better than ±0.5dB.

Since the frequency range of the filterbank is divided into discrete channels whose individual band widths are 5% of the centre frequency, the uncertainty in any one measurement of frequency is ±2.5%. Baker (1974), showed error bands in graphical form of the mean and rms velocities due to the turbulence bandwidth compared to the filter bandwidths; the number of points in the velocity probability distribution was approximately given by;

$$n = (6 \frac{\sigma}{\Delta f} + 1) \qquad 3.4.1$$

where σ and Δf are the turbulence and filter bandwidths respectively. The percentage error in the mean frequency was ±2.5% at zero turbulence intensity and diminished at $\sigma/\Delta f$ greater than 1. The percentage error in the turbulence intensity was shown to be more than 3% at $\sigma/\Delta f$ of 1.3; this percentage error decreased gradually to zero as $\sigma/\Delta f$ increased to 4. According to the above analysis, more than 25 filters are required to build the probability spectrum, in order to reduce the percentage error in the mean and rms velocities to zero.

In the present experimental investigations, each velocity probability distribution was made of more than 20 filters as shown in Appendix A3 and the corresponding error in the turbulence intensity for $\frac{\sigma}{\Delta f} = 3.166$ was less than 0.5%. The above analysis also suggested that in the present investigations, the mean velocity components were obtained within ±3%, and the likely precision of the rms velocity was 8%.

3.4.2 Temperature and heat flux measurements

The measurements of mean gas temperature with a suction pyrometer were subject to radiation errors, which were minimised, in the present work, by enclosing the bright thermocouple bead in a refractory sheath of low thermal conductivity which also minimised the conduction loss through the pyrometer. The errors arising from subjecting the pyrometer to non uniform temperature distribution in the furnace were estimated by treating the pyrometer stem as an extended surface, those errors were found to be less than 0.05%.

This approach enlisted that the suction was not isokinetic and the temperature differences between the true gas temperature and the measured value depend on the suction velocity, gas velocity and specific heat, Braud et al (1972), this difference was less than 5C in the present investigations. Errors can also arise due to variations in the suction rate from the precribed value and precautions were taken to keep the suction rate constant and within ±5% of the calibration rate, the corresponding errors were estimated to be less than ±20K. However, the mean gas temperature can be obtained within ±25K in the range of temperature measurements of the present investigations. Further details on the gas temperature error analysis can be found in references by Khalil (1975), Khalil et al (1976) and Styles (1976).

The furnace wall and cooling water temperatures were measured with chromel-alumel-thermocouples and the precision of those temperatures was around ±0.5°C for mean temperatures up to 150°C. The cooling water flow rate was measured by rotometer which was accurate within ±1.3%. The above analysis suggested that the wall heat flux can be obtained in the present furnace within ±2%.

3.5 Summary

The following conclusions summarize some of the findings of the present experimental investigation.

1. A laser Doppler anemometer with frequency shift has been used to measure the velocity characteristics of turbulent non reacting and reacting flows in furnace type geometries at zero and finite swirl.
2. The filterbank satisfactorily processed the on line Doppler signals in flow situations with and without combustion and swirl. The velocity probability distributions are near Gaussian in non-swirling flows and do not contain any suggestions of the bimodel distribution. The precision of the mean and rms velocities was ±3% and 8% respectively.
3. The mean velocity results in reacting and non reacting swirling flows indicate that the size of the central recirculation region increases

with swirl while the length of the wall recirculation decreases with swirl. The velocity probability distributions demonstrate that at the centreline location, corresponding to zero mean velocity, and at points upstream and downstream of this location, a wide range of negative and positive velocities exist and can render previous measurements of the length of the recirculation region, obtained by other measuring techniques invalid.

4. Mean velocity components in reacting flows were measured to be generally higher than the corresponding component of non reacting flows, due to heat release. Similarly, the magnitude of the rms velocity generally increases with combustion; the results suggest that, in the vicinity of reaction zones, combustion generated turbulence appears.

5. Measured mean velocity components and the corresponding turbulence intensity at the burner exit in reacting and non reacting flows were obtained and used as inlet conditions to the calculation procedure of chapter 2.

6. A suction pyrometer has been used in reacting flows to measure the mean temperature with a precision of ±25K. The mean gas temperature results identify regions of maximum and minimum temperatures corresponding to reaction zones and unpremixed reactant streams. Wall heat transfer distributions were also obtained from estimating the heat added to the cooling water in each of the furnace sections; the likely precision of these measurements was ±2%.

7. The introduction of swirl stabilizes the flame and shortens it. The peak centreline temperature moves upstream and the flame spread is wider at high swirl numbers. The use of quarl burner creates a central recirculation zone downstream of the burner throat which helps in stabilizing the flame and moves the location of peak wall heat flux upstream towards the burner exit.

8. The present experimental techniques enable the extensive measurements of mean velocity components, the corresponding normal stresses, mean gas temperature and the wall heat flux in reacting and non-reacting flows in furnace type geometries with better precision than those obtained by other measuring techniques; particularly for the velocity characteristics near recirculation zones. The present measurements are used in the next two chapters to assess the validity of the computational procedure in reacting and non reacting flows, and yield meaningful comparisons as the measurements are of known precision.

CHAPTER 4

ISOTHERMAL FLOW CALCULATIONS

4.1 Introduction

In this chapter, the validity of the turbulence model and the numerical scheme of chapter 2 for the representation of the properties of turbulent, swirling recirculating flows is assessed. The assessment of the turbulence model is supported by comparisons between measured and calculated flow properties in simple non-reacting flows akin to the present flow configuration, and in non-reacting flows in the present furnace enclosure geometry. Implications of the turbulence models for reacting flow calculations are also discussed.

The turbulence model used in the present work and previously described in chapter 2, introduces the eddy viscosity concept and expresses the Reynolds stresses in terms of an effective viscosity and mean velocity gradients as shown by equation 2.3.7. The effective viscosity expression, proposed by Kolmogorov (1942) and Prandtl (1945) to be proportional to the square root of the turbulent kinetic energy k and to a length scale ℓ characterising the energy containing eddies, was suggested in connection with boundary layer and free shear flows; its application to recirculating flows requires examination. One of the objects of the present experimental investigation is to obtain detailed information to verify the use of the eddy viscosity concept and the two equation turbulence model in recirculating flows. Radial profiles of $\bar{U}/U_{max}$, $\overline{uv}/U^2_{max}$ and k/U^2_{max} were obtained in the present work with the aid of laser Doppler anemometry and are shown in figures 4.1.1 to 4.1.2 for non-swirling and swirling low flow rate measurements. At a location of one annular diameter downstream of the jet exit and for swirling and non-swirling flows, the distributions of mean axial velocity exhibit regions

of positive and negative radial gradient; the corresponding radial profiles of Reynolds shear stress $\overline{uv}$, shown in the figures, display the occurance of changes in the sign of the stress. This is in qualitative agreement with the occurance of the maxima and minima in the mean velocity profiles shown in the same figures. The spacing between consecutive measurement positions does not allow a quantitative assessment of a possible discrepancy between zero mean velocity gradient and zero Reynolds shear stress $\overline{uv}$, and consequently, the eddy viscosity concept and the Kolmogorov-Prandtl assumption was incorporated in the present work as indicated in chapter 2.

In the second section of this chapter, various comparisons with previous experimental measurements in confined flow geometries are described and the numerical details of each test case and the consequent physical implications of the results are discussed. The third section describes the comparisons between the present measurements, outlined in table 3.2, for non-reacting flows and the corresponding calculations. The predicted flow properties, obtained with the aid of the numerical procedure of section 2.2 were discussed in section 4.4. The capability of the calculation procedure to predict the mean flow pattern and turbulence characteristics is then extended to reacting flows, with the consequent implications on the flame structure. The chapter ends with section 4.5, where conclusions on the suitability of the model and its validity for complex flow configurations are shown.

4.2 Flow properties in turbulent recirculating flows

In this section, the capability of the numerical procedure of section 2.2, embodying a two equation turbulence model, to predict the flow patterns and local flow properties for a wide range of non-reacting flow configurations, is assessed. This is done by comparing the calculated results with the corresponding measurements. These flow configurations were selected to represent, both simple flow situations such as swirling pipe flow and flow situations akin to furnaces and combustion chambers, such as coflowing flows and flow

past sudden enlargement where corner recirculation zones are expected. These non-reacting flows simulate most of the possible furnaces, where the knowledge of the aerodynamic pattern is important to establish the possibility of flame stability.

In such flow situations where flow reversal may occur, the elliptic nature of the flow requires an iterative procedure such as that of section 2.2, and solves the conservation equations of mass and momentum for non reacting turbulent flows. The various flow configurations reported in this section are tabulated in table 4.1. In each test case, the flow configuration, measured properties, numerical tests and the obtained comparisons are described and the agreement quantified. In the calculations described in this section, non-uniform grid arrangements which comprised 400 grid nodes were used except for flows behind baffles, where 30x30 grid was employed. The optimum location of the grid nodes is a matter of experience but, as a result of considerable testing, the present calculations are grid independent in the sense that the use of 50% more grid nodes would not result in values of the dependent variables which are significantly different from those presented in this section.

4.2.1 Swirling pipe flow

The experimental investigations of Weske and Sturov (1974) relate to the flow of swirling air in a pipe. The degree of swirl was varied by rotating the inlet pipe at various rotational speeds up to 3,000 r.p.m. This swirl generator made it possible to obtain, at the inlet to the downstream stationary pipe, a radial distribution of tangential velocity which was close to that of the solid body rotation. Measurements of the three velocity components, obtained with hot wire anemometry, were recorded at downstream locations for two values of the ratio of the maximum tangential velocity to the mean axial velocity at the inlet plane. Measurements of mean velocity components and the corresponding turbulence intensities were available at

Table 4.1

Flow situation		measured properties						Re	S	Comments
		U	V	W	k	P	T			
Swirling pipe flow	Weske and Sturov (1974)	✓	✓	✓	✓	-	-	$3x10^4$	1.0,3.0	
	Baker (1967)	✓	-	✓	-	✓	-	$5x10^4$-$2x10^5$	0.55	
Pipe jet with and without swirl	Craya and Curtet (1953)	✓	-	-	-	✓	-	$2x10^5$	0.0	
	Craya and Utrysko(1967)	✓	-	✓	-	✓	-		swirl	varied 0.0 to 0.81
Flow past backward facing step	Abbott and Kline (1962)	✓	-	-	-	-	-	$2x10^4$	0.0	plane flow
Axi-symmetric sudden expansion	Back and Roschke (1972)	✓	-	-	-	-	-	100 to 10^4	0.0	single jet
	Owen (1975)	✓	✓	-	✓	-	-		0.0	coaxial jets
	Beltagui & Maccallum (1974)	✓	✓	✓	-	✓	-	$9x10^5$	swirl	varied 0.0 to 0.6
Flow over roughness rib	Wilkie (1966)	-	-	-	-	✓	✓	$1.92x10^5$	-	axisymmetric flow
	Mantle (1966)	-	-	-	-	✓	-	$0.7x10^5$	-	plane flow
Plane wall jets	Kacker and Whitelaw (1971)	✓	-	-	✓	-	-		-	
Wake flows	Durao and Whitelaw(1974)	✓	-	-	✓	-	-		0.0	
	Assaf (1975)	✓	-	-	✓	-	-	$4.25x10^4$ & $5.10x10^4$	0.0	

the inlet plane and were used as boundary conditions; the rate of dissipation at the inlet plane was calculated from the expression;

$$\varepsilon = k^{3/2}/0.005\ D \qquad 4.2.1$$

which assumes the existance of a constant mixing length across the pipe.

The downstream boundary conditions corresponded to zero gradients and were assigned at x/D of 160. The influence of the grid size and arrangement was found to be sensibly insignificant for grids greater than 16x16.

The measured and calculated radial profiles of mean tangential velocities for swirl W_{max}/U_m of 1.0 and 3.0 and at downstream locations of x/D of 0.35 and 5.1, are shown in figures 4.2.1 and 4.2.2 respectively; the corresponding profiles of kinetic energy of turbulence are also presented in these figures.

The agreement between the measured and calculated mean tangential velocity and kinetic energy of turbulence are reasonably good. Discrepancies shown near the wall of the pipe may be attributed to the two equation turbulence model which is known to be imperfect for asymmetric flows, see for example, Hanjalic et al (1972). These discrepancies may also be attributed, at least partly, to the assumption of 2.3.7 which requires that the location of zero velocity gradient be identical to that of zero local shear stress.

Swirling flow in a pipe can also be generated with vanes imparting rotational action on the fluid. An experiment of that type was carried out by Baker (1967) who measured the mean velocity components, with a directionally sensitive impact probe, at various stations downstream the pipe inlet section. The swirl number had a value of 0.55 and was defined as;

$$S' = 8\rho \int_0^R U\,W\,r^2\,dr / \rho\,U_m^2\,D^3 \qquad 4.2.2$$

Calculations were performed using the present computational procedure and were compared with the measurements. The comparison between mean tangential velocities was carried out at two stations of x/D equals 15 and 35. The

inlet radial velocity profiles were assumed and were found not to influence the calculations of figure 4.2.3 significantly. These results were obtained with the assumption that the inlet radial velocity decreased linearly with the radius. The profile of mean tangential velocity at inlet was assumed to follow a forced vortex variation with radius.

The kinetic energy and dissipation rate profiles at inlet were assumed to correspond to a mixing length assumption and did not have a significant influence on the calculations downstream of x/D = 4.0. The exit boundary condition of $\partial\bar{\Phi}/\partial x_j = 0$ was assumed at x/D = 100. Measured and calculated values of the mean tangential velocity component are shown in figure 4.2.3 at x/D of 15 and 35, and clearly demonstrate that the calculations obtained using a two equation turbulence model lie within the experimental scatter. The discrepancies near the walls and the centreline stem from the imperfection of the turbulence model for near wall flows and to the anisotropic nature of turbulence in the central core of the flow.

The calculations of swirling pipe flow require the solution of elliptic equations, because as can be seen from figures 4.2.1, 4.2.2 and 4.2.3, the tangential velocity component varies significantly in both longitudinal and radial directions. The local gradients in the radial direction are greater than those in the axial direction and hence, the flow has small ellipticity. Once again the discrepancies shown for swirling flow in pipes are mainly due to the turbulence model. Figure 4.2.3 shows the predicted velocity distributions of Roberts (1972) using a streamline vorticity procedure and a two equation turbulence model.

The need for a model to represent the non-isotropic nature of swirling flows has been discussed by Lilley (1974) and partly developed by Morse (1976) and Ribeiro (1976). The Reynolds stress model of Launder (1975) may be appropriate for such flows but no comparisons have so far been reported with recirculating swirling flows.

4.2.2 Pipe jet with and without swirl

The flow of a jet into a coflowing stream is of practical importance, for example, in cement rotary kilns.

This arrangement induces a secondary flow through the annulus formed between the jet nozzle and the pipe diameter and can result in recirculation in the vicinity of the pipe wall for high values of jet to annulus velocity ratio. Many investigations have been carried out for this configuration with various jet to annulus momentum ratios.

The investigations of Barchilon et al (1964) and Craya et al (1967) were carried out in a duct of diameter 162mm and a central nozzle diameter of 12mm. Measured static and total head pressures were recorded at various locations in the flow using a pitot probe. The analytical investigations of Craya and Curtet (1953), for the coflowing geometry, devised a similarity parameter, C_t, which is known as the Craya Curtet number defined as;

$$\frac{1}{C_t^2} = \frac{1}{\bar{U}_m^2 A} \int_A \left(\frac{\bar{P}}{\bar{\rho}} + \bar{U}^2\right) \, rdr - \frac{1}{2} \qquad 4.2.3$$

and

$$U_m = \frac{1}{A} \int_A \bar{U} \, rdr$$

A is the cross sectional flow area.

This number relates the momentum of both jet and annulus flows. In the present calculations, the initial velocity profile was assumed to be that of a turbulent pipe flow i.e.

$$\bar{U} = U_{c.L} \left\{1 - \left(\frac{2r}{d}\right)\right\}^{\frac{1}{7}} \qquad 4.2.4$$

and the corresponding distribution of kinetic energy of turbulence and its dissipation rate were based on a mixing length assumption. The downstream boundary conditions were assigned at x/D of 10 and corresponded to zero

gradients. Tests were carried out to investigate the influence of assumed inlet conditions on the flow pattern and indicated insignificant differences. A detailed investigation of the influences of assumed profiles at inlet has been reported by Khalil (1976).

Figure 4.2.4 shows the location of the wall recirculation zone for various values of C_t. As C_t increases, i.e. the annulus/jet momentum ratio increases, the wall recirculation decreases in size and moves downstream of the inlet section. The influence of C_t on the recirculated mass flow rate is shown in figure 4.2.5; the symbols represent different data obtained from Barchilon et al (1964), while the solid line represents the calculated variation of $M_{r_{max}}/M_{tot}$ for different values of C_t. The ratio of the re-circulated mass to the total mass increases as C_t decreases as would be expected. The measured and predicted values are in very good agreement for the range of C_t reported here; the uncertainty in the experiments was expected to be largest at large C_t, due to the use of pitot tubes. The calculation of El Ghobashi (1974), obtained for the same flow, with the k- ε turbulence model and a different numerical scheme are shown in figure 4.2.4 and 4.2.5 and were in good agreement with the present calculations.

The influence of swirling the inner jet on the flow pattern, momentum exchange, velocity profiles and pressure distributions was investigated by Craya and Utrysko (1967). The velocities were measured using a directionally sensitive pitot probe in the geometry described above but with various degrees of swirl in the central jet. The same inlet profiles used in the non-swirling case were assumed here and, in addition, the tangential velocity profile which was taken from the data of Craya et al (1967). The present comparisons were performed for annulus to jet mass flow rates of 15 and at five different swirl numbers varying from 0.0 to 0.81.

Figure 4.2.6 shows the centreline distribution of mean axial velocity at different swirl numbers. The symbols represent the measurements and the

solid lines the calculated distributions. It can be seen that both measured and calculated velocity distributions are in good agreement at low swirl numbers. The agreement in the initial region deteriorated as the swirl intensity increased; due to the anisotropic nature of the turbulence in the mixing region. These results are shown for Curtet numbers (C_t) between 1.26 and 1.38 and no recirculation zones were observed for this value of C_t as expected from figures 4.2.4 and 4.2.5. Profiles of mean tangential velocity component are shown in figure 4.2.7 for a swirl number of 0.81. The measured and calculated tangential velocities are shown to be in reasonable agreement within the previous comments on experimental accuracy.

The computer storage required for the present grid (20x20) could be estimated from section 2.2.4 and was 27 kilowords and 360 seconds computing time.

4.2.3 Flow over a backward facing step

Abbott and Kline (1962) observed turbulent flow downstream of a plane sudden expansion with the aid of smoke and in the vicinity of reattachment position, with tufts. Similar investigations in laminar flow have been reported by Melling (1975) using laser anemometry. The results of Abbott et al (1962) can only be used as qualitative measures of the capability of the computational procedure. Although Abbott and Kline did not provide detailed measurements in the recirculation region, the present computation procedure can readily provide these by starting the calculation upstream of the step. The exit boundary conditions of zero gradients was assigned at different downstream positions depending on the value of 2h/d, i.e. on the length of the recirculation zone. The step height is h and the small duct width is d. The actual location of the exit was determined by means of trial and error with the criteria that the location of the exit should not influence the upstream calculation.

Comparison between measured and predicted variation of the recirculation zone length (x_r) and the step height (h) is shown in figure 4.2.8 for a range of Reynolds numbers from $2x10^4$ to $5x10^4$. At small expansion ratios; i.e. $\frac{2h}{d}$, it was observed that the recirculation zones on both sides of the symmetry plane were identical; but for larger values of 2h/d, the two recirculation regions appeared to interact and resulted in asymmetric region of recirculation. The comparisons, therefore, were limited to regions of small expansion ratios; i.e. $2h/d<1.0$. For these regions the symmetry prevails and the reattachment location tended to correspond to approximately 8.5h as the value of 2h/d increased above 0.8. Figure 4.2.8 also indicated contours of iso-velocity lines and velocity profiles in the recirculation zone corresponding to different expansion ratio 2h/d of 0.11, 0.2 and 0.56. The computer storage requirements were 25K words and the computer time was 280 seconds.

Although the present comparison is rendered incomplete by the lack of experimental data, two conclusions can be drawn. First, it appears that the length of the recirculation region for symmetric flow on a single step is insensitive to flow properties over a wide range and is well represented by the present calculations: in addition, the calculation procedure can represent properties which have not been measured in a plausible manner. Secondly, it is clear that the present scheme could not represent the asymmetric results of Abbott and Kline and of Durst, Melling and Whitelaw (1974); it is probable that a three dimensional, time-dependent calculation scheme would be required for these asymmetric flows.

4.2.4 Axisymmetric, sudden expansion flow

The flow downstream of an axisymmetric, sudden enlargement is one of the common features of furnace flows since, in general, furnaces are composed of a large duct with small inlet concentric jets for the reactants to enter the furnace. The real furnace configurations have more complicated

inlet geometries of secondary and tertiary inlets which are concentric with the central fuel entry. For simple flow situations, downstream of an axisymmetric sudden enlargement, Back and Roschke (1972) investigated the flow pattern for a range of Reynolds numbers.

Measurements of the reattachment length were obtained using dye traces and encompassed Reynolds numbers from 100 to 10^4 based on the small pipe diameter, the expansion ratio d/D was 0.385. The calculated values of reattachment lengths are compared with measurements at high Reynolds numbers and shown in figure 4.2.8, which also presents the calculations and measurements of subsection 4.2.3, The high Reynolds number measurements of Back and Roschke (1972) corresponded to 2h/d of 1.6 and x_r/h of 8.5.

As an example of the information which can be obtained from the computational procedure, figure 4.2.9 and 4.2.10 were prepared. Figure 4.2.9 represents contours of isovelocity lines, static pressure, turbulence kinetic energy and length scale of turbulence for the flow of Back et al (1972) and at Re= $5x10^4$. Figure 4.2.10 shows contours of mean axial velocity static pressure and kinetic energy of turbulence for an expansion ratio of 0.3 and Re of $5x10^4$. There are no measurements to compare with, but these calculations illustrate the capability of the present procedure. The inlet axial velocity profiles for these calculations were represented by equation 4.2.4, radial and tangential velocity components were assumed zero at inlet. The inlet kinetic energy of turbulence and its dissipation rate were assumed to conform to mixing length hypothesis . The influence of inlet velocity profile assumptions, on the centreline velocity was less than 10.5% and became negligible at x/D of 3.8 and for the test Reynolds number 10^5. The influence of inlet profile of turbulent kinetic energy and dissipation rate on local flow properties was found small except on the wall shear stress which was varied by 9% due to a ten fold change of inlet kinetic energy of turbulence as shown in figure 4.2.11.

Further experimental investigations in sudden enlargement flows were reported by Owen (1975) whose investigations were concerned with the flow in an axisymmetric sudden enlargement with coaxial jets of air. The enclosure diameter was 125mm, while the annulus outer diameter was 87.5mm and the central/annulus diameter ratio was 0.715. Measurements of mean axial and radial velocities, kinetic energy and shear stresses were obtained for free and confined jets and were obtained with a laser Doppler anemometer. The central jet had a peak velocity of 2.44 m/s while the annular one had a peak velocity of 29.5 m/s, hence a negative recirculation zone was created on the centreline due to the momentum exchange ratio of 140; i.e.

$\rho U_a A_a U_a / \rho U_j A_j U_j = 140.$

Measured and predicted velocity profiles at two downstream locations, x/D of 0.25 and 0.6, are shown in figure 4.2.12. the obtained agreement illustrates the capability of the present numerical scheme and the two equation turbulence model to reasonably represent the flow pattern in coaxial jet flow in sudden enlargement; inlet velocity profiles were measured with pitot tube and were used in the calculation scheme. The computer storage and time requirements for this flow and that of Back et al (1972) were similar and corresponded to 25K storage and 280s running time.

The measurements of Beltagui and Maccallum (1974) were obtained downstream of a sudden enlargement in an axisymmetric flow with and without swirl; two swirl generators of the hubless and the annular type were used. A wide range of swirl numbers was investigated for two different expansion ratios of 0.4 and 0.2. The measurements of mean axial, radial and tangential velocity components were obtained by a water cooled three hole probe whose tip outside diameter was 6.35mm. This probe was also used for static pressure measurements, for situations where the flow was principally in the radial direction, a disc probe was used for the pressure measurements. The mean inlet velocity U_o was 15.2 m/s and the corresponding Reynolds number was 9×10^4.

No turbulence quantities were measured and the inlet profiles reported by Maccallum (1975) were used in the calculation procedure. The influence of inlet velocity and kinetic energy profile assumptions, on the mean axial velocity was found to be less than 8% of the inlet mean velocity U_o, in the vicinity of the inlet and diminished at x/D_f of 0.25. Comparisons between measured and calculated mean axial velocity for a hubless swirler of vane angles 22^o (S= 0.239) and d/D_f of 0.2 are shown in figure 4.2.13. Profiles of mean axial velocities at different locations in the enclosure are shown in the figure. They are in good agreement and the discrepancies in the low velocity regions, can be attributed to the precision of the measurements and the anisotropic nature of swirling flows.

The measured and calculated tangential velocity profiles at various locations downstream the step are shown in figure 4.2.14. Figure 4.2.15 shows the radial profiles of static pressure coefficient at various axial locations, for the same swirler. The agreement between the calculations and the measurements is good but discrepancies up to 25% can be observed in regions of steep gradients. In judging these comparisons, the likely precision of the measurements should be considered and is of the order of ±10%.

Radial profiles of mean axial velocities for a swirl vane angle of 15^o and d/D_f of 0.4 are shown in figure 4.2.16. The agreement is reasonable, again except at low velocities, where discrepancies are likely to be significant and are due to the uncertainty of the measurement technique. For an annular swirler, profiles of measured and calculated mean axial velocity are shown in figure 4.2.17 and are in qualitative agreement. A central recirculation zone appeared immediately downstream of the swirler hub and extended to x/D_f of 1.6. The agreement is not very good, as shown in figure 4.2.17, and this can be partly attributed to the inadequacy of the turbulence model to describe anisotropic turbulence and highly swirling flows, but mainly to the inaccuracies associated with the measuring techniques in recirculation zones.

4.2.5 Flow over roughness rib elements

The flow over plates and in channels with surfaces roughened by ribs is relevant to the augumentation of heat transfer and has been examined experimentally, for example, by Wilkie (1966) and Mantle (1966). The increase of the surface area as for example, in the corrugated fire tubes of industrial and domestic boilers, increases the heat transfer to the walls. Wilkie measured the fully developed pressure and Stanton number distributions in an axisymmetric arrangement with various ratios of pitch "P" to rib height "Δ". The inner roughened surface was heated electrically with $T_w/T_b = 1.2$, while the outer smooth wall was not heated, and the temperature distribution along the surface was measured by thermocouples. Pressure tappings were used for the static pressure measurements, for various rib height/width ratios.

No inlet profiles of mean velocity components, kinetic energy of turbulence and dissipation rate were reported by Wilkie. The mean axial velocity profile at inlet was assumed to be that of fully developed channel flow and the influence of this assumption on the centreline velocity was less than 5% and diminished at downstream locations less than one rib height. The radial velocity component at inlet was assumed to be zero and the kinetic energy distribution corresponds to $k/U^2 = 0.005$. The influence of varying k/U^2 between 0.003 and 0.03 on the centreline velocity distribution was less than 4%. The dissipation rate was assumed to follow a mixing length hypothesis and the influence of this assumption diminished at downstream distances less than one rib height.

The measurements of Wilkie for P/Δ of 15 and 7.2 are shown in figure 4.2.18a and 4.2.18b. Figure 4.2.18a shows the variation of Stanton number and pressure coefficient between two ribs on an axisymmetric body, for a Reynolds number of 1.913×10^5. On the same diagram, the calculated distributions are also shown and exhibit good agreement over the flow field. The maximum deviation amounts to 15% at low values of S_t, the pressure coefficient

($C_p = \delta P/\frac{1}{2}\rho\bar{U}^2$) is in good agreement with the measurements whose scatter was in the order of 5%. The average S_t for roughened surfaces, with pitch to height ratios of 15, had a value of 0.0057 corresponding to 0.0025 for smooth surface.

Figure 4.2.18b shows the Stanton number and pressure coefficient variation between the ribs for the geometrical arrangement with P/Δ of 7.2. Measured and calculated Stanton numbers are in good agreement except near the rib faces where high values of S_t are expected. The reattachment length downstream of the upstream rib face coincides with the location of maximum S_t and a small recirculation zone is also observed upstream of the downstream rib. Detailed contours of velocity vectors, mean axial velocity, static pressure, turbulence energy and length scale for P/Δ of 7.2 are shown in figure 4.2.19 and 4.2.20. No measurements exist with which comparisons can be made and these calculations provide an overall description of the local flow properties and heat transfer for flow between ribs on cylindrical surfaces.

The measurements of recirculation zone length obtained by Mantle (1966) are shown in figure 4.2.21 together with the calculated values of the present procedure and the two are in good agreement. Although Mantle did not observe, with his wool tufts, reattachment for values of P/Δ less than 6.6, the calculations indicate reattachment at much lower values of P/Δ. For P/Δ less than 2.5, no reattachment was observed and the flow skims over the surface between ribs. The discrepancies at low values of P/Δ may be due to the inaccuracy of the measuring technique which depended on the wool tuft motion with the flow. The flow Reynolds number was 0.7×10^5 with plane roughened surface, in contrast to Wilkie where the roughened surface was cylindrical.

The effect of the pitch to rib height ratio on the local Stanton number distribution is shown in figure 4.2.21 with the corresponding pressure drop distribution. It can be seen that, as the pitch decreases for the same rib height, the overall Stanton number and, therefore, the total heat flux to

the wall increases. Unfortunately, the required pressure drop, as indicated by the pressure coefficient, also increases and the rate of increase of pressure drop is similar to the rate of increase of heat transfer rate.

4.2.6 Plane wall jet flows

Kacker and Whitelaw (1971) used a hot wire anemometer to measure mean velocity and turbulent kinetic energy downstream of wall jet geometries with four different ratios of slot to free stream velocity. In the particular case of a thick slot lip, there is a substantial region of recirculation immediately downstream of the lip and this requires the solution of elliptic equations. Unlike the recirculation regions of previous flows of 4.2.5, which were bounded by two surfaces, this recirculation zone is bound by one surface.

Measured and calculated values of mean velocity and turbulence kinetic energy are presented on figures 4.2.22a and 4.2.22b for two values of the velocity ratio, i.e. U_C/U_G = 0.75 and 2.30 and at two downstream stations x/y_c of 10 and 150. The region of reversed flow is not large at the first downstream station where measurements are available and, at further downstream stations, the influence of the recirculation disappeared. The calculations, however, encompass the region of recirculation and the results shown on the figures have been influenced by upstream recirculation.

Measured initial conditions were input to the calculation scheme except for the rate of dissipation ε which was calculated with the aid of a mixing length assumption. The downstream boundary conditions of zero gradients was located at a station such that the upstream calculations were uninfluenced.

The measured and calculated values of mean velocity and kinetic energy of turbulence are in reasonable agreement, similar calculations, with a simple turbulence model, were obtained with a computer program based on the solution of equations for stream function and vorticity; Gosman et al (1969) but required relatively longer computation time and storage. In these earlier

computations, the agreement was reasonable and was due to the use of algebraic length scale assumptions formulated from the experimental measurements.

4.2.7 Flow in the wake of a disc

Measurements of mean axial velocity and the corresponding normal stress, reported by Durao and Whitelaw (1974), were obtained by laser anemometry in the wake of a disc surrounded by an annular free jet. Measurements of mean axial velocity and the corresponding normal stress in the confined wake flow behind discs, obtained using laser anemometry, were also reported by Assaf (1975). The present computational procedure was used to calculate these two flows; as for the flow of Durao and Whitelaw, measured axial velocity distributions along the centreline and at a radial profile at x/D of 0.3 are shown in figure 4.2.23 and 4.2.24 together with the calculations obtained with the range of assumed values of the radial velocity component at the exit from the annular jet. Measured initial values of the axial velocity component and the corresponding normal stress were used in the calculations.

The radial velocity component was initially assumed zero and, as can be seen, the agreement between calculation and measurements is imperfect. In particular, the length of the recirculation region is calculated to be around 75% of the measured value and the minimum velocity is overestimated. The influence of finite radial velocity is also shown on the figure and is significant: thus, the absence of measured initial values of this radial component can be serious. In the present case, the radial values are likely to be very close to zero and the discrepancies between calculations and measurement can be attributed more to the turbulence model than to incorrect initial conditions.

There are also differences between calculations and measurements in the decay of the centreline velocity in the jet region and also at the outer edge of the jet. The former can be attributed to the turbulence model, as discussed by Pope and Whitelaw (1976), but the latter is linked to the distribution of grid nodes in the outer region of flow and to the radial location at which the free boundary condition is assigned. For the calculations of figure 4.2.23 and 4.2.24, the outer grid boundary was located at 10D from the centreline and corresponded to $\partial\Phi/\partial r$ of zero: the grid mesh was 30x30 with 16 grid nodes between the velocity maximum of figure 4.2.24 and the centreline. The inner region of the flow was not influenced by the location of the boundary condition and the outer region became less influenced with increasing downstream distance.

The local velocities and turbulence intensities measured by Assaf (1975) in a confined wake flow were obtained for two disc to pipe diameter ratios of 0.25 and 0.5 at the same flow rate and corresponded to Reynolds numbers of $5.1\text{x}10^4$ and $4.25\text{x}10^4$ respectively. The measured inlet velocity and turbulence intensities were applied to the computational scheme as inlet conditions. Previous calculations, Assaf (1975) were obtained with a similar computation scheme and were in reasonable agreement with the measurements away from the recirculation zone. The difference between measurements and predictions was attributed to the deficiency of turbulence model and was consistant with the observations of Pope (1976).

The present comparisons shown in figure 4.2.25 show the measured axial velocity and the corresponding calculations at various axial locations downstream the disc, for the two discs. The size of the grid was also 30x30 similar to that used for figures 4.2.23 and 4.2.24 and grid lines were concentrated in the central region of the flow. The results shown in figure 4.2.25a for d/D of 0.25 and figure 4.2.25b for d/D of 0.5 were obtained with the exit

boundary conditions of zero axial gradient located at x/D of 30; The comparisons between measured and calculated mean velocity indicated qualitative agreement and had similar trends to the previous flow of Durao et al. The deficiency in the vicinity of the recirculation zone is attributed to the inadequacy of the two equation turbulence model to represent wake flows. The detailed investigation of Pope (1976) for wake flows reveals significant defects in the two-equation and Reynolds stress models which were confirmed by the predictions of many wake flows such as those of Durao et al (1974) and Assaf (1975). The calculated length of recirculation zone is 30% less than that measured and the spreading rate, is underpredicted by a factor of four. The application of Reynolds stress closures to near wake flows does not provide significant improvement over the two equation turbulence models; consequently, Pope concluded that the discrepancy is caused by the common factor in the different models; namely, the dissipation equation and suggested a closure based on the spectral energy equation.

4.3 Flow properties in present flow configurations.

The calculations presented in this section were obtained for the flow configuration of the experimental facility of section 3 under non reacting conditions with the inlet and boundary conditions listed in table 3.2. In obtaining these calculations, the measured inlet velocities and turbulence intensities were utilized to specify the initial conditions of the computational scheme. These calculations cover a wide range of flow conditions and comparisons with the corresponding measurements allow an assessment of the validity of the assumptions embodied in the equations solved for the aerodynamic properties, i.e. the turbulence model, and to appraise the present computational scheme for isothermal flow in the geometry investigated for combusting flow.

The implications of the present comparisons in non-reacting flows can be readily extended to include the various effects of combustion and density

variation. These results represent a base line against which the furnace flow predictions under reacting situations should be referred.

Grid independent tests were carried out for the present calculations of non reacting flows and a 20x20 grid was found adequate to yield results which do not depend on the grid size or arrangement in the sense that a 30% increase in the number of grid nodes would not yield significantly different results than those shown in this section. The grid line arrangement was non uniform and the grid line density was the largest in regions of steep gradients; near the centreline, the boundaries of mixing regions and near the enclosure walls.

Comparisons between measured and the corresponding calculated flow properties, carried out for the flow situations of table 3.2 were in reasonable agreement at low flow rate measurements, cases 1 and 2 and are shown in Appendix A6. Calculations were performed and compared with measured velocity profiles of the non swirling flow, case 4 of table 3.2. Measured inlet velocity and kinetic energy profiles were used as initial conditions for the calculation procedure. The exit conditions were located at x/D_f of 3 and were represented by zero axial gradient and satisfied the overall continuity. Measured and predicted mean axial velocity distributions along the centreline are shown in figure 4.3.1 and are in good agreement downstream of the jet exit. Radial profiles of mean axial velocity component $\bar{U}$ at different axial locations are shown in figure 4.3.2 for case 4 of table 3.2. Reasonable agreement was obtained except in the core region where discrepancies occurred and may be attributed to the centreline velocity recovery in the wake of the recirculation zone behind the blocked central jet.

Swirling flow computations were performed for the experimental configuration, case 5 of table 3.2 with the burner of figure 3.1.1a. The radial profiles of mean axial velocity for S = 0.52 are shown in figure 4.3.3 and are in good agreement with the measurements. Details of these computations are

given in Appendix A4. A general comment on the calculations is that the size of the central recirculation zone is smaller than the measured value, which relates to the use of the two equation turbulence model for wake flows. It was found that the calculations of swirling flows are sensitive to the specification of inlet conditions, which were not uniform across the flow at inlet as conveniently assumed in previous calculations. The rate of centreline velocity recovery is slower than the measured one and the maximum discrepancy was less than 25% in regions of steep velocity gradients.

Generally, a qualitative agreement was obtained for swirling flows, provided that the proper inlet conditions were specified or reasonably assumed. The normal axial stress profiles measured with laser anemometry were compared with the corresponding calculations and are shown in Appendix A4. The discrepancies in the normal stresses were observed to be as high as 20% and are attributed to the anisotropic nature of the swirling flow particularly in the mixing regions as shown in Appendix A2 . Provision of modifications to the isotropic viscosity hypothes is required and attempts were made by Lilley (1974) to correlate the directional viscosities and the local swirl number.

Flame stability in reacting flows is influenced by the swirl and the burner geometry as well as the air to fuel stream momentum ratio. The experiments, cases 6, 7 and 8 of table 3.2 were therefore obtained with the burner geometry of figure 3.1.1b with quarl angle of 20° and were compared with the corresponding calculations in figures 4.3.4 and 4.3.5. Two swirl numbers were investigated here; 0.3 and 0.52 with annulus air flow Reynolds number of 4.7×10^{4} and a blocked central jet placed at the burner throat. Inlet velocity profiles were measured at the burner exit for S = 0.3 and 0.52 respectively and were fed into the numerical computation scheme. Figure 4.3.4 shows radial profiles of mean axial velocity for S = 0.3, the solid lines represent the calculated profiles while the solid circles represent

the experiments. The agreement between measured and calculated velocities is reasonably good. The large recirculation zone on the centreline was created due to the effects of swirl and divergent quarl. The size of the central recirculation zone was under-predicted with the maximum discrepancy of 30% in steep velocity gradient zones. The underpredicted size of this recirculation zone can be attributed to the deficiency of the two-equation turbulence model in predicting wake flows and flows with strong anisotropy as in the present situation. This conclusion is consistant with the observations of Pope (1976) and Assaf (1975) for wake flows where the size of the predicted recirculation zone is 20% less than measured.

The profiles of mean axial velocity for a swirl number of 0.52 are shown in figure 4.3.5, where the solid lines represent the calculations and the solid circles represent the measurements of case 8 of table 3.2. The size of the central recirculation zone at the high swirl number is larger than that of figure 4.3.4 but the wall recirculation zone is smaller. The agreement between measured and calculated velocities, shown in figure 4.3.5, is reasonable although the size of the central recirculation zone is under predicted by 25%. The present flow situation, with quarl burner, requires specification of the inclined wall and the computation starts at the burner throat, with the provision of a modified wall function as explained at the end of section 2.3. Inlet velocity profiles were specified at the burner throat from measured profiles obtained at the exit of the straight burner. The grid used for the calculations presented in figures 4.3.4 and 4.3.5 had a 20x20 non uniform grid line arrangement and accounted for the burner's divergent angle.

The introduction of swirl in the annular air jet of the present flow configuration increases the spreading rate of the jet and reduces the length of the wall recirculation zone. This implies rapid mixing and a shorter, well stabilized flame, under firing conditions. The quarl burner geometry

used in cases 6, 7 and 8 of table 3.2 was found to result in a larger central recirculation zone which helped to stabilise the flame under reacting conditions. The mixing zone formed by the quarl downstream of the burner throat enhances the rate of mixing prior to the furnace and the incoming fresh reactants are heated by the recirculated products of combustion.

4.4 Discussion and implications of the present calculations

The previous sections showed that reasonable agreement exists between measurements and predictions in simple and swirling recirculating flows. Discrepancies in predicting the length of recirculation zones and spreading rates may be attributed to inaccurate measurements which may lead to erroneous boundary conditions and to deficiencies in the turbulence models.

An approach which would overcome the first problem is to increase the size of the solution domain so that known boundary conditions may be applied upstream of the burner exit. This approach is in principle, advantageous but may present difficulties in application, especially in complex geometries. The present calculations indicate that the uncertainties of the initial and boundary conditions are insufficient by themselves to explain the observed discrepancies between calculated and measured properties in flow configurations where flow reversal may occur. The effect of assuming the initial conditions was found to be significant in coaxial swirling flows. The measured inlet profiles of mean velocities and kinetic energy of turbulence, obtained with laser anemometry for the flows considered in section 4.3, overcame this uncertainty of the initial and boundary conditions. These measurements isolate the real reasons for any discrepancies between the measured and predicted properties.

Two particular defects which result from the turbulence models, are evident in the predictions of the recirculating and swirling flows. The length of the regions of recirculation is under-predicted as is the rate at which the wake decays. These defects were observed by Assaf (1975), Pope

(1976) and Truelove (1975) for flows with substantial recirculation zones; the results of section 4.2, related to recirculated flows, i.e. those of Owen (1975) and Beltagui et al (1974), illustrate the underprediction of the size of the recirculation zone and the spreading rate. For wake flows, the agreement with the measurements of Durao et al (1974) and Assaf (1975) shown in section 4.2, was unsatisfactory in the immediate vicinity of the disc and the predicted size of the recirculation zone was less than 70% of the measured size. However, qualitative agreement obtained at further downstream locations was better than those in the disc vicinity.

In confined coaxial swirling flows, an increase in the swirl intensity lowers progressively the centreline pressure, close to the exit of the swirler and consequently increases the adverse pressure gradient along the axis until it is too great to be sustained by the shear flow. The flow on the centreline reverses and the central recirculation zone appears. The size of the central recirculation zone depends strongly on the specified swirl number, and hence, improper specification of inlet swirl number can cause significant differences in the predicted length of recirculation as indicated by Khalil (1976). However, the discrepancies observed in predicting the length and the size of the central recirculation zone can not be blamed entirely on improper specifications of inlet profiles but are attributed to the anisotropic nature of the flow and to the use of eddy viscosity concept in strongly swirled flows and flows behind obstacles.

The above discussion illustrates the possible sources of discrepancy in the calculated flow properties akin to non reacting situations. These comparisons set a base line for the likely agreement in reacting flows, although the influence of density variation may dominate the flow and hence improved agreement can be obtained; in these reacting flows, additional problems of density fluctuations and wall heat transfer may arise. The next chapter is devoted to reacting flows in furnace type geometries.

4.5 Concluding Remarks

From the comparisons shown in this chapter, for non reacting recirculating flows, the following concluding remarks are appropriate:

1. The elliptic form of the continuity equation and equations for three components of momentum and the rate of turbulence dissipation have been solved numerically, together with equations for turbulence kinetic energy. The equations, expressed in finite difference form were solved simultaneously at each node in the orthogonal grid incorporated in the computation scheme.

2. The ability of the two equation turbulence model to represent the aerodynamic characteristic of turbulent recirculating flows was also assessed by various comparisons between relevant measurements reported in literature and the corresponding calculations. Reasonable agreement was obtained between measured and calculated mean velocity components and kinetic energy of turbulence in swirling pipe flows and coflowing flows with and without swirl.

3. The validity of turbulence model for flows over roughness ribs and in wall jets was assessed by comparisons which indicated that measured and calculated flow properties were in good agreement. In contrast to these flows, unsatisfactory agreement was obtained in wake flows which is consistant with previous calculations of Assaf (1975), Pope and Whitelaw (1976) and Pope (1976). For these wake flows with recirculation, known turbulence models result in underprediction of the length of recirculation region and the rate of spread of the downstream wake. The latter discrepancy is particularly serious and appears to stem from the modelling of the dissipation equation in recirculation regions behind discs.

4. The validity of the present computational procedure was extended to include furnace type geometries; comparisons were made with measured flow properties, in sudden enlargement non reacting jet

flows and, in the present flow configurations. The corresponding calculations reveal the ability of the solution procedure and the turbulence model to represent the flow properties of a coaxial jet in confined flow with various conditions of swirl, quarl and Reynolds number. The obtained agreement was reasonable for non swirling flows and as swirl intensity increased, the agreement deteriorated and maximum discrepancy in the vicinity of the recirculation zone boundaries was less than 25%.

CHAPTER 5

CALCULATED PROPERTIES IN TURBULENT REACTING FLOWS.

In this chapter,the calculated values of local flow properties in axisymmetric furnaces are compared with the corresponding measurements,to examine the accuracy and width of applicability of the calculation procedure. In the first section,5.1,the experimental data used in the assessment are obtained from the literature reviewed in chapter 1,while in section 5.2 the measured data of the present work are compared with the corresponding calculations.The collected data represent a wide variety of flow situations ranging from pure diffusion flames in coflowing air stream,to fully premixed flames.The corresponding density ratio between fuels and oxidant varied from 0.06 for hydrogen flames to 1.55 for propane flames.The calculations were performed with the two-equation turbulence model of section 2.3,with different combustion models of section 2.4 and the radiation and pollutant models of sections2.5 and 2.6.Generally,the calculations yielded the same qualitative trends as the measurements:the quantitative agreement is discussed for each flow situation in the various subsections of5.1 and 5.2.The implications of the modelling assumptions on the flow pattern, combustion efficiency and pollutant formation are discussed in section 5.3.

Calculations of furnace flames , where no experimental measurements are available,were predicted in various furnace flow configurations and are discussed in section 5.4.These calculations illustrate the extent to which useful information can be obtained and used to provide adequate representation of flame characteristics for engineering design purposes.The chapter ends with section 5.5 which summarises the main conclusions and implications of the present computational scheme as applied to reacting flows in furnace type geometries.

5.1 Comparison between calculated flame properties and the corresponding measurements of previous investigations.

The present section describes the comparisons between measured and calculated flow properties in a wide range of furnace flow configurations. These test cases were performed to assess the validity of the present computational scheme and,in particular the turbulence and combustion models. In each test case, flow configuration and flame type are indicated and the inlet and boundary conditions were specified as in tables 5.1 and 5.2. The collected data includes measurements of mean velocity components, mean gas temperature,mean species concentration,radiative wall heat flux and pollutant emission.

In the calculations described in this section,non uniform grid arrangements with 20x20 grid nodes were used.The optimum location of the grid nodes is a matter of experience but, as a result of considerable testing and special attention to the reaction zones,the present calculations are grid independent in the sense that the use of larger numbers of grid nodes, for example 25x25, did not result in values of the dependent variables which are significantly different from those presented in this section.

In the following subsections, the comparisons between measured and calculated flame properties and wall heat flux distributions are described in furnace geometries of cement kiln and boiler types.These comparisons are discussed in terms of flow pattern,gas temperature,reactants and pollutant distributions and wall heat flux.

5.1.1 The flow of Cernansky and Sawyer(1974).

The flow configuration of Cernansky and Sawyer(1974) consisted of coflowing streams of propane and air introduced to a cylindrical duct. The overall dimensions of the furnace are given in table 1.2.The flow configuration is similar to that of figure 1.3,but with swirl vanes in

Table 5.1

Furnace	Reference	Flame Type	Geometry	Dependent Variables
Berkeley	Cernansky et al (1974)	swirling propane diffusion flame	Cement kiln with swirl 0.31 in air stream	$U,V,W,P,k,\varepsilon,\bar{f},\bar{M}_{fu},\overline{m_{fu}m_{ox}},\overline{m_{fu}^2},\bar{M}_{NO},\overline{m_{N_2}m_{ox}},\overline{T'^2},\overline{\rho u},\overline{\rho v}$ (Model 7)
Delft	Wu et al (1971)	swirling natural gas diffusion flame	boiler type with swirl 0.0 and 0.84	$U,V,W,P,k,\varepsilon,\bar{f},\overline{f'^2},R_x,R_y$ (Model 3)
Glasgow	Beltagui et al (1974,1975)	swirling town gas/ air premixed flame	boiler type with swirl 0.,0.239	$U,V,P,k,\varepsilon,\bar{M}_{fu},\overline{m_{fu}'^2},\overline{m_{fu}m_{ox}},\overline{T'^2}$ (Model 4)
Karlsruhe	Gunther et al (1972) Lenze et al (1974)	Natural & town gas jet diffusion flames	cement kiln without swirl	$U,V,P,k,\varepsilon,\bar{f},\overline{f'^2},\bar{M}_{CO},\overline{T'^2}$ (Model 3)
New Brunswick	Steward et al (1972)	partially pre-mixed propane flame	cement kiln without swirl	$U,V,P,k,\varepsilon,\bar{f},\bar{M}_{fu},R_x,R_y,\overline{m_{fu}m_{ox}},\overline{T'^2}$ (Model 4)
Sydney	Bilger et al (1972,1974)	hydrogen jet diffusion flame	cement kiln without swirl	$U,V,P,k,\varepsilon,\bar{f},\overline{f'^2},\bar{M}_{NO},\overline{m_{N_2}m_{ox}},\overline{T'^2},\overline{\rho'u},\overline{\rho'v}$ (Model 3)
U.T.R.C.	Bowman et al (1975)	Natural gas diffusion flame	boiler type without swirl	$U,V,P,k,\varepsilon,\bar{f},\bar{M}_{fu},\overline{m_{fu}m_{ox}},\overline{m_{N_2}m_{ox}},\bar{M}_{NO},\overline{m_{fu}^2},\overline{T'^2},\overline{\rho u},\overline{\rho v}$ (Model 7)
Delft Conical	Paauw (1974)	Natural gas diffusion flame	boiler type without swirl	$U,V,P,k,\varepsilon,\bar{f},\bar{M}_{fu},\overline{m_{fu}m_{ox}},\overline{m_{fu}^2},\overline{T'^2},\overline{\rho'u},\overline{\rho'v}$ (Model 7)

Table 5.2

Variable	Inlet Profile	Remarks
$\bar{U}$	$U_o \left[1 - \frac{2r}{d}\right]^n$	$0.2 \geqslant n \geqslant o$
$\bar{V}$	$U_o \left[1 - \frac{2r}{d}\right].C$	$0.05 \geqslant C \geqslant -0.05$
$\bar{W}$	$\lambda .r$	λ varies as function of S
k	$\beta \left[\delta \left(\frac{2r}{d}\right)^2 + 1\right]$	$\beta = 1.5 (i_o)^2$, $i_o = \left(\frac{\sqrt{\overline{u^2}}}{\bar{U}}\right)_{inlet}$ $2 \geqslant \delta \geqslant 0$
ϵ	$k^{3/2} / (\lambda_o y_a)$	$5 \times 10^{-4} \geqslant \lambda_o \geqslant 10^{-3}$
$\bar{T}$	$T_o \left(1 \pm \frac{2r}{d}\right)^n$	$0.1414 \geqslant n \geqslant o$ The sign depends on the wall: fluid temperature ratio

the annular air stream,which imparted tangential momentum to the air and the corresponding swirl number at inlet was 0.31.The swirl was used to enhance the stability of the flame but was maintained at a sufficiently low level to avoid recirculation.Fuel and air flows were chosen such that the flame was maintained within the combustion tunnel over the full range of operating conditions.The air to fuel mass flow rate ratio was 1000 and the corresponding central/annulus velocity ratio was 45 with an initial temperature of 300K in the reactant streams.

Measurements of aerodynamic properties were not reported,but radial and axial traverses of the flame were made to measure T and NO,using probes inserted through the downstream end of the combustion tunnel.Temperature traverses were made with a Pt/Pt-13%Rh fine wire thermocouple(120μm diameter bead) coated with a non catalytic coating and were corrected for radiation losses.Gas samples were removed from the flame using a water cooled stainless steel probe and nitric oxide was measured with a chemiluminescence technique.

The assumptions of table 5.2 were made in respect of initial profiles of mean velocity components,turbulent kinetic energy and its dissipation rate as those inlet conditions were not specified by Cernansky et al(1974). Uncertainty bands were imposed on the inlet profile assumptions of the dependent variables shown in table 5.2.When the two extremes of the uncertainty band were used as inlet profiles for the calculations, the results were different in the burner vicinity by less than 3% and diminished at further downstream location of x/D_f =0.1.

Figure 5.1.1 shows centreline distributions of mean temperature,oxygen and fuel concentrations.The calculated flame properties were obtained with the aid of model 7 which was selected on the grounds of preliminary calculations which indicated that the local values of N_D were of the order unity.Models 1,2 and 3 are only applicable when $N_D >> 1.0$,i.e diffusion controlled,while models 4 and 5 are appropriate for very small values of N_D ; i.e kinetically influenced reactions.In this case, pollutant formation details were required

and model 7 was used rather than model 6 as recommended in chapter 2 for NO calculations.A significant point illustrated by the experimental measurements shown in figure 5.1.1 is the overlapping of the propane and oxygen profiles, which is indicative of the strong mixing processes that are occuring.Since these are time average profiles, they merely indicate the average state of fuel rich and fuel lean conditions varying with time.The calculations were in reasonable agreement with the measurements;in particular,the mean temperature distribution indicated discrepancy of less than 130K at 1000K in predicting the location of peak temperature.Fuel and oxygen calculated distributions consistantly indicated the overlapping region along the centreline and are in agreement with the measurements.

Predicted concentrations of pollutant NO were obtained from the relevant conservation equations embodied in the pollution model of section 2.6 and are compared with measurements in figure 5.1.2.The effects of turbulent fluctuations on the formation of pollutant NO were included in the calculation procedure and were found to influence the results significantly,i.e ignoring the effects of turbulent fluctuations resulted in 50% underprediction of NO concentrations.The maximum discrepancy observed was less than 20% and this is reasonable when compared to previous attempts to predict NO concentrations as reported by,for example, Carreto(1975) in similar complex flows. Along the centreline NO concentrations increased downstream from the injector tip reached a maximum in the hot region near the flame tip and then decreased as mixing caused dilution and cooling.The calculated values are lower than measurements even though the effects of temperature fluctuations and superequilibrium have been considered through the use of equations 2.6.6 and 2.6.7.There is,however, insufficient evidence to suggest that the magnitude of superequilibrium is too small or that prompt NO has formed as a result of HCN reactions.

5.1.2 The flow of Wu and Fricker (1971).

The measurements of Wu and Fricker (1971) were obtained in an axisymmetric water cooled furnace with various inlet conditions.The air nozzle had a divergent quarl angle of 35^{o} and the swirl numbers in the air stream were zero and 0.84.The overall dimensions of the furnace are given in table 1.2 in chapter 1.The local gas velocities were obtained with a five hole hemispherical impact tube.The mean gas temperatures were obtained by a suction pyrometer while the total wall heat flux was obtained by a'SHELL'total heat flux meter,described by Braud et al(1972).

The fuel(natural gas) was supplied at a rate of 100 kg/hr through the central jet and corresponded to 1.07 Mw thermal input,while the air flow rate through the divergent quarl throat was 1320kg/hr.The inlet velocity profiles and turbulence characteristics were not measured and thus were specified according to the recommendations of table 5.2.The uncertainty band imposed on the assumed inlet axial velocity,kinetic energy and dissipation rate profiles had insignificant influence on mean axial velocities in the burner vicinity,while the corresponding influence on the mean gas temperature along the centreline was less than 3% and diminished at axial distances less than $0.15D_f$ from the burner exit.

The calculated and measured temperature profiles are shown in figure 5.1.3 at two locations downstream from the burner exit and for swirl numbers of 0.0and 0.84.The symbols of figure 5.1.3 denote the measurements and the solid lines represent the calculated temperature profiles obtained when the assumptions of fast chemical reaction and a clipped Gaussian probability distribution of mixture fraction (model3) were incorporated in the calculation procedure.The choice of this model was based on calculated values of τ_s which were two order of magnitude greater than τ_k in the flame region.The measurements and predictions are in good agreement at various radial locations throughout the flame for both swirl numbers.The relatively higher flame temperature at x/D_f of 0.77 at S=0.0 was caused by the upstream transport

of enthalpy from downstream by the recirculated flow.At the swirl number of0.84 , the reaction zone was remarkably shortened but much more spread out radially which is in agreement with the early reattachment of the corner recirculation with the higher swirl number.

The centreline temperature distributions are shown is figure 5.1.4 for the two swirl numbers,for S=0.84, the maximum temperature occurs in the first furnace diameter downstream the burner exit;for the non-swirling case, the centreline temperature attains a peak at x/D_f of 1.3.The experimental results of wall heat flux indicated that 33% of the wall heat transfer was due to convection for the non-swirling case and increased to 36% for S=0.84. Preliminary calculations of the wall heat flux were carried out with the aid of model R-I which resulted in 50% underprediction of the radiative heat flux to the wall because this model did not couple the radiative fluxes R_x and R_y. Due to the high percentage contribution of radiation to the wall, it was necessary to use model R-II which coupled the radiative fluxes as reviewed in chapter 2.

The calculated wall heat flux distributions for S=0.0 and 0.84 are compared with the corresponding measurements and shown in figure 5.1.5.The experimental results,which were obtained from the water cooled sections, are represented by the histogram and the agreement between the measurements and calculations is fair for both swirl numbers.The total wall heat flux distribution for S=0.0 has a peak value at 1.4 furnace diameter which is consistant with the location of the reattachment point,giving very high heat transfer coefficient at the stagnation point.At the swirl number of S=0.84,the location of the peak wall heat flux moves upstream towards the burner end and attains larger value than the corresponding non-swirling peak.The wall heat flux decreases rapidly downstream of the peak and the average wall heat flux was larger in the swirling flame than without swirl as can be expected from the exit gas temperature, for the same thermal load input.

5.1.3 The flow of Beltagui and Maccallum(1974,1975).

Further comparisons were carried out with the experimental results of Beltagui and Maccallum(1974,1975),from the the two axisymmetric furnaces described in section 4.2.4.A mixture of air and town gas was supplied through a central jet to the furnace with air to fuel volumetric ratio of 8.In the present comparisons,swirl numbers of 0.0and 0.239 were obtained from vane swirlers placed at the jet exit.Mean velocities were generally obtained with a water cooled three hole probe while a disc probe was used where the velocities were principally in the radial direction.Mean gas temperatures were obtained with Pt-5%Rh-Pt-20%Rh thermocouples and were corrected for various sources of error.

Detailed measurements were reported and comprised the three velocity components,pressure coefficient and gas temperatures.A careful examination to the accuracy and reliability of the data is necessary before displaying any comparisons between the measured and calculated properties.The precision of the mean velocity measurements,obtained in the wall and central recirculation zones was difficult to quantify but is likely to deteriorate as the magnitude of the velocities decreased because of the interference caused by the probe tip(6.35 mm in diameter) and the response of the probe to very small velocity changes.In regions where steep velocity gradient, and consequently high turbulence intensity,exist,near the reaction zone, measuring errors in the tangential velocity component can be expected due to the indicated high pressure difference across the probe.When the radial velocity component is considered,readings were liable to be in error in regions where the flow has a high radial component and a low axial component,Beltagui(1974). For reacting flows, the wall temperature distributions were reported,Maccallum(1975); the end walls were at 600C while the maximum wall temperature,at the impingement point was 780C.No inlet conditions were measured,and these were assumed

according to table 5.2;if the two extremes of the uncertainity band imposed on the assumptions were used for the calculations,the results would be different by less than5% and this difference diminished rapidly for x/D_f greater than 0.1.

The calculated flow properties in this furnace were obtained with the aid of model 4.This model assumes finite reaction rate and is appropriate to premixed flame situations,where the time scale of chemical kinetics τ_k is much larger than τ_s ,the mixing time scale; hence N_D is much less than 1 and the reaction is kinetically influenced as reviewed in section 2.4.The mean axial velocity profiles at various axial locations downstream of the burner are shown in figure 5.1.6 for zero swirl number.These profiles are normalised by U_b , the inlet mixture velocity(U_o=15.2 m/s).The dashed and solid lines in the figure denote the measured and calculated profiles respectively and indicate quantitative agreement with discrepancy in the vicinity of the recirculation zone.This discrepancy decreased towards the forward flow regions, and away from the burner exit.Radial profiles of mean gas temperature in the furnace at S=0.0 are shown in figure 5.1.7:the agreement is generally good and the maximum discrepancies are of the order of 15% of the adiabatic temperature rise ΔT_a, ($\Delta T_a = T_a - T$,where T_a is the adiabatic flame temperature).The calculated temperature profiles exhibited peak values at the centreline of the flame and decrease away from the flame reaction zone towards the furnace walls.

In figure 5.1.8,the mean axial velocity profiles at a swirl number of 0.239 are shown at various axial locations downstream the burner.The obtained agreement is reasonable as the calculated velocity profiles correctly predicted the jet's rate of spread and the decay of the centreline mean axial velocity. The length of the wall recirculation zone is nearly $1.4D_f$ which may be compared to a length of $2D_f$ for the non-swirling flame of figure5.1.6:no central recirculation zone was observed for that flame.

Measured and calculated tangential velocity profiles are compared in

figure 5.1.9 and exhibited reasonable agreement except in the vicinity of the burner exit.The calculated decay of the maximum tangential velocity along the furnace is faster than the measured ,which causes a more uniform distribution of W than that measured at the same axial location.Qualitative agreement between the measured and calculated pressure coefficient was obtained in the furnace at various axial locations downstream the burner exit as shown in figure 5.1.10.Pressures in this flow are generally subatmospheric,increasing to nearly atmospheric at the furnace walls.Comparison between the pressure field in figure 5.1.10 for reacting flow and that in figure 4.2.15 for non-reacting flow under the same inlet Reynolds number,reveal that combustion always brings the static pressure closer to atmospheric and , in contrast, the effect of swirl is to lower the centreline pressure in the vicinity of the swirl vanes. Radial profiles of measured and calculated temperature are compared at various locations as shown in figure 5.1.11 and indicate maximum discrepancies of less than 10% of the local temperature in the vicinity of the burner and furnace walls.The temperature profiles for a finite swirl number exhibit more uniform distribution than the corresponding non-swirling profile at the same axial location;this can be readily attributed to the effect of swirl which shortens the flame.

5.1.4 The flow in Karlsruhe furnace.

Turbulent diffusion flames in confined cylindrical furnaces were reported by Gunther et al (1972) for town gas flames and Lenze et al (1974,1975) for natural and town gas flames under various inlet and boundary conditions.The furnace was mounted vertically and was water cooled in ten sections.The overall dimensions of the furnace,given in table 1.2, were common for the two sets of measurements discussed here.The central fuel nozzle supplied town gas at a rate of 23.2 m^3/hr and the coflowing air was supplied through the remaining annular area at a uniform velocity corresponding to a flow rate of 108 m^3/hr.The nozzle diameter was 10mm.

The furnace geometry resembles a cement kiln,where the primary jet entrains

the low momentum secondary flow and recirculation occurs if the mass flow rate of the secondary fluid(annular) is insufficient to meet the entrainment of the jet to the point of impingement with the chamber walls.According to the theory of Thring and Newby(1953), the extent and location of the recirculation zone may be characterised by the parameter C_t(Craya Curtet number) and a backflow parameter,θ,which depends on the jet to chamber diameter ratio and the primary to secondary mass flow rates and density ratio. In the present furnace configuration,significant wall recirculation was observed at x/D_f of 2 and extended further downstream.

No velocity measurements were reported in the furnace.Gas sampling techniques and thermocouples were used to measure the mean species concentrations and temperature profiles respectively.Inlet profiles of mean flow properties were not provided and reasonable assumptions were made according to table 5.2.When the two extremes of the uncertainity associated with these assumptions were used in the calculations,the maximum difference between the results,which was localized in the burner vicinity ,was less than 3%; this difference diminished further downstream.

Mean gas temperatures along the centreline of the town gas flame of Gunther et al (1972) are shown in figure 5.1.12 and correspond to a jet Reynolds number of 3.2×10^4. The calculations were obtained with the aid of model 3 and are shown in figure 5.1.12 with the measured temperature which is represented by the solid symbols .The predicted centreline distribution is in good agreement with the measurements and the maximum discrepancy is less than 12%.This remarkable agreement may be attributed to the ability of model 3 to represent the present flame characteristics.The calculated time scale of turbulence,$\tau_s$was larger than that of chemical reaction τ_K and the assumption of infinitly fast reaction was justified on the basis of the local values of N_D which were in excess of 100 in the reaction region.This agreement is readily complemented by the radial profiles of mean gas temperature shown in figure 5.1.13 at two axial locations.The predicted rate of flame

spread was faster than that obtained from the measurements,due to the basic assumption embodied in model 3; i.e.fast chemical reaction.

Further investigations in the same furnace were carried out by Lenze et al (1974,1975) for various burner arrangements.Two arrangements,one consisting of three burners set in a row, and the other of five burners in a cross, were investigated; all the burners had a diameter of 5 mm.The two arrangements were then replaced by burners of diameters equal to $5\sqrt{n}$ mm, where n is the number of the burners in the arrangement and measurements for these equivalent burners were carried out.The burner diameters equivalent to three and five burner arrangements were 8.65mm and 11.2mm respectively. The calculations were performed with the equivalent single burner and with town gas and natural gas as the fuels for the 8.65mm and 11.2mm burners respectively.Velocity ,temperature and turbulence characteristics were not measured in the inlet plane and were,therefore, assumed in accordance with table 5.2.

Measured and calculated concentrations of CH_4 and CO ,along the flame centreline , are shown in figure 5.1.14.The calculations were obtained with the aid of model 5 and with the procedure of Gordon et al (1971) which accounted for the intermediate reaction steps and made comparison of intermediate radicals such as CO, possible. The agreement is reasonable and demonstrates the ability of model 5 to provide local concentrations of the reaction intermediates. Model 3 could have been used to determine energy properties, but the concentrations of the intermediates would not have been determined. In addition, the calculation of CO concentration resulted in a finite overall heat of reaction which caused local temperatures greater by up to 40C than those obtained from model 3 , which considers a global reaction of the hydrocarbon fuel to CO_2 and H_2O in a single step.The reaction mechanisms for hydrocarbon fuels are very complicated and consist of many intermediate revesible step reachions and a model which solves these intermediate steps is required to estimate the concentrations of these intermediates.The assumption of

single step mechanism, would ,however result in lower temperature than when multistep reaction is considered.The determination of the local radical concentrations was obtained in the present flow configuration by the aid of model 5 and the mechanism shown in figure 2.4.5. A second procedure to calculate the local equilibrium concentrations of any hydrocarbon oxidation, Gordon et al (1971) was also used in the present flame and the corresponding results are compared with the measurements in figure 5.1.14.This procedure requires excessively large coputer storage and provides the local equilibrium concentration on the basis of local pressure,temperature,air to fuel ratio and fuel composition.

5.1.5 The flow of Steward et al(1972)

The flow of Steward et al was different from those mentioned before,as the fuel(propane) was partially premixed with air and was injected through the nozzle in a coflowing , uniformly-distributed air flow.The flow rates were adjusted to allow 20% excess air and the Craya Curtet number,C_t ,was 0.18 , corresponding to large recirculation zones covering 0.6 of the furnace wall length.The furnace was oil cooled and was equiped to measure wall radiative and convective heat fluxes.

The mean velocities were measured with a water cooled pitot tube with its tip constructed of hypodermic tubing of 1.75 mm outer diameter.Gas mean temperatures were measured using bare thermocouple wires of Pt/Pt-10%Rh and were corrected for radiation losses.The gas samples were obtained by means of a water cooled gas sampling probe and analysed to quantify the concentrations of carbon dioxide,carbon monoxide,propane,propoylene,methane, oxygen and nitrogen species.The radiative and total heat fluxes along the furnace wall were measured by a wide angle radiometer.Inlet profiles were not measured and,therefore, were assumed according to table 5.2.The uncertainity band of these assumptions did not influence the calculated results of mean velocities and temperatures by more than 3.5% and this influence

diminished at distances greater than 0.17 D_f downstream the burner exit. The corresponding effect on the wall heat flux was less than 2.2%.

Model 4 ,which assumes finite reaction rate was used to obtain the local flame properties in this partially premixed flame as the assumption of infinite reaction rate(models 1 to 3) is not valid on the grounds that local values of N_D were very small, i.e.<<1.0. A comparison between results obtained with models 3 and 4 is presented and discussed in section 5.3.The mean velocity profiles at two axial locations downstream the jet exit are shown in figure 5.1.15.Generally , the measured and calculated velocities are in reasonable agreement in the central region although discrepancies exist at $2r/D_f$ of 0.16.These discrepancies may be attributed partly to the small magnitude of the velocities at the outer edge of the flame and partly to the slightly overpredicted rate of spread of the jet. Unfortunately, no measurements were obtained in the recirculation zone. The mean temperature distribution along the furnace centreline is shown in figure 5.1.16;the solid line represents the calculated temperature distribution which is in good agreement with the experimental data represented by the solid circles.The location of the peak centreline temperature,indicating the flame length,is predicted slightly upstream the measured location.The maximum deviation in the centreline temperature was 165K at T =1650K and corresponds to a 10% difference.

Radial profiles of mean temperature are shown in figures 5.1.18 a,b and c at various axial locations downstream the burner.The profiles at x/D_f of 0.238 and 0.588 are shown in figure 5.1.18a, at x/D_f=0.238, i.e near the flame base;the central core temperature is low and the peak temperature corresponds to the reaction zone.AT x/D_f =0.588, the flame spreads radially and the peak temperature moves away from the centreline towards the furnace walls.It is clear from the two temperature profiles that the model predicts the location of peak temperature with a maximum deviation of $0.05D_f$ while the rate of spread of the flame is slightly overpredicted.

Similar observations were found at further downstream locations as shown in figure 5.1.18b, where general agreement is apparent except at the outer edges of the flame.The centreline temperature increases to nearly 1850K at the flame tip,which corresponds to x/D_f of 1.64, and gradually decreases away from the reaction zone.The radial temperature gradients decay and the temperature profiles even out to nearly flat profiles.Figure 5.1.18c shows comparison between measured and calculated temperature profiles at x/D_f of 2.65 which is near to the furnace exit; $(L_f = 2.85D_f)$.

The increase of the local gas temperature towards the furnace wall is due to the recirculating hot gases and the growth of the flame as seen from figures 5.1.18a,b and c.The radiative wall heat flux distributions, figure 5.1.17, are in reasonable agreement and provide justifications for the use of model R-II.The ratio of convective to total heat flux to the furnace walls depends on the ratio L_f/D_f, type of fuel and on the furnace loading,i.e full load, half load,...etc.In the present furnace the convective heat flux to the wall was reported to be approximately 30% of the total wall heat flux and the wall heat flux distributions calculated with model R-I resulted in 40% underprediction of the radiative heat flux.This observation supported the conclusion that model R-I is not suitable for flows where radiation contribtes to more than 70% of the total wall heat flux as this would lead to at least 28% underpredicted wall heat flux, hence model R-II is preferable.This underprediction decreases as the proportion of radiative to convective flux decreases.

Calculated wall heat flux distributions were also obtained by Steward et al(1972),by dividing the furnace space into finite elements and using the Mont Carlo method to simulate radiative transfer among the elements using measured temperature distributions.These calculations were based on the assumed flow pattern obtained from similarity criterion,Craya et al(1953), and did not include the effects of turbulent fluctuations and diffusion.

The zone method which incorporates the transfer equation in the integro-differential form can not be easily used with the numerical procedure of section 2.2 as discussed in section 2.5.

5.1.6 The flow of Bilger et al(1972,1974).

Detailed profiles of velocity,temperature and species concentration were reported by Bilger et al (1972,1974) for a variety of jet diffusion flames in large confinement.The experimental test rig comprised a duct of square section of 300x300mm and length of 1800 mm.Hydrogen fuel was injected into a coflowing air stream through a central fuel nozzle of 7.65 mm diameter located at one end of the duct, and the hot products of combustion escaped through the other end.

The axial velocity was measured by means of a pitot probe along the centreline and at the inlet section to the furnace.To determine the chemical composition of the flame,gas samples were removed through a 3.2mm diameter probe and analysed for hydrogen,oxygen and water vapour with a katharometer, an oxygen analyser and lithium chloride cell respectively.Concentrations of nitric oxide,NO, were obtained with a chemiluminescence analyser.The local gas temperatures were obtained with 120μm thermocouples of Pt-5%Rh,Pt-20%Rh with non catalytic coating to avoid catalytic effects.The measured temperatures were corrected for radiation and conduction effects.No wall heat flux measurements were reported since the flame was narrow; the assumption of adiabatic walls was made in the calculations.

In the present comparisons,which relate to hydrogen jet diffusion flames, the fuel to air inlet velocity ratio was 10 and the corresponding mass flow ratiowas less than 0.01.The profiles of inlet turbulent kinetic energy and its dissipation rate at inlet were not measured and were assumed here according to table 5.2,these assumptions had insignificant influence on the comparisons shown later in the subsection.An equivalent furnace diameter was used to replace the square cross section,and the mass flow rate of the air

was the same.This diameter corresponds to nearly forty fuel nozzle diameter, and did not influence the calculated flame properties as the flame was narrow and the influence of the reaction was restricted to radial locations of $2r/D_j$ less than 24.

The present comparisons were obtained with the aid of model 3, which is appropriate to diffusion flames where the time scale of turbulence τ_s is much greater than the chemical kinetic time scale τ_k ,i.e $N_D>>1.0$.Previous theoretical investigations,Bilger (1975b) indicated that,for the particular flame measurements used in the present comparisons,the assumptions of fast chemical reactions were justified on the ground of high local values of N_D. The calculated centreline distribution of mean velocity is shown in figure 5.1.19 together with the available experimental data.Measured and calculated velocities are in good agreement and a maximum discrepancy of less than 10% occured in the burner vicinity.

The calculated hydrogen,oxygen and temperature profiles are shown in figure 5.1.20 and 5.1.21 at various distances downstream of the burner exit; the available experimental data are indicated on the same figures.At an axial location corresponding to x/D_j of 40, figure 5.1.20 shows good agreement between the measurements and calculations.At this location,finite concentrations of oxygen and fuel coexisted in the reaction zone extending between $2r/D_j$ of 4 and 9.The radial temperature profile exhibits a peak which is located in the reaction zone.Radial profiles of mean concentrations of hydrogen and oxygen and local temperature ,obtained at x/D_j of 80 are shown in figure 5.1.21 and exhibit similar trends to those of figure 5.1.20.Both fuel and oxygen concentrations are finite between $2r/D_j$ of 0.5 and 13.The temperature profile at this location exhibits a maximum temperature in the reaction zone at $2r/D_j$ of 7 .Radial profiles of measured mean gas temperature at x/D_j of 120 and 160 are shown and compared in figures 5.1.22 and 5.1.23 with the corresponding calculations.The calculated temperature profiles are in good agreement with the measured temperatures and correctly predicted the flame spread.

Radial profiles of measured and calculated NO concentrations are shown in figure 5.1.21 and exhibit a peak value of NO in the regions of maximum temperature.The predicted distribution of NO at x/D_j of 80,was shown earlier in figure 2.4.11 and depends on the way the density-velocity and density-scalar correlations are included in the pollutant formation model.The present comparisons were obtained with the aid of equation 2.6.6 and considered the influence of the density correlations.The centreline distributions of hydrogen, NO and temperature are shown in figure 5.1.24 and are in reasonable agreement with the corresponding measurements.The quality of the agreement for the results is aided by the boundary layer nature of the diffusion flame.

5.1.7 The flow of Bowman et al (1975)

An axisymmetric sudden expansion furnace with a central fuel injection and annular air was used by Bowman et al (1975) to simulate furnace flows.The furnace diameter was 122mm and its length was 1220mm;the coaxial burner arrangement comprised a central jet of 63mm and an annulus of inner diameter of 63.7mm and outer diameter 93.7mm.The air flow rate through the annulus was adjusted to give air to methane velocity ratio of 22 and to allow for 10% excess air.The furnace walls were water cooled and thermally lagged to prevent heat loss to the atmosphere.

The axial velocity was measured with pitot probes at various locations in the flame.Values of mean gas temperature were obtained from a double sonic orifice probe;the first orifice was choked and stagnation pressure and temperature downstream of the orifice were measured;stagnation pressure at the first orifice was also recorded.From this measured information and previous calibration,the local gas temperature was obtained.This method of temperature measurements is limited to flows containing insignificant concentrations of particulates(soot,liquid droplets) and requires calibration at various Reynolds numbers.Local concentrations of species and products of combustion were measured with standard sampling and gas analysis equipments.

The inlet profiles of mean velocity components,turbulent kinetic energy and its dissipation rate were not measured and were assumed here according to table 5.2.Inthe extreme case , when the uncertainity limits were used in the calculation as inlet conditions,the predicted mean velocity, temperature and wall heat flux were different by less than 4% in the vicinity of the burner exit and this difference diminished at further downstream distances.As discussed earlier in section 2.4,the assumptions of model 3 and 4 are appropriate only when , the ratio τ_s/τ_k i.e N_D attains very large and small values respectively.However, in the present flame configuration, the time scale of turbulence τ_s and that of chemical kinetics τ_k were of the same order of magnitude in the reaction zone and suggested the use of model 7.

Calculated mean axial velocity profiles are shown in figure 5.1.25 together with the corresponding measurements. A recirculation zone exists in the initial region of the coaxial streams as, the annular stream,i.e the air stream, moves rapidly relative to the central fuel jet; this recirculation zone enhances mixing the reactants and was utilized to stabilize the flame. At x/D_f of 0.157, the calculated velocity was in good agreement with the measurements except in the vicinity of the centreline where, the velocity was underpredicted and is consistant with the previous turbulent model deffi-ciencies,Pope(1976), in the predictions of wake flows with two-equation turbulence model.Better agreement is obtained away from the wake of the central recirculation zone as shown in figure 5.1.25.

Calculated profiles of mean gas temperature and the corresponding meas-urements are shown in figure 5.1.26 at various axial locations.In the vicinity of the burner,the mean temperature is low (in the order of 850K) and the calculations indicate a peak temperature which coincides with the reaction zone.Comparisons of mean gas temperature at downstream locations indicate an underprediction of the rate of flame spread which is also observed in the velocity field.The mean gas temperature profiles flatten at further downstream locations and the measurements suggest that only a small portion of the total

available chemical heat release occurs beyond the initial stirred region of $2.5D_f$ and that such heat production is approximately matched by the heat loss to the combustor walls.The predicted gas temperatures at x/D_f of 5.35 and 8.14 exhibit peak values,corresponding to the reaction zone,which move away from the centreline.

By virtue of the rapid momentum transport,relatively high oxygen concentrations are present throughout the fuel stream as shown in figure 5.1.27; the measured and calculated oxygen mole fractions are in reasonable agreement as can be seen from the figure.The oxygen concentration ,at the first measuring location of x/D_f of 0.157,decreases rapidly from the annulus and achieves a constant value in the central core of the flame.The rate of flame spread is underpredicted as shown by the overpredicted oxygen concentrations at the flame edge.At further downstream locations, at x/D_f of 5.35 and 8.14, the agreement is better except in the vicinity of the furnace walls.The overprediction of oxygen concentrations at the outer edge of the flame is consistant with the prediction of a longer flame as discussed earlier.

Radial profiles of mean nitric oxide concentrations are shown at various axial locations in figure 5.1.28:the calculated values were obtained with the aid of the pollutant model described by equation 2.6.6.At the axial location nearest to the injection plane,the NO concentrations are very small as expected from the corresponding temperature profile.Significant levels of NO are achieved within $2.5D_f$ downstream of the injector exit and continue to form at approximately steady rate; the centreline value of NO increases at about 1.36 ppm/cm.The agreement shown by figure 5.1.28 is reasonable for the present calculation in view of the strong temperature dependency of the production of NO.

The agreement shown in figure 5.1.28 was achieved by including the effects of temperature,density , species fluctuations and their correlations.A simple calulation, which did not include the density correlations resulted in very poor agreement and, for example,at x/D_f of 2.56,did predict NO concentrations

to be 25% of the measured values at this location.At the furnace exit section, the measured and predicted NO concentrations, using equation 2.6.6, were in very good agreement;the measured concentration was 156ppm and the calculated value was 150ppm.

The furnace of Bowman et al ,which resembles the main features of the fire tube boiler,is similar to that of the present experimental investigation of chapter 3,but the expansion ratio ,(1:1.3), was smaller than those appropriate for real furnaces,typically 1:5.The resulting flame length was larger than $10D_f$ and the measured overall heat flux to the furnace wall contibuted to nearly 16% of the total heat input and the exhaust gases escape from the furnace exit with very high enthalpy.This is in contrast to the Delft furnace discussed in 5.1.2 where 60% of the heat input is transferred through the walls.

5.1.8 The flow of Paauw(1974)

In many furnace flows, the burner is made of a divergent quarl air nozzle with a central fuel jet;this arrangement can result in improved mixing in the combustion chamber.The flow in a conical furnace was investigated by Paauw; his experimental test rig comprised a conical chamber of 1.4m length and the smallest diameter at entrance was 300mm.The total conical angle was 22°.Methane was supplied centrally through a fuel pipe of 44mm inner diameter and 89mm outer diameter.Air flowed through the remaining part of the upstream surface. The furnace lining was fireproof cement and measurements were made through four holes in the wall at downstream distances of 0.2,0.4,0.6 and 0.8 m.

To obtain uniform velocity at the upstream end of the furnace,settling chambers were used.The flow rate of the fuel,which contained 76% CH_4 ,was $100m^3/hr$; the air flow rate was 5% more than the stoichiometric requirement. The mean inlet air and gas velocities were 5m/s and 28m/s respectively.Measurements of local velocities were obtained with the aid of a five hole pitot probe and Becker gas chromatograph was used to obtain the local gas concentr-

ations,while a suction pyrometer was used to obtain the local mean gas temperature and was shielded to prevent heat losses by radiation.The measured wall temperature was below 700K and the measured heat flux, obtained by a"SHELL" heat flux radiation pyrometer indicated that the radiation heat transfer contributed less than 5%of the total heat release from the fuel.

The inlet velocity and turbulence characteristics profiles were not measured and ,therefore, were assumed according to table 5.2.These assumptions had an insignificant influence on the calculated mean velocities,concentrations and local gas temperatures.The measured radial profiles of axial velocity at various locations are shown in figure 5.1.29 and are compared with the corresponding calculations obtained with the aid of model 7 . This model was selected on the ground that the local values of N_D were of the order of unity and the assumptions of models 3 and 4 are not appropriate.The agreement shown in figure 5.1.29 is reasonable and is helped by the boundary-layer nature of the flow. The calculated rate of centreline velocity decay was slightly smaller than the measured rate and resulted in 15% discrepancy in the centreline region at downstream location 0.8m from the burner exit.

The measured and calculated temperature profiles at various axial locations are shown in figure 5.1.30 and are generally in reasonable agreement;the mean temperatures were low and supported the use of model 7 which accounted for finite reaction rate.The corresponding measurements and calculations of local oxygen concentrations are shown in figure 5.1.31,these oxygen concentrations are underpredicted in the vicinity of the burner and indicate a slower rate of reaction and diffusion of oxygen towards the fuel stream.At the further downstream location of x=0.8 m, the agreement is good and it can be concluded that this model correctly describes the local flow properties in the conical furnace.

5.2 Comparison between calculated flame properties and the corresponding measurements of the present investigations.

The comparisons between measured and calculated flame properties have extended to include the different flames, obtained in the furnace of the present work and listed in table 3.3 of chapter 3.The comparisons fulfilled one of the objects of the present investigation,i.e to use the present flame measurements to allow an assessment of the validity of the numerical scheme to predict flow properties in furnace type geometries.The present comparisons were made to emphasize the significance of the computational procedure in providing quantitative information on the flame structure and its behaviour in confined enclosures.

The comparisons presented in this section include the aerodynamic characteristics of the flow,i.e mean velocity components and the corresponding turbulence intensities;they also include mean gas temperature profiles and the wall heat flux distributions.The comparisons do not include species concentrations ,as no related measurements were carried out.The inlet, velocity components and turbulent kinetic energy profiles were measured in the present work , as shown in chapter 3, and are incorporated in the calculation scheme;in contrast, the dissipation rate was not measured and was assumed according to table 5.2.Figure 5.2.1 illustrates the computational grid used for the present flow configuration

The measured and calculated centreline distributions of mean axial velocity and kinetic energy of turbulence are shown in figure 5.2.2 for the flow situation of flame 1 of table 3.3.The measurements were described in chapter 3 and the calculated distributions were obtained with the aid of model 3.This model was selected because the flow corresponds to a diffusion flame; the calculated values of the time scale of turbulence τ_s were two order of magnitude greater than the τ_k, i.e $N_D >> 1.0$.The discrepancies in the burner vicinity can be attributed to the fact that this flame was not attached to

the burner rim; better agreement was obtained at further downstream locations. The agreement between measured and calculated turbulent kinetic energy profiles was reasonable away from the burner exit and were less than about 12%.Detailed calculations for this flame were obtained by Khalil et al (1974,1975)and are shown in Appendix A6.These calculations were obtained with models 1 and 2 which oversimplify the flame reaction mechanism by ignoring the fluctuations of scalar properties and assuming a square wave temporal distribution respectively.The various combustion models used to predict the flow properties of flame 1 are discussed later in the chapter.

The measured flow properties of flame 2 of table 3.3 obtained at a low flow rate for an air swirl number of 0.52 are compared with the corresponding calculations obtained with the aid of model 3.Typical values of local Damkohler number N_D range between 4 and 1000 in the flame reaction zone and supported the use of the assumption of fast equilibrium chemical reaction, incorporated in model 3 .The calculated centreline distributions of mean axial velocity and kinetic energy of turbulence are shown in figure 5.2.3;the corresponding measurements are shown on the same figure by the solid symbols .The centreline velocity distribution indicates the existance of a central recirculation zone due to the effect of swirl.The size of this zone was underpredicted and this can be attributed to the turbulence model defficiency discussed in chapter 4.The measured and calculated distributions of kinetic energy of turbulence along the centreline of flame 2 are in good agreement;the effect of the swirl was shown to result in higher values of k along the centreline and is consistant with the higher levels of turbulence associated with swirling flows,Baker et al (1974c) and Khalil et al (1974,1975). Detailed comparisons of measured and predicted velocity components and kinetic energy of turbulence for flame 2 , reported by Khalil et al (1974,1975) and obtained with the aid of models 1 and 2 , are discussed in section 5.3 together with those obtained with other models.

Further experiments with the same burner arrangement of flames 1 and 2

were carried out at a higher flow rate which corresponds to Re $=4.7 \times 10^4$ in the annulus flow; these flow conditions correspond to flame 3 obtained with a finite swirl number of 0.52.The comparisons between measured and predicted flow properties were reported by Hutchinson et al(1975) and are shown in detail inAppendix A4. The comparisons,which included mean axial and tangential velocities, mean temperature and wall heat flux, were in good agreement.The calculations were obtained with the aid of a finite reaction rate model with a square wave temporal distribution of species. Calculations of the properties of flame 3 were also carried out using model 3 and the corresponding comparisons with measurements are discussed later in the chapter.

In the experimental investigations of flames 4,5 and 6 ,the influences of burner quarl and swirl number on the local flow properties were considered. Figures 5.2.4 to 5.2.14 illustrate that there is general agreement between the measurements and the calculations.In these calculations, model 7 was used to obtain the local flow properties and was supported by the calculated near unity values of the Damkohler number.Radial profiles of measured and predicted mean axial velocity in flame 4 are presented in figure 5.2.4 and are in good agreement.The agreement is generally satisfactory apart from the size of the central recirculation zone which was 80% of the measured size and was achieved by the inclusion of the density-velocity correlations, whose influence was significant near the reaction zone.

In contrast to the velocity profiles shown in figure 5.2.4, the corresponding non-reacting flow with a blocked central jet and the same air flow rate, exhibited a longer recirculation zone along the centreline of the flow which extended inside the burner quarl.The effect of heat release resulted in higher axial velocities.

Radial profiles of measured tangential velocities are shown in figure 5.2.5 and may be compared with the corresponding calculated profiles.The mean tangential velocity profiles exhibit peak values near the quarl edge and the

calculated velocities are in good agreement with the measurements.The tangential velocity component decays in the axial and radial directions as shown in the figure; the maximum tangential velocity decreased from 6.5 m/s in the burner vicinity to 3.0 m/s at x/D_f of 1.33.

The calculated radial profiles of mean gas temperature in flame 4, shown in figure 5.2.6 , are presented at various axial locations.The measured and predicted temperatures are in good agreement.In the vicinity of the burner, the radial profiles exhibit four different regions:the core region where the local centreline temperature is low because the unburned fuel jet persists downstream of the burner exit;the temperature then increases until it reaches a maximum value at the edge of the reaction zone; it then drops to a minimum value in the wake of the air stream, but rises again in the wall recirculation zone due to the reversed flow of hot gases.Discrepancies of the order of 200K can be observed near the temperature troughs in the burner vicinity and better agreement is obtained at further downstream locations.The temperature in the post flame regions,at $x/D_f > 1.33$, is uniform and the calculated temperatures are in good agreement with the measurements.In flame regions, the location of peak temperature region moves away from the centreline due to the flame spread at downstream distances from the burner exit.

The centreline distribution of kinetic energy of turbulence was deduced from the measured three components of the normal stresses, $\overline{u_i u_i}$ and is shown in figure 5.2.7; the calculated distribution along the centreline is also shown in the figure and qualitatively represents the measurements.The peak kinetic energy of turbulence in the burner vicinity,which exists due to the steep velocity gradient,is well predicted as shown in the figure.

The wall heat flux distribution was obtained from the measured cooling load of the furnace cooling sections at various axial locations of the burner bottom plate inside the furnace;the measured distribution is also represented in figure 5.2.8.The calculated wall heat flux, obtained with model R-II,is also shown in the figure and is in reasonable agreement with the measurements.

The calculated peak wall heat flux,at x/D_f of 0.833,which coincided with the location of the reattachment point, is in agreement with the measurements and previous observations of ,for example,Wu et al(1971),Khalil et al (1974, 1975) and Hutchinson et al (1976).In the burner vicinity discrepancies in the predicted wall heat flux were observed at x/D_f of 0.2 and may be attributed to the finite size of the calorimeter,section D of figure 3.1.4.The radiative heat flux to the furnace black walls was significant and is consistant with previous observations for quarl burner arrangements at the higher flow rate, Hutchinson et al (1975b).

The present calculation procedure was used to predict the local flow properties and heat transfer rates for the turbulent swirling situation of flame 6 which was stabilized by continuously preheating the fresh reactants by the recirculated hot gases in the central recirculation zone.The measured inlet velocity and turbulence kinetic energy at the burner exit were utilized to specify the inlet condition at the burner throat where the calculations started.The dissipation rate of turbulence was not measured at the inlet but was assumed according to table 5.2.The measured profiles of mean axial velocity and the corresponding calculations shown in figure 5.2.9 identify a central recirculation zone extending from the burner throat to a downstream distance of $0.8D_f$.They also indicate the existance of a wall recirculation zone,whose size is smaller than that for S=0.3 under the same flow and geometrical conditions.The mean axial velocities are generally higher than the corresponding non-reacting counterpart due to the heat release.The agreement between the measured and calculated axial velocities is satisfactory except in the vicinity of the central recirculation zone,where the calculated size of this zone was predicted to be 0.8 of the measured size.This discrepancy is in common with previous wake flow calculations and has been attributed to the turbulence model,Pope and Whitelaw(1976).Comparison of the tangential profiles of figure 5.2.10 shows reasonable agreement.The local values of W are higher than those previously shown for S=0.3 and the profiles show peak

values at locations in the wake of the quarl edge and decrease monotonically downstream the burner exit; a maximum value of 10.5 m/s occurs at x/D_f of 0.1 and decreases to nearly 5 m/s at x/D_f of 1.13.

Radial profiles of measured and predicted mean gas temperature, obtained with the aid of model 7 , are shown in figure 5.2.11; and the rapid mixing, caused by the large value of swirl number, resulted in higher temperature at the burner exit.Increasing the swirl number from 0.3 to 0.52 , increased the centreline temperature at the burner exit from 660K to 1280K.The measurements and calculations of the local flame temperature are in reasonable agreement, except in the burner vicinity and near the temperature troughs in the wake of the air stream.This discrepancy is attributed to the under-predicted flame spread rate and partly to the water-cooled bottom plate conditions.The measured flame length was nearly $0.5D_f$ and was shorter than that of flame 4.

In figure 5.2.12, the kinetic energy of turbulence distribtion along the centreline of flame 6 is shown; the measured values were obtained from measurements of the three normal stresses, $\overline{u}^2$, $\overline{v}^2$ and $\overline{w}^2$. The calculated distributions of k are in good agreement with the measurements except at far downstream locations where discrepancies of the order of 25% are observed. Figure 5.2.13, shows the various distributions of k along the centreline of flames 1,2,4 and 6;these were normalized by the average velocity in the air stream at the burner throat for comparison purpose.The measured and calculated distributions of k/U_a^2 along the centreline illustrate the effects of swirl and burner quarl on the peak kinetic energy in the burner vicinity, these peaks correspond to k/U_a^2 of 0.07 and 0.15 for flames 1 and 2 respectively and 0.09 and 0.13 for flames 4 and 6 respectively.The effect of swirl is to increase the peak value of k while the divergent quarl shifts this peak further downstream.

The measured and calculated total wall heat flux distributions are shown in figure 5.2.14 for flame 6;the measured values , obtained from the cooling

water load at the various furnace sections exhibited a peak value which coincided with the reattachment point. The calculated total wall heat flux was in reasonable agreement with the measurements; the radiative heat flux to the wall contributed to nearly 60% of the total wall heat flux; the use of model R-II, accounted for the coupling between the directional radiative fluxes, and resulted in a realistic representation of the radiation transfer. The agreement shown in the figure is satisfactory for the engineering purposes, although discrepancies of the order of 15% were observed. The average wall heat flux, obtained from the measurements was 36.5Kw/m^2 and the corresponding calculated value was 35.2Kw/m^2.

5.3 Assessment of combustion models

The previous sections showed that reasonable agreement can be obtained between measured and calculated local flame properties in complex flow configurations. These comparisons appraise the usefulness of the present computational procedure and the optimum combustion model to predict information about flow pattern, combustion efficiency and pollutant emission which are of great interest to the designer. The present section is prepared to demonstrate the greater discrepancies associated with the use of the non-optimum combustion models although they may be simple and require less computation time. The effect of turbulent fluctuation correlations on the rate of chemical reaction with particular attention to pollutant formation is described and the present section ends with summary of recommended models for various flame configurations in furnace type geometries.

The present comparisons were drawn to illustrate the effect of the use of non-optimum combustion model assumptions on the local flow properties in different flow configurations. Five different furnace geometries were selected to represent a wide variety of industrial applications in boilers and cement kilns. These furnaces include, the present furnace of section 3.1, the furnace of Lockwood et al (1974), the geometry of Bilger et al (1972, 1974),

the furnace of Steward et al (1972) and the furnace flows reported by Beltagui and Maccallum(1974,1975).In the furnace of Lockwood et al, the mixture fractions in a diffusion flame were measured in great detail.In the geometry of Bilger et al ,species concentrations and temperatures were measured in a diffusion flame in a coflowing air stream.The furnace of Steward et al represents a partially premixed flame where detailed measurements of species and temperatures were carried out.The furnace flow of Beltagui et al represents a fully premixed flame.

The calculations of flow properties in the furnace of the present investigations , obtained with different combustion models, are shown in figures 5.3.1 to 5.3.4.In discussing the ability of the various combustion models to represent the flame characteristics,attention is focussed on the predictions of the mean gas temperature with the minimum calculation time.However,the aerodynamic characteristics of the flame, represented by mean axial velocity and kinetic energy of turbulence are shown in figure 5.3.1; the radial profiles of calculated velocity,obtained with models 1,2,3,4and 6 ,are compared with the corresponding measurements of flame 1.Models 2,3,4 and 6 resulted in reasonable agreement with the measurements as they include the effects of turbulent fluctuations on the mean velocity and kinetic energy of turbulence. Model 1 resulted in discrepancies of the order of 26% in the mean velocity and 20% for the kinetic energy of turbulence.These overpredicted values,obtained with model 1,were due to the assumption of infinitely fast chemical reaction without allowance of fluctuations in temperature or any species and led to overpredicted mean temperatures.The obtained agreement improved when the influence of turbulent fluctuations was included,thus,models 3 and 6 resulted in satisfactory agreement.Bearing in mind the limitations of the turbulence model, velocity predictions are adequate when either models 3 or 6 is used; comparisons between the corresponding temperature profiles shown in figure 5.3.2 indicated significant differences between models 1 and 2,while models 3,4 and 6 predicted mean gas temperature within 100K from each other.In this

particular flame, the calculated mixing time scale τ_s is two order of magnitude greater than τ_k the chemical kinetic time scale and the flame is however mixing controlled.The optimum model assumptions are those of model 3, the use of models 1 and 2 gives unsatisfactory results eventhough it is much cheaper;on the other hand model 6 gives similar results to those of model 3 but requires the solution of large number of equations.
Models of combustion used in the previous sections indicate some acheivements and defects which may be used to assess the validity of the assumptions on which they are based:figure 5.3.3 and figure 5.3.4 illustrate the centreline distributions of mean gas temperature for flame 3 as obtained from combustion models that account for turbulent fluctuations but differ in the way they are handled.Figure 5.3.3 shows results with models 4 ,6 and 7 and indicates that model 4 gives lower temperature than measured in the reaction zone due to the incorporation of the smaller of the eddy-break up and Arrhenius reaction rates as the controlling rate.On the other hand,model 5,which is shown in figure 5.3.4 with models 3 and 4, includes intermediate reaction steps and resulted in higher values of temperature than the measurements in regions of formation of CO_2 as the radical CO reactions are considered. Model 3 results in reasonable agreement away from the burner vicinity,where temperature is over predicted by the model's oversimplified fast chemical reaction assumptions.Model 6 results in good agreement away from the burner vicinity while model 7 underpredicted the flame temperature at down-stream distances greater than one furnace diameter.

In the flame situations where straight burners are used,flames 1,2,3, the calculated values of the local N_D ,in the reaction zone, are of the order of 100 and the optimum model,whose assumptions match the physical properties of the flame,is model 3.This model is not suitable for premixed situations or arbitrary fuelled systems as it assumes infinitely fast reaction. Models 6 and 7 attempt to dispense with the assumption of infinite fast chemical reaction by considering slower reaction rate which is controlled

by turbulent fluctuations.The use of such models to diffusion controlled flames requires excessively large computing time and the obtained results are similar to those of model 3.In flame situations where a quarl burner is used,flames4,5 and 6,the calculated values of N_D in the reaction zone are much less than in flames 1,2 and 3and the assumptions of model 3 are not justified.As the fuel and oxygen are not completely mixed,the assumptions of models 4 and 5 are also inappropriate here and the use of model 7 results in reasonable agreement as shown in previous section.

Generally,for each of the flames considered, an optimum combustion model is selected on the basis of N_D and the required properties,other models can also be used which either can be simpler but give unsatisfactory results or give similar results but require more computation time and storage.

A second example of furnace flows where at least two models can be applied is that of Lockwood et al (1974) which is similar to the furnace of the present investigation,but with a smaller expansion ratio.In that particular furnace which fires town gas and the flow Reynolds number is 1.63×10^4, measured centreline and radial profiles of mixture fraction were reported for two fuel to air ratios of 0.072 and 0.0786.The measured centreline distribution of the mixture fraction f for the first flame is shown in figure 5.3.5a.The corresponding calculations were obtained with the aid of models 3 and 7 and are shown in the figure.Both models resulted in reasonable agreement with the measurements, with model 7 giving slightly better agreement in the vicinity of the burner.Contours of isomixture fractions are shown in figure 5.3.5b for a non swirling flame and fuel to air ratio of 0.0786.The agreement between measurements and calculations using model 3 is good although the centreline values of f are slightly overpredicted. Model 1 was used by Lockwood et al(1974) and their calculations overpredicted the measurements by more than 20% as the model did not allow for turbulent fluctuations.However,model 3 is the optimum model as it yields quantitative agreement,in contrast to model 1, and is cheaper than model 7,which

requires 40% more computing time and storage and gives similar results.

The flow of Bilger et al (1972) was discussed earlier in section 5.1 and the calculations were obtained with the aid of model 3.When model 4, which assumes finite reaction rate, is incorporated, slower reaction rate occurs and a longer flame than measured is obtained as shown if figure 5.3.6. Model 3 clearly gives better results in the flame as its basic assumptions are consistant with the measuring conditions.Further calculations were obtained in the same configuration,with velocity ratio U_j/U_a =5 and are shown in figure 5.3.7,with the corresponding measurements.Two models were used,namely model 3 and 6, and result in reasonable agreement,however, model 3 is recommended as it involves the solution of less equations than model 6,to give similar quantitative agreement.

In the flow situation of Steward et al(1972),model 4 was used in the solution procedure and was selected on the basis of calculated local values of N_D .In figure 5.3.8, measured centreline distribution of T is shown with the corresponding predictions obtained with models 3 and 4.Model 4 gives better predictions than model 3;the calculated values of N_D in the reaction zone were very small<<1.0 and do not justify the use of model 3.In this particular flame situation,models 6 and 7 indicate similar predictions to those obtained with model 4.Hence,model 4 is more appropriate than model 3 because of local values of N_D,while models 6 and 7 require 35% more computing time.

The premixed flames of Beltagui and Maccallum(1974 ,1975) were considered in section 5.1 where model 4 was used to predict the flame properties.Comparisons are given here between this model and model 6,to illustrate the benefit,if any, from the use of model 6 which requires 40% more computing time.Figure 5.3.9 is prepared to indicate the type of agreement which can be obtained when both models are used to predict local velocity distributions. The discrepancies shown in the figure are of the order of 12% and were localized in the initial region of the flow where reaction started.The

temperature rise distribution along the centreline was very well predicted with models 4 and 6 as shown in figure 5.3.10.Models 4 and 6 are most appropriate to premixed flames but model 4 is recommended because it requires less computing time to yield similar results to model 6.

It is concluded from the previous comparisons, that an optimum model can be used on the basis of the arrangement of the inlet streams and the calculated values of N_D. Alternative non optimum models can also be used but would give unsatisfactory results if they are simpler than the optimum model, or require more computing time when complicated models are considered.

The capability of a combustion model to calculate local properties in flames rests ultimately on how well the important processes are represented in the conservation equations of mass,momentum, species and energy expressed in terms of average entities.When these conservation equations are averaged by a conventional method,there are the density correlation terms,which when neglected itroduce errors into the equations;these errors vary according to the type of the flame,location in the flame,fuel to air ratio,fuel and density gradients.The effect of these correlations is significant on the mean temperature and nitric oxide concentrations as shown in section 2.4. The modelling of conservation equations for these correlations involve assumptions which have not been directly tested and it is clear, therefore, that uncertainities of the order of ±100K and up to±10 ppm exist from this uncertainity.

The various model assumptions and limitations to real flow situations are indicated in table 5.3 which summarises the basic assumptions,treatment of scalar entities,type of reaction mechanism and applicability of the various combustion models.

5.4 Calculation outside range of measurements.

The comparisons discussed in sections 5.1 and 5.2 between the calculated results obtained using various combustion models and the experimental results

Table 5.3

Model	Basic Assumptions	Scalar temporal distributions	Reactions	Application
1	fastchemical reactions reactants do not coexist ($\tau_s >> \tau_k$)	-	Single step irreversible	General, qualitative, physically controlled diffusion flames.
2	fast chemical reactions reactants can exist at same place but different times ($\tau_s >> \tau_k$)	Square wave	single step irreversible	General, quantitative, physically controlled diffusion flames.
3	fast chemical reactions, reactants can exist at same place but different times ($\tau_s >> \tau_k$)	clipped Gaussian probability distribution	single step irreversible	Quantitative, physically controlled diffusion flames.
4	finite reaction rate Eddy break up expression ($\tau_k >> \tau_s$)	clipped Gaussian probability distribution	single step irreversible	Quantitative, kinetically influenced premixed flames and mixing zones
5	finite reaction rate Eddy break up expression ($\tau_k >> \tau_s$)	clipped Gaussian probability distribution	multi inter-mediate steps reversible	Quantitative, kinetically influenced, detailed chemistry. Premixed flames and mixing zones
6	finite reaction rate correlation expression $\tau_k \simeq \tau_s$	clipped Gaussian probability distribution	single step irreversible	Quantitative, general, diffusion/premixed flames and arbitrary fuelled system
7	finite reaction rate correlation expression cross correlations $\tau_k \simeq \tau_s$	clipped Gaussian probability distribution	single step irreversible	Quantitative, general, diffusion/premixed flames and arbitrary fuelled suitable for pollutant calculations

representing measurements in a wide variety of confined flows,confirm the ability of the computational procedure to predict the local flow properties. The discrepancies between measured and predicted mean velocities are less than 10% of the measured values and increased to 25% in the vicinity of recirculation zones.The mean gas temperature are predicted within±150K from the measured values while the discrepancies in the predicted species concentrations are less than 10%.The corresponding maximum discrepancy in the calculated nitric oxide is ± 20%.

The parameters affecting the flame pattern,combustion efficiency and pollutant emission are numerous and it is very expensive and time consuming to carry out detailed measurements to assess their effects.Calculations are therefore carried out to assess the effects of some of the parameters e.g, inlet flow Reynolds number,air to fuel ratio and swirl intensity on the flame properties.Calculations were also extended to investigate the effects of burner geometry and fuel nozzle geometry on the local flow properties where no experimental results were available.From a practical standpoint, the designer is intrested in the wall heat flux and temperature distribution, stack temperature,unburned hydrocarbons and exit nitric oxide concentrations, which are influenced by the flow inlet conditions(Re,air to fuel ratio and swirl number), and the geometric inlet and boundary conditions(burner and fuel nozzle geometries).These calculations are carried out using model 3 and a 20x20 non-uniform grid arrangement.

5.4.1 Effect of flow and geometric inlet and boundary conditions.

The effect of Reynolds number on the flow properties in the present furnace configuration of flame 2 was considered, and figure 5.4.1 shows the effect of doubling the Reynolds number of the fuel and air.The isovelocity contours did not change largely due to doubling the mass flow rates.The corresponding isotherms are also shown in the figure and the exhaust temperatures at the high Re are higher than at the lower Re.This is consistant

with the observed 48% increase in the wall heat flux due to doubling Re when the swirl number is 0.52.For the non swirling flame,under the same flow conditions, the total wall heat flux distribution increased by a factor of 1.4 due to doubling the Reynolds number in the inlet streams. Hence, doubling the thermal input to the furnace results,in lower furnace efficiency, as indicated by the increase of the exhaust temperature,due to the shorter residence time.This is consistant with the observations of Michelfelder et al (1974);the wall heat flux increases by 60% at twice the burner load for swirl number of 0.5 and by 44% at zero swirl.

Partial loads always tend to give lower NO emission;the reduction in the amount of NO may be the result of several complementary or contradictory effects which should be considered by the designer,namely;

1.Reducing the heat input to the furnace reduces the bulk gas temperature and hence the temperature of the entrained outer recirculation matter is therefore lower than full load.

2.The mean residence time within the furnace is increased,but that will have little relevance to NO formation because the bulk gas temperature is too low to initiate NO formation.

3.Reducing the burner throughput changes the mass exchange at the root of the flame which may promote or inhibit NO formation.

The exhaust NO concentrations for the flames of figure 5.4.1 are 32 and 40 ppm and correspond to the low and high Re.This observation is in agreement with the measurements of Michelfelder et al (1974),where the exhaust NO concentrations increased from 30ppm at half load to 35ppm at full load for S=0.5.

Classical flame theory(see Williams 1965),based on a very crude analysis of mixing, predicts that the shape of a diffusion flame is affected by changing the air to fuel mixture from lean to rich.The present calculation procedure offers the opportunity to predict the effect of such changes on the flame characteristics,as investigated in detail by Khalil et al

(1974) and Khalil(1976).A 15% change in the inlet air to fuel ratio, resulted in changes in the mean velocity of less than6% along the centreline of flame 1.The corresponding changes in the mixture fractions and temperatures were less than 10% and illustrated the importance of the accurate specification of inlet $\left(\frac{air}{fuel}\right)$ ratio.The effect of excess air, on the flame length for example, is more significant than a similar percentage of excess fuel and is due to the dilution associated with the former case. The exhaust NO concentrations do not change significantly for a 15% change in the equivalence ratio and suggest that there are no major differences in the NO formation rate.

The flow pattern and heat transfer rates in furnace flows were greatly affected by the introduction of swirl in the air stream and helped to create a recirculation zone along the centreline to stabilize the flame by the recirculated hot combustion products.The effect of swirl on the centreline mean axial velocity distribution was shown in figure 5.4.2 for a wide range of swirl numbers.The central recirculation zone was created for swirl numbers around 0.4 for the geometry of the burner of figure 3.1.1a and its size was sensitive to changes in swirl number.Beltagui(1974) investigated the influence of swirl number on the flow properties in axisymmetric furnace flows and suggested a critical swirl number of 0.22 at which central recirculation zones started to form in premixed flames.As the swirl number increased,the length of the wall recirculation zone and consequently the flame length decreased as indicated by the location of peak centreline temperature distribution shown in figure 5.4.2.The wall heat flux changed accordingly and more heat flux was transferred in the first half of the furnace as the swirl intensity increased.The total wall heat flux increased with swirl for a given input thermal energy.The flow was characterized by higher combustion rates and locally higher temperatures in the flow field resulting in increased rates of NO formation and lower exhaust concentrations of unburned hydrocarbons.

The method of introducing , and hence mixing ,the fuel and air streams influenced the local heat release patterns, and therefore the temperature distributions,in the flame region.Two aspects were considered for coaxial burner arrangements:the effect of the fuel nozzle diameter and geometry, and the effect of the air nozzle divergent angle.Figure 5.4.3 presents calculated variations of temperature,mixture fraction,wall heat transfer rate and NO concentration for the furnace of section 3.1 and for different diameters of the central fuel jet.The effective initial equivalence ratio was equal to 1.05 and the swirl number was 0.52.The increase in burner diameter results in reduction in the velocity of the fuel jet for the same mass flow rates.Although the thickness of the material between the fuel and air streams is consequently reduced,the smaller fuel jet velocity reduces the flame length: a 27 mm to fuel jet results in a maximum centreline temperature at $0.3D_f$ whereas an 8 mm jet results in a maximum centreline temperature at more than one furnace diameter downstream.This effect is similar to an increase in swirl from 0.0 to 1.75,although other regions of the flow would be more influenced by a change in the swirl than by a change in the geometry of the fuel nozzle.Two consequences of the shorter flame are an increase of the NO concentrations on the centreline and an increase in the wall heat transfer rate in the upstream of the furnace.The increase in the centreline values of NO concentration is large and the increase in the total NO production of the furnace will also be significant.In contrast,the increase in the wall heat transfer rate is comparatively small due to the local influence which the change in the fuel jet has on the temperature distributions in the furnace:the aerodynamic flow characteristics in the near wall region and the stack temperature are uninfluenced by the change in the fuel jet diameter.

The effect of two different fuel nozzles on mixing and heat release is considered; the two fuel nozzles correspond to those of figures 3.1.1a and

3.1.1c and the calculated local flow properties downstream of the burner are shown in figure 5.4.4.Burner 2,led to shorter flame than that of burner 1 since the fuel was directed towards the air stream which improved the mixing and heat release and resulted in lower wall heat flux compared to burner 1. The centreline concentrations of NO indicated that burner 2 resulted in a peak NO upstream that of burner 1 due to the shorter flame and the total production of NO was uninfluenced.

The influence of quarl angle is demonstrated on figure 5.4.5 for a swirl number of 0.52.The burner and furnace geometries are similar to those of section 3.1:the equivalence ratio is 1.05 and the fuel pipe is 12mm. Calculated centreline distributions of mean velocity,temperature,mixture fraction and NO concentration are presented:the corresponding heat transfer rates,for a prescribed wall temperature of 333K are also shown.The effect of decreasing quarl angle is to increase the temperature,mixture fraction, NOconcentration and heat transfer rate in the upstream region of the furnace: this influence is similar to increasing the swirl number.The peak NO along the centreline increases as the quarl angle decreases and the total production of NO increases.

The furnace to burner diameter ratio has a strong influence on the flow pattern and recirculation;as the furnace to burner diameter ratio increases, the wall recirculation zone increases in size and the furnace length should be larger than the wall recirculation zone.Most of the fire tube boiler furnaces have an expansion ratio of nearly 1:5 i.e,the burner to furnace diameter ratio,for example, the furnace of Wu et al (1971) had an expansion ratio of 1:5.13 and furnace diameter of 0.9 m while that the furnace of Beltagui et al had an expansion ratio of 1:5 and furnace diameter of 0.46m. The furnace of the present investigation have an expansion ratio of 1:5.45 and the furnace diameter was 0.3 m.

The influence of the wall temperature on the total heat transfer rate

from the furnace and the consequent changes in the lengths of the flame and of the the recirculation zones is shown in figure 5.4.6.The influence of swirl and the effect of removing the end plates of the furnace of section 3.1, to allow a low velocity,coflowing stream are also demonstrated.As can be seen, an increase in the wall temperature results in decreased heat transfer rate(with consequent increased thermal energy in the exhaust), decreased length of flame and central recirculation region and increased length of the corner recirculation regions.The shorter flame length,however, and particularly in a wall temperature of 450K where the change in length is large,causes an increase in overall NO production,due to increased temperature fluctuations:in general, the more efficient combustion associated with the warmer air entrained by the flame also results in greater production of NO.The influence of swirl is consistant with that demonstrated in figure 5.4.2.In figure 5.4.6c,the end plates of the furnace have been removed and the calculations performed with the same mass flow of air as in the results of figure 5.4.6a and b .There is no corner recirculation zone and the heat transfer to the wall is less than that for the arrangement with end plates for all values of swirl number.

5.4.2 Practical relevance.

The furnace and burner designer is practically interested in total wall heat flux and temperature distributions,stack temperature,unburned hydrocarbons and furnace exit NO concentrations.These properties were influenced by the flow and geometric inlet and boundary conditions of the previous subsection.A shorter flame is obtained with high swirl intensity and results in a large improvement in the furnace efficiency, as the wall heat flux increases and the stack temperature decreases.The amount of unburned hydrocarbons is reduced but the total production of NO increases.A compromise between the combustion efficiency and the NO emission should be made as the increase

of swirl has a desired effect on the first but not on the second.The effect of furnace loading is similar to that of swirl but to a less extent.Partial loads result in lower NO emission and relatively higher furnace efficiency. The burner and fuel nozzle geometry result in a shorter flame, a large wall heat flux distribution but also in a larger NO emission.

In the furnace flows considered in the previous sections,5.1,5.2 and 5.3, the input thermal energy to the burner was less than 1 Mw.These furnaces were selected to assess the validity of the various combustion models by way of comparisons with the detailed experimental data availabe in these furnace flows.The obtained agreement was shown to be satisfactory and the calculation procedure ability to represent these furnace flows was assessed. However,in real furnace situations used in power stations and industry, complicated burner geometries are used and the thermal energy input through the burner is large.Attention was turned to the use of the numerical procedure to investigate the performance of furnaces of practical dimensions and input loads in terms of local flow properties and heat transfer rates. A sample of this type of furnaces where the gaseous fuels are fired at loads of 6 Mw,Rhines(1974) is considered.Measured and calculated flow properties are given in Appendix A7 where comparisons at various locations in the furnace are made and the usefulness of the numerical procedure is appraised.

5.5 Concluding Remarks

The following more important conclusions are appropriate to this chapter;

1. The local flow properties in reacting flows have been calculated using a combustion model appropriate to each flow situation, as argued in Chapter 2. Turbulent, confined non-premixed flames are diffusion controlled to the extent that fast, single step reaction can be assumed together with a clipped Gaussian probability distribution of concentration; this corresponds to the situation where $N_D >> 1$ and model 3 has been used. Premixed flames

are kinetically influenced and, therefore, have been represented by a finite reaction rate in the fuel conservation equation; in this flame situation, $N_D \ll 1$ and model 4 has been used with a single step reaction and model 5 when intermediate radical concentrations were required. In flame situations where the mixing and chemistry have similar magnitudes, i.e. $N_D \simeq 1$, model 7 has been used.

2. In turbulent gaseous flames, the radiative source term in the total enthalpy conservation equation was obtained from a four-flux type radiation model which made use of simplifying assumptions for the angular distribution of radiant intensity and was easily coupled to the numerical solution of the aerodynamic equations. Model R-II, in which the radiation intensities are expressed as Taylor series in distance, has been used for the present calculations. Model R-I, which does not couple the net radiation fluxes, leads to significant underprediction of radiation.

3. The local concentrations of nitric oxides have been calculated from a pollution model which took account of the effects of turbulent fluctuations on the rate of pollutant formation through model 7 and involved a reduced form of the Zeldovich reaction scheme. The numerical grid was modified to give NO_x formation rates, independent of the grid arrangement. As a result, calculated values of NO_x agreed with measurements in within around ± 20 ppm.

4. In the conservation equations of mass, momentum, energy and species, the effect of density, velocity and scalar fluctuation correlations was considered and found to influence the gas temperature in particular; their neglect reduced the calculated concentrations of NO by up to 30 ppm.

5. Comparisons between measured and calculated flow properties discussed in sections 5.1 and 5.2, represent a wide variety of flame situations and show that there is good agreement. This justifies the choice of the various combustion models for the relevant flame situations and supports the use of the calculation procedure for design purposes. The procedure

permits the prediction of: mean velocity with discrepancies less than 10%, kinetic energy of turbulence with discrepancies less than 15%, mean temperature within ± 150K, the wall heat flux with discrepancies less than 15% and the nitric oxide concentration within ± 20%.

6. Calculations, outside the range of measurements in confined furnace flows indicated that short flames and high furnace efficiencies are obtained at high swirl intensities and with divergent quarl burners. The total wall heat flux increases as the swirl intensity increases and exhaust temperature decreases. The information obtained from these parametric investigations has been presented in quantitative form and aids the design of practical and economical furnaces.

CHAPTER 6

SUMMARY OF CONCLUSIONS AND RECOMMENDATIONS

A summary of the main conclusions of the present investigation is given in the first section of this chapter. Recommendations for future furnace flow measurements and the corresponding mathematical modelling of turbulence, combustion and pollutant formation are discussed in the second section.

6.1 Summary of Conclusions

This section provides general conclusions which may be related to the objectives specified in Chapter 1. These conclusions are;

1. Detailed measurements of mean and rms velocities have been obtained in an axisymmetric furnace arrangement using laser anemometry in non-reacting and reacting flow situations with various degrees of swirl and with and without burner quarl. As a result of combustion, the mean velocity increased significantly wherever there was a high proportion of hot combustion products and the rms velocity increased by up to 80% in the reaction zone. The swirl and burner quarl were found to create a central recirculation zone, and to reduce the size of the wall recirculation zone. In reacting flows, the central recirculation zone helped in stabilising the flame.

2. Measurements of mean gas temperature were obtained in reacting flows with the aid of suction pyrometers and the wall heat flux distribution was calculated from the measured cooling water temperatures at the inlet and outlet of each of the furnace cooling sections. The effects of swirl and burner quarl were to shorten the flame and to reduce the exhaust temperature; the peak wall heat flux moved upstream as the degree of

swirl increased and the quarl angle decreased.

3. The elliptic form of the continuity equation and equations for three components of momentum have been solved numerically with equations for kinetic energy of turbulence and its dissipation rate; these equations, expressed in finite difference form were solved simultaneously at each node, in an orthogonal grid incorporated in the computational scheme. The ability of the two-equation turbulence model to represent the aerodynamic characteristics of turbulent non-reacting recirculating flows was assessed by comparison of relevant measurements reported in the literature and in the present work with the corresponding calculations. The agreement was found to be excellent for non swirling flows and worsened slightly as the swirl intensity increased. The magnitude of the discrepancies was judged to be of little importance to combusting calculations where the combustion model was expected to result in significantly larger unknowns.

4. Various combustion models were used to provide closure to the species and energy conservation equations which were solved to yield furnace flame properties. These models varied in complexity from simple models of fast chemical reactions to models considering the temperature and concentration fluctuations and their correlations. The major assumption of fast chemical reaction was modified by the inclusion of the effects of concentration fluctuations, expressed in a clipped Gaussian distribution, and was found to be appropriate to diffusion controlled flames. Finite chemical reaction models were used for premixed flames and expressed the rate of chemical reaction in Arrhenious form with the introduction of the effect of turbulence through an eddy break up rate. These models were appropriate for situations where the reactants are in intimate contact and the reaction is kinetically

influenced.

5. A general combustion model suitable to most flame situations was developed. This model calculated the rate of chemical reaction in the fuel conservation equation by decomposing each entity to its mean and fluctuating components and solving conservation equations for the resulting correlations. The contribution of each term in the resulting rate of reaction expression was governed by turbulent mixing and chemical kinetics. The advantage of this model, over other combustion models, is that it is the most physically appropriate to arbitrary fuelled flames where the reaction is neither diffusion controlled nor kinetically influenced. On the other hand, a disadvantage of this approach is the large number of conservation equations which have to be solved with increase in the correlations considered, and the consequently higher computational cost.

6. Temperature fluctuations, contribute to the generation of nitric oxide over an appropriate part of the reaction zone in furnace flows. An implication of this is that NO concentration levels are substantially higher than the values predicted on the basis of mean temperatures. A model which takes account of the temperature and concentrations effects was successfully used; this model was modified to include the effects of superequilibrium.

7. In variable density flows, additional correlations appear in the conservation equations of mass, momentum, species and energy, due to density fluctuations. These correlations, can be of similar magnitudes to the corresponding mean quantities, in the vicinity of the reaction zone and, therefore, have a significant influence on the mean temperature and NO concentrations, and are incorporated in the present scheme.

8. The ability of the combustion models to predict the flame charac-

teristics in furnace configurations has been assessed by comparing the calculated flame properties with the corresponding measurements reported in the literature and those obtained in the present investigations. Model 3 was used for diffusion flames, models 4 and 5 were used for premixed flames and models 6 and 7 were used for arbitrary fuelled flames. The agreement between the measured and calculated flow properties is reasonably good; the discrepancies in mean velocity were less than 10% and those in the kinetic energy of turbulence were less than 15%. The mean gas temperature was predicted within ±150K, while the maximum discrepancies in the wall heat flux and pollutant concentration were less than 15% and ±20% respectively.

9. A parametric investigation was carried out, using the calculation procedure, to assess the effect of flow, geometric and boundary conditions on wall heat flux and temperature distributions, stack temperature, unburnt hydrocarbon and pollutant concentration at the furnace exit. An increase in the air swirl number shortens the flame, as the energy release rate increases and is evidenced by locally higher temperatures and increased hydrocarbon burnout rates; this is accompanied by an increase in the total wall heat flux and lower exhaust temperature. An increase in flow rate, for the same geometry and equivalence ratio results in an increase in the total wall heat flux and the stack temperature.

Another parameter which significantly affects the flame characteristics is the existance of burner quarl which results, like swirl, in a shorter flame and hence a more compact furnace with higher combustion efficiency.

6.2 Recommendations for future work

The areas recommended for further study are as follows;

1. Further applications of the present procedure to practical furnaces;
2. Improvement to the various models;

3. Extension of the experimental program.

These topics are individually discussed.

6.2.1 Further applications of the present computational procedure

The present computational procedure can be used to examine in detail the influence of the various parameters on the combustion efficiency and pollutant emission of various industrial and commerical furnace geometries. In particular the following are suggested:

1. A parametric study of boiler type furnaces, i.e. determination of the effects of flow Reynolds number, type of fuel, air to fuel ratio, pressure, preheat temperature, wall temperature and swirl. This will facilitate the better understanding of the influences of these parameters and hence allow improved design.

2. For similar purposes, the effects of geometric parameters such as the burner/furnace diameter ratio, shape of the burner and furnace exhaust geometry can and should be determined more extensively than has been done so far. In addition, an attempt should be made to provide the burner geometry and initial flow conditions to the program so that furnace properties can be calculated on the basis of geometric, wall and burner inlet conditions.

3. The procedure should be expanded to calculate the local properties of liquid spray flames. Preliminary calculations, Khalil et al (1976b) Appendix A8, were carried out with the assumption of fully vapourized fuel at the inlet to the solution domain and solved conservation equations for mass, momentum species and energy simultaneously. This procedure is inexact, as it applies only to very small droplet diameters, i.e. less than 25 μm and does not contain any information of the droplet size, trajectory and evaporation; it can and should be extended to take account of droplet characteristics and their interaction with the surrounding gases.

6.2.2 Improvement to the various models

1. During the validation tests of chapters 4 and 5, it emerged that the present turbulence model is adequate for recirculating flows but shows

deficiencies in wake and strongly swirling flows. This is characterised by the underprediction of the size of recirculation zone in the wake of discs and in swirling flows and was attributed to the defects in dissipation equation, Pope (1976). A fresh approach based on the spectral energy equation is a possible means of overcoming the defect of the modelled dissipation equation.

2. The assumption of fast chemical reaction in model 3 is limited to diffusion flames and improvement of the assumed probability distribution to allow for intermittency is needed. This can be obtained from a probability of reaction which depends on the time scales of turbulence and chemistry and on the local air to fuel ratio.

The eddy-break up assumption of model 4 requires further investigations and improvement; the expression of the reaction rate in terms of the reactedness, fuel and oxygen parcel thickness and stretching rate, Spalding (1976), is more physically sound than the original model and deserves further development and testing.

Model 7, which is based on a series expansion of the reaction rate expression, is limited to low temperature fluctuation intensity. To overcome this limitation, the rate of reaction can be expressed in terms of Φ, and the time average rate obtained as $\bar{R}_{fu} = \int R_{fu}(\Phi) P(\Phi)\, d\Phi$. Different forms of $P(\Phi)$ can be assumed, alternatively transport equations of these probability distributions are solved, e.g. Pope (1976).

3. The use of the present radiation model was limited to non scattering grey gas but can be easily extended, using Truelove's (1976) model to account for multigas components, soot and particulate radiation which are dominant in oil flames.

4. More work is required to evaluate the effect of the correlations $\overline{\rho'\phi}$, by solving conservation equations for these correlations and comparing the time and mass averaged entities, particularly in the reaction zone.

6.2.3 Extension of the experimental study

On the basis of the work reviewed in chapter 1 and that performed in the present investigation, it is suggested that the aerodynamics of small

axisymmetric furnace models has been adequately covered by experiments up to a swirl number of 0.5. There are important areas which need experimental investigation, namely;

1. extension of the range of swirl number.
2. measurements in spray flames.
3. measurements in large-scale furnaces.

In spray flames, measurements of flame characteristics such as heat release pattern, droplet size and distribution and soot concentration are required to supplement the small number presently available. In particular, measurements are needed:

(a) to establish the interaction of the droplets and the main gas flow

(b) to examine the effect of swirl and pressure on the flame characteristics

(c) to explore the spray flame behaviour in confined geometries and particularly the heat release pattern, wall heat flux and soot formation.

As regards the large furnace measurements, little work has been reported in this area, as the problem associated with optical measuring techniques in such flow configurations is difficult. Laser anemometry measurements in a large scale furnace were reported by Baker et al (1974a), and several problems were encountered, e.g. alignment of the optical arrangement, beam flickering and the steep temperature gradients along the measuring probe. Further improvements were carried out by Wigley (1976) and preliminary measurements were carried out. Further work is necessary to improve the techniques and, thus, in conjunction with temperature and species concentrations, velocity and turbulence measurements should be effected in large scale furnaces, to contribute to physical understanding and to provide quantitative confidence in the present procedure.

Generally, measurements of joint probability distributions of velocity and temperature in reacting flows are needed, to aid further advances in turbulence and combustion modelling including alternative methods such as the probability approach of Pope (1976) and to quantify the correlations between the aerodynamic and thermal properties in reacting flows.

REFERENCES

Abbott, D.E. and Kline, S.J. (1962) Experimental investigations of subsonic turbulent flow over single and double backward facing steps. J. Basic Eng. D84, 317.

Afrasimova, N.V. (1967) Study of the aerodynamics of a furnace space. Thermal Engineering, 14, 10.

Anasoulis, R.F., McDonald, H. and Bugglen, R.C. (1973) Development of a combustor flow analysis, Part 1: Theoretical studies. AF APL-TR-73-98.

Andrews, G.E., Bradley, D. and Lwakabamba J.B. (1975) Turbulence and turbulent flame propagation - a critical appraisal. Combustion and Flame, 24, 285.

Antonopoulos, K. (1975) A comparison of finite difference and finite element methods of solution of convective transport equation. M.Sc. Thesis, London Univ.

Arrhenius, S. (1889) Uber die Reaktionsgeschwindigkeit bei der inversion von rohrzucken durch sauren. Z. Phys. Chem. 4, 226.

Asalor, J. and Whitelaw, J.H. (1975) The influence of combustion induced particle concentration variations in laser Doppler anemometry. LDA-Symposium, 115, Denmark.

Assaf, H. (1975) Measurements and calculations of flow properties downstream of blunt body flame stabilisers. M.Sc. thesis, London Univ.

Back, L.H. and Roschke, E.J. (1972) Shear layer flow regimes and wall instabilities and reattachment lengths downstream of an abrupt circular channel expansion. J. Appl. Mech, 94, 677.

Baker, R.J. (1974a) The application of filter bank to measurements of turbulence in fully developed jet flow. Proc. 2nd International workshop on laser velocimetry, Purdue Univ.

Baker, R.J. (1974b) Private communications.

Baker, R.J., Hutchinson, P. and Whitelaw, J.H. (1974a) Preliminary measurements of instantaneous velocity in a 2 m square furnace using laser anemometry. J. Heat Transfer, C96, 410.

Baker, R.J Hutchinson, P. and Whitelaw, J.H. (1974b) Velocity measurements in the recirculation region of an industrial burner flame by laser anemometry with light frequency shifting. Combustion and Flame, 23, 57.

Baker, R.J., Hutchinson, P., Khalil, E.E. and Whitelaw, J.H. (1974c) Measurements of three velocity components in a model furnace with and without combustion. Proc. 15th Symposium (International) on Combustion, 553, Combustion Institute, U.S.A.
See also,
Measurements of three orthogonal velocity components in confined coaxial jet flows with and without swirl and combustion. Imperial College, Dept. of Mech. Eng. Report HTS/74/29, and U.K. AERE Report AERE-R 7776.

Baker, R.J. and Wigley, G. (1975) Design, evaluation and application of a filter bank signal processor. LDA Symposium, 350, Denmark.

Baker, D.W. (1967) Decay of swirling, turbulent flow of incompressible fluid in long pipes. Ph.D. Thesis, Univ. of Maryland.

Barchilon, M. and Curtet, R. (1964) Some details of structure of an axisymmetric confined jet flow. Symposium on fully separated flow, Philadelphia, see also, J. Basic Eng. D86, 777.

Barrère, M. (1973) Modelisation des foyers de turboreacteur en vue de l'etude de la pollution. AGARD meeting, CP 125.

Baulch, D.L., Drysdale, D.D. and Horne, D.G. (1968-1970) High temperature reaction rate data. Univ. of Leeds, reports Nos. 1-5.

Becker, H.A. (1974) Effects of concentration fluctuations in turbulent flames. Proc. 15th Symposium (International) on Combustion, 601, the Combustion Institute, U.S.A.

Beer, J.M. and Chigier, N.A. (1964) The flow near the nozzle in double concentric jets. J. Basic Eng., D86, 797
See also,
Velocity and static pressure distributions in swirling air jets issuing from annular and divergent nozzles. J. Basic Eng., D86, 788.

Beer, J.M. and Chigier, N.A. (1972) Combustion Aerodynamics Applied Science Publishers, London.

Beltagui, S.A. (1974) Aerodynamics and modelling of vane swirled flames in furnaces. Ph.D. thesis, Glasgow Univ.

Beltagui, S.A. and Maccallum, N.R.L. (1974) Aerodynamics of vane swirled flames in furnaces. Glasgow Univ., Dept. of Mech. Eng. Report,
See also
The modelling of vane swirled flames in furnaces. Glasgow Univ. Dept. of Mech Eng, Report.

Beltagui, S.A. and Maccallum, N.R.L. (1975) Vane swirled flames in furnaces. Proc. 2nd European symposium on Combustion, 672.

Bilger, R.W. (1975a) A note on Favre averaging in variable density flows. Combustion Science and Technology, 11, 215.

Bilger, R.W. (1975b) Turbulent jet diffusion flames. Proc. Progress in energy and combustion science., 1, 87.

Bilger, R.W. and Beck, R.E. (1974) Further experiments on turbulent jet diffusion flames. Sydney Univ., Dept. of Mech. Eng. Report F.67.

Bilger, R.W. and Kent, J.H. (1972a) Measurements in turbulent diffusion flames. Sydney Univ. Dept. of Mech. Eng. report F41.

Bilger, R.W. and Kent, J.H. (1972b) Concentration fluctuation in turbulent jet diffusion flame. Sydney Univ. Dept. of Mech Eng. Report F46.

Borghi, R. (1973) Etude theorique de l'evolution residuelle des produits pollutants dans les jets de turboreacteurs. AGARD meeting CP 125.

Borghi, R. (1974a) Computational studies of turbulent flow with chemical reaction. Presented at Project SQUID on turbulent mixing, U.S.A.

Borghi, R. (1974b) Methode analytique de prevision de taux de reaction chemique en presence d'une turbulence non homogene. O.N.E.R.A. publication, T.P. 1343.

Bousingisque, V.J. (1877) Theorie de l'ecoulement tourbillant Mem. Pres. Acad. Sci. 23, 46.

Bowman, C.T. and Cohen, L.S. (1975) Influence of aerodynamic phenomena on pollutant formation in combustion Vol 1: Experimental results. EPA-650/2-75-061-2, U.S.A.

Bradshaw, P., Ferriss, D.H. and Atwell, N.P. (1967) Calculation of boundary layer development using turbulent energy equation. J. Fluid Mechanics, 28, 593.

Bray, K.N.C. (1973) Equations of turbulent combustion, 1. Fundamental equations of reacting turbulent flows. Univ. of Southampton, A.A.S.U. Report 330.

Bray, K.N.C. (1974) Kinetic energy of turbulence in flames. Univ. of Southampton, A.A.S.U. Report 332.

Braud, Y. and Chedaille, J. (1972) Industrial Flames,vol 1:Measurements in Flames, Edward Arnold

Bush, W.B., Feldman, P.S. and Fendell, F.E. (1975) On diffusion flames in turbulent shear flows, modelling reactant consumption in a mixing layer. Univ. of California, San Diego, La Jolla.

Carreto, L.S., Gosman, A.D., Patankar, S.V. and Spalding, D.B. (1972) Two calculation procedures for steady three dimensional flows with recirculation. Proc. 3rd International Conference on numerical methods in fluid dynamics, Paris.

Carreto, L.S. (1975) Mathematical modelling of pollutant formation. Proc. Progress in Energy and Combustion Science, 1, 1.

Cernansky, N.P. and Sawyer, R.F. (1974) NO and NO_2 formation in a turbulent hydrocarbon/air diffusion flame. Proc. 15th Symposium (International) on Combustion, 1039, The Combustion Institute, U.S.A.

Chedaille, J., Leuckel, W. and Chesters, A.K. (1966) Aerodynamic studies carried out on turbulent jets by the International flame research foundation. J. Inst. fuel, 39 , 311.

Chigier, N.A. and Dovork, D. (1974) Laser anemometer measurements in flames with swirl. Proc. 15th Symposium (International) on Combustion, 573, the Combustion Institute, U.S.A.

Chou, P.Y. (1945) On velocity correlations and the solution of the equations of turbulent fluctuations. Quart. Appl. Math., 3, 38.

Craya, A. and Curtet, R. (1953) Sur l'evolution d'un jet en espace confine, C.R.A.S., 236, 1134, 153, Paris.

Craya, A. and Utrysko, B. (1967) Jets tournants en espace confine,service de documentation scientifique et technique de l'ormenents, Paris.

Daly, B.J. and Harlow, F.H. (1970) Transport equations of turbulence. Phys. of Fluids, 13, 2634.

Damkohler, G.Z. (1947) On the effect of turbulence on the flame velocity in gas mixtures. NACA, T.M.1112.

Davidov, B.J. (1961) On the statistical dynamics of an incompressible turbulent fluid. Dokl. ANSSSR, 136, 47.

Demarco, A.M. and Lockwood, F.C. (1975) A new flux model for the calculation of three dimensional radiation heat transfer. La Reivesta du Combusteble, 5, 29, 184.

Donaldson, C. dup, Sullivan, R.D. and Rosenbauum, M. (1972) A theoretical study of the generation of atmospheric clean air turbulence. AIAA Journal, 10, 2, 162.

Donaldson, C. dup and Hilst, G.R. (1972) Chemical reactions in inhomogenous mixtures, the effect of the scale on turbulent mixing. Presented, Proc. 1972 Heat Transfer and Fluid Mechanics Institute.

Donaldson, C. dup and Varma, A.K. (1976) Remarks on the construction of a second order closure description of turbulent reacting flows. Combustion Science and Technology, 13, 1-6, 55.

Dopazo, C. and O'Brien, E.E. (1973) Isochoric turbulent mixing of two rapidly reacting chemical species with chemical heat release. Phys. of Fluids, 16, 12, 2075.

Durão, D.F.G. and Whitelaw, J.H. (1974a) Measurements in the region of recirculation behind a disc. Proc. 2nd International Workshop on laser velocimetry, Purdue Univ.

Durão, D.F.G. and Whitelaw, J.H. (1974b) Instantaneous velocity and temperature measurements in oscillating diffusion flames. Proc. Roy. Soc. (London), A338, 479.

Durão, D.F.G. (1976) The application of laser anemometry to free jets and flames with and without recirculation. Ph.D. Thesis, Univ. of London.

Durst, F., Melling, A. and Whitelaw, J.H. (1972) Laser anemometry, a report on EUROMECH 36, J. Fluid Mech., 56, 143.

Durst, F., Melling, A. and Whitelaw, J.H. (1974) Low Reynolds number flow over a plane symmetric expansion. J. Fluid Mech., 64, 111.

Durst, F., Melling, A. and Whitelaw, J.H. (1976) Principles and Practice of Laser Doppler Anemometry. Academic Press, London.

Edelman, R.B. and Fortune, O.F. (1969) A quasi-global chemical kinetic model for the finite rate combustion of hydrocarbon fuels with application to turbulent burning and mixing in hypersonic engines and nozzles. AIAA Paper 69-86.

ElGhobashi, S.E. (1974) Characteristics of gaseous turbulent diffusion flames in cylindrical chambers, a theoretical and experimental investigation. Ph.D. thesis, London Univ.

ElGhobashi, S.E. and Pun, W.M. (1974) A theoretical and experimental study of turbulent diffusion flames in cylindrical furnaces. Proc. 15th Symposium (International) on Combustion, 1353, the Combustion Institute, U.S.A.

ElGhobashi, S.E., Pun, W.M.and Spalding, D.B. (1975) Concentration fluctuations in isothermal turbulent confined coaxial jets. Imperial College, Dept. of Mech. Eng., report HTS/75/23.

El Mahallawy, F.M., Lockwood, F.C. and Spalding, D.B. (1975) An experimental and theoretical study of the turbulent mixing in a cylindrical gas fired furnace. Proc. European Symposium on Combustion, 633.

Evans, D.G. and Matthews, K.J. (1973) Computer predictions of burner fluid flow and heat release. C.E.G.B. report R/MR 179, U.K.

Farmer, W.M. (1973) Measurements of particle size, number density and velocity using a laser interferometer. Applied Optics, 11, 2603.

Favre, A. (1969) Statistical equations of turbulent gases, Problems of hydrodynamics and continum mechanics, Society of Industrial and Applied Mathematics, Philadelphia, 231.

Fenimore, C.P. (1970) Formation of nitric oxide in premixed hydrocarbon flames. Proc. 13th Symposium (International) on Combustion, 373, the Combustion Institute, U.S.A.

Fricker, N. and Leuckel, W. (1970) Draft report on trails NG-1. I.F.R.F. DOC. nr F35/2/4.

Fricker, N., Van Hyden, L. and Michelfelder, S (1971) Investigations into the combustion of natural gas in multiple burner systems. I.F.R.F. DOC. nr F35/2/5.

Fristrom, R.M. (1962) Radial concentrations and reactions in a methane oxygen flame. Proc. 9th Symposium (International) on Combustion, 560, the Combustion Institute, U.S.A.

Ghazzi, U., Orlalani, C.U. and Silvano, Pasini (1975) Nitric oxide formation in gas turbine combustion chambers. Italian flame days, San Remo.

Gordon, S. and McBride, B.J. (1971) Computer program for calculation of complex chemical equilibrium composition, rocket performance, incident and reflected shocks and Chapman-Jouguent detonations. NASA SP 273.

Gosman, A.D., Pun, W.M., Runchal, A.K., Spalding, D.B. and Wolfshtein, M. (1969), Heat and mass transfer in recirculating flows. Academic Press, London.

Gosman, A.D. and Lockwood, F.C. (1972) Incorporation of a flux model for radiation into a finite difference procedure for furnace calculations. Proc. 14th Symposium (International) on Combustion, 661, the Combustion Institute, U.S.A.

Gosman, A.D. and Lockwood, F.C. (1973) Predictions of the influence of turbulent fluctuations on flow and heat transfer in furnaces. Imperial College, Dept. of Mech. Eng. report HTS/73/52.

Gosman, A.D. and Pun, W.M. (1974) Calculation of recirculating flows. Imperial College, Dept. of Mech. Eng. report HTS/74/2.

Gosman, A.D., Khalil, E.E. and Launder, B.E. (1975) Computation of flows in ducts with sudden enlargements. Pennsylvania State University, College of Eng. report.

Gunther, R. and Simon, H. (1969) Turbulence intensity, spectral density fluctuations and Eulerion scales of emission in turbulent diffusion flames. Proc. 12th Symposium (International) on Combustion, 1069, the Combustion Institute, U.S.A.

Gunther, R. and Lenze, B. (1972) Exchange coefficients and mathematical models of jet diffusion flames. Proc. 14th Symposium (International) on Combustion, 687, the Combustion Institute, U.S.A.

Hanjalic, K. and Launder, B.E. (1972) A Reynolds stress model of turbulence and its application to asymmetric shear flows. J. Fluid Mechanics, 52, 609.

Harlow, F.H. and Nakayama, P.I. (1967) Turbulent transport equations. Phys. fluids, 10, 323.

Hawthorne, W.R., Weddell, D.S. and Hottel, H.C. (1949) Mixing and combustion in turbulent gas jets. 3rd Symposium on combustion, flame and explosion phenomena, 266.

Hilst, G.R., Donaldson, C. dup, Teske, M., Contilano, R. and Freiberg, J. (1973) The development and preliminary application of an invariant coupled diffusion and chemistry model. NASA CR 2295.

Hottel, H.C. and Sarofim, A.F. (1967) Radiative transfer. McGraw Hill Book Company, New York.

Hutchinson, P., Khalil, E.E., Whitelaw, J.H. and Wigley, G. (1975a) The calculation of furnace flow properties and their experimental verification. ASME paper 75-HT-8. See also, J. Heat Transfer, C98, 276, 1976.

Hutchinson, P., Khalil, E.E., Whitelaw, J.H. and Wigley, G. (1975b) Influence of the burner geometry on small scale furnaces performance. Proc. 2nd European Symposium on Combustion, 675.

Hutchinson, P., Khalil, E.E. and Whitelaw, J.H. (1976) The calculation of wall heat transfer rate and pollution formation in axisymmetric furnaces. Presented at 4th Members Conference of the IFRF, Ijmuiden.

Iverach, D., Basden, K.S. and Kirov, N.Y. (1972) Formation of nitric oxide in fuel-lean and fuel rich flames. Proc. 14th Symposium (International) on Combustion, 767, the Combustion Institute, U.S.A.

JANAF, Thermochemical tables, (1971) National Bureau of Standards, U.S.A. NSRDS 37, COM-71, 50363.

Jones, W.P. (1975) The effect of temporal fluctuations in temperature on nitric oxide formation. Combustion Science and Technology, 10, 93.

Jones, W.P. and Launder, B.E. (1973) Predictions of low Reynolds number phenomena with a two equation model of turbulence. Int. J. Heat and Mass Transfer, 16, 1119.

Kacker, S.C. and Whitelaw, J.H. (1971) The turbulence characteristics of two dimensional wall jet and wall wake flows. J. Appl. Mechanics, E 93, 239.

Kemp's (1975) Engineers Year Book, vol. 2.

Khalil, A.K., El Mahallawy, F.M. and Rafat, N.M. (1974) Theoretical and experimental study of mixing of two coaxial non swirling confined jets. Cairo Univ, Dept. of Mech. Eng., Report 18.

Khalil, E.E., Spalding, D.B. and Whitelaw, J.H. (1975) The calculation of local flow properties in two dimensional furnaces. Int. J. Heat and Mass Transfer, 18, 775. See also Imperial College, Dept. of Mech. Eng. report HTS/74/38, 1974.

Khalil, E.E. (1976) Effect of initial and boundary conditions on the computation of two dimensional recirculating flows. Imperial College, Dept. of Mech. Eng. report

Khalil, E.E. and Wigley, G. (1976a) Analysis of the experimental error in the laser anemometer velocity measurements and the temperature measurements in a small scale natural gas furnace. AERE report R/8470.

Khalil, E.E. and Whitelaw, J.H. (1976b) Aerodynamic and thermodynamic characteristics of kerosene spray flames. Proc. 16th Symposium (International) on Combustion.

Khalil, M.B. (1975) Analysis of different factors affecting the accuracy of temperature measurements in flames. M.Sc. Cairo Univ. Dept. of Mech. Eng.

Kolmogorov, A.N. (1942) Equations of turbulent motion of an incompressible fluid. Itr. Ak. Nauk, SSSR, 1942 (Translation from Russian by D.B. Spalding, 1968).

Kondratiev, V.N. (1964) Chemical kinetics of gas reactions. Pergamon Press, Oxford.

Launder, B.E. and Spalding, D.B. (1972) Mathematical models of turbulence. Academic Press, London.

Launder, B.E. and Spalding, D.B. (1973) The numerical computations of turbulent flows. Imperial College, Dept. of Mech. Eng. report HTS/73/2. See also Computer Methods in Applied Mechanics and Engineering, 3, 269, 1974.

Launder, B.E., Reece, G.J. and Rodi, W. (1975) Progress in the development of Reynolds stress turbulence closure. J. Fluid Mechanics, 68, 537.

Lenze, B., Milano, M.E. and Gunther, R. (1974) The mutual influence of multiple jet diffusion flames. Proc. 3rd Members Conference of the IFRF. See also Combustion Science and Technology, 11, 1, 1975.

Leuchter, O. (1974) Analyse numerique de la phase D'inflammation dans une couche de melange turbulente. AGARD meeting, Cp 164.

Leuckel, W. (1969) The effect of swirl on ignition and combustion behaviour of turbulent diffusion flames. IFRF DOC. nr K20/2/44.

Lilley, D. (1974) Swirl flow modelling for combustors. AIAA paper 74-527.

Lockwood, F.C. and Spalding, D.B. (1971) Predictions of a turbulent duct flow with significant radiation. Presented at Thermodynamics Colloquium, Societe Francaise de Physique, Evian, France.

Lockwood, F.C., El Mahallawy, F.M. and Spalding, D.B. (1974) An experimental and theoretical investigation on turbulent mixing in cylindrical furnaces. Combustion and Flame, 23, 283.

Lockwood, F.C. and Shah, N. (1976) Improved flux model for the calculation of radiation heat transfer in combustion chambers. ASME Paper 76-HT-55.

Lowes, T.M., Heap, M.P., Michelfelder, S. and Pai, B.R. (1972) Mathematical modelling of combustion chamber performance. Presented 4th Symposium on flames and industry, London.

Maccallum, N.R.L. (1975) Private Communication.

Mantle, P.L. (1966) A new type of roughened transfer surface selected by flow visualization techniques. Proc. 3rd Int. Heat Transfer Conference, 45, Chicago.

Mason, H.B. and Spalding, D.B. (1973) Prediction of reaction rates in turbulent premixed boundary layer flows. European Symposium on Combustion, 601.

Matthews, L. and Whitelaw, J.H. (1971) The prediction of film cooling in the presence of recirculating flows with a 2-equation model of turbulence.Imperial College,Dept.of Mech.Eng.Report HTS/71/31.

Mathur, M. and Maccallum, N.R.L. (1967) Swirling air jets issuing from vane swirlers. J. Inst. Fuel, Part 1, Free Jets, 40, 214, See also, J. Inst. fuel, Part 2, Enclosed Jets, 40, 317.

McLaughlin, D.K., and Tiederman, W.G. (1973) Biasing correction for individual realization of laser anemometer measurements in turbulent flows. Phys. fluids, 16, 2082.

McGuirk, J.J. (1971) Flame stabilization by recirculation. M.Sc. thesis, Univ. of London.

Melling, A. (1973) The influence of velocity gradient broadening on mean and rms velocities measured by laser anemometry. Imperial College, Dept. of Mech. Eng. report HTS/73/33.

Melling, A. (1975) Investigation of flow in non circular ducts and other configurations by laser Doppler anemometry. Ph.D. thesis, Univ. of London.

Michelfelder, S. and Lowes, T.M. (1974) Report on the M-2 trails. IFRF DOC. nr F36/2/4.

Monin, A.S. and Yaglom, A.M. (1971) Statistical fluid mechanics. Edited by J. Lumley, The MIT Press, Cambridge.

Morse, A.P. (1976) Private communication.

Naguib, A.S. (1975) The prediction of axisymmetrical free jet, turbulent reacting flows. Ph.D. Thesis, Univ. of London.

Odidi, A.O.O., (1974) The influence of turbulence on the time mean rate of chemical reactions. Ph.D. Thesis, Univ. of London.

Owen, F.K. (1975) Laser velocimeter measurements in free and confined coaxial jets with recirculation. AIAA paper 75-120.

Paauw, T.N.T.A. (1974) Some measurements and numerical calculations on turbulent diffusion flames. AGARD Meeting CP 164.

Pai, B.R. and Lowes, T.M. (1972) The predictions of flow, mixing and heat transfer in the Ijmuiden furnace. IFRF DOC nr G 02/2/22.

Palmer, H.B. and Beer, J.M. (1974) Combustion Technology, Some Modern Developments. Academic Press, New York.

Patankar, S.V. and Spalding, D.B. (1972) Mathematical models of fluid flow and heat transfer in furnaces, a review. Proc. 4th Symposium on flames and industry, London.

Pope, S.B. and Whitelaw, J.H. (1976) The calculation of near wake flows. J. of Fluid Mech., 73, 9.

Pope, S.B. (1976) The calculation of the flows behind bluff bodies with and without combustion. Ph.D. Thesis, London Univ.

Prandtl, L. (1925) Uber die Ausgebildete turbulenz. Zamm, 5, 136.

Prandtl, L. (1945) Uber ein neues formel System fur de Ausgebildete Turbulenz. Nachr. Akad. Wiss., Gottingen, Math-Phys. kl. p6.

Pun, W.M. and Spalding, D.B. (1967) A procedure for predicting the velocity and temperature distribution in confined, steady, turbulent, gaseous, diffusion flame. 18th International Astranautical Congress, Belgrade.

Rhines, J.M. (1974) Aerodynamic and heat transfer characteristics of proprietary burners fired with natural gas in a cylindrical furnace. 3rd Members Conference of the IFRF, Ijmuiden.

Rhines, J.M. (1975) Private communications.

Rhodes, R.P. and Harsha, D.T. (1972) On putting the turbulent in turbulent reacting flow. AIAA paper 72-68.

Ribeiro, M.M.M. (1976) The turbulence structure of free jet flows with and without swirl. Ph.D. thesis, Univ. of London.

Richardson, J.N., Howard, Jr. H.C. and Smith, Jr. R.W. (1953) The relation between sampling-tube measurements and concentration fluctuations in a turbulent gas jet. Proc. 4th Symposium (International) on Combustion, 814, The Combustion Institute, U.S.A.

Richter, W. (1976) Dissertation, Universitat Stutgart, (in vorbereitung).

Roberts, L.W. (1972) Turbulent swirling flows with recirculation. Ph.D. Thesis, London Univ.

Rotta, J.C. (1951) Statistische theorie nichthomogener turbulenz. Zeitsch F. Physik, 129, 541.

Self, S.A. and Whitelaw, J.H. (1976) Laser anemometry for combustion research. Combustion Science and Technology, 13, 171.

Schuster, A. (1905) Radiation through a foggy atmosphere, Astrophys. J., 21,1.

Shah, N. (1976) Private Communication.

Shvab, V.A. (1948) Relation between the temperature and velocity fields of the flame of a gas burner. Gos. Engerg.izd. Moscow, Leningrad.

Siddall, R.G. and Selquk, N. (1976). Two flux pherical harmonies modelling of two dimensional radiative transfer in furnaces. Int. J. Heat and Mass Transfer, 19, 313.

Singh, V.P. (1976) A study of turbulent flames stabilised in a high-velocity, high temperature flow. Combustion Science and Technology, to be published.

Spalding, D.B. (1970) Mixing and chemical reaction in steady confined turbulent flame. Proc. 13th Symposium (International) on Combustion, 649, the Combustion Institute, U.S.A.

Spalding, D.B. (1971) Concentration fluctuation in a round free jet. Chem. Engng, Sci., 26, 95.

Spalding, D.B. (1975) Lecture notes on combustion. Imperial College, Dept. of Mech. Eng.

Spalding, D.B. (1976) Models of turbulent flames, a review. Combustion Sciences and Technology, 13, 3.

Steward, F.R., Osuwan, S. and Picot, J.J. (1972) Heat transfer measurements in cylindrical test furnaces. Proc. 14th Symposium (International) on Combustion, 651, the Combustion Institute, U.S.A.

Styles, A.C. (1976) Application of suction pyrometer to two phase spray combustion. Univ. of Sheffield, Dept. of Chem. Eng. report.

Takagi, T., Ogaswara, M., Fujii, K. and Duizo, M. (1974) A study of nitric oxide formation in turbulent diffusion flames. Proc. 15th Symposium, (International) on Combustion, 1051, the Combustion Institute, U.S.A.

Thompson, D., Brown, T.D. and Beer, J.M. (1972) Formation of NO in a methane air flame. Proc. 14th Symposium (International) on Combustion, 787, the Combustion Institute, U.S.A.

Thompson, D., Vince, I.M. and Chigier, N.A. (1975) Effect of temperature fluctuations on NO formation. Proc. 2nd European Symposium on Combustion, 303.

Thring, M.W. and Newpy, M.P. (1953) Combustion length of enclosed turbulent jet flames. Proc. 4th Symposium (International) on Combustion, 789, the Combustion Institute, U.S.A.

Tribus, M. (1961) Thermostatics and Thermodynamics. D. Van-Nostrand, Co. Inc.

Truelove, J. (1975) Mathematical modelling of radiant heat transfer in furnace. AERE Report R 7817.

Truelove, J. (1976) Private communication.

Waldman, C.H., Wilson, R.P. and Engleman, V.S. (1974) Analyses of the kinetic mechanism of methane-air combustion with pollutant formation. EPA-68-02-0270-WSS/CI74-2, U.S.A.

Weinberg, F.J. (1963) Optics of Flames, Butterworth, London.

Weske, D.R. and Sturov, G. Ye (1974) Experimental study of turbulent swirled flows in cylindrical tube. Fluid Mechanics, Soviet research, 3, 77.

Whitacre, G.R. and McGann, R.A. (1975) Comparison of methods for the prediction of radiant heat flux distribution and temperature. ASME paper 75-HT-9.

Wigley, G. (1974) The application of radial diffraction gratings to laser anemometry. AERE report R-7886.

Wigley, G. (1976) Private communication.

Wilkie, D. (1966) Forced convection heat transfer from surfaces roughened by ribs. Proc. 3rd Int. Heat transfer conference, 1, Chicago.

Williams, F.A. (1965) Combustion theory, Reading Mass. Adison-Wesley.

Wu, H.L. and Fricker, N. (1971) An investigation of the behaviour of swirling jet flames in a narrow cylindrical furnace. 2nd Members Conference of the IFRF.

Yanta, W.J. (1973) Turbulence measurements with laser-Doppler velocimeter. Naval Ordnance Laboratory, Silver Spring, Maryland, NOLTR-73-94.

Zeldovich, Y.B. (1949) On the theory of combustion of initially unmixed gases. Zhur. Tekhn. Fiz., 19, No. 10. English translation, N.A.C.A. Tech. Mem, 1296, 1950.

APPENDIX A1

CALCULATION OF SWIRL NUMBER

The most commonly used parameter to characterize swirling flows is the swirl number defined by the equation;

$$S = 2\, G_\Phi / G_x\, D_e \qquad \text{A1.1}$$

where

$$G_\Phi = 2\pi \int_{R_1}^{R_2} Wr\, \rho U\, rdr$$

$$G_x = 2\pi \int_{R_1}^{R_2} U\, \rho U\, rdr$$

R_1, R_2 are the inner and outer diameters of the swirler and D_e is the burner exit throat diameter. In the present work, the swirl vanes were placed upstream the burner annulus exit as shown in figure 3.1.1 and hence the swirl number was determined at the annulus exit, 170 mm from the swirler, from measured distributions of U and W at the burner exit, obtained with laser anemometry. Two swirl vanes were used in the present work and the corresponding profiles of U and W are shown in figures A 1.1 and A 1.2. The swirl numbers for the individual swirlers were obtained by integrating the momentum fluxes and substituting in equation A1.1. The corresponding swirl numbers were 0.3079 and 0.52.

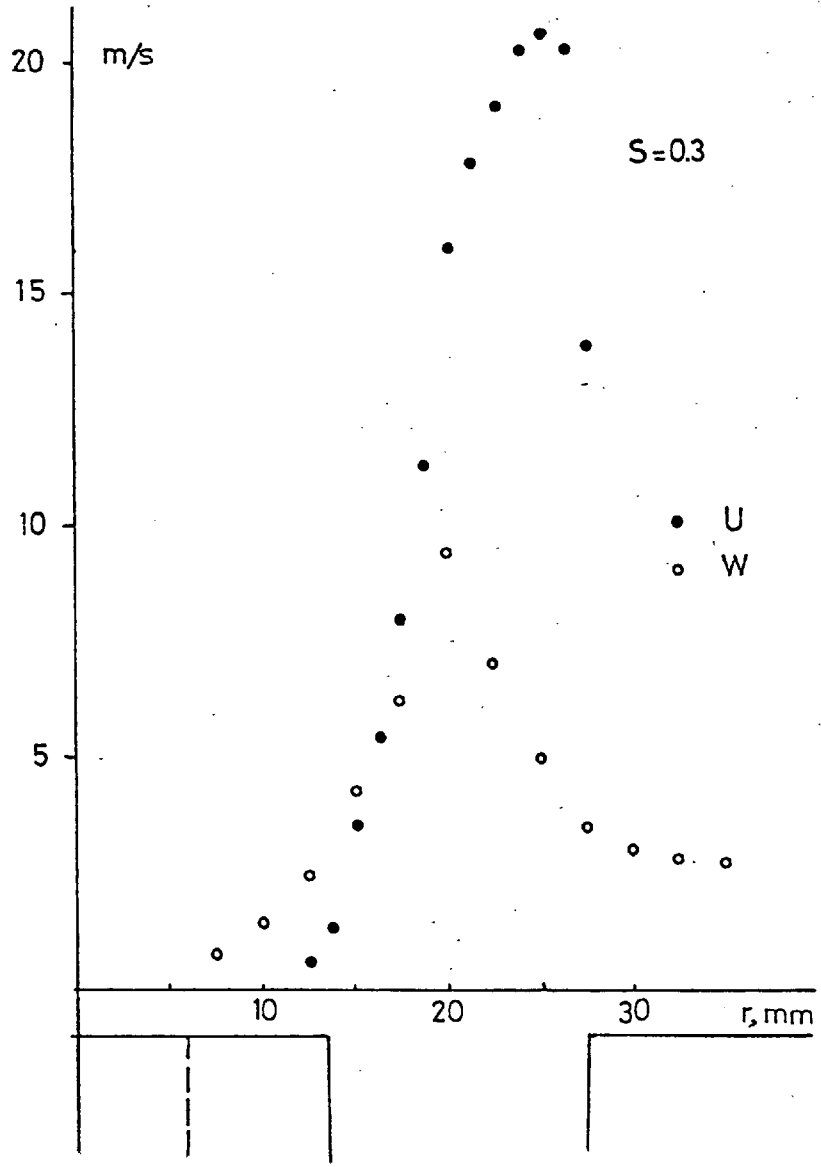

Figure A1.1:Measured profiles of U and W at burner exit
S= 0.3

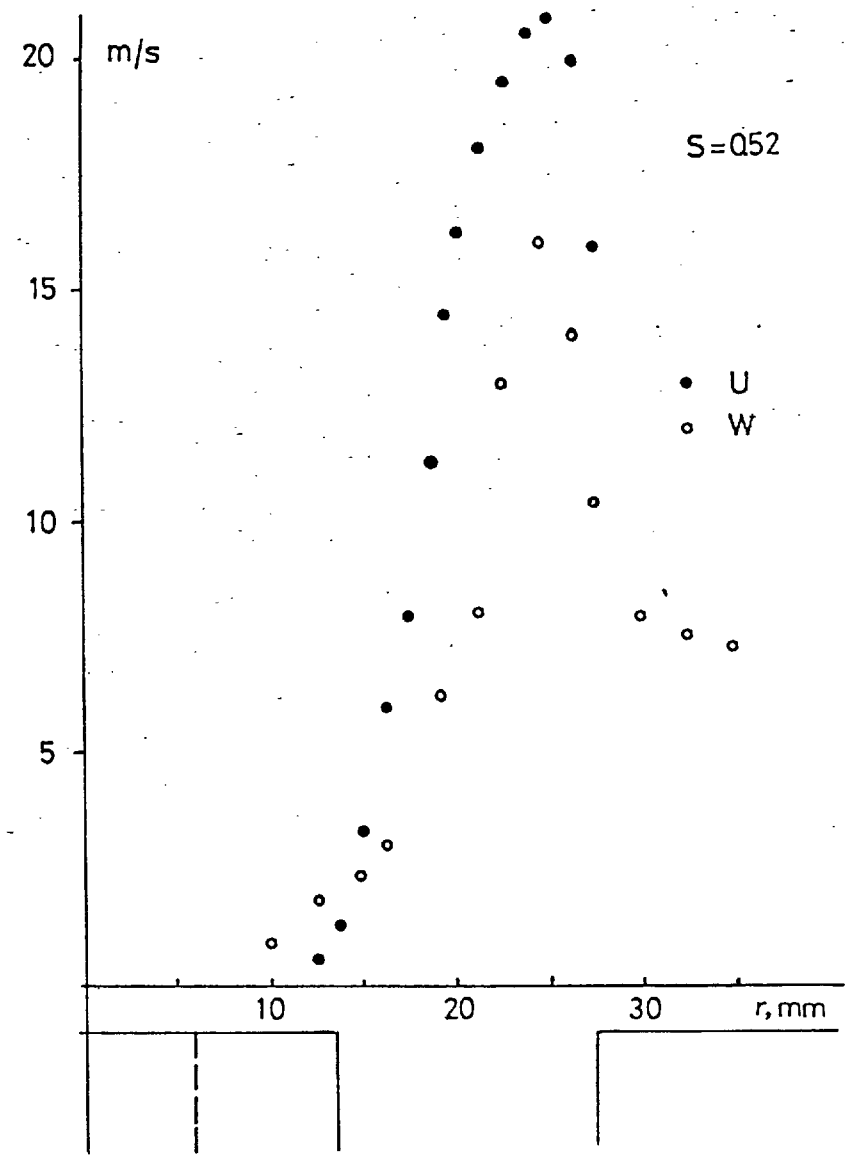

Figure A1.2:Measured profiles of U and W at burner exit
S= 0.52

APPENDIX A2

MEASUREMENTS OF THREE VELOCITY COMPONENTS IN A MODEL FURNACE WITH AND WITHOUT COMBUSTION

R. J. BAKER,* P. HUTCHINSON,† E. E. KHALIL,‡ AND J. H. WHITELAW§

Measured values of three components of mean velocity and the corresponding normal stresses are reported in the flow within an enclosure which is representative of a small-scale furnace with an axi-symmetric, swirling flow configuration. The measurements were obtained in isothermal air flow and in a combusting mixture of air and natural gas, exit swirl numbers of zero and 0.52 were investigated for both the isothermal and combusting cases. A laser anemometer was used to obtain the measurements and comprised an argon-ion laser, a rotating diffraction grating as beam splitter and frequency shifter, transmission and collection optical components, a photomultiplier and a filter-bank signal processor. The grating provided a frequency shift of ±0.54 MHz and allowed measurements in regions of high turbulence intensity and negative mean velocity. The filter bank consisted of 50 filters spanning the range from 0.6 to 6 MHz which, with the frequency shift indicated above and the optical arrangement employed, corresponded to a measurable velocity range of −2 m/sec to 23 m/sec.

Measured values of mean axial velocity and the corresponding normal stress are presented for the four flow conditions of zero and finite swirl, with and without combustion. The turbulent-kinetic energy is presented for the isothermal cases and the regions of near-isotropic turbulence identified, only the axial and tangential normal stresses were measured for the combusting cases. The measurements were designed to be used for the evaluation of turbulent-flow prediction procedures. They demonstrate, for example, that the regions of recirculation are substantially different for the combusting measurements and that the turbulence is far from isotropic over most of the flow fields; similarly, the velocity-probability-density distributions indicate that Gaussian turbulence exists in only negligible regions of the flows.

Introduction

The measurements presented in this paper were obtained in four flow configurations downstream of a co-axial jet and contained within a cylindrical enclosure, as shown on Fig. 1. The enclosure was designed to result in flow configurations which closely resemble those in an axi-symmetric furnace and the experiment is intended to provide data against which two-dimensional flow-modelling calculation procedures can be tested. The four flows correspond to isothermal air emerging from the annulus and jet with swirl numbers of zero and 0.52 and to air and natural gas emerging from the annulus and jet with swirl numbers of zero and 0.52 and burning in the enclosure.

A laser anemometer was used to obtain measurements of the three velocity components and their correlations in each of the above flows. In particular, this instrumentation allowed detailed measurements in regions of flow recirculation without disturbance of the flow. It made use of a bank of filters to process the signal from the photomultiplier and this allowed velocity-probability-density distributions to be obtained at each measuring station. These distributions yielded values of mean velocity and of all single-point correlations of the fluctuating velocity, though with a precision which worsens with increasing order of correlation. The results reported

* Formerly Research Associate at Imperial College, London. Now at Electro Watt Engineering Services, London W1.

† Principle Scientific Officer, AERE, Harwell.

‡ Research Student, Imperial College, London.

§ Professor of Convective Heat Transfer, Imperial College, London.

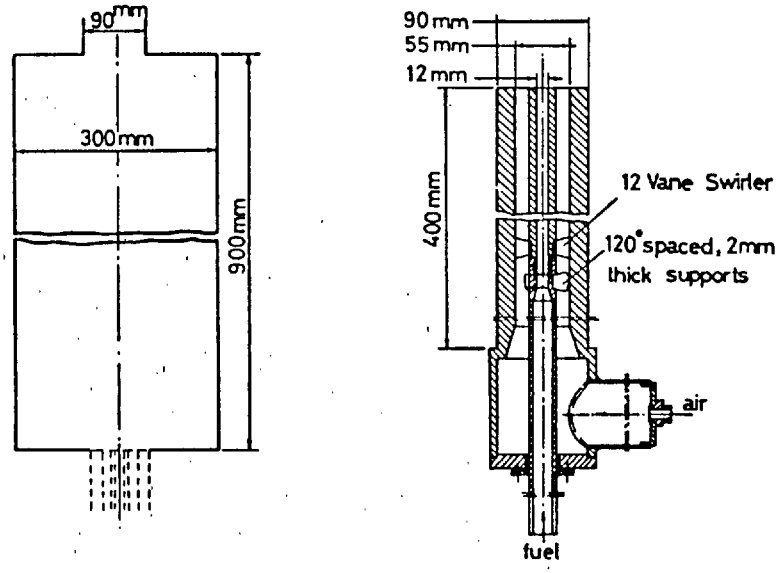

FIG. 1. Flow enclosure and co-axial burner.

here are restricted to mean velocity components and the corresponding normal stresses due to space limitations and because these properties are most urgently needed for testing purposes.

Previous measurements, in flow configurations similar to those investigated have been reported, for example, by Afrosimova,[1] Mather and MacCallum,[2] Wingfield,[3] Wu and Fricker,[4] and Beltagui and MacCallum.[5] These measurements are reported in less detail than is necessary for present purposes and, because of the lack of suitable instrumentation, do not include measurements of velocity correlations in regions of recirculation or combustion.

The following sections of the paper describe the equipment and associated procedures and the results; the equipment is not described in detail where reference can be made to a previous publication. The Results section includes relevant discussion and assessment of errors arising from the instrumentation. The paper ends with a summary of relevant conclusions.

Equipment and Experimental Procedures

The present section describes, in turn, the furnace arrangement, the instrumentation and the experimental procedure.

Furnace Arrangement

The furnace arrangement is shown on Fig. 1 together with relevant dimensions. For measurements with isothermal air, compressed air was supplied through pressure regulators to the core and annulus of the burner. The volumetric flow rates were measured with rotameters and adjusted to provide a mass axial–velocity ratio similar to that necessary to ensure overall stoichiometry when the air through the central tube was replaced by natural gas (CH_4 81.3%; N_2 14.4%: C_2H_6 2.9%). For the particular case of isothermal flow with zero swirl, the central tube was blocked off at its exit. With this exception the central jet Reynolds numbers were 0 and 0.21×10^4 for the isothermal flows and 0.4×10^4 for the combusting flows: the annulus Reynolds number was 1.75×10^4 for all measurements. The annulus flows were seeded with small concentrations of titanium dioxide particles obtained from a fluidized bed: the seeding rate corresponded to a volumetric concentration of approximately 5×10^{-12}, i.e., 100 particles of 0.5 μm diameter per ml of air, and was of the same order in both isothermal and combusting flows.

For the isothermal-air measurements, a perspex enclosure was used and was replaced by a water-cooled, steel enclosure for the combusting measurements. The steel enclosure was fitted with diametrically opposed 100 mm diameter quartz windows. This enclosure and the optical arrangement were moved axially with respect to the burner and the end plates and allowed measurements at all axial locations within the enclosed space. The thermal-wall boundary condition for the steel enclosure closely approximated a uniform temperature of 570°K.

Instrumentation

The laser anemometer and its signal-processing system was similar to that described by Baker.[6] It comprised an Argon-ion laser, operating at 488 nm and 200 mW, a rotating diffraction grating and an integrated transmission optical arrangement. The forward-scattered light was collected and passed, through a pin hole to a photomultiplier. The circular grating had a total of 10 800 lines and was rotated at 3000 rpm by a synchronous motor. The first order diffraction patterns were, therefore, shifted by ± 0.54 MHz from the laser-light frequency to give a total frequency difference between the beams of 1.08 MHz. The angle between the light beams was 8.6°.

The signal-processing system comprised a bank of filters with an oscilloscope display and digital-voltmeter read out of the content of each filter. It consisted of fifty filters in the frequency range 0.631 to 6.025 MHz and, with the frequency shift provided by the rotating grating and the present optical geometry, corresponds to a velocity range from approximately -2 m/sec to 23 m/sec. The velocity distribution was displayed on the oscilloscope and the stored integrator amplitudes corresponding to each filter read from the digital voltmeter and supplied to a computer program which evaluated the true velocity-probability-distribution from which the mean frequency, its rms and corresponding skewness and flatness factors were determined. Further details of the performance and operating functions of the filter bank have been reported by Baker.[7]

Experimental Procedures

The optical arrangement was aligned in its fixed position and the centre-line of the burner and the enclosure aligned with the three-dimensional traverse arrangement in the vertical position. The air and gas supplies were adjusted, with the aid of rotameters, to give the required velocity ratio between the central-jet and annulus flow. The air passed through a fluidised bed of titanium dioxide particles. The signal from the photomultiplier was monitored on an oscilloscope and processed by the filterbank.

The measuring-control volume was located in the desired position and the frequency distribution accumulated. After a total of approximately 5×10^5 signal bursts, the amplitude corresponding to each filter was recorded, in turn, from the digital voltmeter. The results were subsequently punched on computer cards for further analysis. The burner and end plates were traversed to allow measurements at different locations in the flow field. Each probability distribution was evaluated to provide the values of mean velocity and normal stresses presented in the next section: skewness and flatness factors were also obtained but are not presented.

Before making the detailed measurements of the next section, the symmetry of the axial velocity was tested on two orthogonal diameters at values of x/R_o of 1.11 and 8.8 and for a swirl number of 0.52; the maximum deviation in mean velocity between any set of four radial traverses at the same value of x/R_o was less than 0.1%. For each of the flow conditions of the results presented in the next section, the measured profiles included the exit plane of the central-jet and annulus flows and led to measured values of the swirl number: this is in contrast to the results of previous authors where swirl numbers were estimated rather than measured.

Results

Contours of measured values of mean-axial velocity are presented on Fig. 2 for swirl numbers of zero and 0.52 and for isothermal flow and combusting natural gas. A comparison between the isothermal flows indicates that the swirling flow has a substantial region of recirculation on the axis in contrast to the non-swirling flow, the size of the recirculation region in the corner of the enclosure is, however, larger in the case of the non-swirling flow. For the combusting flows, a comparison between the zero-swirl and finite-swirl flows indicates similar behaviour to that for the isothermal flows. It can also be seen that the regions of recirculation are generally longer with combustion: this observation is consistent with the larger values of axial velocities which are to be seen and which stem from the combustion and the associated reductions in density.

Figure 3 presents axial normal stresses corresponding to the mean-velocity measurements of Fig. 2. Very large values of normal stress can be observed particularly in regions of low mean velocity and, indeed, the magnitude of all recorded values of normal stress exceed 0.2.

Figure 4 presents values of turbulent kinetic energy obtained with the two isothermal flows and identifies regions where the flow was close to isotropic $[1.2 \geq (\overline{v^2})^{1/2}/(\overline{u^2})^{1/2},\ (\overline{w^2})^{1/2}/(\overline{u^2})^{1/2} \geq 0.8]$, on this occasion, and because of the absence of a predominant mean velocity, the contours are presented in dimensional form. The contours of turbulent kinetic energy for the case of zero

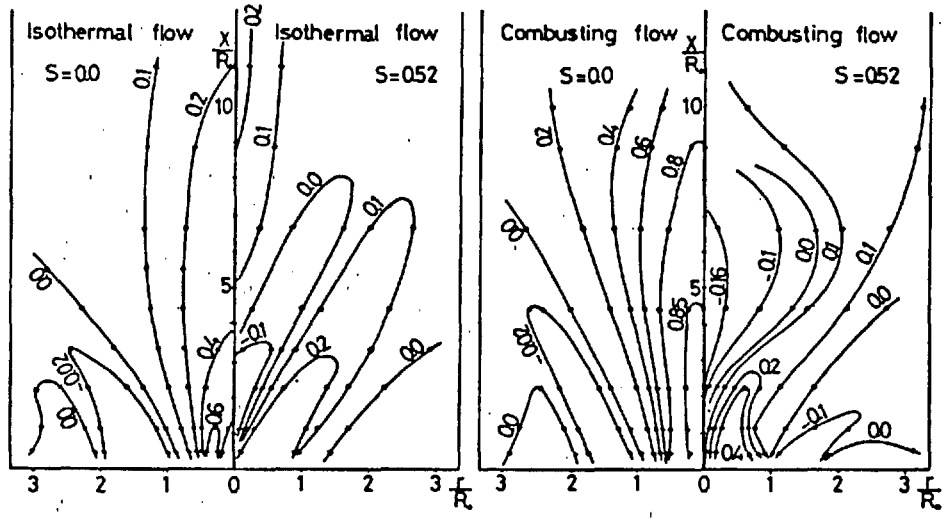

FIG. 2. Contours of constant velocity (U/U_a) for swirl numbers of 0.0 and 0.52 and for isothermal and combusting flow.

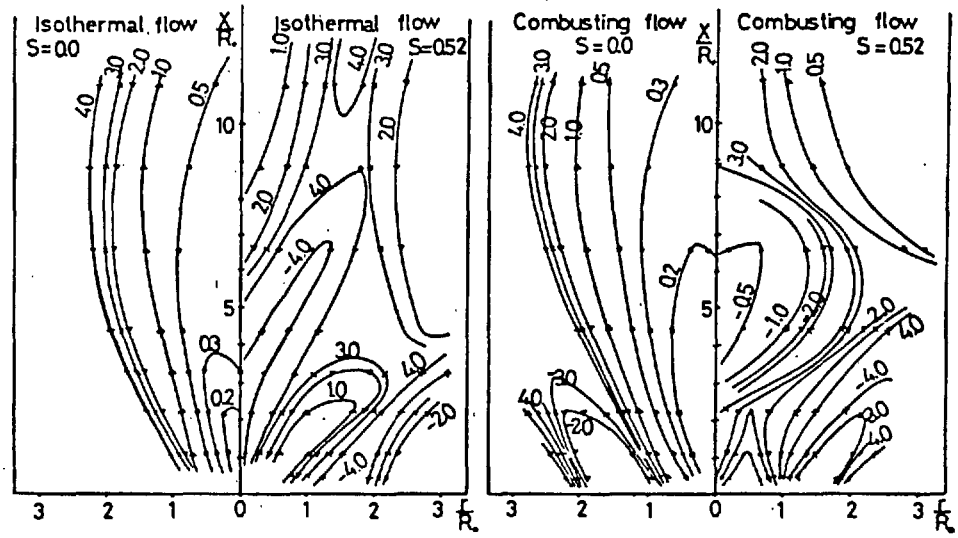

FIG. 3. Contours of normal stress $[(\overline{u^2})^{1/2}/U]$ for swirl numbers of 0.0 and 0.52 and for isothermal and combusting flow.

swirl are similar to the corresponding contours of axial normal stress shown on Fig. 3. In contrast, the contours of turbulent kinetic energy for a swirl number of 0.52 are very different to those of the axial normal stress and demonstrate the need for the separate consideration of the three normal stresses in any model of the turbulent flow. The extent of the isotropy of the flow is indicated by the hatched region of Fig. 4 and can be seen, even within the specified limits, to be comparatively small for the case of finite swirl and only slightly larger for zero swirl.

In the case of combusting flows, the finite dimensions of the windows prevented extensive measurements of the radial velocity component and it is, therefore, not possible to present values of turbulent kinetic energy. It is possible to indicate regions of the flow where the criterion, $1.2 \geq (\overline{w^2})^{1/2}/(\overline{u^2})^{1/2} \geq 0.8$, is satisfied and these are identified on Fig. 5, the corresponding flow

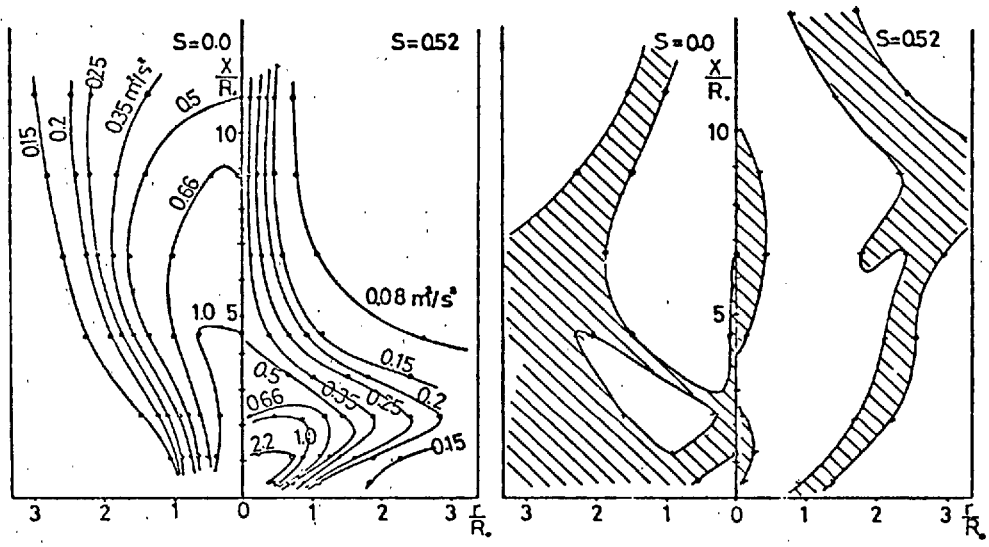

FIG. 4. Contours of turbulent kinetic energy for swirl numbers of 0.0 and 0.52 and flow regions of near isotropy-isothermal flow. Hatched area represents $1.2 \geq (\bar{v}^2/\bar{u}^2)^{1/2}$, $(\bar{w}^2/\bar{u}^2)^{1/2} \geq 0.8$.

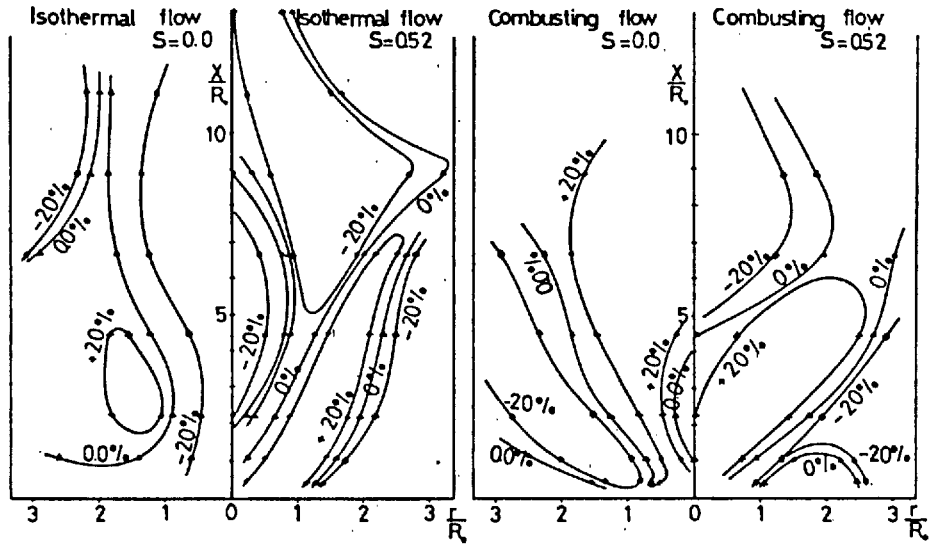

FIG. 5. Contours representing deviations between the axial and circumferential normal stresses.

regions for isothermal flow are identified for comparison. The effect of the combustion, with zero swirl, is to reduce the regions of the flow for which the axial and tangential stresses are within 20% of each other: this reduction is much less for the case of a swirl number of 0.52.

It is also of interest to note that the velocity probability distributions measured along the center line of the non-swirling flows were more Gaussian with combustion than without. This was not so evident with the swirling flows but, in all cases, substantial regions of the flow had probability distributions which were far from Gaussian. No bimodality was observed.

The results described in the previous paragraph, and presented in greater detail in Ref. 8 are subject to some uncertainty and the following comments relate to the likely magnitude of errors arising from known sources. Possible errors due to velocity-gradient broadening, refractive-index variations and the filterbank were considered and, where appropriate, corrections applied. The procedures suggested by Melling[9] were used to estimate the magnitude of gradient-

broadening corrections and showed that the maximum error in the mean-velocity values was less than 0.1%, the corresponding errors in normal stresses were less than 1% except close to the wall where a correction of 4.5% was required. The plexiglass wall of the isothermal-flow enclosure caused refraction of the light beams and resulted in displacements of the measuring control volume: the maximum calculated displacement was 1.5 mm and corrections were applied. Possible errors associated with the use of the filterbank have been discussed in Ref. 7, in the present case, each measured probability distribution was made up of 5×10^5 values of instantaneous velocity and the analysis of Ref. 7 suggests that the maximum error in rms frequencies should not exceed 0.5% and that the mean frequency is not subject to any significant error.

The sources of error discussed in the previous paragraph are of little significance to the conclusions which can be extracted from the present data and to their value for comparison with turbulent-flow calculation procedures. In the region of the reaction zone and in the mixing region immediately downstream of the burner exit, the measurements may be subject to additional uncertainties associated with the particle distribution and its correlation with temperature. In the case of the swirling flame, both regions represent a very small part of the total flow regime, in the non-swirling flow the reaction zone extended to a value of x/R_o of approximately 8 but again represented a comparatively small region of the flow.

Conclusions

1. The laser anemometer has been used to obtain measurements of three components of velocity and the corresponding correlations in non-swirling and swirling flow, with and without combustion: the measurements were obtained mainly to facilitate the evaluation of two-dimensional calculation procedures embodying turbulence and combustion models.

2. The isothermal results quantify the effect of a change from a swirl number of zero to one of 0.52 and demonstrate that swirl results in the presence of a region of recirculating flow on the burner axis with a smaller corner region of recirculation. The non-isotropy of the isothermal flows is indicated as is the need for consideration of the three normal stresses in appropriate turbulence models.

3. The combustion results also quantify the effect of a change from a swirl number of zero to one of 0.52. They reveal larger forward velocities than the isothermal measurements and correspondingly larger regions of recirculation. As expected the swirl substantially reduced the length of the flame but also tended to increase the non-isotropic region of the flow.

Nomenclature

- k turbulent kinetic energy $\frac{1}{2}(\bar{u}^2+\bar{v}^2+\bar{w}^2)$, m^2/sec^2
- r radius, m
- R_o outer radius of the co-axial burner, m
- S swirl number (angular momentum of flow in exit plane of burner/axial momentum of flow in exit plane of burner $\times R_o$)
- U mean axial velocity, m/sec
- U_a average mean axial velocity at exit from annulus, m/sec
- u fluctuating axial velocity, m/sec
- v fluctuating radial velocity, m/sec
- w fluctuating tangential velocity, m/sec
- x axial distance along centre line from burner exit, m

REFERENCES

1. Afrosimova, V. N.: Thermal Engineering (USSR) *14*, 10 (1967).
2. Mather, M. L. and MacCallum, N. R. L.: J. Inst. Fuel. *40*, 238 (1967).
3. Wingfield, G. J.: J. Inst. Fuel. *40*, 456 (1967).
4. Wu, H. L. and Fricker, N.: An investigation of the behaviour of swirling jet flames in a narrow cylindrical furnace, International Flame Research Foundation, Document K20/a/61 (1971).
5. Beltagui, S. A. and MacCallum, N. R. L.: Combustion Institute European Symposium, 559 (1973).
6. Baker, R. J.: The application of a filterbank to measurements of turbulence in a fully-developed jet flow, Atomic Energy Research Establishment Report 7648 (1974). See also Proc. of Laser Velocimetry Workshop, Purdue University (1974).
7. Baker, R. J.: A filterbank processor for laser anemometry, Atomic Energy Research Establishment Report 7652 (1974).
8. Baker, R. J., Hutchinson, P., Khalil, E. E. and Whitelaw, J. H.: Measurements of three velocity components and their correlations in a model furnace with and without combustion and swirl, Imperial College, Mechanical Engineering Report HTS/74/29 (1974).
9. Melling, A. The influence of velocity-gradient broadening on mean and rms velocities measured by laser anemometry, Imperial College, Mechanical Engineering Department, Report HTS/73/33 (1973).

COMMENTS

A. K. Gupta, Sheffield University, England. Would the authors like to comment on the term "combustion generated turbulence"?

R. Gunther, University of Karlsruhe, F.R. Germany. Have your fluctuations of velocities been higher in flames or in isothermal flow? Please give data.

Authors' Reply. Professor Gunther and A. Gupta have asked the same question in different ways. The experiments show that the rms of the velocity fluctuations tends to increase at any particular location in the flow as a consequence of combustion. It is, however, unsatisfactory to attempt to compare the fluctuations obtained with and without combustion at the same location since the characteristics of the entire flow are significantly different. A more satisfactory procedure, though still far from perfect, is to compare the integral of the rms of the velocity fluctuations over the entire furnace volume for the isothermal and combustion cases. In the present case, measured profiles of the rms values of the axial and tangential velocity fluctuations were integrated over the radius at each measurement station and summed: the results indicate an increase from .0140 m^3/sec to .0175 m^3/sec for the non-swirling flow and 0.0220 m^3/sec to 0.0360 m^3/sec for the swirling flow. Thus it is clear that, as a consequence of the combustion, the velocity fluctuations have increased significantly.

Possible explanations for increases in velocity fluctuations in combusting flows are not difficult to find but are difficult to substantiate. Bray[1] has shown that the equation for turbulent kinetic energy contains terms which take account of combustion but whose magnitude remains to be quantified. It is clear, however, that the mean velocity gradients are greater in the present combusting flows and this would suggest that the production term, i.e., $\langle u_i u_i \rangle (\partial U_i / \partial X_i)$ would be greater in the combusting case.

REFERENCE

1. Bray, K. N. C.: Equations of Turbulent Combustion, PART 1, University of Southampton, Department of Aeronautics and Astronautics, Report AASU 330, 1973.

APPENDIX A 3

The experimental results of the present work are listed in this Appendix. Eight non-reacting flow cases and six reacting flow situations were considered. The table of this appendix lists the flow Reynolds number, burner geometry, swirl number and the figures displaying the results relevant to each case.

Flow situations	Type	R_e	Burner Quarl	S	Figures
Case 1	I	1.75×10^4	-	0.0	1 to 7
2	I	1.75×10^4	-	0.52	8 to 14
3	I	1.75×10^4	-	0.3	see Khalil (1976)
4	I	4.70×10^4	-	0.0	15
5	I	4.7×10^4	-	0.52	see Hutchinson et al (1975)
6	I	4.7×10^4	20^o	0.0	see Khalil (1976)
7	I	4.7×10^4	20^o	0.3	16 to 18
8	I	4.7×10^4	20^o	0.52	19 to 21
Flame 1	B	1.75×10^4	-	0.0	22 to 26
2	B	1.75×10^4	-	0.52	27 to 31
3	B	4.7×10^4	-	0.52	see Hutchinson et al (1975)
4	B	4.7×10^4	20^o	0.3	32 to 40
5	B	4.7×10^4	20^o	0.52	see Hutchinson et al (1975)
6	B	4.7×10^4	20^o	0.52	41 to 49

I. non reacting

B. reacting

Table A.3.1

	Case 1	Case 2	Case 4	Case 7	Case 8
R_e	1.75×10^4	1.75×10^4	4.7×10^4	4.7×10^4	4.7×10^4
Swirl number	0.0	0.52	0.0	0.3	0.52
Inlet profiles	1	8	-	16	19
mean axial velocity	2	9	15	17	20
r.m.s. axial velocity	3	10	-	17	20
mean radial velocity	4	11	-	-	-
r.m.s. radial velocity	4	11	-	-	-
mean tangential velocity	-	12	-	-	-
r.m.s. tangential velocity	5	12	-	-	-
kinetic energy	6	13	-	-	-
probability distribution	7	14	-	18	21

Case 3 see Khalil (1976)

Case 5 see Hutchinson (1975)

Case 6 see Khalil (1976)

Table A.3.2

	flame 1	flame 2	flame 4	flame 6
R_e Swirl number	1.75×10^4 0.0	1.75×10^4 0.52	4.7×10^4 0.3	4.7×10^4 0.52
Inlet profiles	-	-	32	41
mean axial velocity	22	27	33	42
r.m.s. axial velocity	23	28	34	43
mean tangential velocity	-	29	35	44
r.m.s. tangential velocity	24	29	35	44
kinetic energy	25	30	36	45
probability distribution	26	31	37	46
wall temperature	-	-	38	47
mean gas temperature	-	-	39	48
wall heat flux	-	-	40	49

flame 3 see Hutchinson et al (1975)

flame 5 see Hutchinson et al (1975)

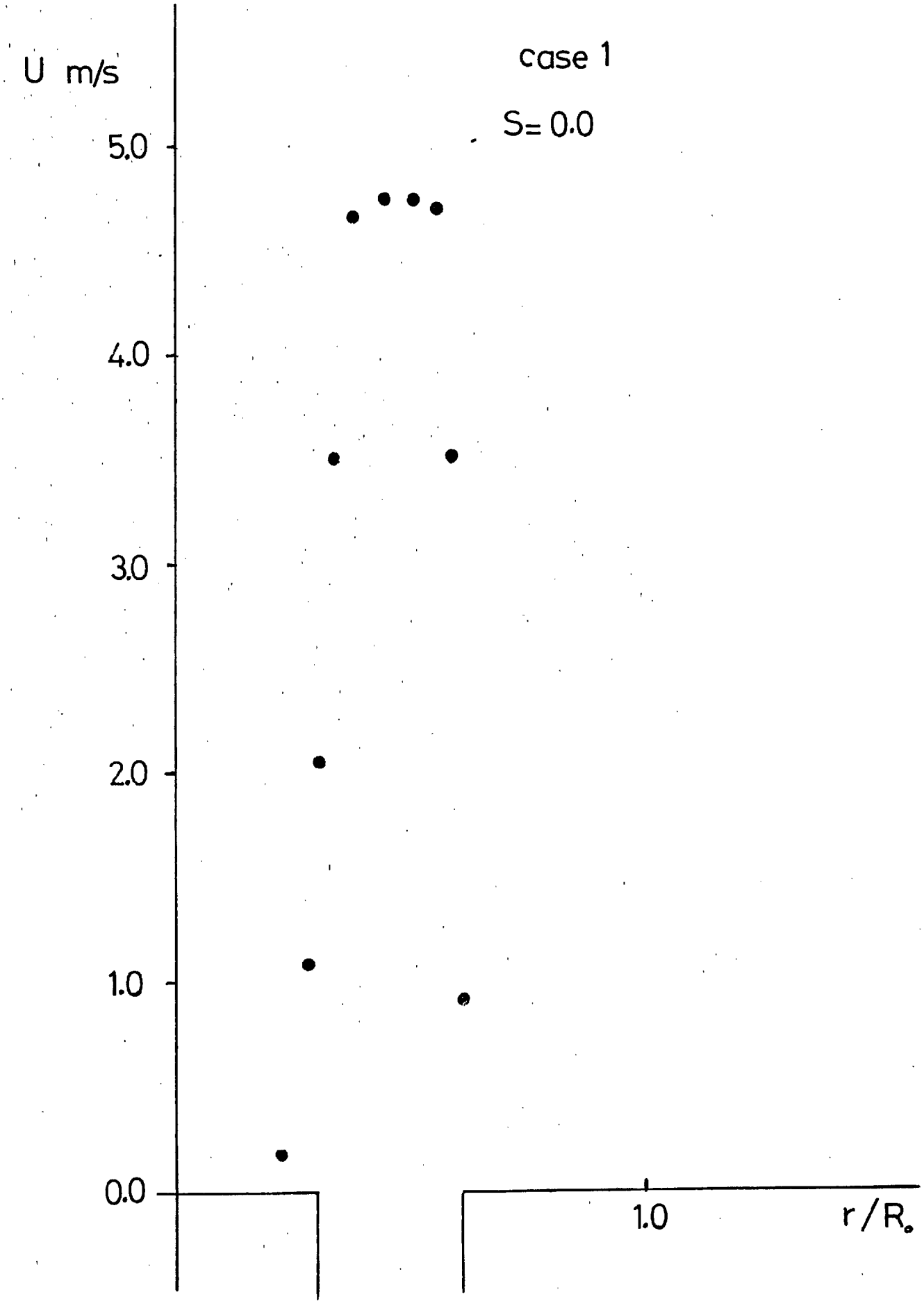

Figure A3.1 :Measured axial velocity profile at burner exit (S=0.0)

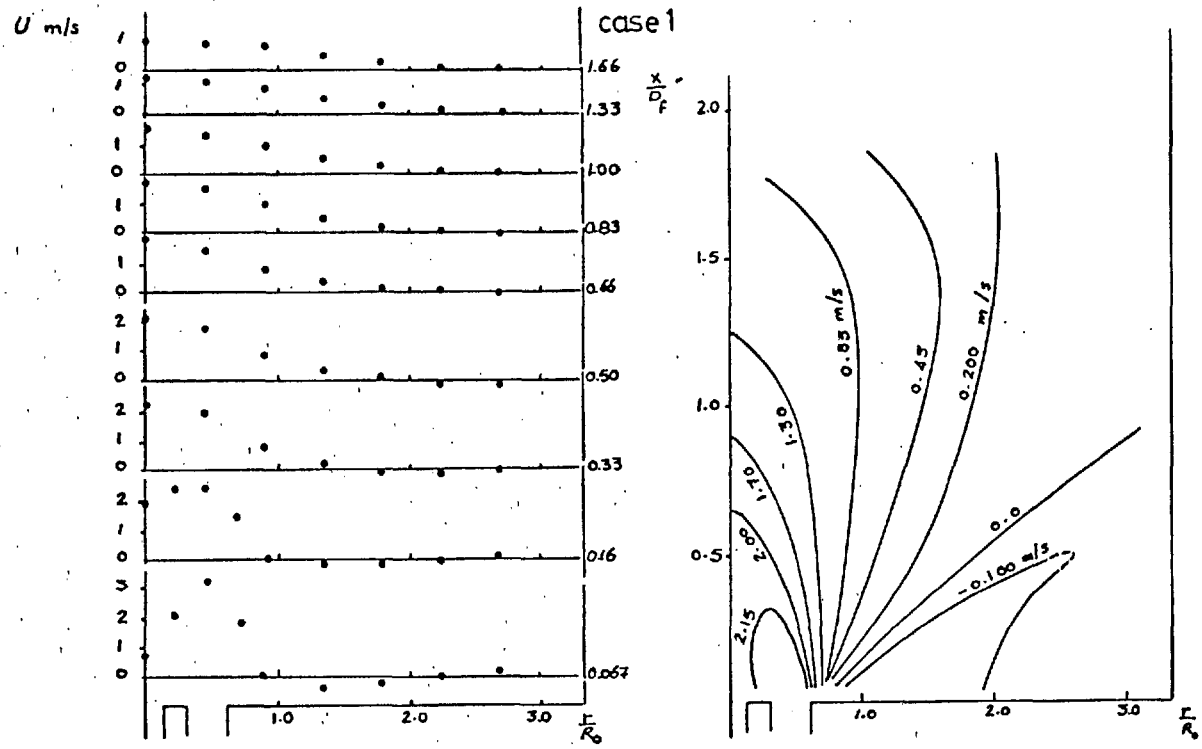

Figure A3.2:Measured mean axial velocity profiles and contours (isothermal flow,S=0.0)

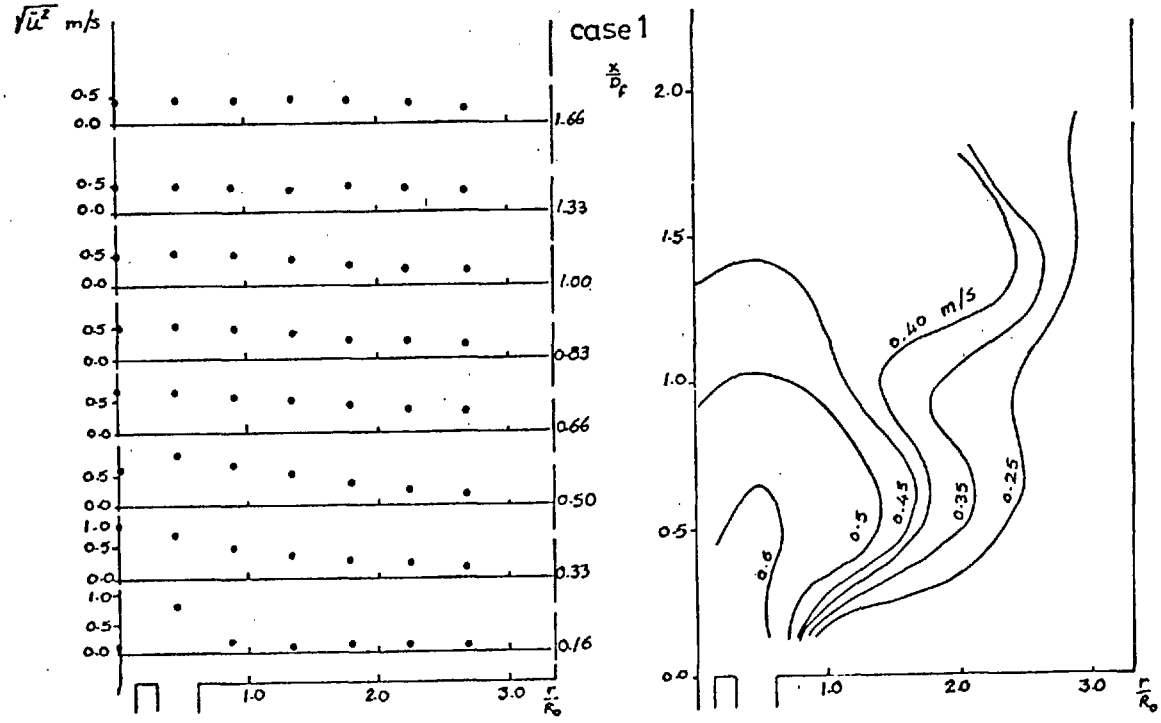

Figure A3.3:Measured axial normal stress profiles and contours (isothermal flow,S=0.0)

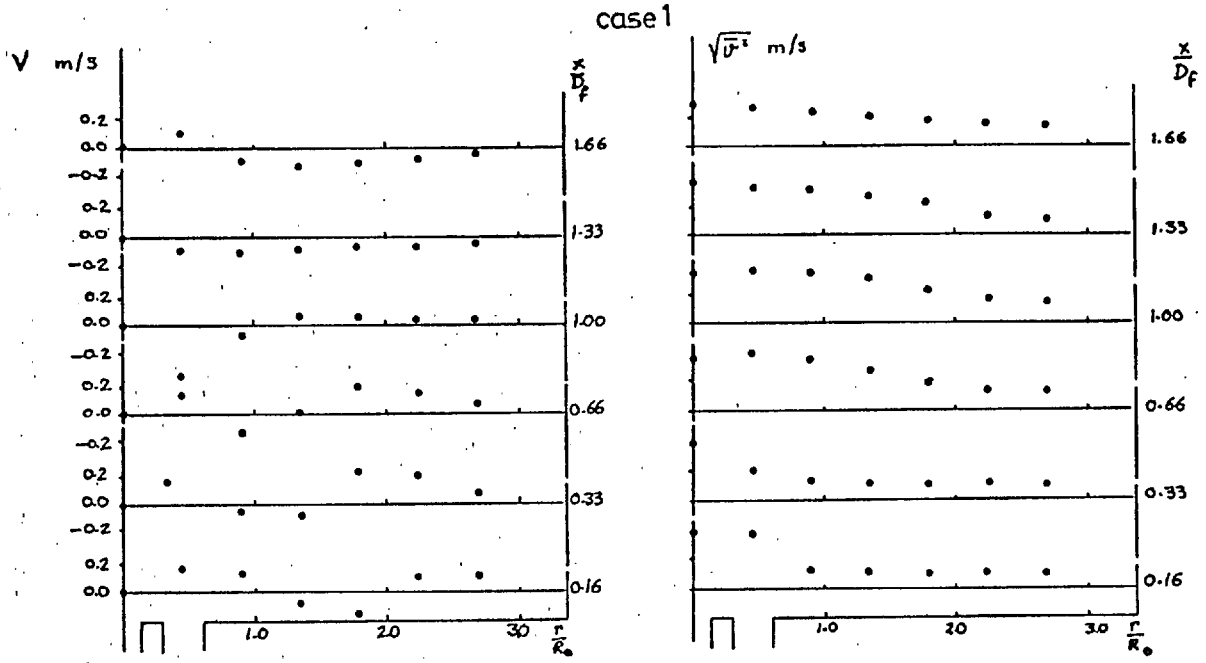

Figure A3.4:Measured mean radial velocity and normal stress profiles (isothermal flow,S=0.0)

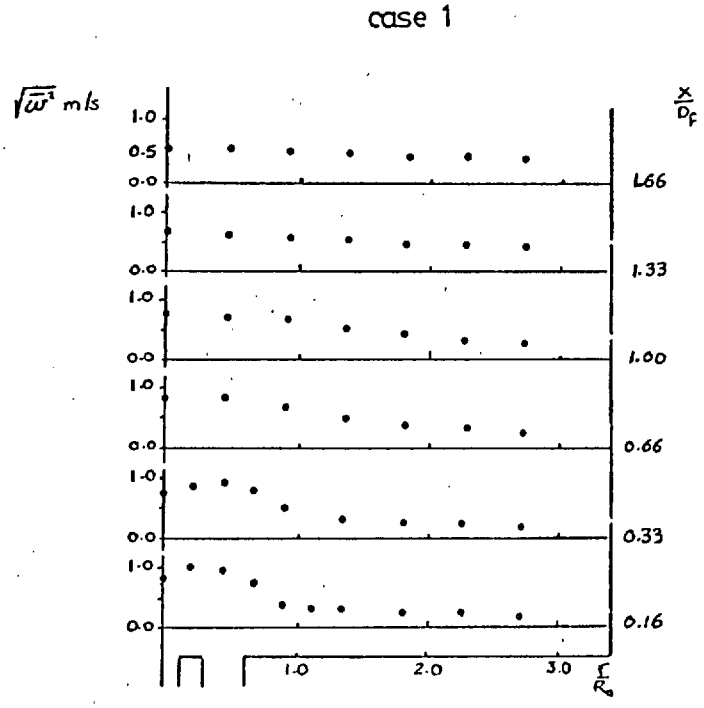

Figure A3.5:Measured tangential normal stress profiles (isothermal flow,S=0.0)

N.B. No mean tangential velocity component.

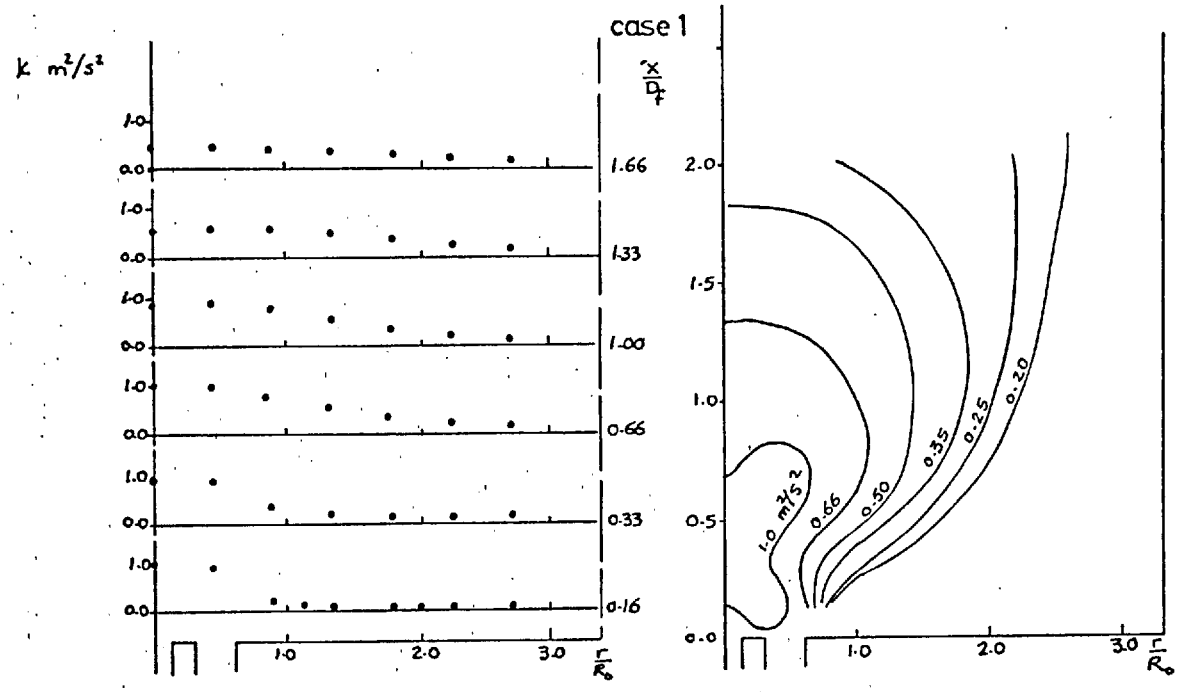

Figure A3.6:Measured kinetic energy of turbulence profiles and contours.
(isothermal flow,S=0.0)

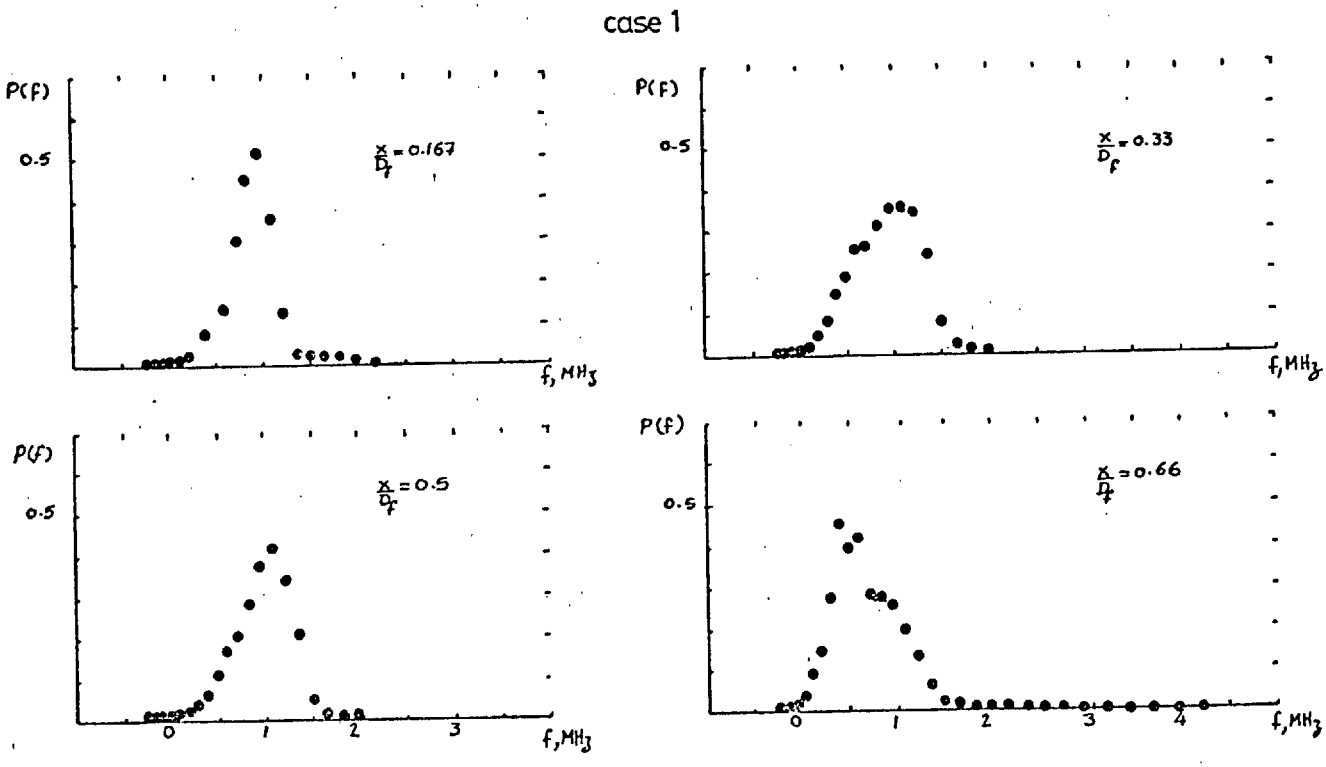

Figure A3.7:Velocity probability distribution along the centreline.
(isothermal flow,S=0.0)

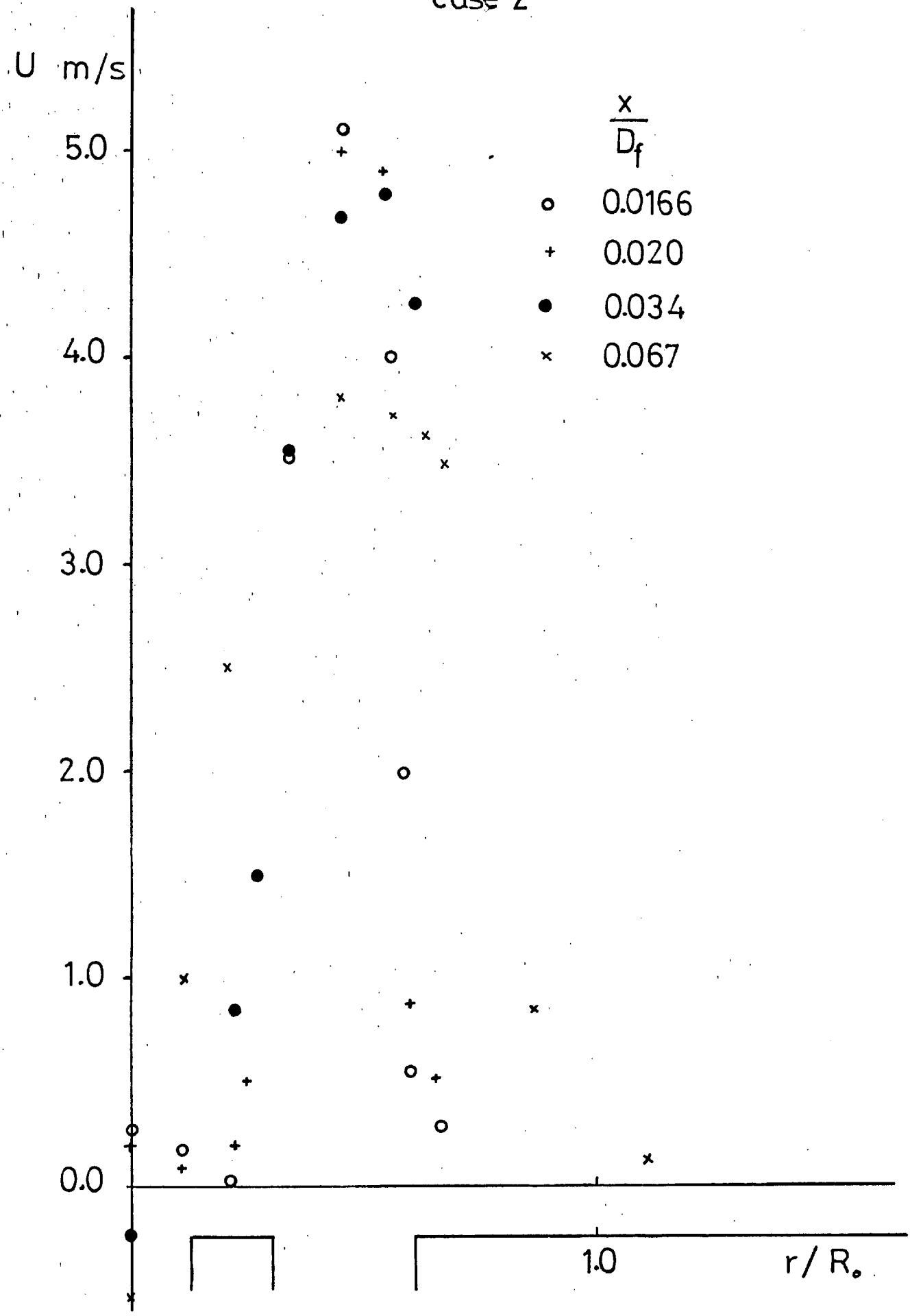

Figure A3.8:Measured axial velocity profile at burner exit(S=0.52)

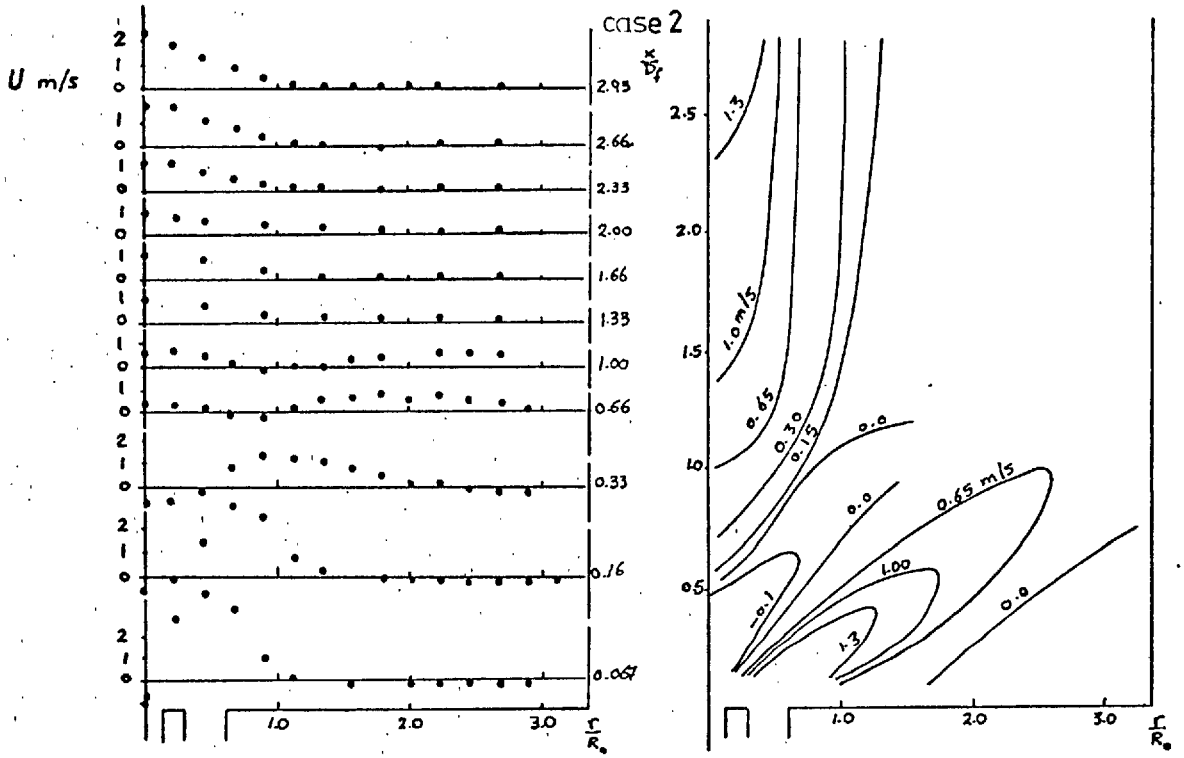

Figure A3.9:Measured mean axial velocity profiles and contours (isothermal flow,S=0.52)

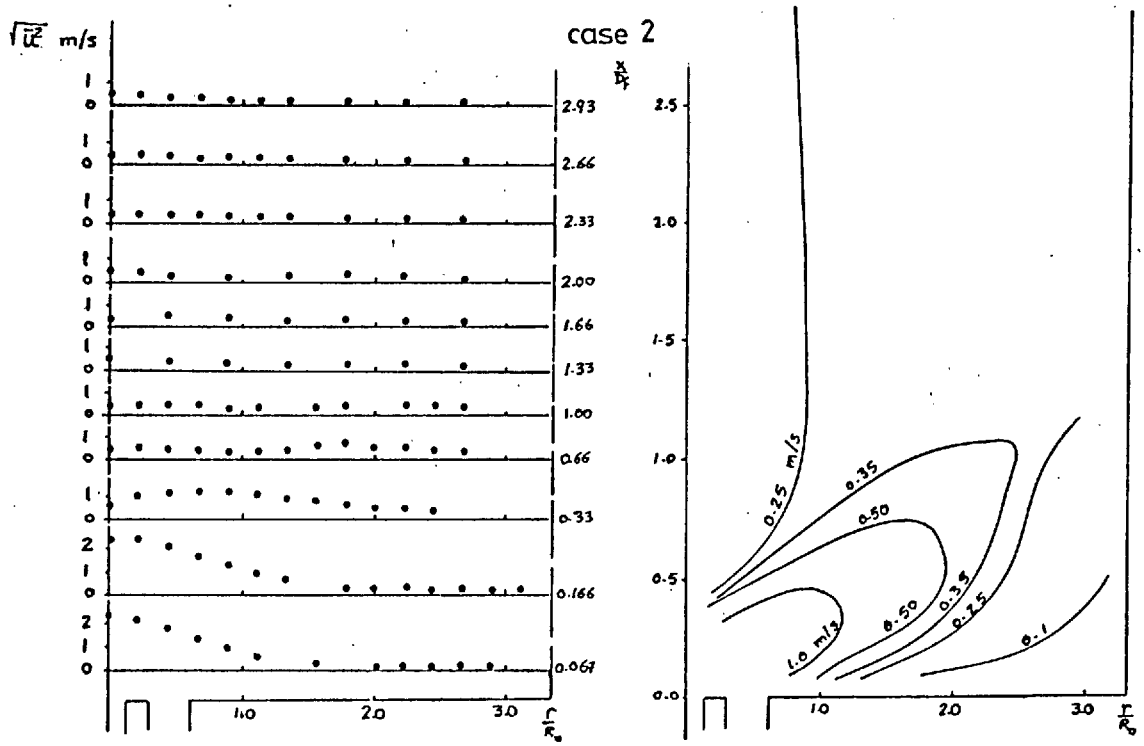

Figure A3.10:Measured axial normal stress profiles and contours (isothermal flow,S=0.52)

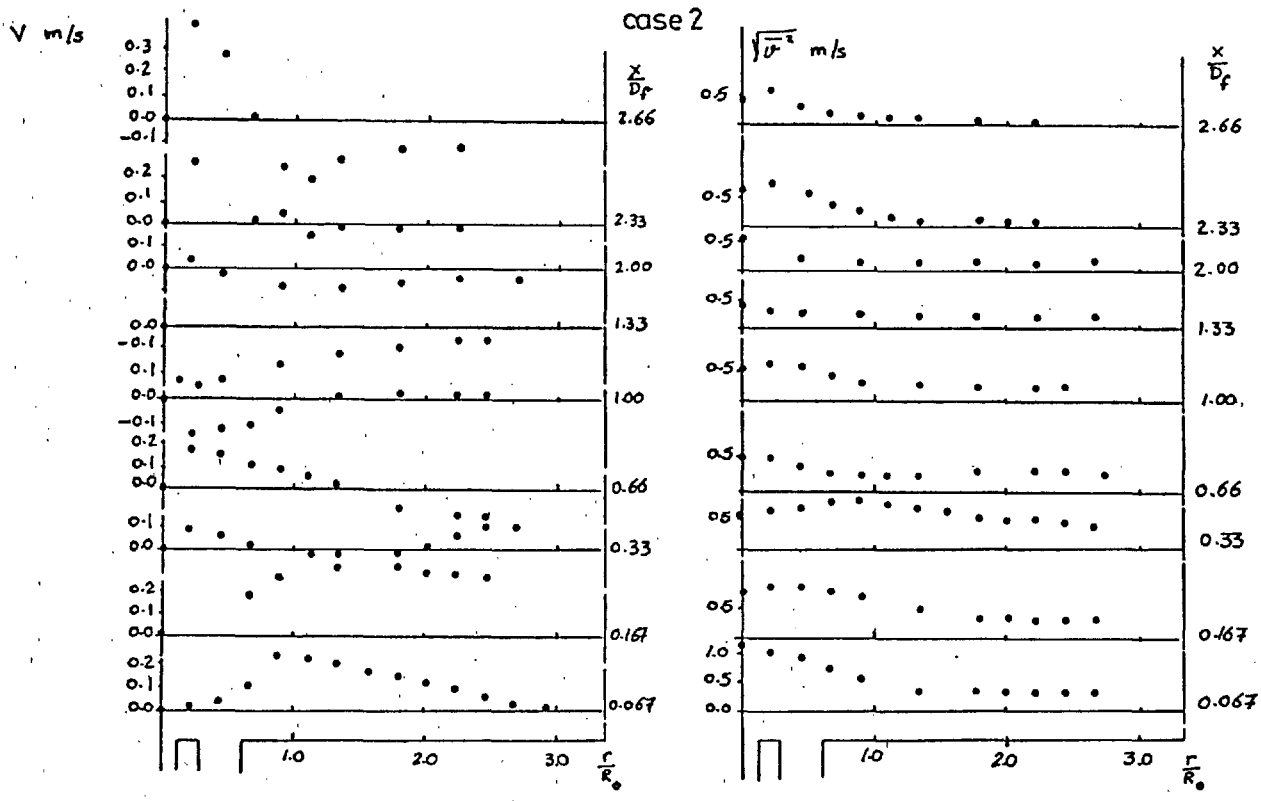

Figure A3.11:Measured mean radial velocity and normal stress profiles.
(isothermal flow,S=0.52)

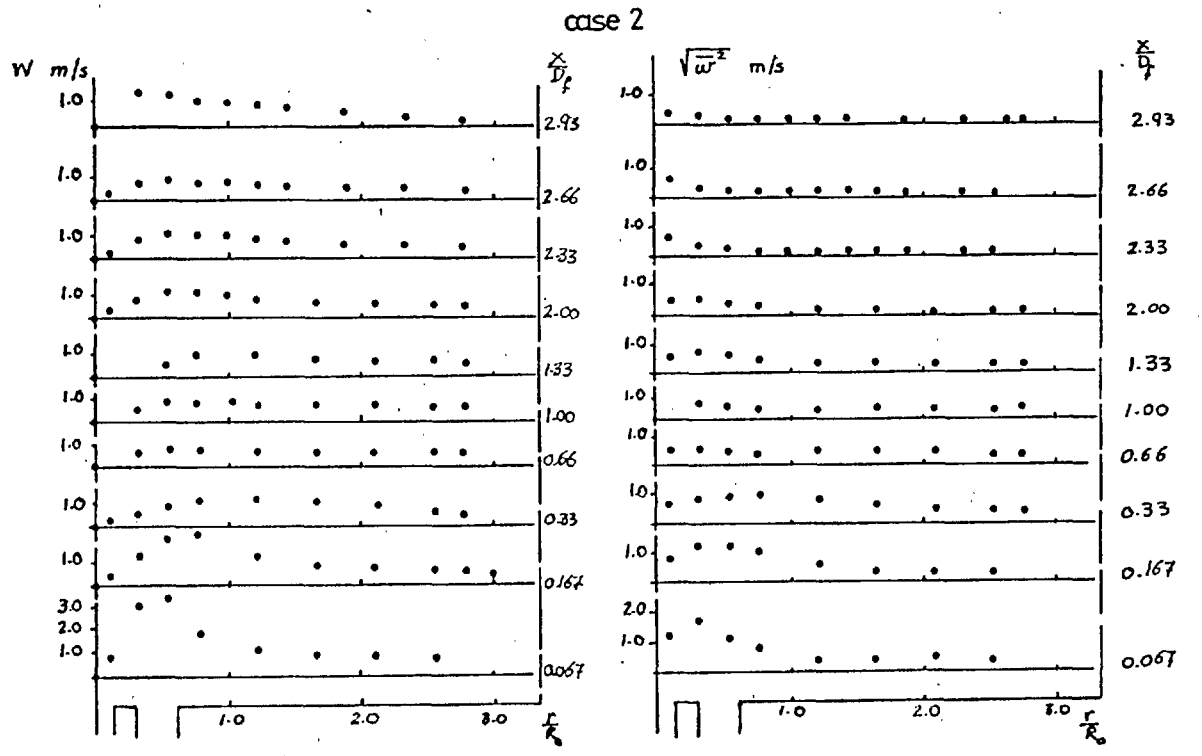

Figure A3.12:Measured mean tangential velocity and normal stress profiles.
(isothermal flow,S=0.52)

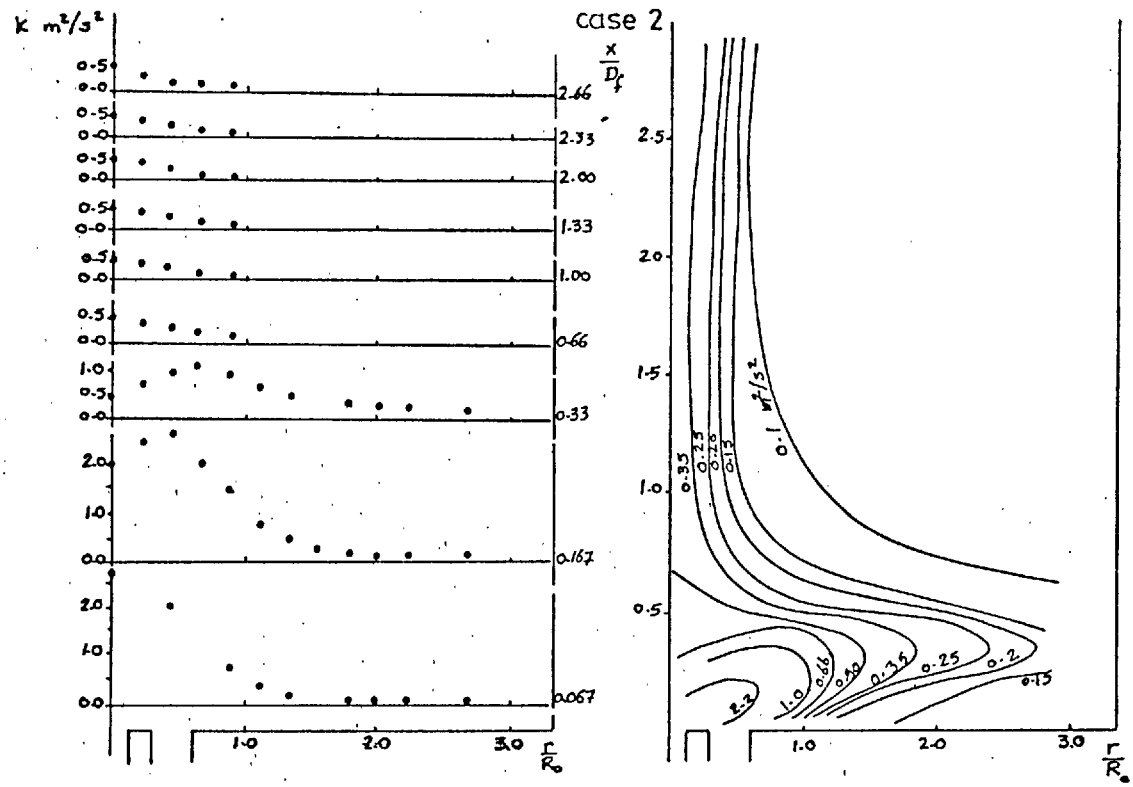

Figure A3.13:Measured kinetic energy of turbulence profiles and contours (isothermal flow,S=0.52)

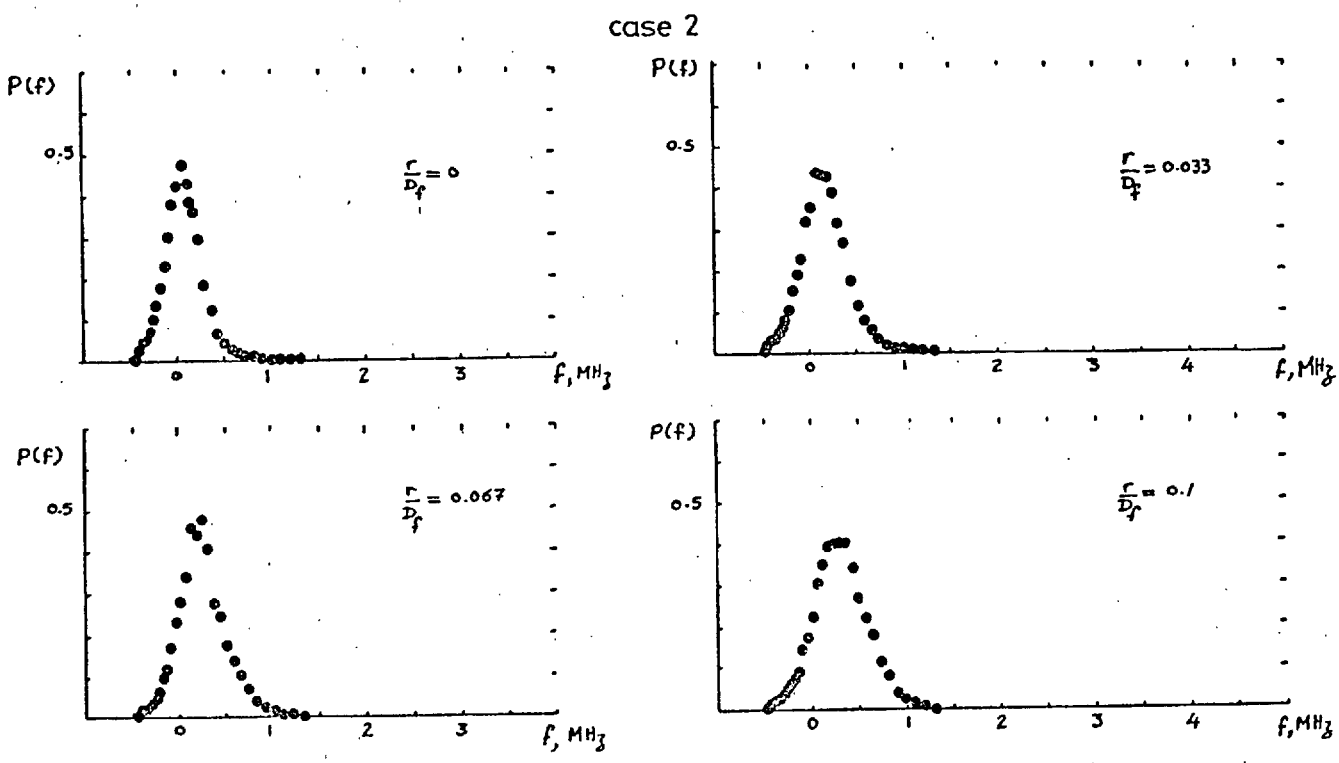

Figure A3.14:Velocity probability distributions at various locations. (isothermal flow,S=0.52,x/D_f=0.5)

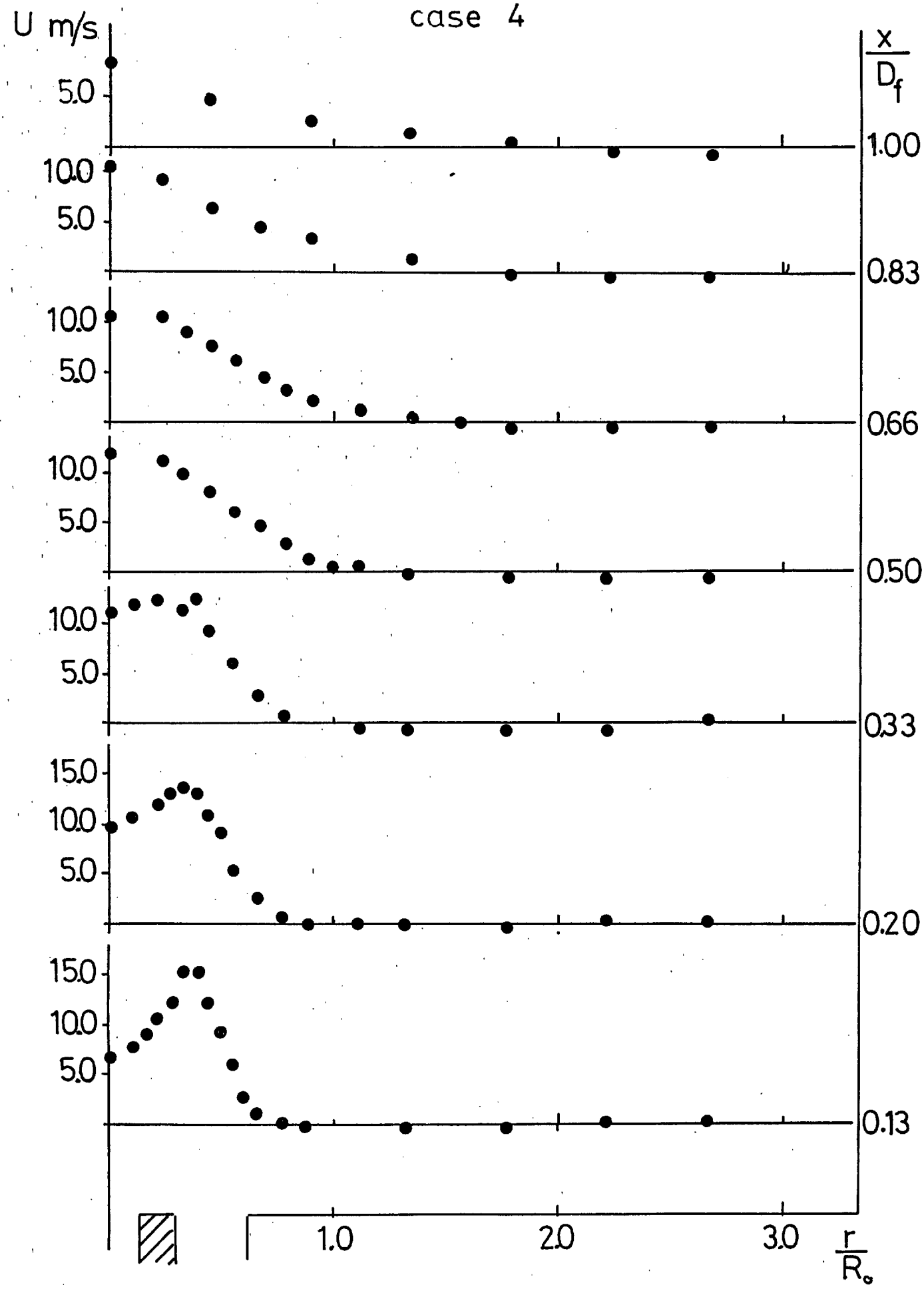

Figure A3.15:Measured mean axial velocity profiles.

(isothermal flow,S=0.0)

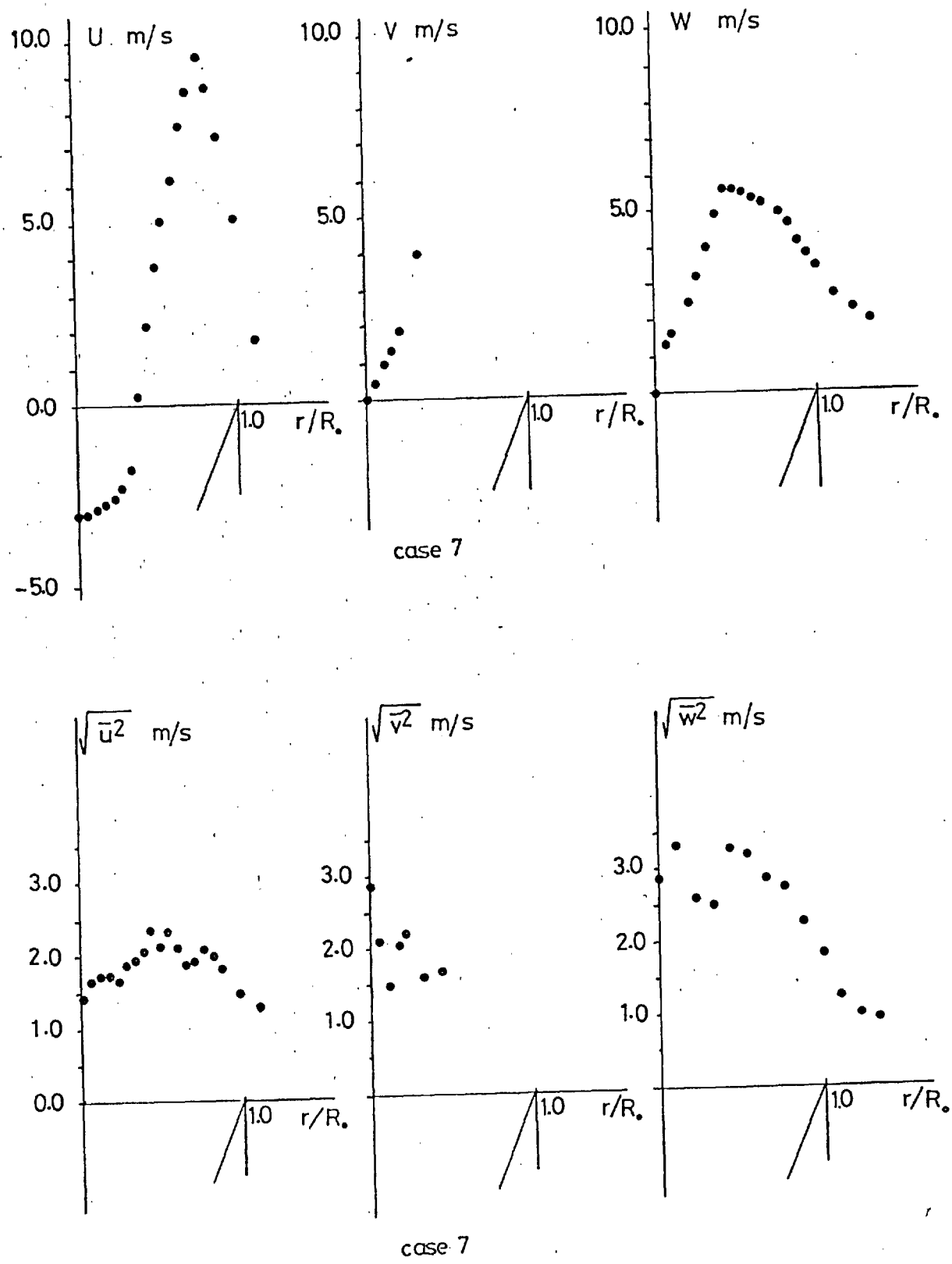

Figure A3.16:Measured velocity profiles at burner exit (S=0.3)

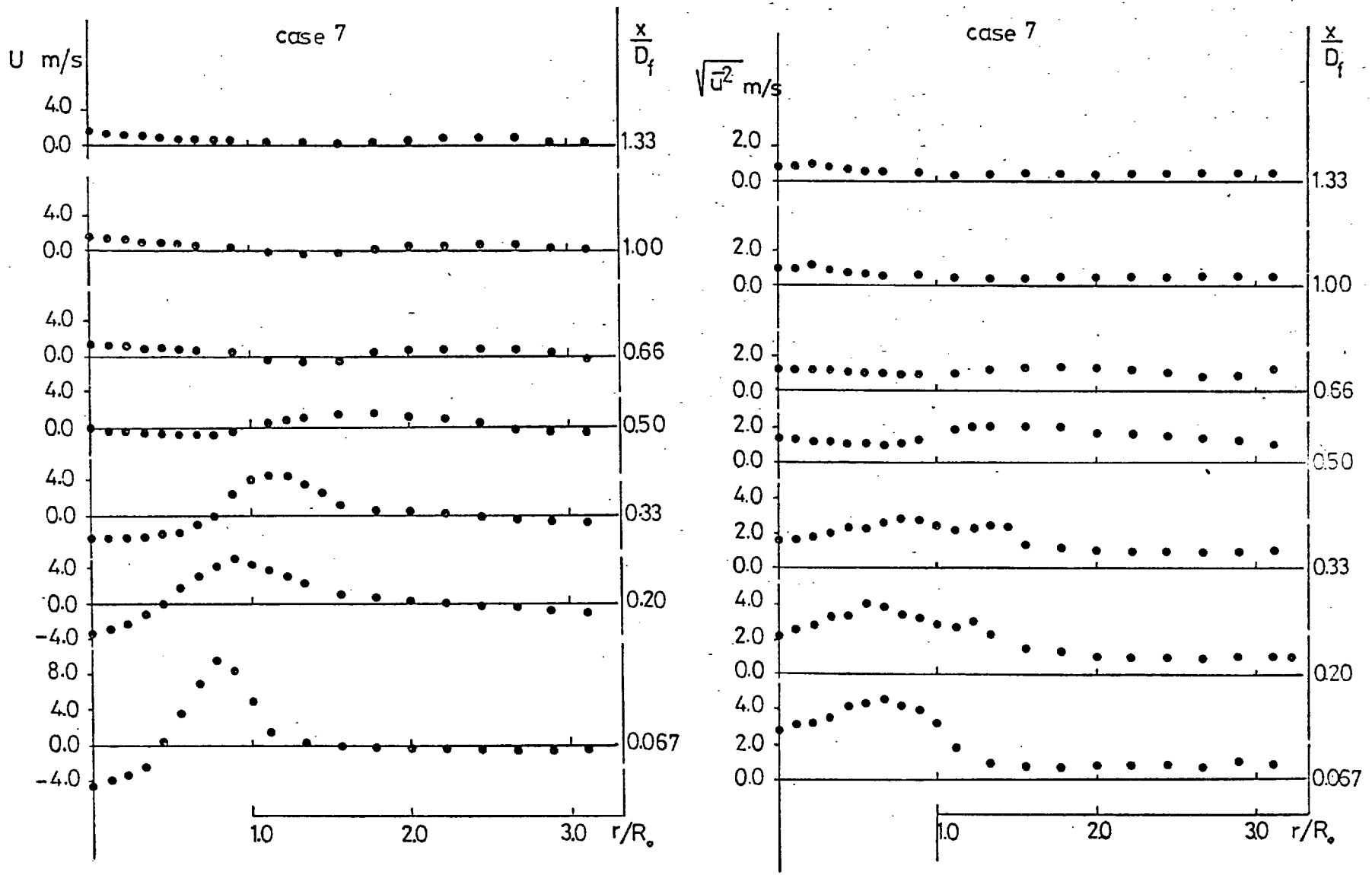

Figure A3.17:Measured mean axial velocity and the corresponding normal stress profiles.
(isothermal flow,S=0.3)

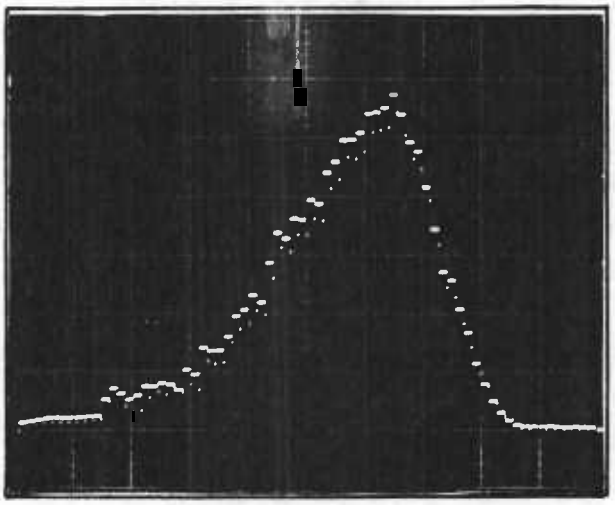

$\frac{x}{D_f}=0.067$, $\frac{r}{D_f}=0.1$

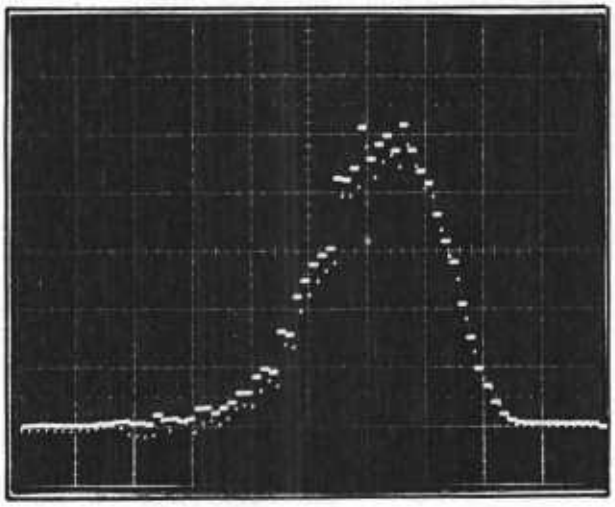

$\frac{x}{D_f}=0.067$, $\frac{r}{D_f}=0.13$

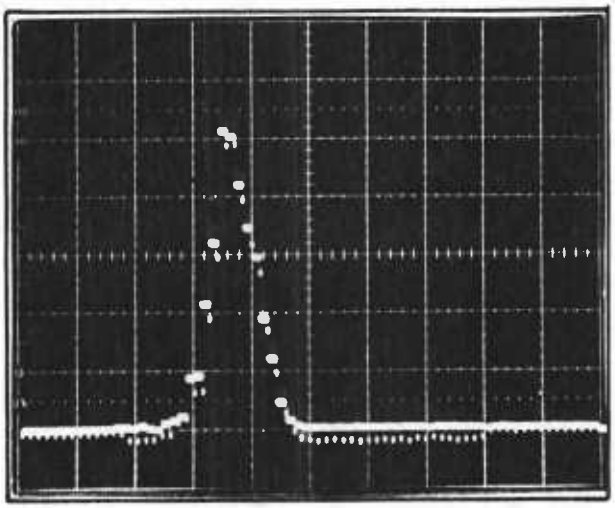

$\frac{x}{D_f}=0.067$, $\frac{r}{D_f}=0.43$

Figure A3.18 :Measured velocity probability distributions

(isothermal flow,S=0.3)

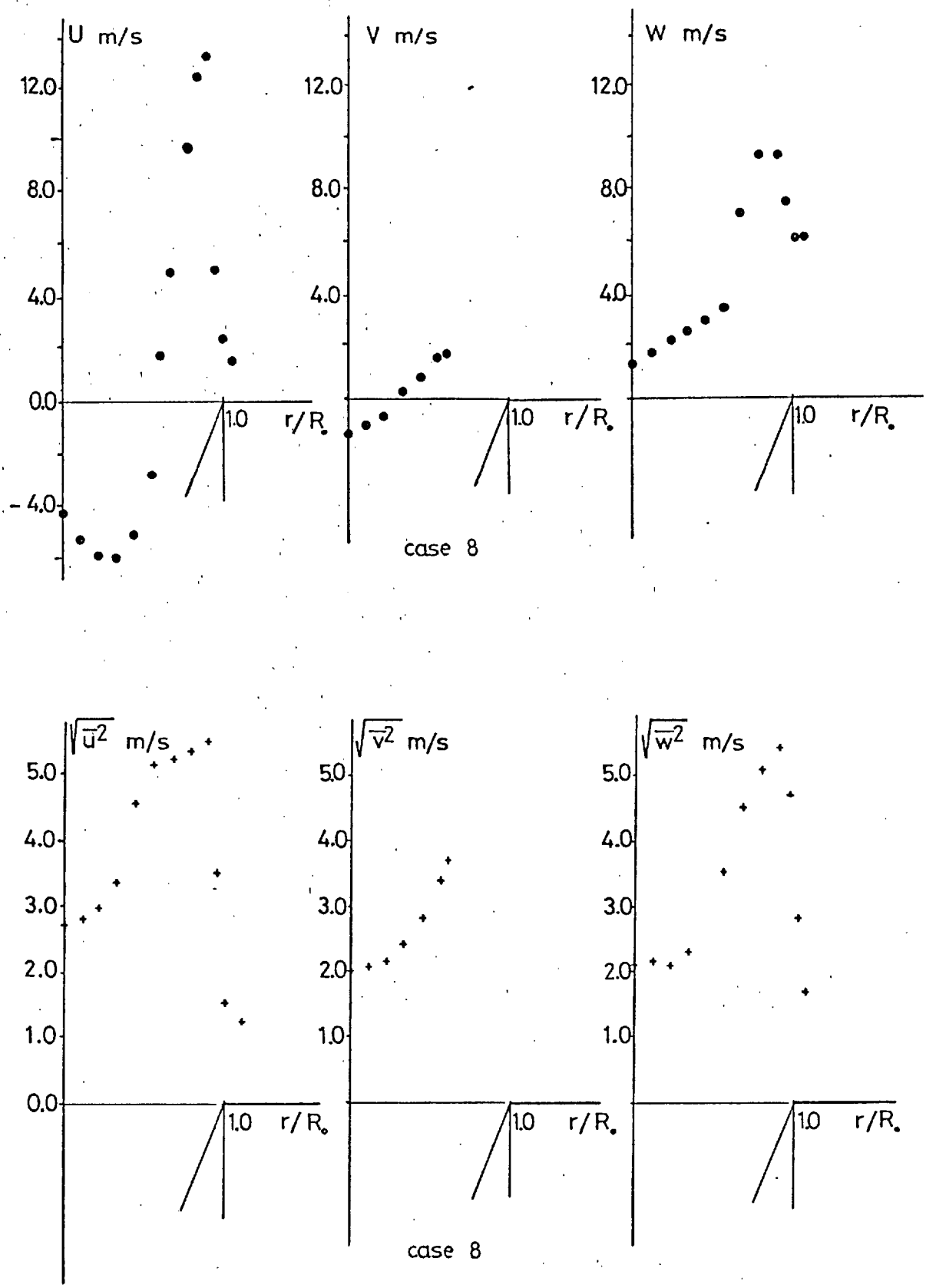

Figure A3.19:Measured velocity profiles at burner exit(S=0.52)

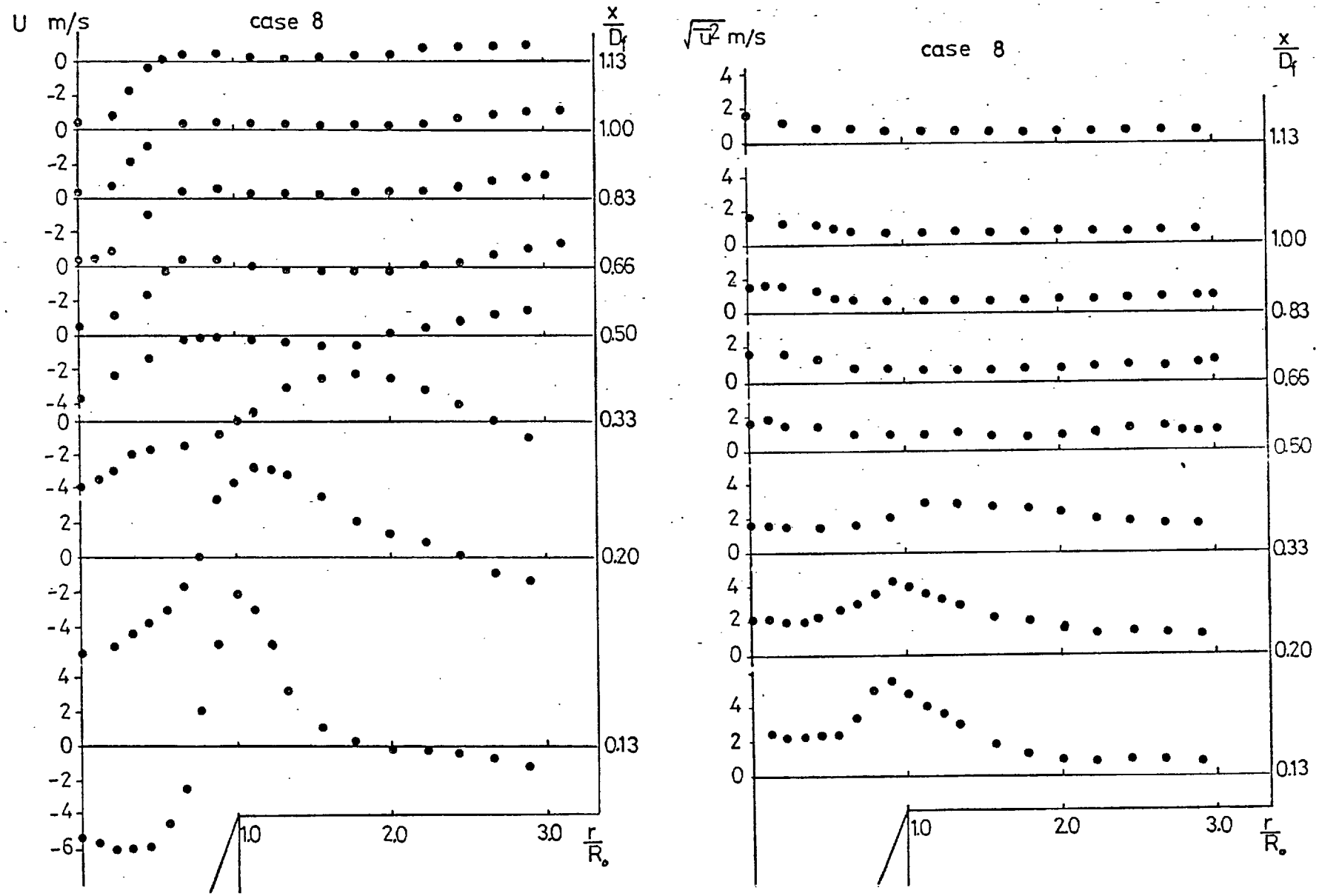

Figure A3.20:Measured mean axial velocity and the corresponding normal stress profiles.
(isothermal flow,S=0.52)

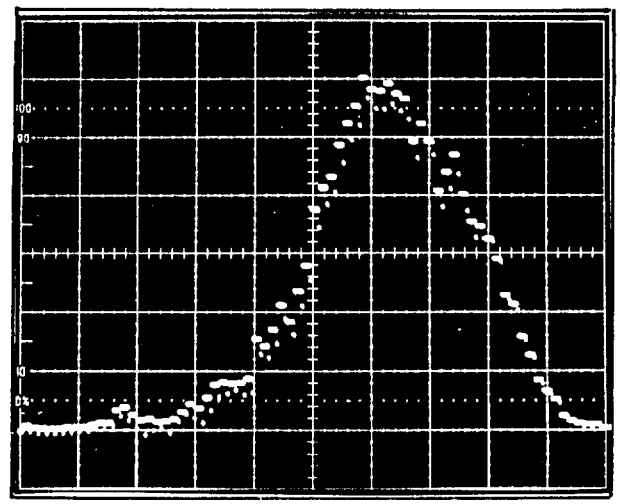

$\frac{x}{D_f}=0.067,\ \frac{r}{D_f}=0.1$

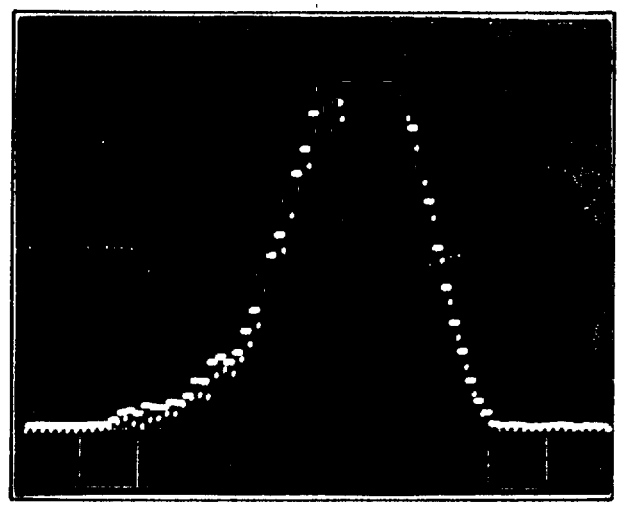

$\frac{x}{D_f}=0.067,\ \frac{r}{D_f}=0.2$

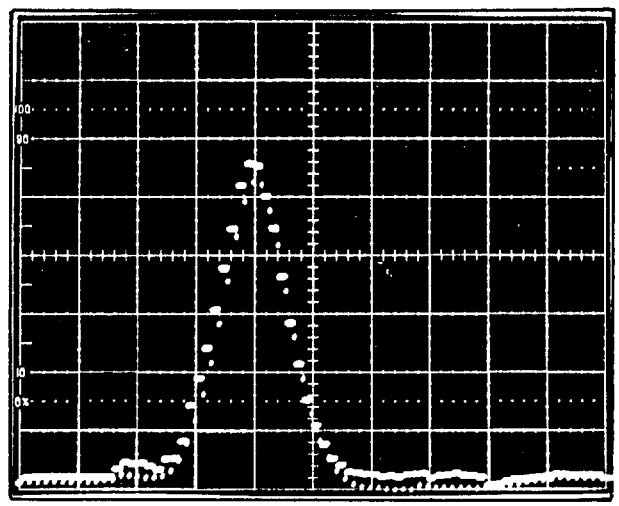

$\frac{x}{D_f}=0.067,\ \frac{r}{D_f}=0.33$

Figure A3.21:Measured velocity probability distributions

(isothermal flow,S=0.52)

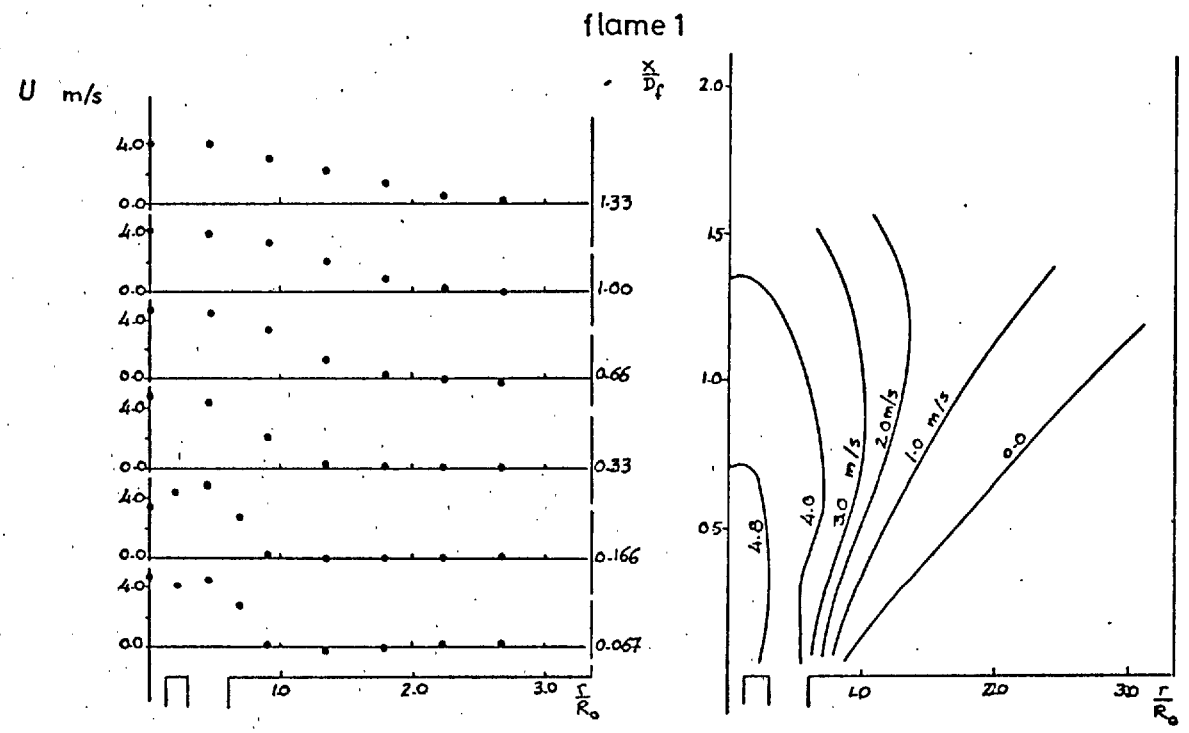

Figure A3.22:Measured mean axial velocity profiles and contours (reacting flow,S=0.0)

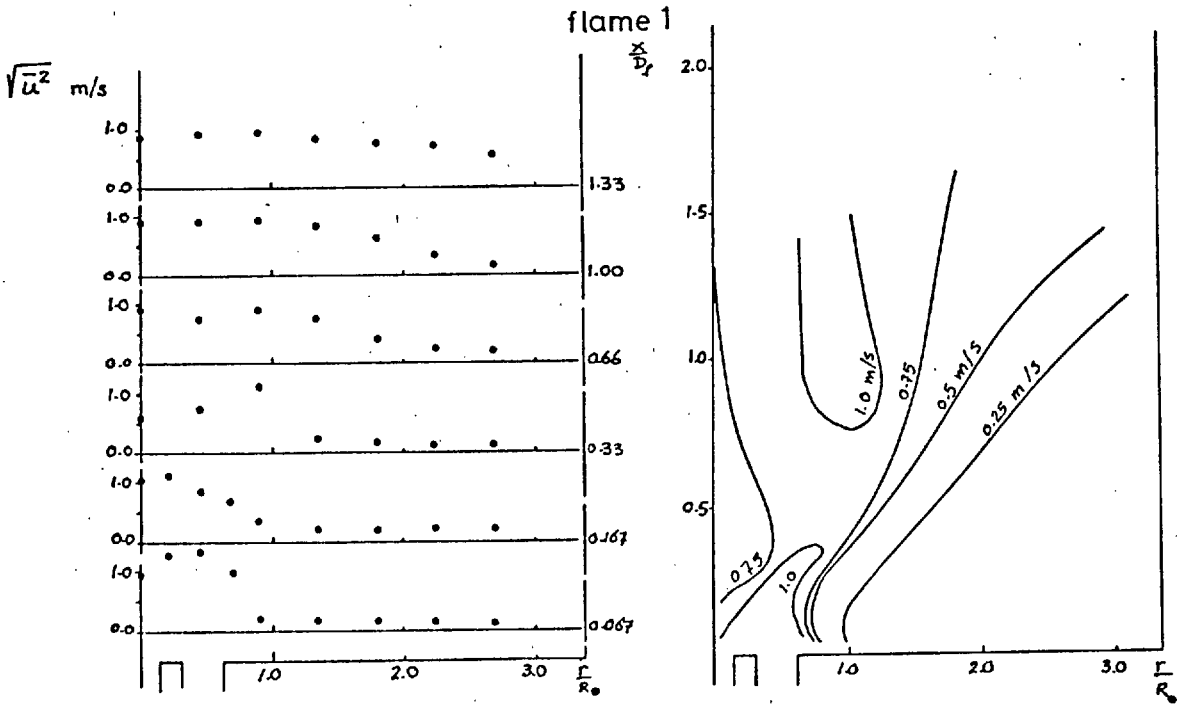

Figure A3.23:Measured axial normal stress profiles and contours (reacting flow,S=0.0)

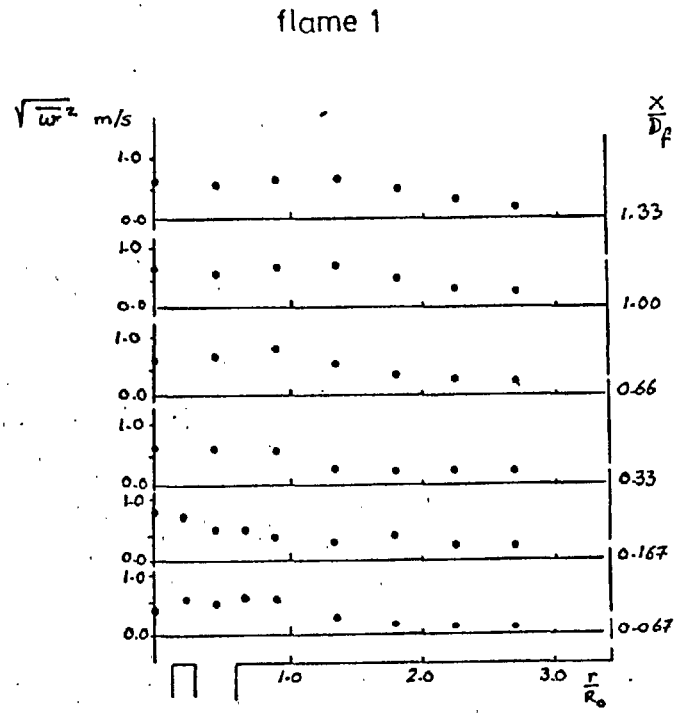

Figure A3.24:Measured tangential normal stress profiles.
(reacting flow,S=0.0)
N.B. No mean tangential velocity component.

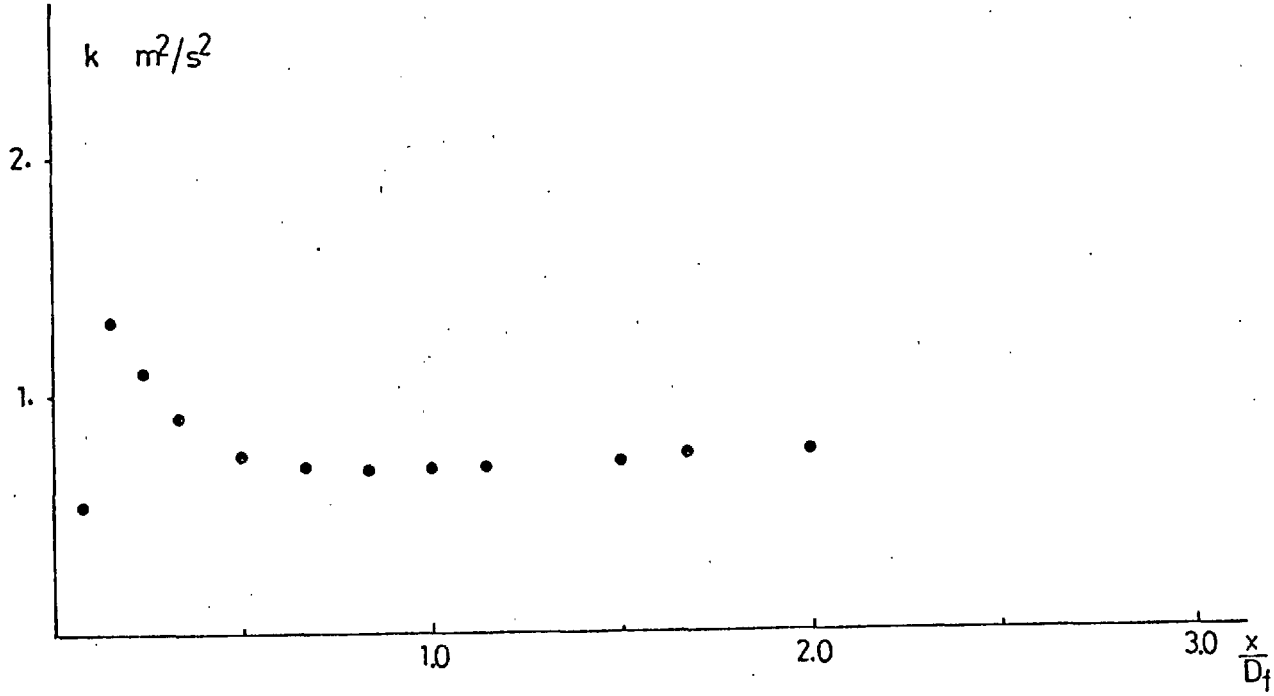

Figure A3.25:Measured centre-line distribution of kinetic energy of turbulence(reacting flow,S=0.0)

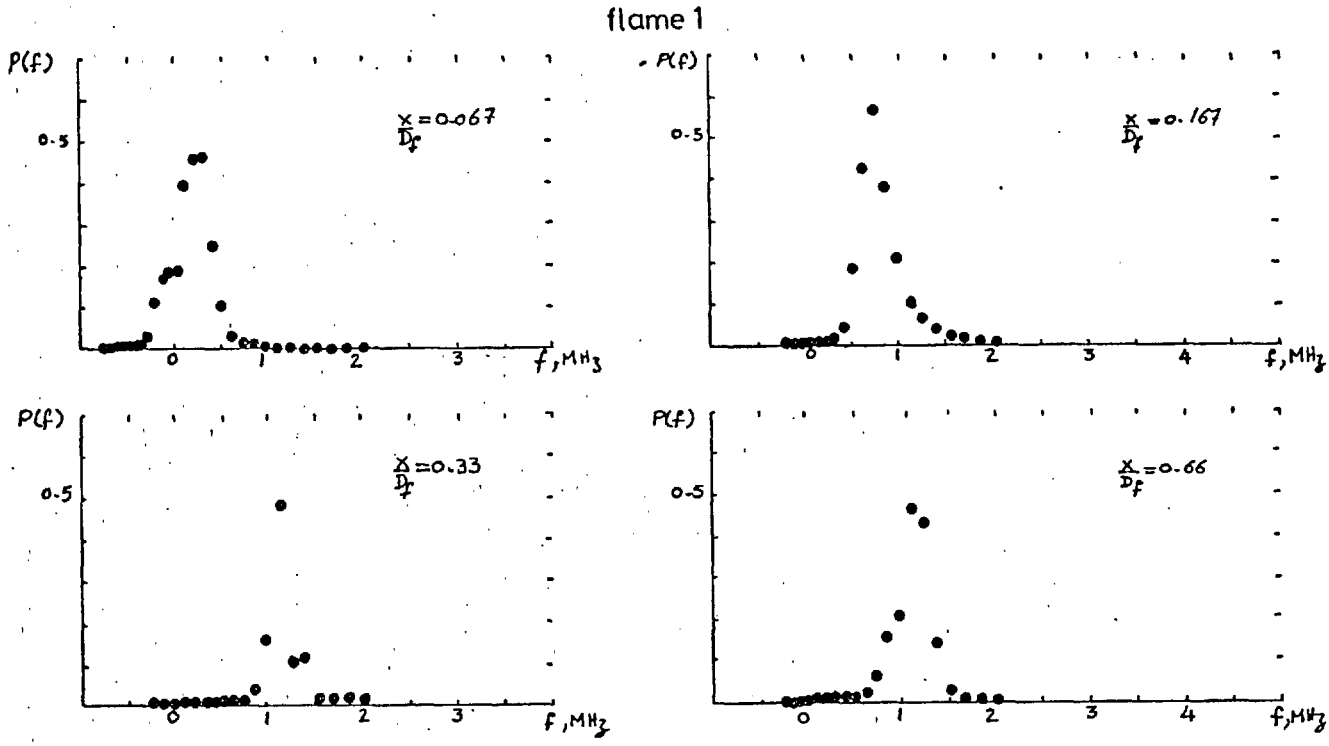

Figure A3.26:Velocity probability distribution along the centreline (reacting flow,S=0.0)

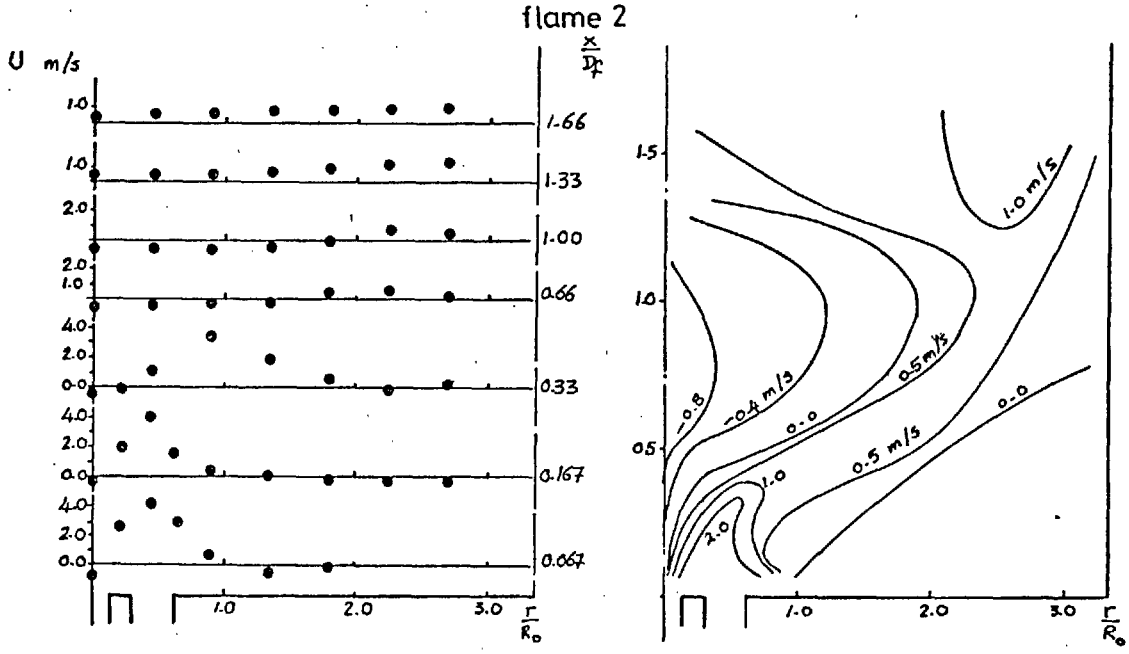

Figure A3.27:Measured mean axial velocity profiles and contours (reacting flow,S=0.52)

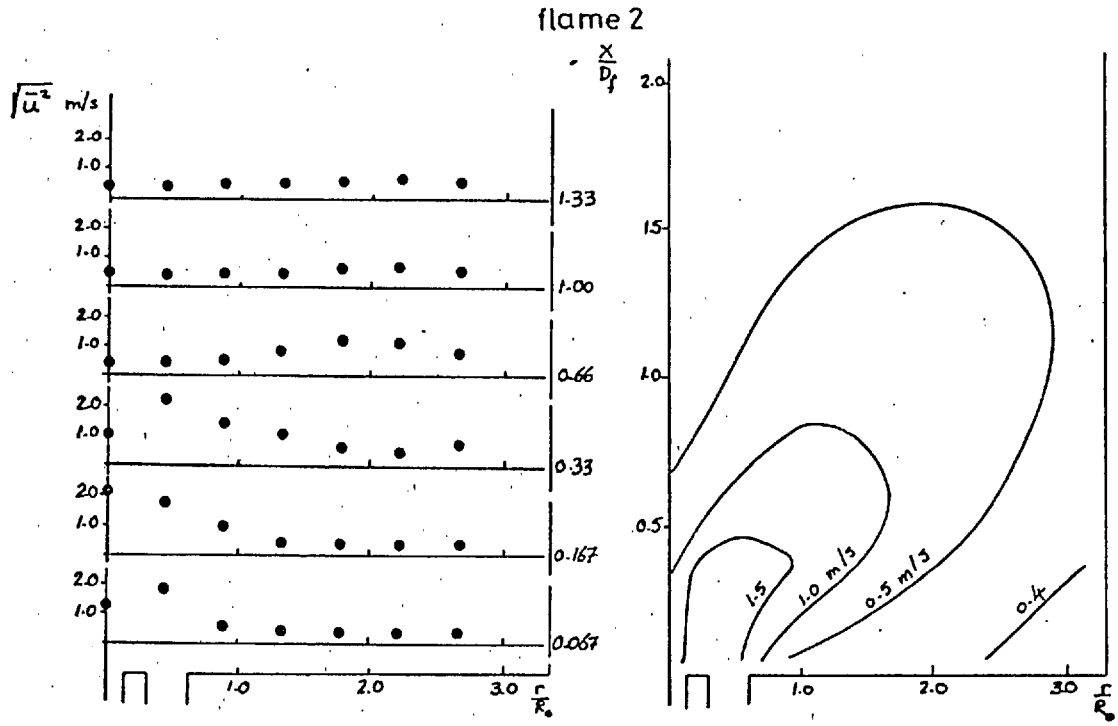

Figure A3.28:Measured axial normal stress profiles and contours (reacting flow,S=0.52)

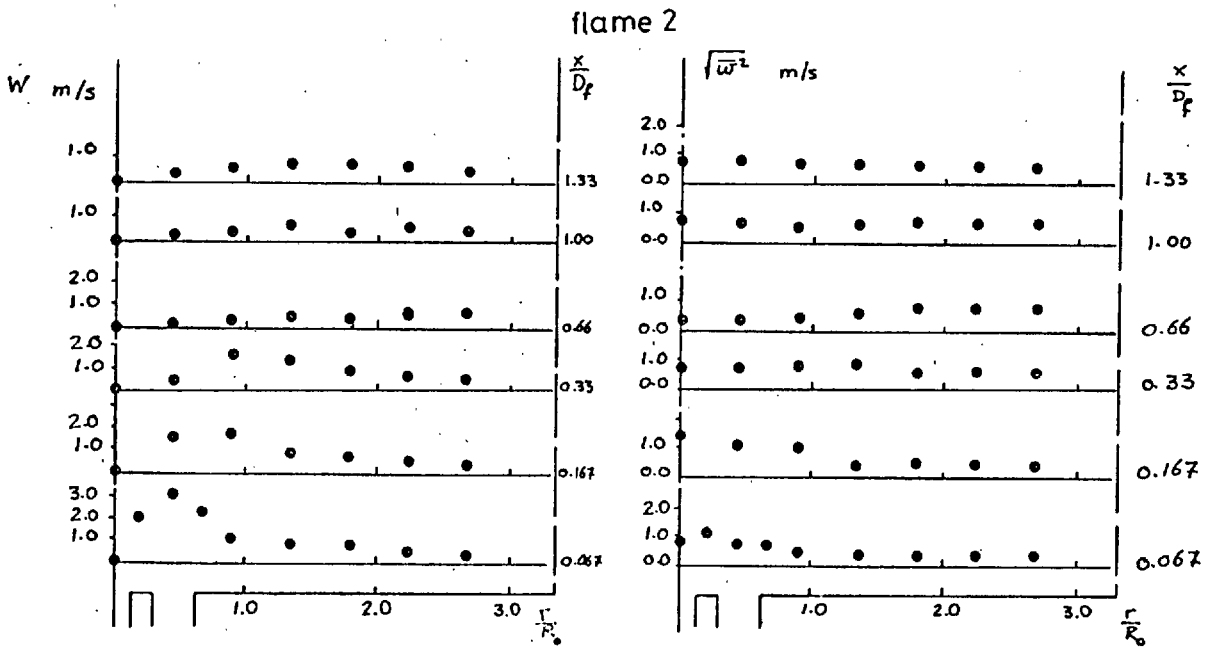

Figure A3.29:Measured mean tangential velocity and normal stress profiles. (reacting flow,S=0.52)

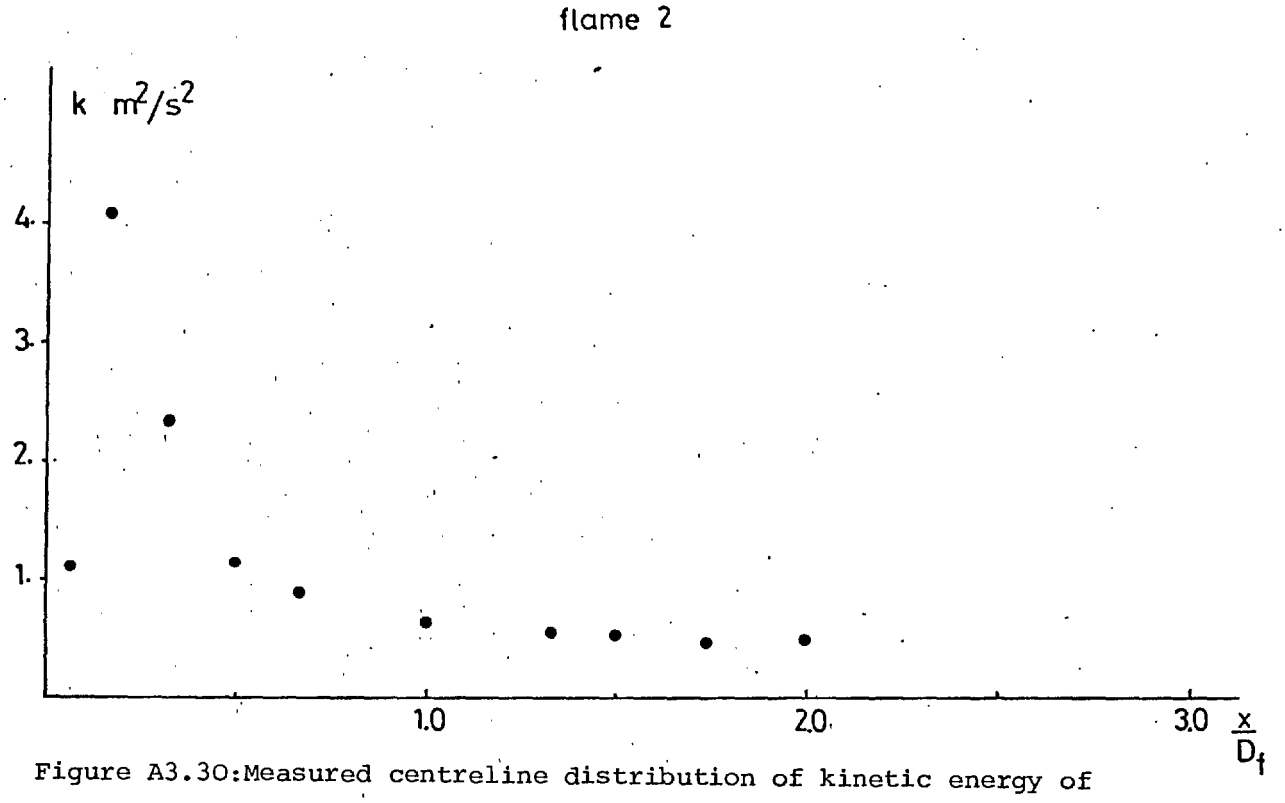

Figure A3.30:Measured centreline distribution of kinetic energy of turbulence(reacting flow,S=0.52)

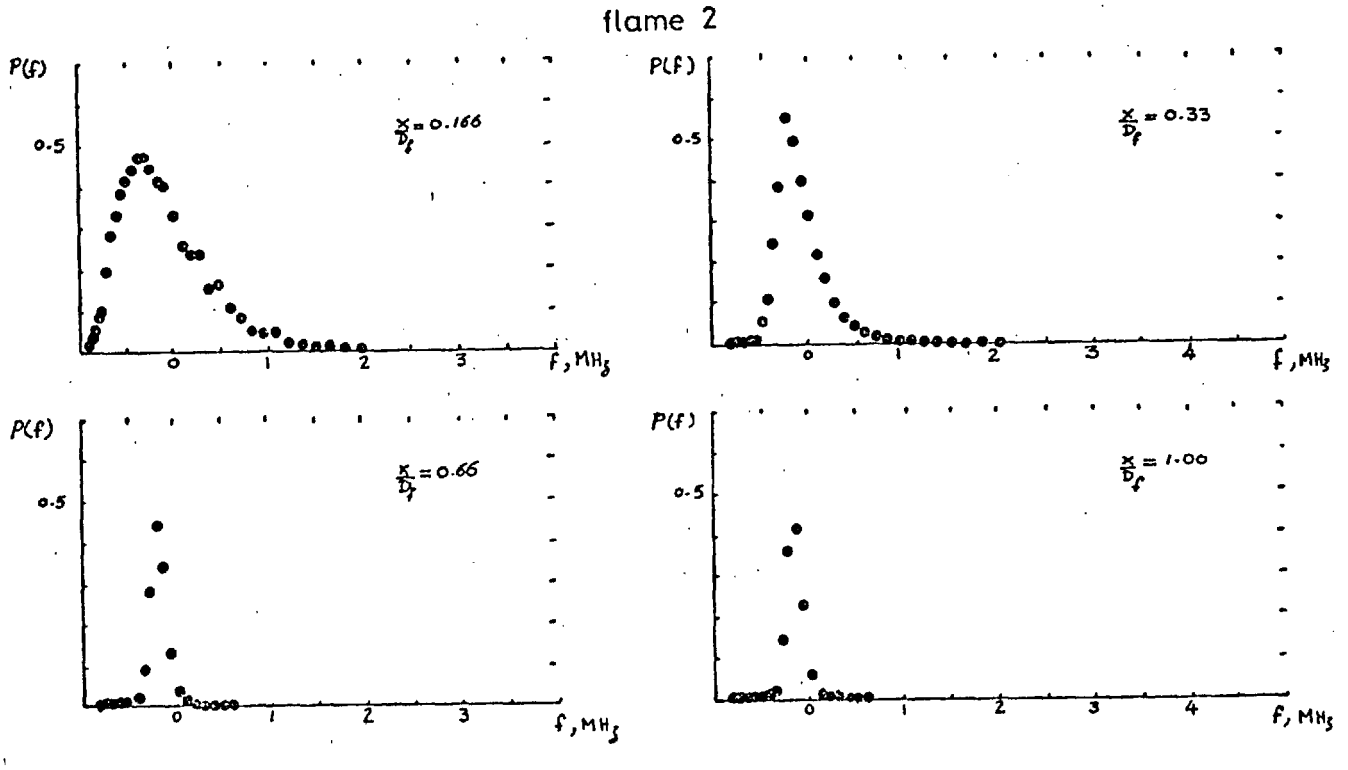

Figure A3.31:Velocity probability distribution along the centreline (reacting flow,S=0.52)

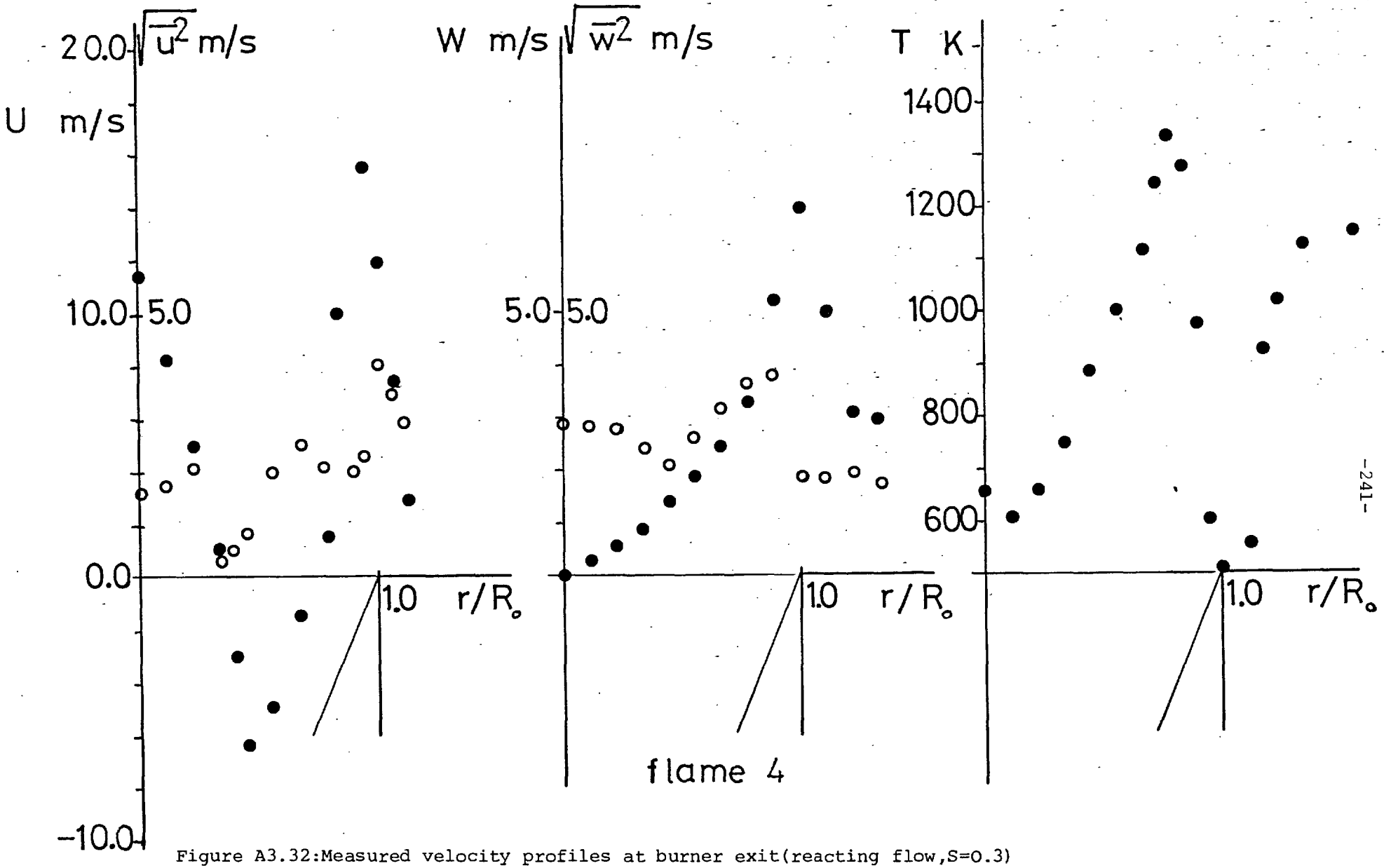

Figure A3.32:Measured velocity profiles at burner exit(reacting flow,S=0.3)

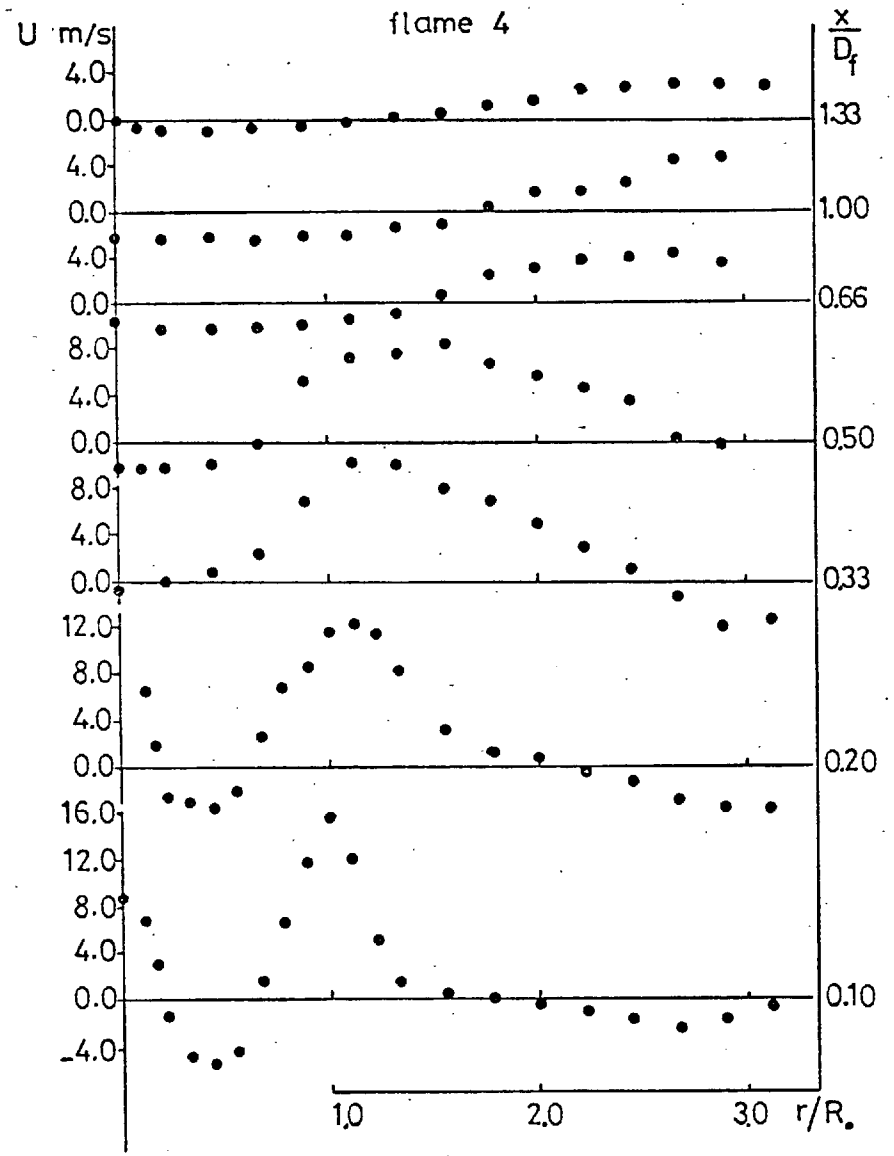

Figure A3.33:Measured mean axial velocity profiles.

(reacting flow,S=0.3)

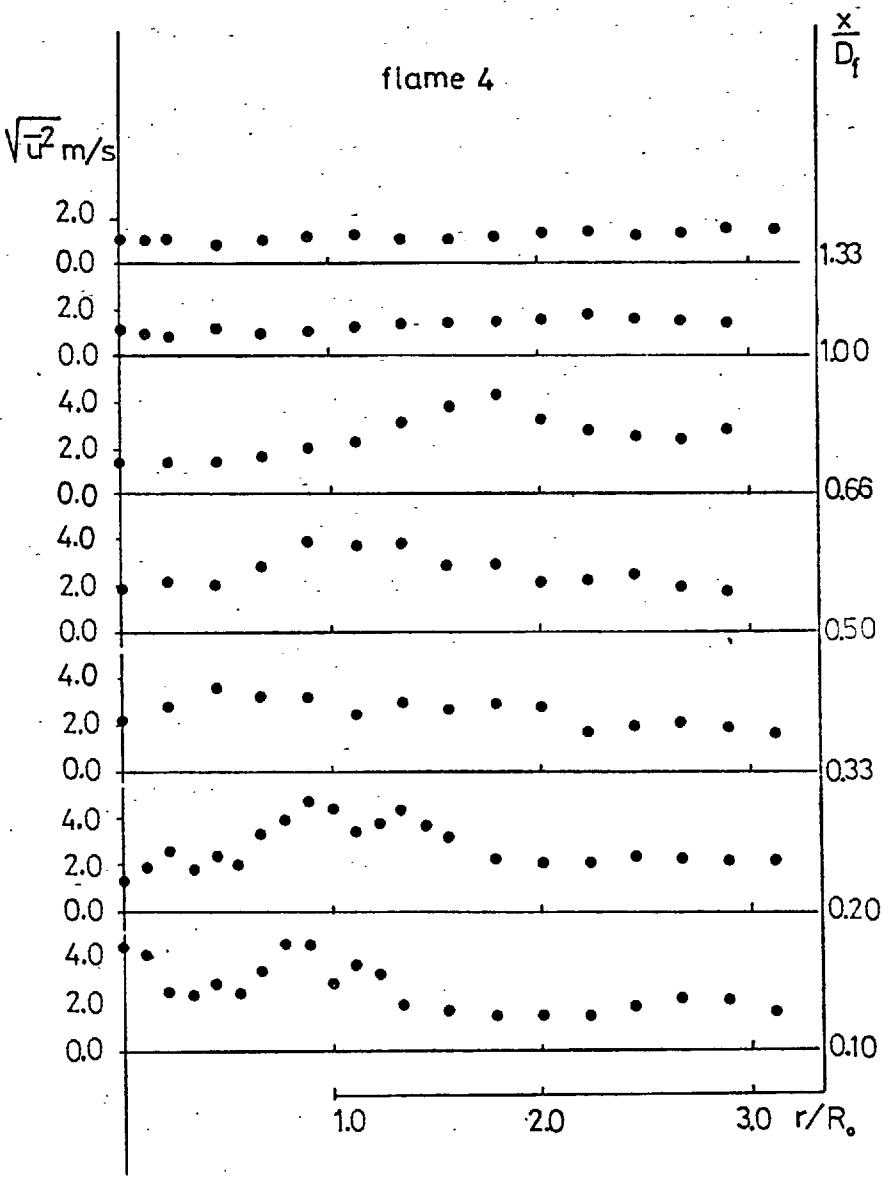

Figure A3.34:Measured axial normal stress profiles.

(reacting flow,S=0.3)

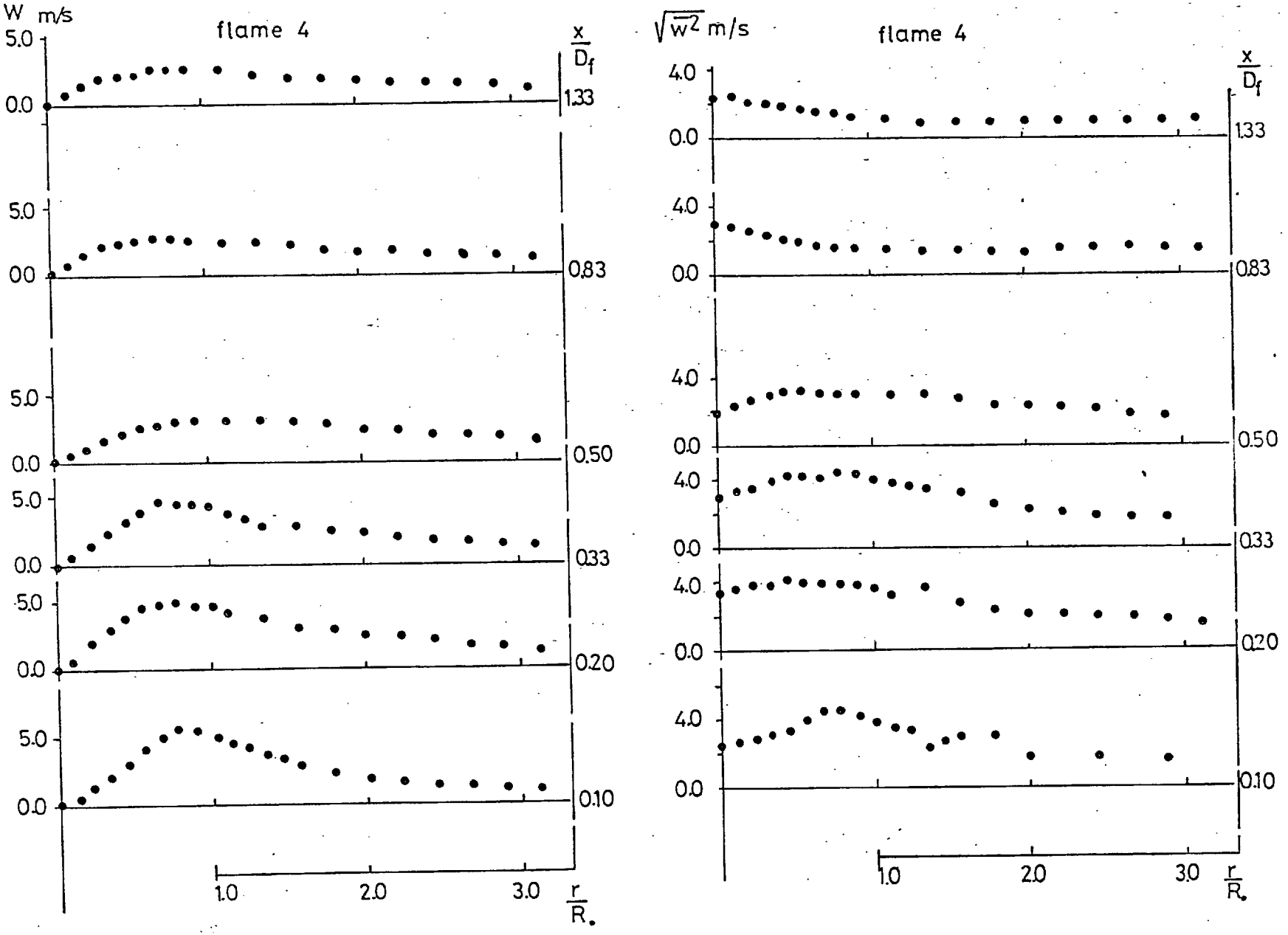

Figure A3.35:Measured mean tangential velocity and the corresponding normal stress (reacting flow,S=0.3)

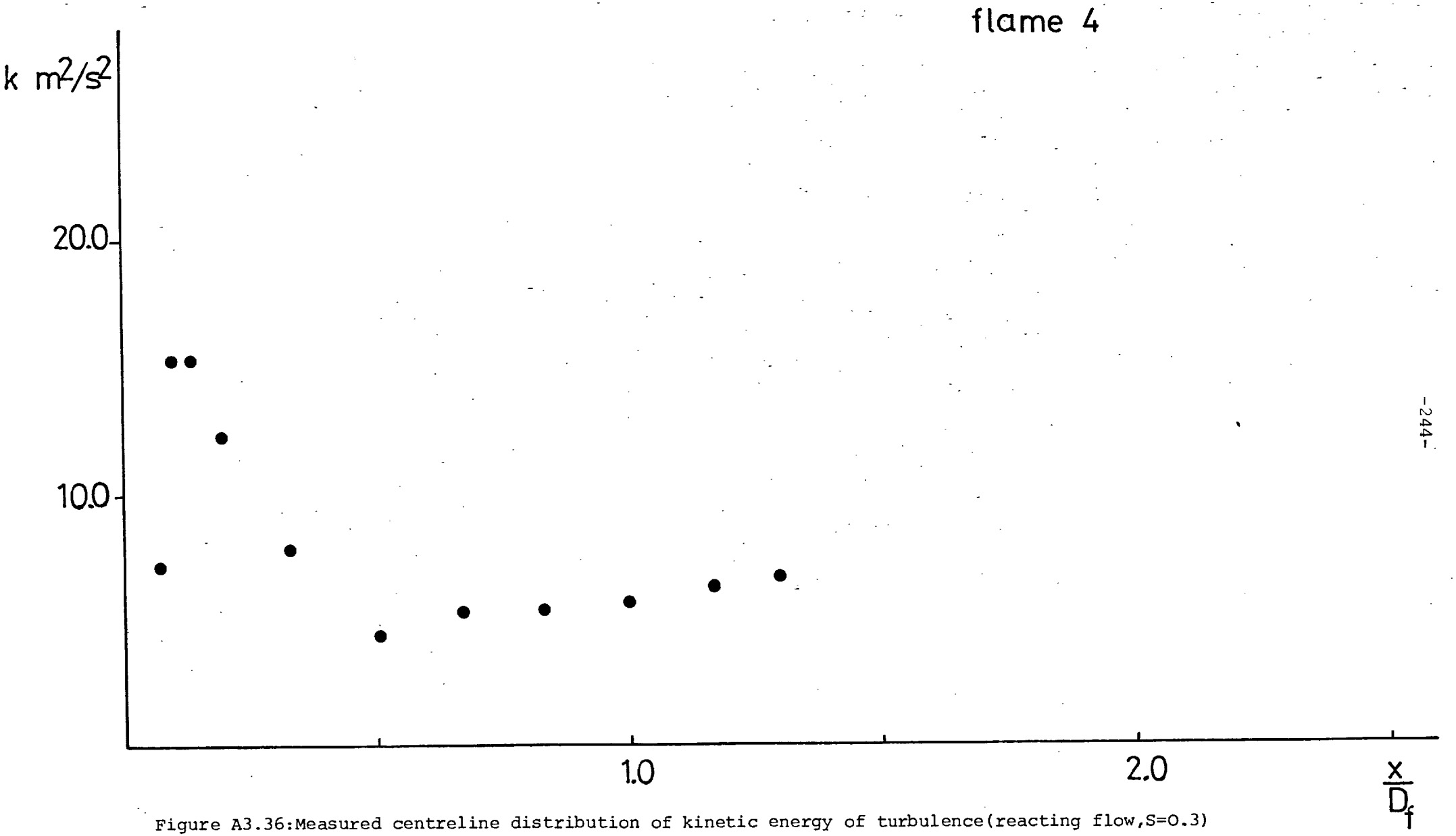

Figure A3.36:Measured centreline distribution of kinetic energy of turbulence(reacting flow,S=0.3)

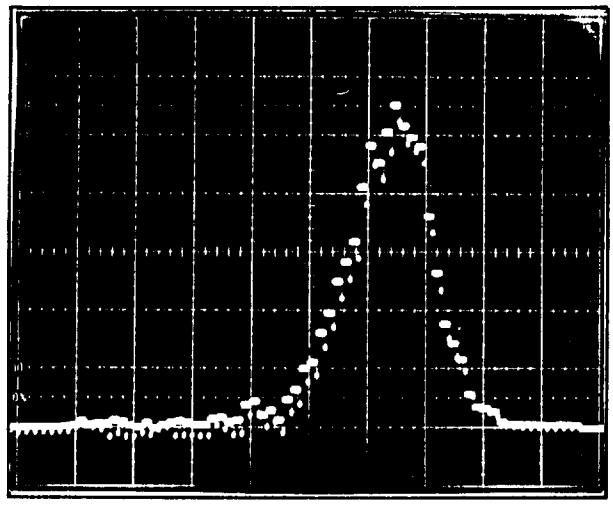

$\frac{x}{D_f}=0.067,\ \frac{r}{D_f}=0.1$

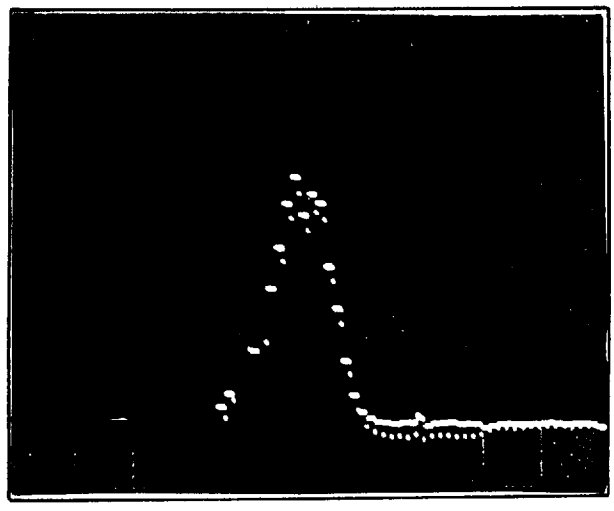

$\frac{x}{D_f}=0.067,\ \frac{r}{D_f}=0.26$

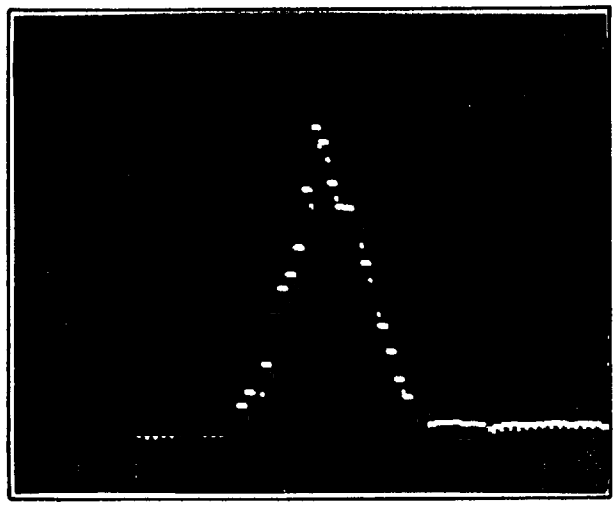

$\frac{x}{D_f}=0.067,\ \frac{r}{D_f}=0.43$

Figure A3.37:Measured velocity probability distributions.

(reacting flow,S=0.3)

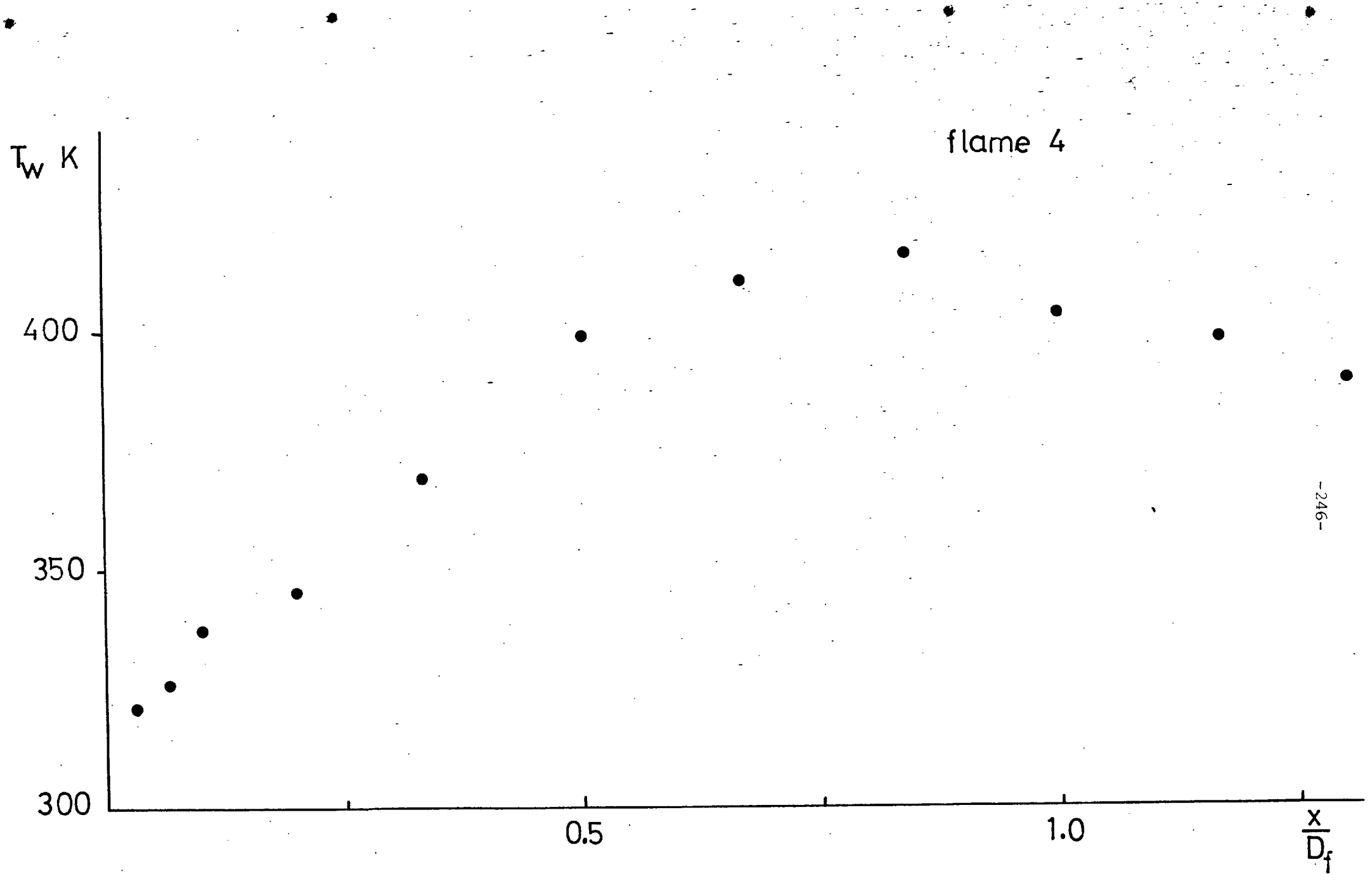

Figure A3.38:Measured wall temperature distribution,(reacting flow,S=0.3)

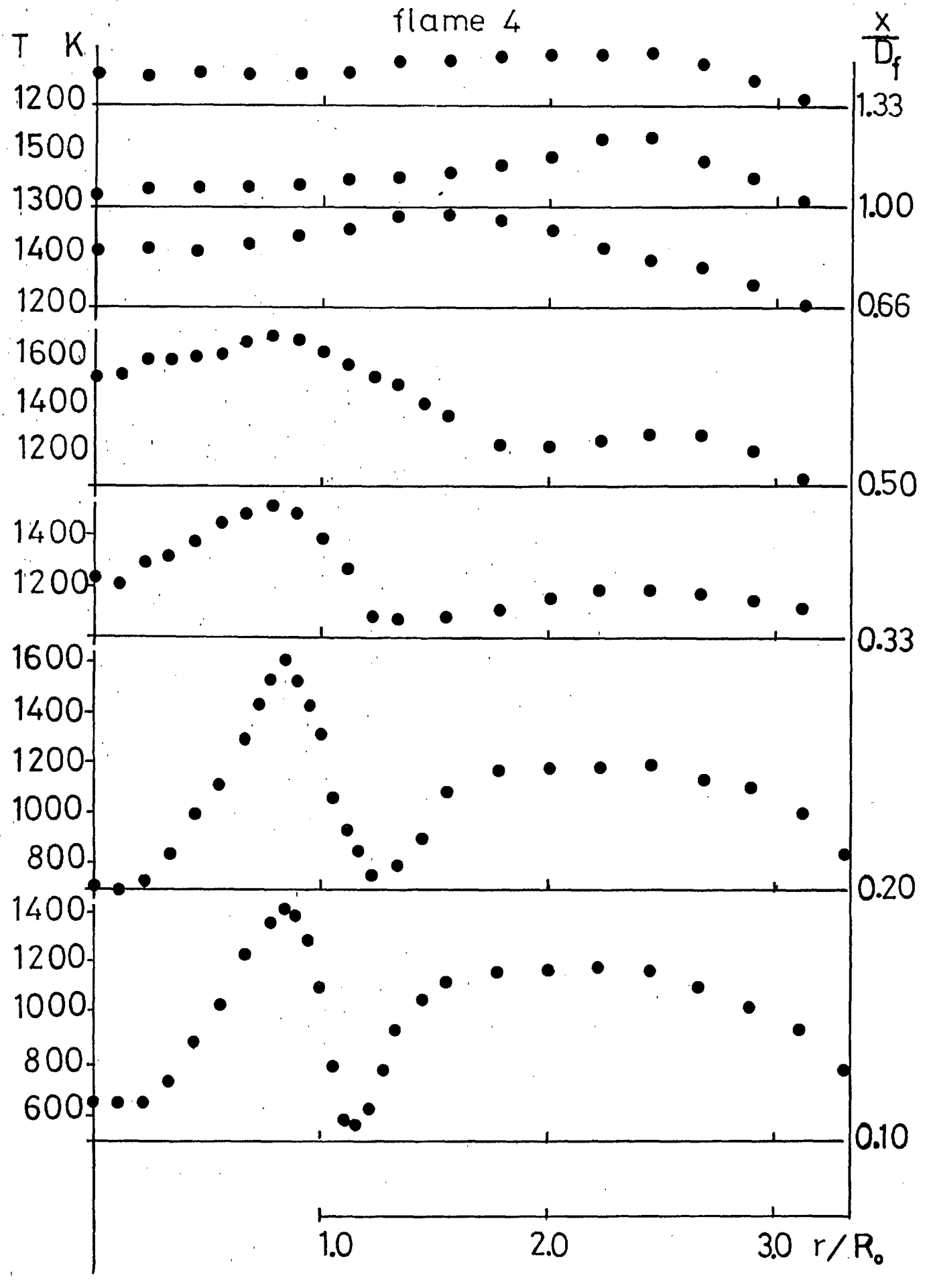

Figure A3.39:Measured mean gas temperature profiles.

(reacting flow,S=0.3)

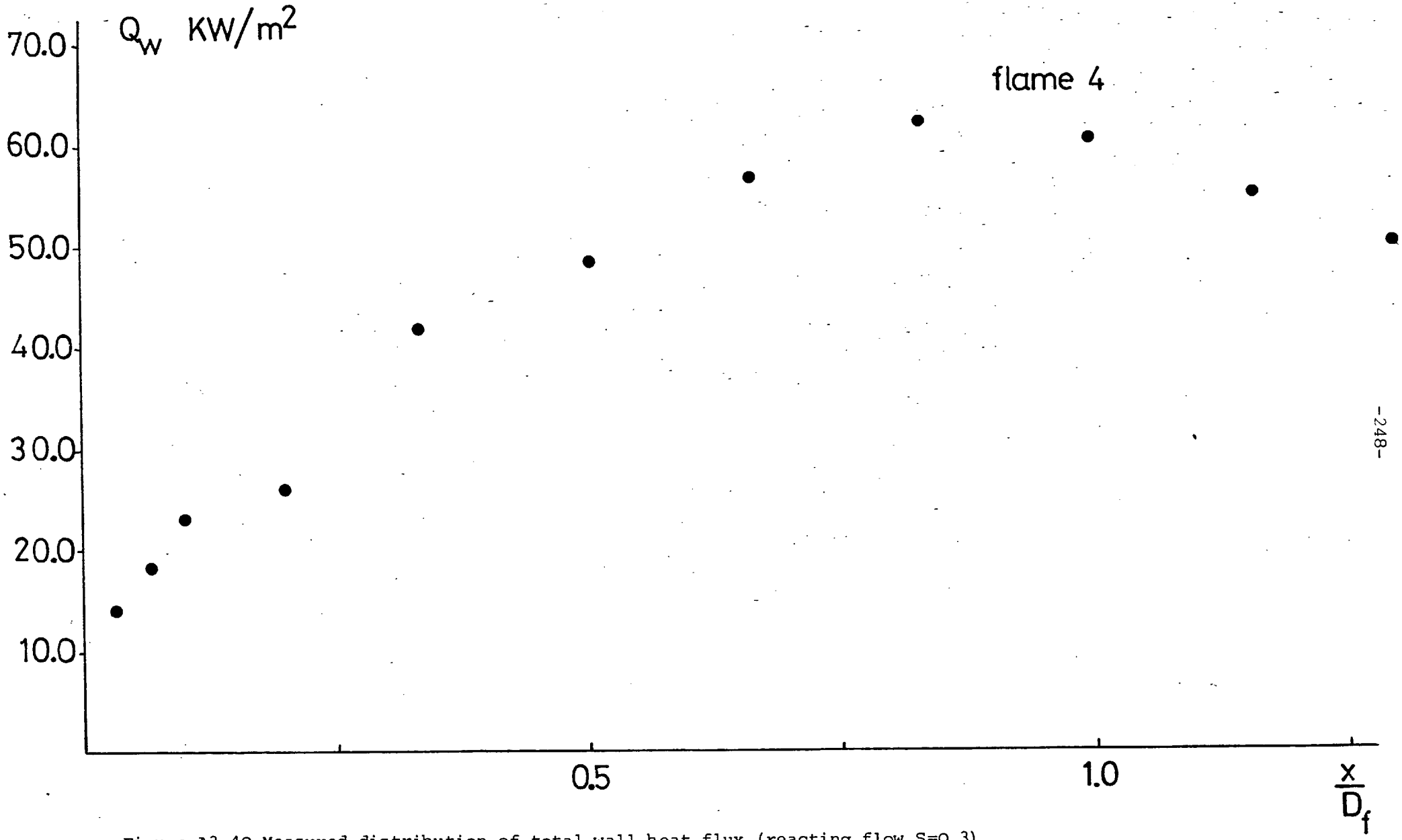

Figure A3.40:Measured distribution of total wall heat flux,(reacting flow,S=0.3)

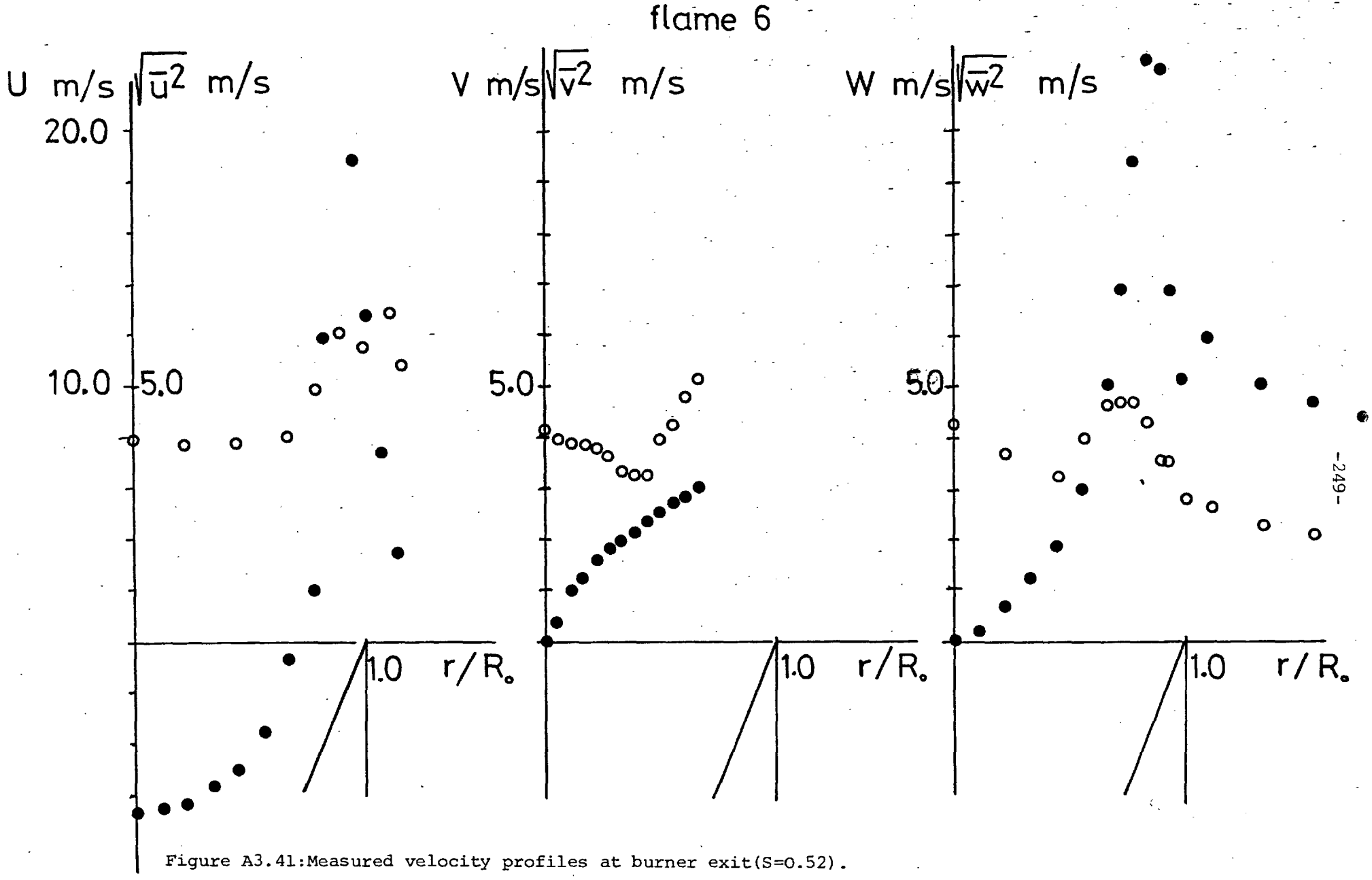

Figure A3.41:Measured velocity profiles at burner exit(S=0.52).

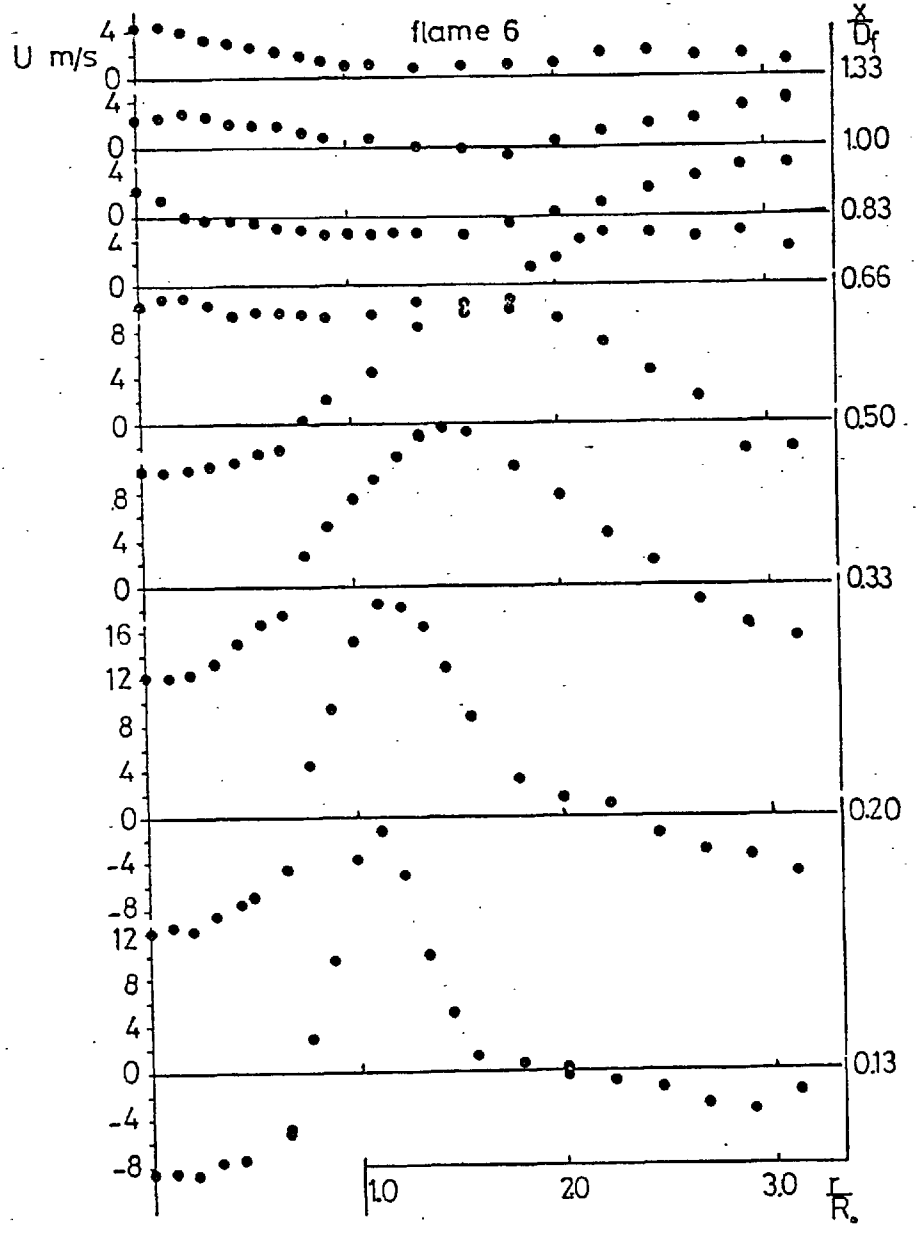

Figure A3.42:Measured mean axial velocity profiles.

(reacting flow,S=0.52)

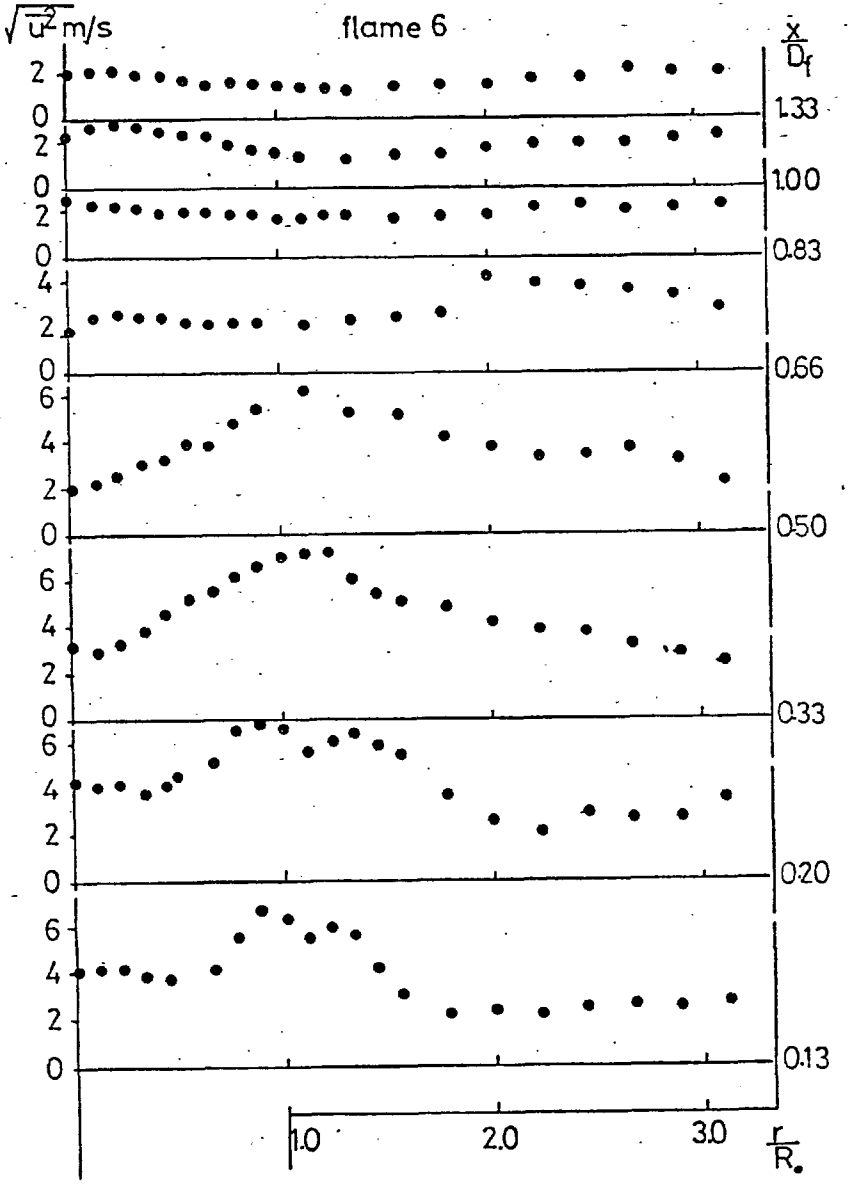

Figure A3.43:Measured axial normal stress profiles

(reacting flow,S=0.52)

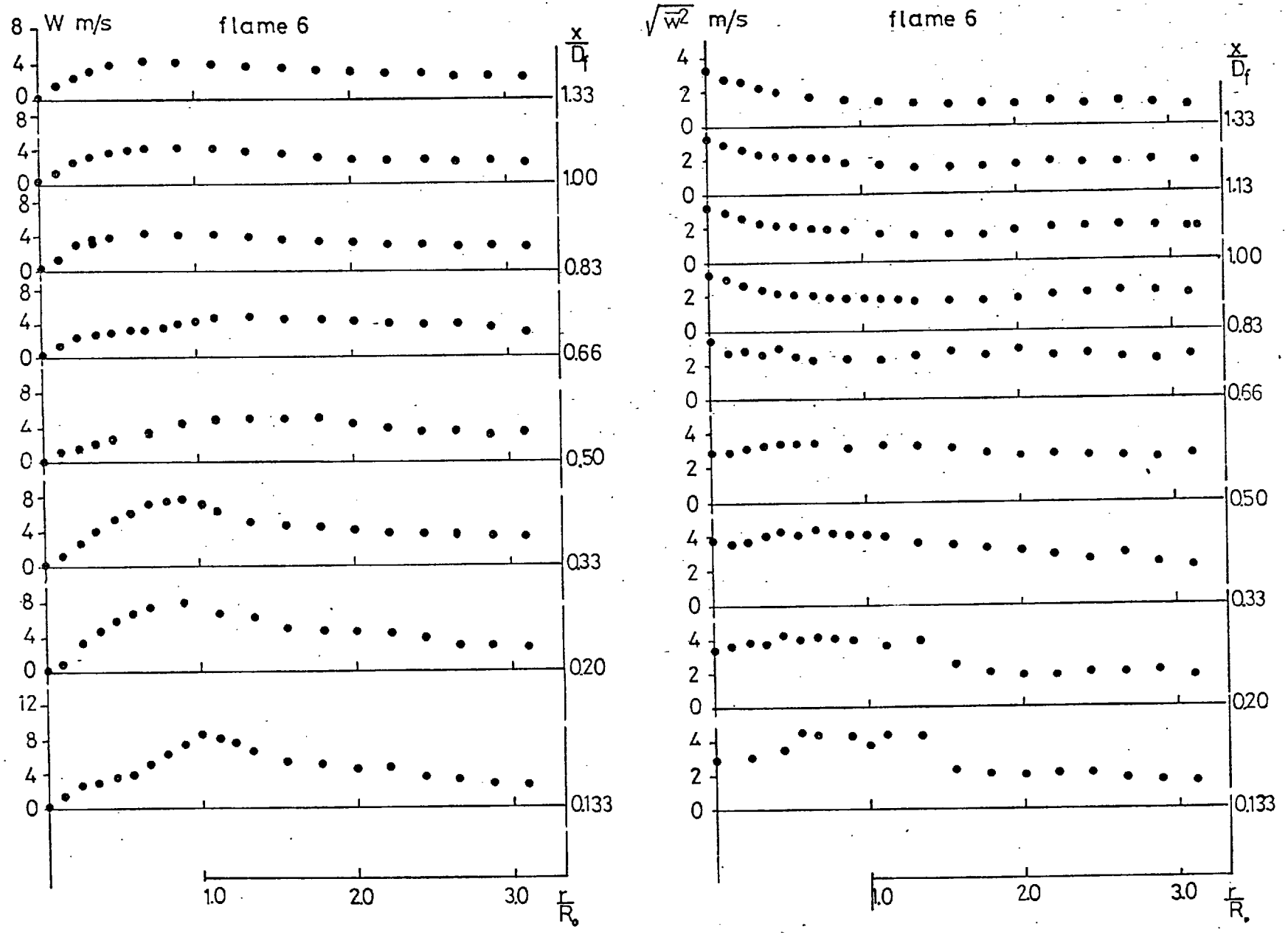

Figure A3.44:Measured mean tangential velocity and the corresponding normal stress(reacting flow,S=0.52)

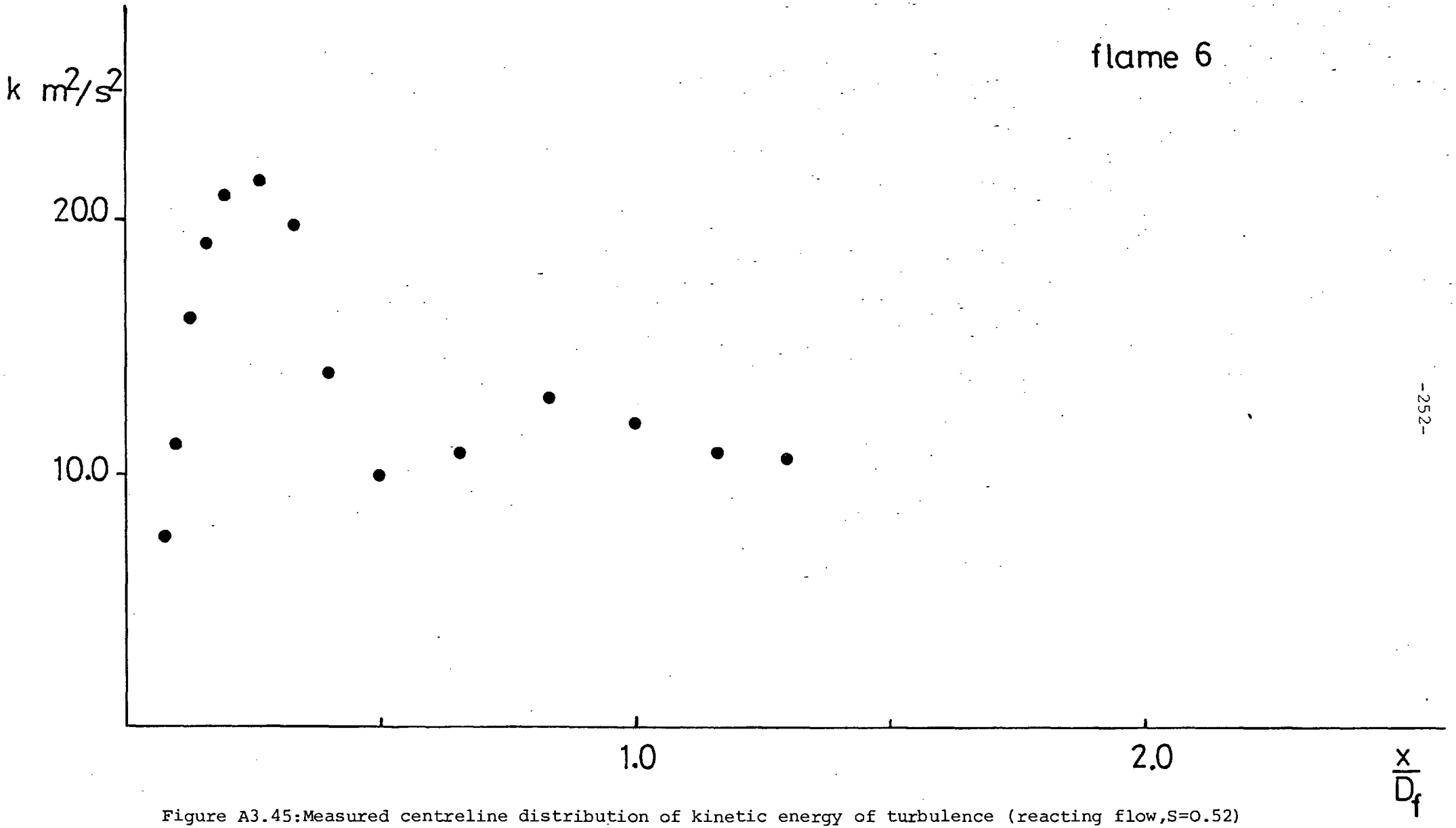

Figure A3.45:Measured centreline distribution of kinetic energy of turbulence (reacting flow,S=0.52)

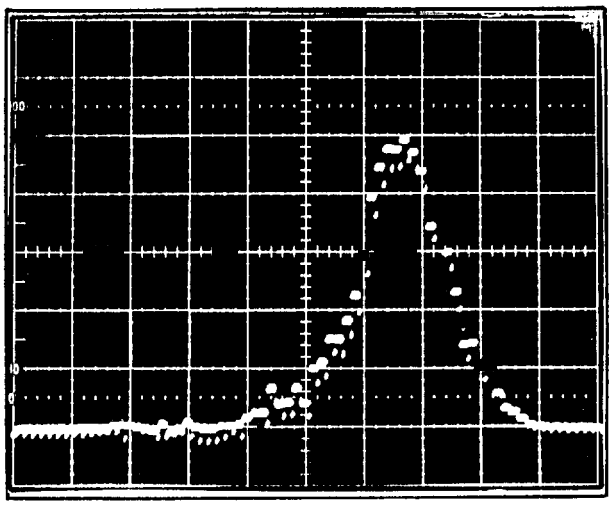

$\frac{x}{D_f}=0.33$, $\frac{r}{D_f}=0.33$

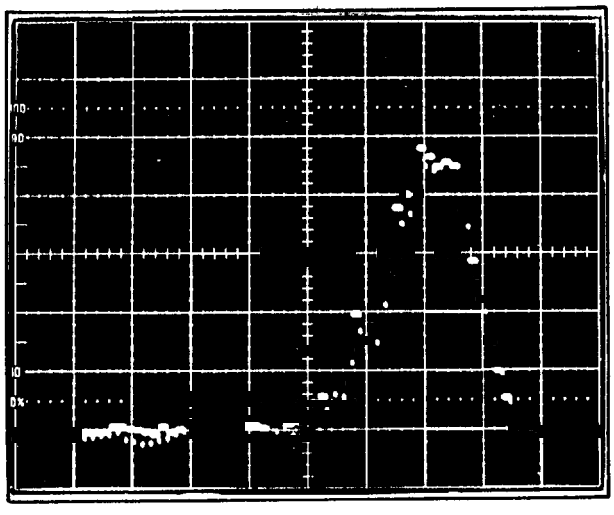

$\frac{x}{D_f}=0.50$, $\frac{r}{D_f}=0.33$

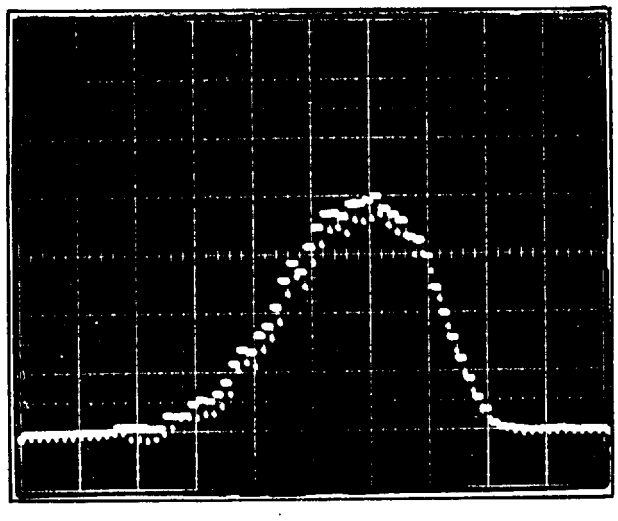

$\frac{x}{D_f}=0.66$, $\frac{r}{D_f}=0.33$

Figure A3.46:Measured velocity probability distributions.

(reacting flow,S=0.52)

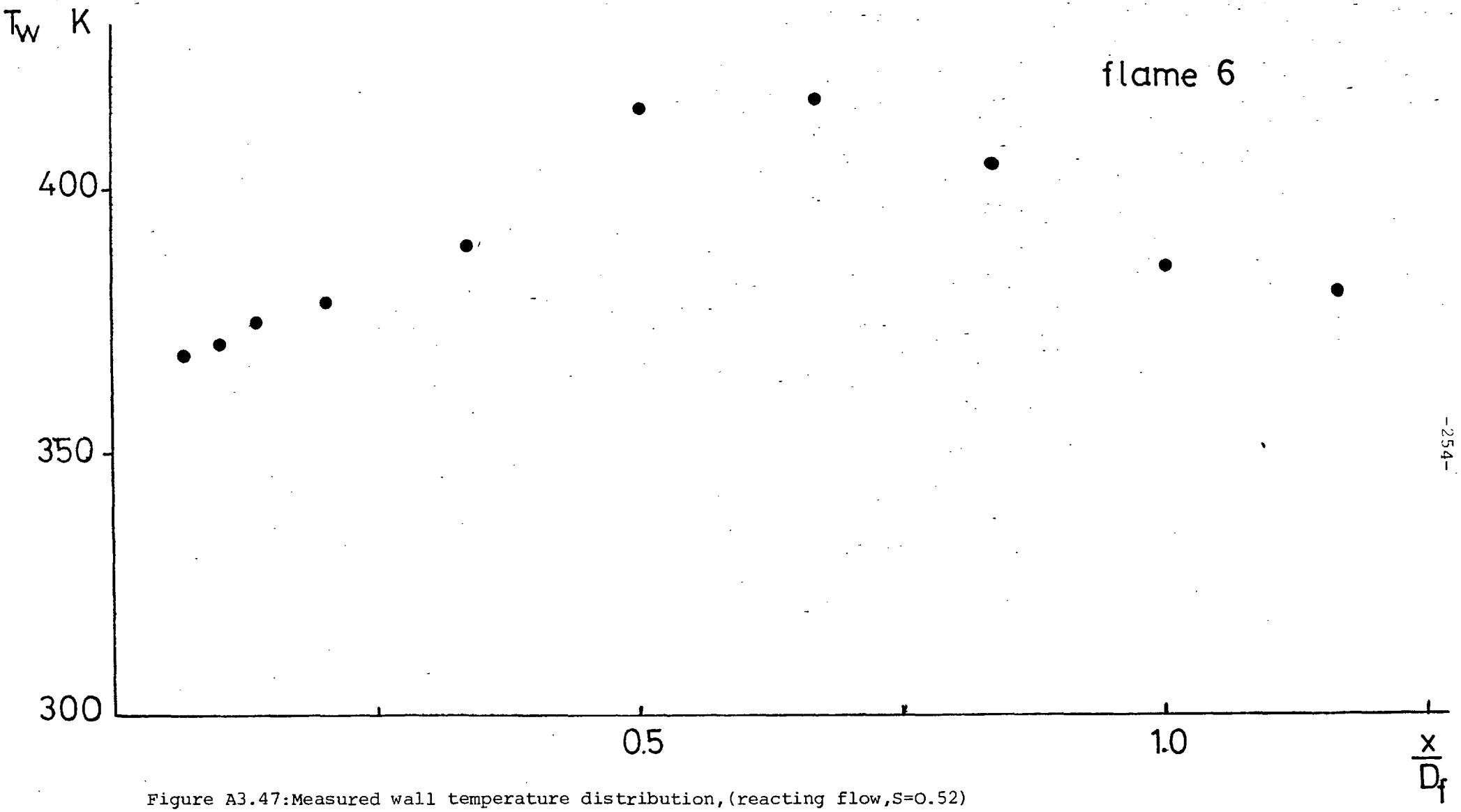

Figure A3.47:Measured wall temperature distribution,(reacting flow,S=0.52)

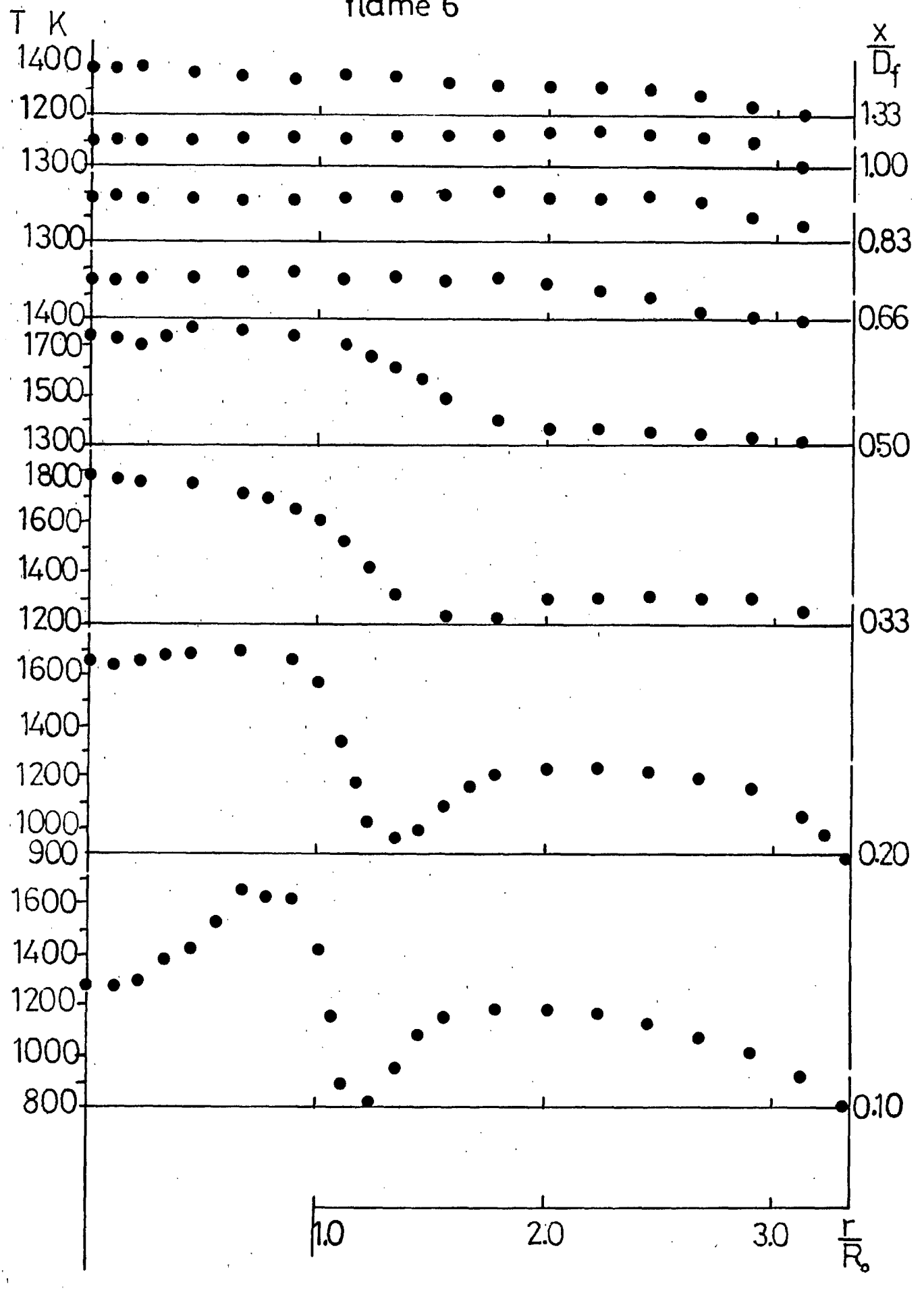

Figure A3.48:Measured mean gas temperature profiles.

(reacting flow,S=0.52)

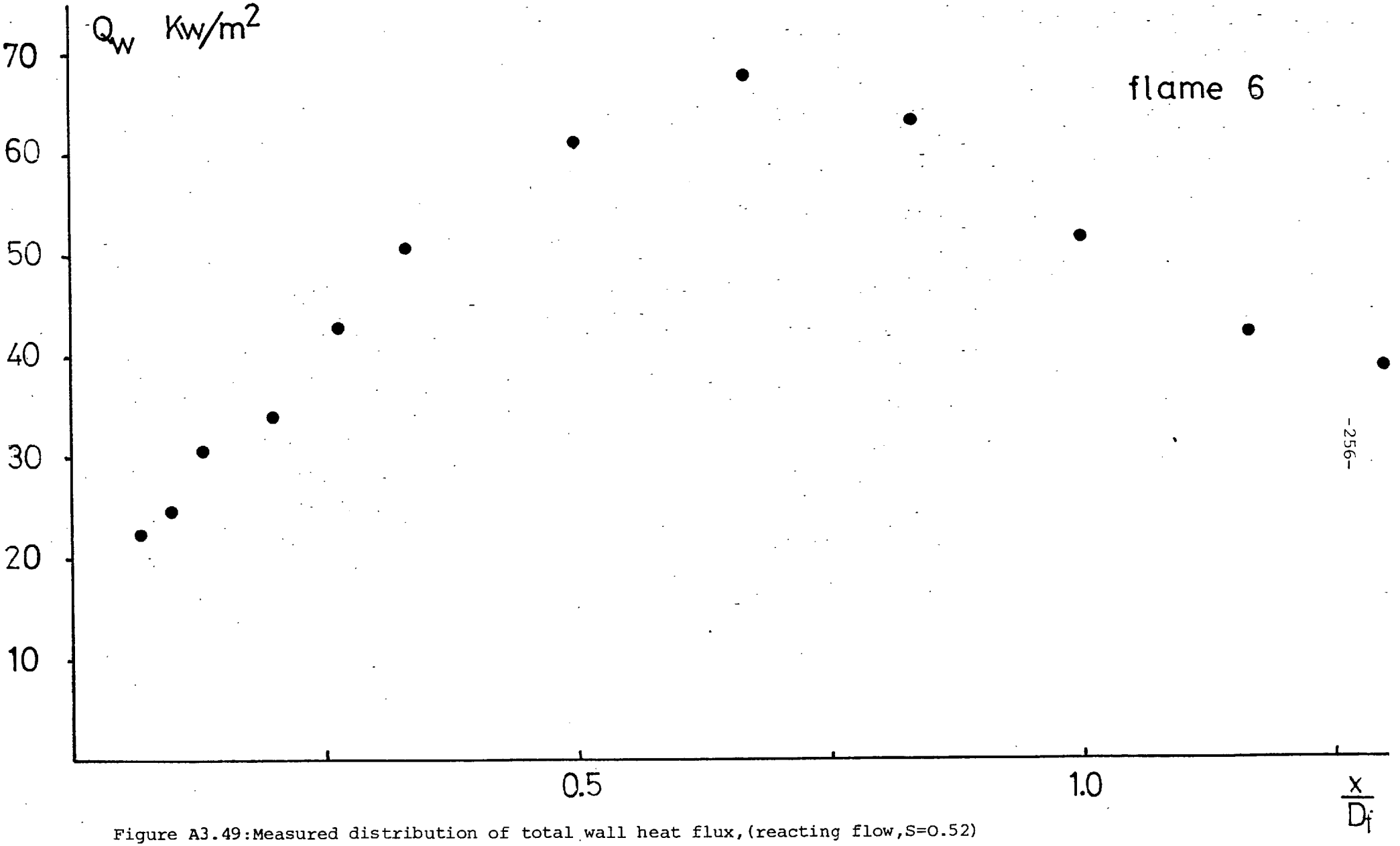

Figure A3.49:Measured distribution of total wall heat flux,(reacting flow,S=0.52)

APPENDIX A4

P. Hutchinson
Theoretical Physics Division,
A. E. R. E. Harwell,
Oxfordshire, England.

E. E. Khalil
J. H. Whitelaw
G. Wigley

Department of Mechanical Engineering,
Imperial College,
London, England

The Calculation of Furnace-Flow Properties and Their Experimental Verification

Measurements of mean axial velocity, and the corresponding normal stress are reported for the isothermal flow of air and for a combusting mixture of natural gas in an axisymmetric furnace enclosure with a coaxial burner. Temperature and wall heat flux measurements were also obtained for the combusting flow. The swirl number of the flow was 0.5. The measurements are compared with the results of a calculation procedure incorporating a two equation turbulence model and a one step reaction model. The combustion model allowed fuel and oxygen to coexist at the same place but not at the same time. The comparison indicates that the calculation procedure qualitatively represents the measurements but that quantitative differences exist. The argument is sufficiently close, however, to justify the use of the method for some design purposes.

Introduction

In an earlier paper, reference [1],[1] the authors reported measurements of velocity components and the corresponding normal stresses obtained in a model furnace by laser-Doppler anemometry. This paper reports new measurements obtained in the same furnace at a higher flow rate and, in addition, compares them with values obtained with a numerical design method. The measurements have been extended to include values of mean temperature and wall-heat flux. The inlet, swirl numbers of the flow were zero and approximately 0.52 for the isothermal air flow and, for reasons of flame stability, the zero swirl flow was not measured for the combusting mixture of natural gas and air. The calculations were ohtained with the aid of a computer program originated by Gosman and Pun [2] and developed by Khalil and Whitelaw [3] for furnace configurations. The program solves, in finite-difference form, the two-dimensional elliptic forms of appropriate conservation equations.

The purpose of the research program, of which the present work forms a part, is to develop a design procedure for cylindrical furnaces. Since the conservation equations embodied in this procedure have been time averaged, the equations are not exact and include assumptions which may be classified as belonging to the turbulence or combustion models. It is, therefore, necessary to quantitatively assess the reliability of the procedure by comparison with experiments and the present experimental program is designed to meet this need. In contrast to previous experimental investigations, for example references [4–6], the present use of laser-Doppler anemometry allows the determination of Reynolds stresses and these provide a more sensitive test of the turbulence model than does the mean velocity. The previous computational investigations of Khalil and Whitelaw [3, 7] demonstrated, by comparison with the experiments of references [1, 4–6], that a two equation turbulence model allowed reasonable prediction of velocity and normal stresses and that a one step representation of the chemical reaction was also satisfactory. The comparisons of references [3, 7] were deficient in that only the data of reference [1] provided measured initial conditions but they did not include temperature or heat flux information. The measurements described here include initial conditions and provide velocity, temperature and heat-flux information obtained in the same flow configuration.

The following sections of the paper consider, in turn, the computational method and its physical assumptions; the flow configuration, associated instrumentation and procedures; and the results of computational and experimental investigations. The implications

[1] Numbers in brackets designate References at end of paper.

Contributed by the Heat Transfer Division of THE AMERICAN SOCIETY OF MECANICAL ENGINEERS and presented at the AIChE-ASME National Heat Transfer Conference, San Francisco, Calif., August 10-13, 1975. Revised manuscript received by the Heat Transfer Division November 12, 1975. Paper No. 75-HT-8.

Table 1

Variable ϕ	a_1	b_1	b_2	S_ϕ
U	1	μ_{eff}	μ_{eff}	$\frac{\partial}{\partial x}(\mu_{\text{eff}}\frac{\partial U}{\partial x})+\frac{1}{r}\frac{\partial}{\partial r}(\mu_{\text{eff}}r\frac{\partial V}{\partial x})-\frac{\partial P}{\partial x}$
V	1	μ_{eff}	μ_{eff}	$\frac{\partial}{\partial x}(\mu_{\text{eff}}\frac{\partial U}{\partial r})+\frac{1}{r}\frac{\partial}{\partial r}(\mu_{\text{eff}}r\frac{\partial V}{\partial r})-\frac{2\mu_{\text{eff}}V}{r^2}+\frac{\rho W^2}{r}-\frac{\partial P}{\partial r}$
W	1	μ_{eff}	μ_{eff}	$-(\frac{\mu_{\text{eff}}}{r^2}+\frac{\rho V}{r}+\frac{1}{r}\frac{\partial\mu_{\text{eff}}}{\partial r})W$
k	1	$\frac{\mu_{\text{eff}}}{\sigma_k}$	$\frac{\mu_{\text{eff}}}{\sigma_k}$	$G_{k_1}-\rho\epsilon$
ϵ	1	$\frac{\mu_{\text{eff}}}{\sigma_\epsilon}$	$\frac{\mu_{\text{eff}}}{\sigma_\epsilon}$	$\frac{\epsilon}{k}(C_1G_{k_1}-C_2\rho\epsilon)$
f	1	$\frac{\mu_{\text{eff}}}{\sigma_f}$	$\frac{\mu_{\text{eff}}}{\sigma_f}$	0
h	1	$\frac{\mu_{\text{eff}}}{\sigma_h}$	$\frac{\mu_{\text{eff}}}{\sigma_h}$	0
g	1	$\frac{\mu_{\text{eff}}}{\sigma_g}$	$\frac{\mu_{\text{eff}}}{\sigma_g}$	$C_{g_1}G_{g_1}-C_{g_2}\rho\frac{\epsilon}{k}g$
m_{fu}	1	$\frac{\mu_{\text{eff}}\mu}{\sigma_{\text{fu}}}$	$\frac{\mu_{\text{eff}}}{\sigma_{\text{fu}}}$	R_{fu}

$$G_{k_1}=\mu_{\text{eff}}\left[2\left(\left(\frac{\partial U}{\partial x}\right)^2+\left(\frac{\partial V}{\partial r}\right)^2+\left(\frac{V}{r}\right)^2\right)+\left(\frac{\partial W}{\partial x}\right)^2+\left(r\frac{\partial}{\partial r}\left(\frac{W}{r}\right)\right)^2+\left(\frac{\partial U}{\partial r}+\frac{\partial V}{\partial x}\right)^2\right]$$

$$G_{g_1}=\mu_{\text{eff}}\left[\left(\frac{\partial m_{\text{fu}}}{\partial x}\right)^2+\left(\frac{\partial m_{\text{fu}}}{\partial r}\right)^2\right]$$

of the comparisons are discussed and specific conclusions stated in the closing sections.

Calculation Procedure

The present section presents the conservation equations and corresponding boundary conditions and comments briefly on the thermodynamic properties, the turbulence model, the combustion models, and the solution procedure. Further details of the solution procedure may be found in references [2, 3]. The equations and physical assumptions are given in detail in references [3, 7].

Equations and Boundary Conditions. The conservation equations, apart from mass continuity, had the common form:

$$a_1\left[\frac{\partial}{\partial x}(\rho U\phi)+\frac{1}{r}\frac{\partial}{\partial r}r(\rho V\phi)\right]=\frac{\partial}{\partial x}\left(b_1\frac{\partial\phi}{\partial x}\right)+\frac{1}{r}\frac{\partial}{\partial r}\left(rb_2\frac{\partial\phi}{\partial r}\right)+S_\phi \quad (1)$$

where the corresponding values of a_1, b_1, b_2 and S_ϕ are given in Table 1. The dependent variables include three components of the time-averaged velocity, total enthalpy and species properties and are to be calculated at values of the independent variables x and r. The use of time-average equations and the effective viscosity hy-

Nomenclature

a_0, b_0, c_0, d_0 = constants in specific heat equation
b_1, b_2 = constants
C_p = specific heat at constant pressure
C_1, C_2 = constants in turbulence model
C_{g1}, C_{g2} = constants in combustion model
C_D = constant
C_R = eddy-break-up constant
D = diameter
E = constant of law of wall
f = mixture fraction = $(\varphi-\varphi_A)/(\varphi_F-\varphi_A)$
g = square of the fluctuation of concentration
h = stagnation enthalpy
H_{fu} = heat of reaction of fuel
i = stoichiometric mass of oxygen per unit mass of fuel
k = kinetic energy of turbulence = $\frac{1}{2}(u^2+v^2+\bar{w}^2)$
K = constant in log law
M = molecular weight
m = mass fraction
P = pressure
Q = heat flux
R = universal gas constant
r = radial distance from axis of symmetry
R_0 = burner outer radius
Re = Reynolds number
R_ϕ = residual value
S = swirl number defined as; $\int\dot{W}U\rho r^2dr/(\int\rho U^2rdr)R_0$
s_ϕ = source or sink term of any variable
T = absolute temperature
U = fluid mean velocity in the axial direction
u = fluctuation component of axial velocity
V = radial mean velocity
v = fluctuation component of radial velocity
W = mean tangential velocity
w = fluctuation component of tangential velocity
x = axial distance from burner exit
y = radial distance from burner centre line
y_a = width of burner annulus
μ = viscosity
ρ = density
σ_ϕ = Schmidt and Prandtl numbers for any variable ϕ
ϵ = dissipation of energy
φ = $(m_{fu}-m_{ox}/i)$
ϕ = general dependent variable
eff = effective (including the effects of turbulence)
fu = fuel
i = species
ox = oxidant
f = furnace
A = air stream
F = fuel stream
w = wall

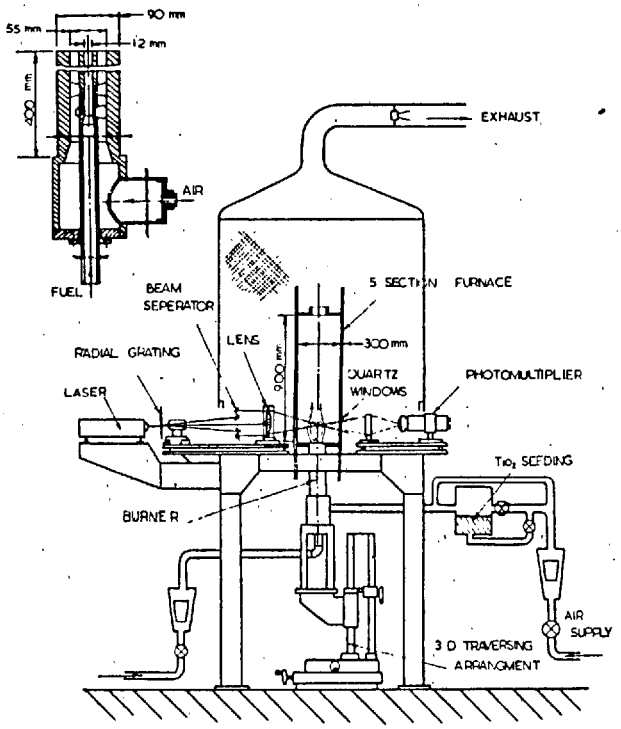

Fig. 1 Arrangement of furnace, burner and laser—Doppler anemometer

pothesis implied by Table 1 requires equations for turbulent kinetic energy and dissipation rate and constitute a model of turbulence. The equations for species concentration and species concentration fluctuations represent the combustion processes and will be referred to as the combustion model.

Boundary conditions are required for each of the equations of Table 1 and, wherever possible, these were obtained by measurement. Fig. 1 shows the geometry of the present furnace and shows a symmetry axis; this provides a boundary condition of the form $\partial\phi/\partial r = 0$ for one boundary of the solution domain. The velocities were assumed zero at all walls and the measurements provided the corresponding wall temperature conditions. The gradients of m_i, f, and g were assumed zero at all walls. At the inlet, the dissipation rate was determined from the equation

$$\epsilon = C_D \frac{k^{3/2}}{0.03 y_a} \tag{2}$$

which stems from a mixing length assumption: all other properties were taken from measurements. At the exit, all gradients were assumed to be zero; as was shown in references [3, 7], this assumption has a negligible influence on the upstream flow.

Thermodynamic Properties. The local density of the gaseous mixtures was obtained from the perfect gas law and Dalton's law of partial pressures. Values of specific heat were obtained from equations of the form:

$$\bar{C}_{pi} = a_{0_i} + b_{0_i}T + c_{0_i}T^2 + d_{0_i}T^3 \tag{3}$$

$$\bar{C}_{p\,\mathrm{mix}} = \sum_i m_i \bar{C}_{pi} \tag{4}$$

with the constants suggested in reference [8]. The total enthalpy of the mixture was defined as

$$h = m_{\mathrm{fu}} H_{\mathrm{fu}} + m_i \bar{C}_{pi} T + (U^2 + V^2 + W^2)/2 \tag{5}$$

with the heat of reaction, H_{fu}, taken as 4.97×10^4 kJ/kg.

Turbulence Model. The turbulence model involves the solution of the equations for k and ϵ together with the equations

$$-\rho\overline{uv} = C_D \rho \frac{k^2}{\epsilon}\left(\frac{\partial U}{\partial y} + \frac{\partial V}{\partial x}\right), \quad -\rho\overline{uw} = C_D \rho \frac{k^2}{\epsilon}\left(\frac{\partial W}{\partial x}\right) \tag{6}$$

The diffusion and dissipation terms in the k and ϵ equations are simplified representations of the exact terms and, although based on reasonable assumptions, have not been tested directly. The validity of this two-equation turbulence model has been tested by comparing calculations, obtained from the solution of boundary-layer equations including appropriate forms of the k and ϵ equations, with measurements also obtained in boundary-layer type flows. It has not been extensively tested in elliptic flows and the comparison of Section 4 help to meet this need.

Combustion Models. A one step, finite reaction rate model has been assumed for all calculations of section 4. It requires the solution of equations for f, g, and m_{fu} and represents the source term in the fuel equation by

$$R_{\mathrm{fu}} = m_{\mathrm{fu}} \rho^2 m_{0x} 10^{10} \exp(-1.84 \times 10^4/T) \tag{7}$$

$$\text{or } R_{\mathrm{fu}} = C_R g^{1/2}(\rho\epsilon/k) \tag{8}$$

whichever is the smaller.

The time variation of f was assumed to have a square wave form, corresponding to a double delta function probability distribution, i.e.

$$f_+ = f + g^{1/2}, f_- = f - g^{1/2} \tag{9}$$

except where the value of f_+ would exceed unity or f_- fall below zero. In these regions, the factor α defined by

$$f = \alpha f_+ + (1 - \alpha) f_- \tag{10}$$

was adjusted to insure that f_+ was unity or f_- zero. This procedure allowed fuel and oxygen to exist at the same place but at different times. The local temperature of the mixture was determined from the enthalpy obtained from the simultaneous solution of the h-equation. From the definition of h given in equation 5, T_+ and T_- are calculated corresponding to values of $m_{\mathrm{fu}+}$ and $m_{\mathrm{fu}-}$. Values of mean temperature were then obtained from an equation similar to equation (10).

The values of constants in the turbulence and combustion models are listed in Table 2 and are consistent with those proposed in reference [9]: they have not been modified for the present calculations.

Solution Procedure. The differential equations represented by equation (1) and Table 1 were expressed in the finite-difference form of reference [2] and solved by the algorithm of that paper. The present calculations were performed with a grid composed of 20×20 nodes and allowed the solution of the 10 equations in approximately 8 min of CDC 6600 cp time; in the absence of swirl, this time reduced to 6 min and in the absence of swirl and combustion to 4 min. These times were achieved with the help of wall functions which linked the wall value to first grid nodes located in the logarithmic region of the boundary layer [9].

The distribution and number of grid nodes was investigated in reference [3] and the present arrangement was based on that experience. Convergence was assumed when the maximum residual, i.e.

$$[\text{convection} + \text{diffusion} + \text{source}]_{j+1}/\phi_j$$

was less than 10^{-4} at any grid node. After 30 iterations, all calculations were observed to converge monotonically. Approximately 250 iterations were required to satisfy the above convergence criterion.

Table 2 Turbulence and combustion model constants

Constant	Value
C_1	1.44
C_1'	1.92
C_D	0.09
K	0.42
E	8.8
C_{g_1}	2.8
C_{g_2}	2.0
C_R	1.0

$\sigma_\epsilon = 1.22$; $\sigma_k = \sigma_h = \sigma_{\mathrm{fu}} = \sigma_g = \sigma_f = .9$

Experimental Procedure

The model furnace and burner arrangements, the instrumentation and the experimental procedures are described briefly and separately in the following paragraphs. With the exception of temperature and heat-flux measurements, the instrumentation is similar to that described in reference [1]; the furnace and burner are also similar but were operated at higher flow rates and, as a consequence, the furnace cooling water was directed to a heat exchanger.

Furnace and Burner Arrangements. Fig. 1 shows, in line-diagram form, the outline and dimensions of the furnace enclosure and the layout of the laser-Doppler anemometer. For the isothermal measurements, a plexiglass enclosure was used and allowed measurements of the three orthogonal velocity components at all locations in the enclosure except in the vicinity of the wall. For the combusting measurements, a double-skinned steel enclosure of the same internal dimensions was used; it was water cooled in five separate axial sections and one section was fitted with windows to allow the transmission of light beams. The bottom plate of the furnace was also water cooled. The finite dimensions of the windows limited the range of locations at which the radial velocity component could be measured.

The burner arrangement is also shown on Fig. 1. For the isothermal measurements, the Reynolds number of the flow in the annulus was 4.7×10^4, corresponding to a mean axial velocity of 12.85 m/s, and that of the central jet flow 0.55×10^4; vane swirlers were added to produce a swirling annulus flow with a swirl number of 0.52. For the combusting measurement, natural gas (CH_4—94.4 percent, N_2—1.40 percent C_2H_6—3.1 percent); was supplied through the central jet to provide an initial mixture fraction corresponding to stoichiometric combustion.

The furnace and burner arrangement was traversed with respect to the laser-Doppler anemometer. The precision of translation in the horizontal plane was of the order of 1.0 mm and, in the vertical plane 2 mm. In this vertical plane, the burner top and bottom plates were moved vertically within the fixed steel enclosure.

The measurements were obtained without seeding the flow although residual titarium dioxide particles in the pipework did contribute to the particulate content of the flow.

Instrumentation. Velocity measurements were obtained with a laser-Doppler anemometer comprising an argon ion laser, a bleached radial diffraction grating and a focussing lens, a light collection arrangement, a photomultiplier and a bank of filters whose output was read automatically and transferred to paper tape. The laser was operated at 488 nm with a power output of approximately 130 MW. The radial grating had a total of 18,000 lines, equispaced in angle. on a radius of 130 mm and was rotated at velocities up to 5000 rpm. The bleaching process allowed 55 percent of the incident light energy to be concentrated into the two first order beams; further details of the performance characteristics of bleached gratings have been provided by Wigley [10]. Measurements were made with frequency shifts from −3.01 MHz to 3.01 MHz. The focussing lens had a focal distance of 400 mm and the forward-scattered light was collected by a lens of diameter 25 mm and focal length 200 mm: it was passed through a 0.75 mm pinhole to the photomultiplier (EMI 9635QB) cathode. The resulting control volume dimensions corresponded to a length of 2.4 mm and a diameter of 0.21 mm. The signal from the photomultiplier was high pass filtered at 600 kHz, amplified, low pass filtered at 10 MHz; limited to 100 mV and supplied to the filter bank described in detail by Baker [11]. In the filter bank the input signal was presented to 60 parallel filters with centre frequencies ranging from 0.631 MHz to 9.55 MHz in a logarithmic progression. After a threshold level had been set to reduce system noise, the filter bank logic established the most resonant of the filters and provided a voltage proportional to this frequency. The voltage analogue signal was supplied to a time analyser which time averaged the signal, and its square, to give values of the mean and rms velocities. The voltage analogue was further used to trigger a constant current which charged a capacitor, associated with a resonant filter, for the length of time of the Doppler burst. By scanning and logging the accumulated charges in the sixty individual capacitor stores, a histogram display was produced and is related to the probability distribution of Doppler frequencies. Statistical analysis of the histogram yielded the mean and rms velocities and higher moments.

The local temperature of the combusting gas was measured with a miniature suction pyrometer. The gas was sucked isokinetically into the probe and over a platinum–platinum 13 percent rhodium thermocouple calibrated between 1100 and 1800 K with a precision of ±20 K: at temperatures below 1100 K, the instrument was at least as precise on this calibration. The temperature of the furnace wall was obtained from chromel alumel thermocouples welded to the surface. The flow rates of water to each of the five sections of the enclosure were measured by rotameter and, together with the temperature of the water at inlet and outlet, allowed the calculation of the wall heat flux.

Results

The measurements presented in this section relate to a swirl number of 0.5 and to isothermal and combusting flow. Preliminary measurements with a swirl number of zero indicated that the flame was not stabilised on the burner and, since this was physically undesirable and could not be satisfactorily represented by the calculation method, they were not persued. The swirl number was determined by assuming profiles of nondimensional velocity and normal stresses, similar to those of reference [1] and calculating the profiles of velocity and normal stresses at downstream locations: the profiles at 0.1 D_f and 0.166 D_f, shown on the following figures were in closest agreement with a swirl number of 0.5 for both isothermal and combusting flow and confirm the measurement of reference [1].

Figs. 2 and 3 present measured profiles of the axial mean velocity and the corresponding normal stress at locations downstream of the burner with isothermal air flow. The calculated profiles are also shown and the general agreement supports the view that the calculation method is satisfactory for isothermal flows and may be applied to combusting flows with the knowledge that the turbulence model is likely to be adequate. As can be seen, the distribution of mean axial velocity is complex with a substantial region of recirculation which begins at the burner exit and extends, away from the centre line, to one furnace diameter downstream. The corresponding fluctuation velocity is comparatively large close to the burner and tends to a uniform and lower value at downstream locations. The calculated normal stress is, of course, based on the solution of an equation for turbulence kinetic energy and assumes that $\bar{u}^2 = \frac{2}{3}k$.

Figs. 4 and 5 present measurements corresponding to those of Figs. 2 and 3 but relate to the combusting flow. The axial velocity and corresponding normal stress are larger in the combusting case, particularly in the region of the reaction zone. Indeed the region of the reaction zone can readily be recognized from the measurements. Once again, the calculated profiles are in general agreement with the measurements although quantitative differences, particularly in the reaction zone, are present. Mean and rms tangential velocity profiles are presented in Fig. 6 at two axial locations close to the burner exit for the burning case; they show that the larger tangential velocities are only slightly smaller than the corresponding axial velocities and that the normal stresses have a similar relationship.

The center-line velocity distributions for the isothermal and combusting flows are shown on Fig. 7. Only two measurements were obtained for the isothermal flow due to the very low particle concentration in this region. Comparison of the measured and calculated distributions indicates general agreement although the measured wake development is faster than that calculated. The region of center-line recirculation is substantial for the combusting flow and the comparison of the two distributions is similar to those reported in reference [1]. The figure also presents calculated distributions of axial velocity for a range of swirl numbers and shows

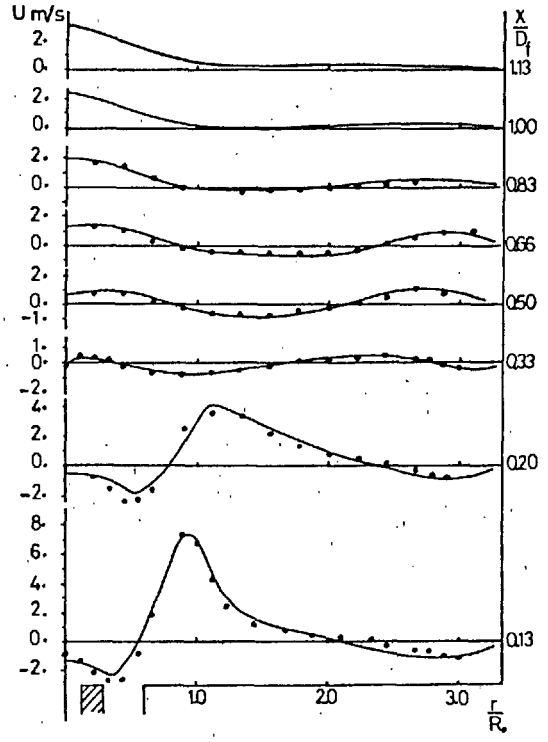

Fig. 2 Measured and calculated profiles of mean axial velocity: isothermal flow . . . measured values, —calculated values

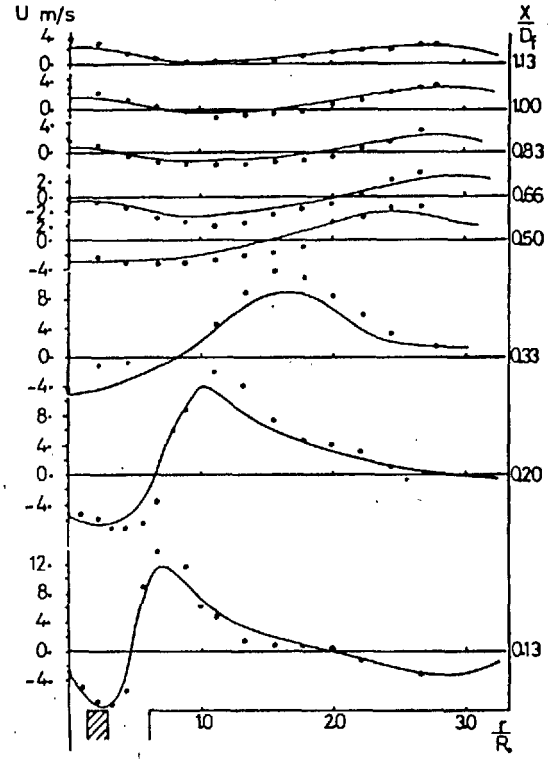

Fig. 4 Measured and calculated profiles of mean axial velocity: combusting flow . . . measured values, —calculated values

that the location and magnitude of the recirculation region are very dependent on the swirl number.

Measured and calculated temperature profiles are presented in Fig. 8 and can be related to the recirculation regions indicated by Fig. 4. They reveal temperature minima, close to the water-cooled base plate and in the region of forward velocity. The two temperature maxima, on either side of the minimum values, represent the edges of the reaction zone.

Figs. 9 and 10 present center-line distributions of mean temper-

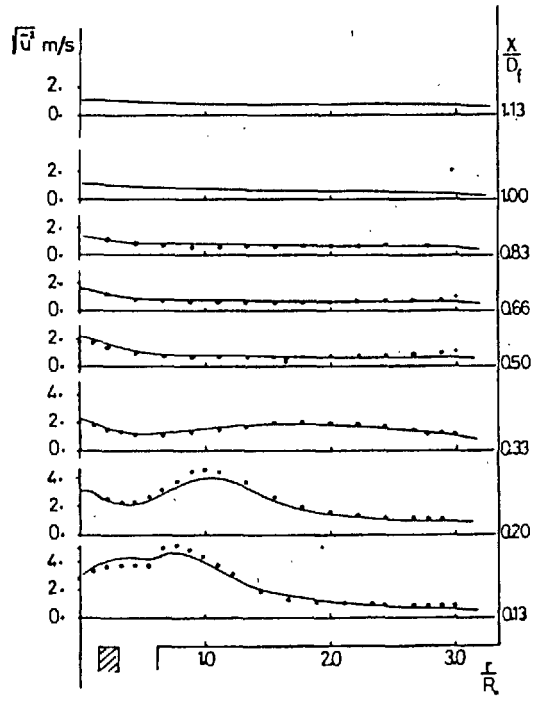

Fig. 3 Measured and calculated profiles of axial normal stress: isothermal flow . . . measured values, —calculated values

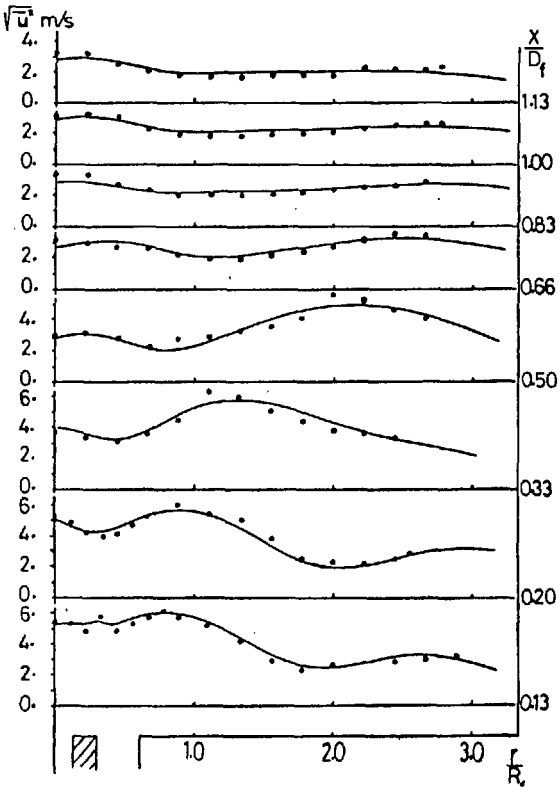

Fig. 5 Measured and calculated profiles of axial normal stress: combusting flow . . . measured values, —calculated values

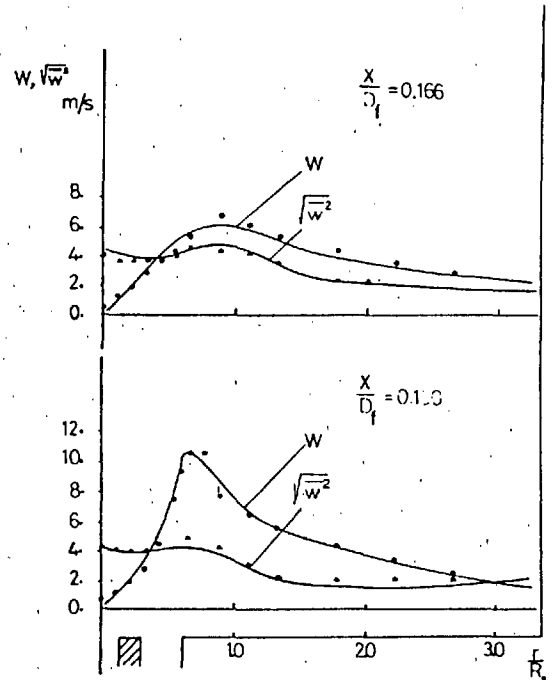

Fig. 6 Measured and calculated profiles of mean tangential velocity and the corresponding normal stress: combusting flow ... measured values, —calculated values

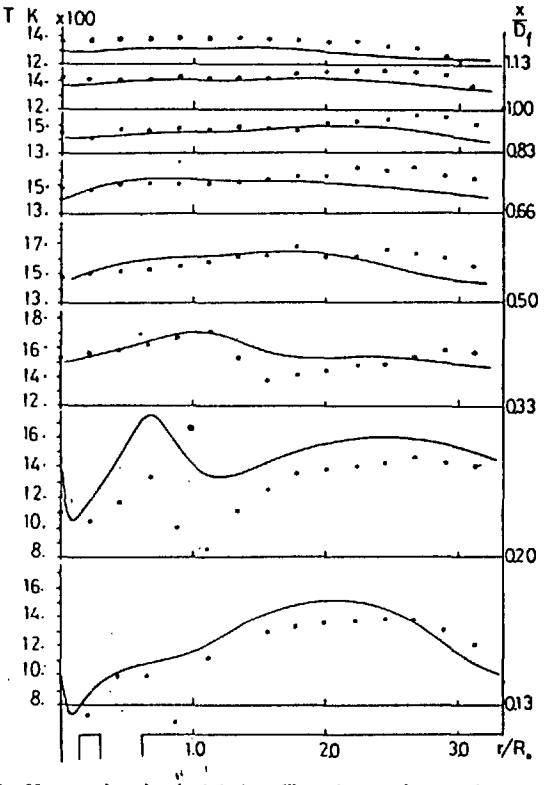

Fig. 8 Measured and calculated profiles of mean temperature ... measured values, —calculated values

ature and wall-heat flux respectively. Measured and calculated values may be compared for the case of a swirl number of 0.5 and the influence of swirl deduced from the calculations. The temperature results indicate that, as far as the center line is concerned the highest swirl number leads to the most rapid rise in temperature. The heat-flux results confirm this and suggest that the present furnace would be operated more effectively with higher flow rates of air and fuel.

Discussion and Conclusions

The comparisons of the previous section show that the calculated results are in general agreement with the measurements but that quantitative differences remain to be explained. Similar calculations, performed with the same physical information but with a different numerical scheme [7] show that differences of up to 15 percent can be introduced by the numerical arrangement although the rms difference was less than 5 percent. It must be presumed, therefore, that a substantial part of the differences indicated on the previous figures must be attributed to the physical content of the calculation method or to errors of measurement, with the former as the main source.

The turbulence model may be assessed from the results of Figs. 2 and 3 and appears to result in differences from the measurements which exceed the experimental scatter and which amount to up to 40 percent of the maximum velocity in the appropriate axial plane. The largest disagreements are in the wake and suggest that the two-equation turbulence model is inadequate in such regions. This conclusion is substantiated by the calculations of Pope and Whitelaw [12] for separated—wake flows. It is noteworthy that the two equation model also assumes isotropy of the normal stresses which is undoubtedly incorrect.

The major source of imprecision for the furnace calculations is the combustion model. The present calculations were repeated

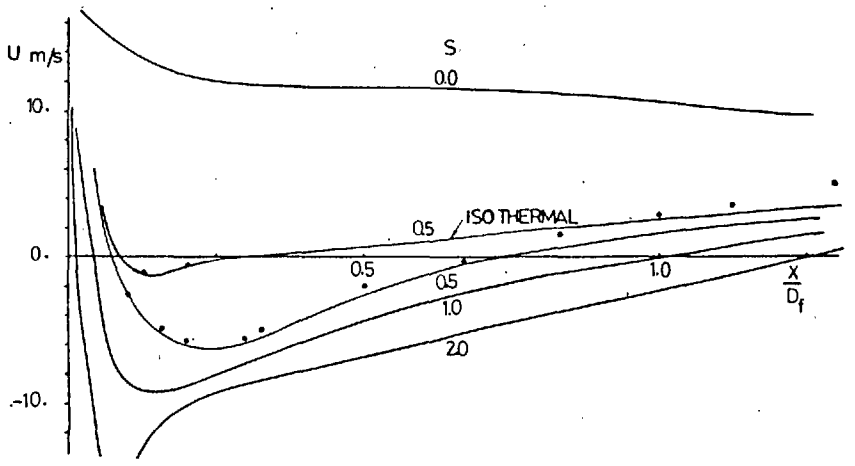

Fig. 7 Measured and calculated center-line distributions of axial mean velocity ... measured values, —calculated values

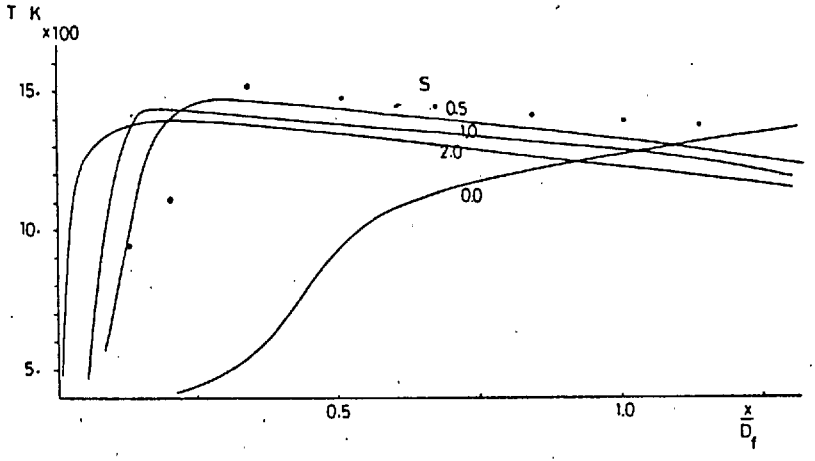

Fig. 9 Measured and calculated center-line distributions of mean temperature . . . measured values, —calculated values

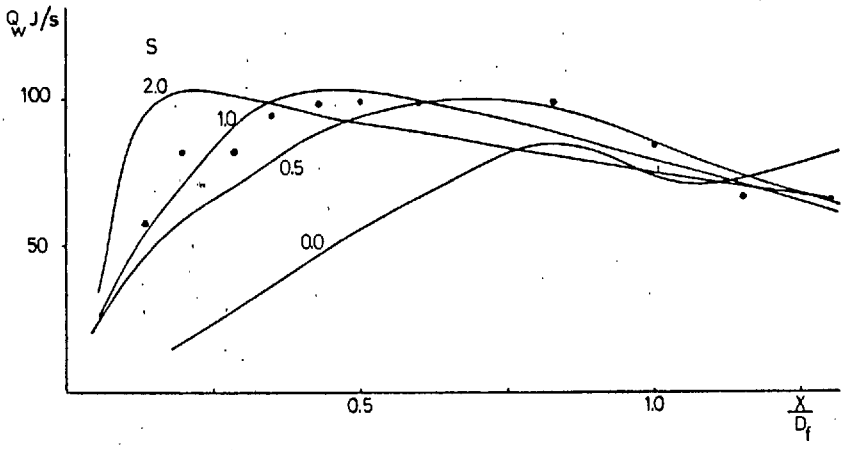

Fig. 10 Measured and calculated distributions of wall-heat flux . . . measured values, —calculated values

with the alternative assumption of infinite-reaction rate and the results were different from those presented here; the differences were not, however, significant when compared with the differences from the experimental data. Instant reaction is undoubtedly an over simplification and the faults in the present model must he traced and corrected. Since the eddy-break up equation controls the reaction for most of the solution domain it may be concluded that it is in need of improvement. Also, the square-wave variation of the mixture fraction with time is a simplification which has not been directly tested for flows of this type. These two assumptions are the most likely reasons for the discrepancies of, for example, Fig. 8 and work is presently in hand to improve them.

In spite of the emphasis of the previous paragraphs on the need to improve the calculation procedure, the results show that trends have been predicted correctly with the present assumptions and consequently the calculation procedure contribute to design in its present form. This is the major conclusion of the present investigation.

Acknowledgments

The present work was carried out with the financial assistance of the AERE, Harwell. Grateful thanks are due to Dr. J. Rhines of British Gas Corp., Solihull for assistance and advice on suction pyrometer measurements.

References

1 Baker, R. J., Hutchinson, P., Khalil, E. E., and Whitelaw, J. H., "Measurements of Three Orthogonal Velocity Components in Confined Coaxial Jet Flows With and Without Swirl and Combustion," *Proceedings 15th Symposium on Combustion*, 1974, p. 533.

2 Gosman, A. D., and Pun, W. M., Lecture notes for course entitled "Calculation of Recirculating Flows," Imperial College, Mechanical Engineering Department, 1973.

3 Hutchinson, P., Khail, E. E., and Whitelaw, J. H., "The Calculation of Wall Heat-Transfer Rate and Pollution Formation in Axi-Symmetric Furnaces," Fourth Members Conference of the IFRF, 1976.

4 Fricker, N., van Heyden, L., and Michelfelder, S., "Investigations Into the Combustion of Natural Gas in Multiple Burner Systems," International Flame Research Foundation document F35/a/5, 1971.

5 Fricker, N., and Wu, H. L., "An Investigation of the Behaviour of swirling Jet Flames in a Narrow Cylindrical Furnace," International Flame Research Foundation, 2nd Members Conference, 1971.

6 Gunther, R., and Lenze, B., "Exchange Coefficients and Mathematical Models of Jet Diffusion Flames," *Proceedings 14th Symposium on Combustion*, 1972, p. 675.

7 Khalil, E. E., and Whitelaw, J. H., "The Calculation of Local-Flow Properties in Two-Dimensional Furnaces," Imperial College, Mechanical Engineering Department Report HTS/74/38, see also I.J.H.M.T. Vol. 18, 1975, p. 775.

8 JANAF thermochemical tables, National Bureau of Standards, USA; NSRDS NBS 37, COM-71-50363, 1971.

9 Launder, B. E. and Spalding, D. B. *Mathematical Models of Turbulence*. Academic, 1972.

10 Wigley, G., "The Application of Radial Diffraction Gratings to Laser

Anemometry," AERE Report 7886, 1974.
11 Baker, R. J., "The Application of a Filter Bank to Measurements of Turbulence in a Fully Developed Jet Flow, *Proceedings of 2nd International Workshop on Laser Velocimetry*, Purdue University, 1974.
12 Pope, S. B., and Whitelaw, J. M., "The Calculation of Near-Wake Flaws," *Journal of Fluid Mechanics*, Vol. 73, 1976, p. 9.

APPENDIX A5

INFLUENCE OF BURNER GEOMETRY ON THE PERFORMANCE OF SMALL FURNACES ++

P. Hutchinson,* E.E. Khalil,** J.H. Whitelaw** and G. Wigley**

Introduction

In recent papers, for example references 1, 2 and 3, it has been shown that calculation methods based on the numerical solution of appropriate conservation equations can result in values of important furnace flow properties which are in reasonable agreement with measurements. In general it can be said that these methods have been shown to correctly represent measured trends and, in some cases, to correctly represent the magnitudes of measured values.

The calculations reported in references 1, 2 and 3 were concerned with two-dimensional arrangements and dimensions appropriate to the furnaces of references 4, 5, 6 and 7. Implicitly, therefore, different geometrical configurations of the burner exit flame were considered but not in the systematic manner necessary to demonstrate their influence. The main purpose of this paper is to remove this deficiency and it is achieved first by comparing calculations with new experiments designed to demonstrate the influence of a burner quarl and then, with this comparison as a guide to the precision of calculation, by presenting calculations for a practically relevant range of geometrical parameters.

The following section describes the experimental arrangement and instrumentation used to obtain the measurements with and without a burner quarl: the results are presented and discussed briefly. The following section outlines the calculation procedure, presents the results obtained for comparison with the experiments of section 2 and discusses the extent of the agreement. Calculated results, outside the range of measurements are also presented. The paper ends with a brief statement of conclusions.

* Theoretical Physics Division, A.E.R.E., Harwell, Oxfordshire.

** Department of Mechanical Engineering, Imperial College of Science and Technology, London.

++ Proc. 2nd European Symposium on Combustion, 675, 1975.

Experimental Investigation

The furnace was axi-symmetric with an internal diameter of 300mm and length of 900mm: the walls were water cooled in five separate axial sections. The co-axial burner was operated with swirl vanes, which resulted in a swirl number of 0.5, and with an annulus flow rate of 23 litres/s of air and a central jet flow of 1.7 litres/s of natural gas; this corresponded to an air/fuel ratio of 13.5. The diameters of the annulus were 55mm and 27mm and of the central jet 12mm. The present measurements were obtained with the burner exit flush with the base plate of the furnace and with a quarl piece removed to create a 20 degree angle at exit from the annulus. The temperature of the furnace wall varied from 328K 20mm above the base plate to a maximum of 383K.

Measurements of mean axial velocity and the corresponding normal stress were obtained with the laser-Doppler anemometer described in references 2 and 4. It combined an argon laser operated at approximately 100mW, a bleached radial diffraction grating to split the laser beam and to provide frequency shifting, focussing and collection lenses, a pinhole, photomultiplier and signal-processing arrangement based on a bank of filters. The filters covered a range from 0.631 MHz to 9.55 MHz in a logarithmic progression.

The local temperature of the combusting gas was measured with a miniature suction pyrometer of outside diameter 5mm. The gas was sucked isokinetically into the probe and over a platinum-platinum/13% rhodium thermocouple calibrated between 1620 and 2000K with a precision of ± 20K; at the temperatures below 1620K, the precision was of the same order of magnitude.

The temperature of the furnace wall was measured with chromel-alumel thermocouples imbedded in the wall. The flow rate of water to each of the five sections of the enclosure was measured with a rotameter and, together with the temperature of the water at inlet and outlet, allowed the calculation of the total heat flux to each section.

The measured values of mean axial velocity and the corresponding normal stress are shown on figure 1 for the two flowscorresponding to with and without quarl: figures 2 and 3 show the temperature and heat flux measurements for the same two flows. It can readily be seen that the presence of the quarl results in stabilisation of the flow

within the quarl and a corresponding movement of the recirculation zone towards the burner exit. The temperature and wall-heat flux distributions show, as might be expected, that a greater proportion of the total heat flux is transferred in the part of the furnace nearer to the burner.

Numerical Investigation

The calculation procedure solved, in finite-difference form, equations for the conservation of mass, three components of momentum, turbulent kinetic energy (k), turbulence dissipation rate (ϵ), total enthalpy, mass fraction of fuel, the mixture fraction $m_{fu} - \frac{m_{ox}}{i}$, and the fluctuation of a scalar quantity (g). The general form of conservation is:

$$\left[\frac{\partial}{\partial x}(\rho U\varphi) + \frac{1}{r}\frac{\partial}{\partial r} r(\rho V\varphi)\right] = \frac{\partial}{\partial x}\left(b\frac{\partial\varphi}{\partial x}\right) + \frac{1}{r}\frac{\partial}{\partial r}\left(rb\frac{\partial\varphi}{\partial r}\right) + S_{\varphi}$$

where U is the axial mean velocity
V is the radial mean velocity
φ is the general dependent variable
x and r are the axial and radial coordinates
ρ is the density
S_{φ} is the source of φ
i is the stoichiometric mass of oxygen per unit mass of fuel
b is the effective diffusivity of φ.

The specific heat was specified according to the suggestions of reference 8 and the heat of reaction was taken as 4.07×10^4 kJ/kg.

A finite reaction rate was assumed with the source term in the fuel equation given by

$$R_{fu} = m_{fu}\ \rho^2\ m_{ox}\ 10^{10} \exp(-1.84 \times 10^4/T)$$

or

$$R_{fu} = g^{\frac{1}{2}}(\rho\epsilon/k)$$

whichever is the smaller. The time variation of the mixture fraction was assumed to have a square wave form and the mean temperature was, therefore, determined as the

temperature corresponding to the mean of the temperatures at the maximum and minimum mixture fractions and not to the mean mixture fraction.

The source term of the enthalpy equation represented a four flux radiation model with the form described in reference 9. It took account of the effects of gas and solid-body radiation.

The solution procedure was described in reference 10 which also provides a detailed evaluation of the ability of the procedure to calculate isothermal flows. The present calculations were carried out with a finite-difference mesh of 20 x 20 nodes and required approximately 8 minutes of CDC6600 time per run.

The results of the calculations, for boundary conditions corresponding to those of the experimental data, are also shown on figures 1, 2 and 3 and are clearly in general agreement with the measurements. Differences of magnitude can be seen but are seldom greater than 15% and never result in a misrepresentation of the measured trend. The comparison provides confidence in the use of the procedure for calculating furnace properties for burner geometries different from those used for the measurements.

Distributions of total wall-heat flux, for a range of quarl angles similar to those used in the IJmuiden furnace (5), are shown on figure 3. The corresponding flame lengths are also indicated and are based on the mean-maximum temperature on the furnace centre line. Clearly a decrease in quarl angle results in a shortening of the flame within the furnace and greater heat release in the near burner region. The influence of the inner diameter of the annulus is also indicated on figure 3: for these calculations, the jet diameter, the outer annulus diameter and the mass flows of air and gas were maintained at the previously quoted values.

The proportion of convective to total heat flux in the calculations of figures 1 to 3 varied with the flow. In general, the convection heat transfer was of the same order as the radiative heat transfer and, for example, in the case of with-quarl flow used for present measurements the proportion of convection to total heat flux was 0.39.

Conclusions

1. Comparison between measurements and calculations of mean axial velocity and the corresponding normal stress, mean temperature and wall-heat flux in a model furnace with and without a burner quarl indicates close agreement. The flame for the with-quarl case is considerably shorter with increased wall-heat flux in the near burner region.

2. The calculation procedure has been used to quantify the influence of quarl angle and of solid material between jet fuel flow and annulus air flow over a range of practically relevant dimensions. In general, an increase in either results in a shorter flame.

Acknowledgement

The financial support of the Atomic Energy Research Establishment, Harwell, is gratefully acknowledged. The British Gas Corporation kindly made available the suction pyrometer used for temperature measurements.

References

1. E.E. Khalil and J.H. Whitelaw. The calculation of two-dimensional, turbulent recirculating flows. Part 2: with combustion. Imperial College, Mech. Eng. Dept. Report, 1975.

2. P. Hutchinson, E.E. Khalil, J.H. Whitelaw and G. Wigley. The calculation of furnace-flow properties and their experimental verification. Paper submitted to ASME/ AIChE Summer Meeting, 1975.

3. E.E. Khalil, D.B. Spalding and J.H. Whitelaw. The calculation of local flow properties in two-dimensional furnaces. To be published in Int. J. Heat and Mass Transfer.

4. R.J. Baker, P. Hutchinson, E.E. Khalil and J.H. Whitelaw. Measurements of three orthogonal velocity components in confined co-axial jet flows with and without swirl and combustion. Proc. 15th Symposium on Combustion. See also Imperial College, Mech. Eng. Dept. Report HTS/74/29, 1974.

5. S. Michelfelder and T.M. Lowes. Report on the M-2 trials. IFRF Doc. Nr. F36/a/4, 1974.

6. N. Fricker and H.L. Wu. An investigation of the behaviour of swirling jet flames in a narrow cylindrical furnace. IFRF 2nd Members Conference, 1971.

7. R. Gunter and B. Lenze. Exchange coefficients and mathematical models of jet diffusion flames. Proc. 14th Symposium on Combustion, 675, 1972.

8. JANAF thermochemical tables, National Bureau of Standards, Washington, D.C., NSRDS NBS 37, COM-71-50363, 1971.

9. A.D. Gosman and F.C. Lockwood. Incorporation of a flux model for radiation into a finite-difference procedure for furnace calculations. Proc. 14th Symposium on Combustion, 661, 1972.

10. A.D. Gosman, E.E. Khalil and J.H. Whitelaw. The calculation of two-dimensional, turbulent recirculating flows. Part 1: isothermal. Imperial College, Mech. Eng. Dept. Report 1975.

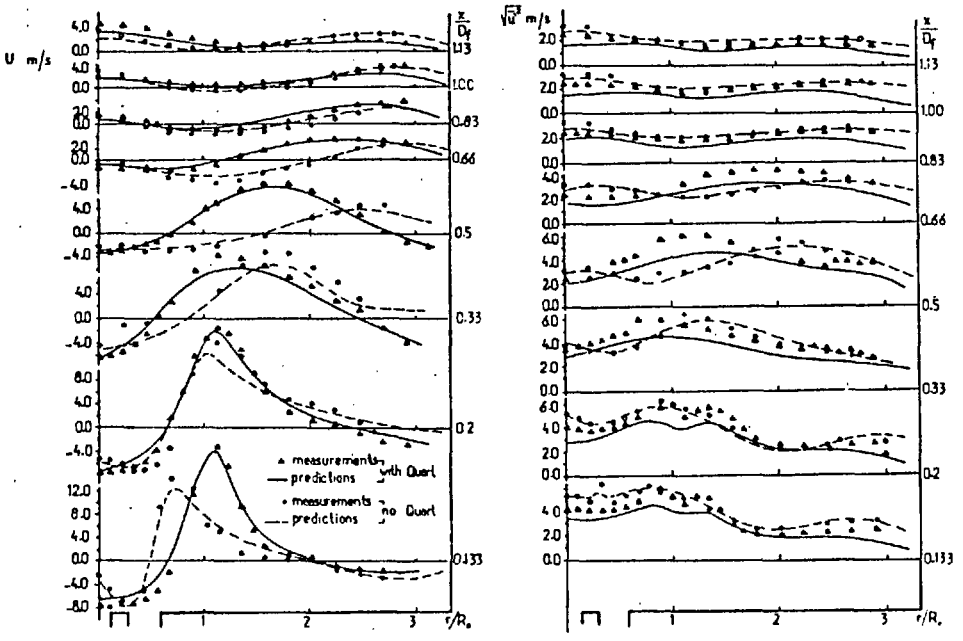

FIG 1. Axial mean velocity and normal stress distributions with and without quarl.

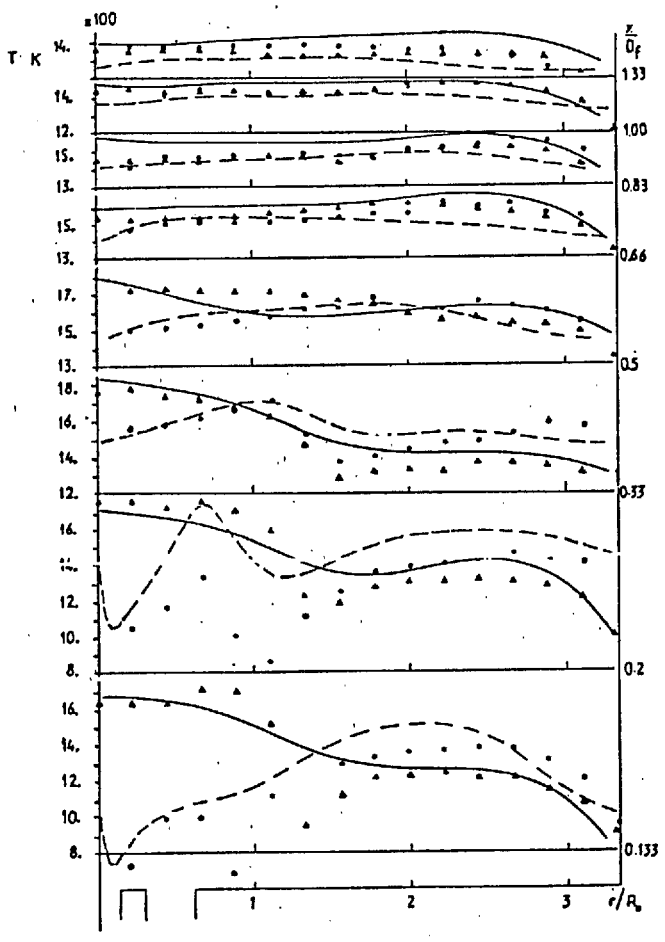

FIG 2. Distributions of mean temperature with and without qural.

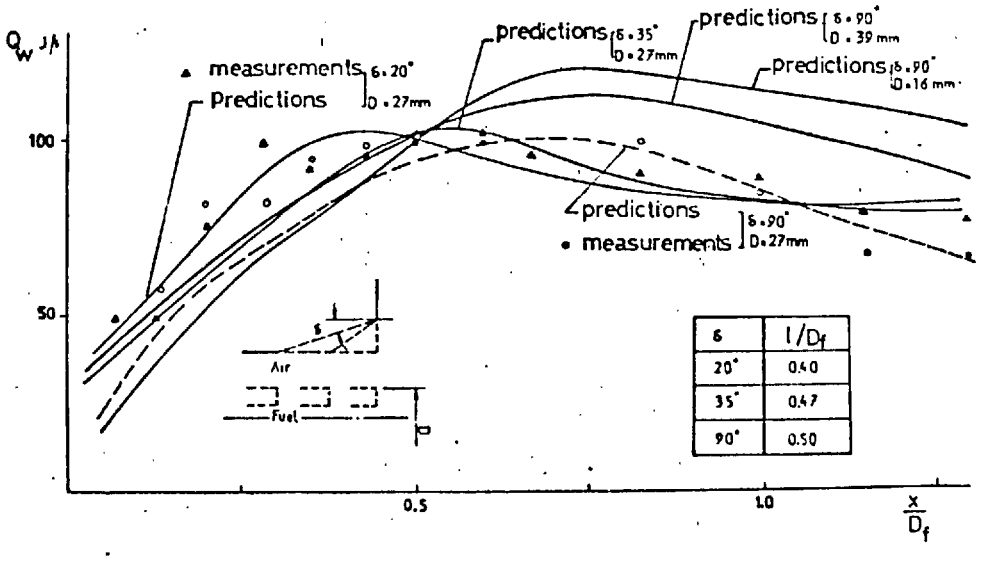

FIG 3. Distributions of wall heat flux as a function of quarl angle and burner dimensions.

APPENDIX A6

Int. J. Heat Mass Transfer. Vol. 18, pp. 775–791. Pergamon Press 1975. Printed in Great Britain

THE CALCULATION OF LOCAL FLOW PROPERTIES IN TWO-DIMENSIONAL FURNACES

E. E. KHALIL, D. B. SPALDING and J. H. WHITELAW
Imperial College of Science and Technology, Department of Mechanical Engineering, London SW7 2BX, England

(*Received 5 February* 1975)

Abstract—Values of local flow properties, obtained by solving appropriate conservation equations in finite-difference form and with boundary conditions corresponding to four furnace arrangements, are presented and compared with measurements.

The calculation procedure employs a two-equation turbulence model, so that calculations can be compared with measurements of turbulence energy as well as mean-velocity components.

Calculations were performed with three combustion models, characterised by instant reaction, instant reaction with scalar fluctuations and Arrhenius reaction or eddy-break up with scalar fluctuations: comparisons with measurements obtained in the Delft, Harwell, Ijmuiden and Karlsruhe furnaces indicate that the last two lead to reasonably correct results.

NOMENCLATURE

A, pre-exponential coefficient;
a, flux-model absorption coefficient;
a_0, constant in the specific heat;
b_0, constant;
b_1, b_2, constants;
C_p, specific heat at constant pressure;
C_1, C_2, constants in turbulence model;
C_{g1}, C_{g2}, constants in combustion model;
C_D, constant;
C_R, eddy-break-up constant;
D, diameter;
E, activation energy;
E, constant of law of wall;
E, black body emissive power, σT^4;
f, mixture fraction, $=(\varphi-\varphi_A)/(\varphi_F-\varphi_A)$;
g, square of the fluctuation of concentration;
h, stagnation enthalpy;
H_{fu}, heat of reaction of fuel;
i, stoichiometric mass of oxygen per unit mass of fuel;
k, kinetic energy of turbulence, $=\frac{1}{2}(\bar{u}^2+\bar{v}^2+\bar{v}_\theta^2)$;
K, constant in log law;
M, molecular weight;
m, mass fraction;
P, pressure;
Q, heat flux;
R, universal gas constant;
r, radial distance from axis of symmetry;
R_o, burner outer radius;
R_f, furnace radius;
Re, Reynolds number;
R_{fu}, rate of chemical reaction;
R_ϕ, residual value;
R_x, R_y, net radiation fluxes in the x and y directions;
S, swirl number defined as: $\int WU\rho r^2\,dr/(\int \rho U^2 r\,dr)R_o$;
s_ϕ, source or sink term of any variable;
T, absolute temperature;
U, fluid mean velocity in the axial direction;
u, fluctuating component of axial velocity;
V, radial mean velocity;
v, fluctuating component of radial velocity;
V_θ, normal tangential velocity;
v_θ, fluctuating component of tangential velocity;
$\mathbf{V}_0$, velocity vector;
x, axial distance from burner exit;
y, radial distance from burner centre line;
y_1, distance normal to the wall;
y_a, width of burner annulus.

Greek symbols

Γ, exchange coefficient;
μ, viscosity;
ρ, density;
σ_ϕ, Schmidt and Prandtl number for any variable ϕ;
σ, Stefan–Boltzmann constant;
ε, dissipation of energy;
φ, the dependent variable $(m_{fu}-(m_{ox}/i))$;
ϕ, general dependent variable;
τ, shear stress.

Subscripts

A, air stream;
eff, effective (including the effects of turbulence);
F, fuel stream;
f, furnace;
fu, fuel;
i, species;
ox, oxidant;
pr, product;
t, turbulent;
w, wall.

1. INTRODUCTION

THE DESIGN of furnaces would be greatly facilitated by a procedure for calculating wall heat transfer and local flow properties as a function of furnace geometry and burner conditions. Such a calculation procedure would allow the influences of air/fuel ratio, mass flow rates, burner-exit geometry and enclosure dimensions on the distribution of heat flux to be determined; the regions of unburnt fuel could be located and reduced; and regions of high temperature and of consequent NO_x formation could be avoided. Design changes leading to improved performance could then be made.

The main purpose of this paper is to test one particular calculation procedure, based on the solution of conservation equations in differential time averaged form. The equations "model" the turbulent flow and the combustion processes; and so require checking by comparisons of calculated results with experimental data. Of course, experiments are also subject to uncertainty and this must be considered in the assessment.

The equations used to model the aerodynamic turbulence have been tested in several flow configurations in the past and the uncertainties which they introduce are unlikely to be as important for furnace calculations as those introduced by the combustion model. Therefore only one turbulence model is considered; but three combustion models are examined, and their results are compared with each other and with measurements.

Attempts to calculate furnace or combustion chamber performance have been reported by, among others, Pai and Lowes [1], Evans and Matthews [2], Gosman and Lockwood [3], Elghobashi and Pun [4] and Anasoulis, McDonald and Buggeln [5]. The present calculations differ from these earlier contributions in that they: (i) make use of a numerical procedure which, although used here solely in the context of two-dimensional flows, can be and has been extended to three-dimensional flows (Patanker and Spalding [6,7]); (ii) take account of recent developments in combustion models; and (iii) include comparisons with the recent and extensive measurements of Baker, Hutchinson, Khalil and Whitelaw [8]. It should be emphasised that the turbulence model and the combustion models have been suggested previously; the turbulence model has been described by Launder and Spalding [9] and the combustion models by Spalding [10, 11].

The experimental data used for comparison purposes, in addition to those of [8], are those of: Michelfelder and Lowes [12]; Wu and Fricker [13]; and Gunther and Lenze [14]. Reference [8] is concerned with the measurement of velocity and its correlations: by contrast, [12-14] present measurements of scalar properties. Relevant details of the geometrical features of these furnaces are indicated in Section 6 where the comparison between calculations and measurements is presented. These computational experiments have been performed at a cost which is very much less than the equivalent furnace-measurement program. The validity of the calculation procedure and the three combustion models is considered in the Discussion (Section 7). The earlier parts of the paper describe the conservation equations, the physical assumptions including the turbulence and combustion models, the solution procedure and the influence of boundary conditions. A knowledge of the sensitivity of the boundary conditions is important because the designer seldom has detailed knowledge of them; indeed, the results presented in [12-14] do not provide a complete specification of boundary conditions.

2. CONSERVATION EQUATIONS AND BOUNDARY CONDITIONS

The geometry of the furnace arrangements considered here results in flows with substantial regions of recirculation and with swirl. The equations used to represent conservation of the flow properties were, therefore, elliptic in form and were expressed in cylindrical coordinates. The general form of the equation was:

$$\left[\frac{\partial}{\partial x}(\rho U\phi)+\frac{1}{r}\frac{\partial}{\partial r}r(\rho V\phi)\right] = \frac{\partial}{\partial x}\left(b\frac{\partial\phi}{\partial x}\right)+\frac{1}{r}\frac{\partial}{\partial r}\left(rb\frac{\partial\phi}{\partial r}\right)+S_\phi \quad (1)$$

with the corresponding values of b and S_ϕ indicated in Table 1.

The use of time-average equations and of the isotropic effective-viscosity hypothesis, implied by Table 1, is complemented by conservation equations for turbulent kinetic energy and dissipation rate. The advantages and limitations of the use of these equations, and a particular effective-viscosity hypothesis, are discussed in Section 3.2.

The elliptic form of the conservation equations represented by equation (1) necessitates the specification of boundary conditions, for each dependent variable, at each surface of the solution domain. This domain was a symmetrical half-section of a furnace and symmetry conditions were, therefore, imposed on the axis. The solid-wall boundary, inlet and outlet conditions corresponded to experiment wherever known: the influence of assumed boundary conditions is quantified in Section 5.

3. PHYSICAL ASSUMPTIONS

Various assumptions are implied in the equations or must be added to them. The representation of the thermodynamic properties, i.e. density, specific heat and heat of reaction are considered in the following subsection. The use of time-average equations and the present model of the turbulence are justified and explained in the second subsection. The various combustion models, the testing of which represents a major part of the contribution of the present paper, are described in the third sub-section which also contains a brief indication of the four-flux model used to represent the radiative heat transfer.

Table 1. Conservation equations corresponding to equation (1)

Conservation of	ϕ	b	S_ϕ
Mass	1	0	0
Axial momentum	U	μ_{eff}	$\frac{\partial}{\partial x}\left(\mu_{eff}\frac{\partial U}{\partial x}\right)+\frac{1}{r}\frac{\partial}{\partial r}\left(\mu_{eff} r\frac{\partial V}{\partial x}\right)-\frac{\partial P}{\partial x}$
Radial momentum	V	μ_{eff}	$\frac{\partial}{\partial x}\left(\mu_{eff}\frac{\partial U}{\partial r}\right)+\frac{1}{r}\frac{\partial}{\partial r}\left(\mu_{eff} r\frac{\partial V}{\partial r}\right)-2\mu_{eff}\frac{V}{r^2}+\frac{\rho V_\theta^2}{r}-\frac{\partial P}{\partial r}$
Tangential momentum	rV_θ	μ_{eff}	$-\frac{2}{r}\frac{\partial}{\partial r}(\mu_{eff} V_\theta r)$
Kinetic energy	k	$\frac{\mu_{eff}}{\sigma_k}$	$G_{k_1}-\rho\varepsilon$
Dissipation rate	ε	$\frac{\mu_{eff}}{\sigma_\varepsilon}$	$\frac{\varepsilon}{k}(c_1 G_{k_1}-c_2\rho\varepsilon)$
Stagnation enthalpy	h	$\frac{\mu_{eff}}{\sigma_h}$	$2a[R_x+R_y-2E]$
Mass fraction of fuel	m_i	$\frac{\mu_{eff}}{\sigma_{fu}}$	R_{fu}
Mixture fraction	f	$\frac{\mu_{eff}}{\sigma_f}$	0
Concentration fluctuation	g	$\frac{\mu_{eff}}{\sigma_g}$	$C_{g_1}G_{g_1}-C_{g_2}\rho\frac{\varepsilon}{k}g$

$$G_{k_1}=\mu_{eff}\left[2\left(\left(\frac{\partial U}{\partial x}\right)^2+\left(\frac{\partial V}{\partial r}\right)^2+\left(\frac{V}{r}\right)^2\right)+\left(\frac{\partial V_\theta}{\partial x}\right)^2+\left(r\frac{\partial}{\partial r}\left(\frac{V_\theta}{r}\right)\right)^2+\left(\frac{\partial U}{\partial r}+\frac{\partial V}{\partial x}\right)^2\right]$$

$$G_{g_1}=\mu_{eff}\left[\left(\frac{\partial f}{\partial x}\right)^2+\left(\frac{\partial f}{\partial r}\right)^2\right] \quad \text{in Model 2.}$$

$$G_{g_1}=\mu_{eff}\left[\left(\frac{m_{fu}}{\partial x}\right)^2+\left(\frac{\partial m_{fu}}{\partial r}\right)^2\right] \quad \text{in Model 3.}$$

3,1. *Thermodynamic properties*

The density of mixtures of air, the combusting gas and the combustion products can be represented with adequate precision for present purposes, by the equation of a perfect gas

$$\rho=\frac{MP}{RT} \tag{2}$$

with M and P determined with the aid of the appropriate mass fractions and Dalton's law of partial pressures.

The specific heat was calculated from the expressions

$$\bar{C}_{p_i}=a_{0_i}+b_{0_i}T \tag{3}$$

and

$$\bar{C}_{p_{mix}}=\sum_i m_i\bar{C}_{p_i}. \tag{4}$$

The definition of the stagnation enthalpy of the mixture is

$$h=m_{fu}H_{fu}+\sum m_i\bar{C}_{p_i}T+\rho[U^2+V^2+V_\theta^2]/2 \tag{5}$$

and includes the heat of reaction, H_{fu} which must be specified from a knowledge of the fuel. In the present case, single-step reactions are assumed and the values of H_{fu} for methane, and ethane (regarded as the only combusting components of the fuel) were taken from [15] and combined according to the mass fractions of the two gases in the fuel.

The constants in equations (3) and (5) are given in Table 2 and were taken from [15].

Table 2. Gas property values; constants in equations (3) and (5)

Gas	Composition	Molecular weight	$a_{0_i}\times10^{-3}$ (kJ/kg K)	$b_{0_i}\times10^{-3}$ (kJ/kg K^2)
Natural gas	CH_4–81·3%, N_2–14·4%, C_2H_6–2·9% + traces	16·04	1000	2·055
Oxygen	O_2	32·0	888·1	0·0977
Carbon dioxide	CO_2	44·0	1740·2	0·3072
Nitrogen	N_2	28·0	823·8	0·1983
Water vapour	H_2O	18·0	1002·3	0·0865

$H_{fu}=4{\cdot}07\times10^4$ kJ/kg.

3.2. *Turbulence model*

The turbulence model used for the present calculations involves the solution of the equations of conservation of turbulent kinetic energy and dissipation rate together with the definition

$$-\rho\overline{uv} = \mu_t\left(\frac{\partial U}{\partial y}+\frac{\partial V}{\partial x}\right); \quad -\rho\overline{uv}_\theta = \mu_t\left(\frac{\partial V_\theta}{\partial x}\right) \tag{6}$$

and the assumption

$$\mu_t = C_D\rho k^2/\varepsilon = \mu_{\text{eff}} - \mu. \tag{7}$$

Equation (7) implies an isotropic turbulent viscosity and, together with equation (6) and the assumed forms of the diffusion and dissipation terms contained in the equations for turbulent kinetic energy and dissipation rate, represents a limitation on the precision of the calculation of aerodynamic flow properties. It has already been shown, for example in [8], that the normal stresses vary considerably throughout the flow and these variations and any implication which they may have for the values of mean velocity will not be represented by the present model. On the other hand, the model has previously been shown to allow good predictions in a wide range of boundary-layer flows, [16, 17]; only a small amount of testing has been attempted in strongly elliptic flows, for example [4, 18]. Consequently, a purpose of this paper is to compare predictions obtained with the two-equation model with experiments and to allow the merits of the model to be appraised for use in connection with furnace–enclosure flows.

It can be expected that the turbulence model has deficiencies, but it is desirable to quantify its abilities before attempting to introduce the additional equations required by a Reynolds stress closure.

The values of the constants in the turbulence–model equations and used for the present calculations are given in Table 3 and are identical to those of [17].

Table 3. Turbulence and combustion model constants

Constant	Value
C_1	1·44
C_2	1·92
C_D	0·09
K	0·42
E	8·8
C_{g_1}	2·8
C_{g_2}	2·0
C_R	1·0

$\sigma_k = \sigma_h = \sigma_{fu} = \sigma_f = \sigma_g = 0{\cdot}9$
$\sigma_\varepsilon = K^2/[(C_2-C_1)C_D^{\frac{1}{2}}] = 1{\cdot}22$

To avoid the need for detailed calculations in the near-wall regions, equations were introduced to link the values of dependent variables on the wall to those in the logarithmic region. The wall functions (9), corresponding to the equations for the three velocity components, kinetic-energy, dissipation rate and enthalpy are:

$$\mathrm{V}_0\frac{(C_D^{\frac{1}{4}}k^{\frac{1}{2}})}{\tau_w/\rho} = \frac{1}{K}\ln[EC_D^{\frac{1}{4}}k^{\frac{1}{2}}y_1\rho/\mu] \tag{8}$$

$$k = \tau_w/\rho C_D^{\frac{1}{2}} \tag{9}$$

$$\varepsilon(y_1/k^{\frac{1}{2}}) = C_D^{\frac{3}{4}}/K \tag{10}$$

$$(T_w-T)[C_{p_{\text{mix}}}\rho C_D^{\frac{1}{4}}k^{\frac{1}{2}}/q_w] = \frac{\sigma_{h,t}}{K}\ln[EC_D^{\frac{1}{4}}k^{\frac{1}{2}}y_1\rho/\mu]+9{\cdot}24\sigma_h\left[\frac{\sigma_h}{\sigma_{h,t}}-1\right]\left[\frac{\sigma_{h,t}}{\sigma_h}\right]^{\frac{1}{4}}. \tag{11}$$

In the case of the equations for m_i, f and g, the wall values were made equal to the values at the first grid node. The values of specific heat, Prandtl number and viscosity were evaluated at the wall temperature. The values used for K and E are given in Table 3. At the symmetry axis, the gradients $\partial\phi/\partial r$ were set to zero.

3.3. *Combustion models*

Three combustion models are referred to in this paper and are described and discussed in turn.

Model 1. The first model postulates a physically controlled, one-step reaction, with fuel and oxygen unable to coexist at the same location. The only species equation to be solved is that for the mixture fraction f, this equation has no source.

Model 2. In the second model, the infinitely fast, one-step reaction is retained; but fuel and oxygen may exist at the same location, although at different times. Equations for f and for the corresponding fluctuations, i.e. g, are solved and the maximum and minimum values of f at any point, f_+ and f_-, are represented by:

$$\begin{aligned} f_+ &= f+g^{\frac{1}{2}} \\ f_- &= f-g^{\frac{1}{2}} \end{aligned} \tag{12}$$

except where the value of f_+ exceeds unity and where the value of f_- is less than zero. Equation (12) represents a symmetrical square-wave variation of f, i.e. f_+ and f_- exist for equal times; but, in regions where f_+ exceeds unity or f_- is less than zero, the factor α defined by

$$f = \alpha f_+ + (1-\alpha)f_-, \tag{13}$$

represents the proportion of time spent in the f_+ state. Values of temperature and the mass fractions of fuel and oxygen are calculated corresponding to f_+ and f_- and the mean quantities obtained from the corresponding T_+, T_-, m_{fu_+}, m_{fu_-}, m_{ox_+}, m_{ox_-} together with α. This leads, for example, to lesser values of T than would be obtained from model 1 and influences the density values used in the continuity and momentum equations. As in model 1, the f-equation has no source term but the g-equation includes a source term for generation. Further information is contained in [10, 11].

Model 3. In contrast to models 1 and 2, a finite reaction rate is introduced in model 3. It is represented by an Arrhenius-type source term or by an eddy-break up term in the fuel equation: the reaction is chosen according to which of these terms leads to the smaller rate of generation of combustion products. The Arrhenius source term may be written in the form

$$R_{fu} = m_{fu}\rho^2 m_{ox}A\exp(-E/RT) \tag{14}$$

and it can be seen that values for A and E/R are required to complete the specification: these values were assumed to be constant and equal to 10^{10} m^3/kgs and $1{\cdot}84\times10^4$ K respectively, in accordance with the recommendation of [19]. The eddy-break-up term may be written in the form

$$R_{fu} = C_R g^{\frac{1}{2}}(\rho\varepsilon/k). \tag{15}$$

In terms of the number of differential equations considered, model 3 requires the solution of the same equations as model 2 and in addition, the solution of an equation for m_{fu}. The equation for g has been solved but, for comparison purposes, some calculations have been performed with an explicit form of the g-equation obtained by neglecting the diffusion and convective terms. It should be noted that the source term in the g-equation is based on m_{fu} rather than on f as in the case of model 2. This is in recognition of the contribution which m_{fu} makes to the fluctuations and is allowed by the solution of the m_{fu}-equation. It should be stressed that, in proposing the use of an eddy-break-up model, Spalding [11] regarded it as a preliminary attempt to take some account of the influence of the eddy-structure of turbulence on combustion. Radiation was considered through a four-flux model incorporated in the source term of the enthalpy equation. The model is described in [20] and incorporates a flux model absorption coefficient expressed as $a = 0{\cdot}2m_{fu}+0{\cdot}1m_{pr}$.

4. SOLUTION PROCEDURE

The differential equations represented by equation (1) and Table 1 were expressed in the finite-difference form of [21] and solved by the algorithm described in the same paper. Calculations were performed with several arrangements of grid nodes and with different number of nodes: Fig. 1 displays the locations of the 20×20 nodes used for the final calculations performed in connection with the furnace geometry of [8]. The influence of node location is indicated in Section 5.

The use of a grid composed of 20×20 nodes allowed the solution of ten equations in approximately 9 min of CDC6600 CP time: in the absence of swirl, this time reduced to approximately 4 min and in the absence of swirl and combustion to 2·5 min.

To aid the solution of the finite-difference forms of equation (1), together with the boundary conditions of Section 3.1, under-relaxation was used, in the form:

$$\phi = \beta\phi_{\text{new}}+(1-\beta)\phi_{\text{old}}. \tag{16}$$

The values of β were set to increase with the number of iterations from values of 0·3 to 0·6 for the velocity components; 0·8 to 0·9 for k and ε; and from 0·9 to 1·0 for other scalar variables.

The solutions were assumed to have converged when the maximum residual defined as

$$R_\phi \equiv \frac{[\text{convection}+\text{diffusion}+\text{source}]_{j+i}}{\phi_j}$$

was less than 10^{-4} at any grid node and for any of the ϕ equations. After thirty iterations, all calculations were observed to converge monotonically.

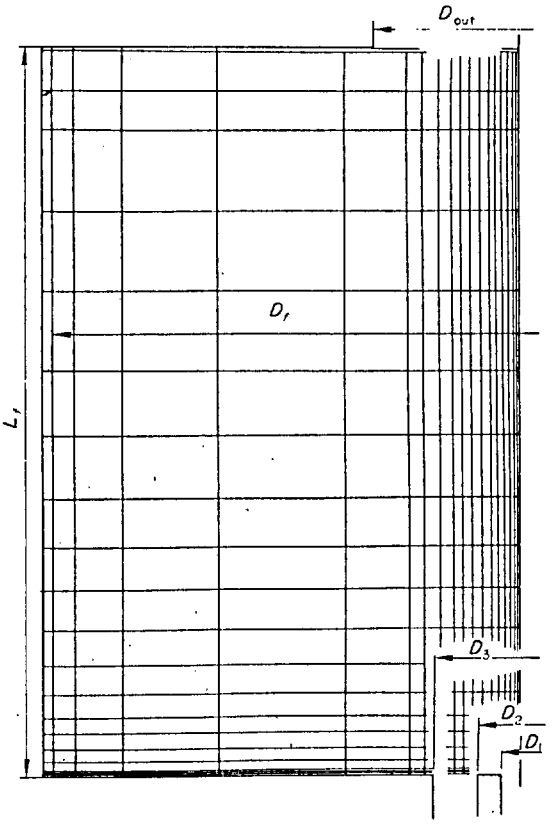

FIG. 1. Furnace and grid arrangement.

5. INFLUENCE OF INITIAL AND BOUNDARY CONDITIONS

The purpose of this section is to indicate the influence of initial and boundary conditions on calculated values of dependent variables. As indicated in Section 2, the elliptic form of the conservation equations requires that values of the dependent variables or their gradients be specified at each boundary of the solution domain. The wall functions provide this information at the solid boundaries although the value of wall temperature is required and the influence of its assumed values must be determined. In addition to the wall temperature also required are: the values of velocity, turbulent kinetic energy, dissipation rate, enthalpy, and species concentration, at the burner exit and at the exit from the furnace; these are not normally known. The influences of the assumed values are indicated here.

Figure 2 indicates the influence of the assumed shape of the velocity profile on the centre-line velocity distribution for each of three flow conditions. The mass flows and total enthalpy flux entering the furnace are the same for the upper two sets of curves and correspond to a stoichiometric condition for the combustion calculation and to the equivalent mass flow ratio for the isothermal calculation. The lower two curves correspond to the isothermal, experimental conditions of [8], i.e. the annulus mass velocity is identical to that for each of the other curves but the central jet is blocked off. The entry profiles of turbulent kinetic energy and dissipation rate were identical for each of the calculations.

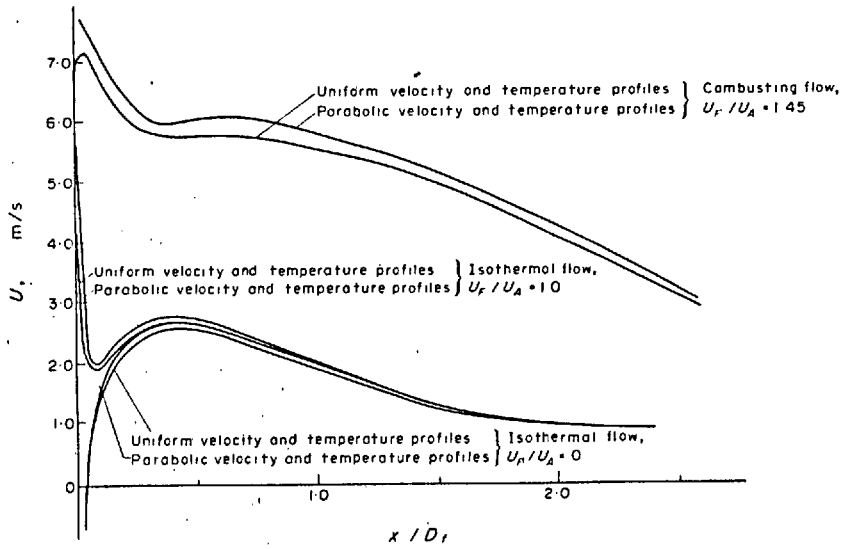

FIG. 2. Influence of initial profiles of mean velocity and temperature; swirl number = 0, isothermal and combusting flows.

The isothermal calculations show that the assumption of constant velocities in the annulus and central jet leads to downstream values of the centreline velocity which are around 2 per cent lower than those obtained with a near-parabolic profile (based on four node points). This influence was found to be considerably smaller for swirling flows. It is unlikely that, in a practical situation, the profile would be near parabolic and the influence of the initial velocity profile can therefore be neglected.

The influence of the presence of a central jet velocity can also be deduced from the lower two sets of curves and is considerable over an axial distance of six central-jet diameters. The two upper curves of Fig. 2 correspond to a combusting flow with uniform and parabolic velocity profiles for the annulus and central-core flows. The calculations show that the increase in centre-line velocity, associated with the parabolic profile, is maintained throughout the furnace although the difference appears to level off at around 0·2 m/s. This difference is reflected in the flow at locations away from the centre line. For example, in the case of the parabolic initial profiles, the recirculation zone is significantly longer and the negative velocities attain higher values. Once again, the influence was negligible for swirling flows.

Similar tests were carried out to determine the influence of the temperature distribution specified in the plane of the burner exit. It was found that, provided the total enthalpy of the incoming fluid was maintained constant, changes in the radial distribution of the fluid temperature were very small. For example, an increase in the fluid temperature of the incoming fluid from 300 to 400 K resulted in a maximum difference in fluid velocity of less than 1 per cent for downstream positions beyond three jet diameters: this influence was less in the swirling case. The temperature of the enclosure was, on the other hand, found to have a more significant influence. Tests were carried out, for the combusting flows, and demonstrated that the influence of an increase in the wall temperature of the circular enclosure from 600 to 1000 K resulted in a small increase in the dividing stream line of the recirculation zone but a more significant change in the velocity and temperature profiles: The results for the non-swirling case are shown on Fig. 3. The two sets of results shown on Fig. 3 correspond to a change in the integrated enthalpy of the flow due to the different wall temperatures: they are particularly relevant to the results of [8] where the wall temperature was not measured.

The influence of the turbulence properties, i.e. k and ε, specified in the plane of the annulus and jet exits has also been investigated. In practice, these properties are

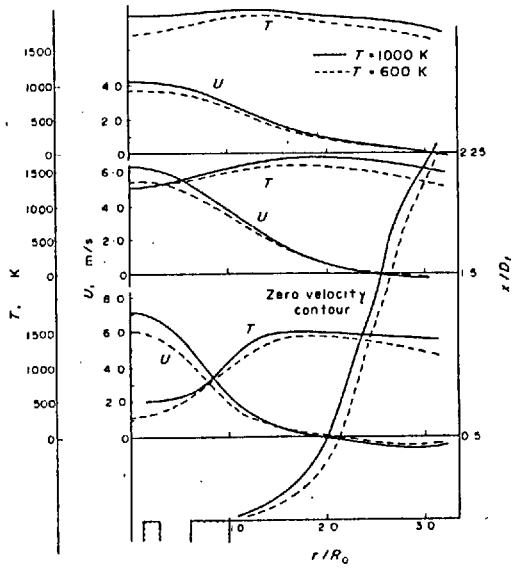

FIG. 3. Influence of wall temperature on mean velocity profiles and on the recirculation zone; swirl number = 0, combusting flow.

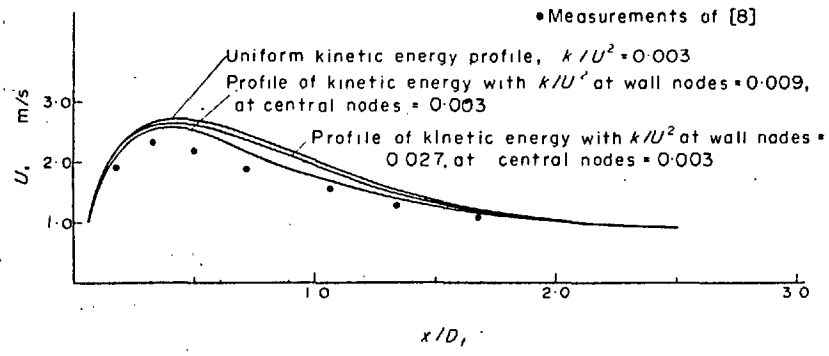

FIG. 4. Influence of initial profiles of turbulent kinetic energy and dissipation rate on mean velocity; swirl number = 0, isothermal flow.

often not known from experiment but are required by the calculation procedure as initial conditions. Figure 4 presents results for the non-swirling, isothermal flow for which the influence is greatest. These calculations were performed with a uniform distribution of mean velocity and three distributions of turbulent kinetic energy corresponding to a uniform distribution with $(\bar{u}^2)^{\frac{1}{2}}/U$ equal to 0·045 (i.e. $k/U^2 = 0{\cdot}003$); a distribution with 0·003 at the two central nodes and 0·009 ($(\bar{u}^2)^{\frac{1}{2}}/U = 0{\cdot}08$) at the two near-wall nodes; and a distribution with 0·003 at the two central nodes and 0·027 ($(\bar{u}^2)^{\frac{1}{2}}/U = 0{\cdot}135$) at the two near-wall nodes. These figures refer to the annulus flow: the central-jet velocity was zero in this case. The corresponding values of dissipation were determined from the equation:

$$\varepsilon = C_D k \frac{k^{\frac{1}{2}}}{l_{mix}} = C_D k \frac{k^{\frac{1}{2}}}{0{\cdot}03 y_a};$$

The results show that the influence of the kinetic energy and coupled dissipation rate is appreciable and, indeed, further calculations have shown that the influence upon the centre-line mean velocity of an increase in the normalized kinetic energy from 0·003 to 0·01 at the two near-wall grid nodes is greater than a decrease in the value at the two central nodes from 0·003 to 0·0006.

Boundary conditions must be specified at the outlet from the flow and the sensitivity of these specifications was also tested for the furnace arrangement of [8]. Independent tests were carried out for U, h, f and g. In each case, calculations were compared with two specifications of the outlet conditions: in one case, the gradient $\partial\phi/\partial x$ was set to zero and in the other the gradient at the exit was set equal to that at the upstream grid node ($0{\cdot}166 D_f$ upstream of the exit plane). No significant differences in upstream calculations were observed for the four flow conditions tested, i.e. isothermal and combusting with and without swirl.

6. COMPARISON OF CALCULATIONS AND EXPERIMENTS

The calculations presented in this section are presented in a sequence which allows the reader to assess the validity of the assumptions embodied in the equations solved for aerodynamic properties, i.e. the turbulence model, and then the overall procedure embodying the turbulence model and a combustion model. In this second stage, the relative advantages of the three combustion models described in Section 3.3 will be assessed. Finally, calculations made with the preferred combustion model will be presented and appraised in order to determine the overall precision with which calculations may be performed.

The basis for the appraisal and validation indicated in the previous paragraph is largely comparison with experiments and it should be recognized that those data cannot be regarded as complete or as of known precision. Four sets of data have been selected as the basis for this comparison and were obtained in furnaces with dimensions indicated in Table 4. Those of Baker *et al.* [8] are the most complete in that they include the velocity components and corresponding normal stresses in detail and included profiles which can be used as initial values. These measurements are probably the most precise available but do not allow comparisons with those properties which are most relevant to furnace heat transfer, i.e. temperature and wall heat

Table 4. Dimensions of furnaces of [8, 12–14]

Furnace of reference	D_f (mm)	L_f (mm)	D_1 (mm)	D_2 (mm)	D_3 (mm)	D_{out} (mm)	Swirl number	Remarks
[8]	300	900	12	27	55	90	0·0 0·52	Isothermal & combusting
[14]	450	2500	10	16	81	450	0·0	Combusting
[13]	900	5000	46	60	131	270	0·0 0·84	Divergent air nozzle: combusting
[12]	2000	6000	46	60	176	900	0·0 0·5	Square cross section: combusting

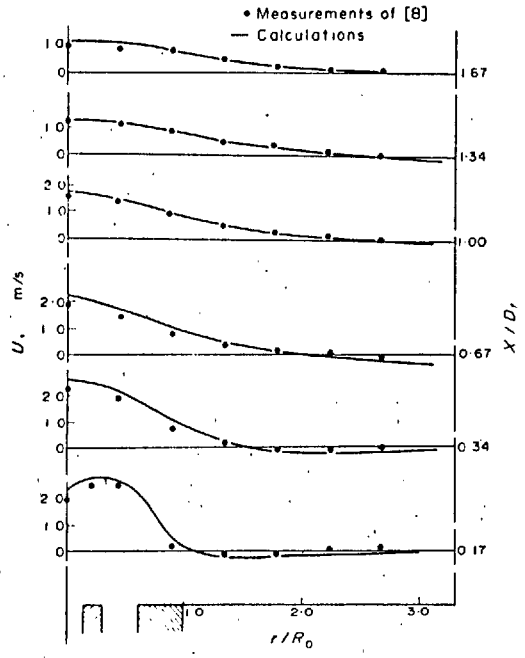

FIG. 5. Radial profiles of mean axial velocity: swirl number = 0, isothermal flow.

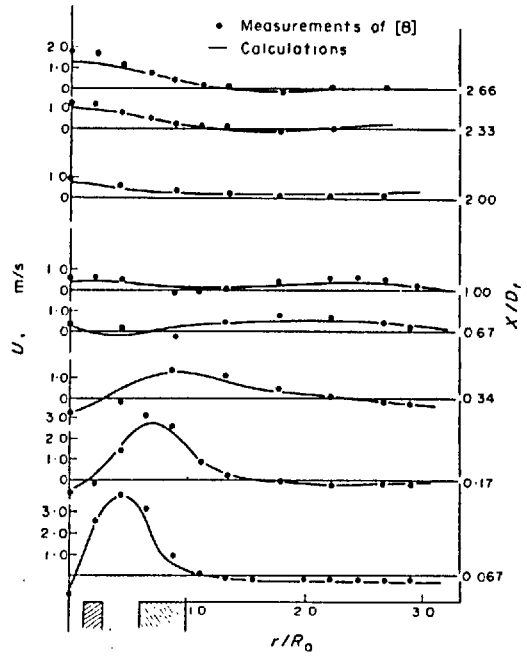

FIG. 7. Radial profiles of mean axial velocity: swirl number = 0·52, isothermal flow.

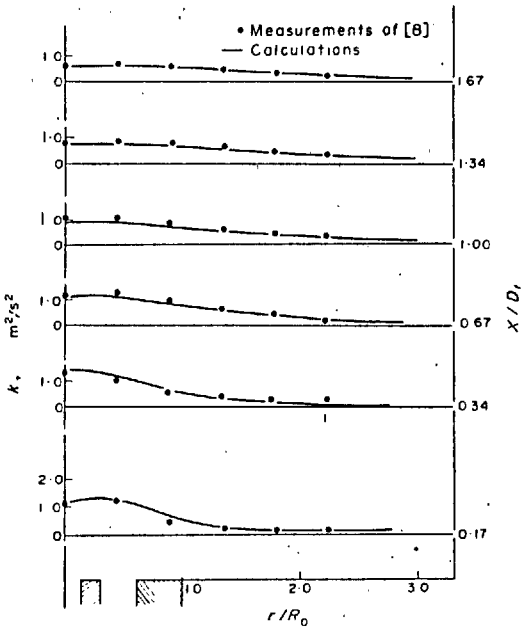

FIG. 6. Radial profiles of kinetic energy of turbulence: swirl number = 0, isothermal flow.

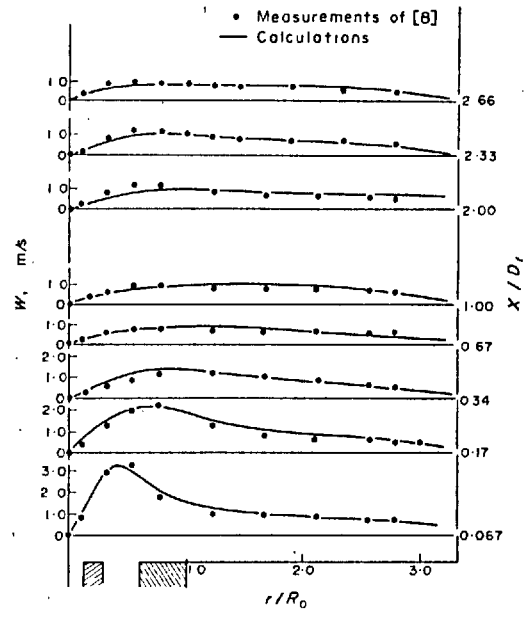

FIG. 8. Radial profiles of mean tangential velocity: swirl number = 0·52, isothermal flow.

flux. In contrast, references [12–14] relate to scalar properties and do not include detailed information of the initial values. Also, the precision of measurements is finite; further comments on this point will be made when the comparisons are presented.

6.1. *Isothermal calculations*

Calculated values of axial velocity and turbulent kinetic energy are compared with measurements on Figs. 5 and 6. The two sets of data are in good agreement with a maximum centre-line deviation of 10 per cent in the mean velocity and a maximum centre-line deviation of 15 per cent in the turbulent kinetic energy. The initial profiles corresponded as closely to the non-swirl experiments as the four grid nodes allowed with values of turbulence intensity at the near wall nodes of 0·08. There was no central jet velocity. In general, it can be said that the turbulence model provides satisfactory predictions for the non-swirling case.

The Figs. 7–9 relate to a swirling flow and compare calculated and measured values of mean-axial and circumferential velocity components and turbulent

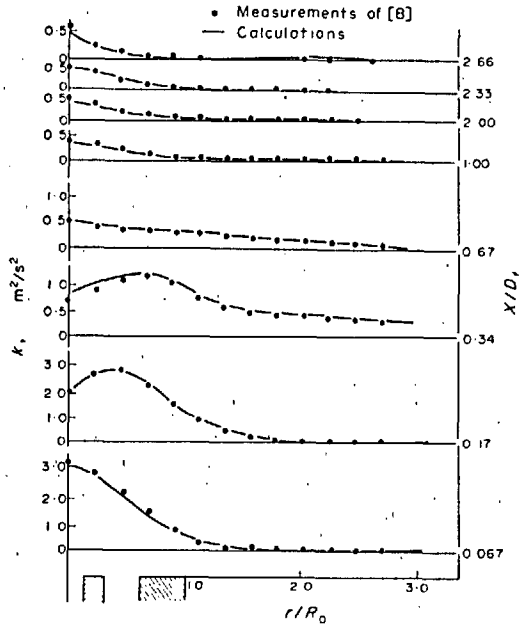

FIG. 9. Radial profiles of kinetic energy of turbulence: swirl number = 0·52, isothermal flow.

kinetic energy. The agreement is not as good as that of Figs. 5 and 6 and this may be attributed to the isotropic nature of the turbulence model. The largest discrepancy occurs in the axial mean velocity which, for example, suggests that the distribution of centre-line velocity is less well calculated in the downstream region; this may be associated with the downstream separation region where the circumferential velocity component is significantly greater than the axial component and, therefore, the probable effects of an erroneous assumption of isotropic viscosity would be most significant. Although the turbulence model appears to be less satisfactory in this swirling case, the agreement between the calculations and measurements may be regarded as satisfactory for engineering purposes: the maximum deviation between centre line calculated and measured velocities is 15 per cent.

6.2. *Combustion calculations*

6.2.1. *Comparison with velocity information and calculated temperatures.* (a) Non-swirling flame—The results presented on Figs. 10–14 correspond to the combustion measurements of [8] and indicate the extent to which the combustion models described in Section 3.3 allow realistic calculations. Figures 10 and 11 present centre-line values of mean velocity and turbulent kinetic energy obtained without swirl: corresponding distributions of mean temperature and the rms of the temperature fluctuations are presented on Fig. 12. Examination of Fig. 10 shows that there are significant differences in the magnitude of the two sets of results. In the initial region, say up to $0{\cdot}3D_f$, the discrepancy can be explained by the slight lift-off of the flame observed in the experiments: this resulted in the acceleration, due to the combustion, being delayed to a region around $D_f/6$. In contrast, the calculations indicate an initial acceleration very close to the burner followed by a decay as the lower density central jet penetrates the surrounding and burning fluid. A comparison of the calculations with the three combustion models indicates that Model 2 agrees most closely with the measurements. It is interesting to note, however, that the results obtained with model 3 are greatly influenced by the form of the g-equation: the figure includes one curve obtained with model 3 but with an algebraic solution of a form of the g-equation in which production and dissipation are assumed equal. The calculations of Fig. 11 again with the exception of the initial region, are in acceptable agreement with measurements. It is difficult to state which model is to be preferred but model 2 does again appear to be

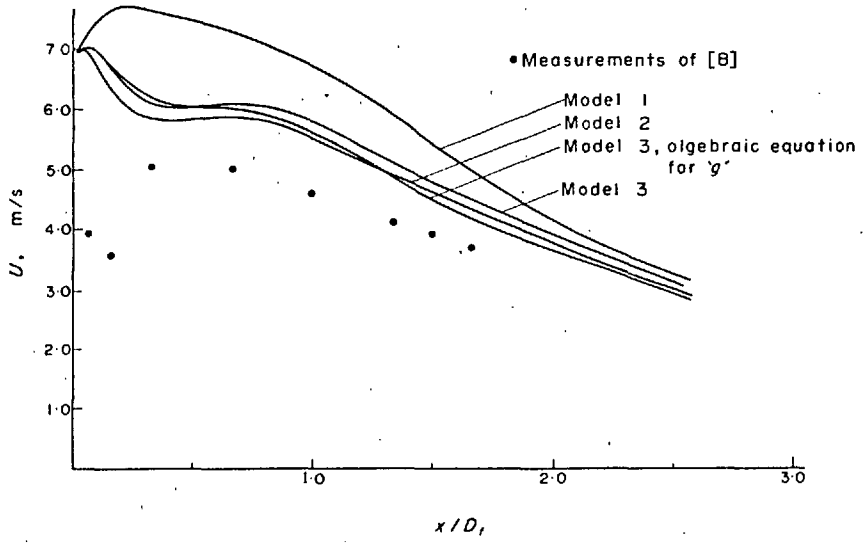

FIG. 10. Centre-line distribution of mean axial velocity: swirl number = 0, combusting flow.

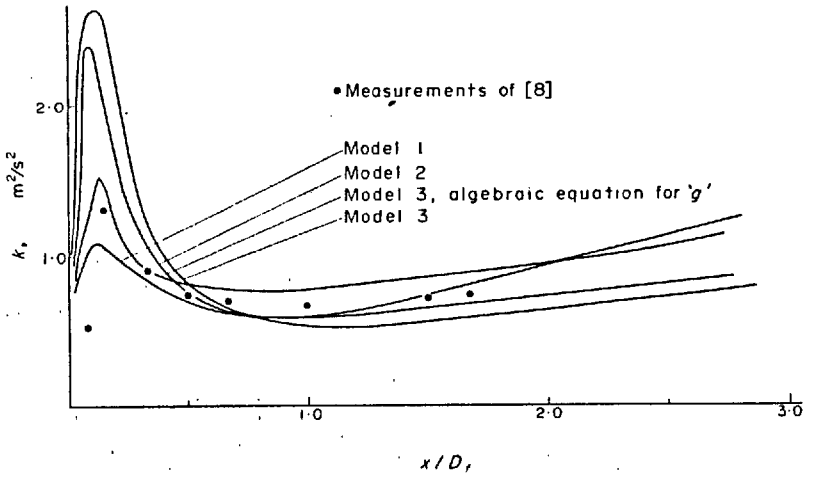

FIG. 11. Centre-line distribution of kinetic energy of turbulence: swirl number = 0, combusting flow.

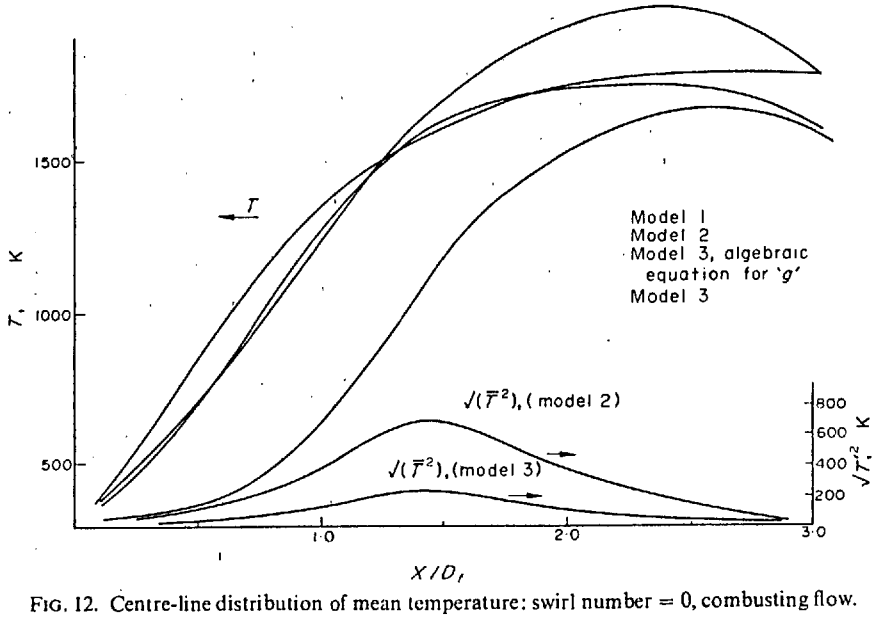

FIG. 12. Centre-line distribution of mean temperature: swirl number = 0, combusting flow.

marginally better than the others. The calculated values of mean temperature and rms of the temperature fluctuations, shown on Fig. 12, cannot be compared with experiments. The mean values indicate, however, that model 2 results in a lower maximum centre-line temperature since the maximum attainable value, the adiabatic-flame temperature, can only be attained in the case of model 1: in the other cases, the adiabatic-flame temperature will correspond to the mean value plus the fluctuation. The distributions of the RMS of the temperature fluctuations are presented in dimensional form and indicate an increase which levels off some half way along the furnace; thereafter, they decay. The shape of the distribution is significantly different from the turbulent kinetic energy distribution of Fig. 11. Comparison of the values of $(\bar{u}^2)^{\frac{1}{2}}/U$ and $(\overline{T'^2})^{\frac{1}{2}}/T$ indicates that the magnitude of the latter is very much greater than that of the former except very close to the burner and the exit. The non-dimensional temperature fluctuation attains a value of 0·95 around x/D_f of 0·4; the maximum value of $(\bar{u}^2)^{\frac{1}{2}}/U$ is around 0·25 and occurs close to the burner exit. The location of the maximum temperature fluctuation corresponds approximately to the end of the luminous zone of the flame.

The differences between the mean and RMS values of temperature obtained with models 2 and 3 are worthy of further comment. It can be seen that the sum of the mean and RMS values will result in temperature values which will be similar but with model 3 providing the larger values over the first two-thirds of the furnace. The aerodynamic patterns of the two flows are different and small differences in the values of $T+(\overline{T'^2})^{\frac{1}{2}}$ are to be expected even though the use of Arrhenius over all but the initial region of the flow might be expected to result in model 3 producing lower values. The differences in $\overline{T'^2}$ are interesting and stem from the different

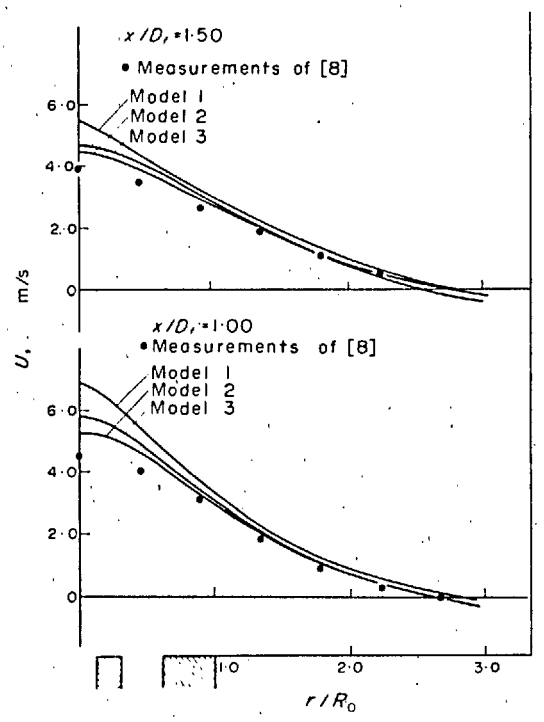

FIG. 13. Radial profiles of mean axial velocity: swirl number = 0, combusting flow.

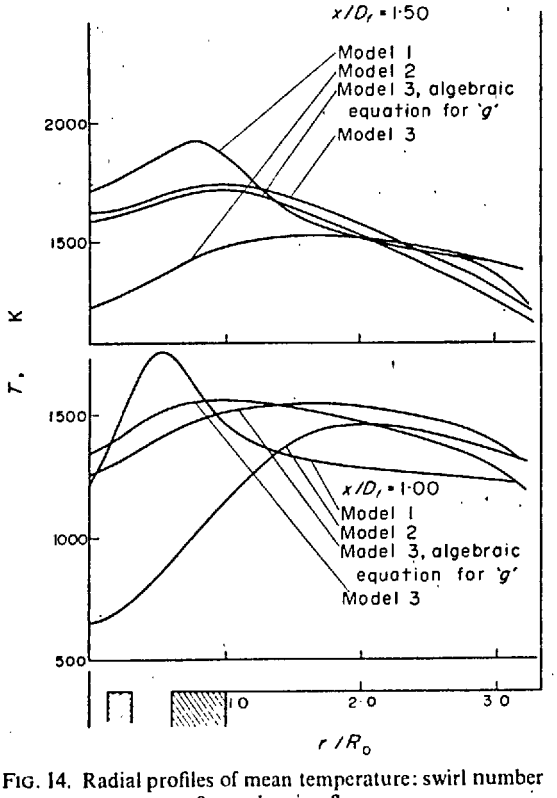

FIG. 14. Radial profiles of mean temperature: swirl number = 0, combusting flow.

source terms in the g-equations for the two models. The maximum values of $(\overline{T'^2})^{\frac{1}{2}}/T$ downstream of the immediate vicinity of the jet, achieved with models 2 and 3 are 0·64 and 0·11 respectively: measurements of Odidi [21] would suggest that the results of model 2 are closer to the truth.

Figures 13 and 14 present sample calculations of mean velocity and temperature obtained at values of x/D_f of 1·0 and 1·50. The mean velocity values may be compared with the measurements and suggest that models 2 and 3, embodying the scalar fluctuations, are to be preferred. This suggestion was supported by comparing profiles at other downstream locations, away from the initial region. The high velocity values associated with model 1 relate to the high values of mean temperature and the correspondingly low values of density used in the solution of the momentum equation for the hotter regions of the flow.

(b) *Swirling flame*—Figures 15–20 relate to the swirling measurements of [8] and present comparisons with calculations. Figure 15 presents centre-line distributions of the axial component of mean velocity and Fig. 16 the turbulent-kinetic energy. In this case, the flame was stabilized on the burner with no apparent lift off and the models should, therefore, more accurately reflect the experiments. It is clear that model 2 represents the data of both figures very well and significantly better than for the non-swirling case. The mean temperature results of Fig. 17 are similar to those of Fig. 12 although the velocity results are very different and the temperature fluctuations are only similar in general form. Thus, although in one case there is no apparent region of recirculation on the centre line and in the other region of flow recirculation exists over the upstream half of the furnace, the mean temperature distributions along the centre line are similar in shape and in magnitude. It is clear, therefore, that the radial temperature distributions must be different and this will be confirmed by results presented in the following section (Fig. 22).

The radial profiles indicated on Figs. 18–20 correspond to axial mean velocity, swirl velocity and temperature and to axial distances from the burner of 1·0 and 1·50. The calculated velocity values may be compared with measurements and again indicate that model 2 results in slightly better agreement than model 3 with model 1 a poor third. Models 2 and 3 also allow temperature calculations which are in close agreement: unfortunately there are no experiments with which to compare them.

6.2.2. *Comparison with temperature information.* The previous paragraphs allow an assessment of the merits of the present turbulence model in terms of velocity and velocity correlations but, because measured values of scalar properties were not presented in [8] any assessment of the overall calculation procedure and of the combustion model in particular is incomplete. References [12]–[14] do report temperature and wall heat flux measurements and, in an effort to improve the basis for assessment, the following six figures compare calculations with measurements. In contrast to the data of [8], however, that in [12–14] does not include adequate information of boundary conditions and reasonable assumptions have had to be made.

The furnace of Gunther and Lenze [14] has a length to diameter ratio of 5·5 but is otherwise similar to that of [8]. The centre-line distributions of mean tempera-

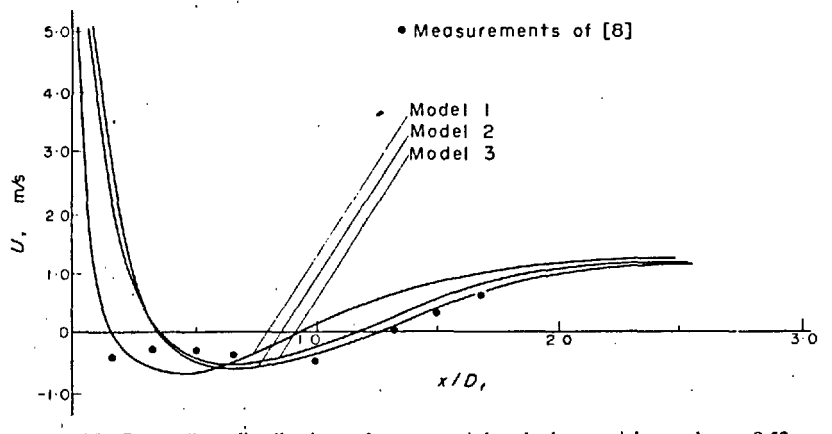

FIG. 15. Centre-line distribution of mean axial velocity: swirl number = 0·52, combusting flow.

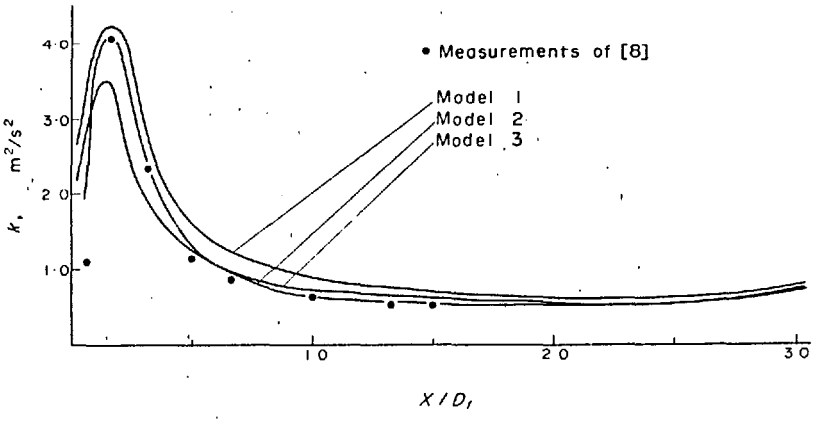

FIG. 16. Centre-line distribution of kinetic energy of turbulence: swirl number = 0·52, combusting flow.

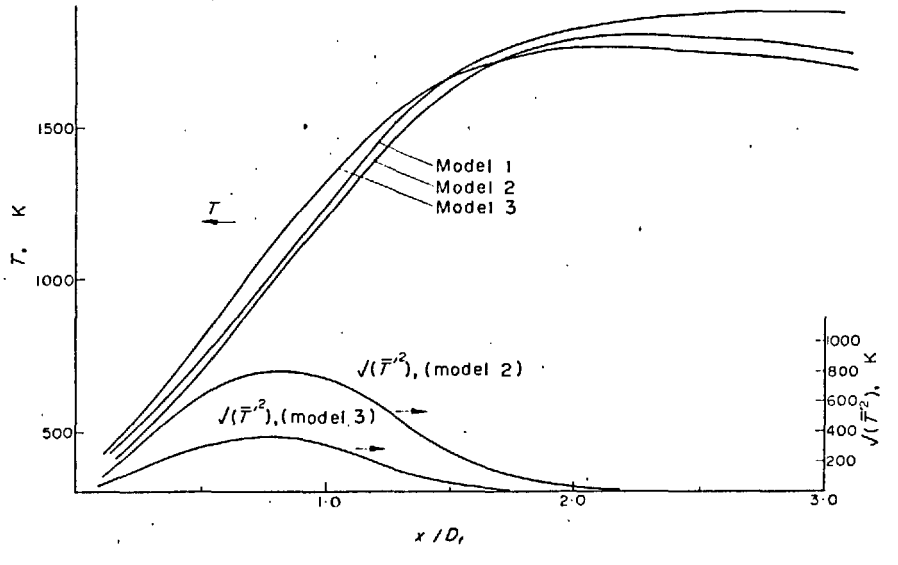

FIG. 17. Centre-line distribution of mean temperature: swirl number = 0·52, combusting flow.

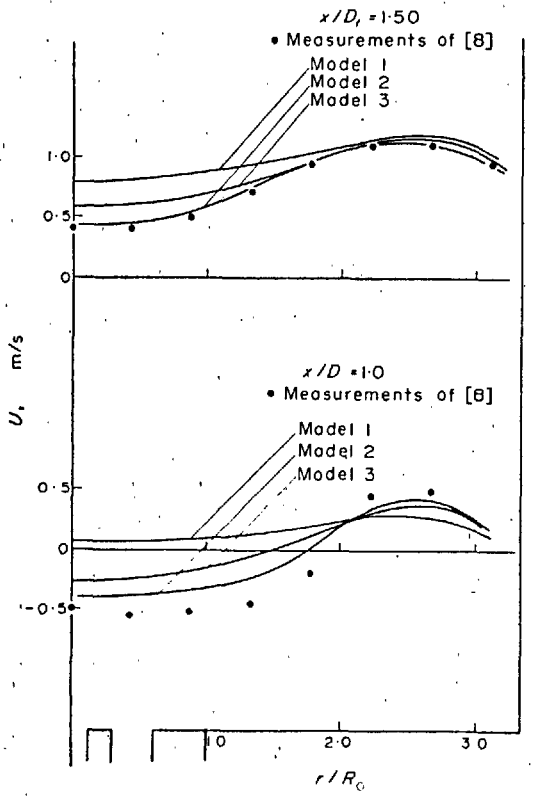

FIG. 18. Radial profiles of mean axial velocity: swirl number = 0·52, combusting flow.

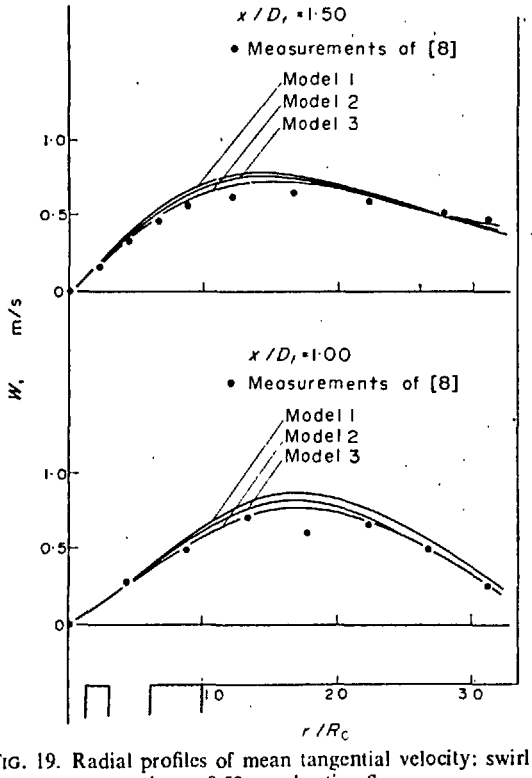

FIG. 19. Radial profiles of mean tangential velocity: swirl number = 0·52, combusting flow.

ture shown on Fig. 21 are similar to those of Fig. 12 but provide the additional information that the results obtained with model 2 are significantly lower than the measurements as well as the results of the other models.

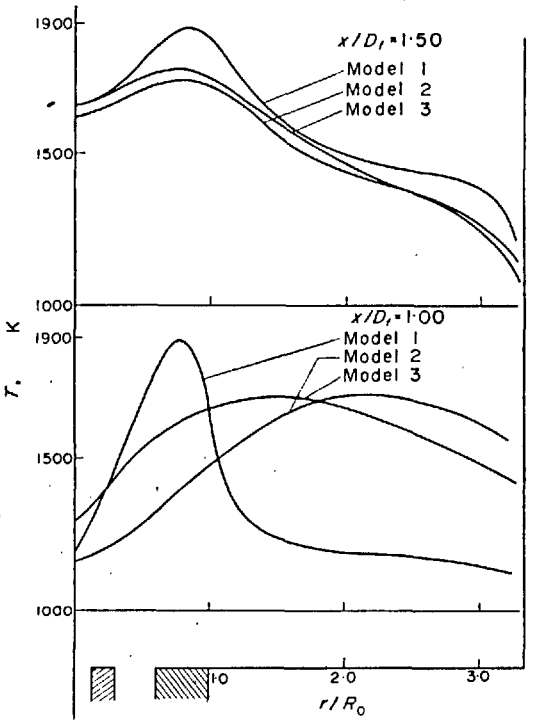

FIG. 20. Radial profiles of mean temperature: swirl number = 0·52, combusting flow.

The large difference between the temperatures calculated with model 2 and the data of models 1 and 3 stems, respectively from the consideration of temperature fluctuations and the form of the source term in the g-equation.

The additional information of Fig. 22 indicates that, although the results of models 1 and 3 were in passable agreement with experiment on the centre line they deviate considerably at other locations: the differences between the predictions obtained with the different models are again of the same magnitude as those of Fig. 14. A more complete picture of the temperature calculations is shown on Fig. 23 which compares the data provided in [14] with temperatures calculated with model 2. This figure shows that the overall pattern of the isotherms is similar but the measured flame is considerably narrower and larger than the calculated flame. The results of Figs. 4–6 suggest that the discrepancy is unlikely to stem from the turbulence model and it must, therefore, result from the combustion model or from erroneous experiments.

The furnace used for the experiments of [13] was also axisymmetric and had a length to diameter ratio of 5·17; it differed significantly from the furnaces of [8] and [14] in that the burner had a quarl exit. Figures 24 and 25 show that the results obtained with model 2 are in particularly close agreement with experiment: they also show that the predictions of the three models are in closer agreement with each other than they were on Figs. 21 and 22. This is consistent with the calculations made in connection with the results of [8] since the results of Figs. 24 and 25 correspond to a swirl number of 0·84 and those of Figs. 21–23 to a swirl number of zero.

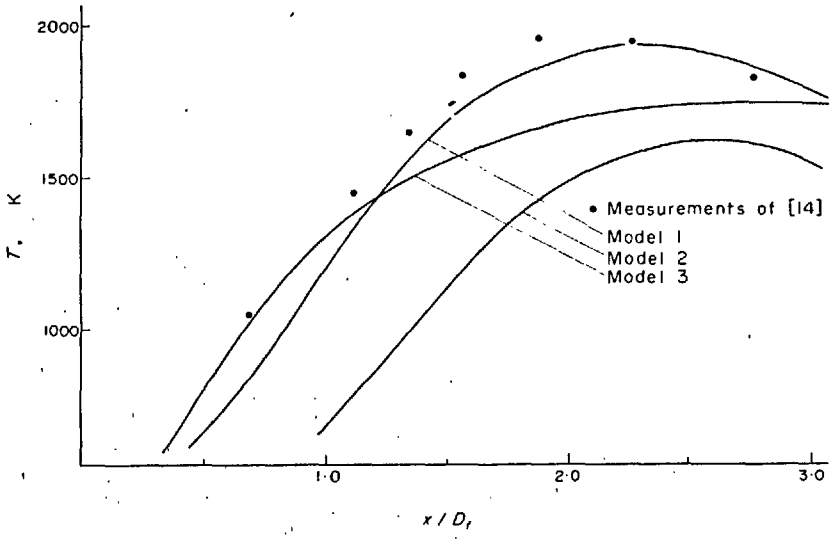

FIG. 21. Centre-line distribution of mean temperature: comparison with results of [14].

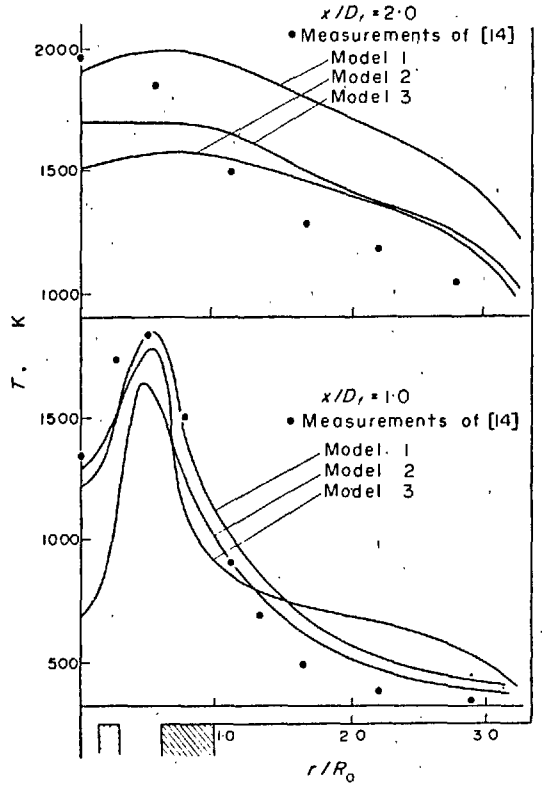

FIG. 22. Radial profiles of mean temperature: comparison with results of [14].

6.2.3. *Comparison with wall heat flux information.* Figure 26 presents values of the non-dimensional wall heat flux corresponding to the furnaces of [12] and [13]. The calculations were made using the measured distribution of wall temperature. Once again, the calculations are in agreement with the experiments for the finite swirl cases but, in general, the agreement is satisfactory for all three configurations except close to the burner and to the furnace exit: the former discrepancy could well be due to the assumed boundary conditions.

The calculated net heat flux was made up of convective and radiative components. In the case of the calculations of Fig. 26, the radiative flux was greater than the convective flux and suggests that the four flux model is a reasonable representation of the physical processes.

7. DISCUSSION AND CONCLUSION

The comparisons presented in Section 6 show that results obtained with the present procedures are in general agreement with measurements but that deficiencies still remain. The agreement is sufficient to justify calculations for many engineering purposes, although it is clear, however, that improvements can be made and the following paragraphs discuss them.

The limitations of the turbulence model can, in principle, be reduced by increasing the number of equations used to characterize the turbulence model.

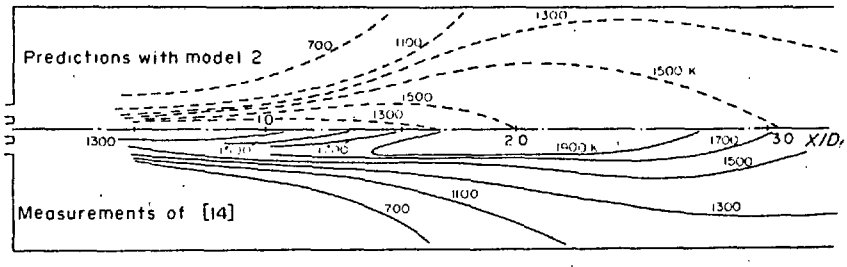

FIG. 23. Contours of isotherms; comparison with results of [14].

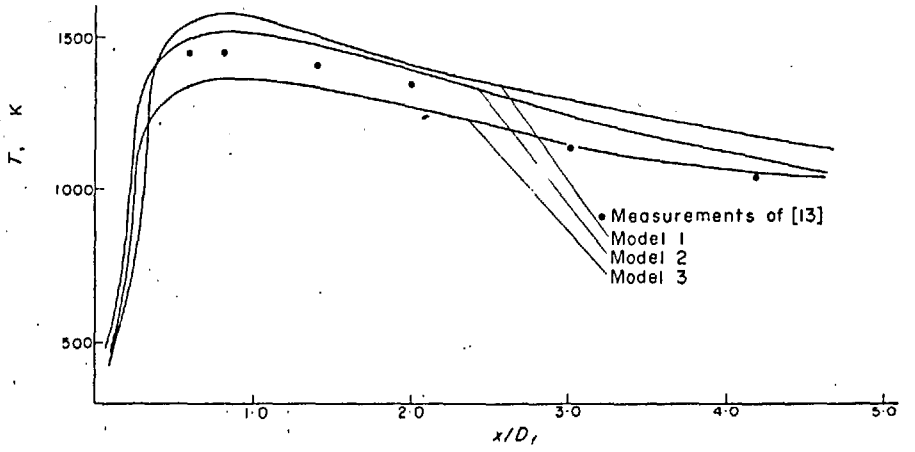

FIG. 24. Centre-line distribution of mean temperature: comparison with results of [13].

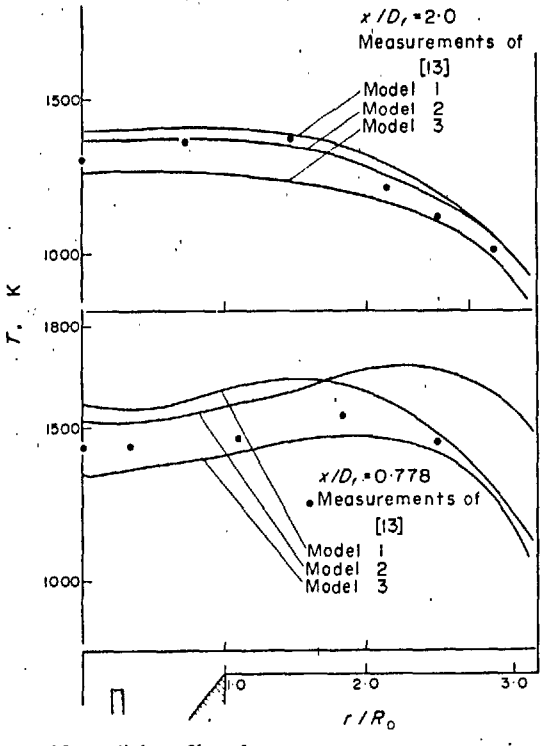

FIG. 25. Radial profiles of mean temperature: comparison with results of [13].

Equations for the normal stresses can be introduced to replace the equation for turbulent kinetic energy and additional shear stress terms represented to improve the characterization of the swirl. The present calculations indicate, that the measurements with swirl are only marginally less well calculated by the procedure and that much larger differences occur as a result of the combustion model. It seems desirable, therefore, to turn attention to the improvement of the combustion model rather than to the aerodynamic turbulence model.

A tentative conclusion which may be drawn from Section 6 is that model 2 represents the available measurements at least as well as model 3. This must result from inadequacies in the detail of model 3 rather than from the concept of recognizing finite-rate reactions. In both models 2 and 3, the square-wave form of the scalar distribution in time is the simplest possible arrangement and is a major candidate for improvement. The form of the eddy-break-up term is also in need of further consideration particularly since the eddy-break-up reaction rate controlled most of the combustion in the furnaces considered in Section 6.

The most important present need is, however, for precise measurements of velocity, temperature, species concentration and the corresponding correlations. The investigations described in [8, 12–14] are deficient for present purposes. In particular [8] does not provide

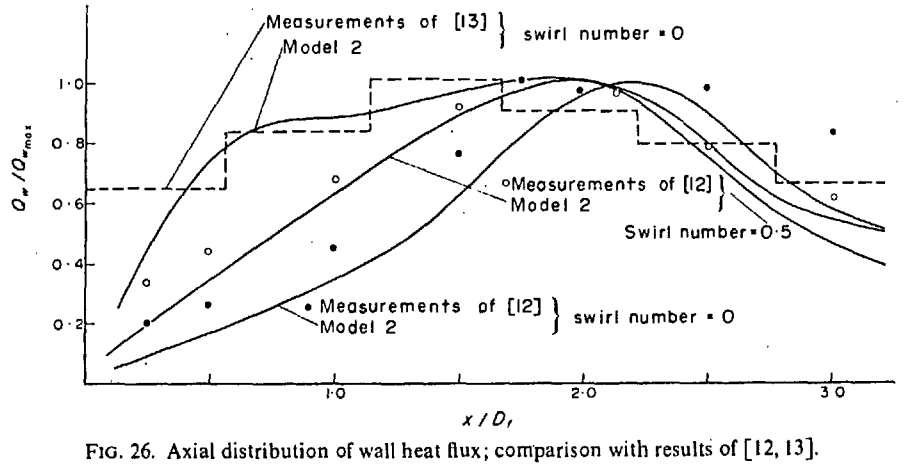

FIG. 26. Axial distribution of wall heat flux; comparison with results of [12, 13].

measurements of temperature or concentration and [12–14] provide no measurements of fluctuating properties and inadequate descriptions of the boundary conditions.

It may be concluded that the present procedure with its two-equation turbulence model, instant reaction with scalar fluctuations and four-flux radiation model is able to represent furnace flows of the type described in [8, 12–14] with a certainty which is of similar magnitude to that of the measurements. There is an immediate need for more comprehensive measurements and for the improvement of the time-fluctuation and eddy-break-up assumptions in the combustion models.

Acknowledgements—We are glad to acknowledge the technical support provided by colleagues at the AERE, Harwell and at Imperial College. Financial support was provided by the AERE, Harwell in the form of a contract to Imperial College: Dr. P. Hutchinson has monitored this contract in a constructive and helpful manner and we are particularly glad to record our appreciation and thanks to him.

The present calculations were performed with the aid of a specially adapted form of a computer program developed by Devraj Sharma for Combustion, Heat and Mass Transfer Ltd.

REFERENCES

1. B. R. Pai and T. Lowes, The prediction of flow, mixing and heat transfer in the Ijmuiden furnace, IFRF, Doc. No. 602/a/22 (1972).
2. D. G. Evans and K. J. Matthews, Computer predictions of burner fluid flow and heat release, C.E.G.B. report, R/MR 179 (1973).
3. A. D. Gosman and F. C. Lockwood, Predictions of the influence of turbulent fluctuations on flow and heat transfer in furnaces, Imperial College Mech. Eng. Dept. Report HTS/73/52 (1973).
4. S. E. Elghobashi and W. M. Pun, A theoretical and experimental study of turbulent diffusion flames in cylindrical furnaces, Proc. 15th Symposium on Combustion, see also Imperial College, Mech. Eng. Dept. Report HTS/74/16 (1974).
5. R. F. Anasoulis, H. McDonald and R. C. Buggeln, Development of a combustor flow' analysis, Part 1: Theoretical studies, AFAPL–TR–73–98 (1973).
6. S. V. Patankar and D. B. Spalding, Simultaneous predictions of flow pattern and radiation for three dimensional flames, in *Heat Transfer in Flames* Edited by N. Afgan and J. Beer. Scripta, Washington, 1974.
7. S. V. Patankar and D. B. Spalding, A computer model for three-dimensional flow in furnaces, in *Proceedings 14th Symposium (International) on Combustion*, pp. 605–614. Combustion Institute, U.S.A. (1972).
8. R. J. Baker, P. Hutchinson, E. E. Khalil and J. H. Whitelaw, Measurements of three orthogonal velocity components in confined co-axial jet flows with and without swirl and combustion, Proc. 15th Symposium on Combustion. See also Imperial College, Mech. Eng. Dept. Report HTS/74/29 (1974).
9. B. E. Launder and D. B. Spalding, *Mathematical Models of Turbulence*. Academic Press, London (1972).
10. D. B. Spalding, Concentration fluctuations in a round free jet. *Chem. Engng Sci.* 26, 95 (1971).
11. D. B. Spalding, Mixing and chemical reaction in steady confined turbulent flame, in *Proceedings 13th Symposium (International) on Combustion*. pp. 649–657, Combustion Institute, U.S.A. (1971).
12. S. Michelfelder and T. M. Lowes, Preliminary report on M-2 trials, IFRF, Doc. nr. F 36/a/4 (1972).
13. N. Fricker and H. L. Wu, An investigation of the behaviour of Swirling jet flames in a narrow cylindrical furnace, 2nd Member Conference, IFRF (1971).
14. R. Gunther and B. Lenze, Exchange coefficients and mathematical models of jet diffusion flames Proc. 14th Symposium (International) on Combustion, pp. 675–687, Combustion Institute, U.S.A. (1972).
15. S. Glasstone, *Thermodynamics for Chemists*. D. Van Nostrand, Princeton, N.J. (1946).
16. K. Hanjalic and B. E. Launder, Fully developed asymmetric flow in a plane channel, *J. Fluid Mech.* **51**, 301 (1972).
17. B. E. Launder, A. Morse, W. Rodi and D. B. Spalding, The prediction of free shear flows—a comparison of the performance of six turbulence models, NASA Conference on free shear flow, Langley field, Hampton (July 1972).
18. L. Matthews and J. H. Whitelaw, Plane-jet flow over a backward facing step. *Proc. Instn Mech. Engrs* **187**, 447 (1973).
19. V. N. Kondratiev, *Chemical Kinetics of Gas Reactions*. Pergamon Press, Oxford (1964).
20. A. D. Gosman and F. C. Lockwood, Incorporation of a flux model for radiation into a finite difference procedure for furnace calculation, Proc. 14th Symposium (International) on Combustion, pp. 661–671, Combustion Institute, U.S.A. (1972).
21. S. V. Patankar and D. B. Spalding, A calculation procedure for heat, mass and momentum transfer in three dimensional parabolic flows, *Int. J. Heat Mass Transfer* **15**, 1787 (1972).
22. A. O. Odidi, The influence of turbulence on the time-mean rate of chemical reaction, Ph.D. Thesis, University of London (1974).

CALCUL DES PROPRIETES LOCALES DE L'ECOULEMENT DANS LES FOURS BIDIMENSIONNELS

Résumé—Les valeurs des propriétés locales de l'écoulement, obtenues par résolution d'équations de conservation appropriées écrites sous forme de différences finies sont présentées et comparées aux mesures expérimentales pour plusieurs types de conditions aux limites correspondant à quatre configurations de fours.

La méthode de calcul utilise un modèle de turbulence à deux équations, si bien que les calculs peuvent être comparés aux mesures d'énergie turbulente aussi bien qu'à celles des composantes de vitesse moyenne.

Les calculs sont effectués pour trois modèles de combustion caractérisés par: une réaction instantanée, une réaction instantanée avec fluctuations scalaires et une réaction d'Arrhénius ou un émiettement des tourbillons avec fluctuations scalaires. Des comparaisons effectuées avec les mesures obtenues dans les fours de Delft, Harwell, Ijmuiden et Karlsruhe, indiquent que les deux derniers conduisent à des résultats raisonnablement corrects.

DIE BERECHNUNG DER ÖRTLICHEN STRÖMUNGSEIGENSCHAFTEN IN ZWEIDIMENSIONALEN FEUERUNGEN

Zusammenfassung—Die durch numerische Lösung der zugehörigen Bilanzgleichungen mit vier verschiedenen Feuerungsanordnungen und entsprechenden Randbedingungen gewonnenen Werte der örtlichen Strömungseigenschaften wurden mit denen aus Messungen verglichen. Die Berechnungsmethode verwendet ein Zwei-Gleichungs-Turbulenzmodell, so daß die Berechnungen mit Messungen sowohl der Turbulenzenergie als auch Komponenten der mittleren Geschwindigkeiten verglichen werden können. Die Berechnungen wurden mit drei Modellen der Verbrennung durchgeführt, die charakterisiert sind durch sofortige Reaktion, sofortige Reaktion mit skalaren Fluktuationen und Arrhenius-Reaktion oder Wirbelauflösung mit skalaren Fluktuationen. Vergleiche mit Messungen aus Feuerungen in Delft, Harwell, Ijmuiden und Karlsruhe zeigen, daß die beiden letzten Modelle zu ausreichend genauen Ergebnissen führen.

РАСЧЕТ ЛОКАЛЬНЫХ ХАРАКТЕРИСТИК ТЕЧЕНИЯ В ПЛОСКИХ ПЕЧАХ

Аннотация — Приводятся значения локальных характеристик течения, полученные путем решения соответствующих уравнений сохранения в конечных разностях при граничных условиях, соответствующих печам четырех конструкций. Полученные значения сравниваются с результатами измерений.

При расчете используется математическая модель турбулентности, представленная двумя уравнениями, так что сравнение расчетных данных с результатами эксперимента производится по энергии турбулентности и составляющим средней скорости.

Расчеты проводились на трех моделях процесса горения, характеризуемых мгновенной реакцией, мгновенной реакцией с флуктуациями скалярных величин и реакцией Аррениуса с флуктуациями скалярных величин. Сравнение численных данных с результатами измерений, полученными для печей исследователями в Дельфте, Харуэлле, Ймюдене и Карлсруэ показывает хорошее совпадение для двух последних случаев.

APPENDIX A.7

Calculation of local flow properties in a Large Scale Furnace

Flow pattern, species concentrations, heat transfer and pollutant emission were calculated for various furnace arrangements with the aid of numerical solution scheme. These calculations, described and discussed in the thesis were concerned with small scale furnace models and were aimed at an assessment of the combustion and radiation models. These models were appropriate to the flow situations considered in chapter 5 and yielded satisfactory results in many furnace flows within the limitations of the turbulence model and the implications of combustion models. It is necessary, however, to assess the validity of the numerical procedure under practical furnace applications and to extend the use of this scheme to large scale furnaces. A replica of a boiler fire tube was constructed by British Gas to measure the local flow properties and to investigate the various factors affecting flow, mixing pattern, combustion and heat transfer in the fire tube under real conditions and was reported by Rhines (1974).

The test furnace consists of a shell boiler fire tube 1.07m inside diameter and 5.48m long, mounted horizontally with the burner welded at one end and the exhaust system at the other. The furnace was surrounded by a water bath to transfer the wall heat load. Mean axial velocities were obtained with the aid of three hole pitot probe which was water cooled. A water cooled suction pyrometer was employed as a sampling probe as well as a temperature measuring device. The combustion gases were withdrawn from the furnace, partially cooled, their temperature measured then further cooled in the probe before the dry gas is analysed after the separation of condensed water. The inside surface of the fire tube was fitted with 40 heat flux gauges welded into the fire tube wall. The wall temperature at various locations was measured with Chromel-alumel thermocouples brazed onto

the inside surface of the fire tube. The firing rate of the burner was 566.4m^3/hr of natural gas (6Mw), which corresponded to 2/3 of the maximum load. The excess air was 4% and the natural gas contained 94.4% CH_4 and 1.48% N_2. Fuel was mixed with air prior to the furnace chamber through fuel orifices.

The procedure of chapter 2 was used to calculate the local flow properties in this furnace and incorporated the two equation turbulence model and the combustion characteristics were represented by model 4 with a clipped Gaussian probability distribution. The radiation model was of the flux type indicated in section 2.5. The inlet conditions were not measured and were assumed in accordance with the recommendations of Khalil (1976), therefore the present attempt to model the furnace should be regarded as preliminary and more refinement is required. The numerical non-uniform grid shown in figure A7.1 comprised 400 grid nodes and yielded grid independent results.

The mean axial velocity profiles across the fire tube at various axial locations are shown in figure A7.2 for burner 2 reported by Rhines (1974) without swirl in the air stream. In the burner vicinity, the reported measurements were not symmetrical at any station, and hence a full measured radial profile was shown at each station. The agreement was poor in that region due to the absence of the measured inlet velocity, kinetic energy profiles and generally due to the incomplete specification of the inlet conditions to the furnace space. At further downstream locations, i.e. x/D_f of 1.68 and 2.8, the agreement is reasonable and discrepancies are attributed to the precision of the measurements. Radial profiles of mean gas temperature are shown in figure A7.3 at various locations downstream the burner exit. The solid circles represent the measurements which were not symmetrical, while the symmetrical profiles calculated by the present procedure are shown by solid lines. The agreement was generally reasonable with maximum deviation of 400 K at 1250 K. The discrepancies associated with the temperature profiles are due mainly to the aerodynamic pattern which was not satisfactorily

predicted.

This comparison was not devised to assess the validity of the present numerical procedure, but was mainly to illustrate its advantage in qualitatively describing the behaviour of full scale flows, even with the minimum specifications of inlet and boundary conditions.

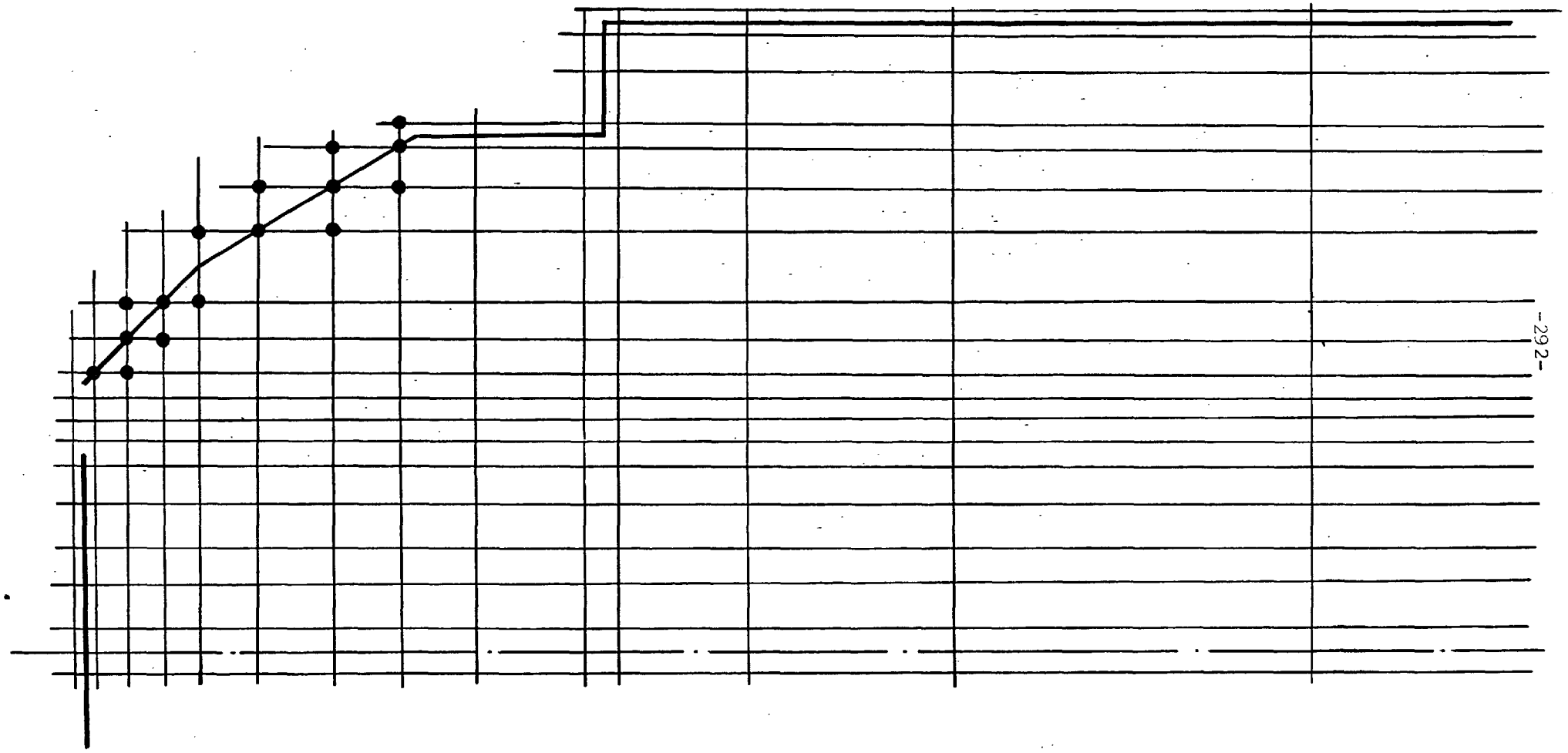

Figure A7.1 :Grid arrangement.

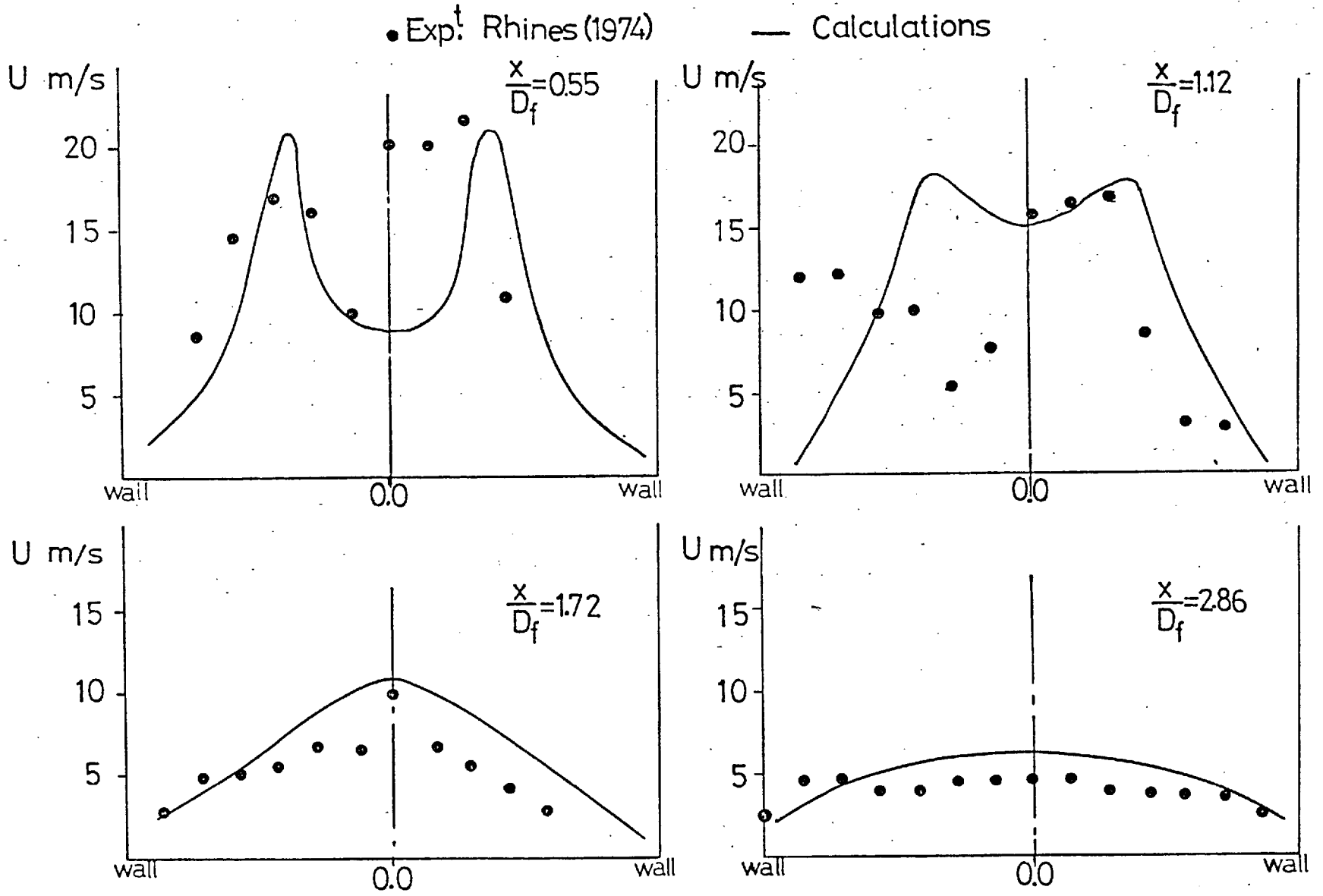

Figure A7.2:Measured and calculated profiles of mean axial velocity.

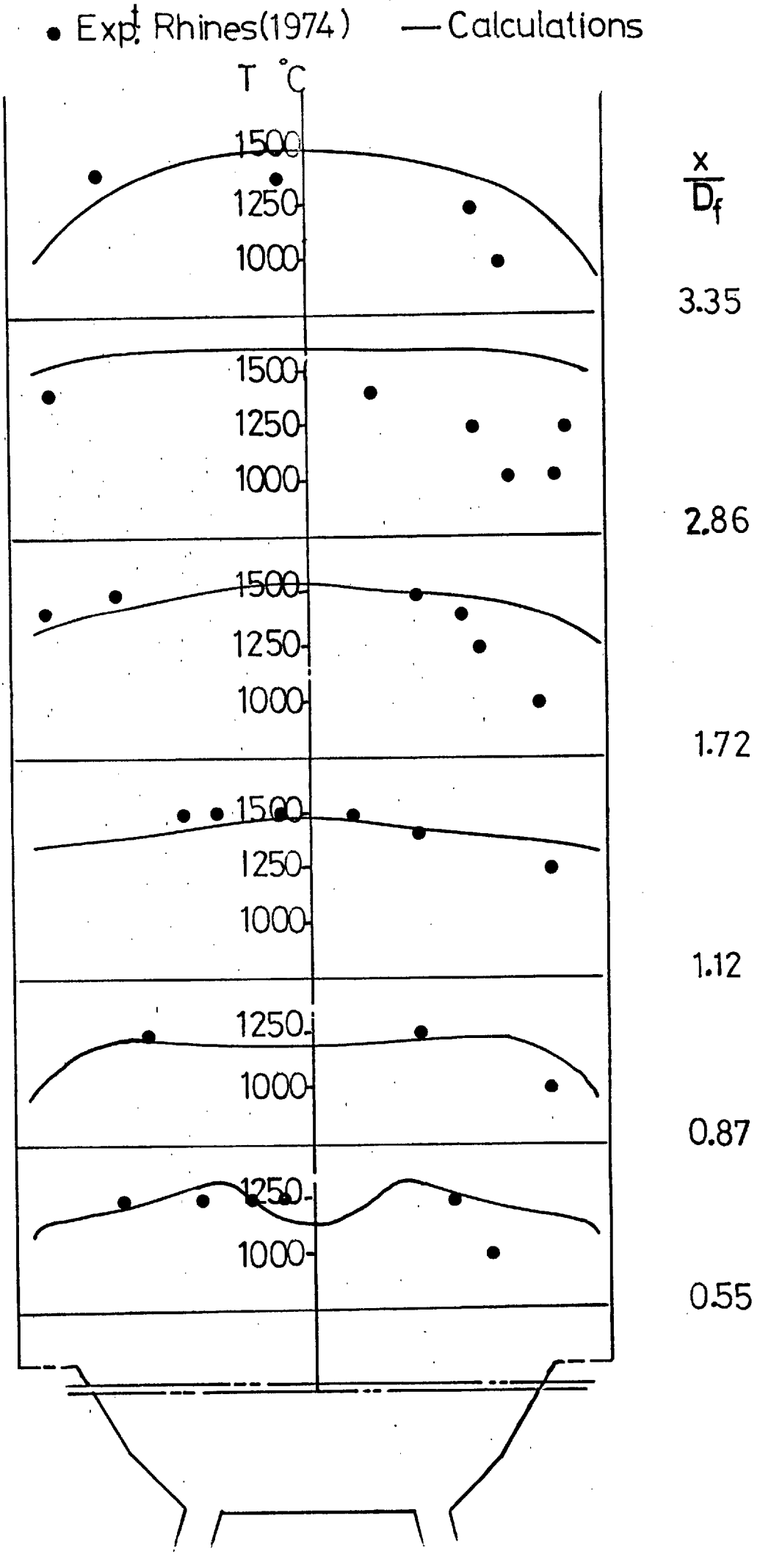

Figure A7.3:Measured and calculated mean gas temperature profiles.

APPENDIX A8

Department of Mechanical Engineering

Imperial College, London SW7 2BX

Aerodynamic and thermodynamic characteristics of kerosene-spray flames

by

E. E. Khalil and J. H. Whitelaw

Paper for presentation at the 16th International Symposium on Combustion and publication in the Symposium Volume

March, 1976

SUMMARY

Measured values of velocity, turbulence intensity, temperature, temperature fluctuations and droplet concentration are reported in four kerosene spray flames burning vertically in atomospheric air. The results are compared with calculated values, obtained with the aid of a numerical solution of modelled conservation equations in differential form, and appropriate to a gaseous flame of the same available enthalpy. Velocity, turbulence intensity and droplet measurements were obtained with a laser anemometer operating in forward scatter: a frequency tracking demodulator provided the velocity information and the number of particles crossing the control volume at a given time were measured with the aid of a digital counter. Measured mean and fluctuating temperature were obtained with platinum-rhodium thermocouple wires of bead diameters 180 and 40 μm respectively. Corrections were made for conduction and radiation effects on the mean temperature and for the effect of the thermal inertia of the smaller wire on the rms measurements.

The comparison between measurements and simulated gaseous flames, indicates that the flames have properties which are similar in general but significantly different in detail. The length of the flame decreases significantly from a spray of 100 μm to 50 μm droplets; and the simulated gaseous flame is still shorter and is not, therefore, a good approximation to spray flames. The measurements of rms velocity and temperature indicate values in excess of 0.75 and 0.30 respectively and the maxima appear to be coincident with the inflection points of the corresponding mean distributions.

INTRODUCTORY REMARKS

In earlier papers, references 1 to 4, the authors have reported measurements in gaseous, turbulent diffusion flames. These measurements have included velocity, velocity correlations and temperature measurements and have aided the development of calculation methods for combustion systems as well as contributing to the understanding of turbulent reacting flows. The present paper relates to kerosene spray flames and reports similar measurements, with the addition of distributions of droplet concentration. The results have been obtained to allow a comparison between the local aerodynamic and thermal characteristics of gaseous and spray flames of similar available enthalpy and to provide data for the testing of calculation methods which incorporate models for droplet combustion.

Four kerosene spray flames, corresponding to two nozzles and two shroud air arrangements, have been investigated with laser-Doppler anemometry and thermocouples. The sprays were designed to give kerosene droplets with Sauter mean diameters of approximately 45 and 100 μm and to allow an experimental comparison between the characteristics of the resulting flames. The anemometer allowed measurements of mean axial velocity and the corresponding normal stress and also provided a quantitative indication of the droplet-number concentration. Thermocouples provided measurements of mean temperature and an indication of the corresponding rms value.

The experimental results obtained from the kerosene-spray flames are compared with calculated values corresponding to gas flames with similar boundary conditions, apart from the finite-diameter droplets. The calculation procedure, which solved conservation equations in finite-different form, is a modified version of that described in references 3 to 5; the updated version is described in reference 6. It incorporated a two-equation turbulence model, one-step fast chemical reaction and a clipped Gaussian probability distribution

of species concentration. To demonstrate the suitability of this procedure for present purposes, a sample number of flow properties calculated for a gaseous flame are compared with measured values.

Previous measurements, in spray flames, have been reported for example in references 7 to 12 and are complementary to the present investigation. In general, the previous investigations aid the development of understanding spray flames but are insufficiently complete to aid the detailed development of computational methods. The present investigation is also deficient in that it does not report measurements of droplet size.

EQUIPMENT AND EXPERIMENTAL PROCEDURES

This section describes, in sequence, the burner arrangements, the instrumentation and the experimental procedure; the magnitude of possible error sources are discussed in a fourth subsection.

Burner arrangement

Figure 1 shows the arrangement of the spray atomizer used for the present experiments and nozzle diameters of 0.25 mm and 0.5 mm. Liquid kerosene was supplied to the nozzles under pressure, through the tangential ports, and discharged vertically into free surroundings: the air flow passed through one of the two shrouds, also shown on figure 1, and impinged on the fuel jet.

The droplet size distribution may be expressed in the form (12, 13)

$$\frac{\delta n}{n} = 6600 \left(\frac{d}{\bar{D}}\right)^6 \exp\left(-9\frac{d}{\bar{D}}\right) \delta\left(\frac{d}{\bar{D}}\right)$$

The Sauter mean diameter (dimension based on the mean surface volume), $\bar{D}$, can be expressed in the form

$$\bar{D} \simeq 75 \left(\dot{m}_{fu}\right)^{0.25} / (\Delta P)^{0.4}$$

where $\dot{m}_{fu}$ is the mass flow rate of fuel (kg/hr) and ΔP is the pressure drop, in the fuel stream across the atomizer. For the present arrangements this relationship suggests that $\bar{D}$ has values of 45 μm and 100 μm for the small and

large nozzle respectively. The air shrouds are likely to result in secondary atomisation and, therefore, in smaller droplets (12): it is difficult to quantify this reduction in size though it is to be expected that the affect will be greater with the larger pressure drops.

Instrumentation

Velocity, velocity correlations and droplet number concentration were obtained with the laser anemometer also shown in figure 1. It comprised a 5mW He-Ne laser (Spectra-Physics Model 120) an integrated optical unit (14), a light-collection arrangement, a photomultiplier (EMI 9558B) and a frequency-tracking demodulator (Cambridge Consultants Model MK2). The 200 mm focal length of the transmission and collection lenses and an aperture of diameter 0.58mm allowed a measuring volume of approximate diameter and length 0.15 mm and 2 mm: the fringe spacing was approximately 4 μm. The tracking filter had a band width of 3% and its output signal was passed to a true integrator and digital voltmeter and to an rms meter: the mean signal voltage and its rms were directly proportional to the mean velocity and the rms of the velocity fluctuations.

The number of particles crossing the central region of the measuring volume was measured with a digital counter (Type TSA6636/2 Venner Electronics) over periods between 10 and 60s and adjusted on the basis of the local mean velocity. The discrimination level of the counter was the same at all positions and, as a result, the measured concentrations are influenced by possible variations in signal amplitude due to particle size and velocity: these effects are presumed small in comparison with the variations in number density.

Values of mean temperature were obtained with a Pt-40%Rh, Pt-20% Rh thermocouple of bead diameter 180 μm. The emf was amplified, integrated and displayed on a digital voltmeter. The radiation losses were determined by heating the thermocouple electrically in a vacuum, recording and plotting the temperature against the heating power. The thermocouple was then placed in the flame and heated at various powers at each location; temperature and heating

powers were again recorded and plotted. The intersection of the two curves gave the gas temperature.

Values of the rms of temperature fluctuations were determined with a thermocouple of bead diameter 40 μm and Pt-30% Rh &Pt-6% Rh wires. The compensation circuit of Odidi (15) was used and the resulting rms value recorded on an rms meter (DISA Type 55D35). The time constant of the thermocouple was determined as a function of temperature by electrically heating the wire in different regions of the flame and solving the equation

$$\frac{\bar{T}_g - \bar{T}}{\tau} + \eta I^2 = 0$$

Experimental Procedure

The spray atomiser was screwed to a 200 mm diameter tray and mounted in an approximately vertical position. The measuring volume of the anemometer and the thermocouples were fixed in space and the nozzle moved in relation to them. Vertical traverse was ensured by aligning the measuring volume and the thermocouple with respect to the centre of the spray nozzle and to the apex of a machined cone located concentric with the nozzle for this purpose. Radial traverses of the nozzle with respect to the anemometer and the thermocouple indicated profiles of mean velocity and temperature which was symmetrical to within 0.4% and 1.8% respectively of the local centre-line values.

The flow rate of kerosene was adjusted, with the aid of a rotometer, to 7.2 kg/hr at a supply pressure of 15 atm. The air supply rate to the shroud of the nozzle was 0.55 kg/hr. Measurements were obtained in four flames corresponding to the information of Table 1.

Table 1

Geometric and initial flow conditions

Flame	I	II	III	IV
nozzle diameter, mm	0.25	0.25	0.50	0.50
Sauter mean diameter, μm	45	45	100	100
type of shroud	a	b	a	b
air pressure, atm	3.5	2.0	3.5	2.0
cone angle*, degrees	52	78	68	90

*footnote: measured in isothermal flow.

Error Analysis

The measured values of mean velocity are probably precise to better than ± 1% in the upstream region of each flame: far downstream the precision may be slightly worse due to the comparatively high values of signal dropout. Corrections to measured values of the rms of Doppler frequency fluctuations, resulting from velocity-gradient and transit-time effects, were considered and found to be less than 3%. The precision of the rms velocity values is limited, in the upstream region by the finite response of the particles to the flow and, in the downstream region by the lack of light frequency shifting and the increasing dropout. At values of $x/D \lesssim 5$, the precision is of the order of ± 5% of the local value and far downstream the appropriate figure is ± 10%.

The measurement of particle number concentration is subject to error due to gradient effects and to the use of a constant threshold level with a signal whose amplitude is an unknown function of particle size and velocity. The gradient and velocity effects are likely to be very small in the present case and the particle size effect was effectively eliminated by basing each measurement of concentration on a large sample, i.e. more than individual signals.

The result is a distribution of particle concentration which is normalised by the initial particle size distribution.

Measurements of mean temperature are subject to conduction and radiation errors. These were estimated and, as a result, the precision of measurement is considered to be better than $\pm$ 1%. The precision of the rms temperature measurements is probably of the order of $\pm$ 15%, as suggested by Odidi.

RESULTS

Measured values of mean axial velocity, turbulence intensity, particle number density and mean temperature along the centre lines of flames I and II are shown on figures 2 and 3 respectively. The characteristics of the two flames are similar and it can be seen that the different shroud arrangements influence the cone angle of the spray. The droplet number density dropped rapidly from the nozzle exit, largely because of the angle of the spray, and a maximum mean temperature of around 1900K was attained around 10D downstream for flame I; for flame II the different shroud arrangement resulted in a maximum centre line temperature of 1760K at a location around 13D downstream.

For both flames, the maximum centre-line velocity was attained upstream of the maximum centre-line temperature and the maximum value of $\tilde{u}/U$ was achieved at the x-location corresponding to the inflection in the mean velocity distribution. The maximum value of $\tilde{T}/T$ was also achieved in the vicinity of the inflection in the mean temperature distribution but the precision of measurement of $\tilde{T}$ makes this less clear. These characteristics are similar to those observed previously in laminar gaseous diffusion flames (16) and are probably common to a wide range of diffusion flames.

Measurements of U, $\tilde{u}/U$ and T were also obtained at values of $r/D > 0$ and yielded contours which are presented on figure 4 for flame I. The outline of

the reaction zone can be identified from the U and T distributions and corresponds with the spray angle of table 1. Measurements of U and $\tilde{u}/U$ in the vicinity of the reaction zone are subject to greater uncertainty than elsewhere due mainly to the combination of high turbulence intensity and signal dropout. It is also clear from the figure that the velocity profile is considerably wider than would be found in an isothermal free jet. Several radial distributions of droplet number density were also measured but, due to the low numbers involved, were imprecise. They did, however, show higher concentrations in the vicinity of the maximum mean temperature and on the centre line.

Figures 5 and 6 present measurements of U, $\tilde{u}/U$ and T along the centre lines of flames III and IV. The T-distributions suggest that the influence of the different shroud-air arrangements is less significant in this case, as might be expected, and the general flame characteristics are similar to those of flames I and II. The larger droplet size, associated with the larger nozzle, has caused the maximum value of U, $\tilde{u}/U$ and T to occur further downstream than for flames I and II and the maximum temperature is correspondingly less. The contours of figure 7 confirm that the maximum temperature is achieved further downstream than for flame I and that the measured temperatures are considerably smaller than those of flame I at the same geometric locations.

The calculation procedure, with the assumptions of fast reaction and a clipped Gaussian probability distribution of scalar fluctuations (6) was used to allow comparison between the characteristics of the present spray flames and a gaseous flame of similar initial conditions and the same available enthalpy. To demonstrate the validity of this procedure, figure 8 presents a comparison between measured and calculated values of centre-line velocity and mean temperature for the hydrogen diffusion flame of Bilger and Kent (17). The agreement is similar in magnitude to that observed in several flows, i.e. local normalised velocity values agree to within 5% and local temperature values

to better than 200K.

To allow comparison with the spray flames, the calculation procedure was arranged with initial conditions corresponding to gaseous kerosene issuing from a jet with cone angles corresponding to those of table 1 and with mass velocity similar to that of the spray flames. The shroud air was simulated by a corresponding mass and tangential momentum injected in the flame of the burner exit and at the outer edge of the jet. This procedure is inexact, since the geometric features of the spray nozzle cannot be represented in detail but the general arrangement is in accord with the experiments and the available enthalpy of the gaseous and spray arrangements are the same.

Figure 9 compares the centre line velocity and temperature distributions of flame I and the corresponding gaseous simulation and shows, as expected, that the gaseous simulation attains a maximum temperature before the spray flame. The distance between the two temperature maxima is similar to that between those of flames I and II and less than that between those of flames I and III. The maximum centre-line temperature of the gaseous simulation is less than that of the spray flame but, as can be seen from figure 10, the maximum temperatures in all three flames are achieved some distance from the centre line: this stems from the tendency to a 'hollow cone' flow caused by the angle of the spray and the corresponding gaseous simulation. The inexact nature of the comparison is indicated by the centre line temperature of flame I at x/D of 7.15: this value is a maximum in the radial profile and stems from the nature of the spray which, as the droplet concentration measurement revealed, produced a similar concentration profile.

DISCUSSION

It is not possible to separate completely the effects of the detailed spray characteristics from that of droplet size but the measurements do suggest

a significant shortening of the flame length as the droplet size is decreased from a Sauter mean diameter of 100 μm to 45 μm. The different arrangements of shroud air also influence the flame properties but significantly less than the droplet size. Similarly, the simulated gaseous flame is still shorter than the 50 μm droplet flame. The differences in the flame resulting from the fuel arrangement are also reflected in the detailed measurements but the relationships between the flow characteristics of each flame are similar.

These observations imply that the representation of spray flames by calculation methods such as that used to determine the properties of the simulated gas flame must be extended to take account of droplet characteristics even with droplet diameters less than 50 μm. The trajectory of droplets and flow need to be specified as initial conditions and, thereafter, the more rapid burning of the smaller droplets must be represented in a droplet-model.

The comparatively high level of the observed velocity and temperature fluctuations require further investigation. The normalised rms of velocity fluctuations achieved a maximum value in excess of 0.75 in flame I and, although this measurement must be regarded as approximate, it clearly corresponds to the inflection in the mean-velocity distribution and may, therefore, stem from an aerodynamic instability. The normalised rms of temperature fluctuations reached 0.30 in flame II and is significantly higher than the values measured by Odidi (15) in his town gas flame: for a random distribution of fluctuations, this implies instantaneous maximum and minimum temperatures of 2100K and 1120K respectely. Future measurements of temperature probability density distributions, in the region of the maxima fluctuations are desirable.

REFERENCES

1. BAKER, R.J., BOURKE, P. AND WHITELAW, J.H.: Fourteenth Symposium (International) on Combustion, p.699, The Combustion Institute, 1973.
2. BAKER, R.J., HUTCHINSON, P., KHALIL, E.E. AND WHITELAW, J.H.: Fifteenth Symposium (International) on Combustion, p. 553, The Combustion Institute, 1975.
3. HUTCHINSON, P., KHALIL, E.E., WHITELAW, J.H. AND WIGLEY, G.: A.S.M.E. Paper 75-HT-8, 1975. To be published in J. Heat Transfer, 1976.
4. HUTCHINSON, P., KHALIL, E.E., WHITELAW, J.H. AND WIGLEY, G.: Second European Symposium on Combustion, p. 659, 1975.
5. KHALIL, E.E., SPALDING, D.B. AND WHITELAW, J.H.: Intern. J. Heat Mass Transfer, 18, 775 (1975).
6. HUTCHINSON, P., KHALIL, E.E. AND WHITELAW, J.H.; The calculation of wall heat-transfer rate and pollution formation in axi-symmetric furnaces. To be presented at the 4th Members Conference of the International Flame Research Foundation, Ijmuiden, 1976.
7. CHIGIER, N.A., McCREATH, C.G. AND ROETT, M.F.: Acta Astronitica, 1, 687 (1974).
8. MIZUTANI, T. AND NISHIMOTO, T.: Combustion Science and Technology, 6, 1 (1972).
9. ONUMA, Y. AND OGASAWARA, M.: Fifteenth Symposium (International) on Combustion, p. 453, The Combustion Institute, 1975.
10. KOMIYAMA, K. FLAGAN, R.C. AND HEYWOOD, J.B.: Second European Symposium on Combustion, p. 641, 1975.
11. CHIGIER, N.A. AND STYLES, A.C.: Second European Symposium on Combustion, p. 563, 1975.
12. ABU ELLEIL, M.M.: Theoretical and Experimental Investigation of the Pre-Combustion Period Events of Fuel Droplets in Gas Turbine Combustion Chambers, Ph.D. Thesis, CAIRO UNIV, Dept. of Mech. Eng. CAIRO, 1974.

13. TANASAWA, Y. AND TESHIMA, T.: On the theory of combustion role of liquid fuel spray, Bulletin of JSME, 1, 36, 1958.

14. BURST, F. AND WHITELAW, J.H. J. Phys. E 4, 804 (1971).

15. ODIDI, A.O.: The influence of turbulence on the time-mean rate of chemical reation, Ph.D. Thesis, London Univ., Dept. of Mech. Eng., 1974.

16. DURAO, D.F.G. AND WHITELAW, J.H.: Proc. Roy. Soc. (London), A 338, 479, 1974.

17. BILGER, R.W. AND KENT, J.H.: Measurements in turbulent jet diffusion flames, Univ. of Sydney, Charles Kolling Research Laboratory, Tech. Note. F-41, 1972.

Acknowledgements

The authors gratefully acknowledge financial support from the A.E.R.E., HARWELL and for the continuing interest of Dr. P. Hutchinson. The spray nozzle was kindly provided, on loan, by Mr. H. Clare of the National Gas Turbine Establishment.

NOMENCLATURE

d	droplet diameter, mm
D	burner outer diameter, mm
$\bar{D}$	sauter mean diameter, mm
I	current, amp.
m_{fu}	fuel mass flow rate, Kg/hr
δn	number of droplets whose diameter lies between d and d + δd
n	total number of droplets
Δp	injector pressure drop, atm
r	radial distance, mm
T	temperature K
$\tilde{T}$	fluctuating temperature K
U	mean axial velocity, m/s
$\tilde{u}$	fluctuating axial velocity, m/s
x	axial distance along the centreline from the burner exit, mm
η	constant involving density, specific heat, resistance and diameters of thermocouple wires.
τ	thermocouple time constant

Subscripts

j	jet
c.l.	centreline
g	gas

Figure Captions

Figure 1 : Optical arrangement and burner geometry.

Figure 2 : Measured centreline distribution of mean velocity, turbulence intensity, droplet concentration and mean temperature (flame I).

Figure 3 : Measured centreline distribution of mean velocity, turbulence intensity, droplet concentration, mean and fluctuating temperature (flame II).

Figure 4 : Contours of iso-velocity, iso-turbulence and isotherms for flame I.

Figure 5 : Measured centreline distribution of mean velocity, turbulence intensity and temperature (flame III).

Figure 6 : Measured centreline distribution of mean velocity, turbulence intensity and temperature (flame IV).

Figure 7 : Contours of iso-velocity, iso-turbulence and isotherms for flame III.

Figure 8 : Comparison between measured and calculated centreline values of U and T

—— calculations

● measured U)
) Bilger and Kent (17)
○ measured T)

Figure 9 : Centreline distribution of velocity and temperature

—— simulated gas flame

▼ measured values of U) Flame I
● measured values of T)

Figure 10 : Radial profiles of temperature

—— simulated gas flame

● flame I

○ flame III

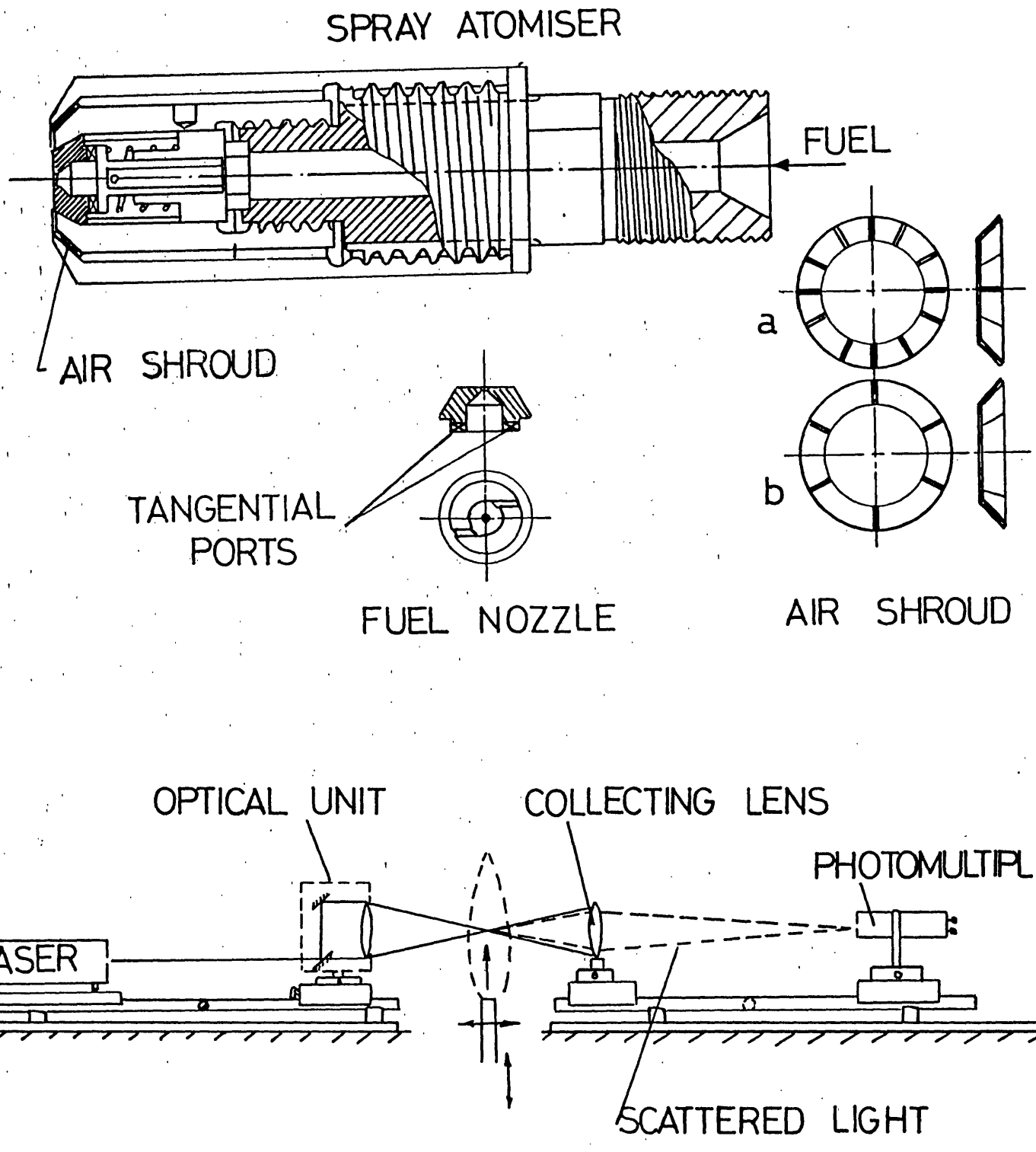
SPRAY ATOMISER
FUEL
AIR SHROUD
a
b
TANGENTIAL PORTS
FUEL NOZZLE
AIR SHROUD
OPTICAL UNIT
COLLECTING LENS
PHOTOMULTIPLIER
LASER
SCATTERED LIGHT

Figure 1

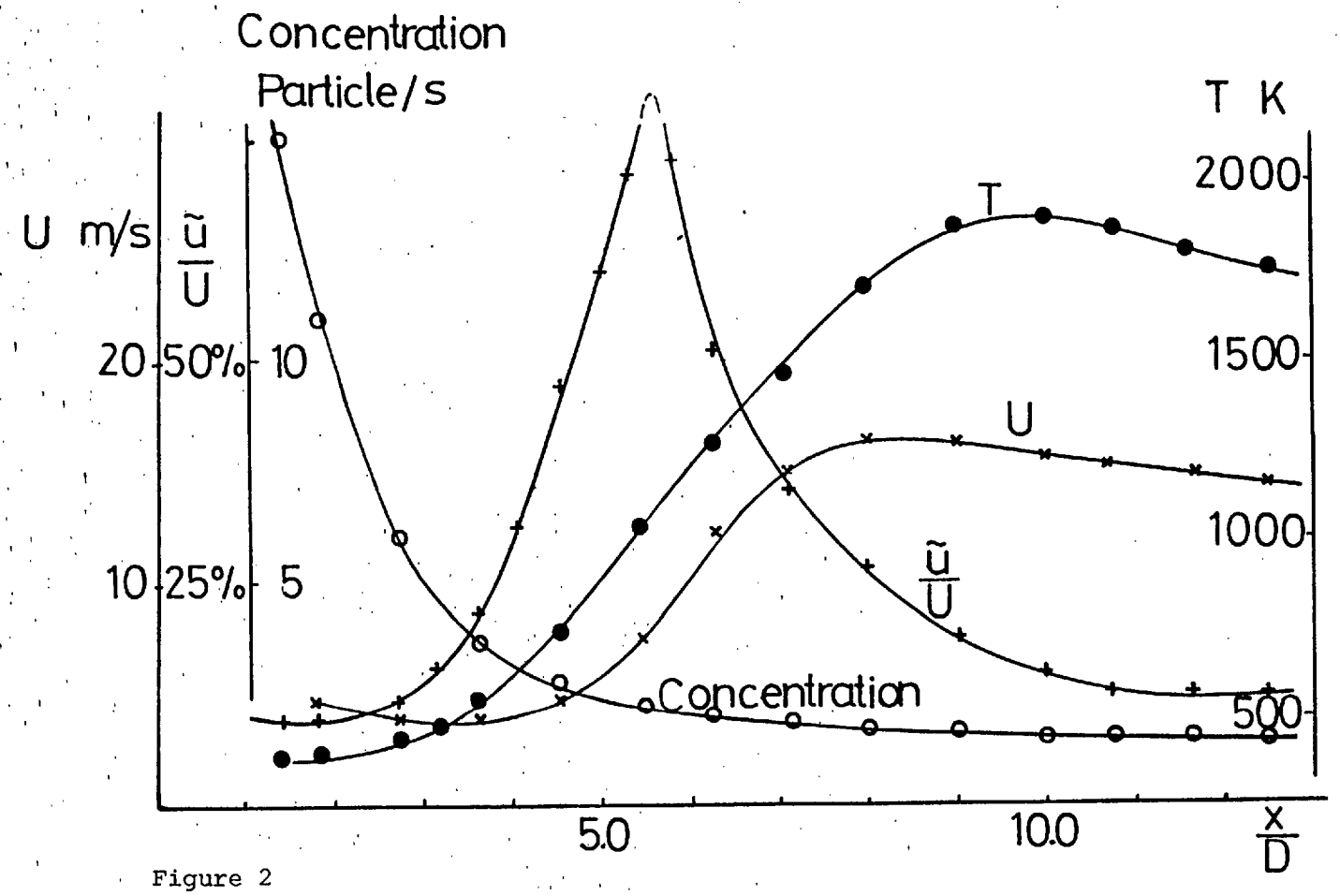

Figure 2

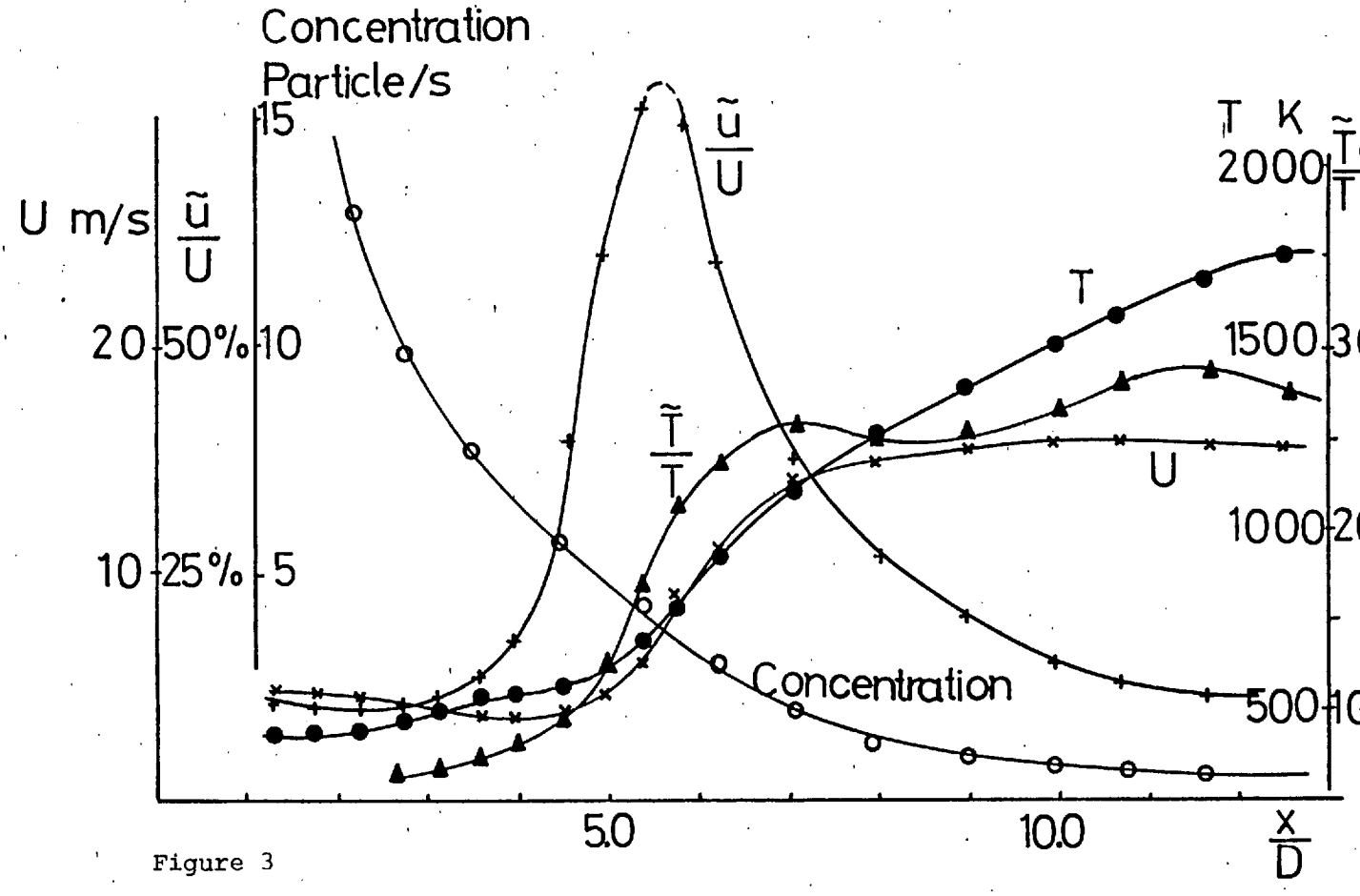

Figure 3

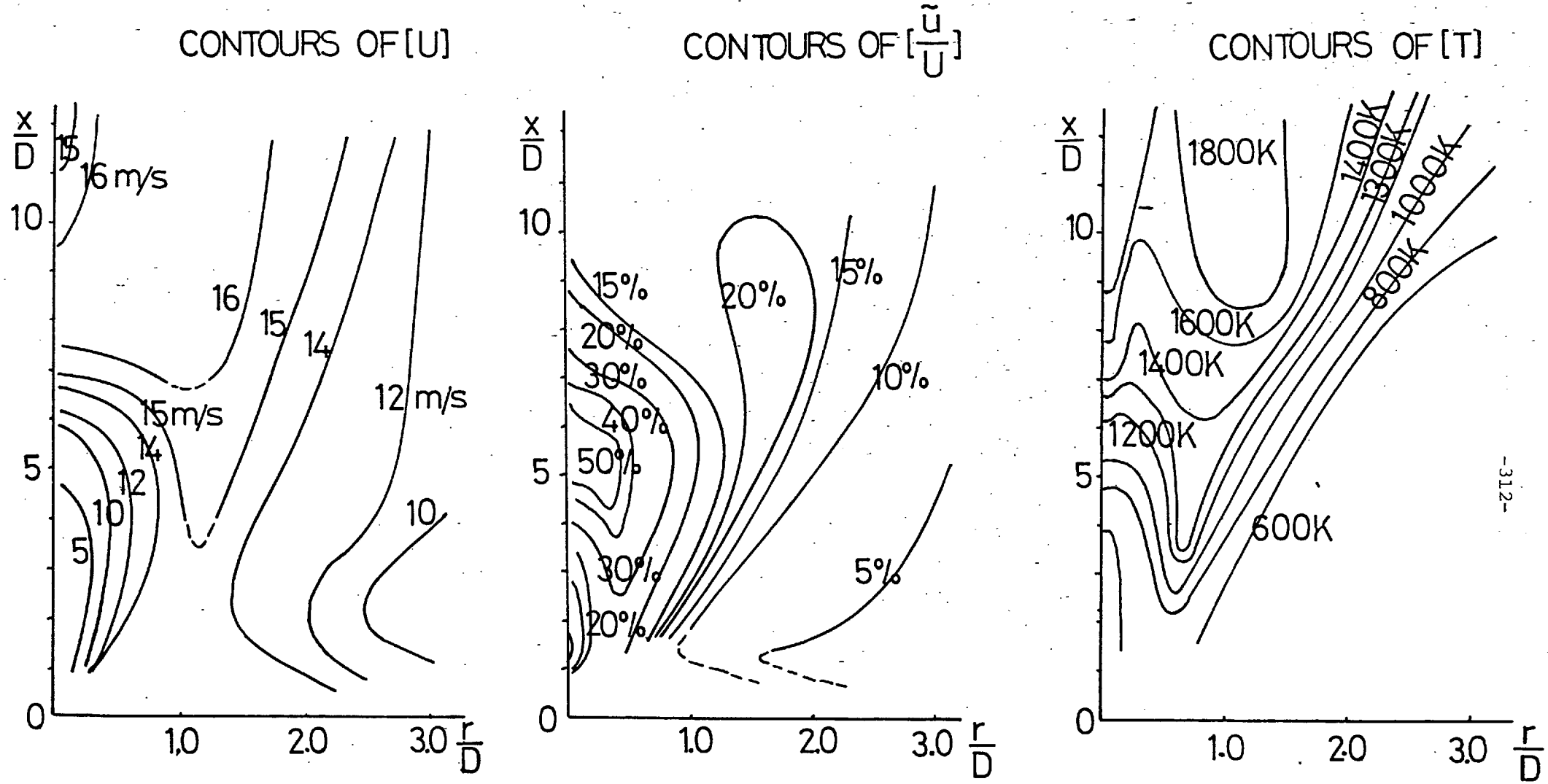
CONTOURS OF [U]
CONTOURS OF [ũ/U]
CONTOURS OF [T]
x/D
r/D
16 m/s
15 m/s
12 m/s
1800K
1600K
1400K
1200K
1000K
800K
600K
15%
20%
30%
40%
50%
10%
5%

Figure 4

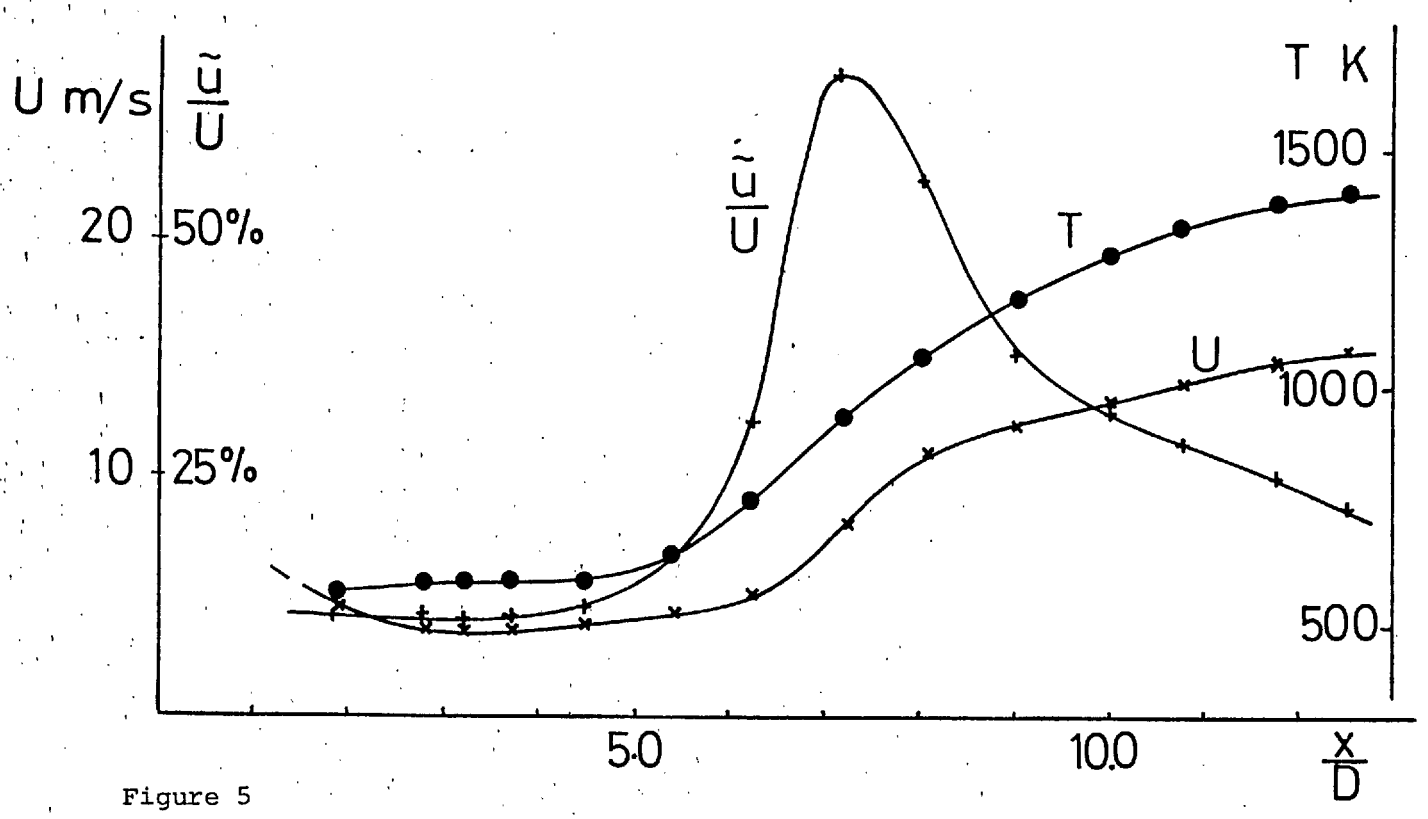

Figure 5

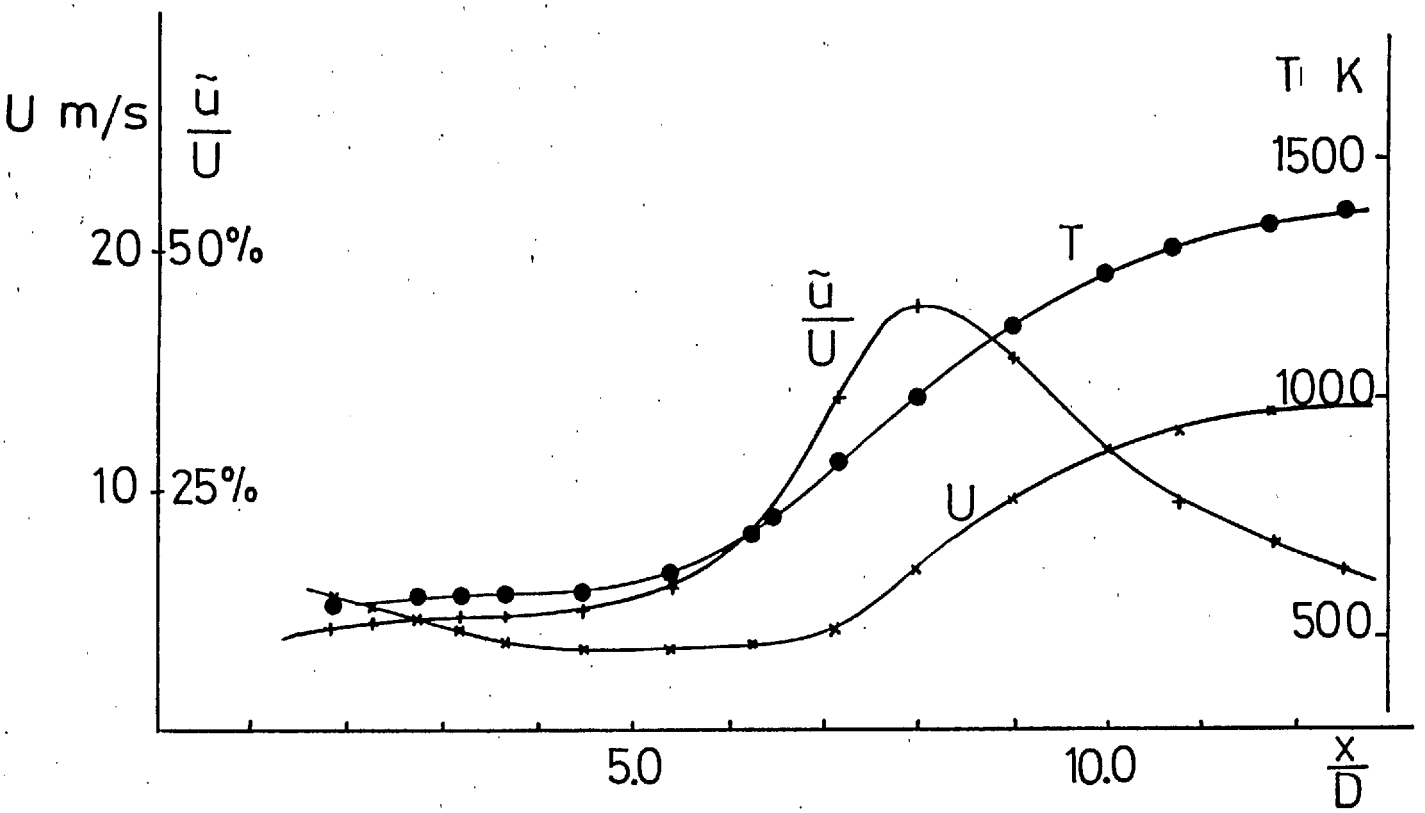

Figure 6

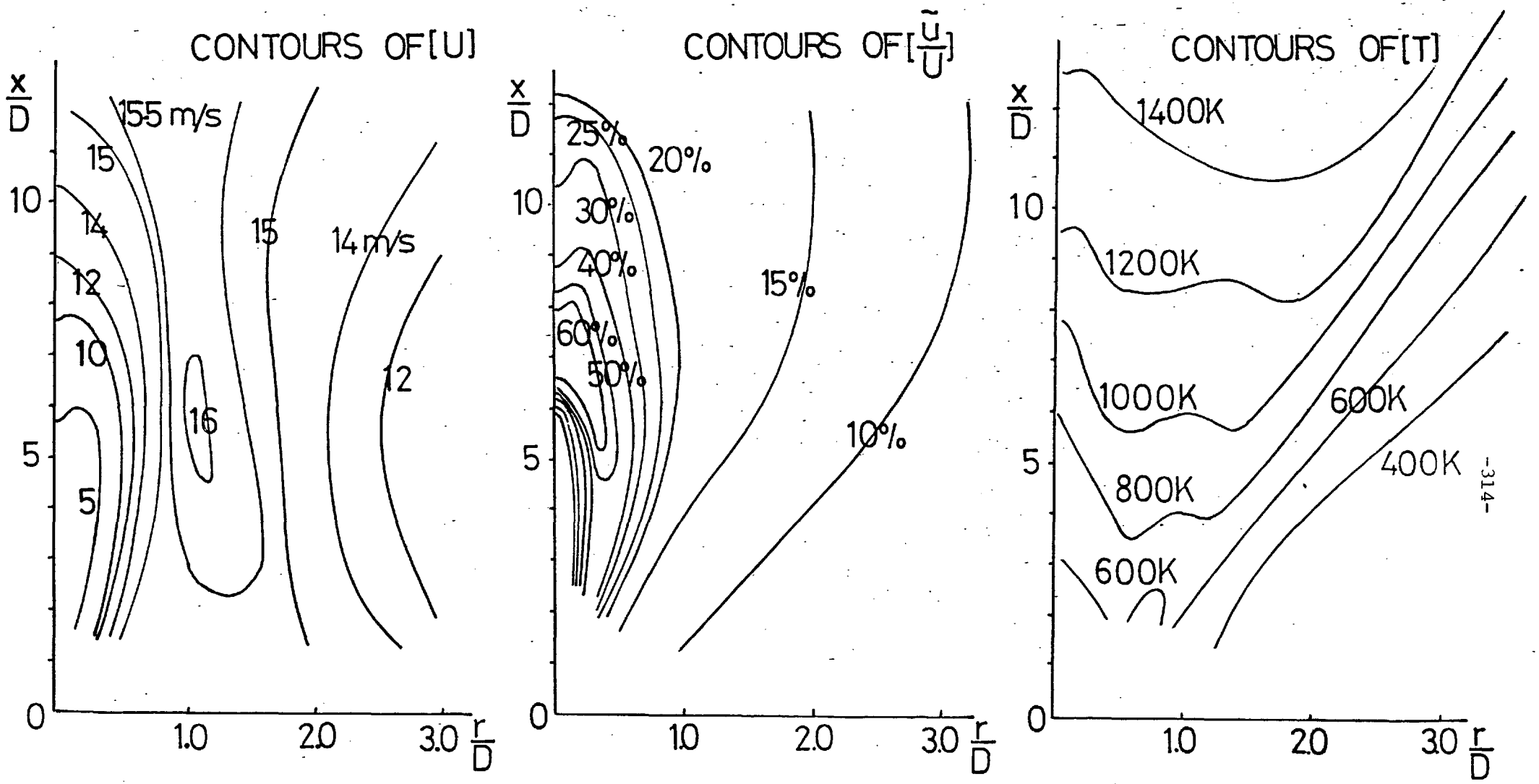
CONTOURS OF[U]
x/D
155 m/s
15
14
12
10
16
15
14 m/s
12
5
0
1.0
2.0
3.0 r/D
CONTOURS OF[ũ/U]
x/D
25%
20%
30%
40%
60%
50%
15%
10%
0
1.0
2.0
3.0 r/D
CONTOURS OF[T]
x/D
1400K
1200K
1000K
800K
600K
600K
400K
0
1.0
2.0
3.0 r/D

Figure 7

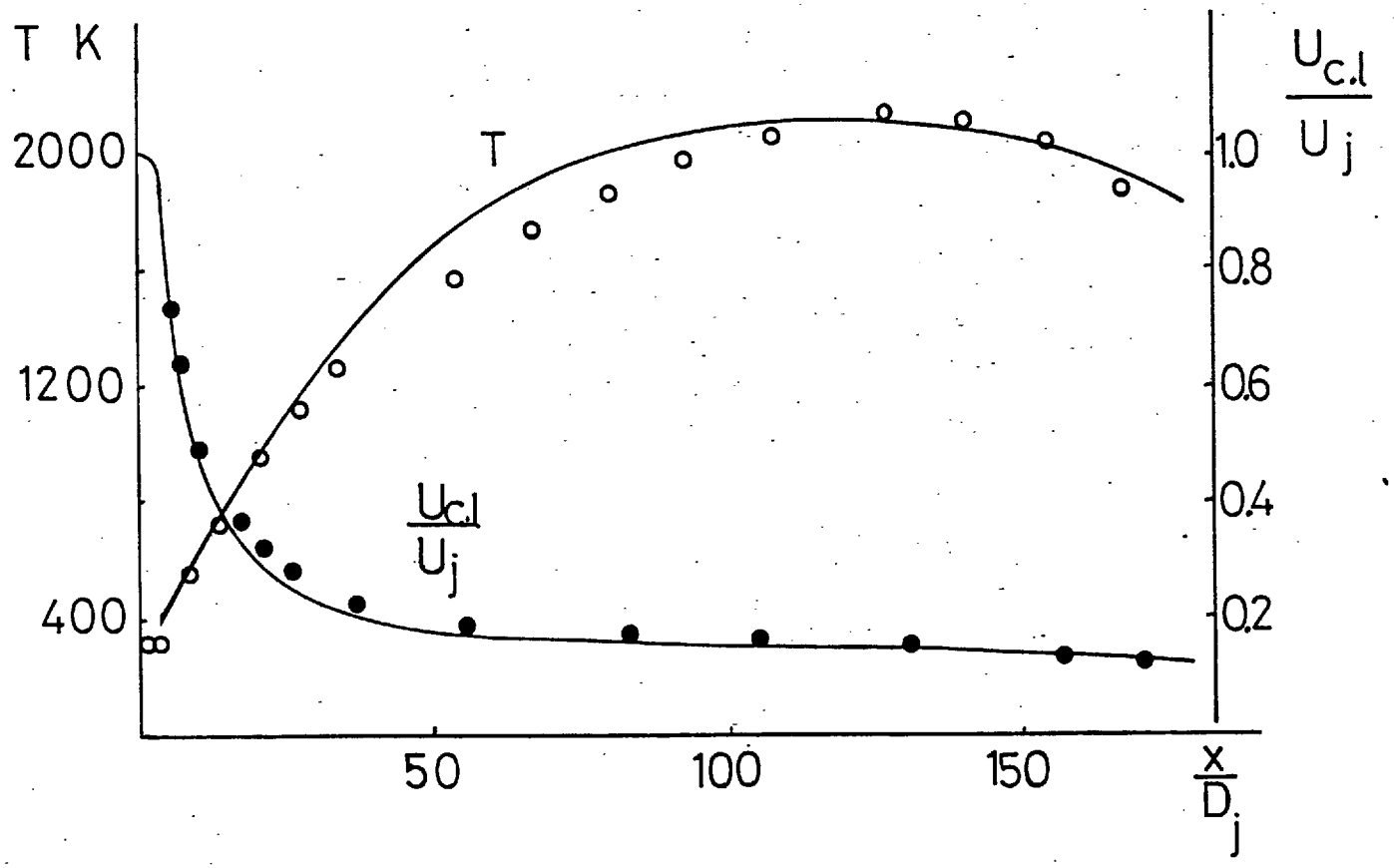
T K
2000
1200
400
T
$\frac{U_{c.l}}{U_j}$
50
100
150
$\frac{x}{D_j}$
$\frac{U_{c.l}}{U_j}$
1.0
0.8
0.6
0.4
0.2

Figure 8

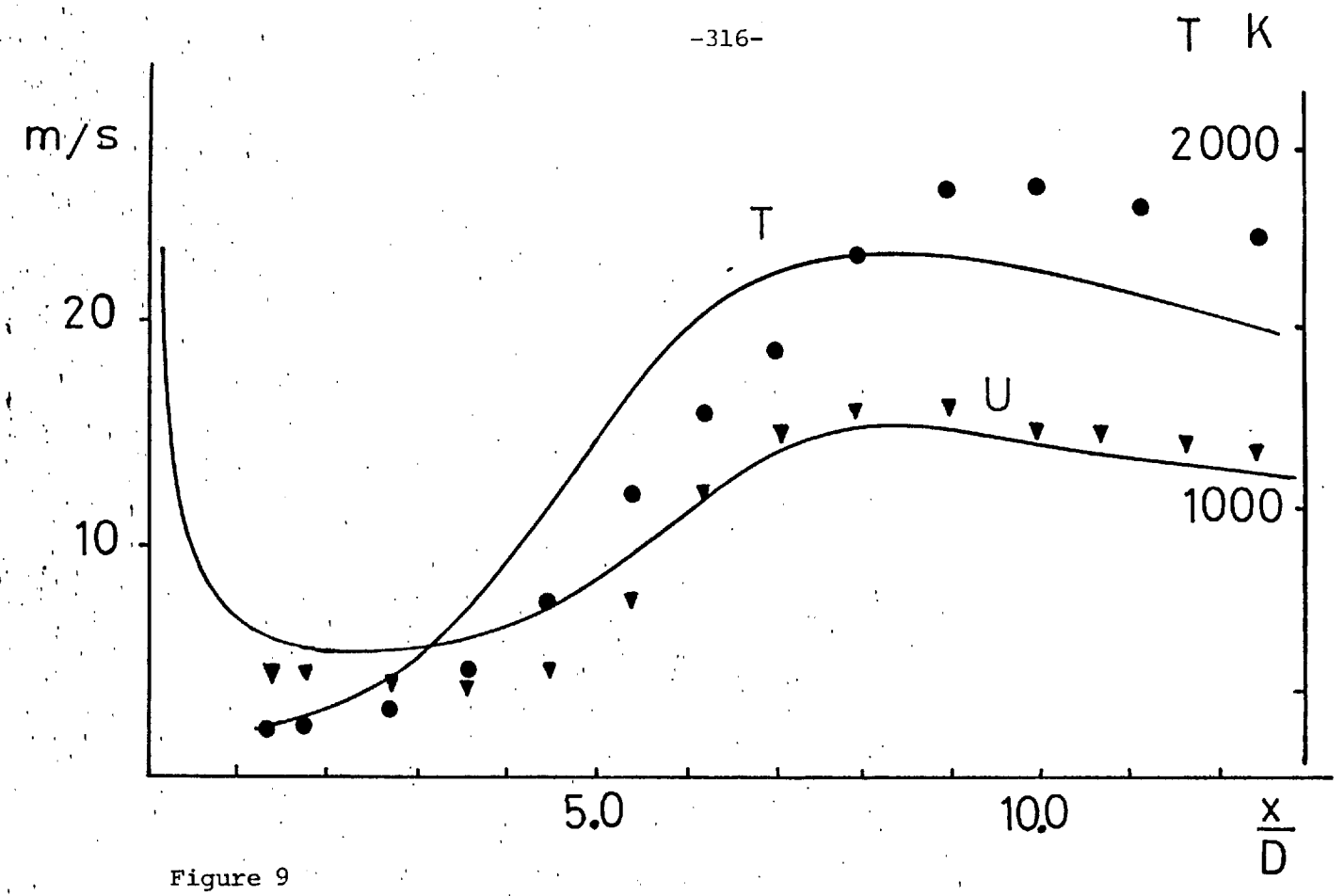

Figure 9

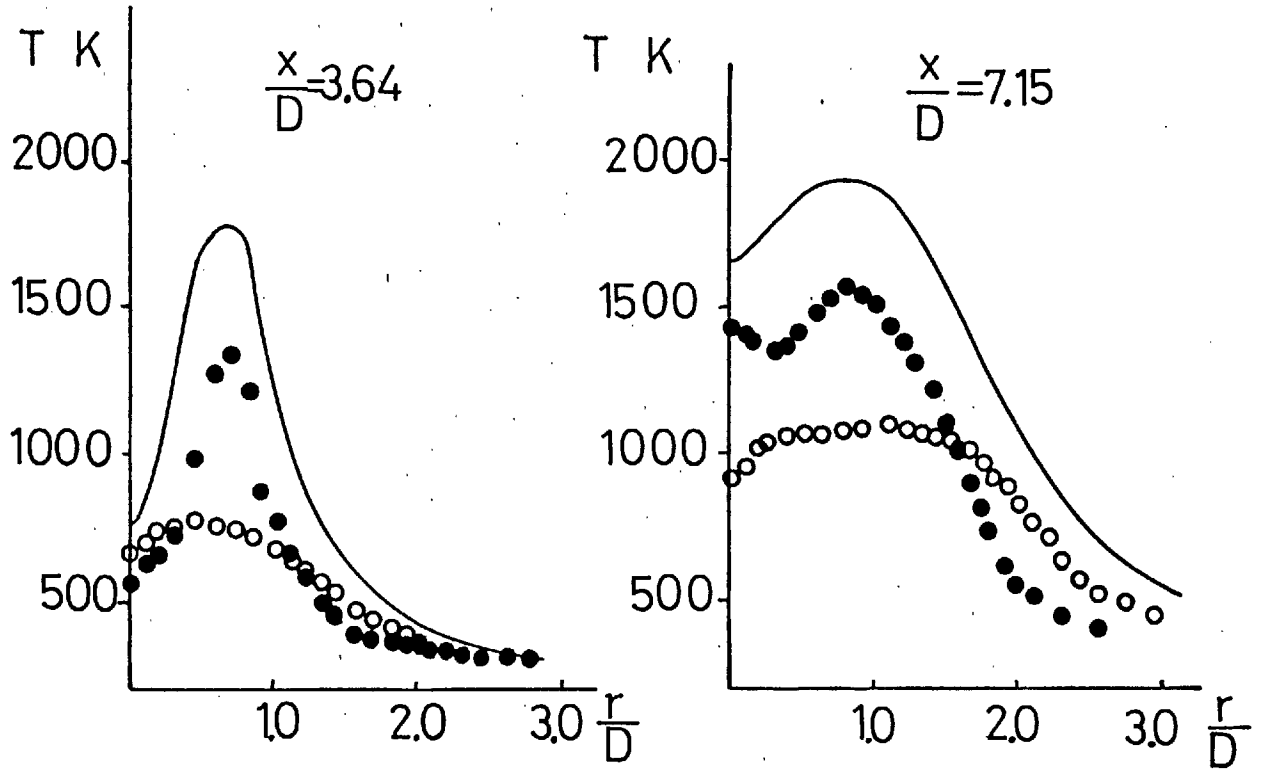

Figure 10

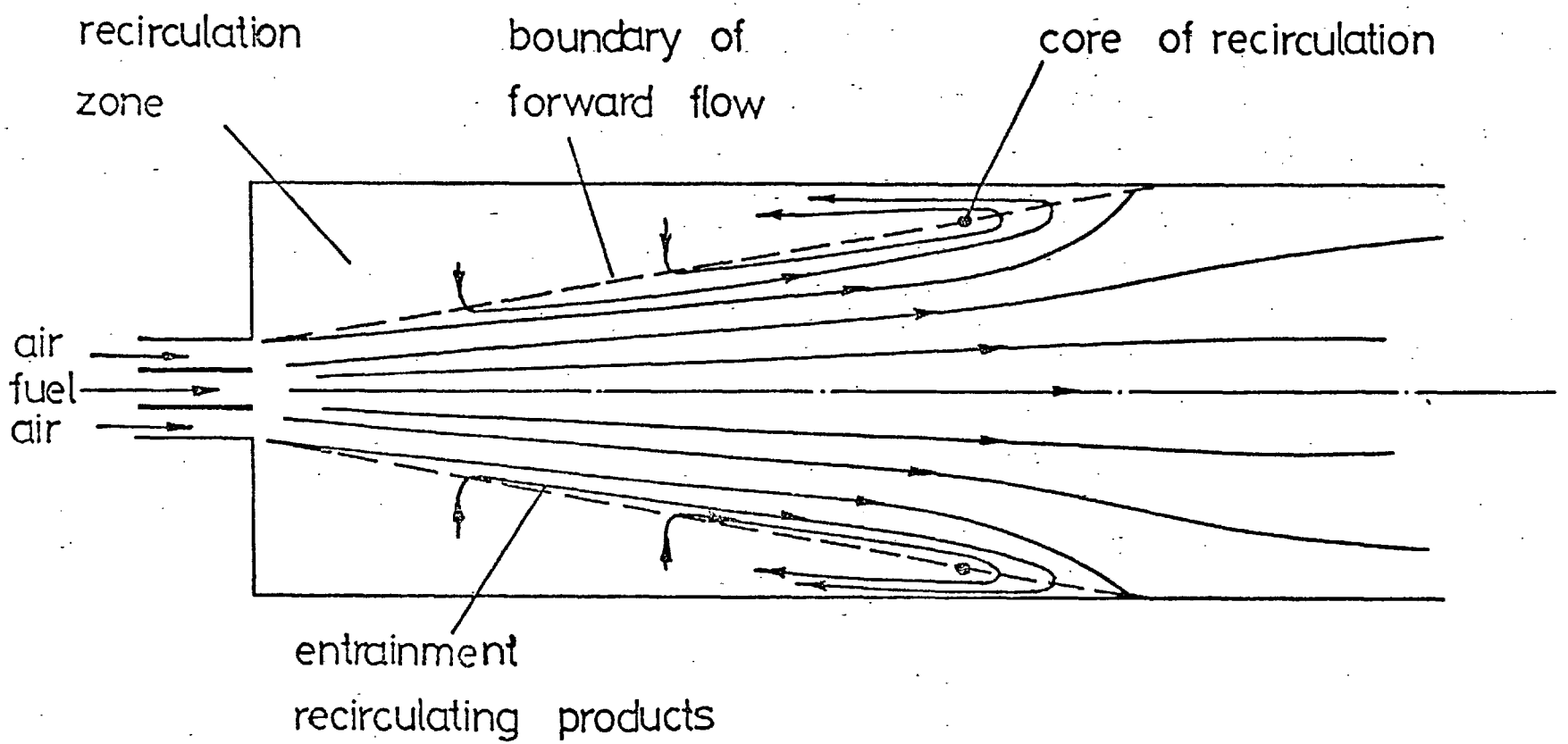

Figure 1.1: Flow pattern for a coaxial jet issuing in an axisymmetric confinement.

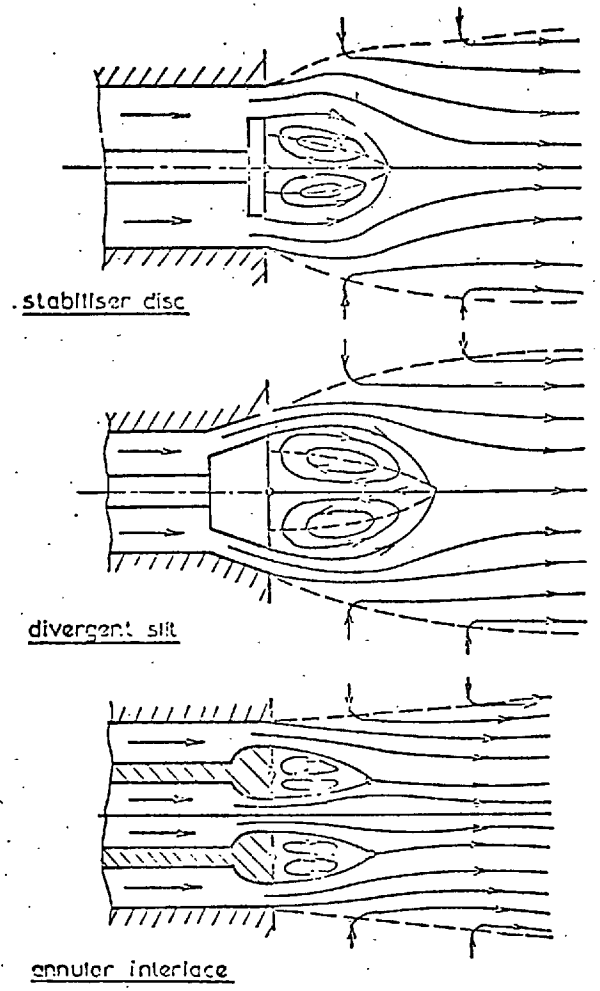

: Internal recirculation in the wake flow behind bluff bodies

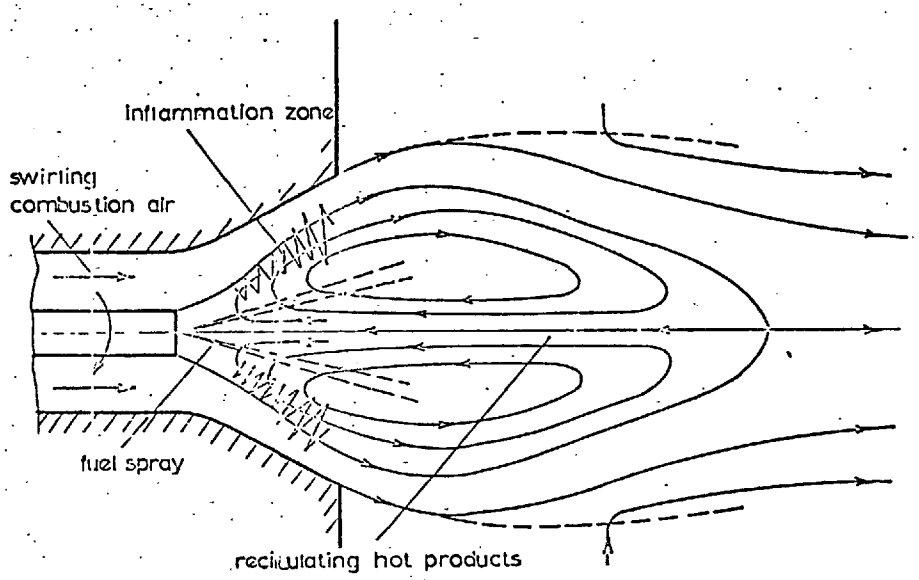

Self-stabilising mechanism of ignition in a swirling flame jet with internal recirculation (Leuckel, 1969)

Figure 1.2: Flow pattern in central recirculation zones.

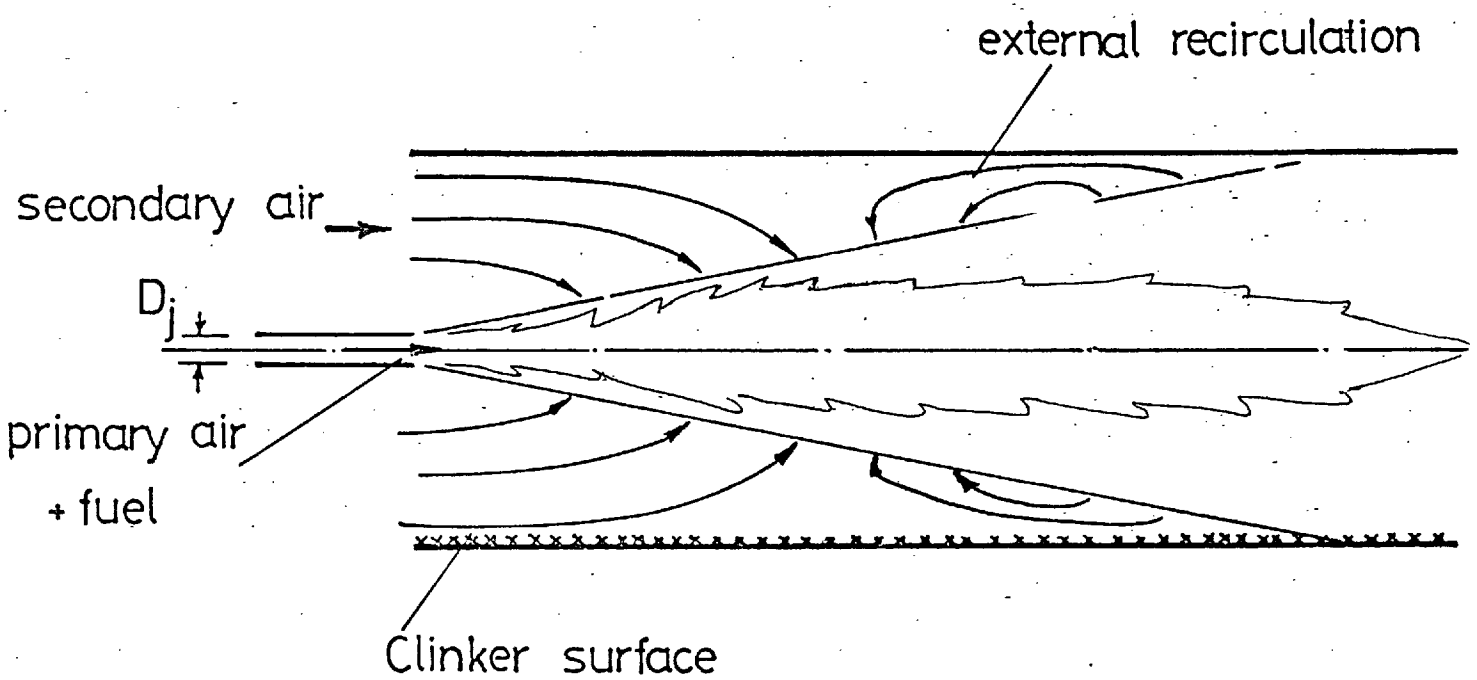

Figure 1.3: Flow pattern in a cement kiln.

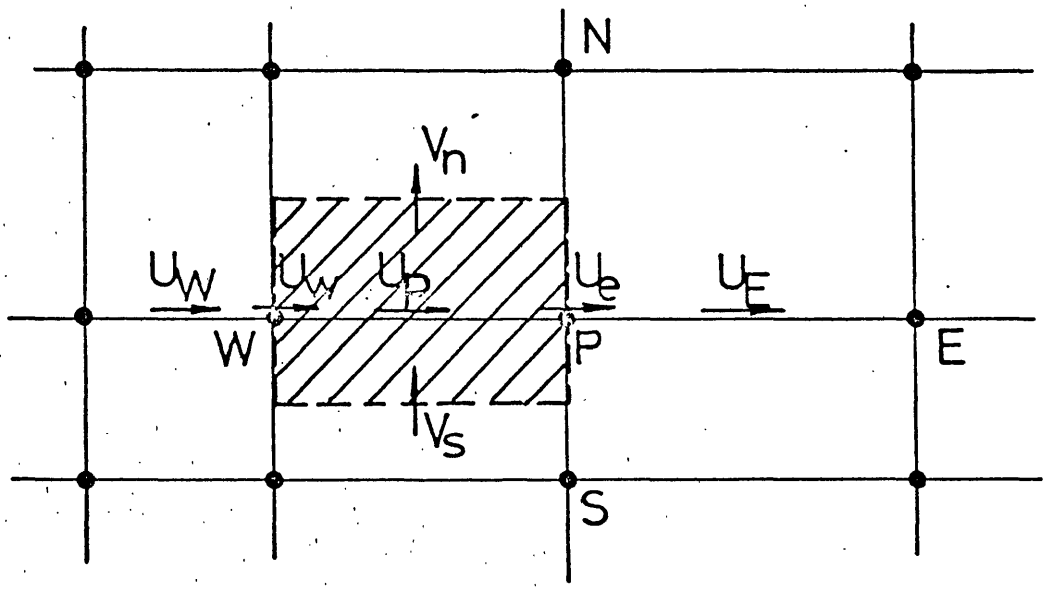

U-cell

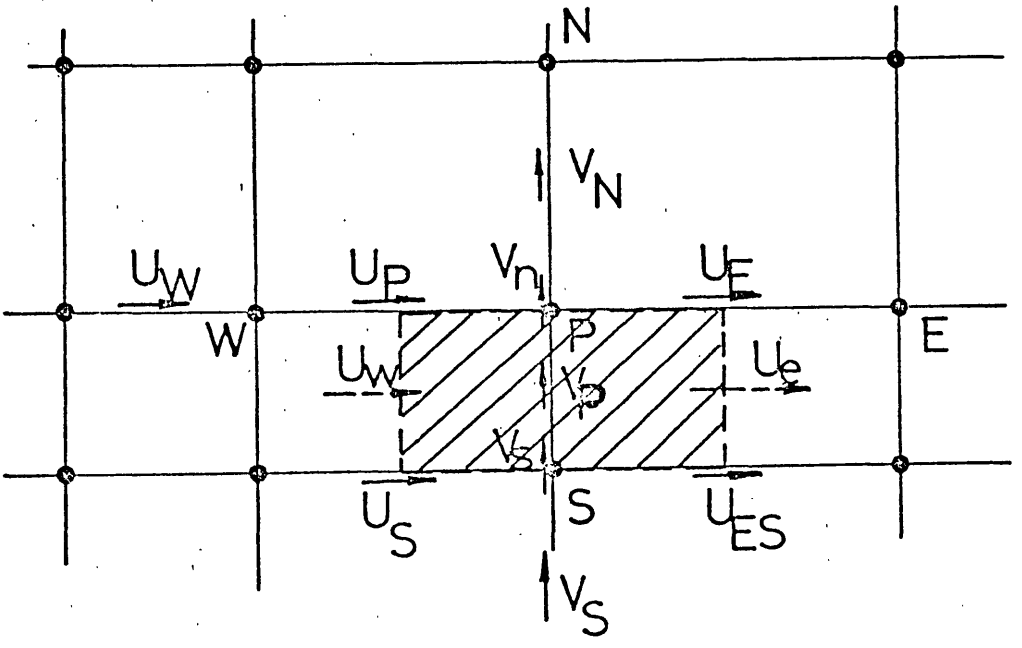

V-cell

Figure 2.2.1: Finite difference grid

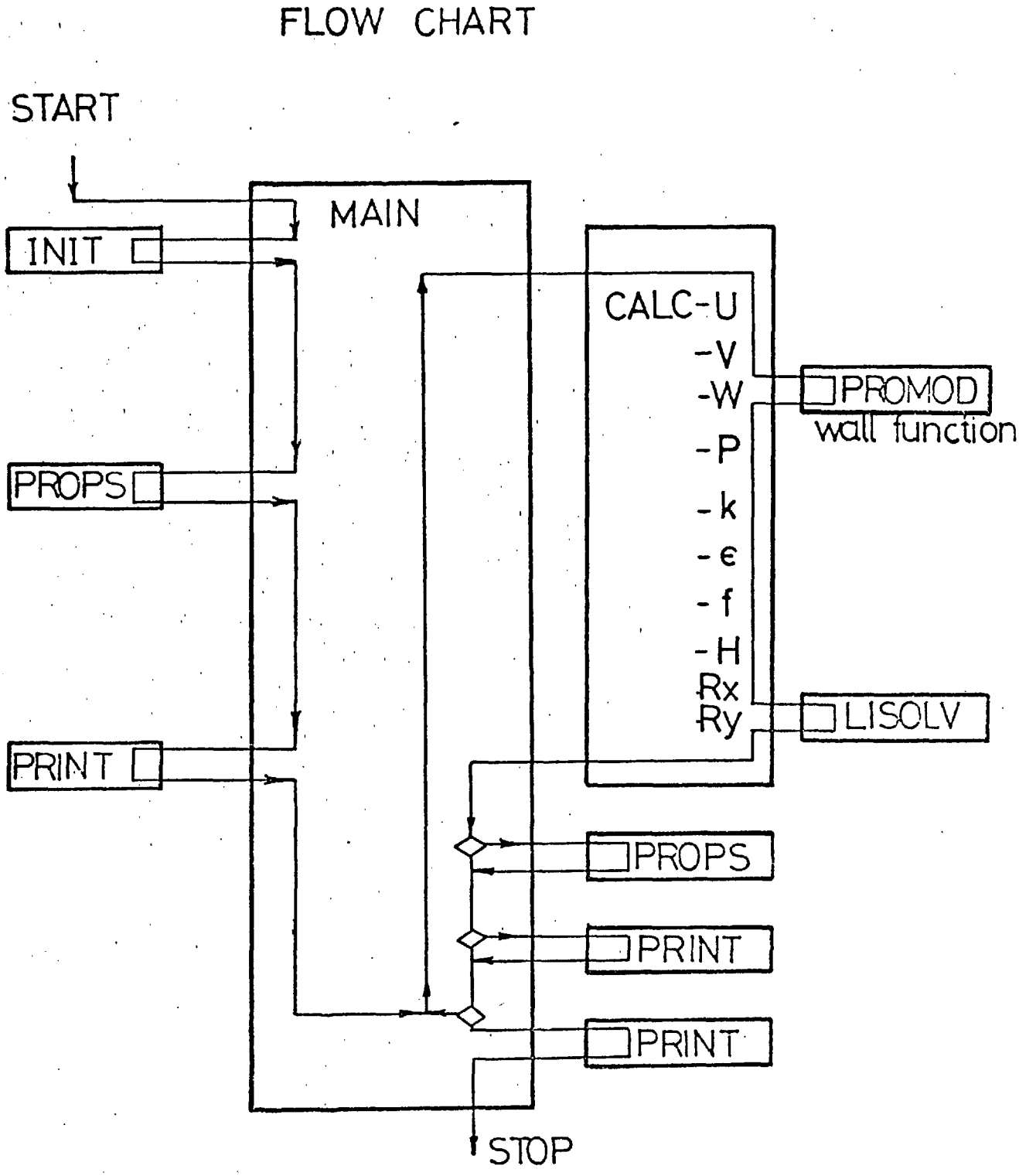

Figure 2.2.2: Flow chart of computational scheme.

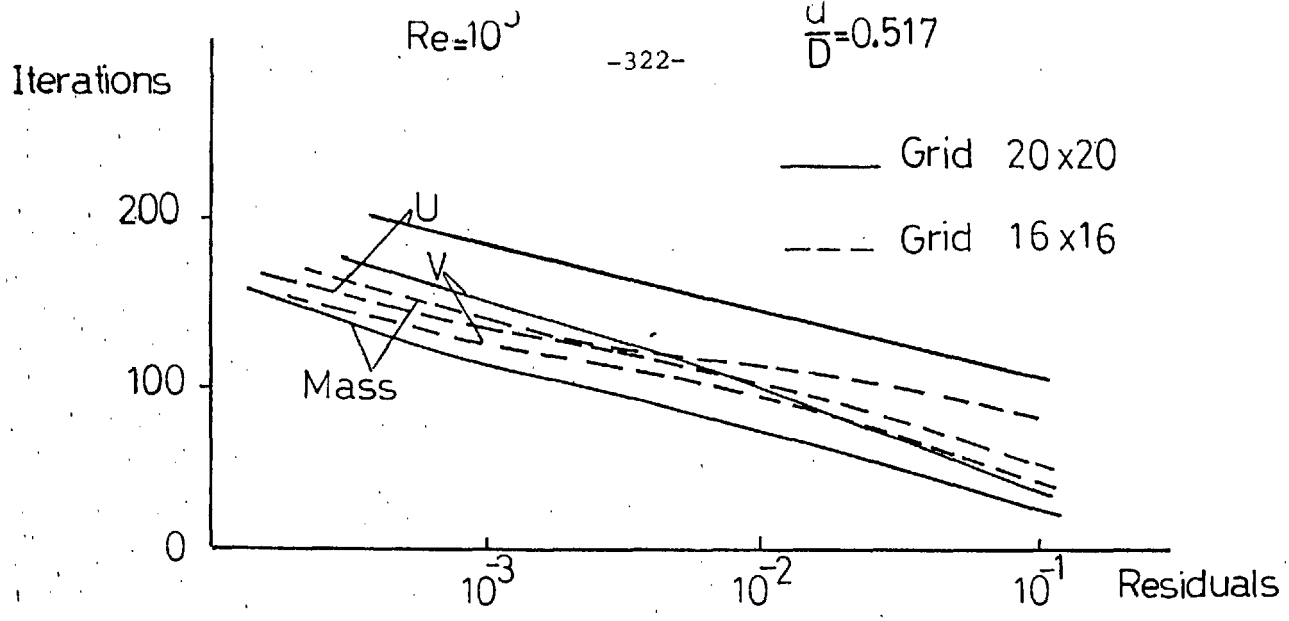

Figure 2.2.3: Residuals variation with number of iteration (sudden expansion flow).

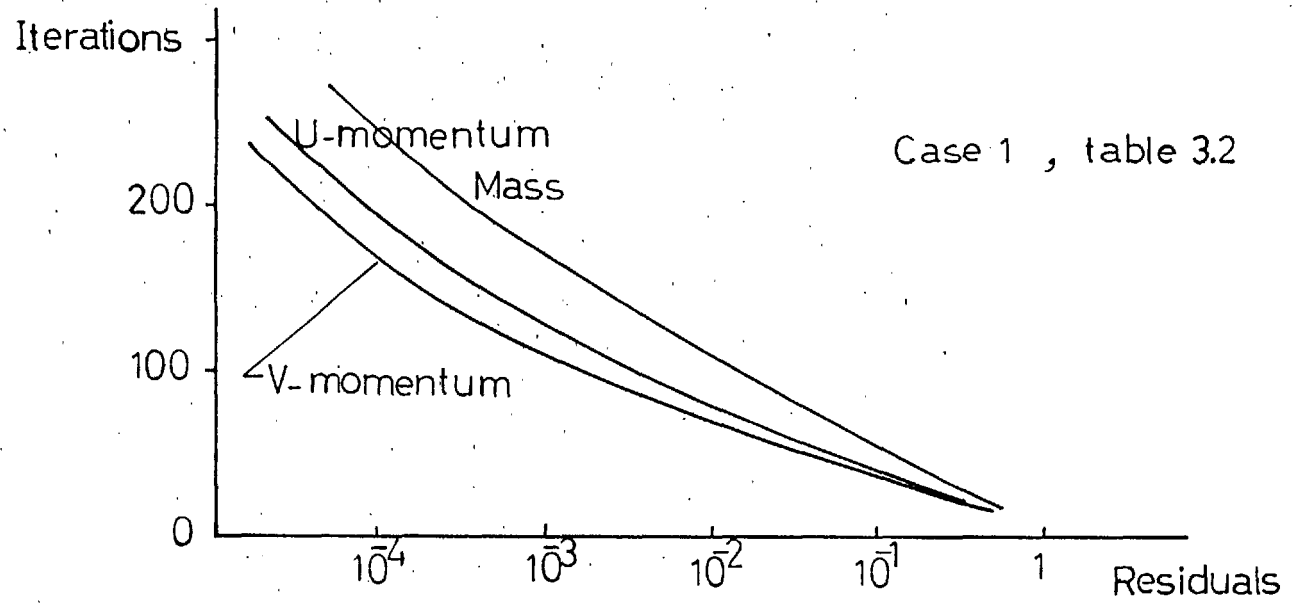

Figure 2.2.4: Residuals variation with number of iteration (coaxial flow).

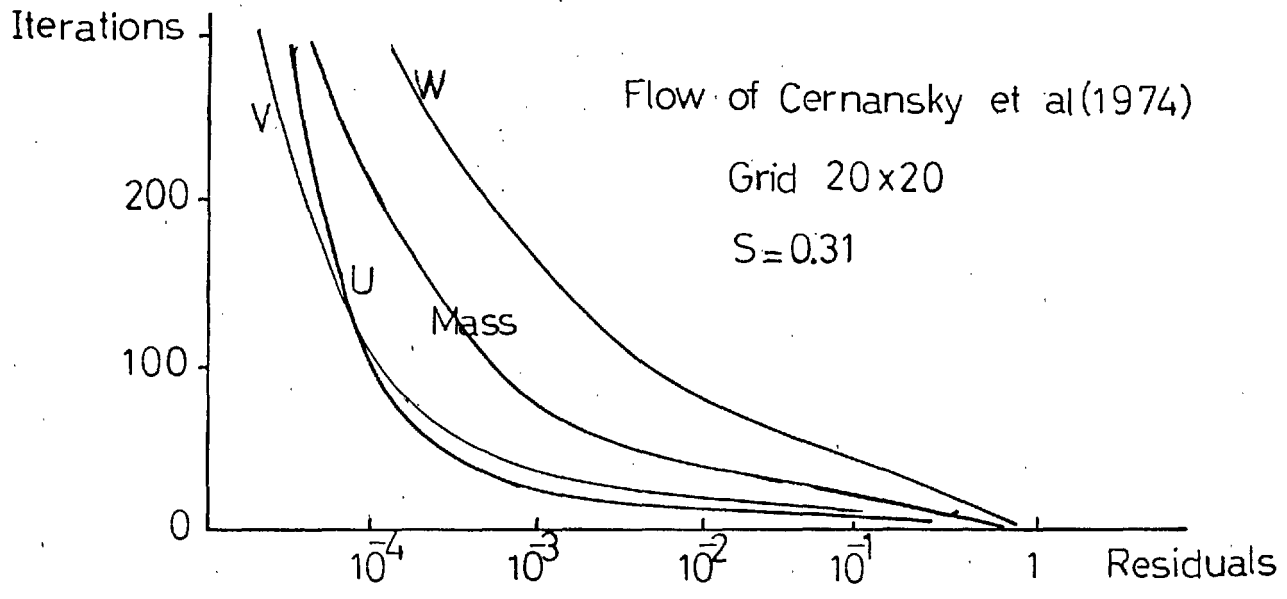

Figure 2.2.5: Residuals variation with number of iteration (swirling flame).

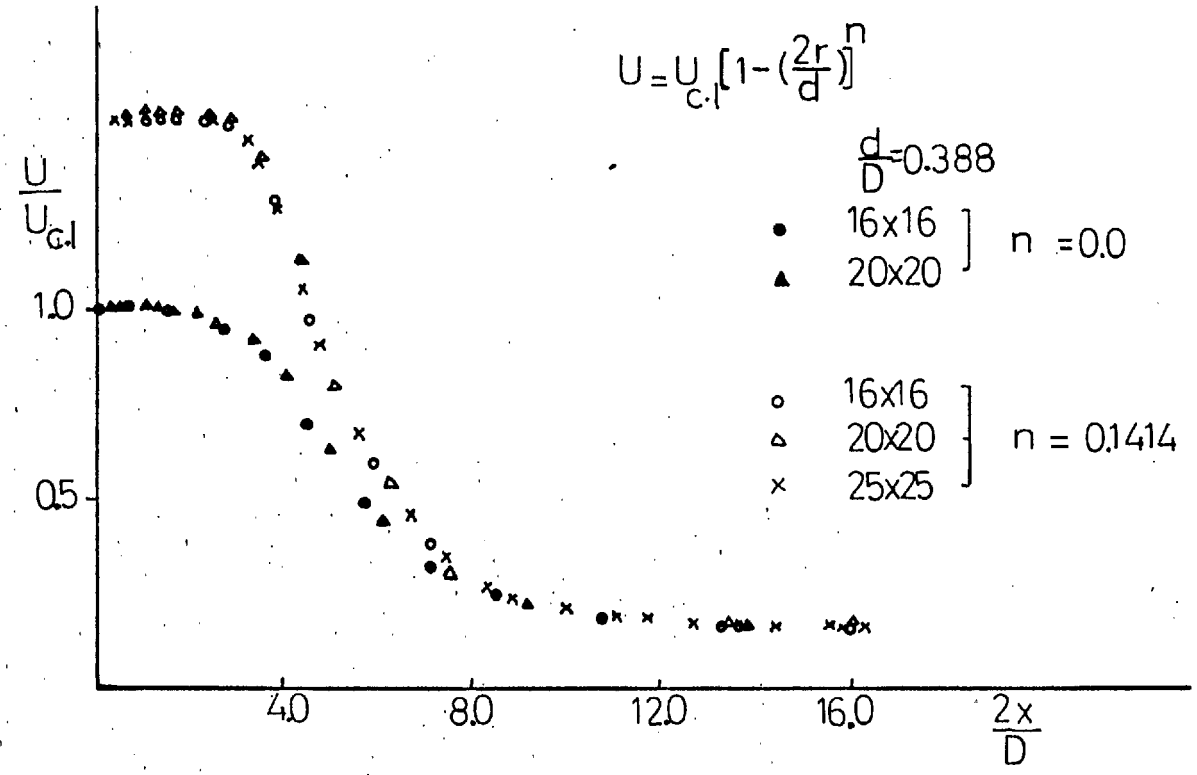

Figure 2.2.6: Effect of inlet velocity profile and grid size on centreline velocities (axisymmetric sudden expansion flow).

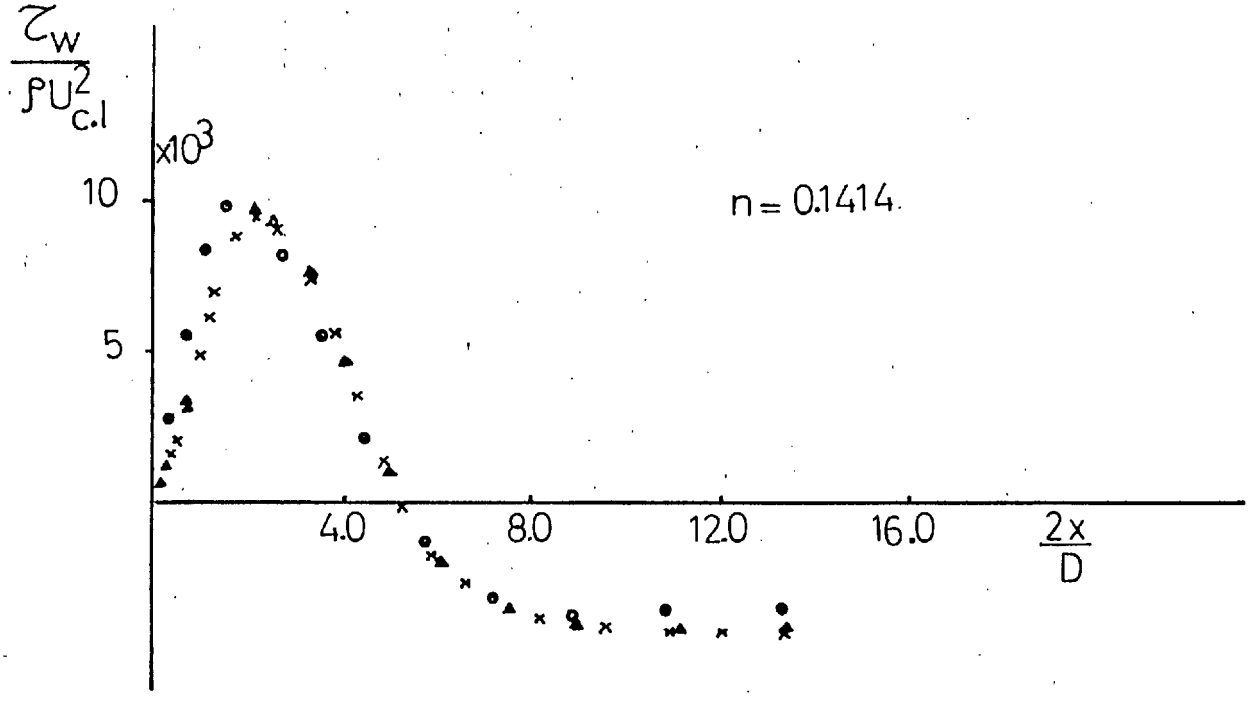

Figure 2.2.7: Effect of grid size on shear stress distribution along the wall (axisymmetric sudden expansion flow).

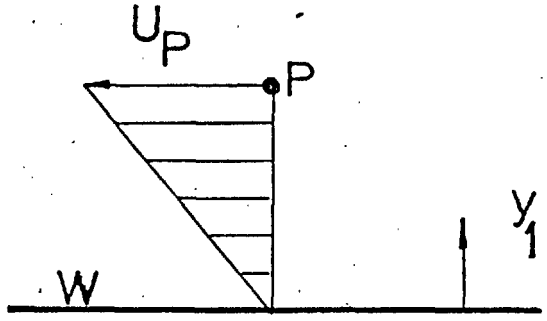

Figure 2.3.1: Near wall grid node.

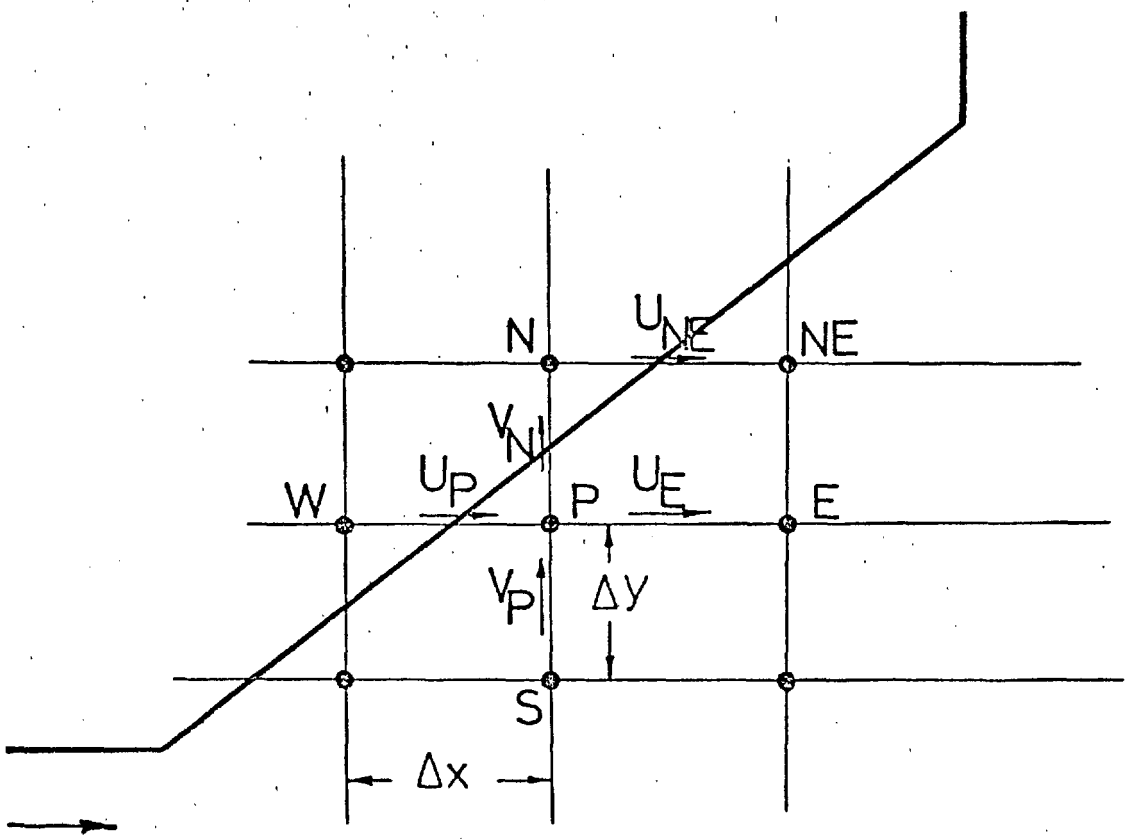

Figure 2.3.2: Grid arrangement near inclined walls.

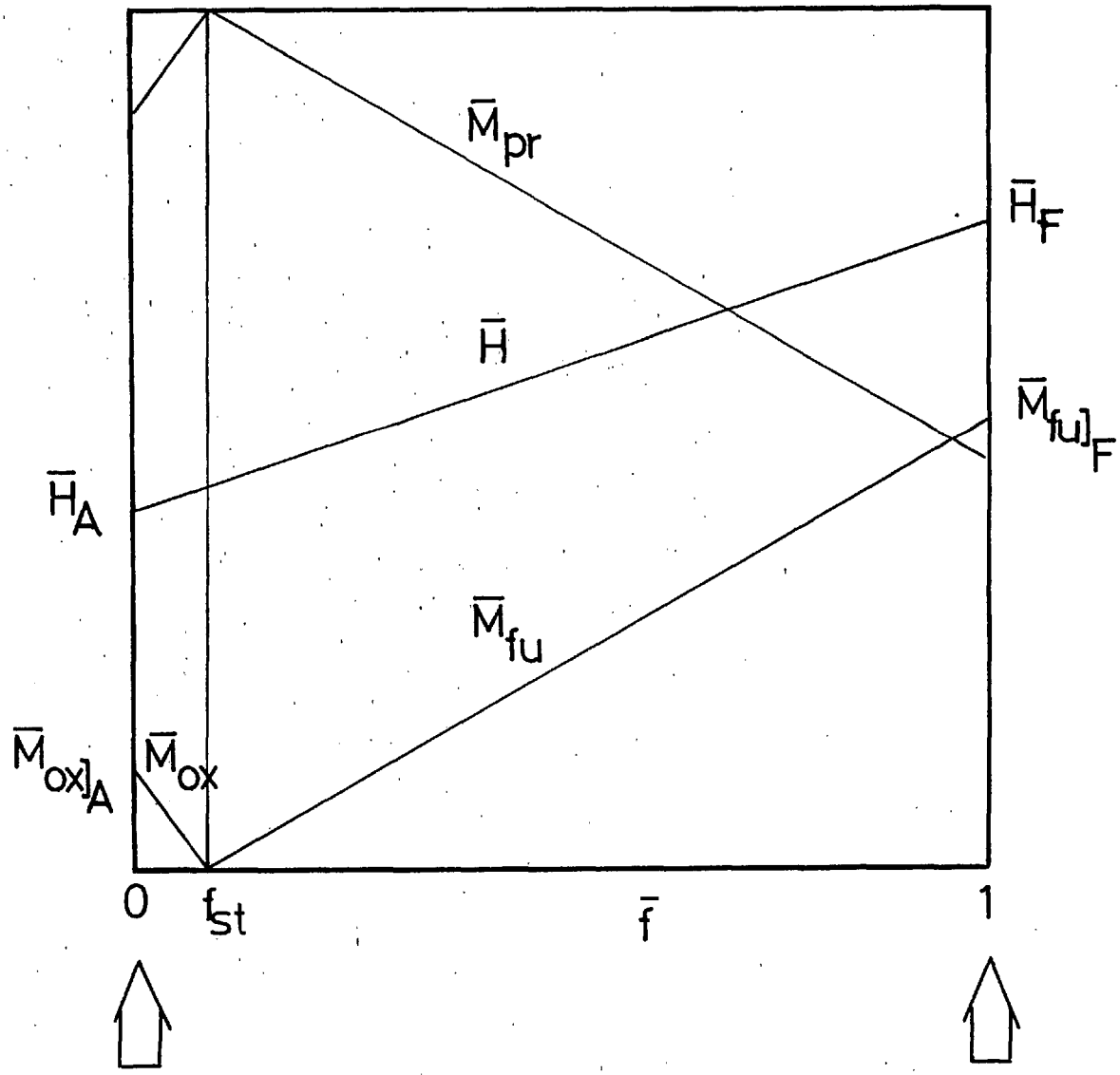

Figure 2.4.1: Relation between f and scalar properties.

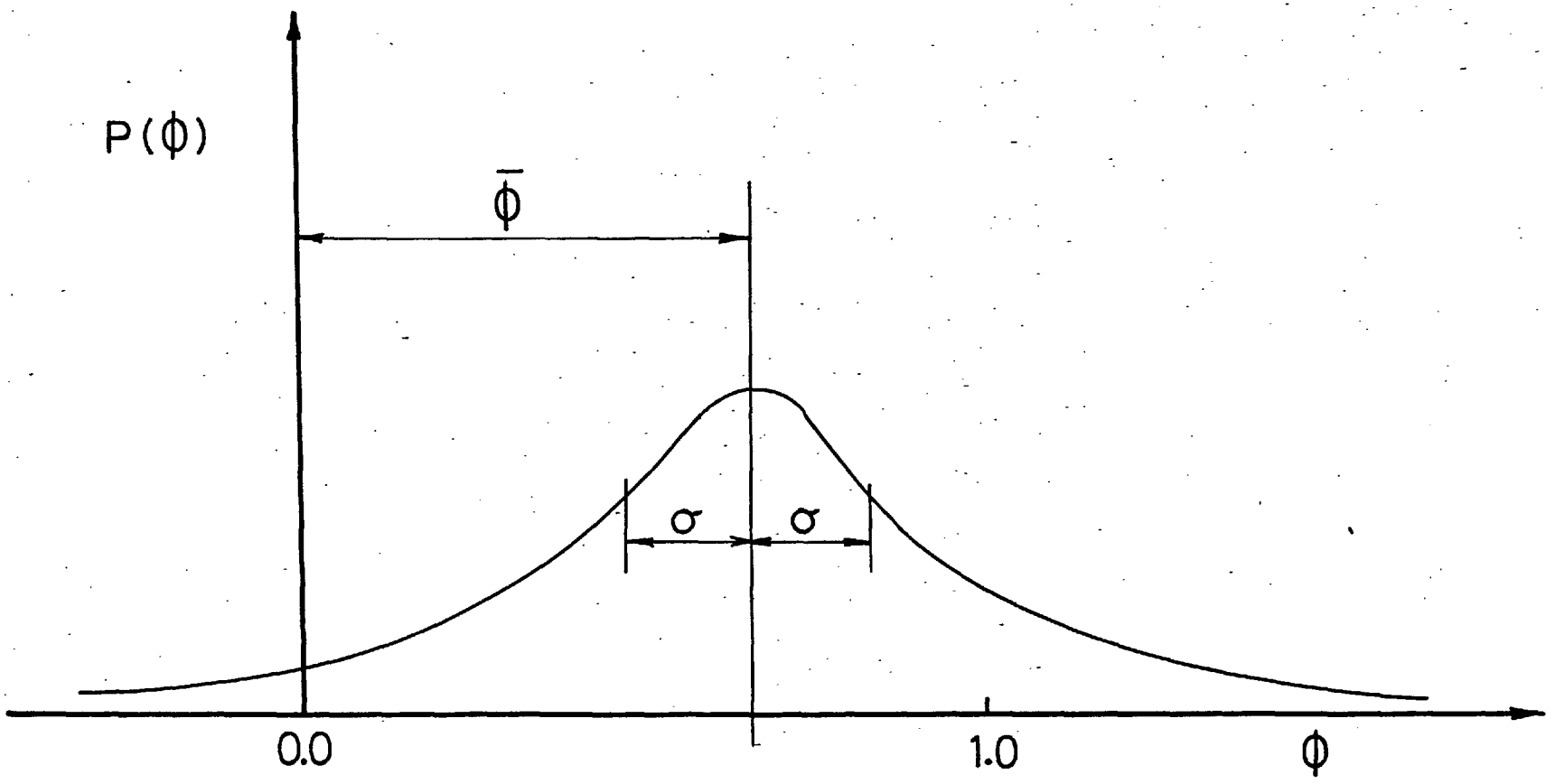

Figure 2.4.2: General single probability distribution of Φ.

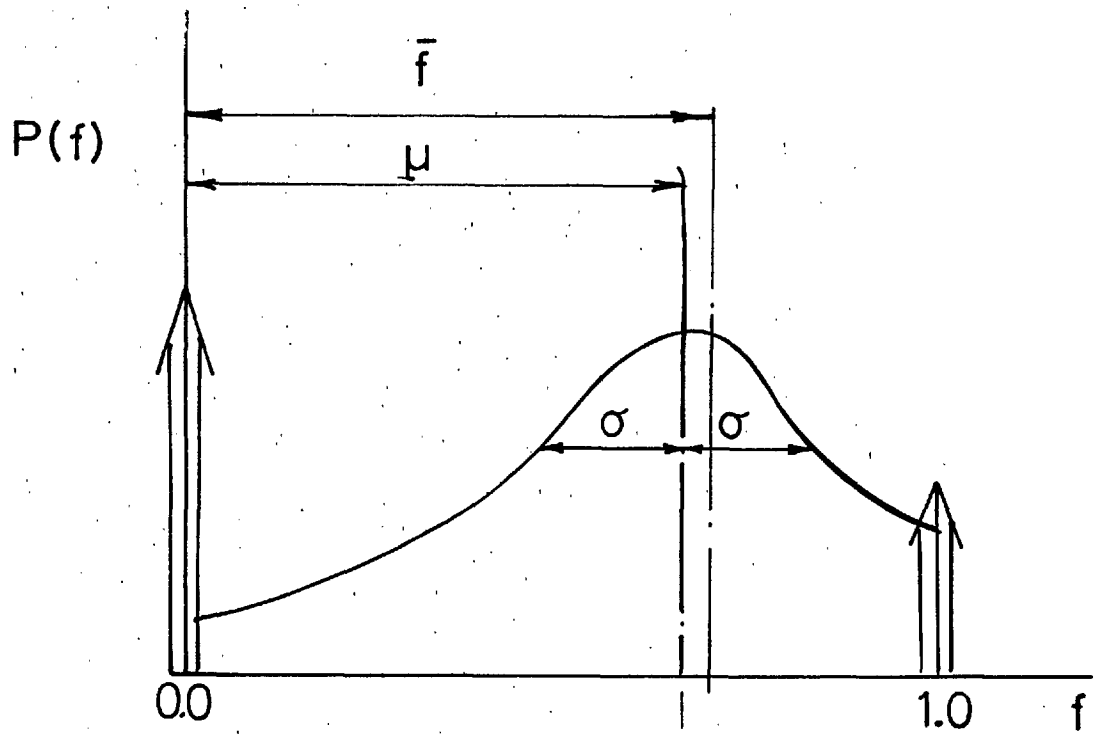

Figure 2.4.3: Clipped Gaussian probability distribution of mixture fraction.

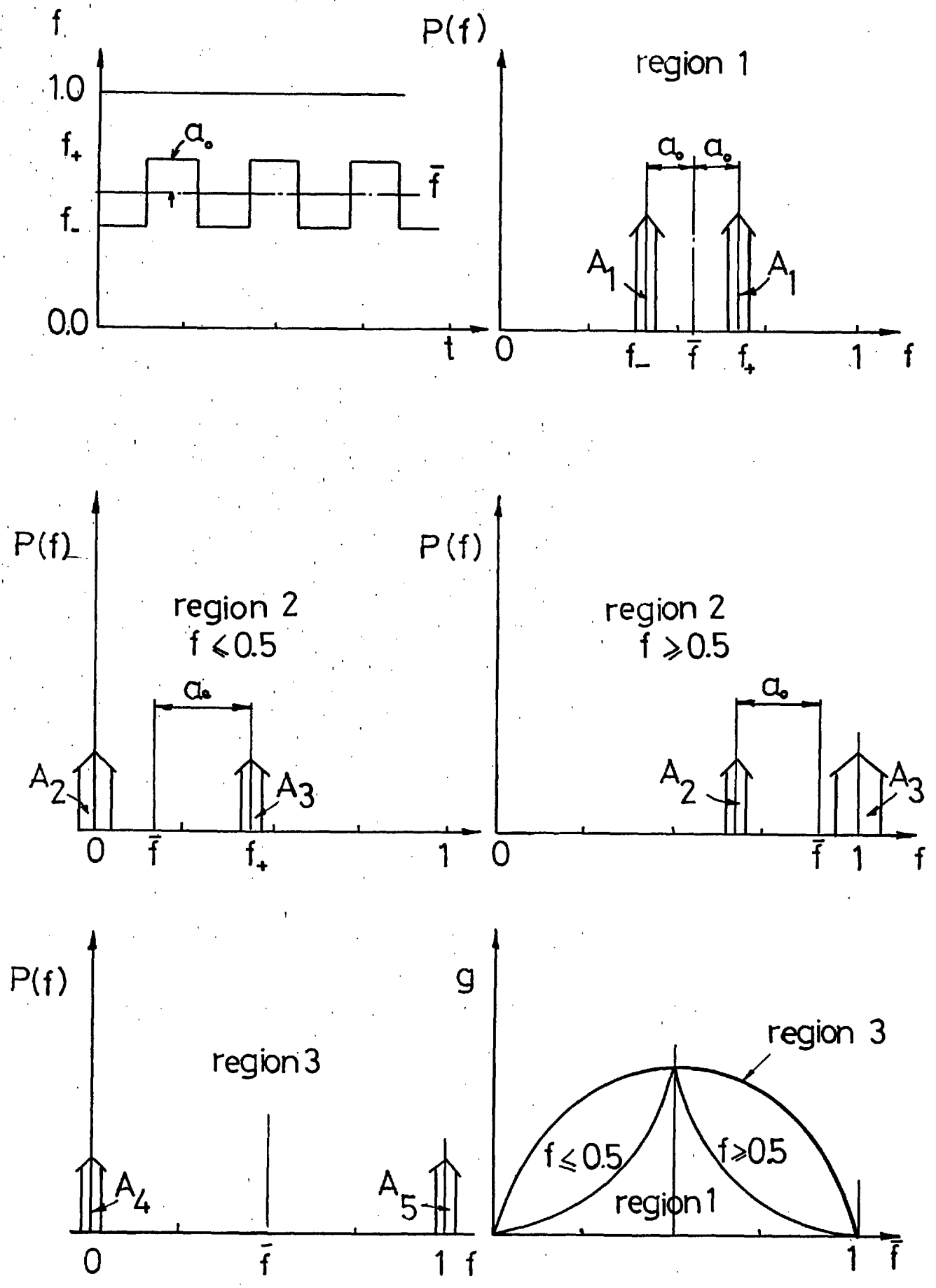

Figure 2.4.4: Probability distributions for a square wave temporal variation of mixture fraction.

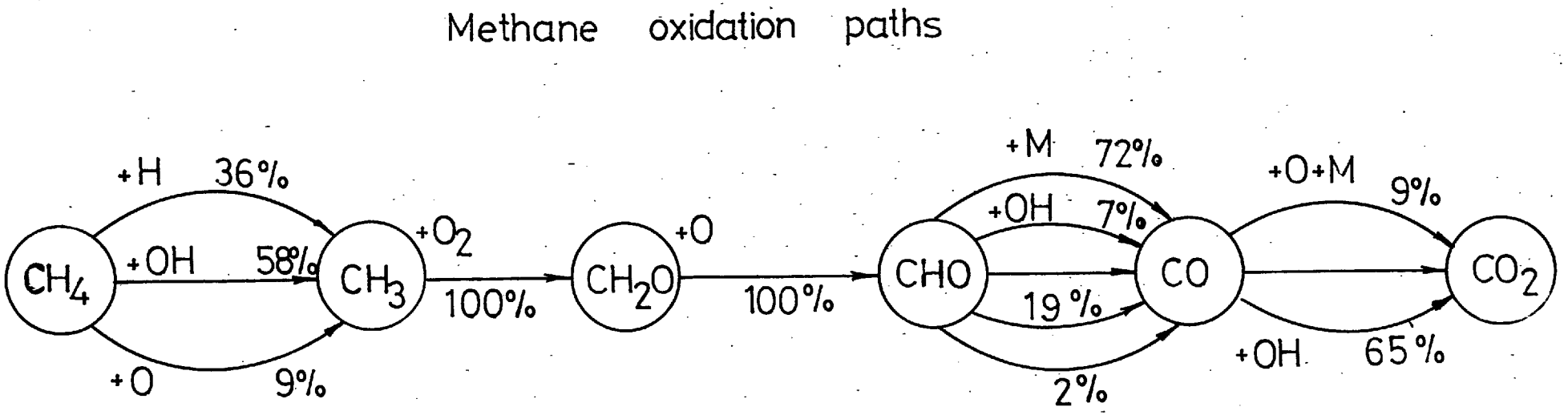

Figure 2.4.5: Methane oxidation paths.

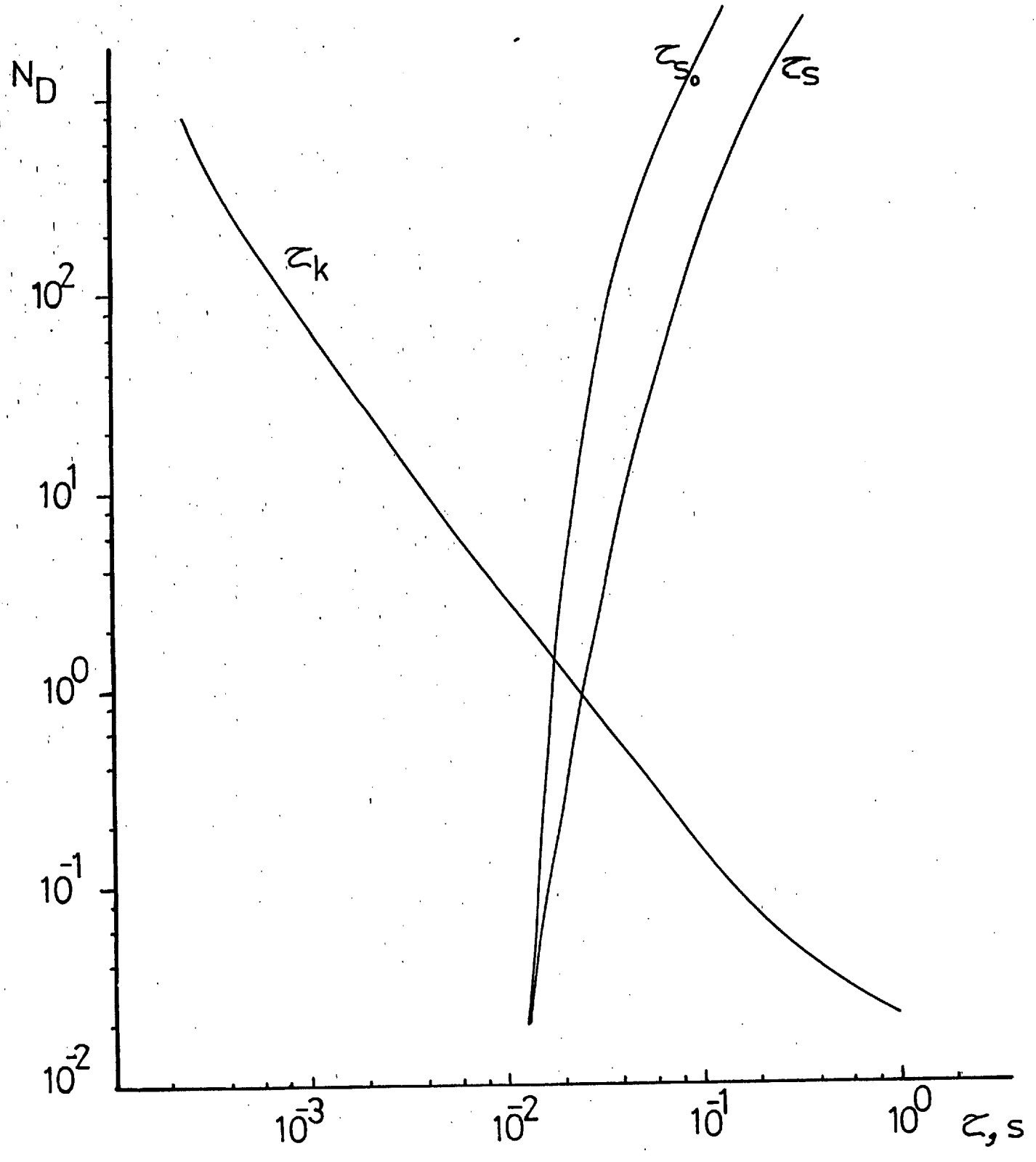

Figure 2.4.6: Relation between various time scales and N_D.

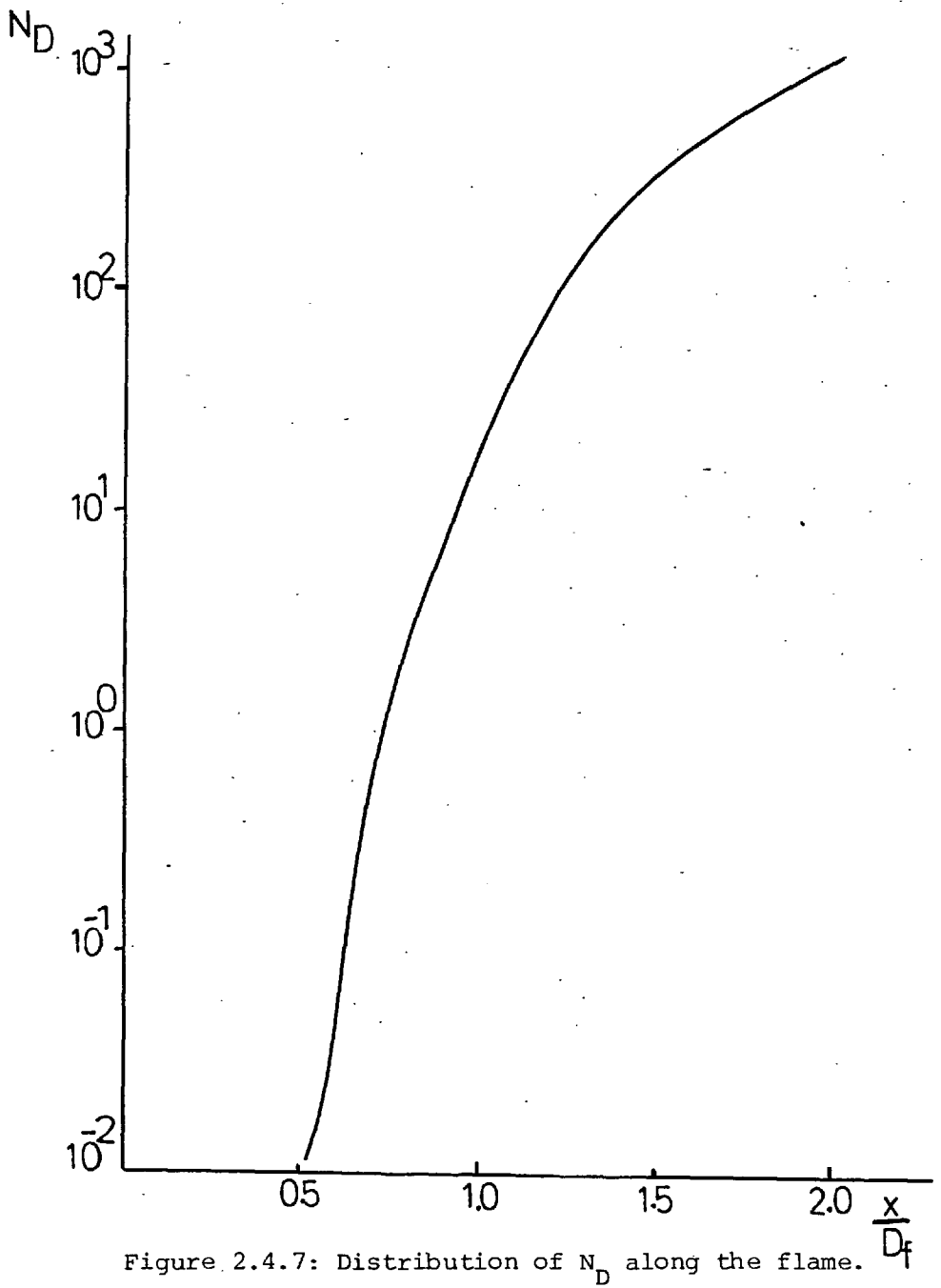

Figure 2.4.7: Distribution of N_D along the flame.

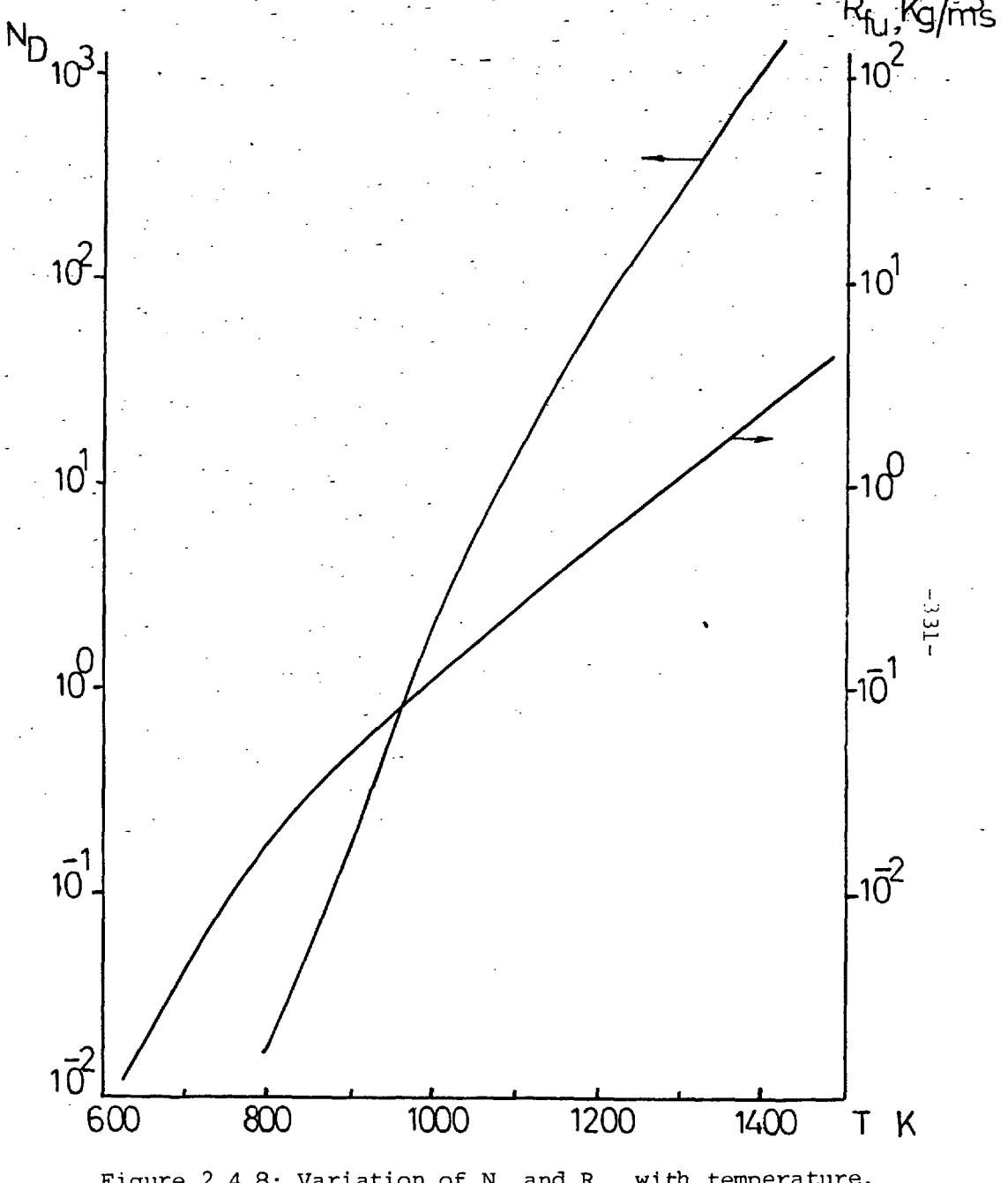

Figure 2.4.8: Variation of N_D and R_{fu} with temperature.

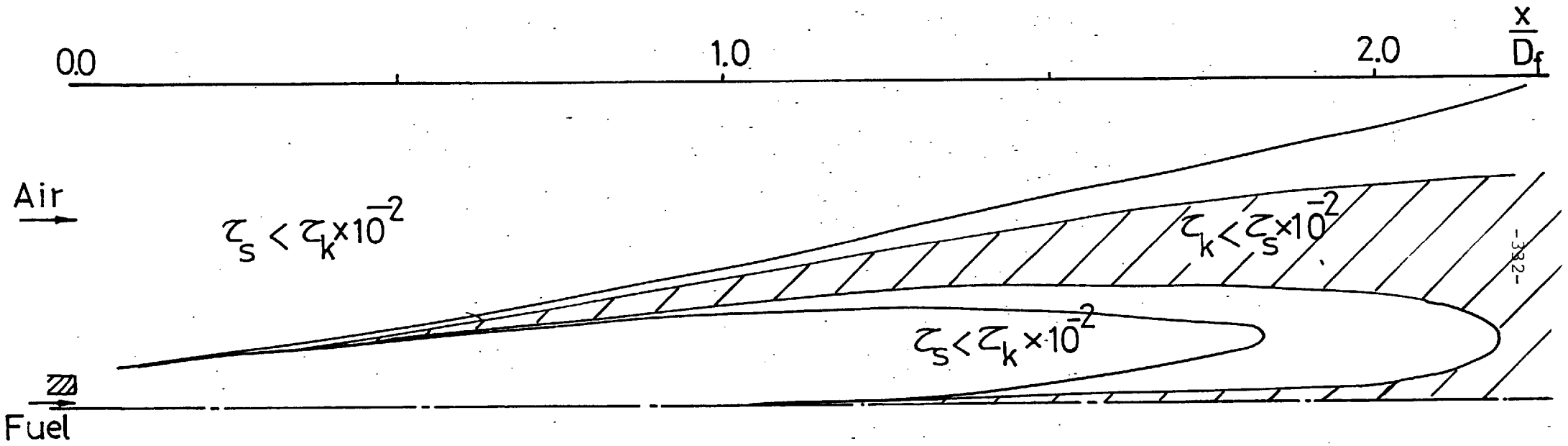

Figure 2.4.9: Variation of τ_s, τ_k in a coflowing methane air flame.

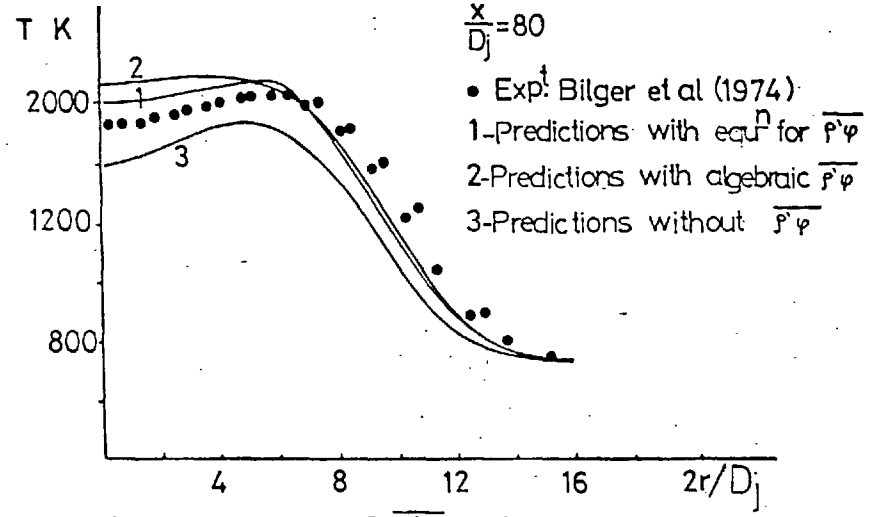

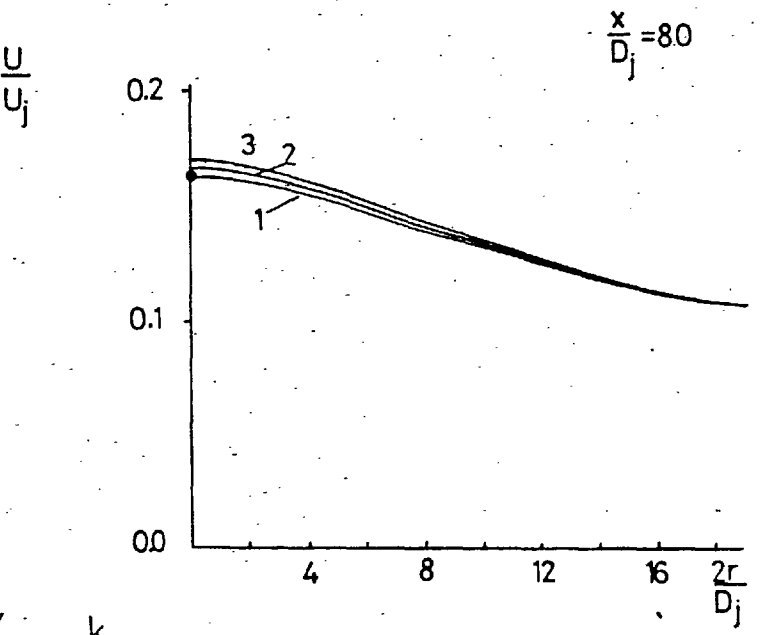

Figure 2.4.10: Effect of $\overline{\rho'\phi}$ on the mean temperature and velocity

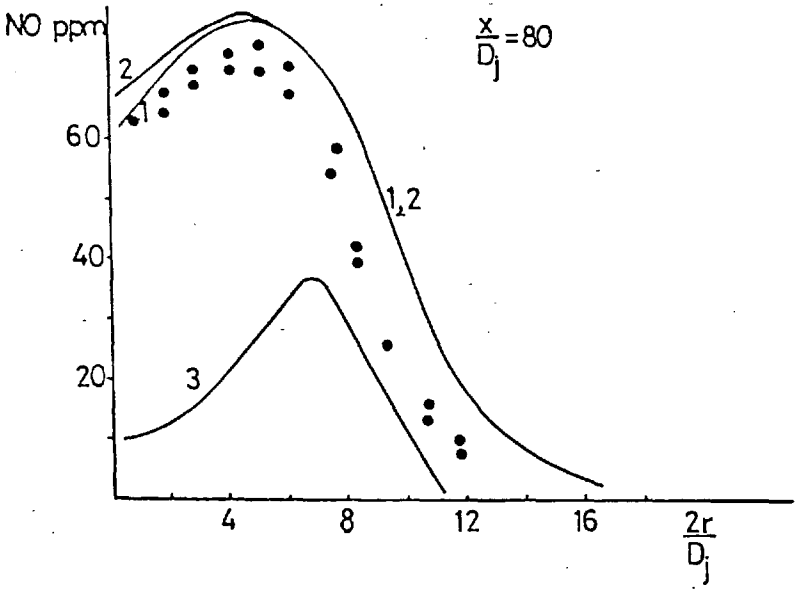

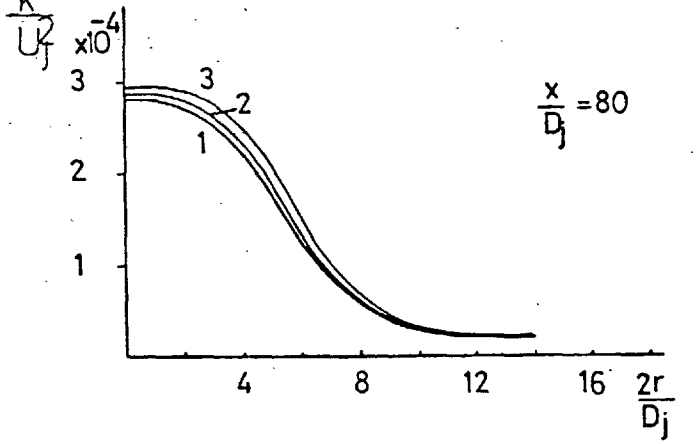

Figure 2.4.11: Effect of $\overline{\rho'\phi}$ on the NO concentration and kinetic energy of turbulence.

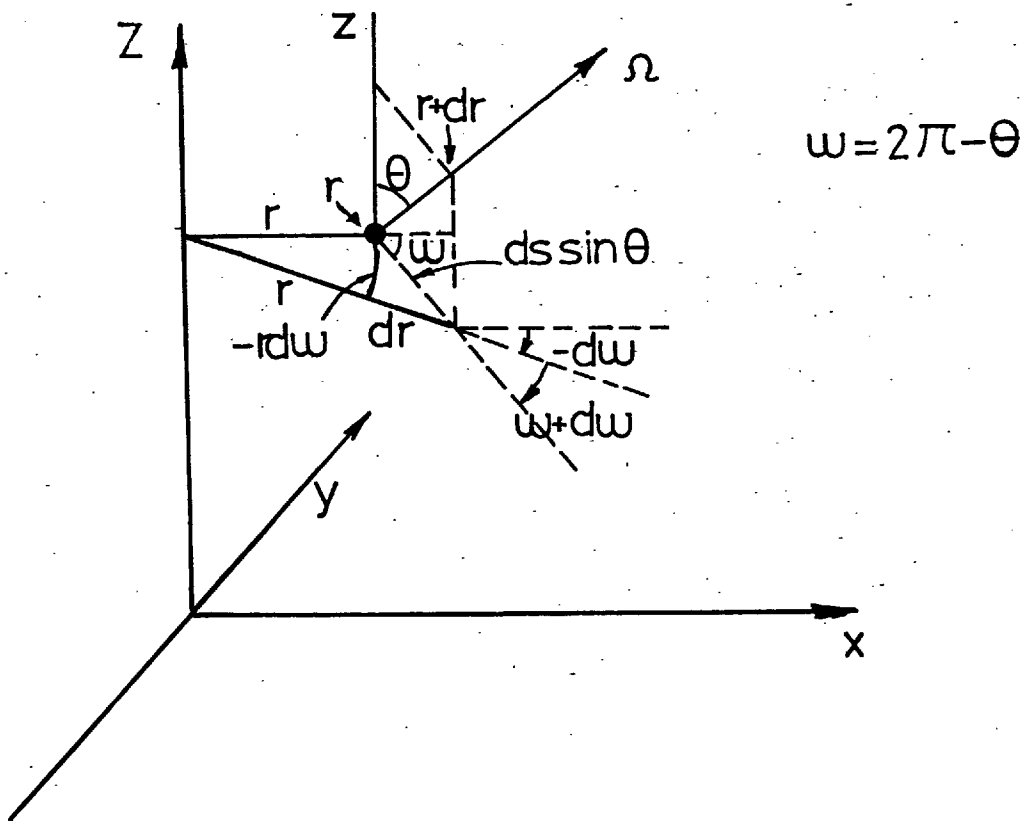

Figure 2.5.1: Radiation intensity distribution.

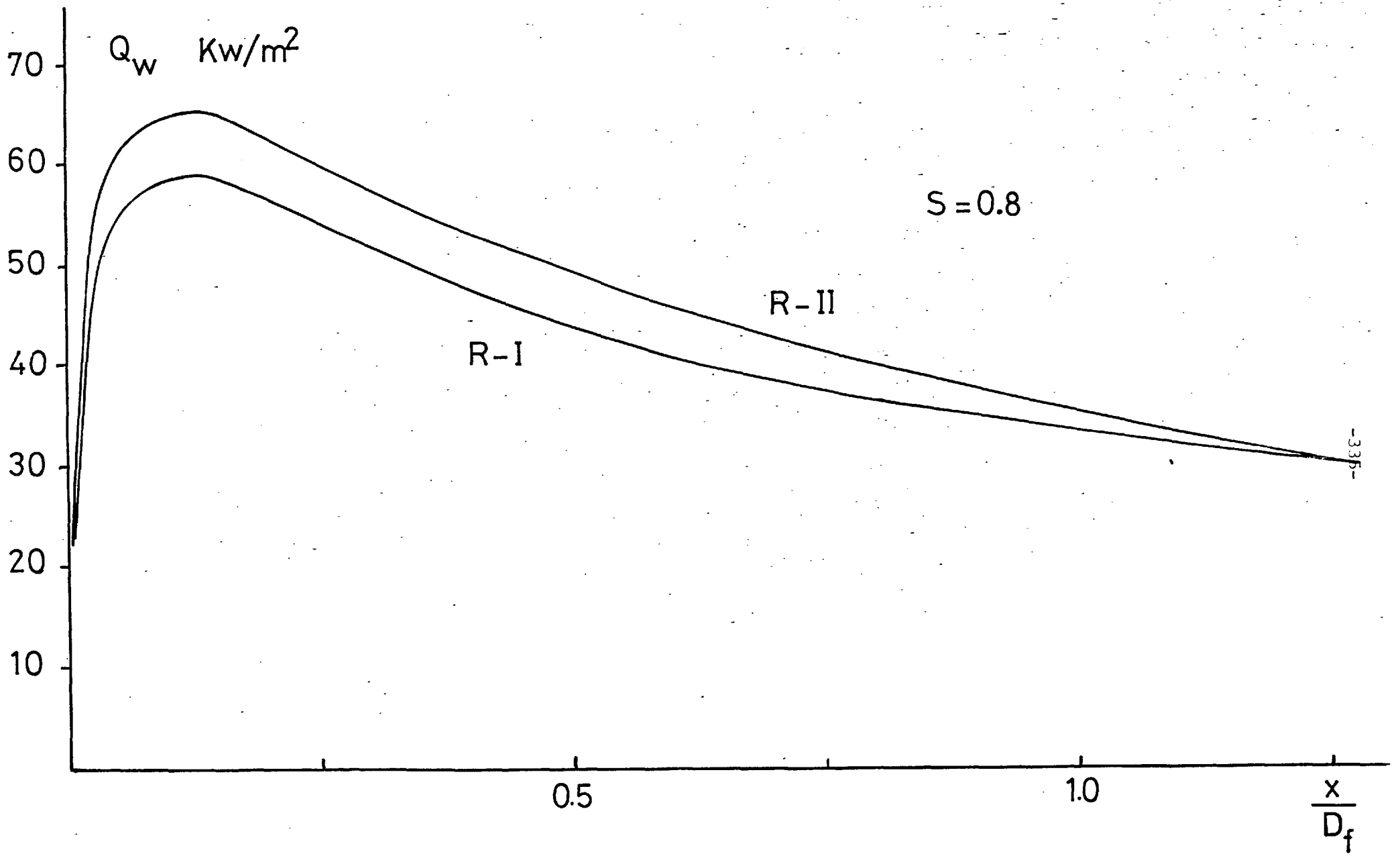

Figure 2.5.2: Wall heat flux distribution for a swirling coaxial flame.

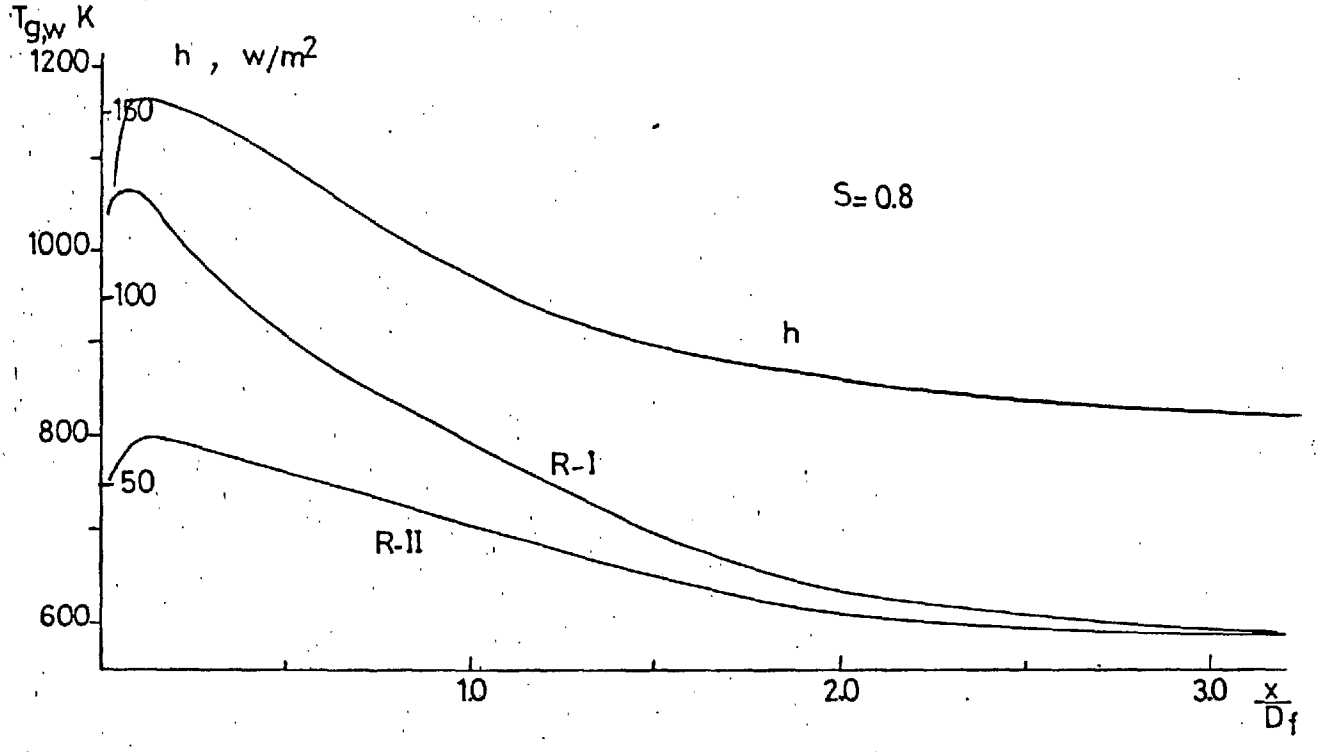

Figure 2.5.3: Near wall temperature and heat transfer coefficient distribution.

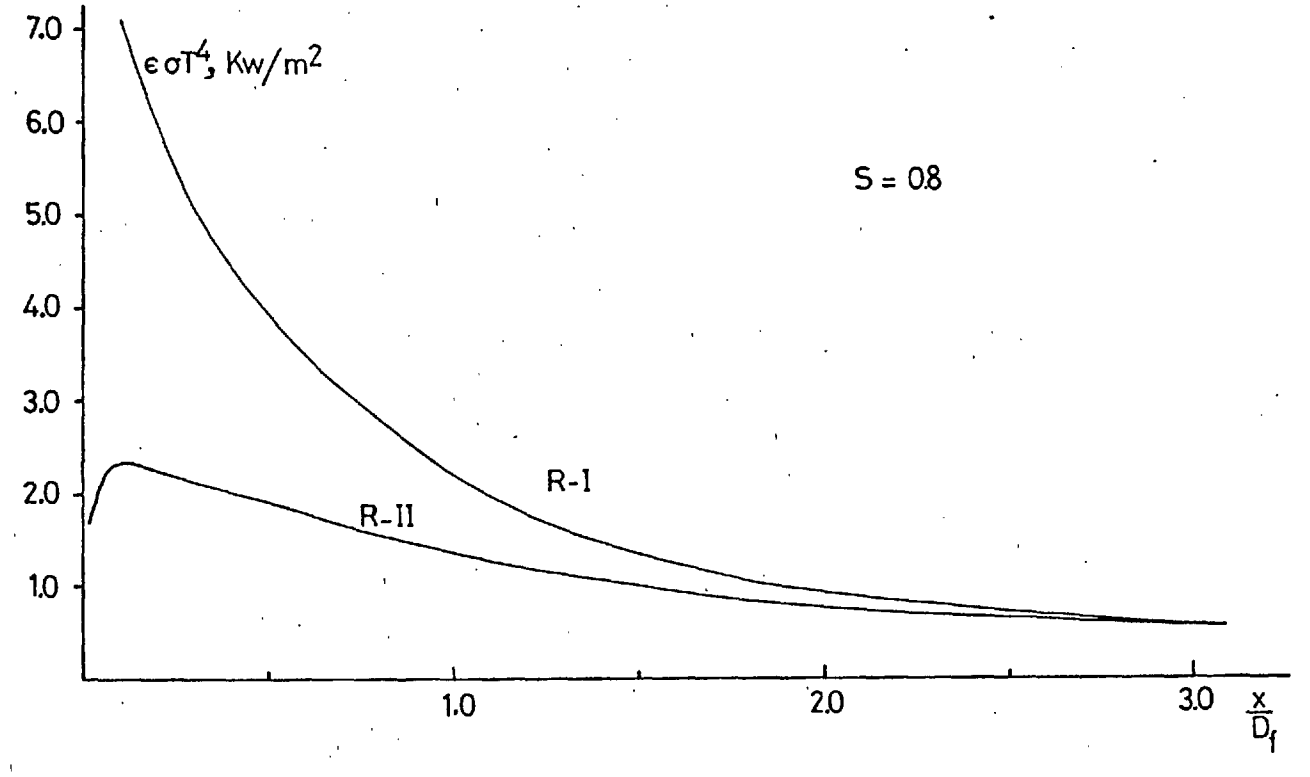

Figure 2.5.4: Emissive power distribution in the vicinity of the wall.

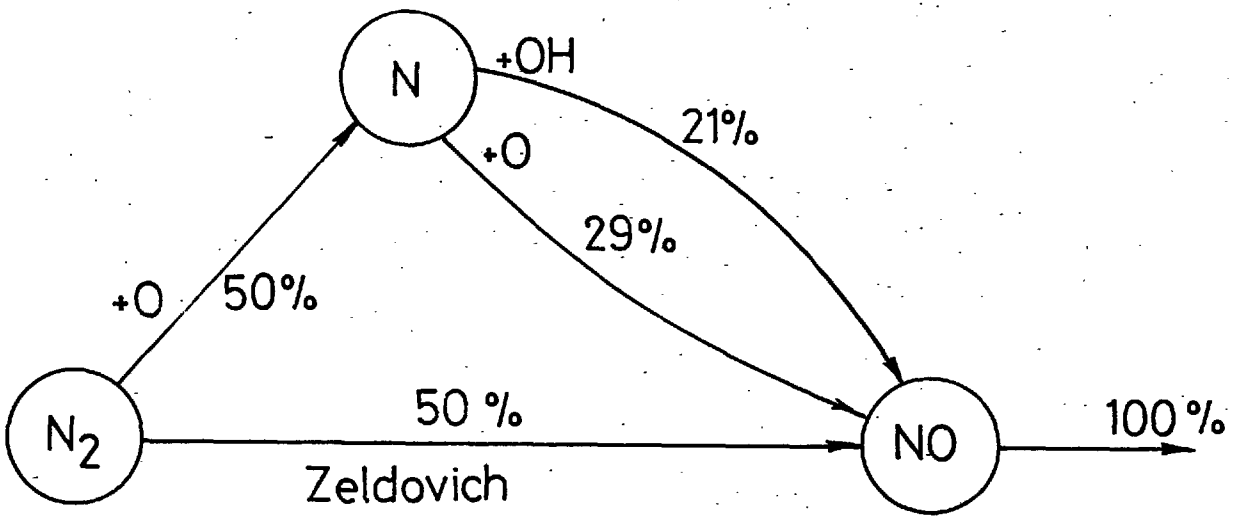

Figure 2.6.1: Nitric oxide formation mechanism.

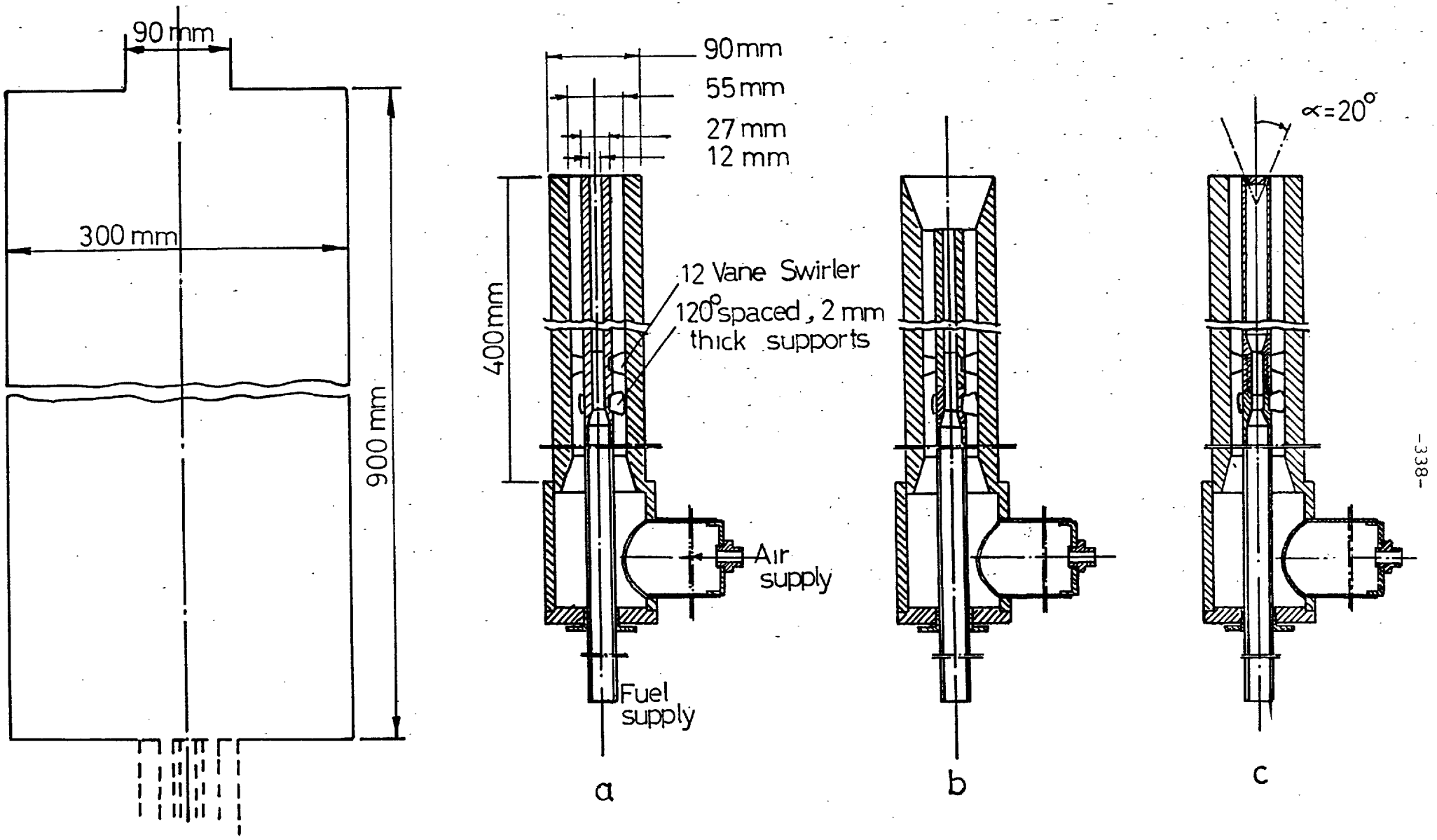

Figure 3.1.1: Burner and furnace arrangements.

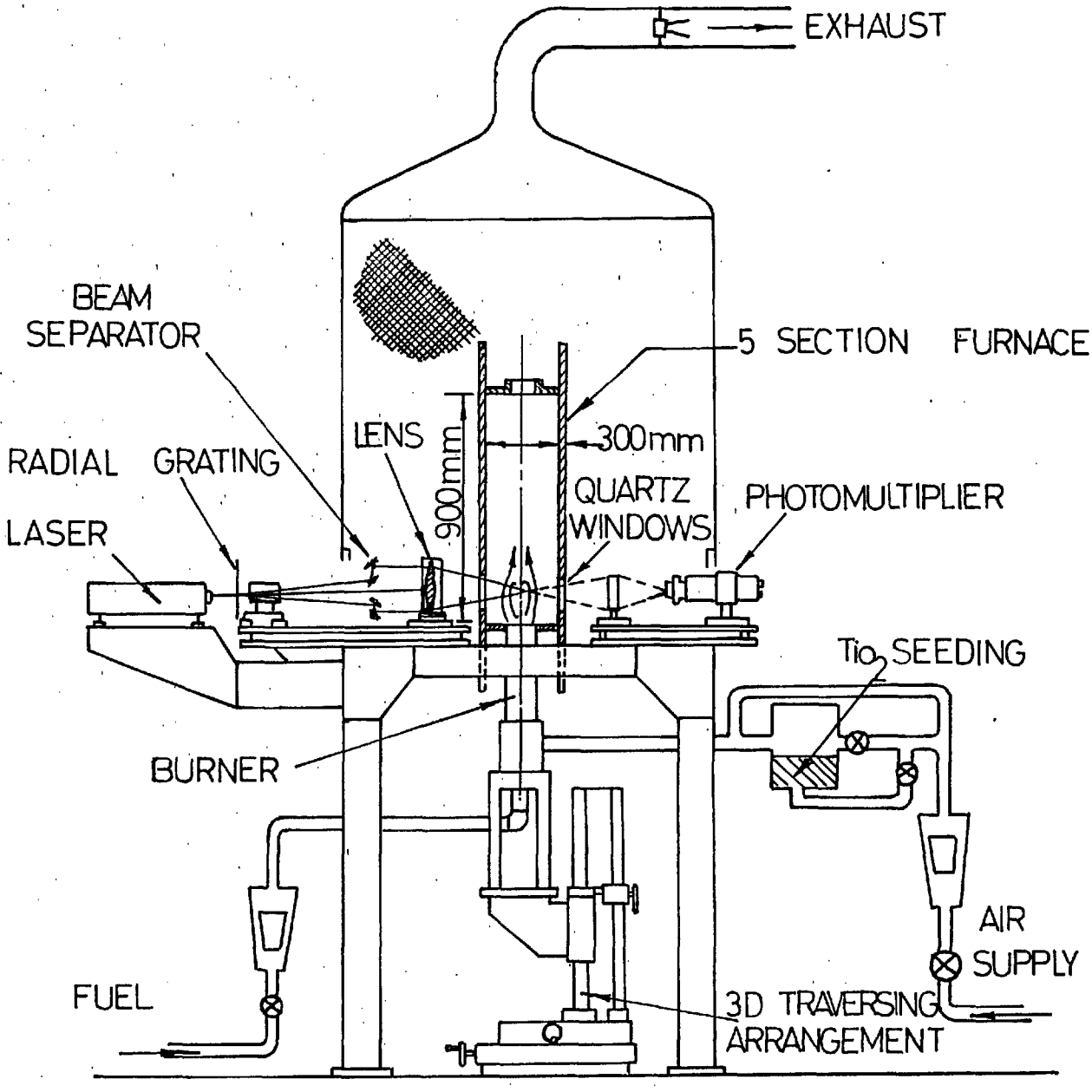

Figure 3.1.2: Layout of experimental rig.

Figure 3.1.3: Photographs of furnace and plexiglass enclosures.

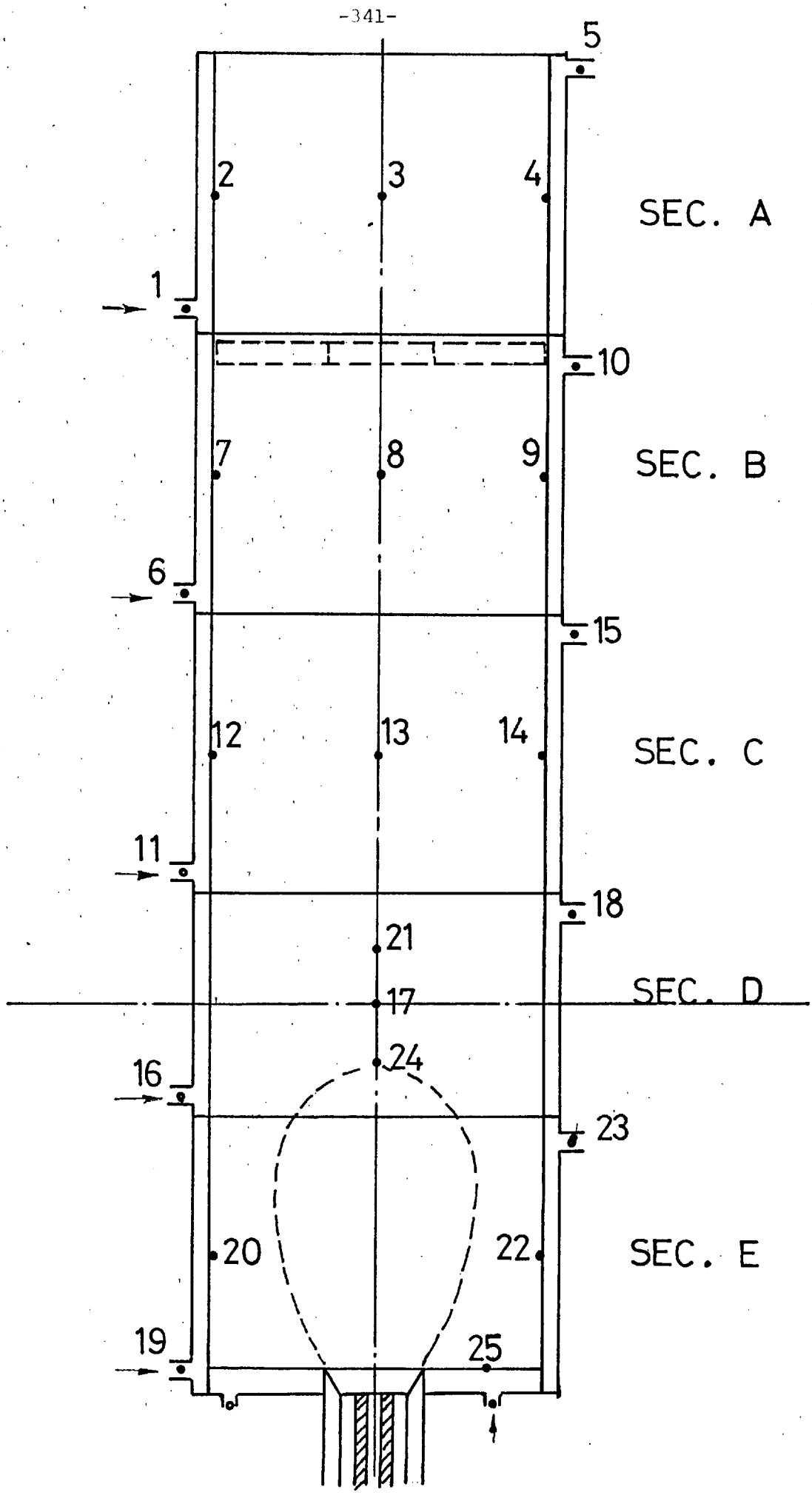

Figure 3.1.4: Locations of thermocouples for wall and cooling water temperature measurements.

Figure 3.1.5: Typical flame in a diverged burner arrangement with S = 0.52, as viewed through the quartz windows.

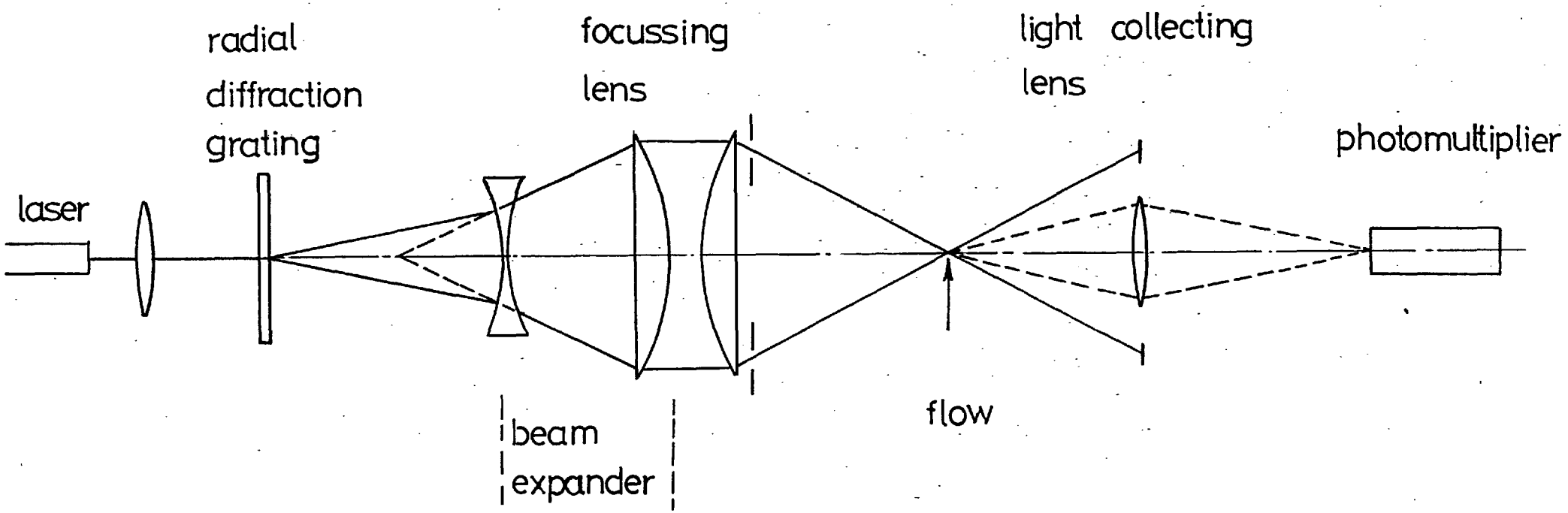

Figure 3.2.1: Optical arrangement.

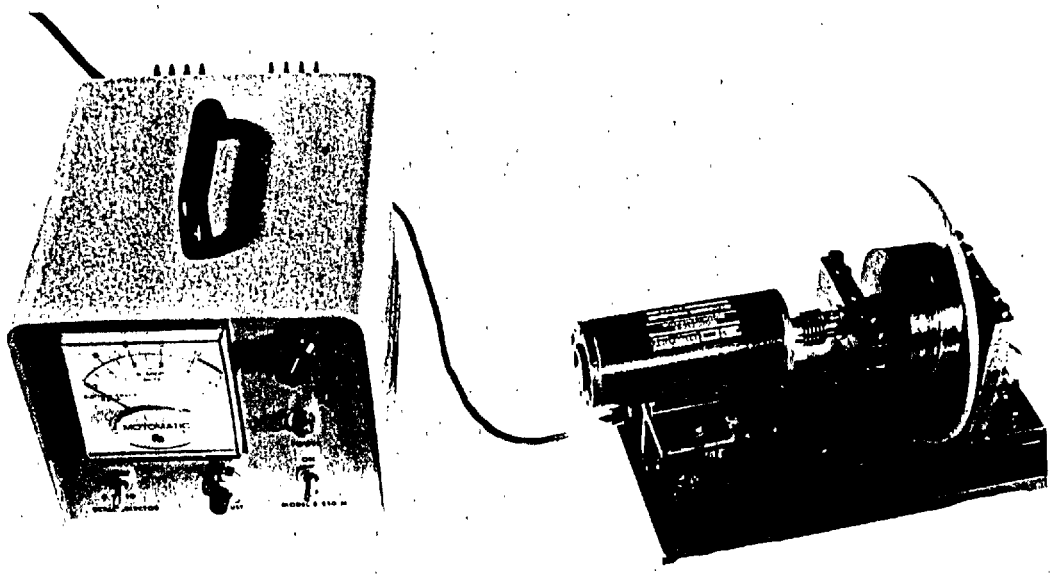

Figure 3.2.2: Optical frequency shifter.

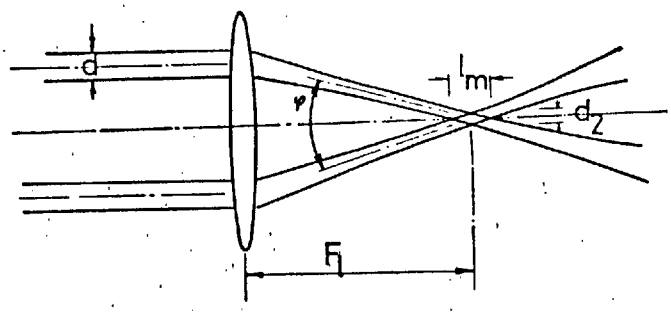

Figure 3.2.3: Beams intersection

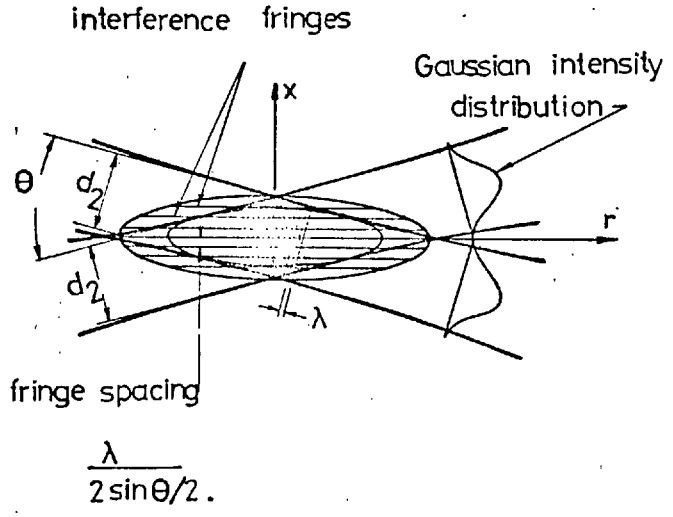

Figure 3.2.4: Fringe pattern in the control volume.

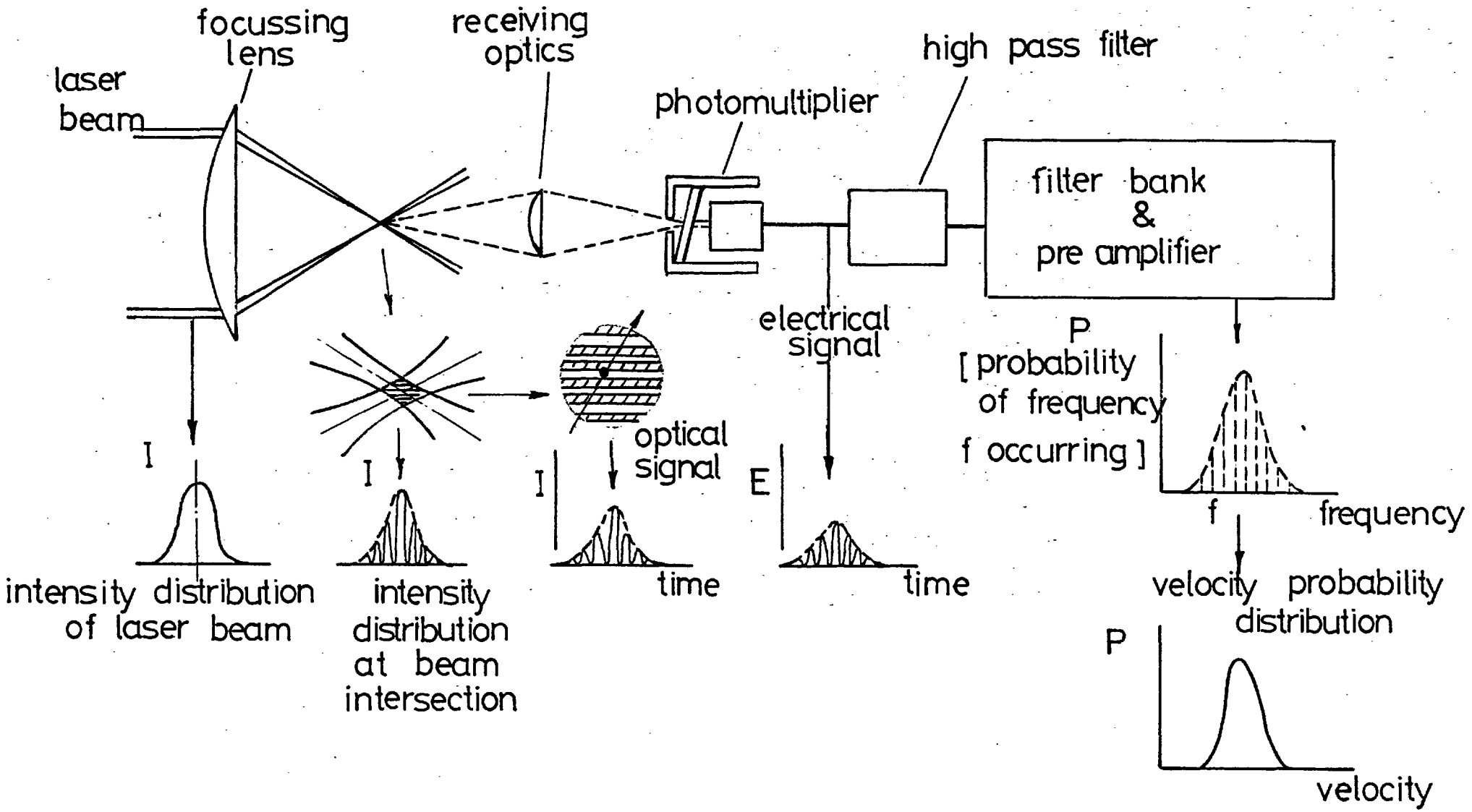

Figure 3.2.5: Block diagram of signal processing.

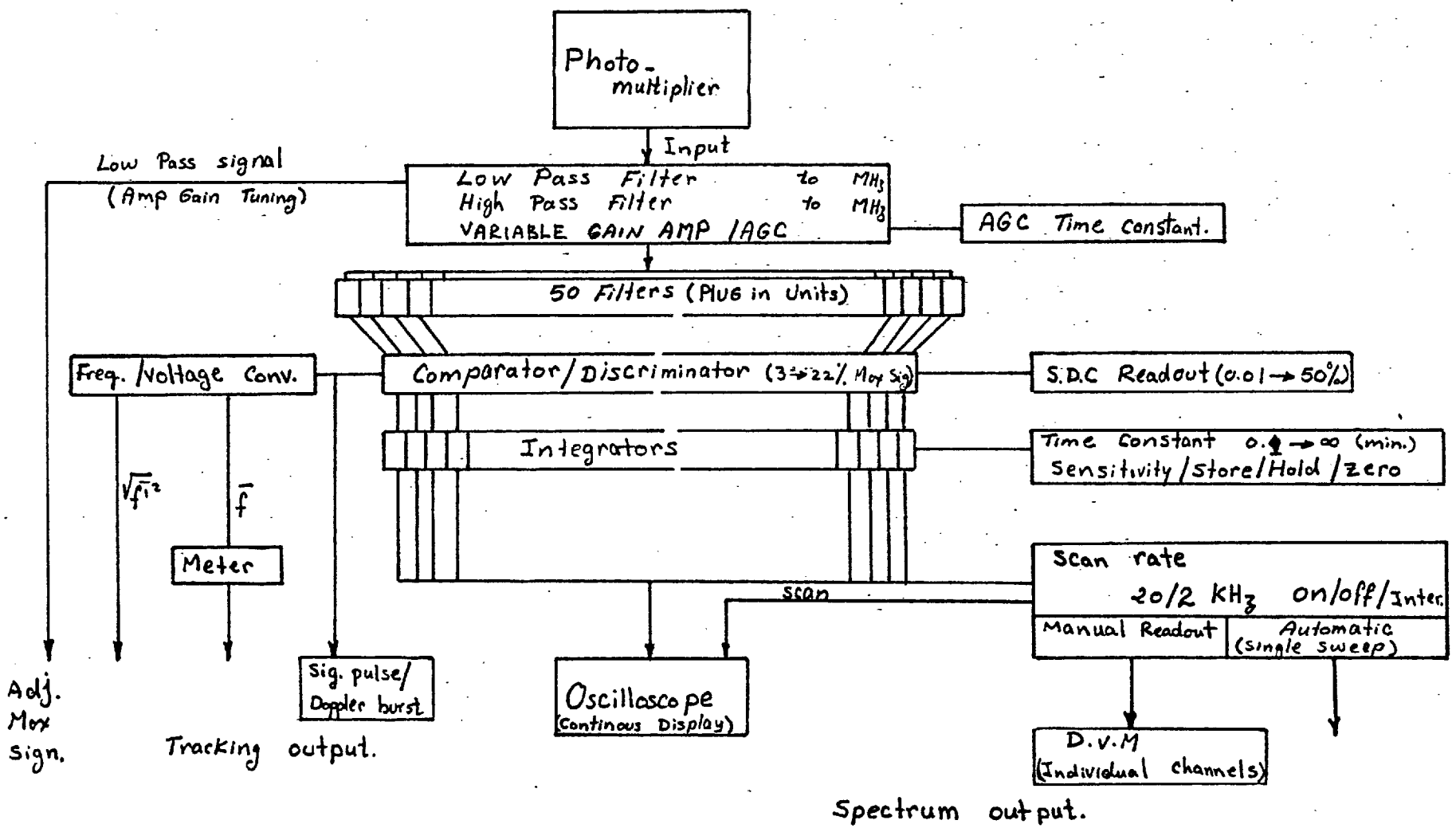

Figure 3.2.6: Block diagram of filter bank.

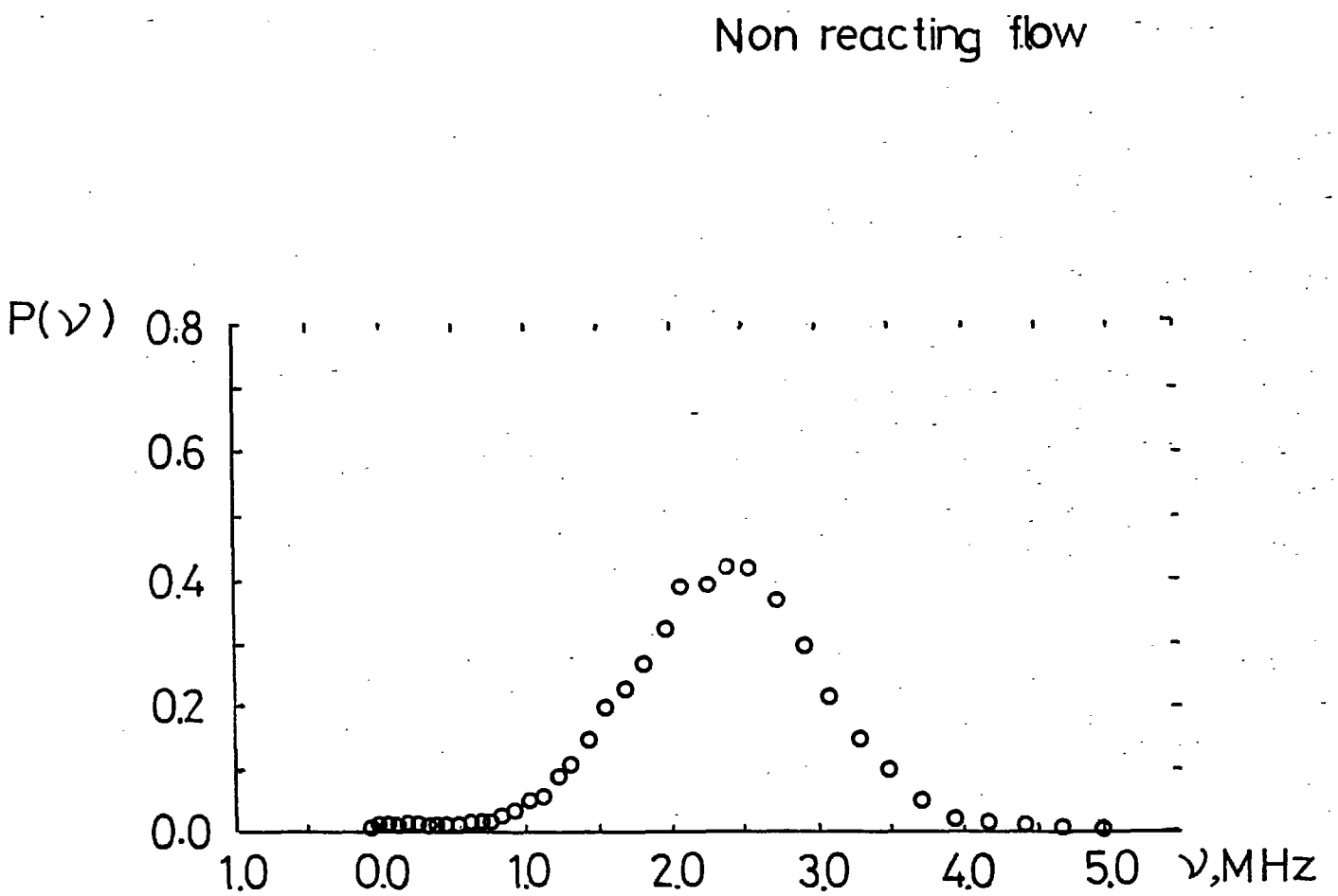

Figure 3.2.7: Measured velocity probability distribution.

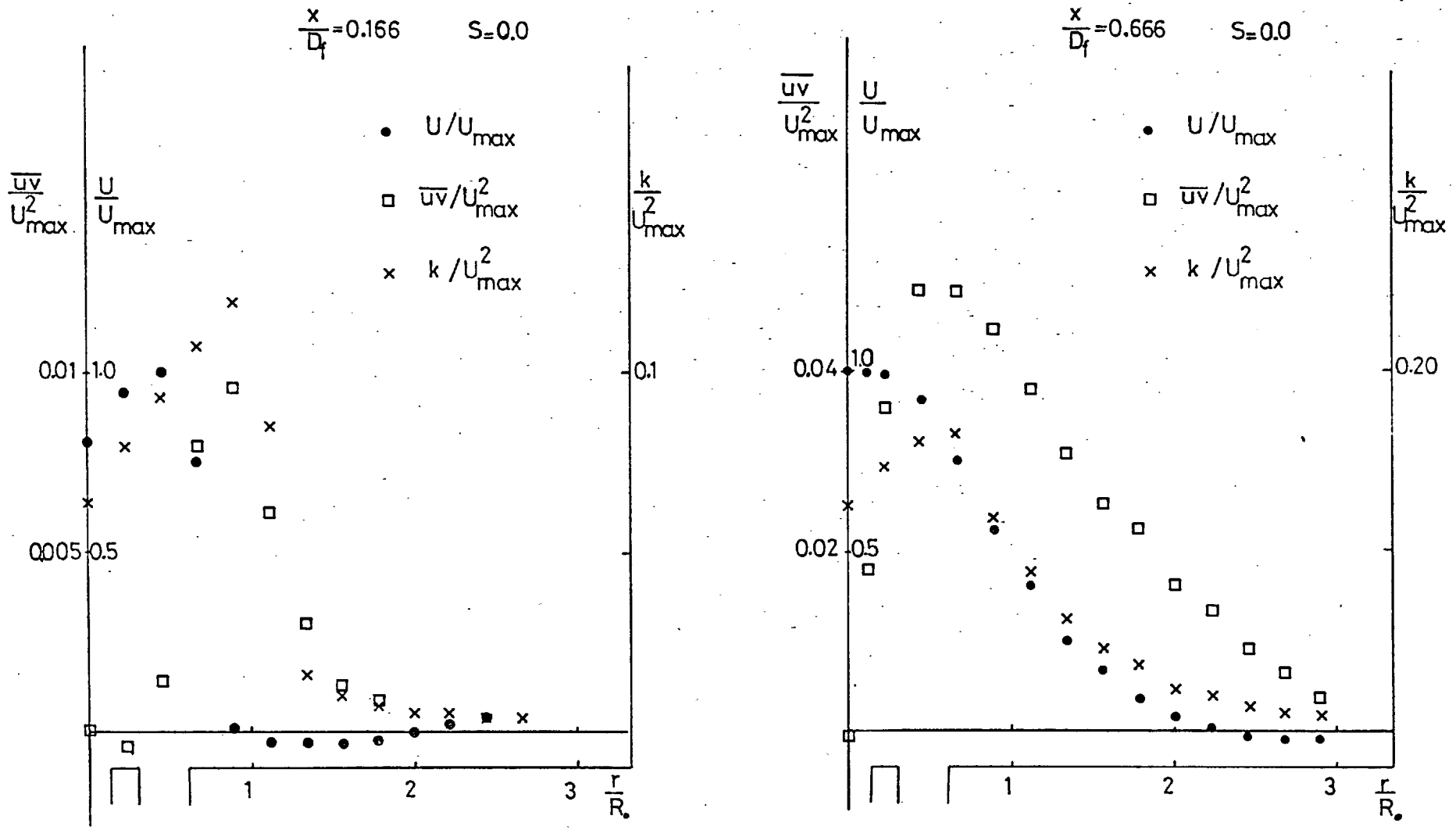

Figure 4.1.1: Radial profiles of mean velocity, shear stress and kinetic energy of turbulence. (isothermal flow).

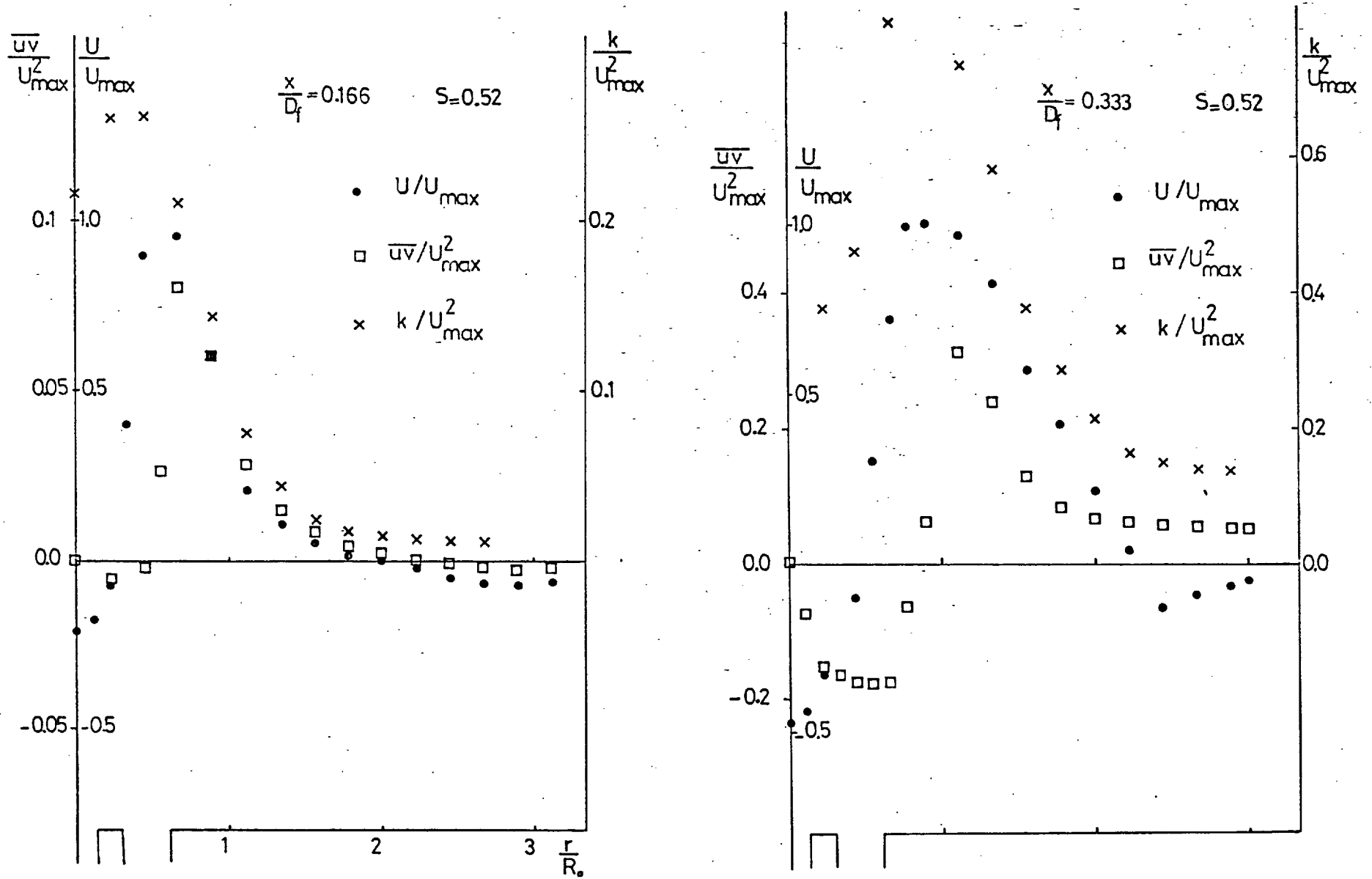

Figure 4.1.2: Radial profiles of mean velocity, shear stress and kinetic energy of turbulence. (isothermal flow).

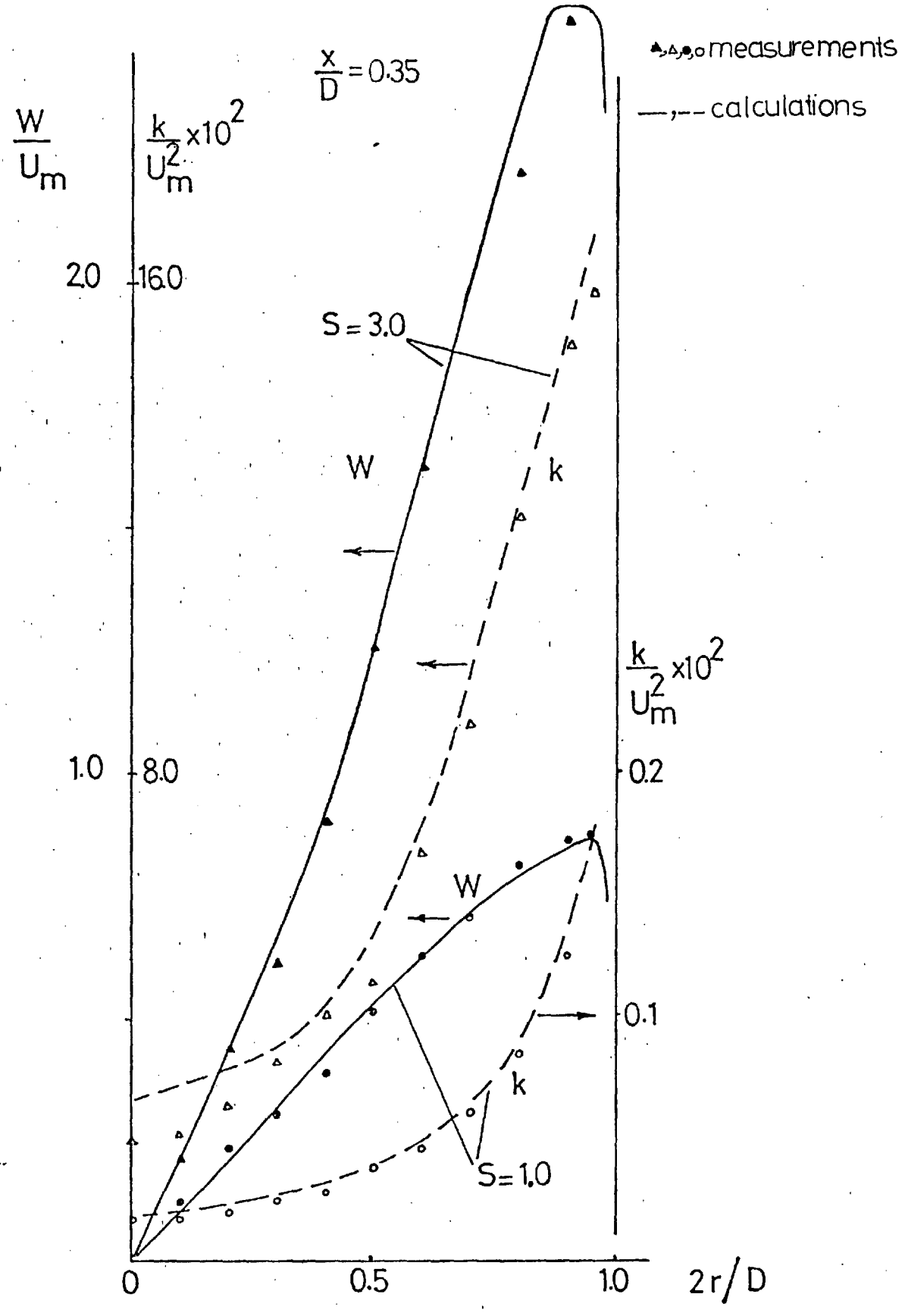

Figure 4.2.1: Measured and calculated profiles of tangential velocity and kinetic energy of turbulence in the swirling pipe flow of Weske et al (1974).

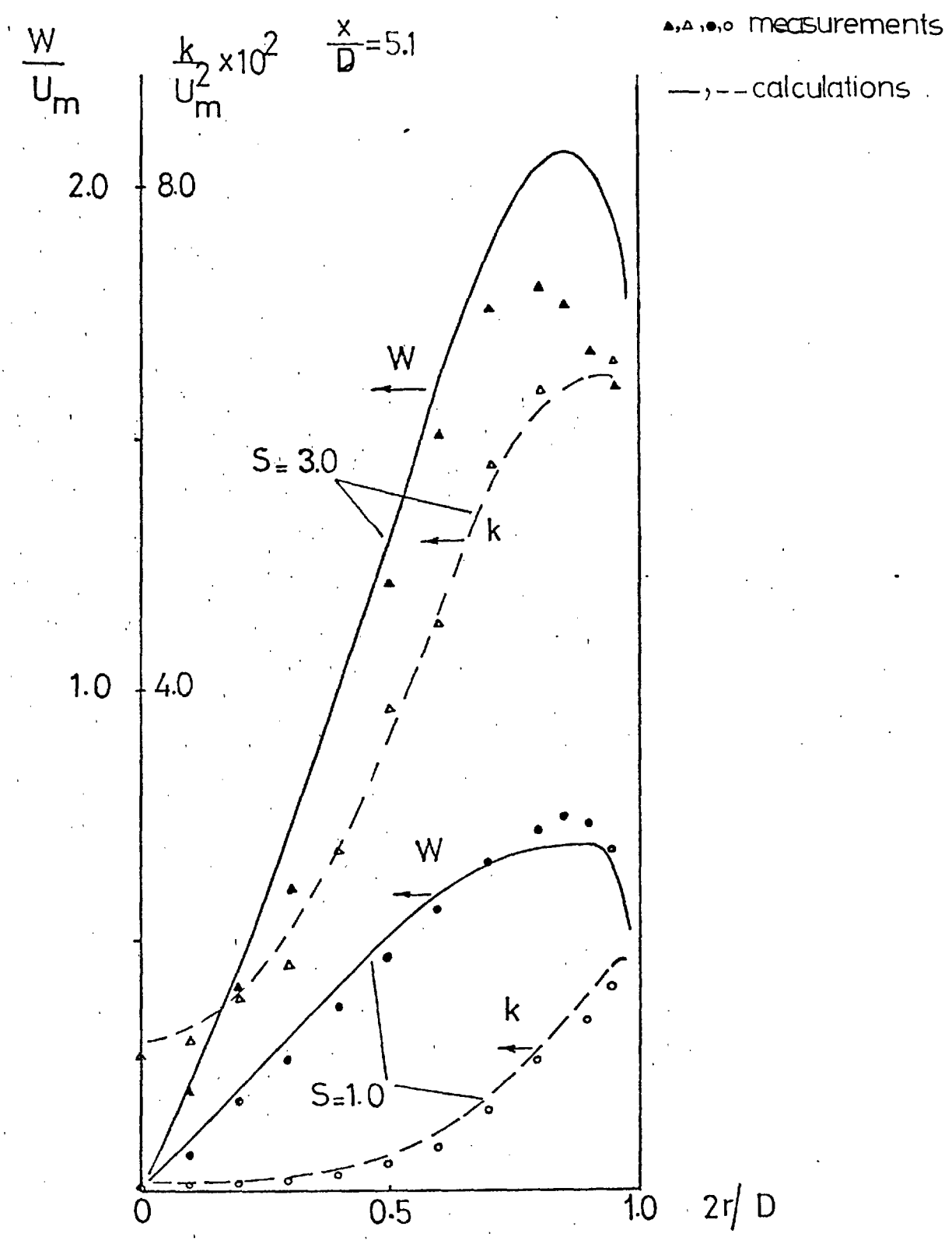

Figure 4.2.2: Measured and calculated profiles of tangential velocity and kinetic energy of turbulence in the swirling pipe flow of Weske et al (1974).

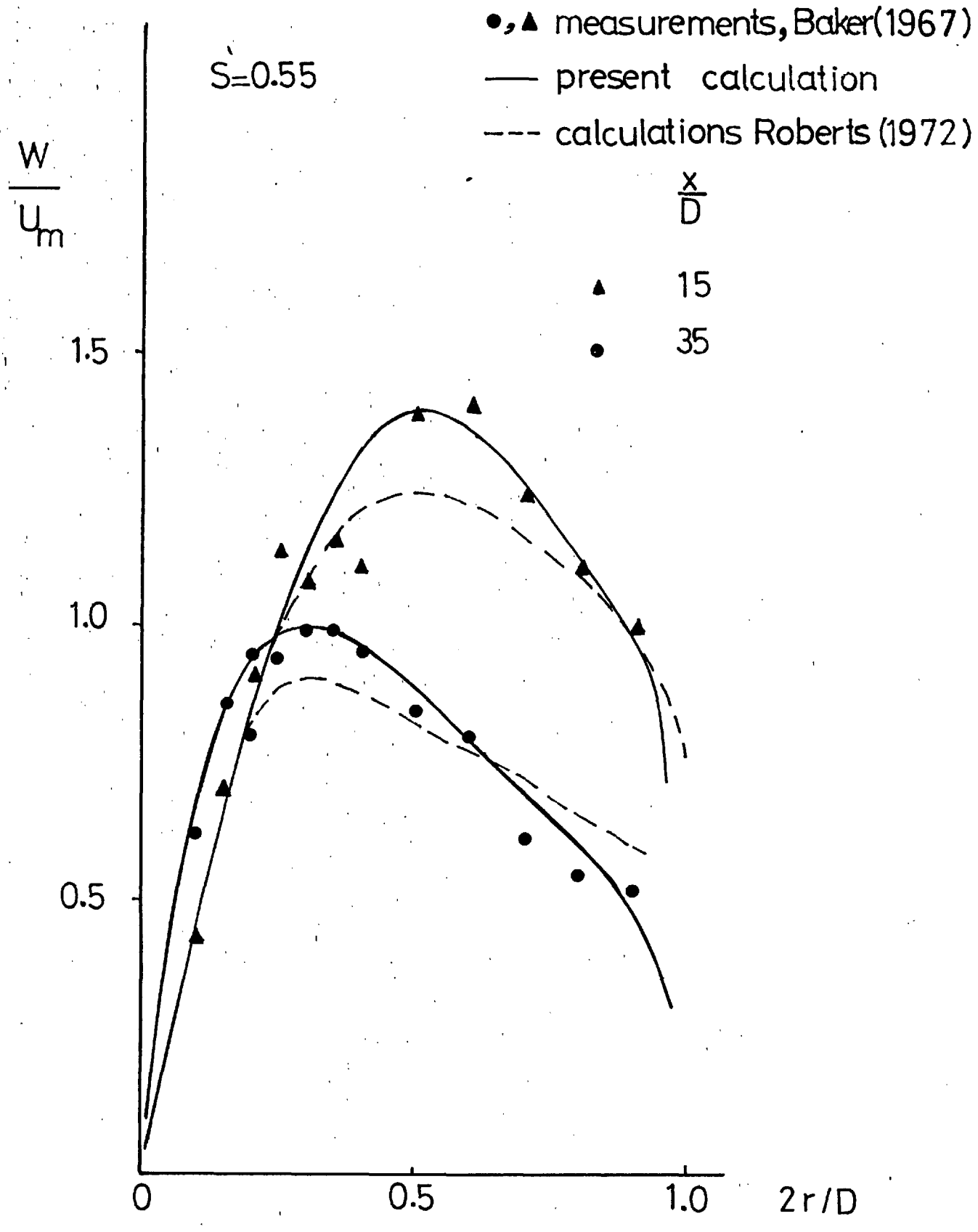

Figure 4.2.3: Measured and calculated profiles of tangential velocity in the swirling pipe flow of Baker (1967).

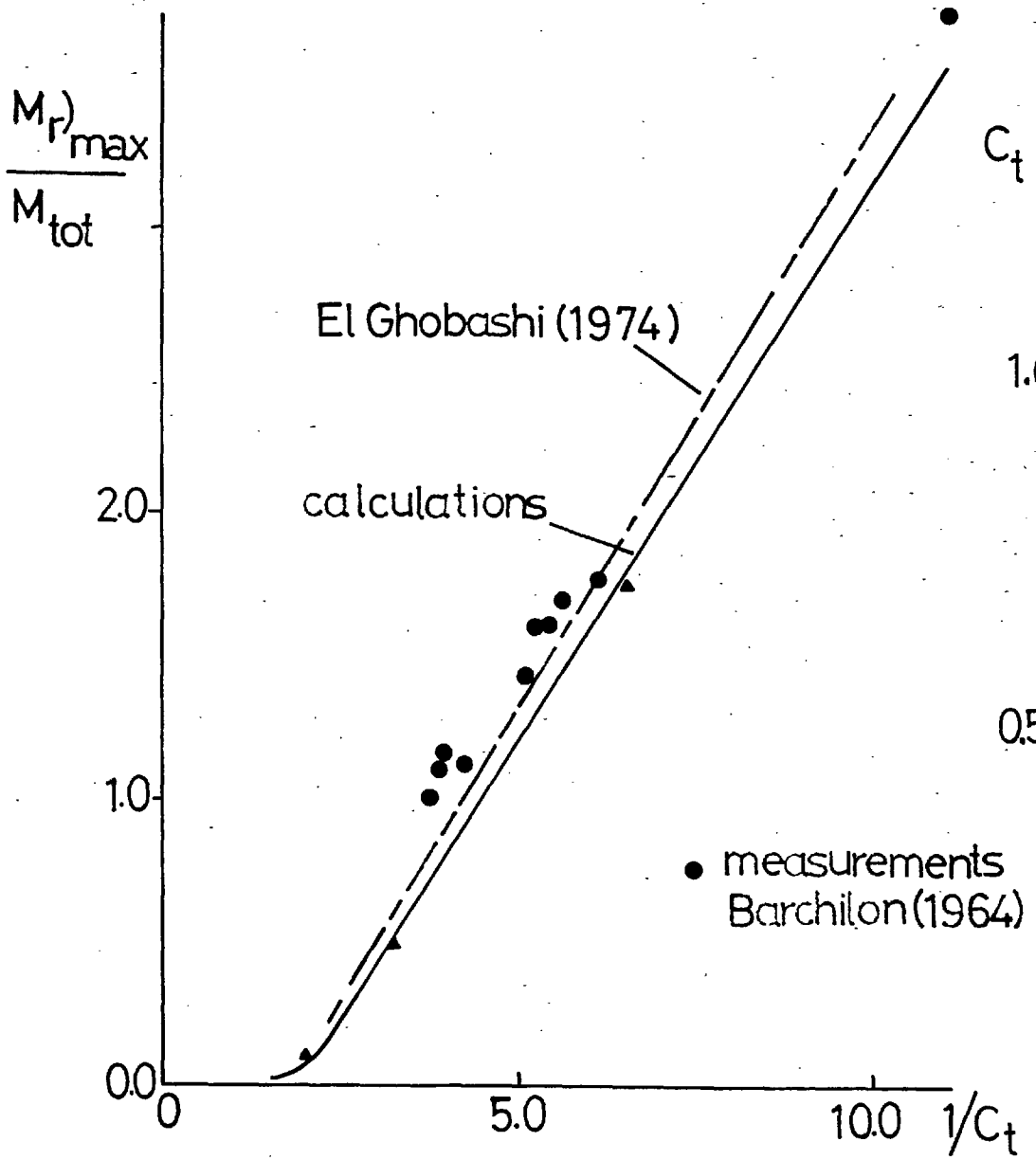

Figure 4.2.5: Measured and calculated relation between recirculated mass and C_t in a coflowing duct.

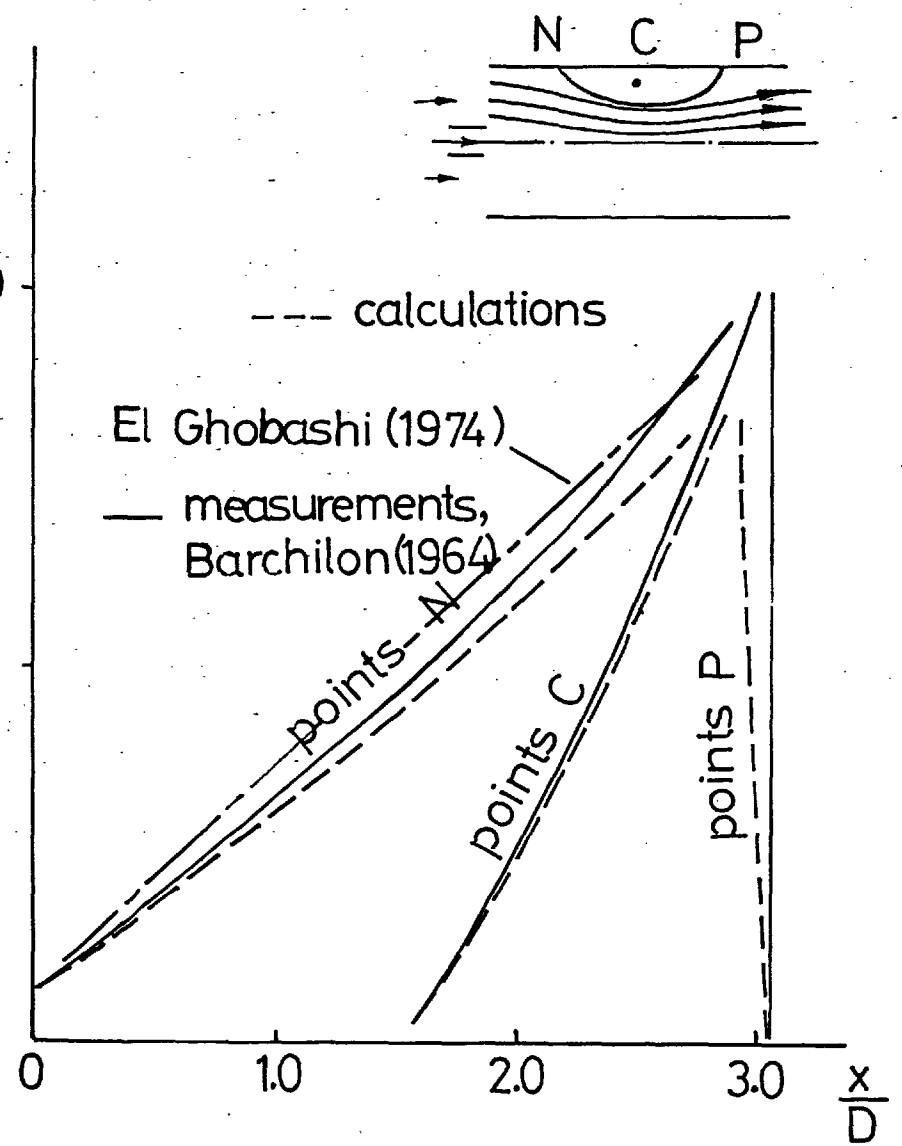

Figure 4.2.4: Measured and calculated size and location of wall recirculation zone in a coflowing duct.

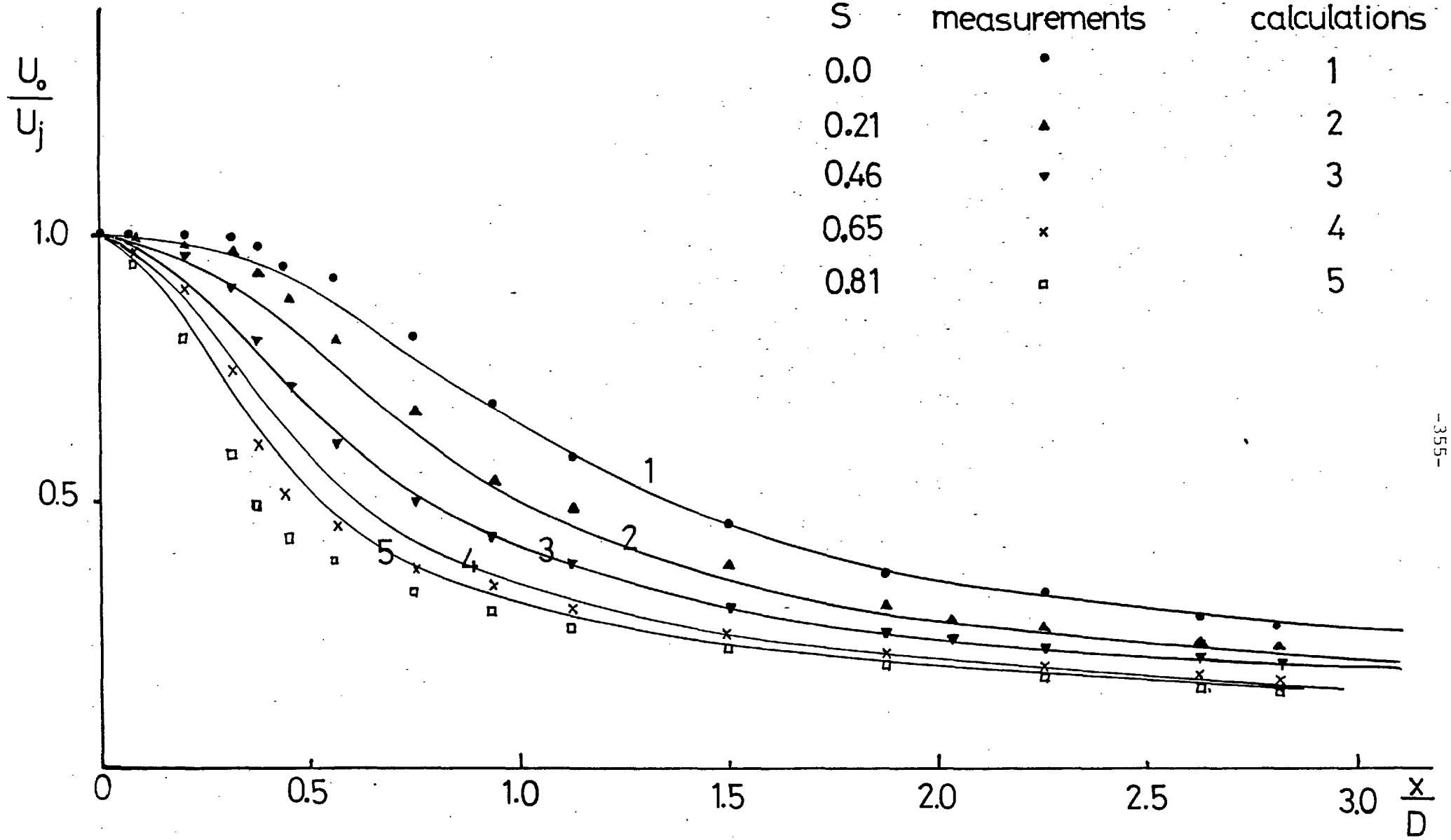

Figure 4.2.6: Measured and calculated velocity distribution along the centreline of a coflowing swirling jet measurements of Craya et al (1967).

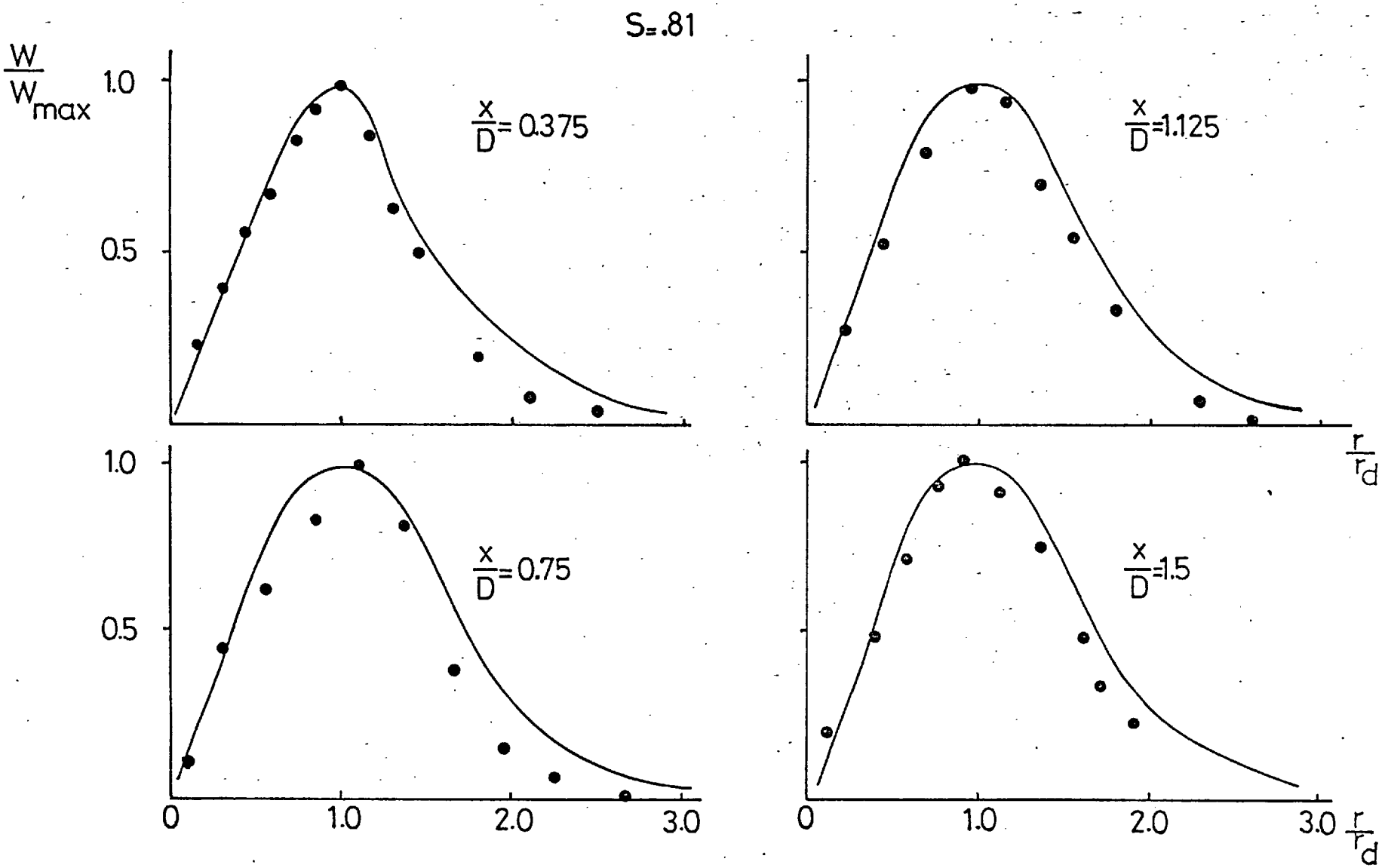

Figure 4.2.7: Radial profiles of measured and calculated tangential velocity in a coflowing swirling jet (measurements of Craya et al (1967).

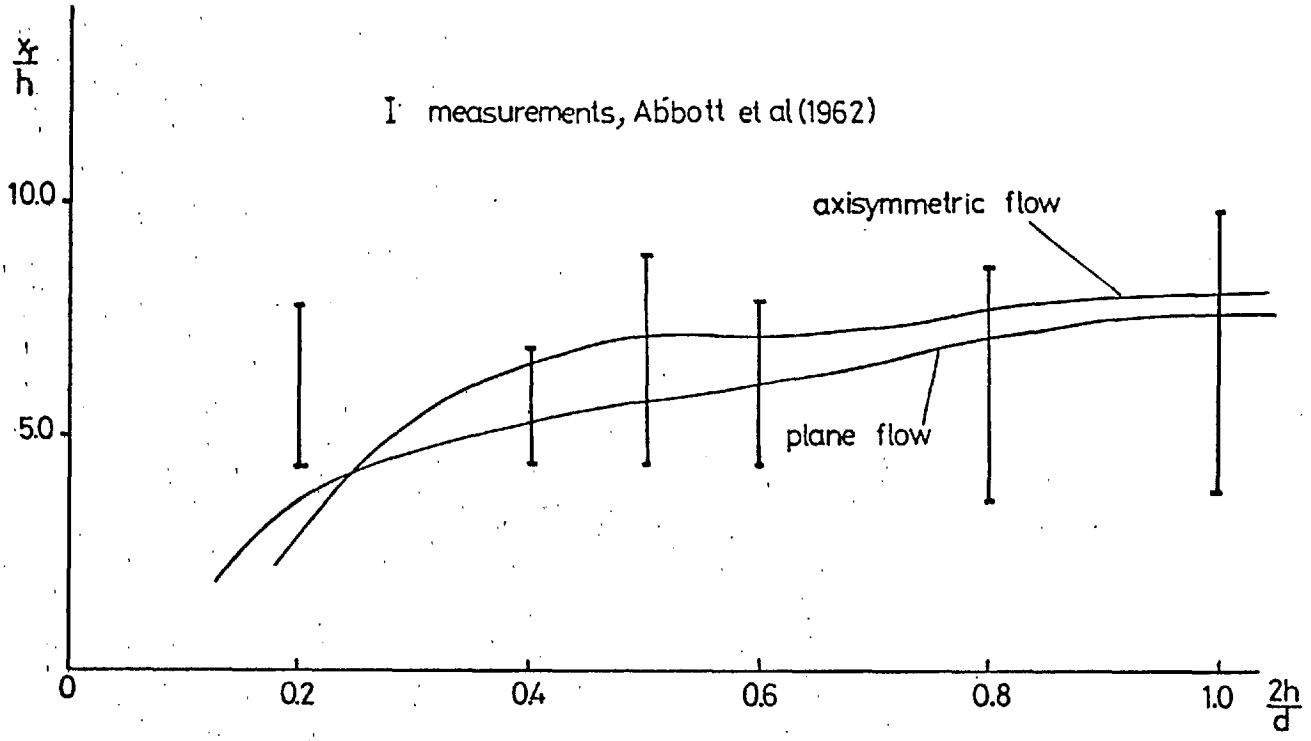

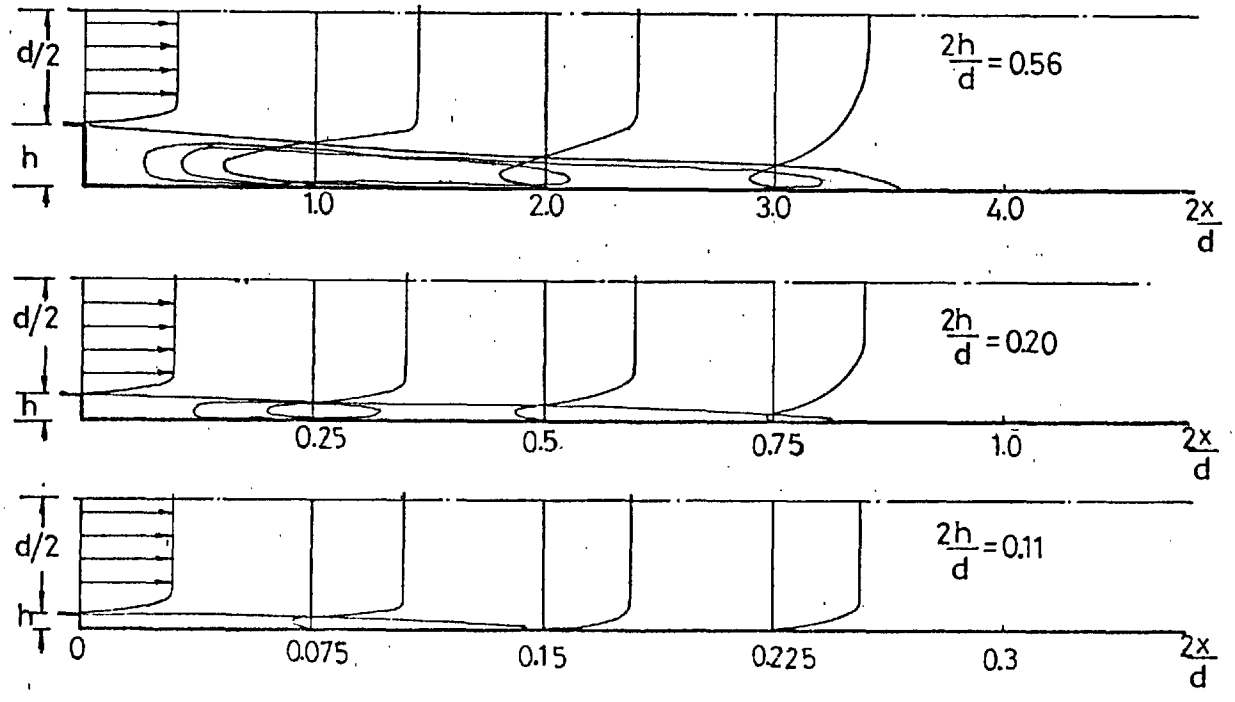

Figure 4.2.8: Measured and calculated variation of recirculation zone length with expansion ratio in plane and axisymmetric flows.

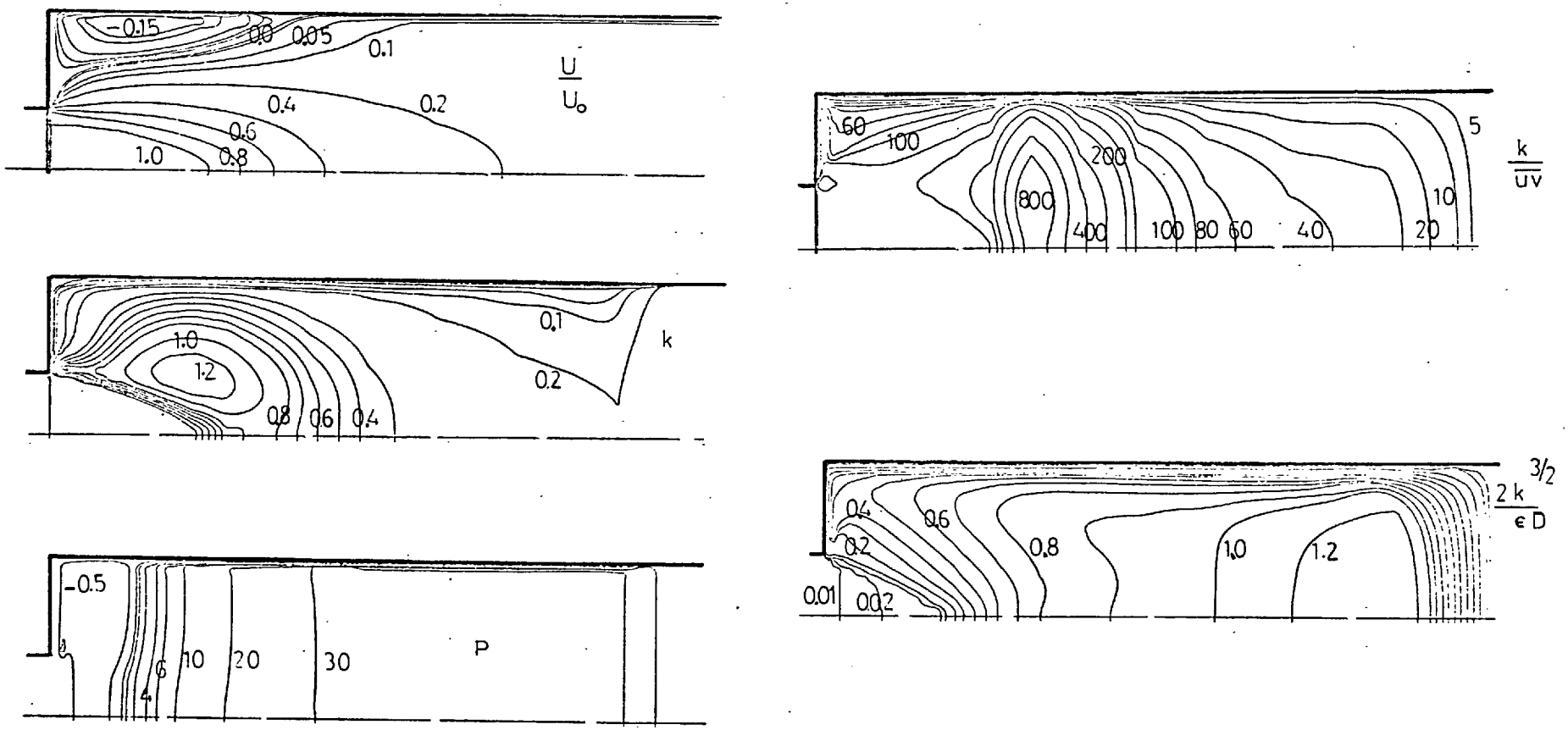

$\frac{d}{D}=0.385$ $\quad Re=5\times10^4$

Figure 4.2.9: Contours of mean velocity, kinetic energy of turbulence; $\frac{k}{uv}$ and $\frac{2k}{\varepsilon D}^{3/2}$ in an axisymmetric sudden expansion flow.

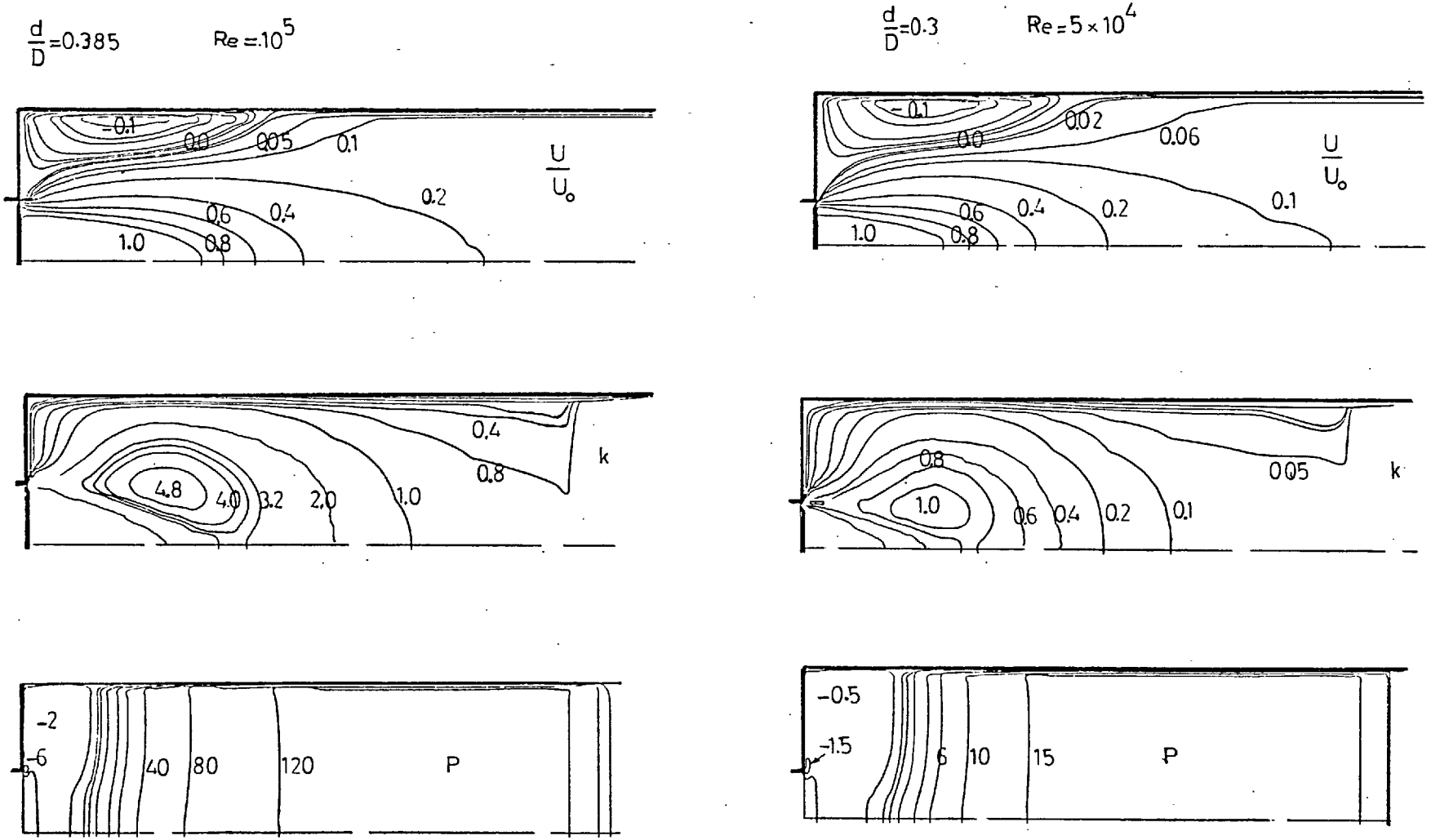

Figure 4.2.10: Effect of Reynolds number and expansion ratio on the local flow properties in an axisymmetric flow.

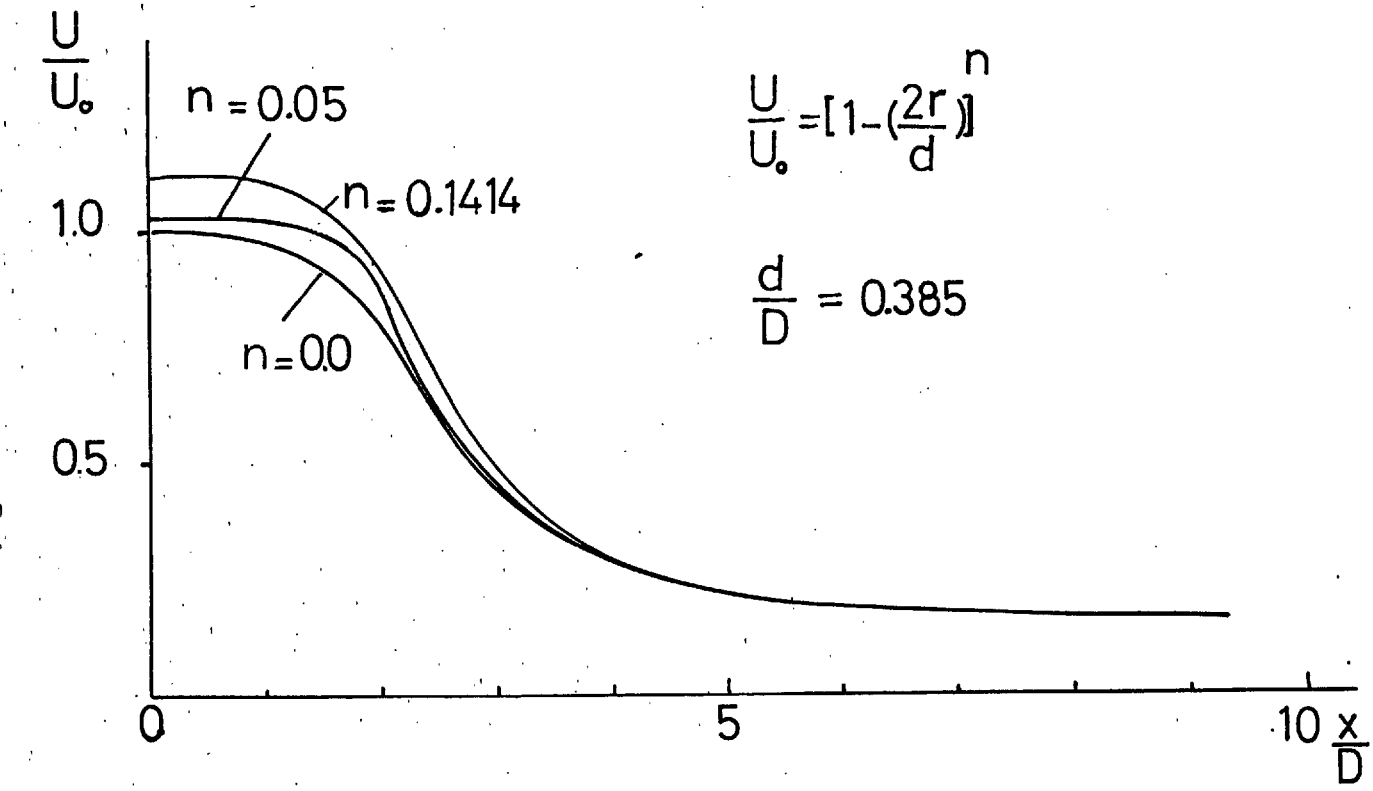

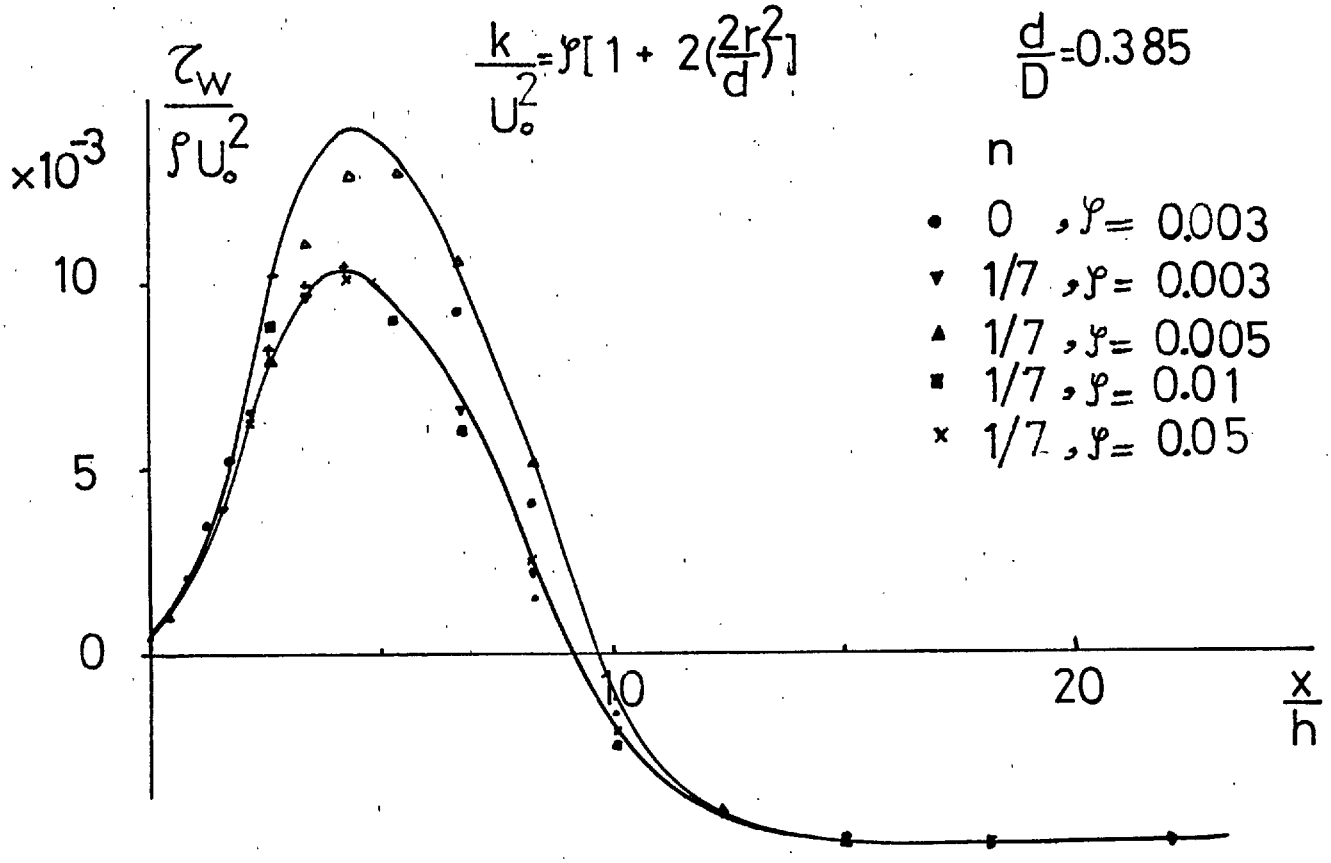

Figure 4.2.11: Effect of inlet velocity and kinetic energy profile assumptions on centreline velocity and wall shear stress.

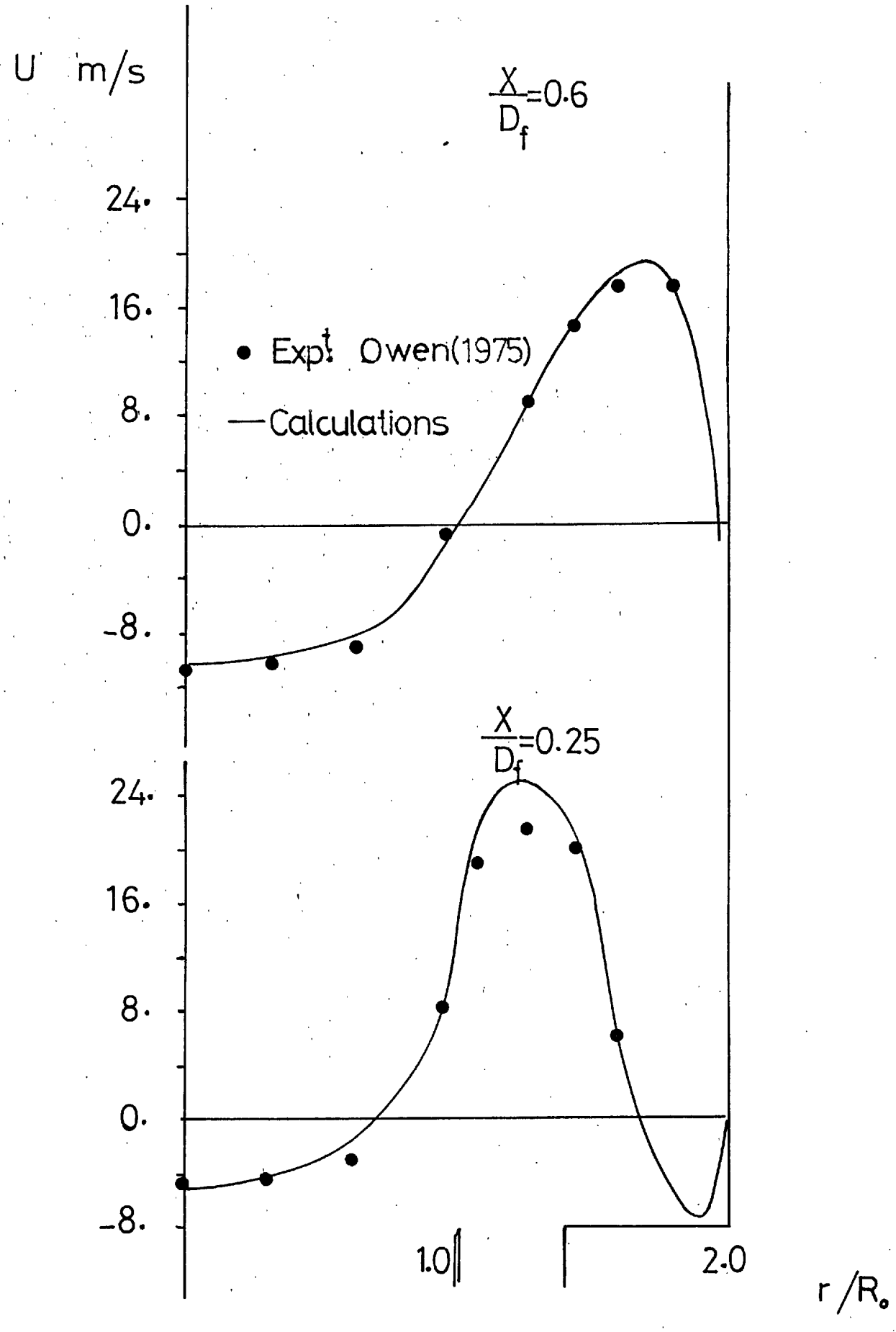

Figure 4.2.12: Radial profiles of measured and calculated mean velocity in a coaxial sudden expansion.

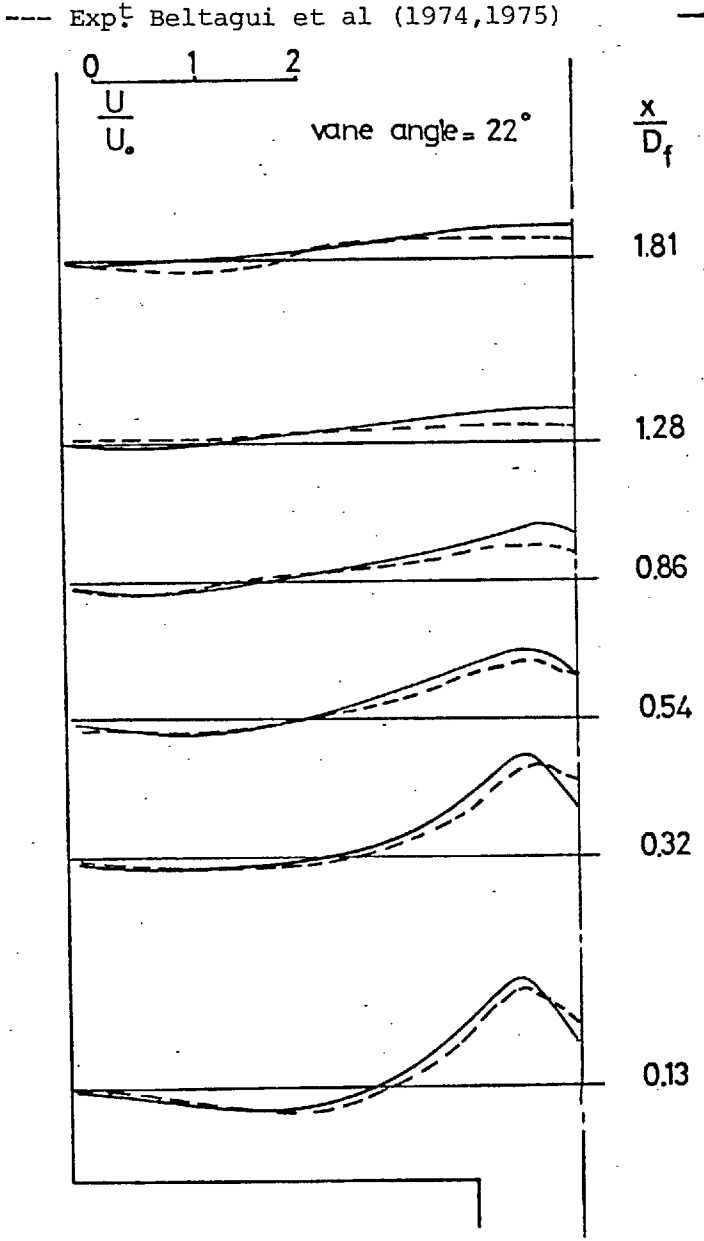

Figure 4.2.13:Measured and calculated mean axial velocity profiles.

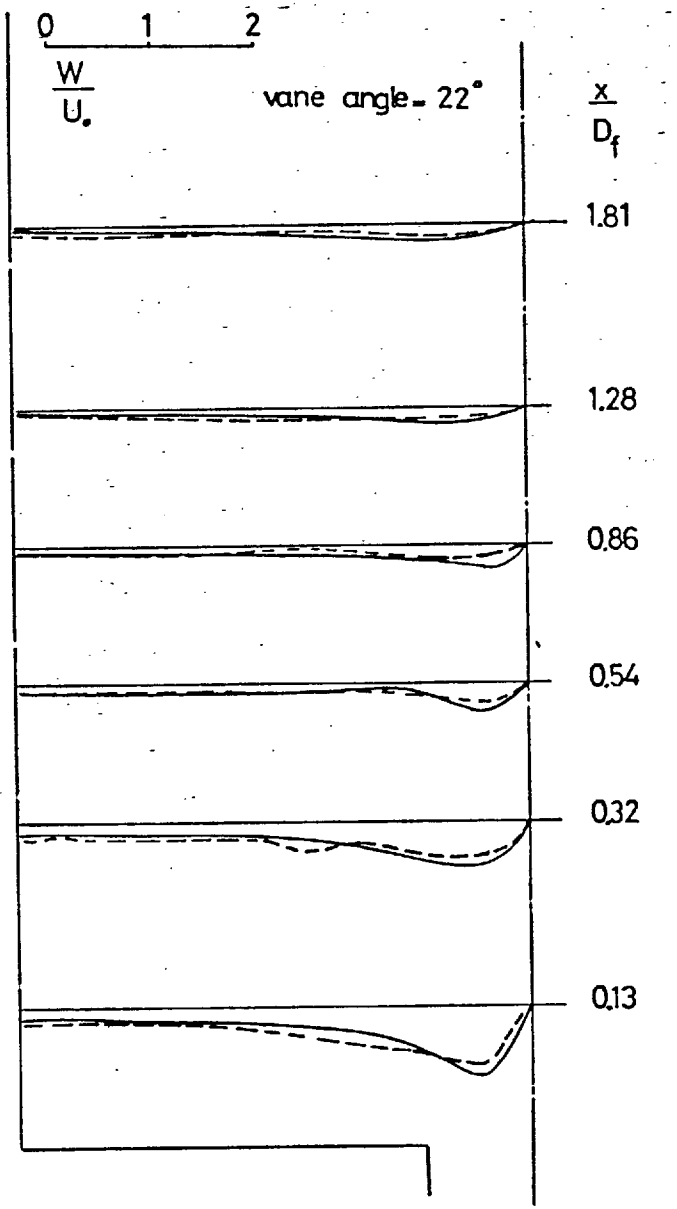

Figure 4.2.14:Measured and calculated mean tangential velocity profiles.

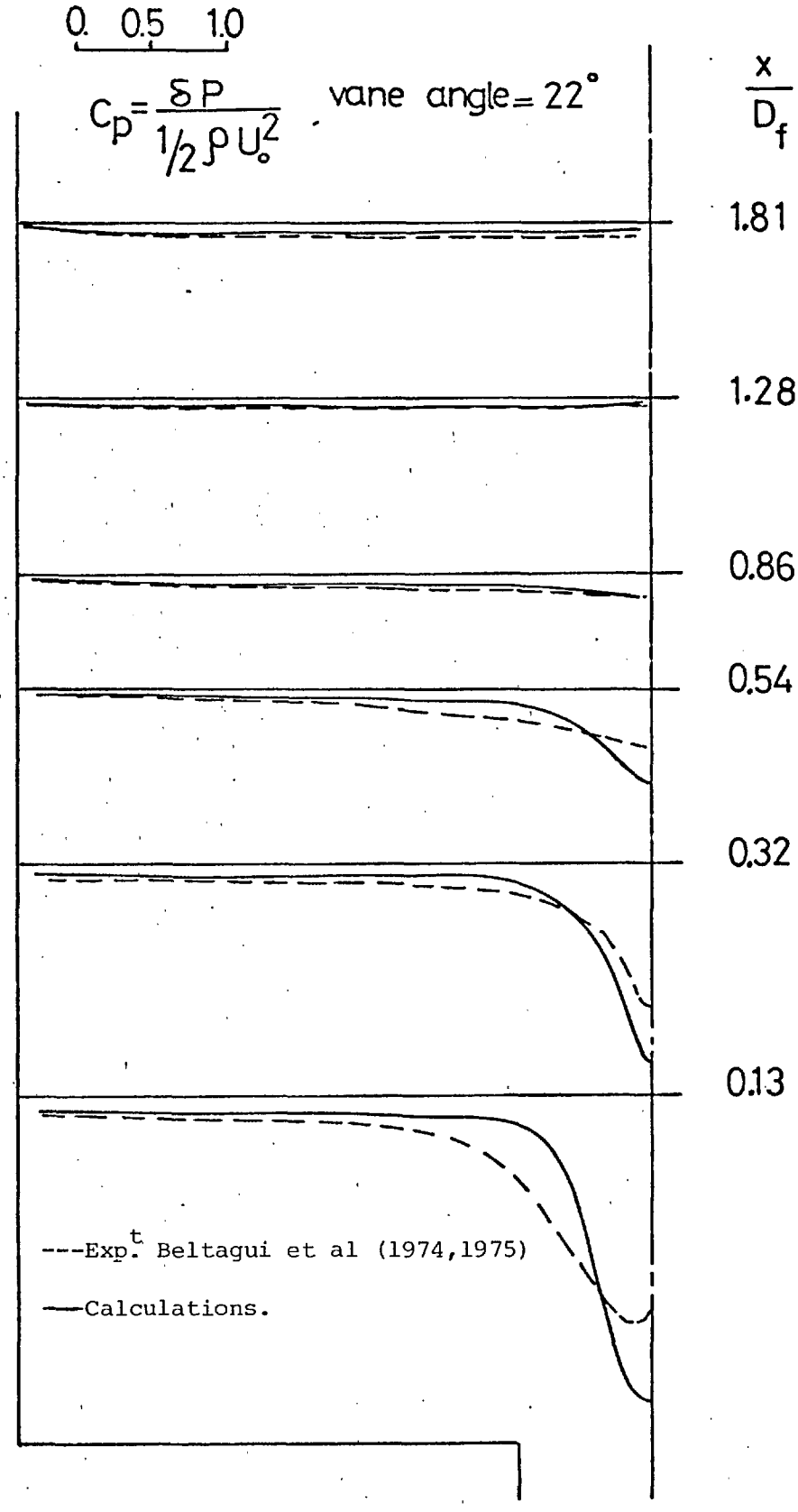

Figure 4.2.15:Measured and calculated pressure coefficient profiles.

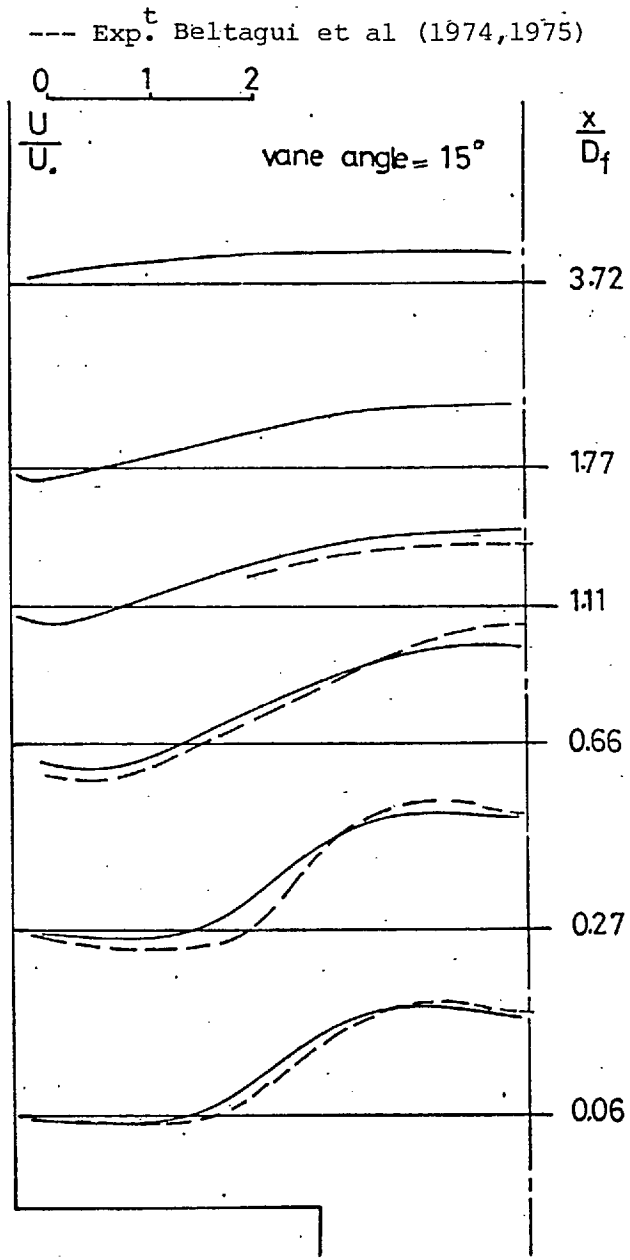

Figure 4.2.16:Measured and calculated mean axial velocity profiles.

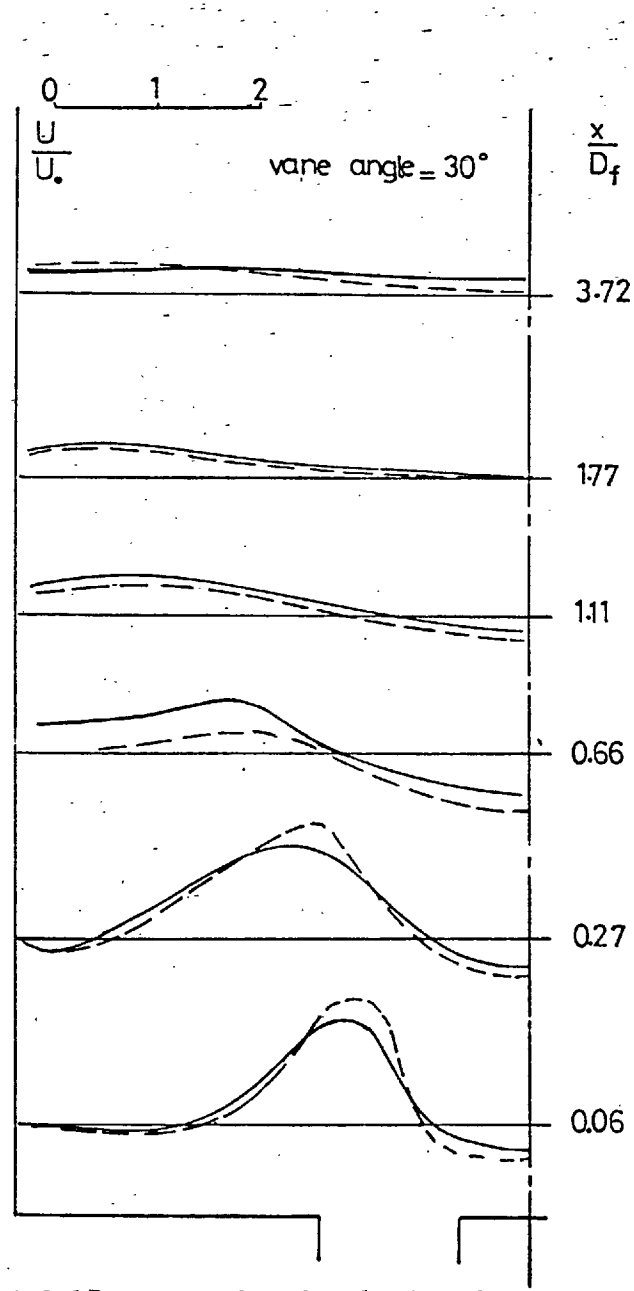

Figure 4.2.17:Measured and calculated mean axial velocity profiles.

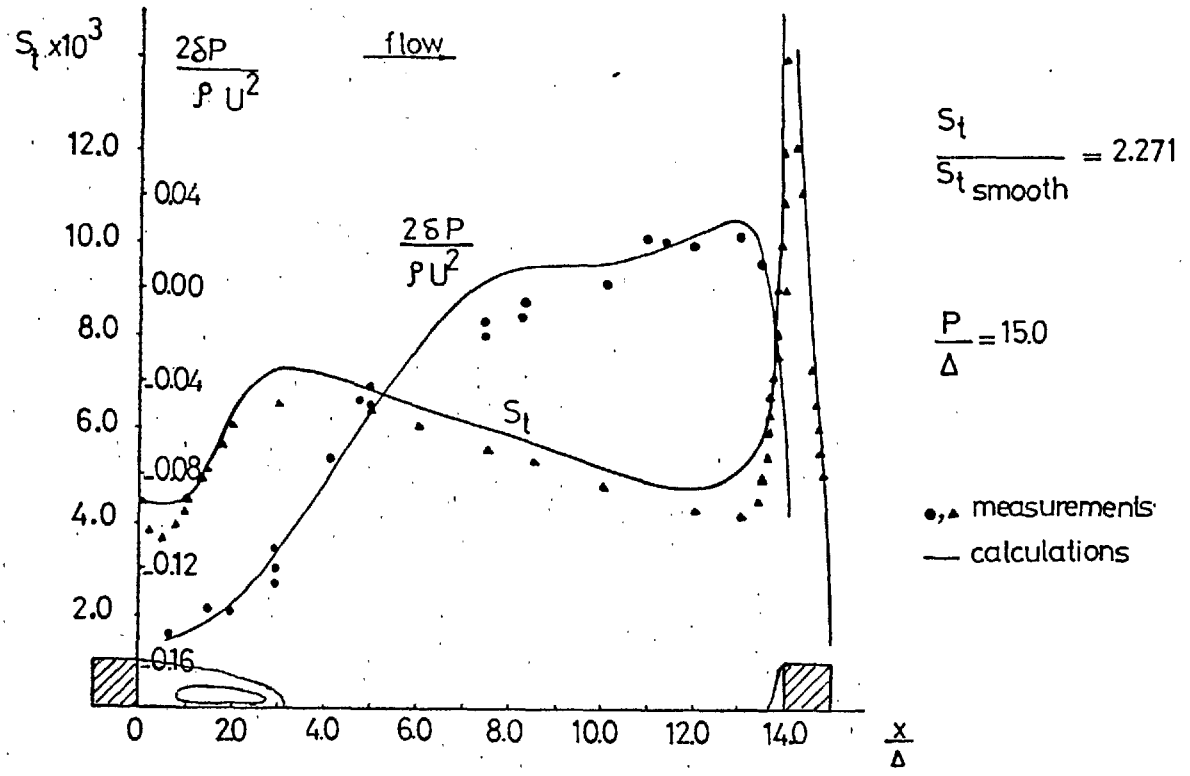

(a)

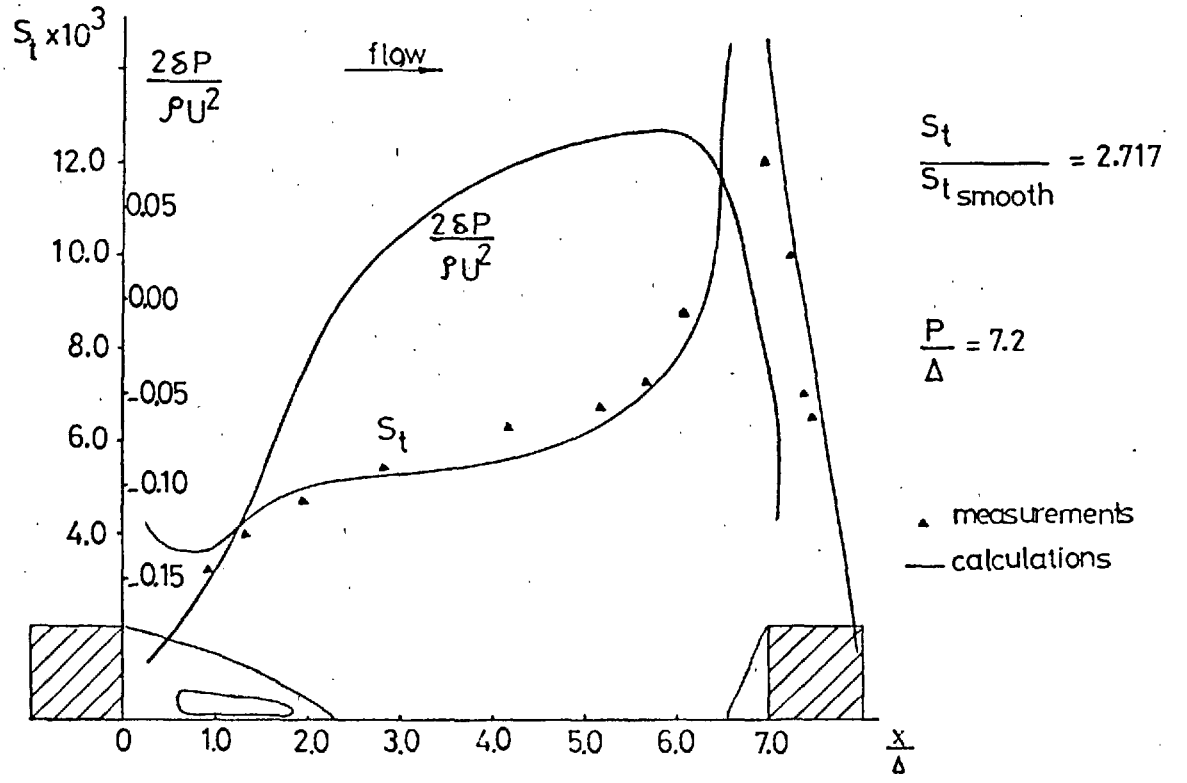

(b)

Figure 4.2.18: Variation of S_t and pressure coefficient between two ribs, measurements of Wilkie (1966).

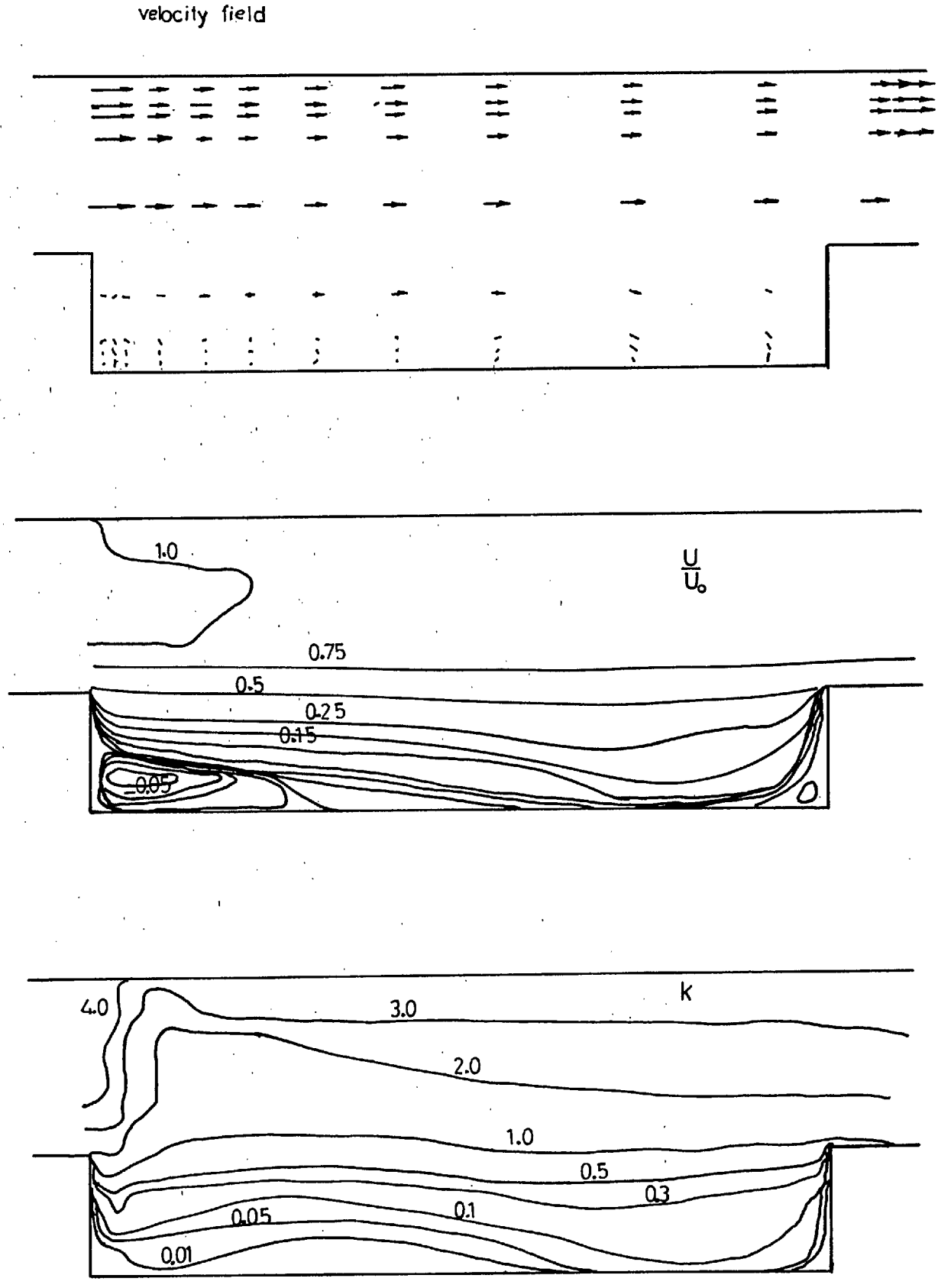

Figure 4.2.19: Calculated velocity vector, iso velocity and iso kinetic energy contours, for flow past roughened axisymmetric surface, $P/\Delta = 7.2$.

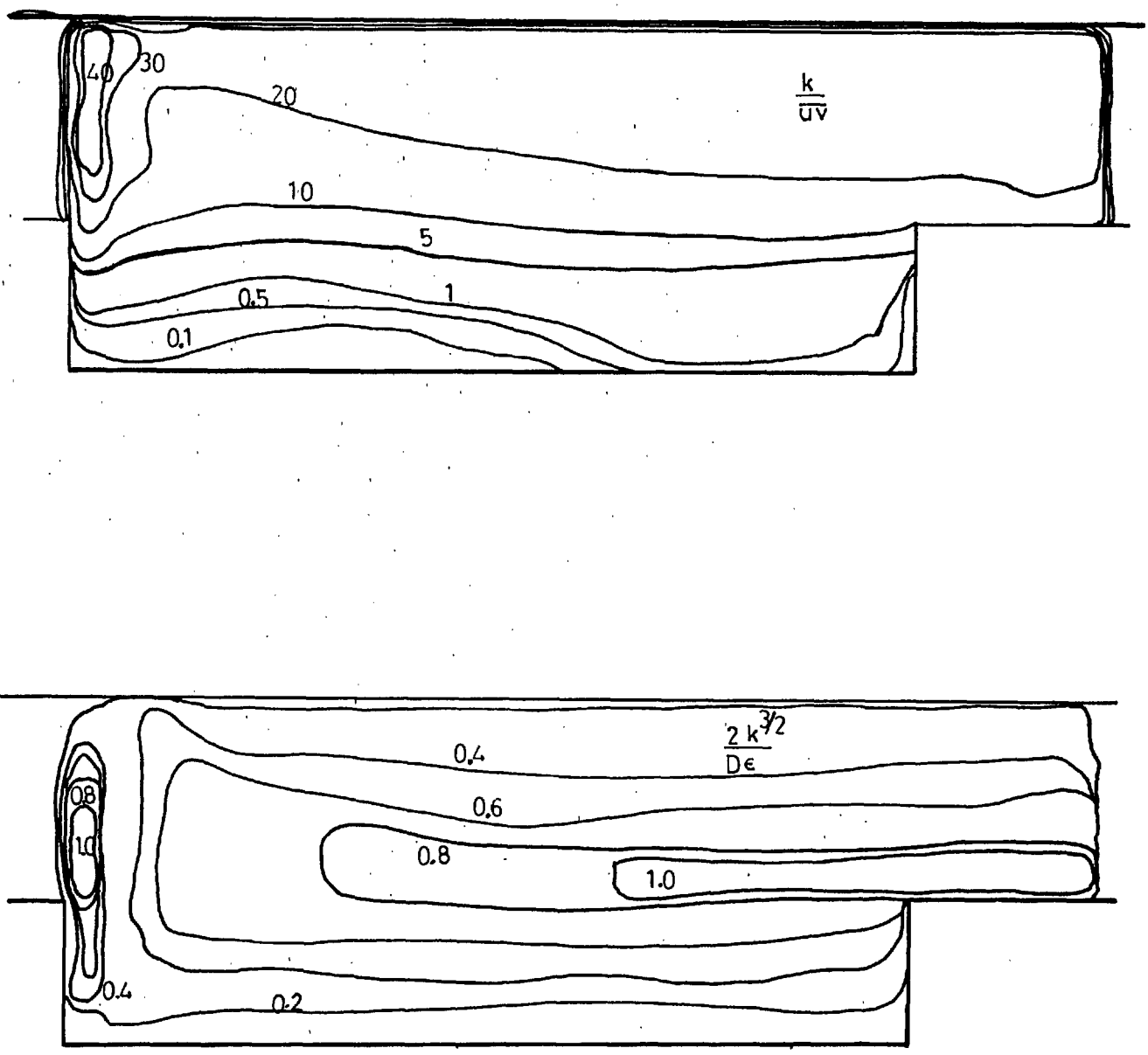

Figure 4.2.20: Calculated contours of $\frac{k}{uv}$ and $\frac{2k^{3/2}}{\varepsilon D}$ for flow past roughened axisymmetric surfaces, $P/\Delta = 7.2$.

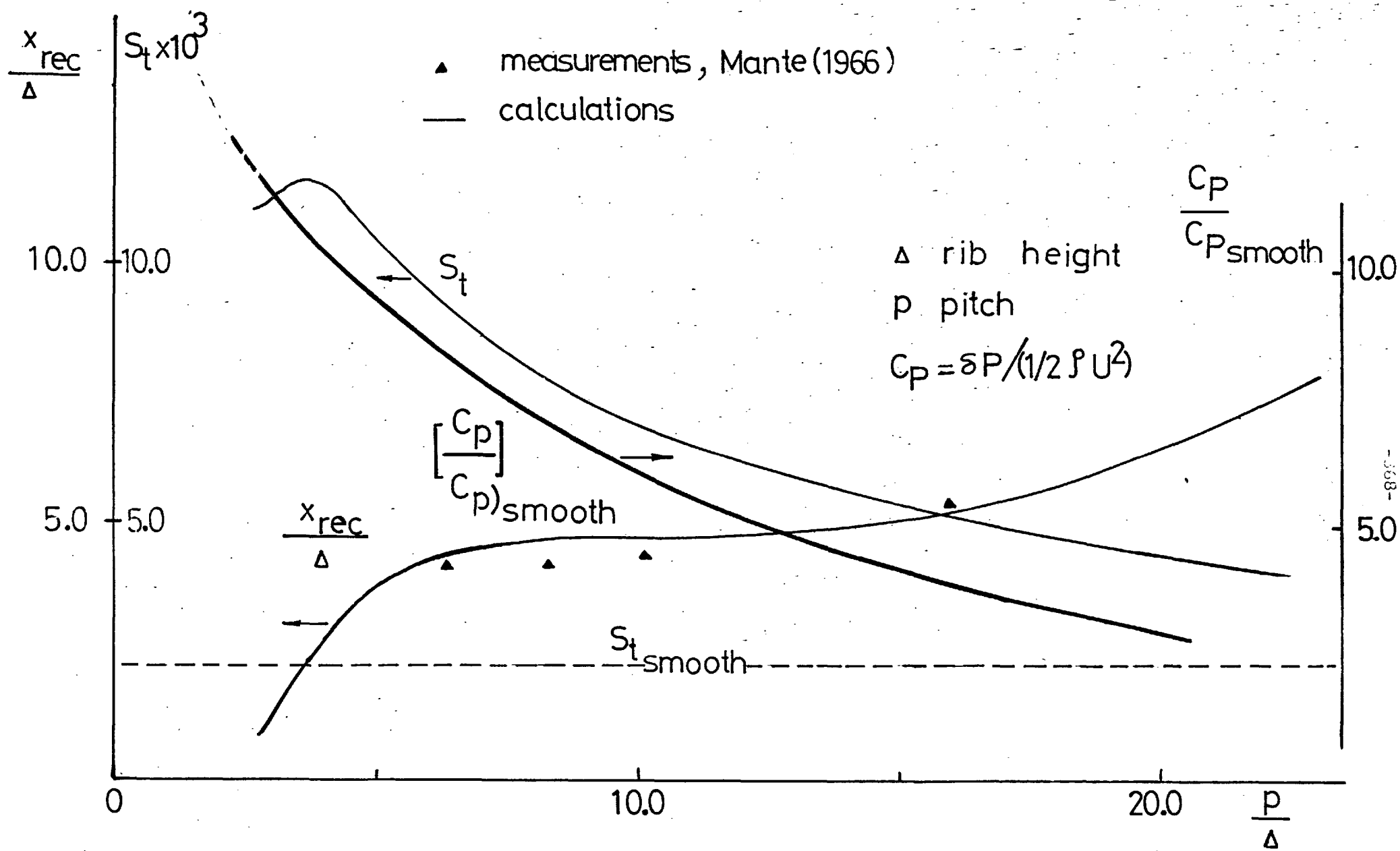

Figure 4.2.21: Variation of recirculation zone length, overall Stanton number and pressure coefficient as a function of the ratio of rib pitch to height.

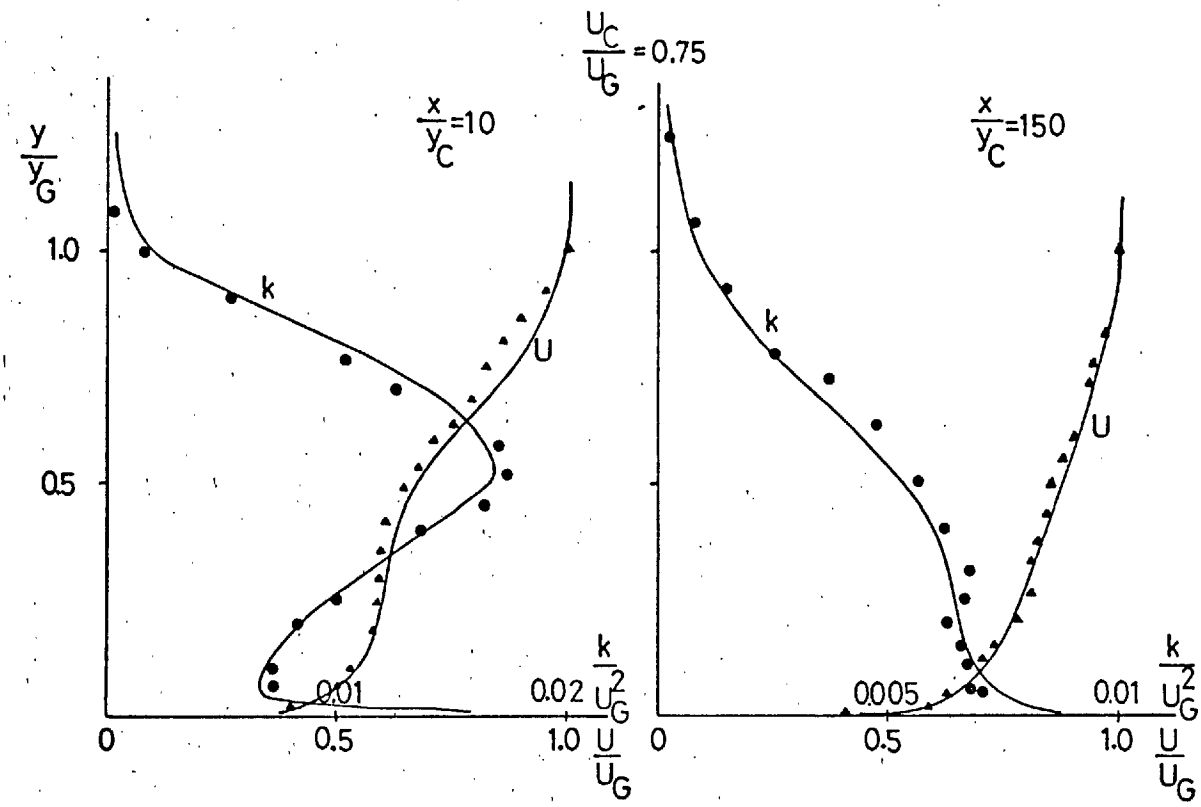

(a)

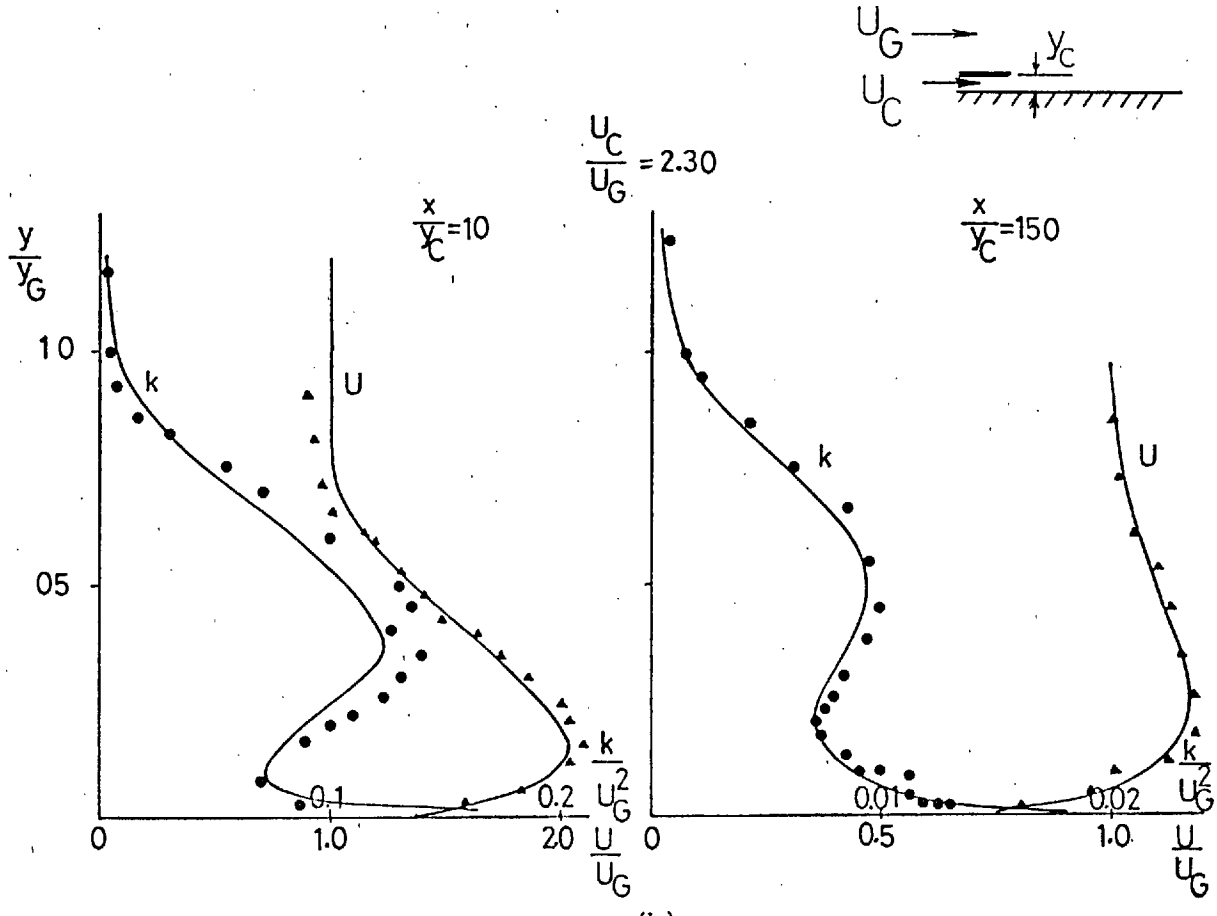

(b)

Figure 4.2.22: Measured and calculated profiles of mean velocity and kinetic energy of the wall jet of Kacker et al (1971).

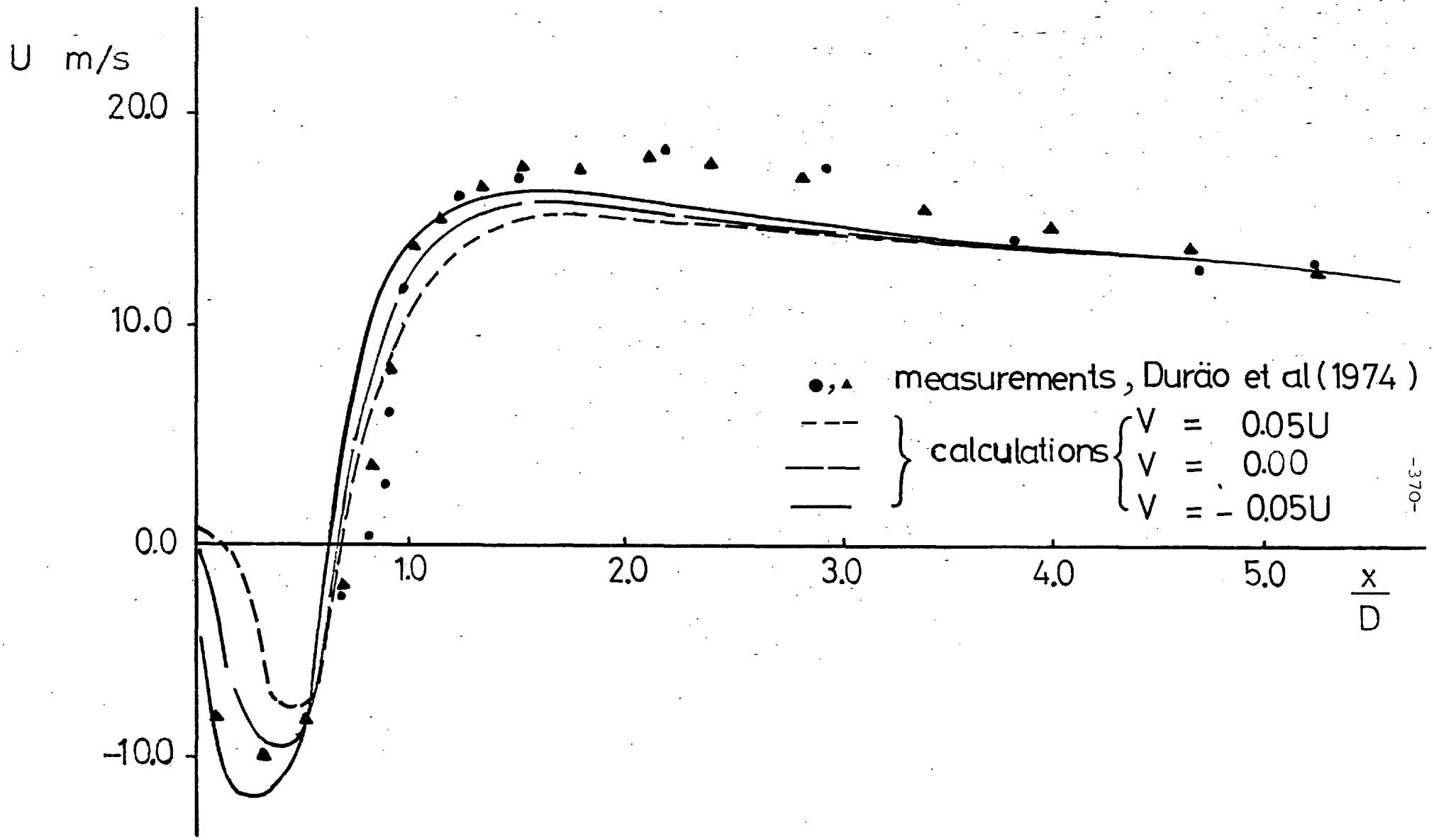

Figure 4.2.23: Measured and calculated values of mean axial velocity in the wake behind the disc of Durao et al.

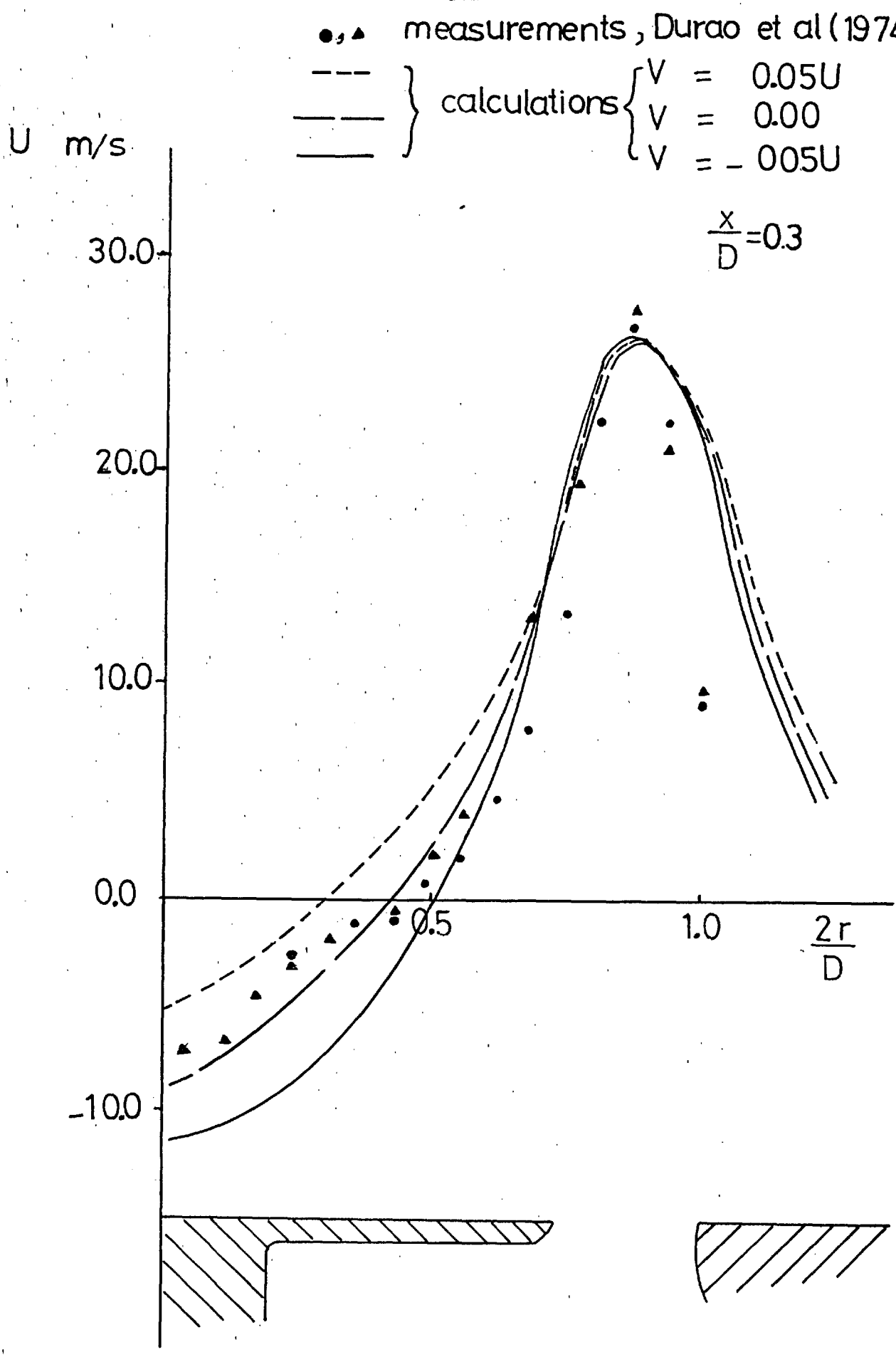

Figure 4.2.24: Measured and calculated radial profiles of mean axial velocity in the wake behind the disc of Durao et al.

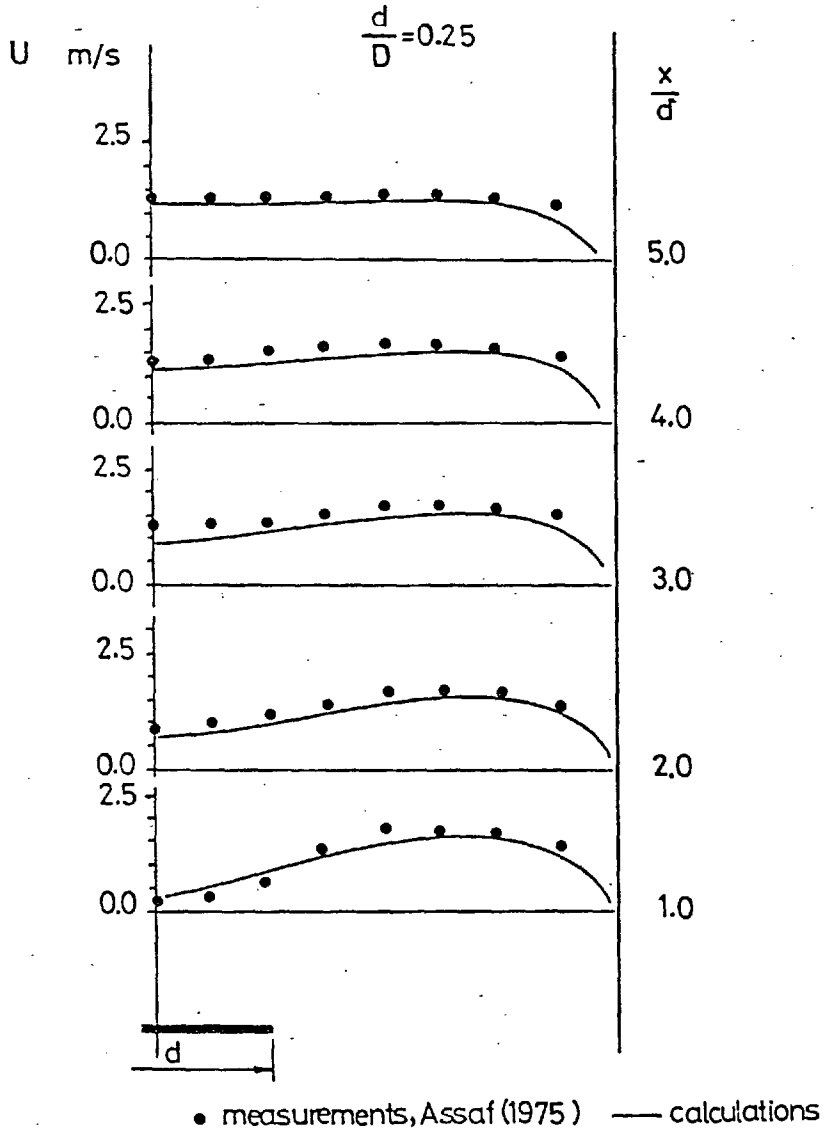

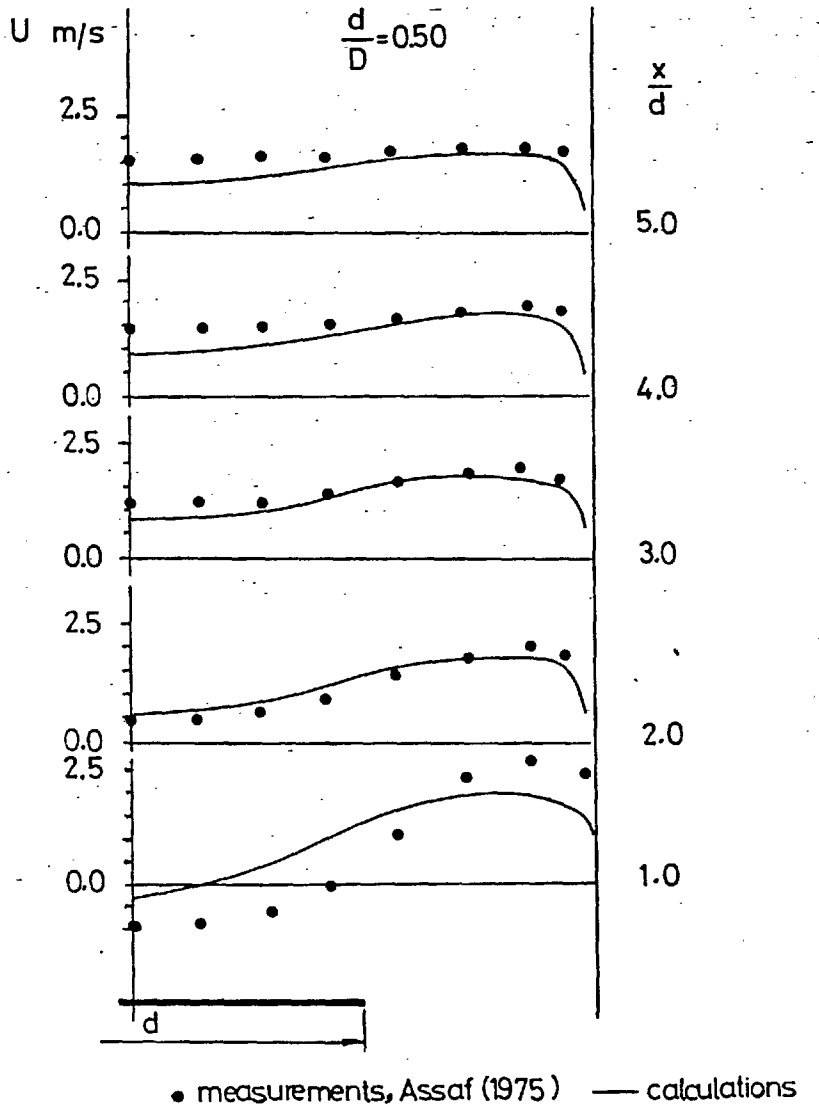

Figure 4.2.25: Radial profiles of measured and calculated mean axial velocity in the wake behind a disc in a confined pipe flow.

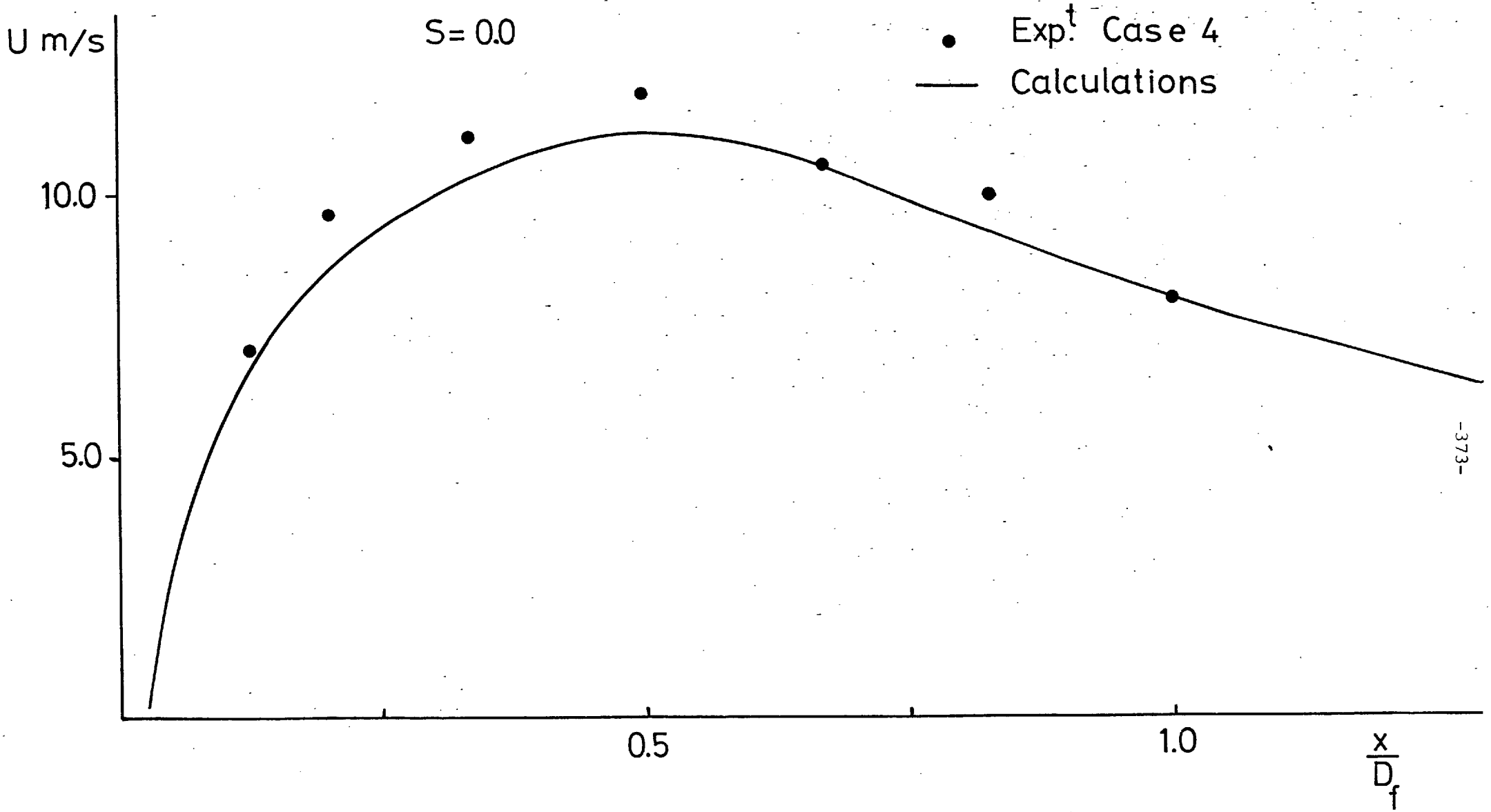

Figure 4.3.1: Centreline distribution of mean axial velocity (case 4).

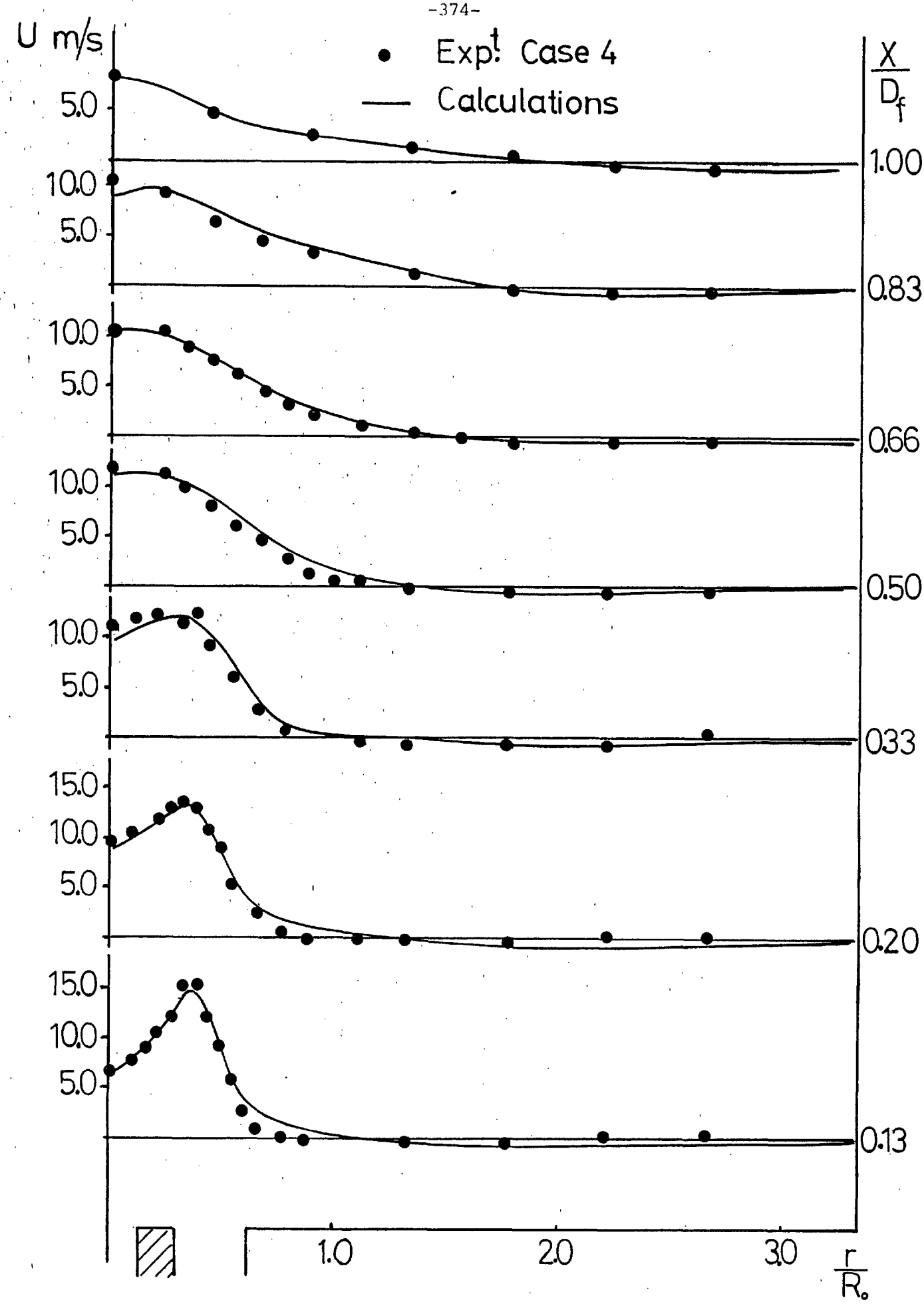

Figure 4.3.2: Measured and calculated profiles of mean axial velocity (case 4).

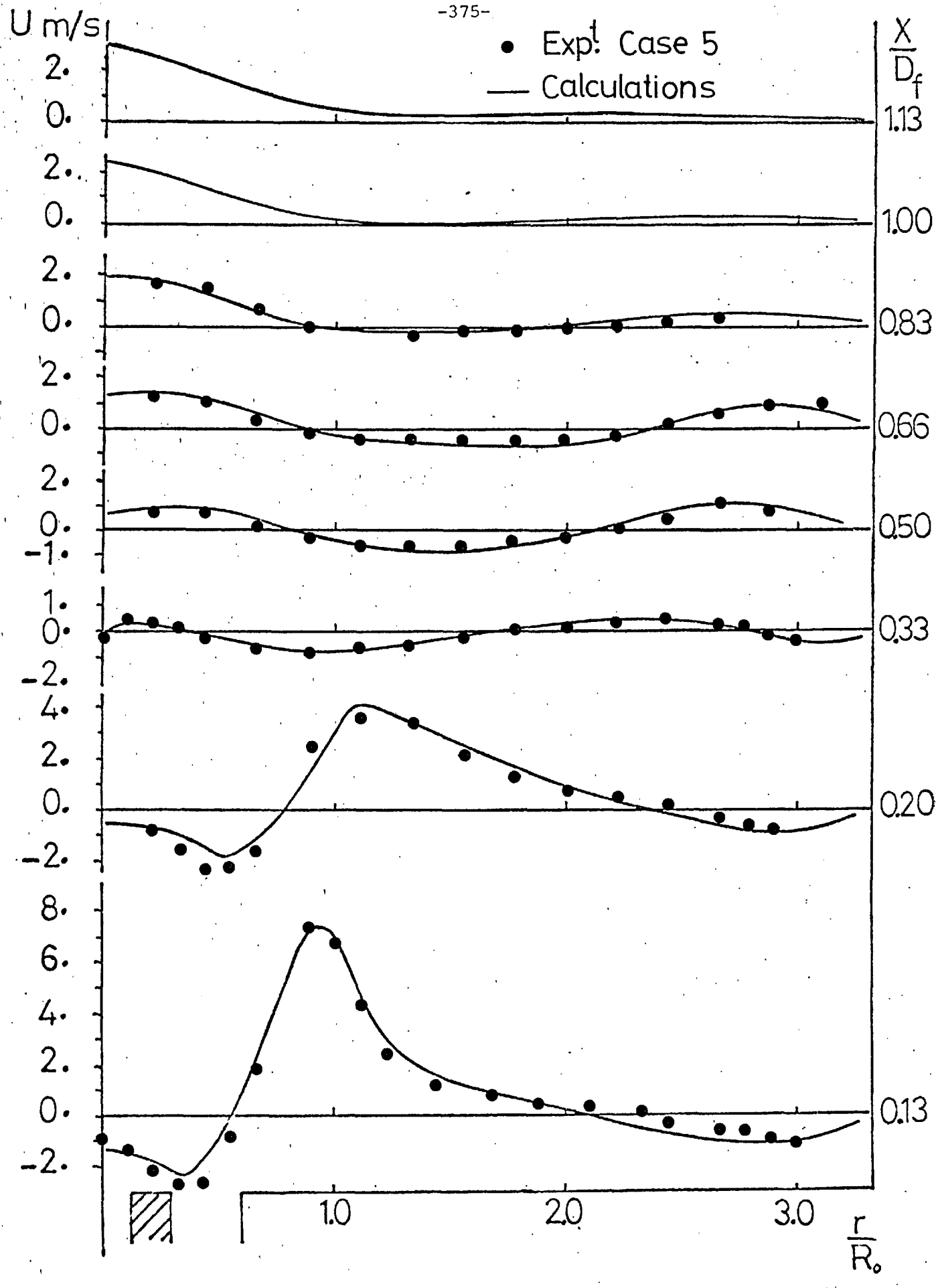

Figure 4.3.3: Measured and calculated profiles of mean axial velocity (case 5).

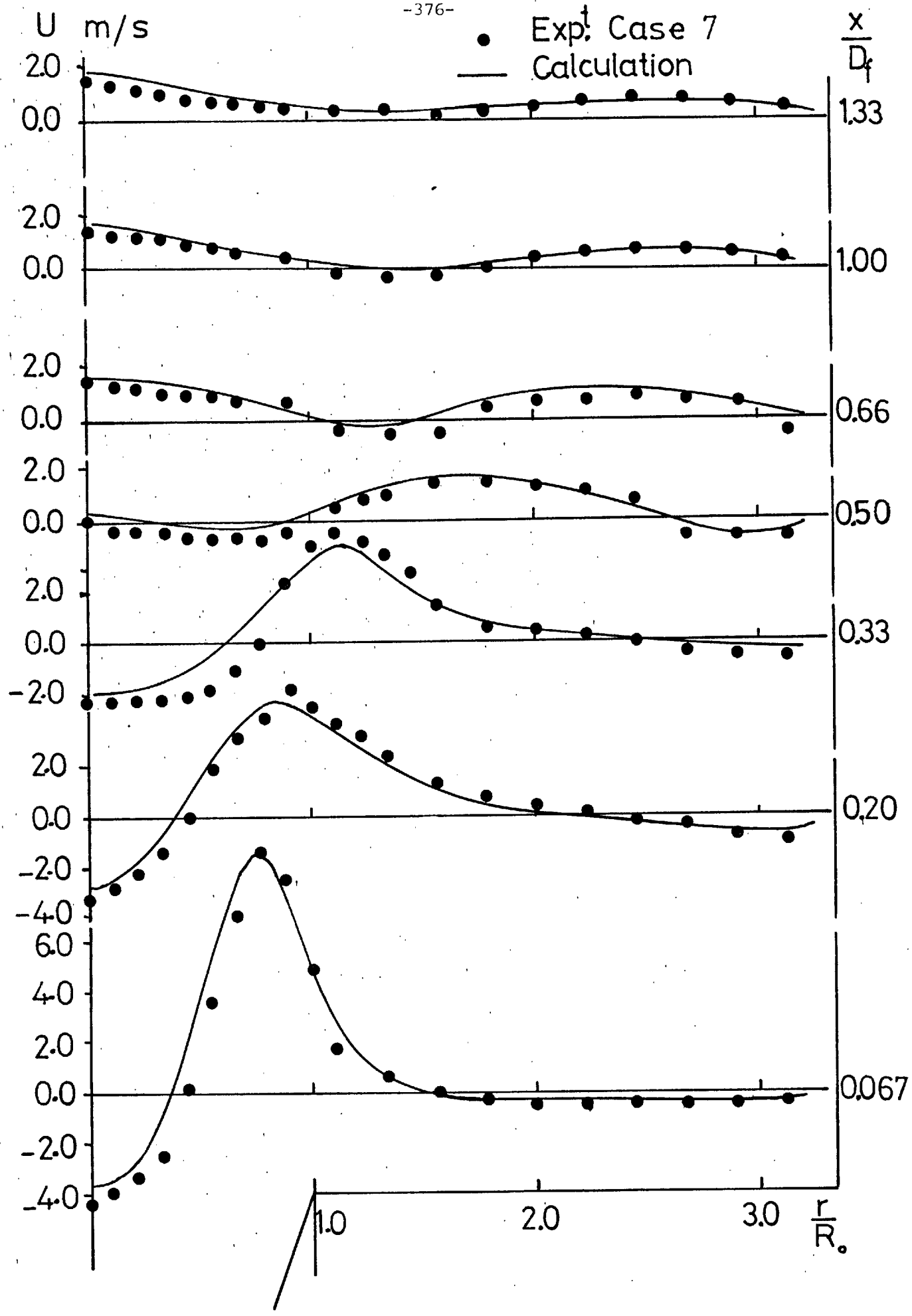

Figure 4.3.4: Measured and calculated profiles of mean axial velocity (case 7).

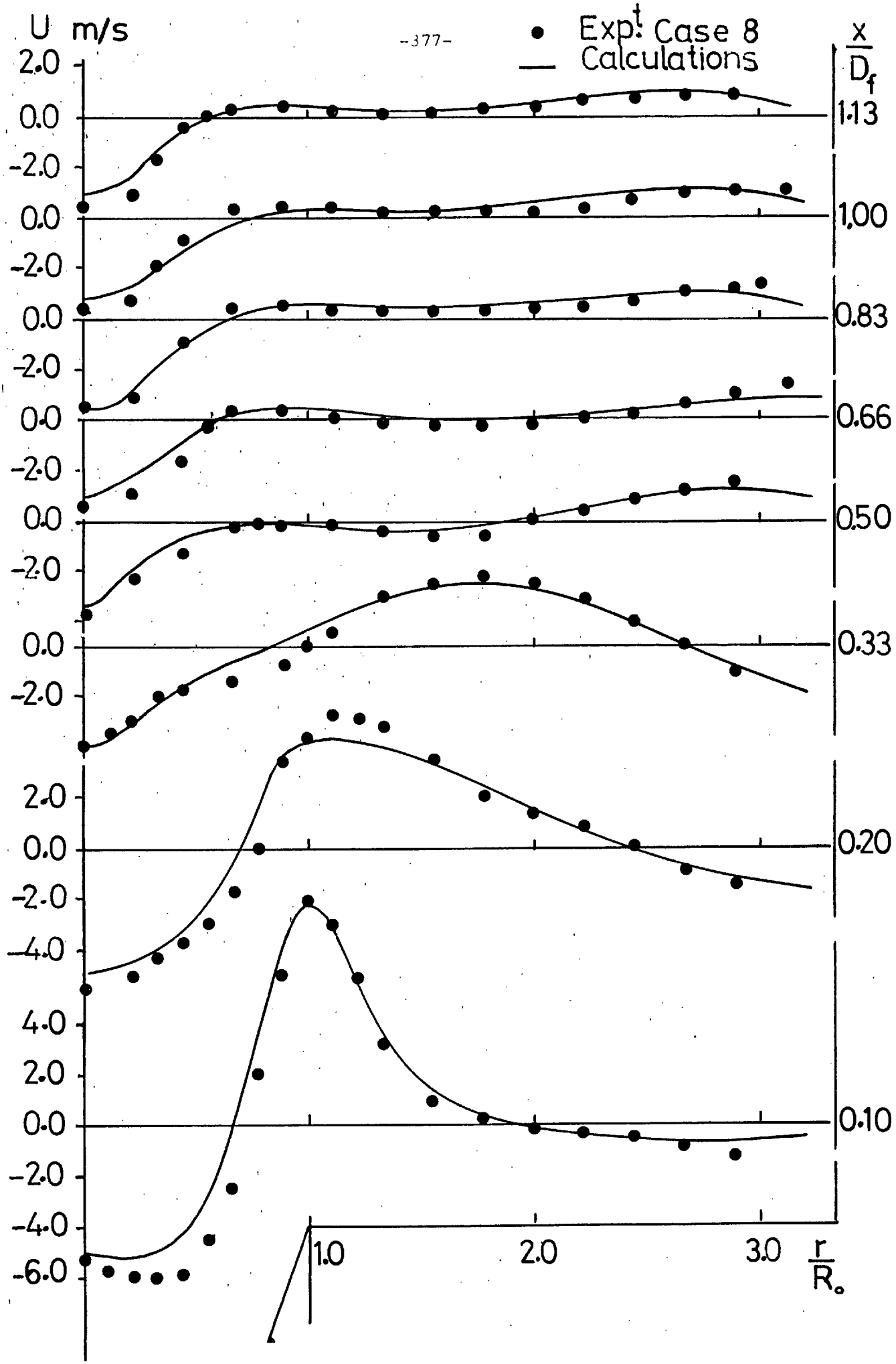

Figure 4.3.5: Measured and calculated profiles of mean axial velocity (case 8).

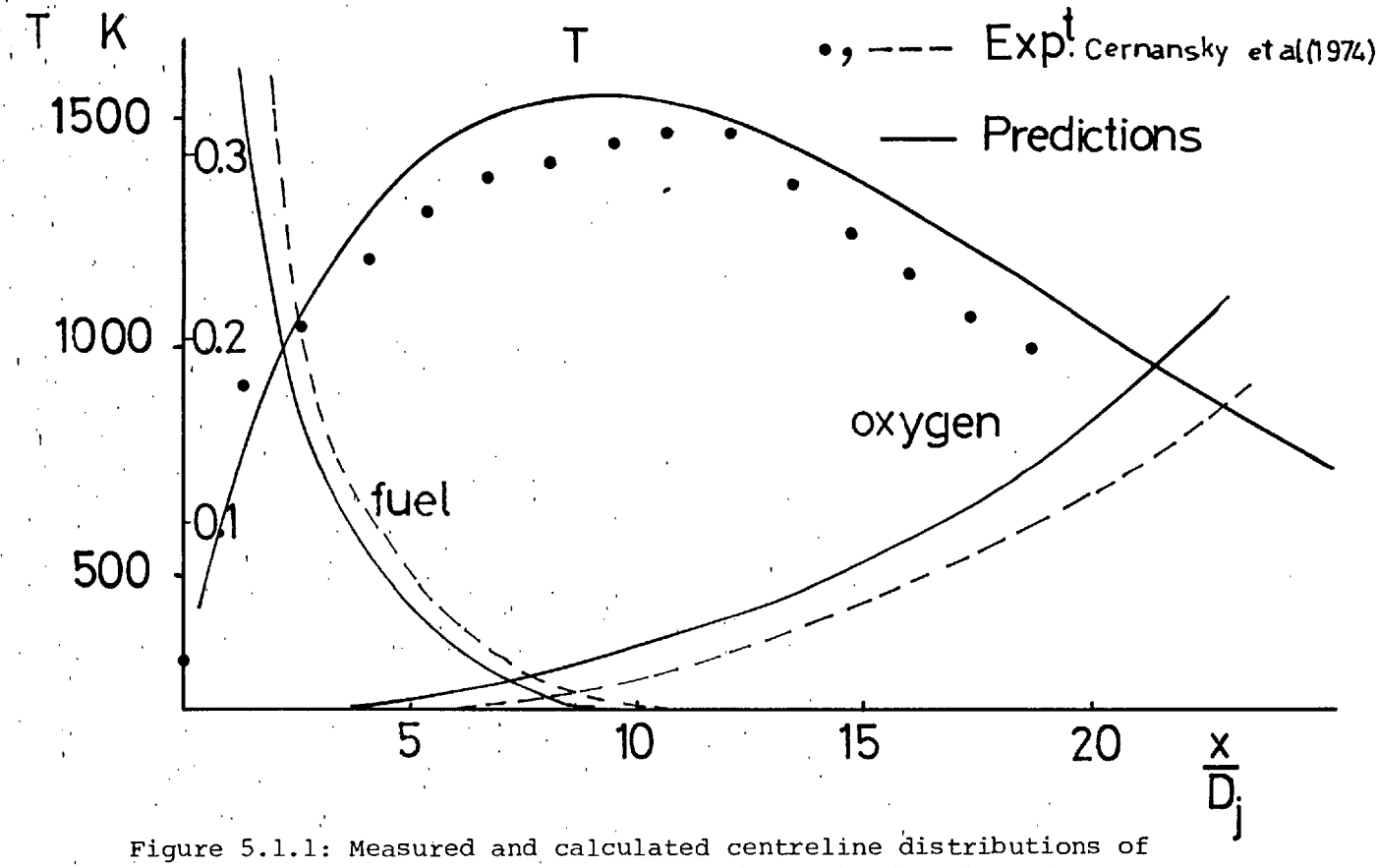

Figure 5.1.1: Measured and calculated centreline distributions of temperature, fuel and oxygen mole fractions in the furnace of Cernansky et al.

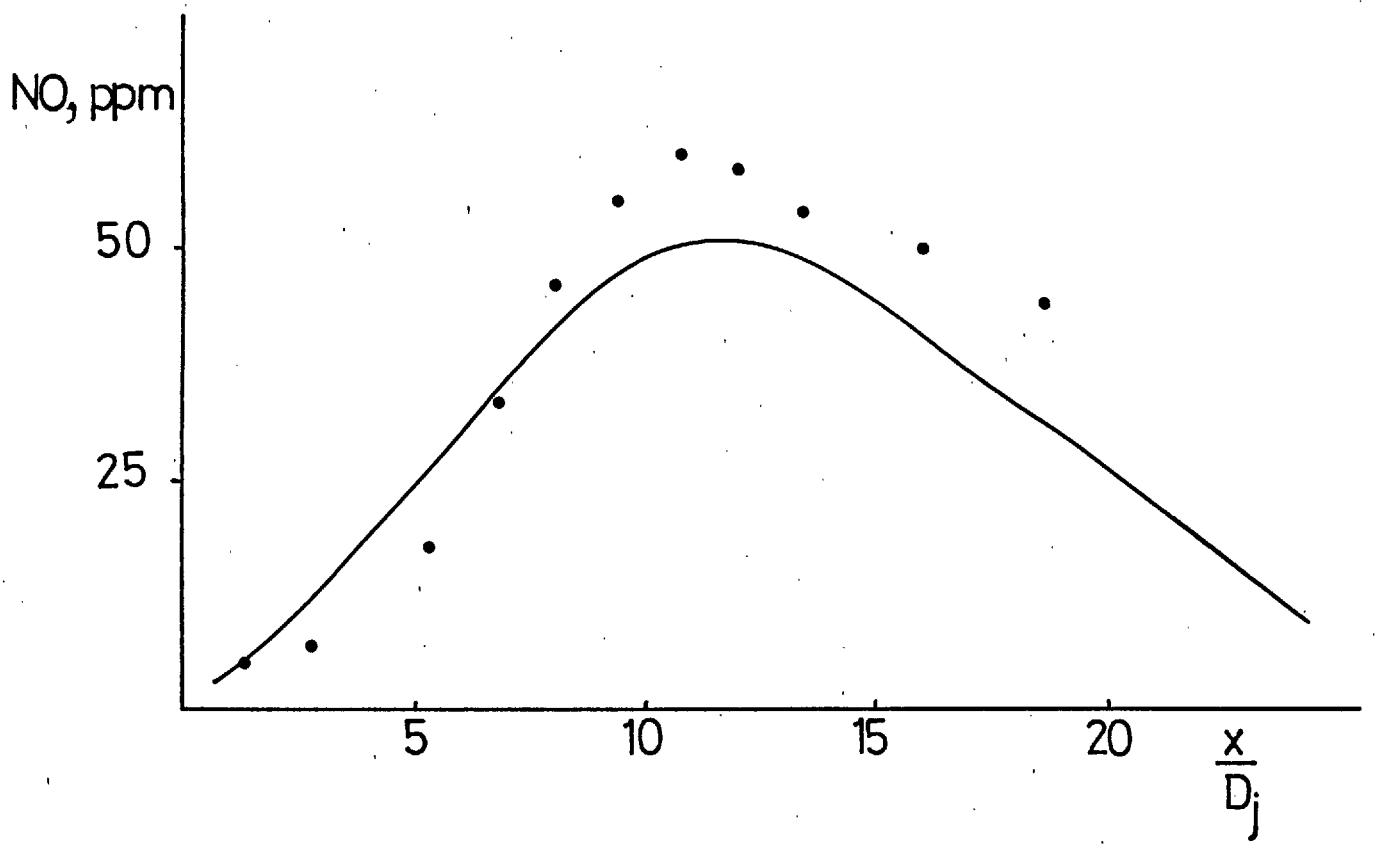

Figure 5.1.2: Measured and calculated centreline distributions of nitric oxide concentrations in the furnace of Cernansky et al.

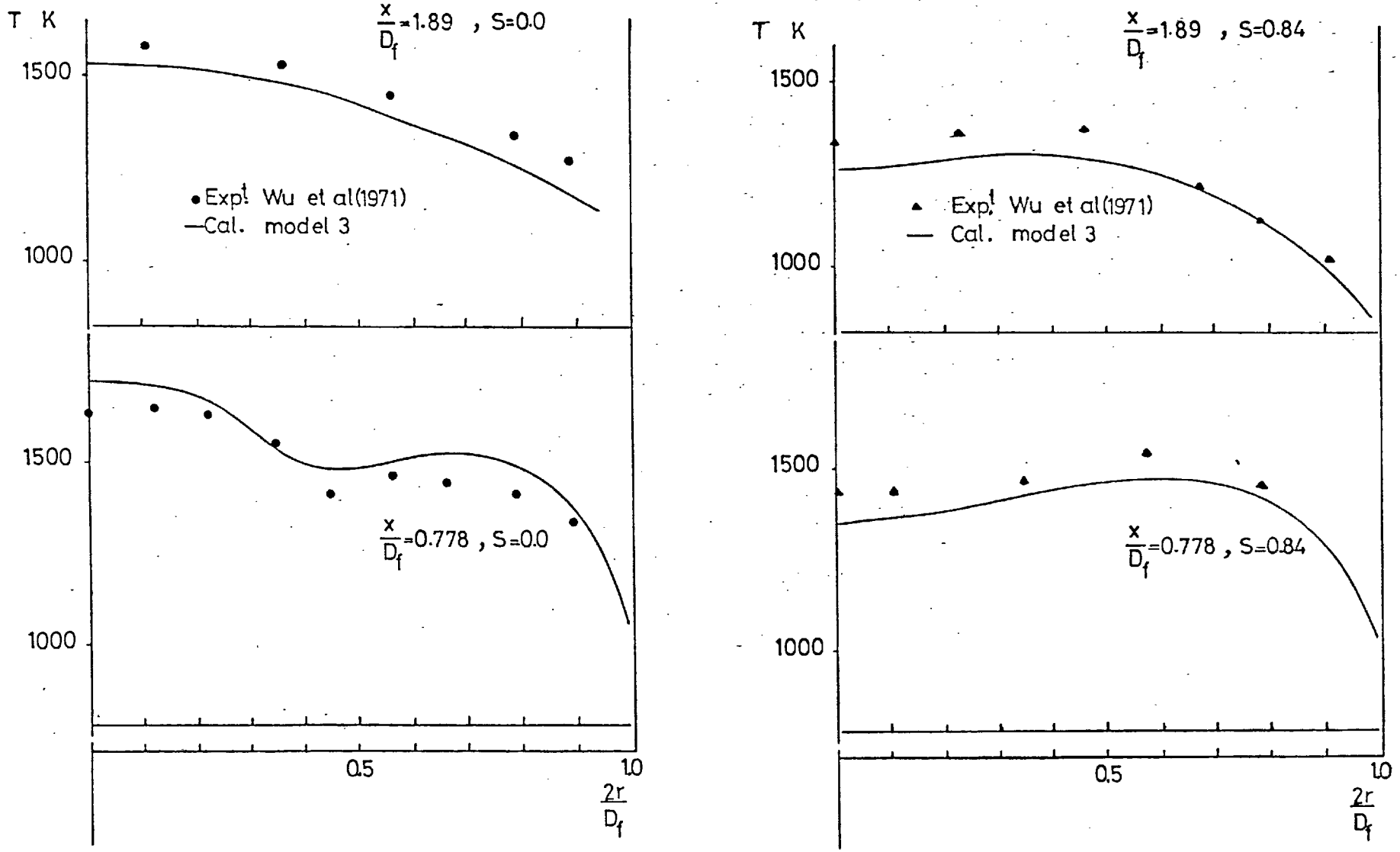

Figure 5.1.3: Measured and calculated profiles of mean temperature at zero and finite swirl in Delft furnace.

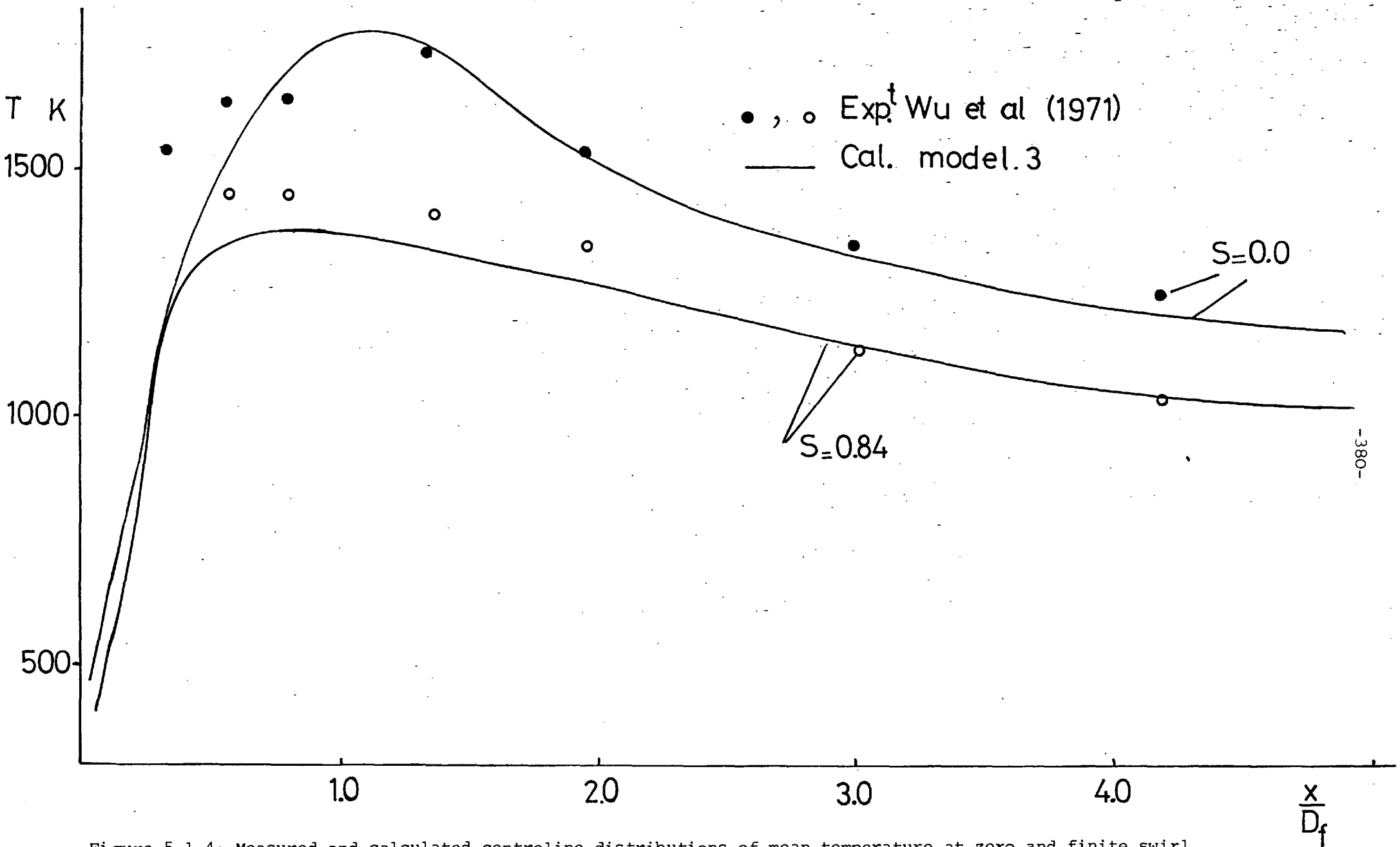

Figure 5.1.4: Measured and calculated centreline distributions of mean temperature at zero and finite swirl in Delft furnace.

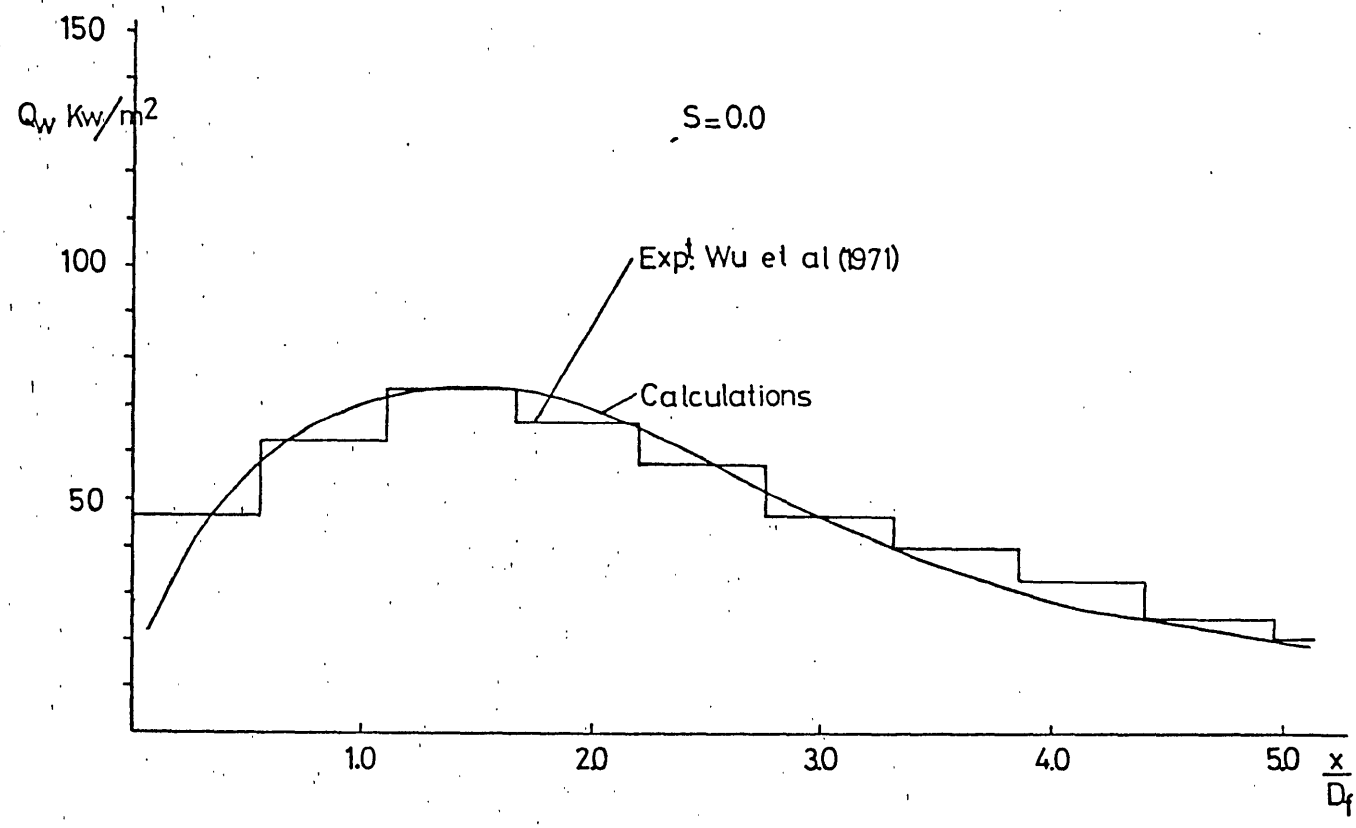

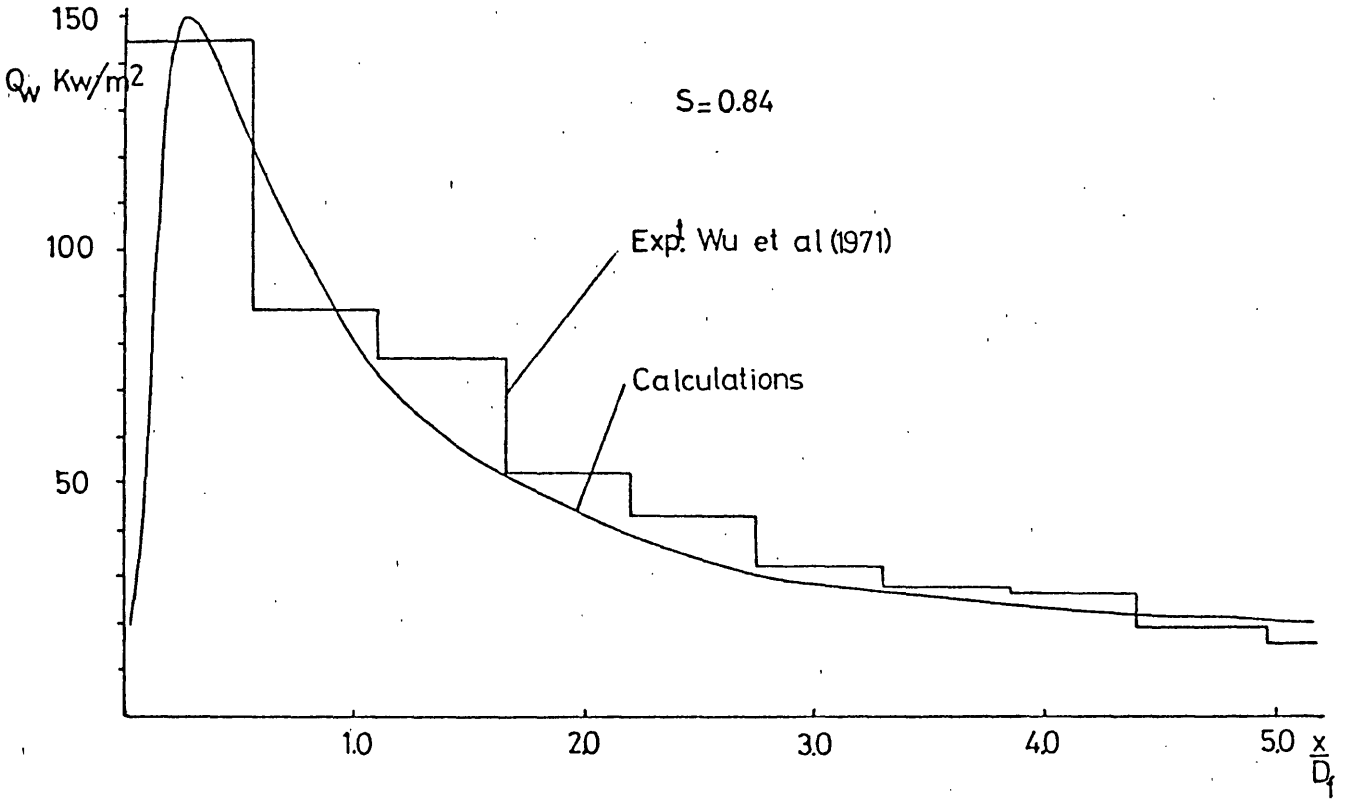

Figure 5.1.5: Measured and calculated distributions of wall heat flux in Delft furnace.

--- Exp.^{t} Beltagui et al (1974,1975)

—— Calculations.

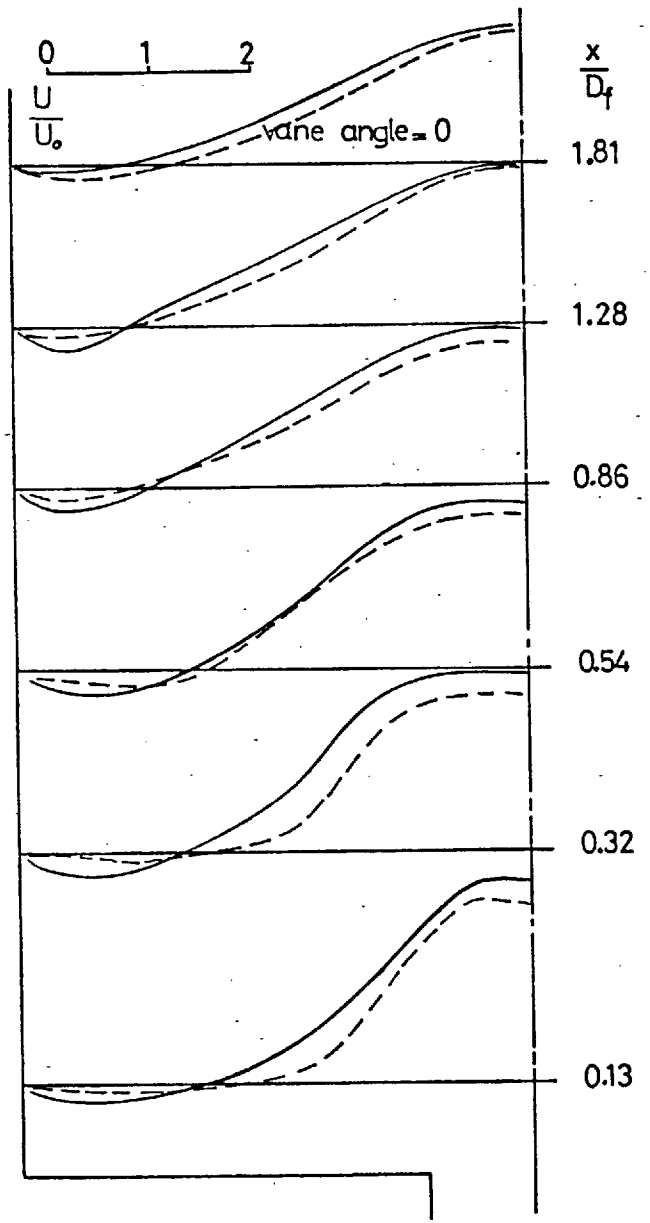

Figure 5.1.6:Measured and calculated mean axial velocity profiles

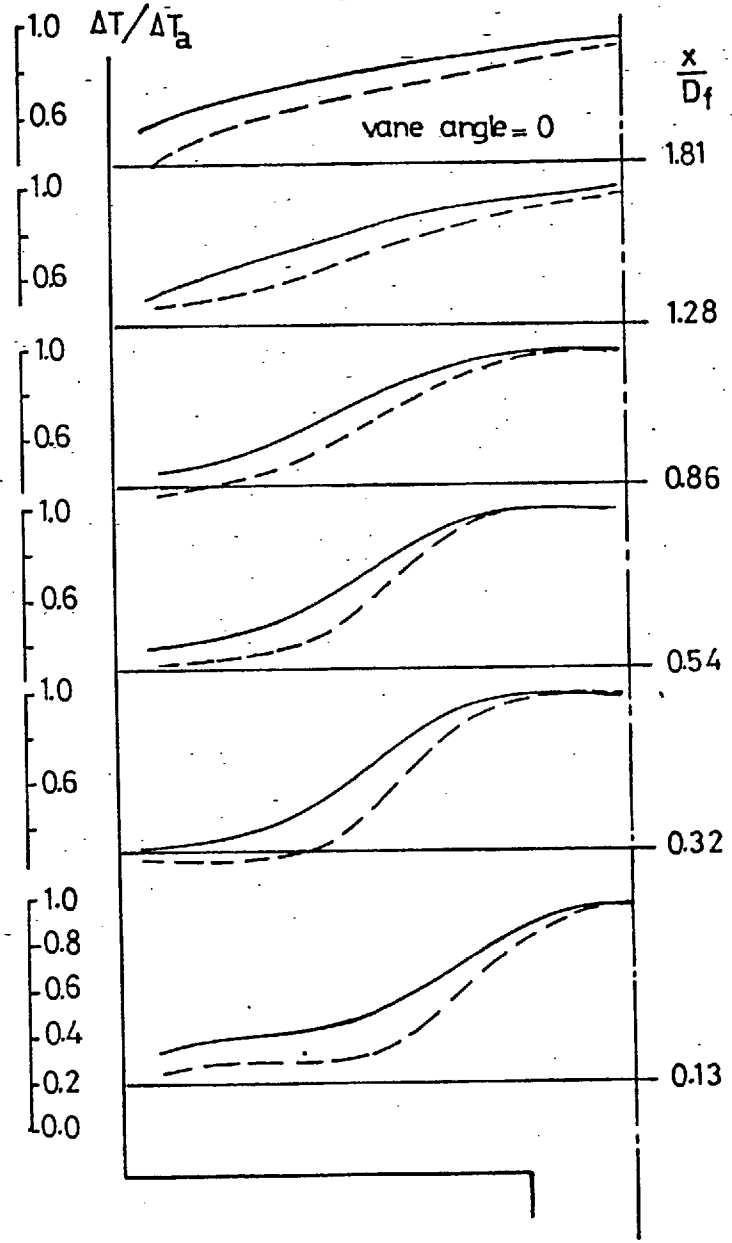

Figure 5.1.7:Measured and calculated mean gas temperature profiles.

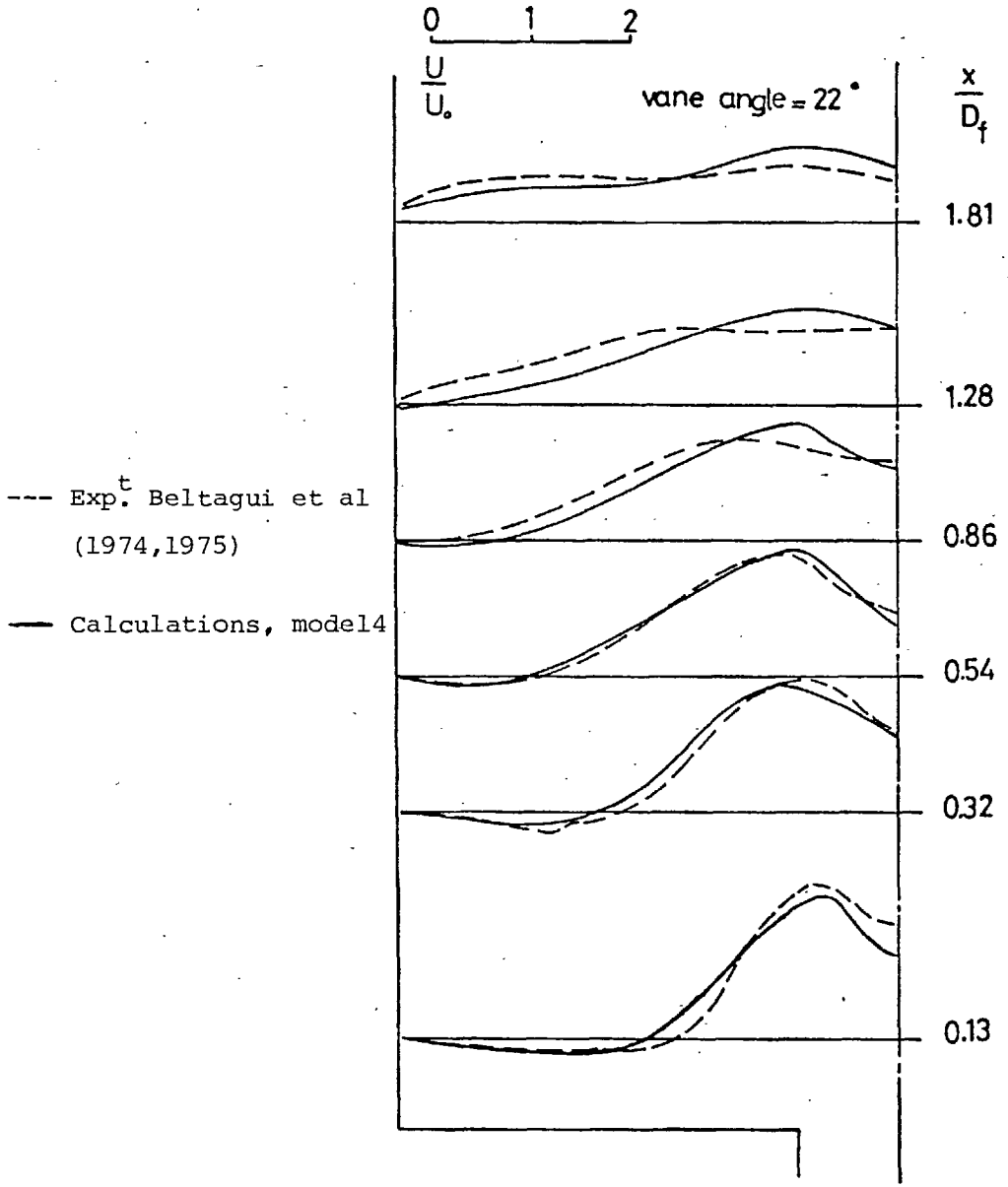

Figure 5.1.8:Measured and calculated mean axial velocity profiles.

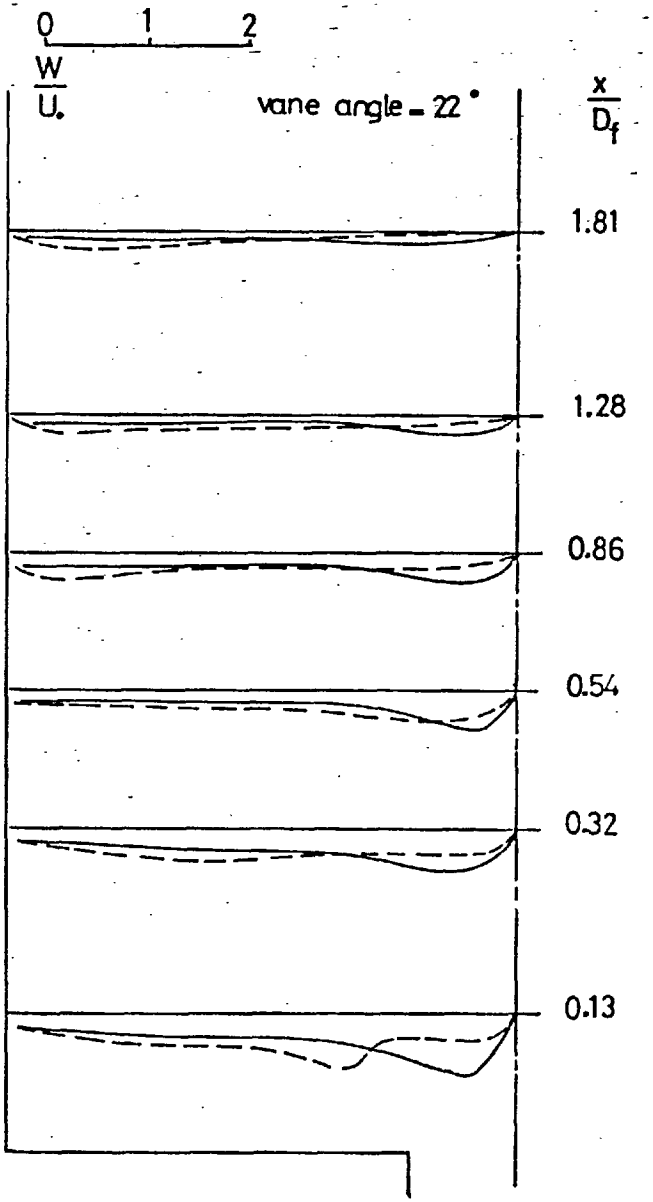

Figure 5.1.9:Measured and calculated mean tangential velocity profiles.

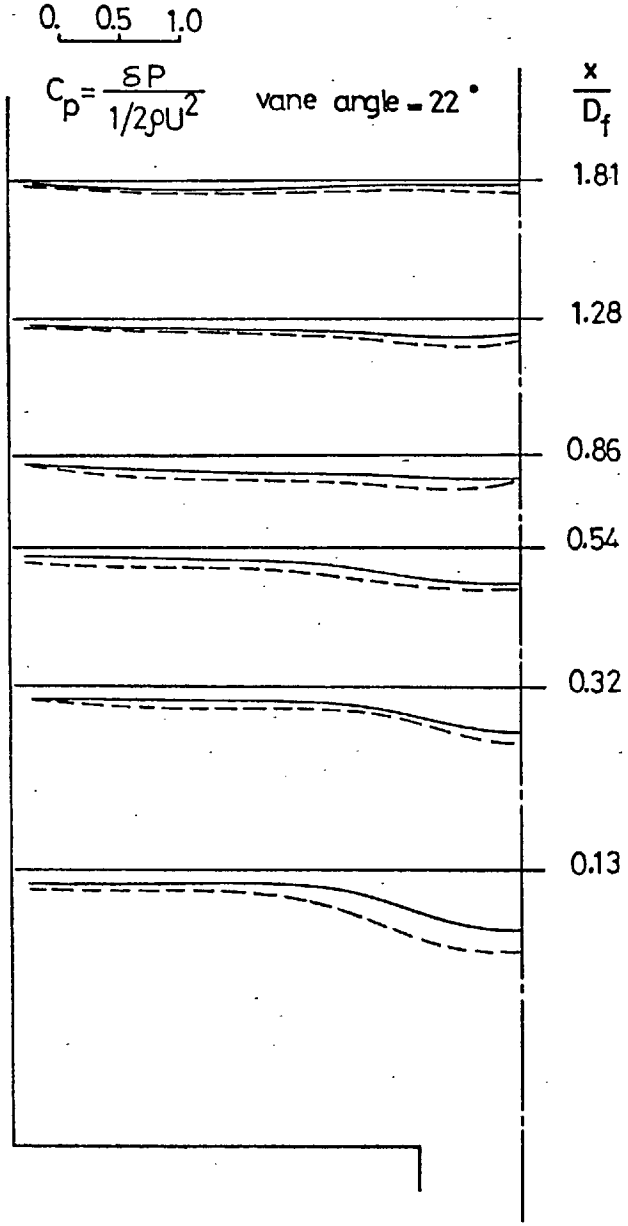

---Exp.[t] Beltagui et al (1974,1975)

——Calculations,model4

Figure 5.1.10:Measured and calculated pressure coefficient profiles

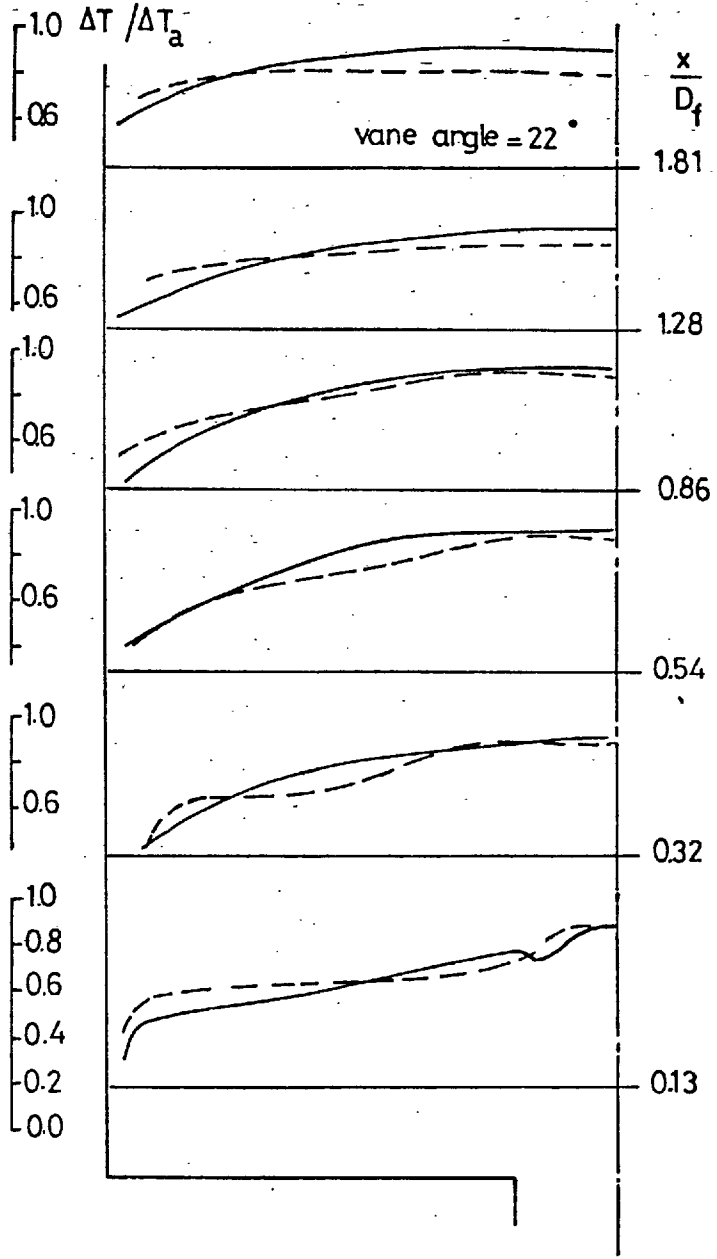

Figure 5.1.11:Measured and calculated mean gas temperature profiles.

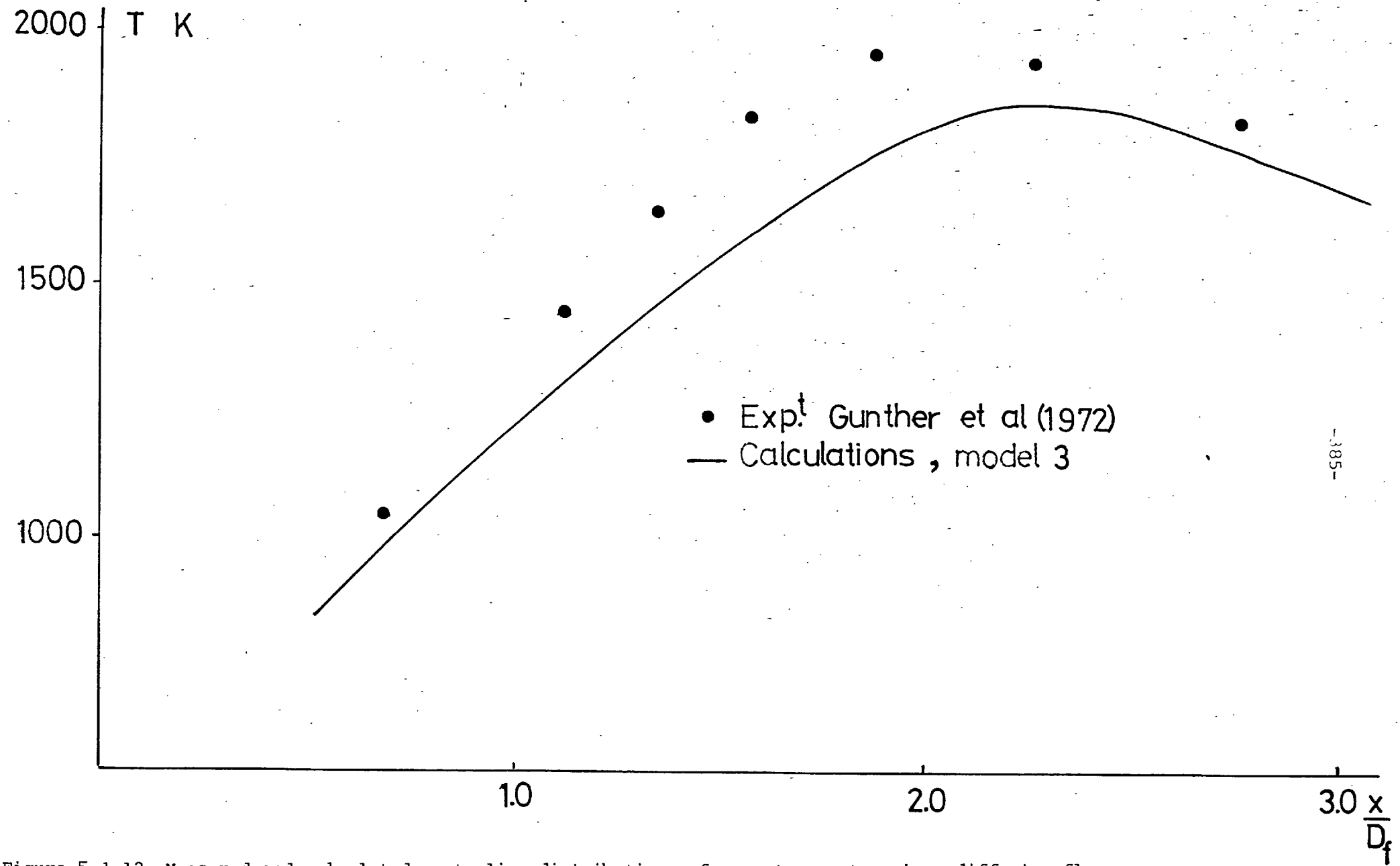

Figure 5.1.12: Measured and calculated centreline distributions of mean temperature in a diffusion flame.

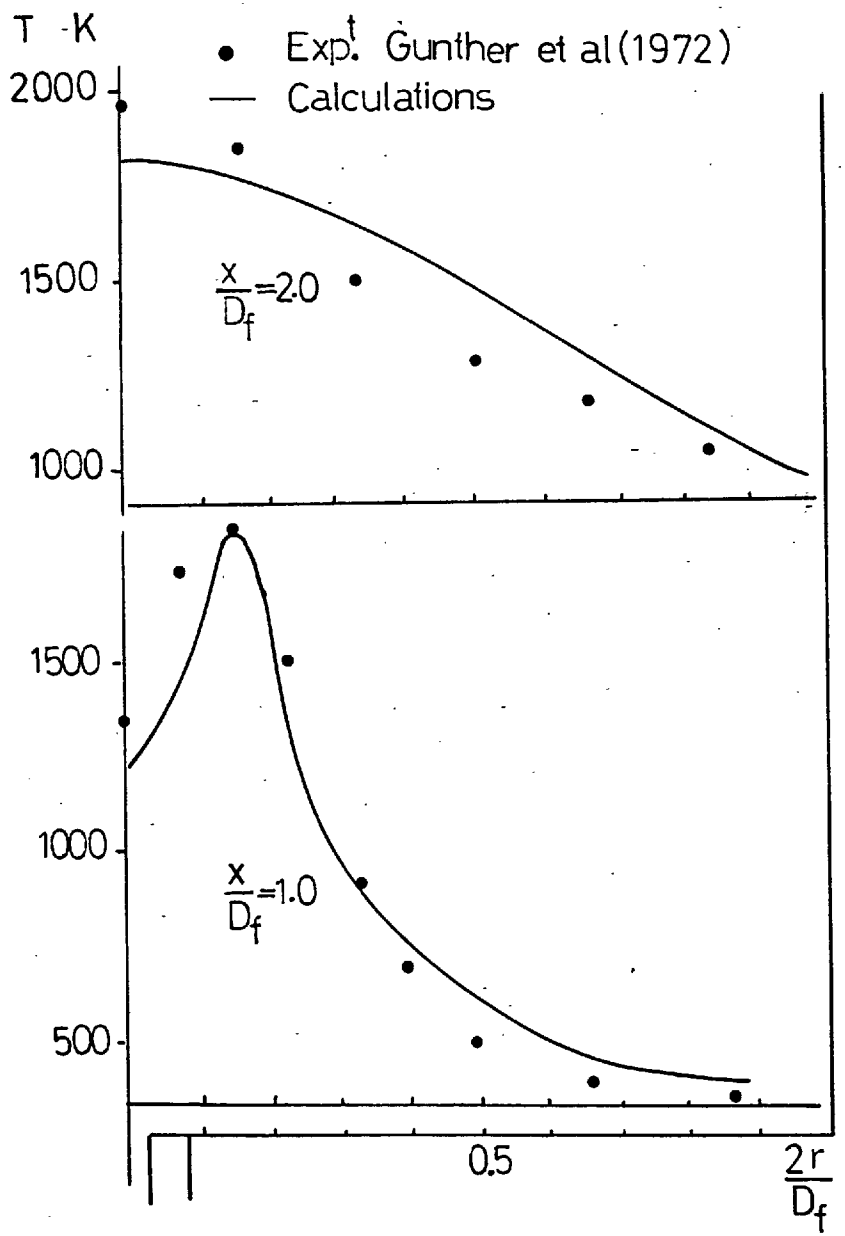

Figure 5.1.13: Measured and calculated profiles of mean temperature.

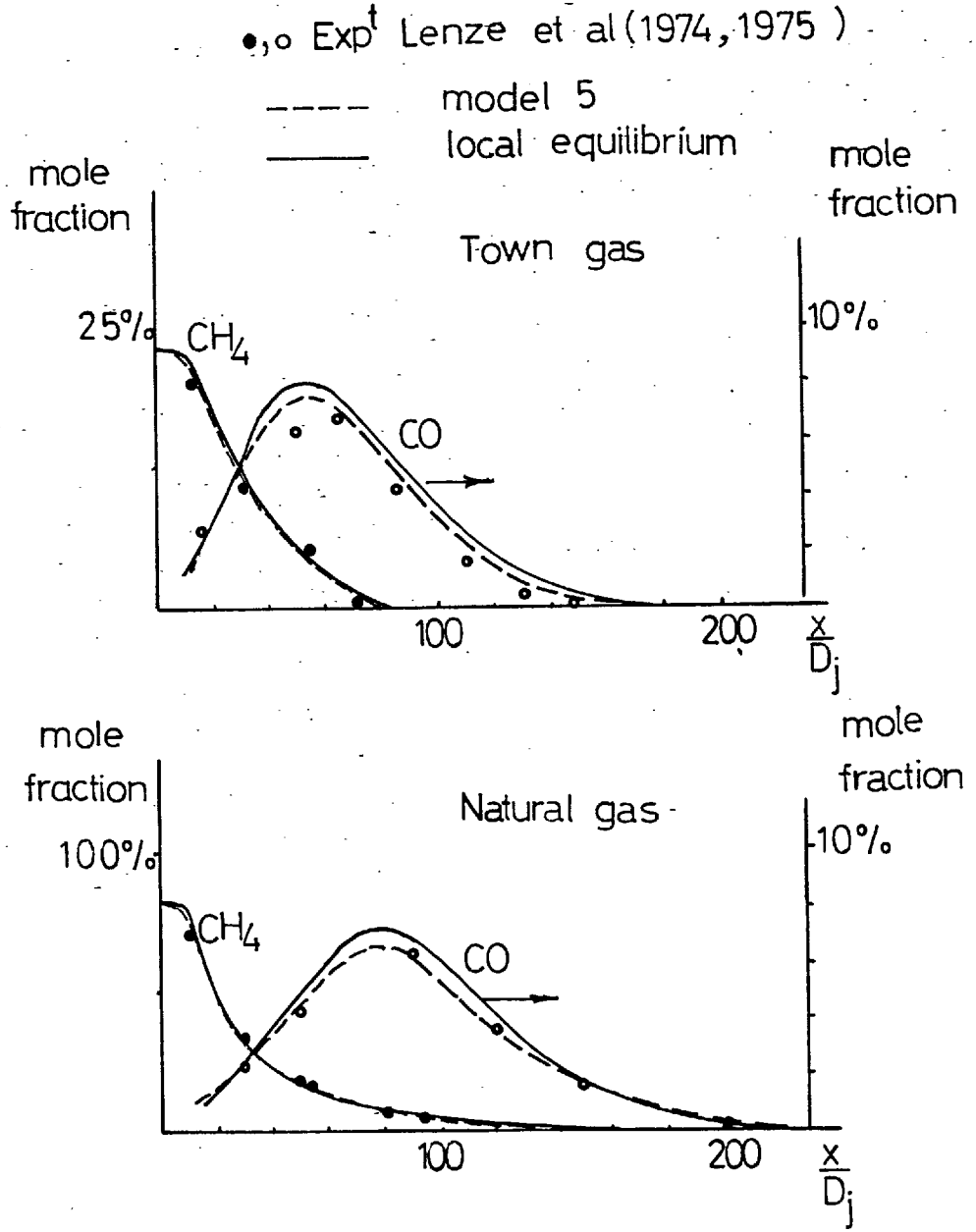

Figure 5.1.14: Measured and calculated centreline distributions of CO and CH_4.

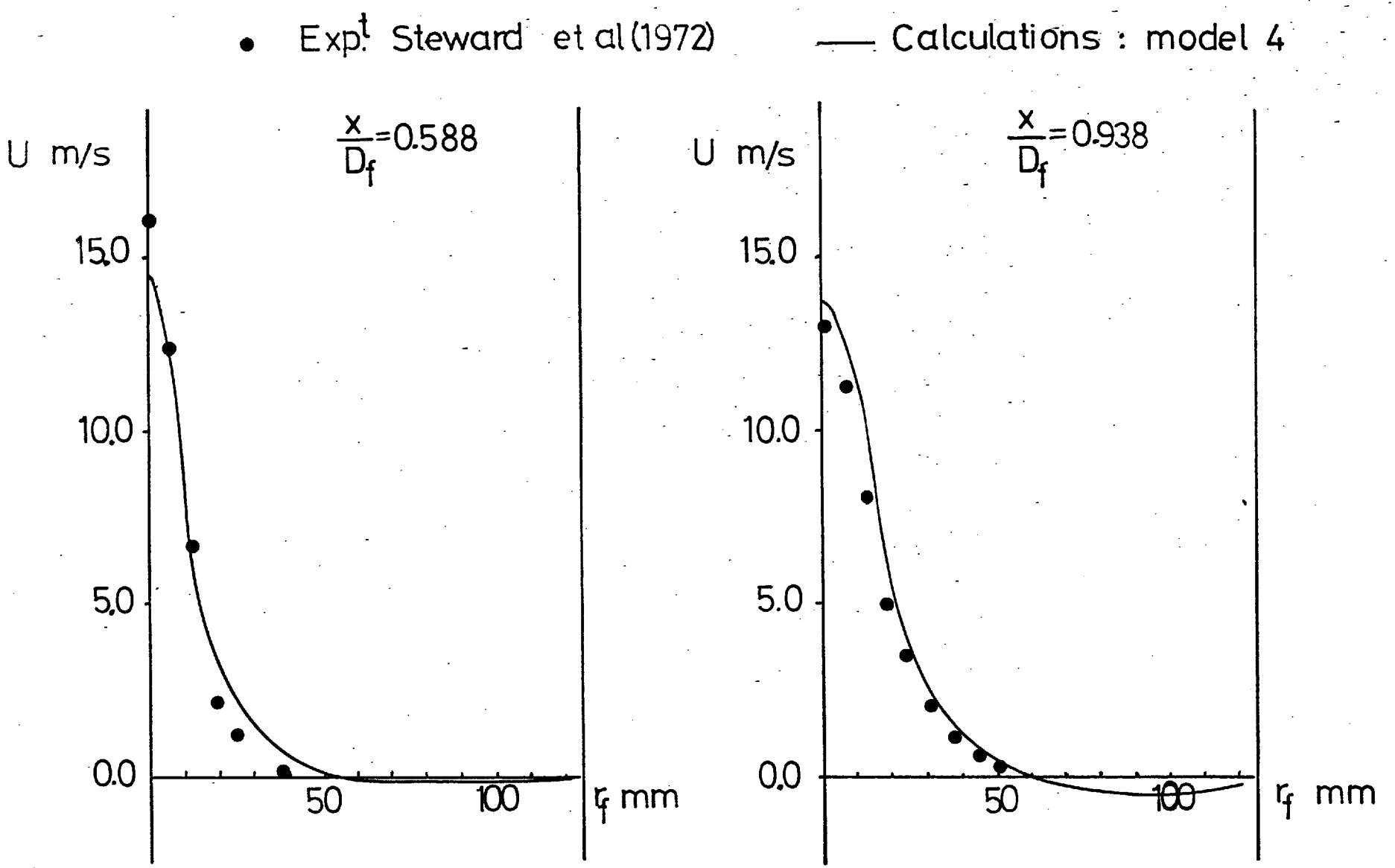

Figure 5.1.15: Measured and calculated profiles of mean axial velocity in the furnace of Steward et al(1972).

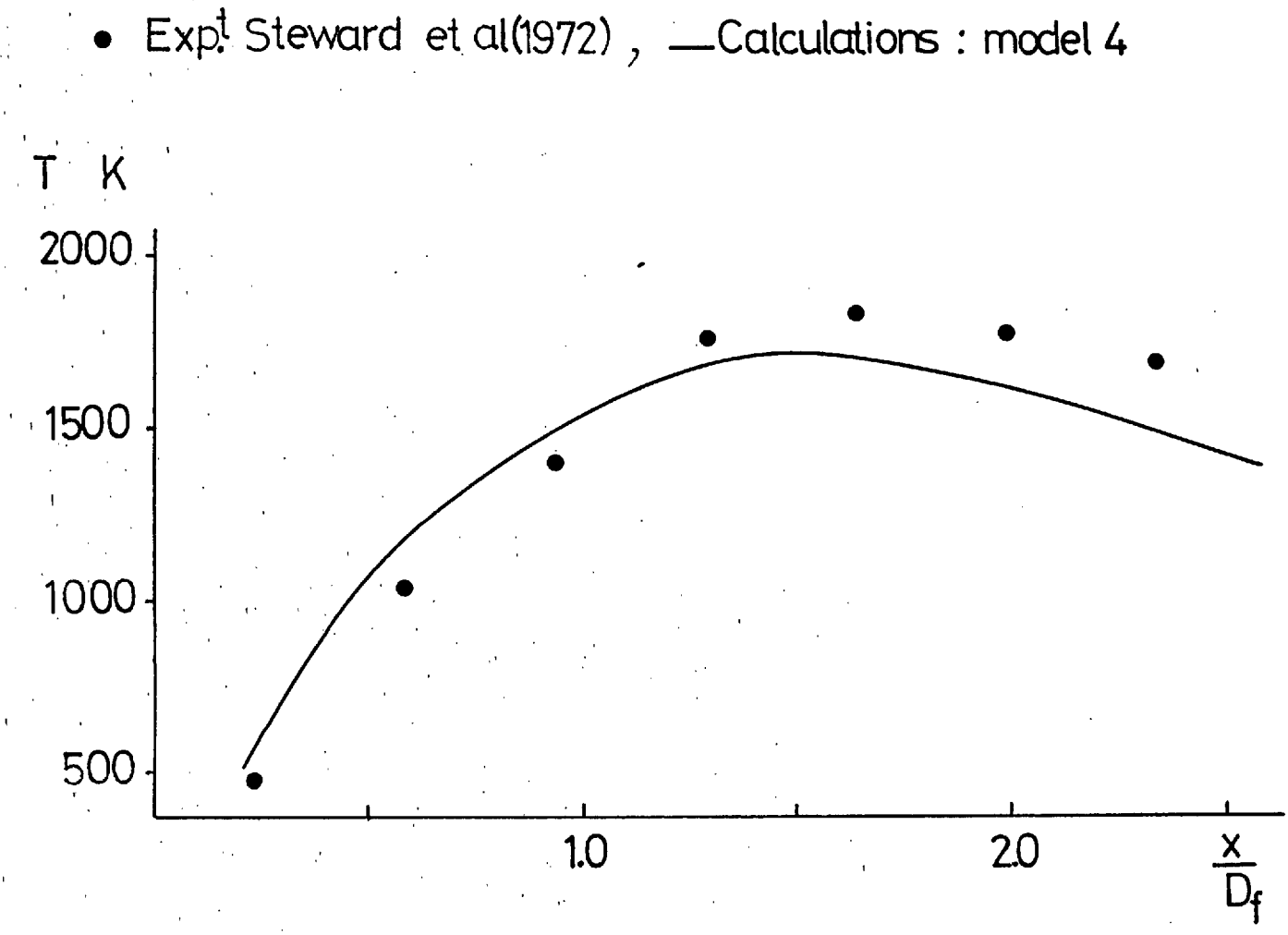

Figure 5.1.16: Measured and calculated centreline distribution of mean temperature in the furnace of Sreward et al (1972).

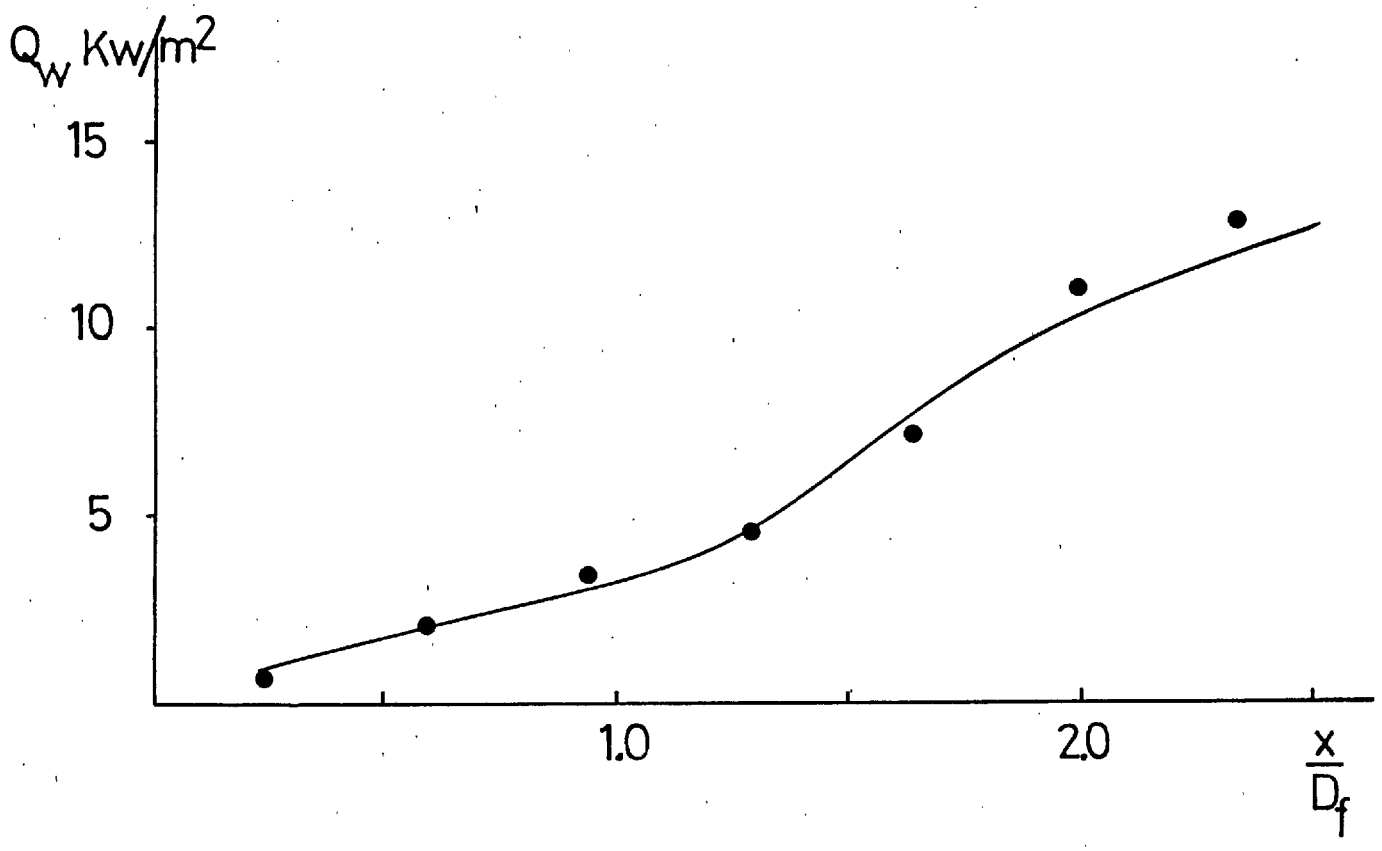

Figure 5.1.17: Measured and calculated distribution of wall heat flux in the furnace of Steward et al(1972).

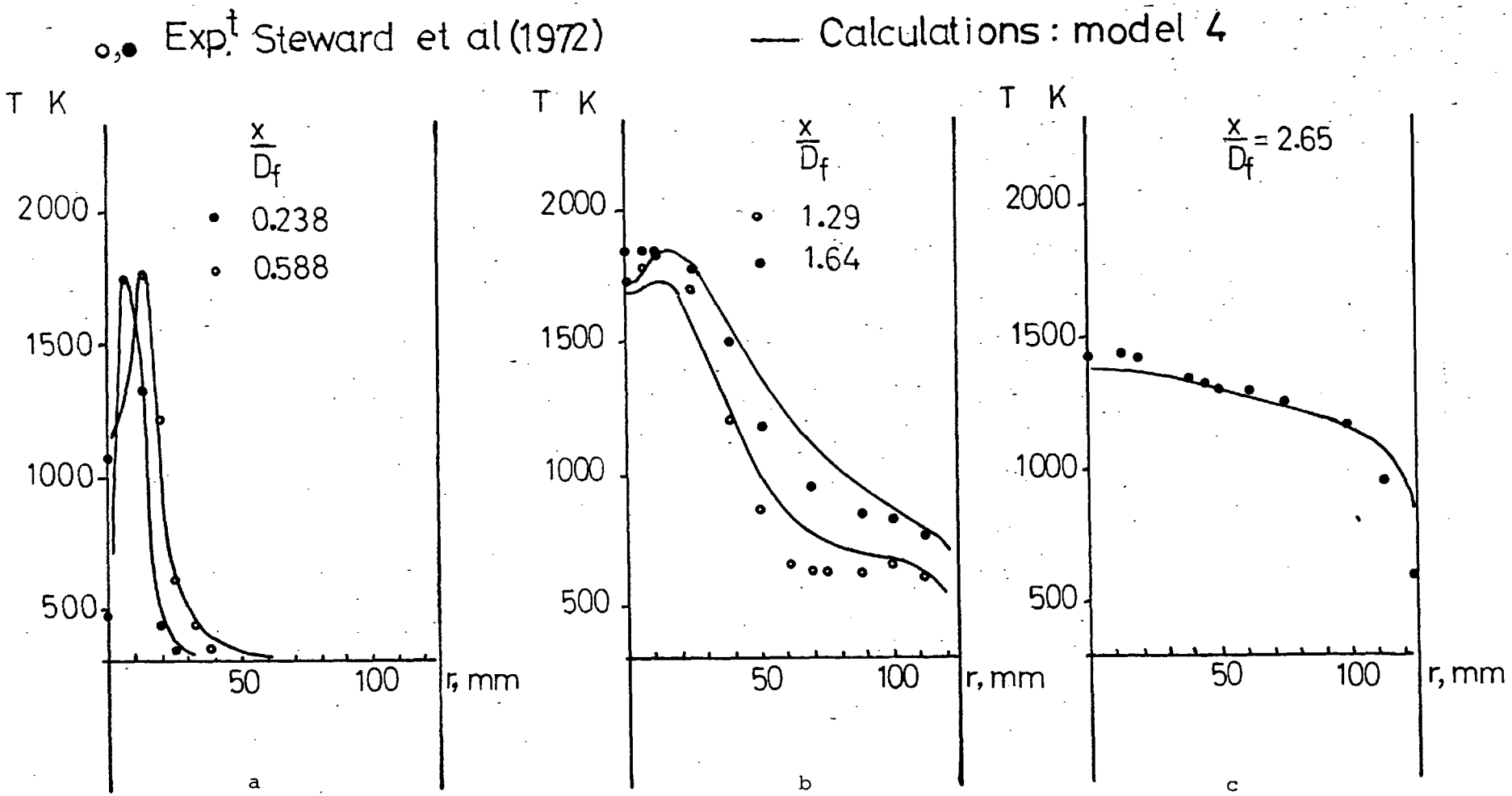

Figure 5.1.18: Measured and calculated profiles of mean temperature in the furnace of Steward et al(1972).

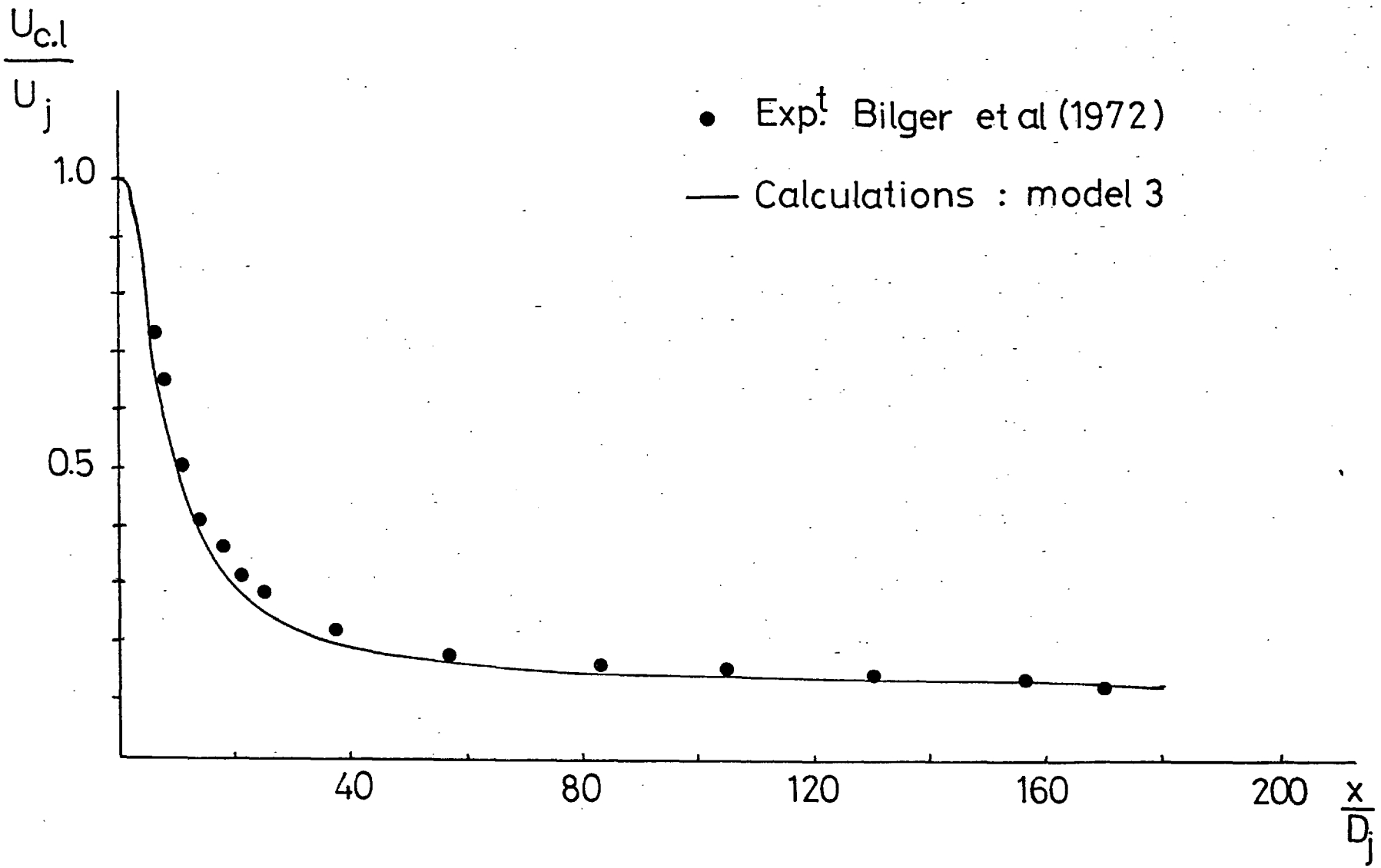

Figure 5.1.19:Measured and calculated centreline distribution of mean axial velocity in the furnace of Bilger et al.

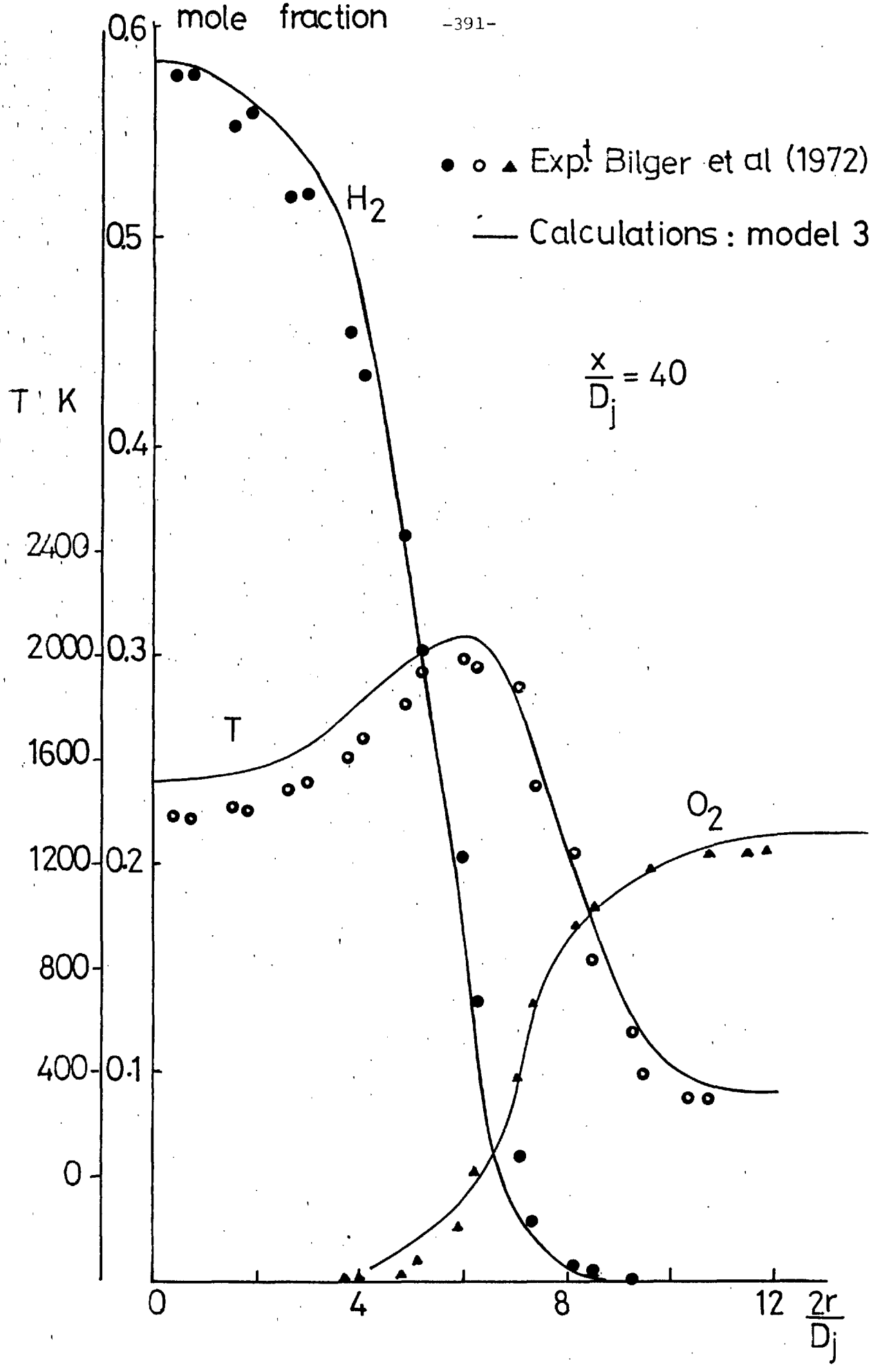

Figure 5.1.20:Measured and calculated profiles of hydrogen and oxygen mole fractions and temperature in the furnace of Bilger et al.

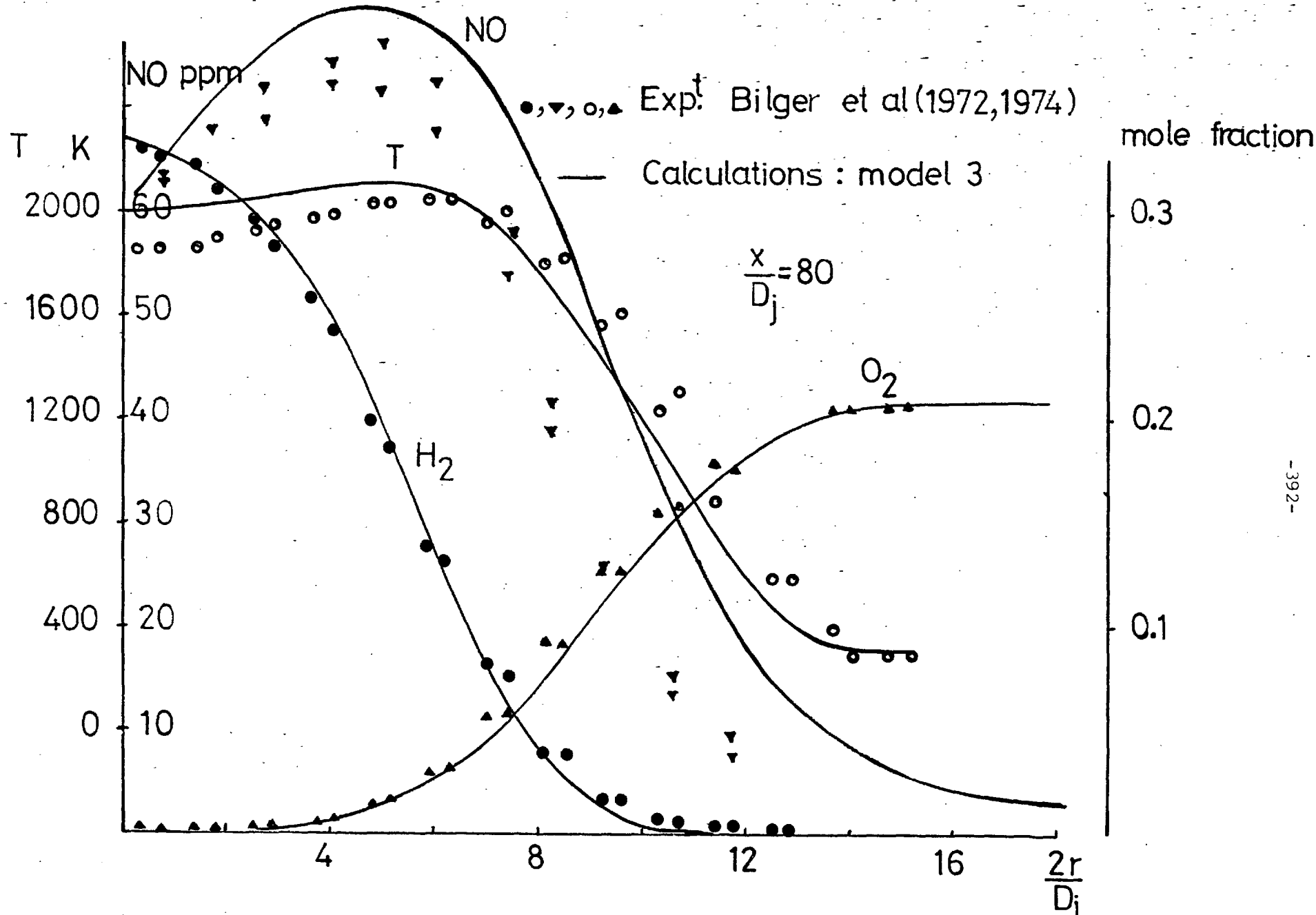

Figure 5.1.21:Measured and calculated profiles of hydrogen and oxygen mole fractions,mean temperature, and nitric oxide concentrations in the furnace of Bilger et al.

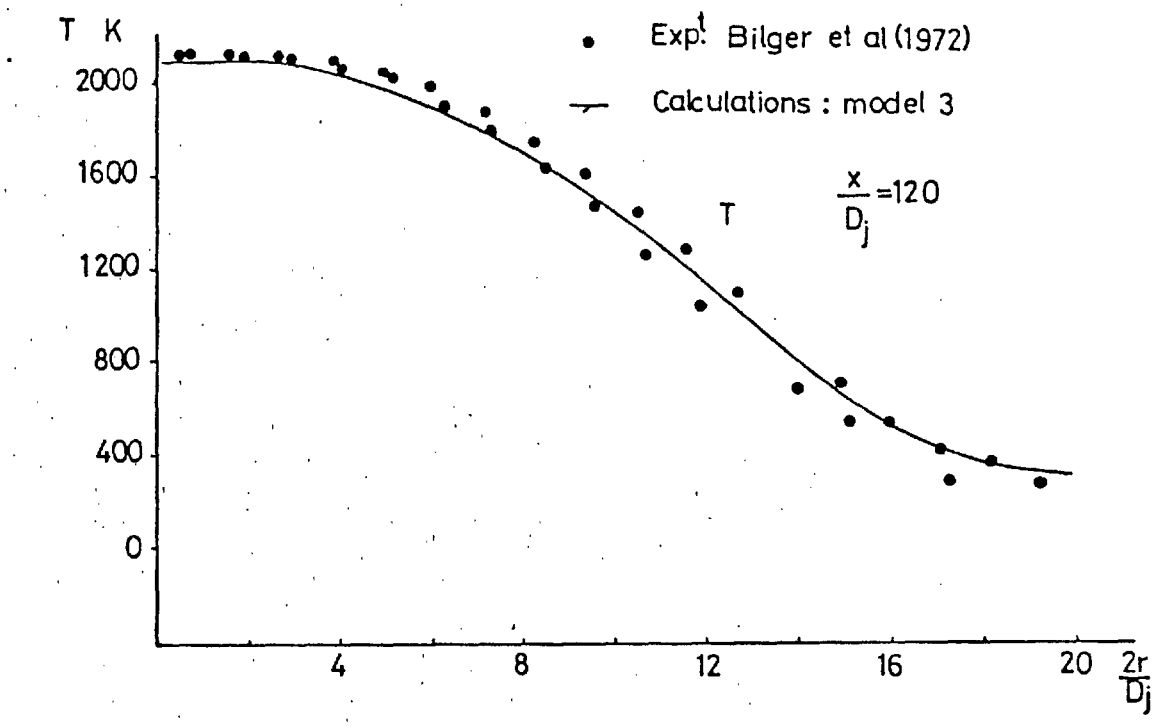

Figure 5.1.22:Measured and calculated profiles of mean gas temperature in the furnace of Bilger et al.

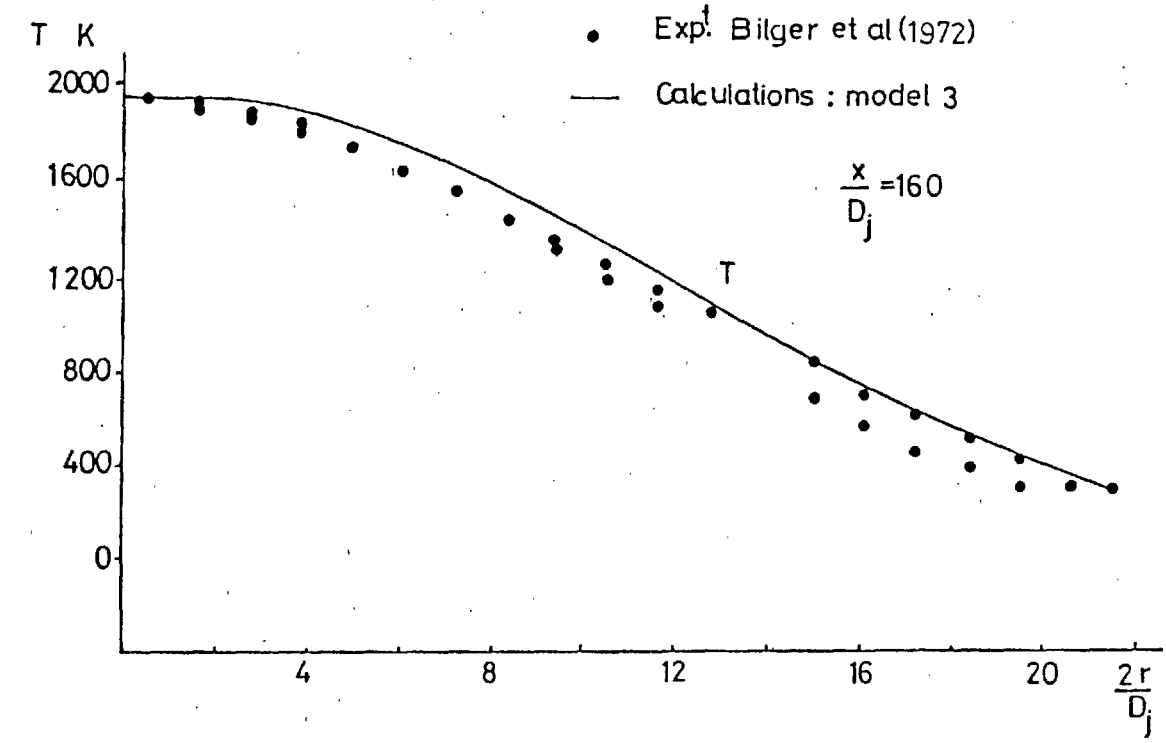

Figure 5.1.23:Measured and calculated profiles of mean gas temperature in the furnace of Bilger et al.

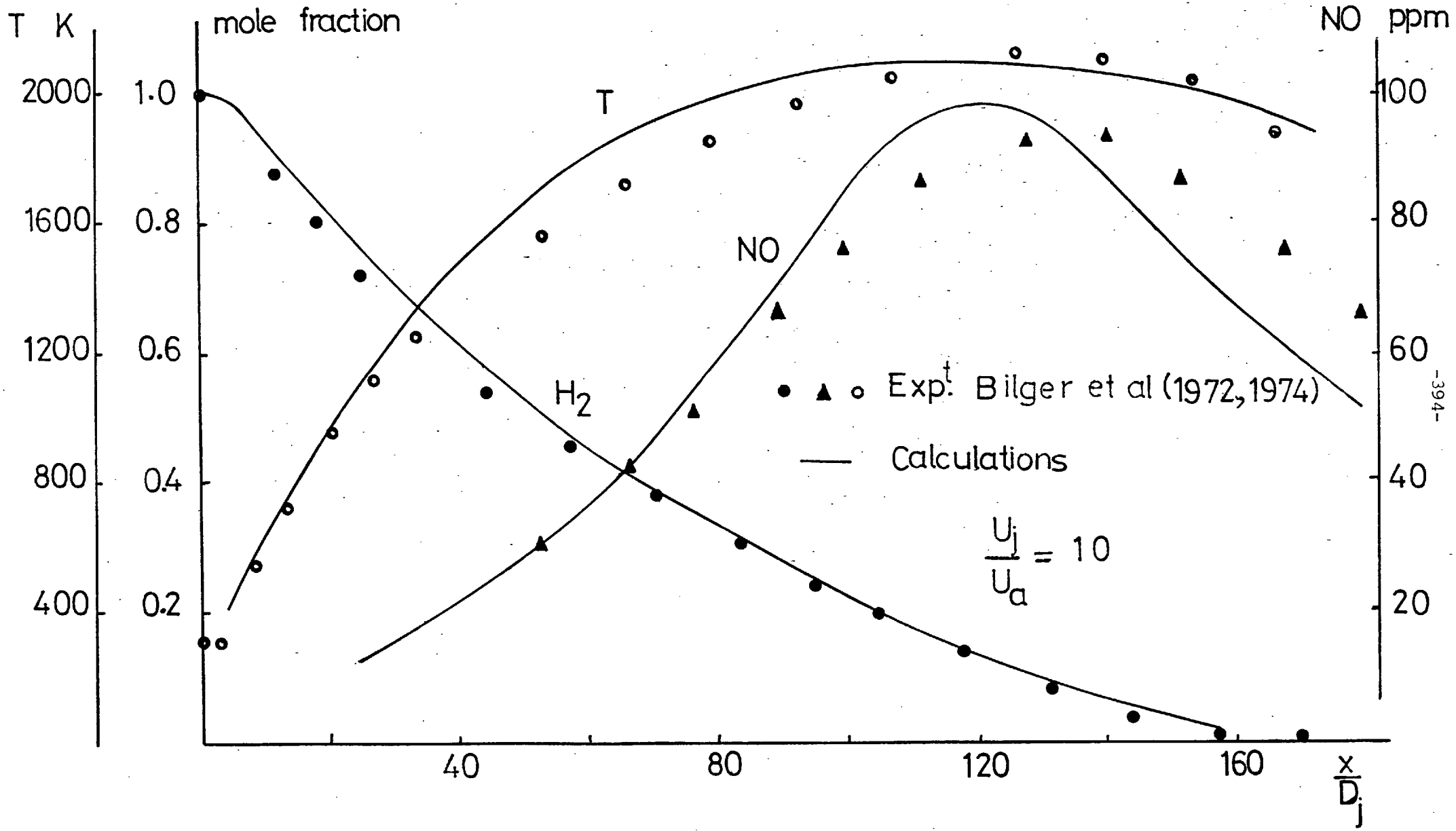

Figure 5.1.24:Measured and calculated centreline distributions of temperature,hydrogen and NO in the furnace of Bilger et al

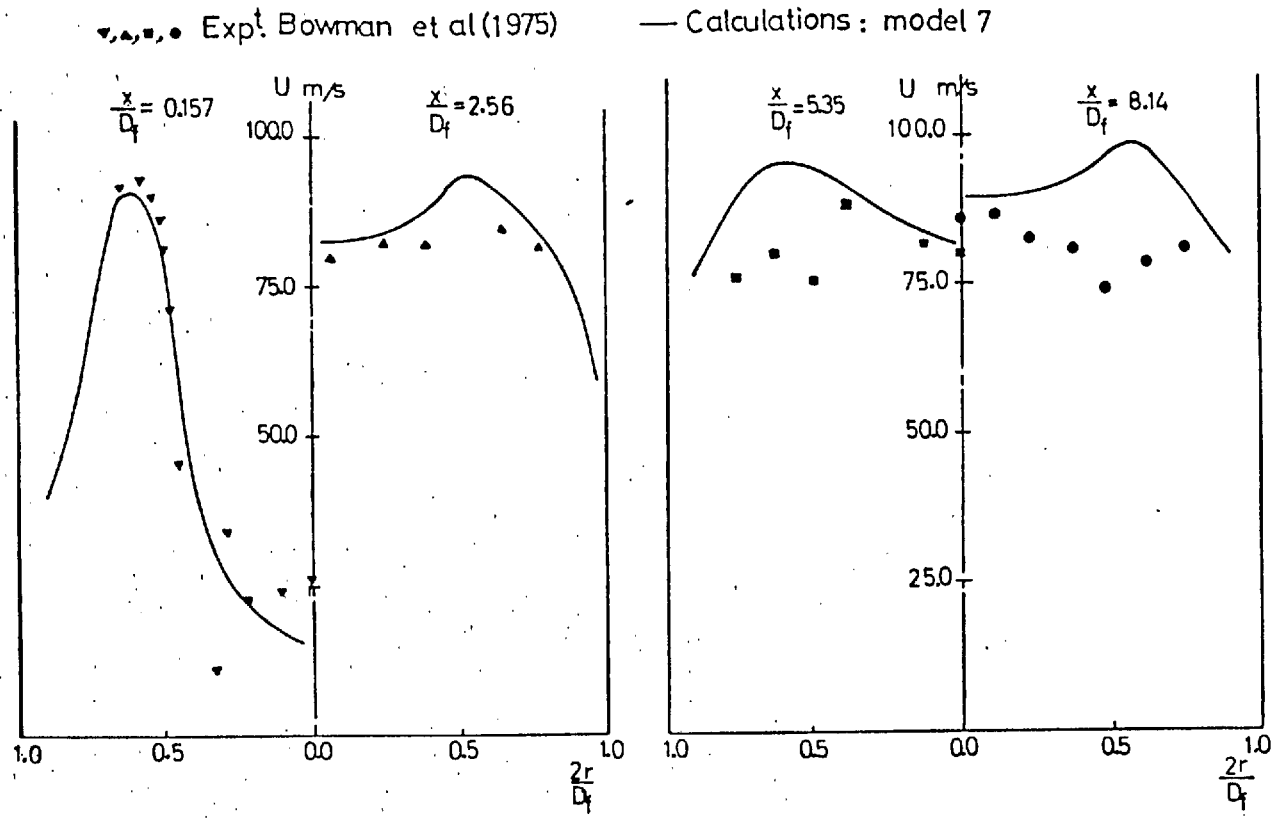

Figure 5.1.25:Measured and calculated profiles of mean axial velocity in the furnace of Bowman et al (1975).

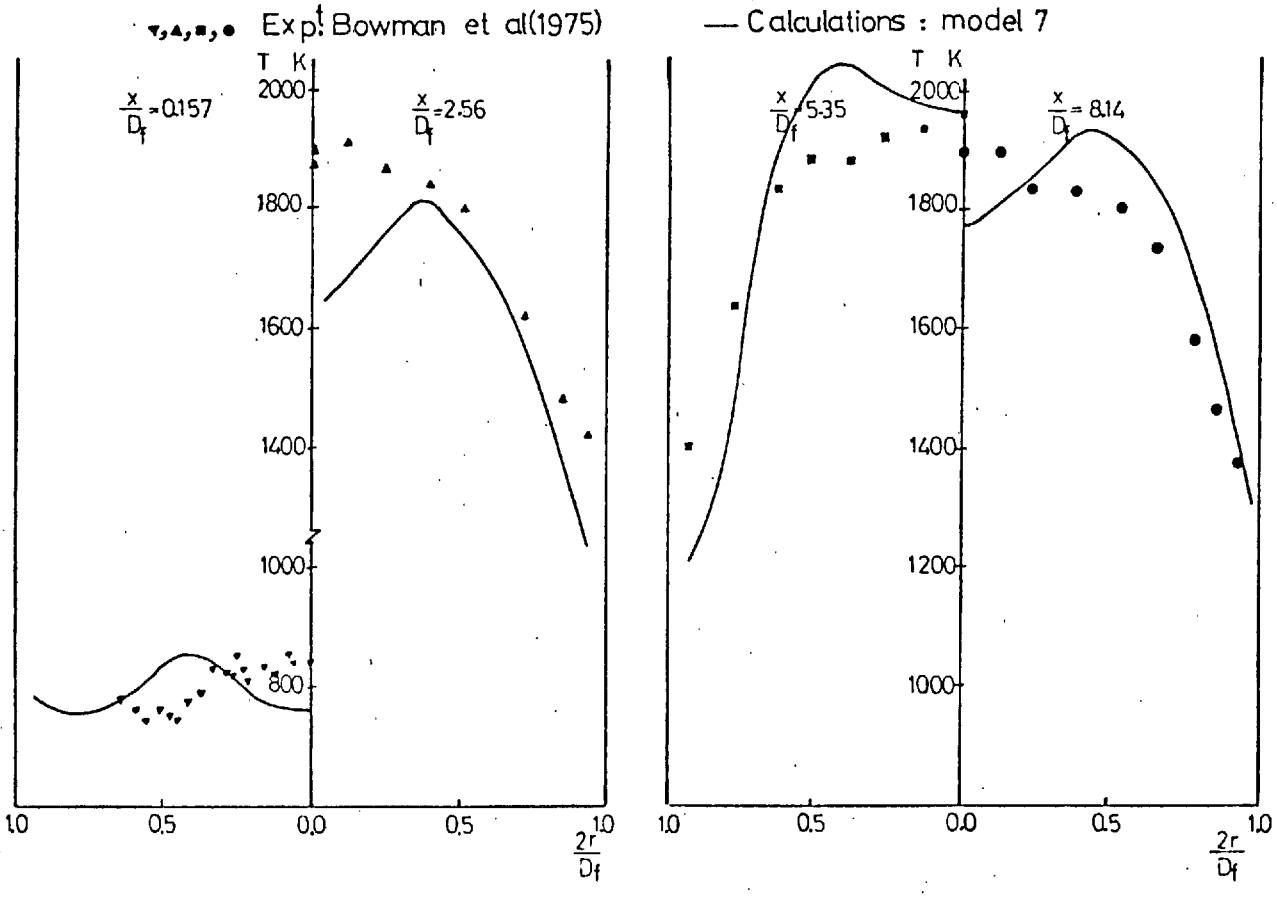

Figure 5.1.26:Measured and calculated profiles of mean gas temperature in the furnace of Bowman et al (1975).

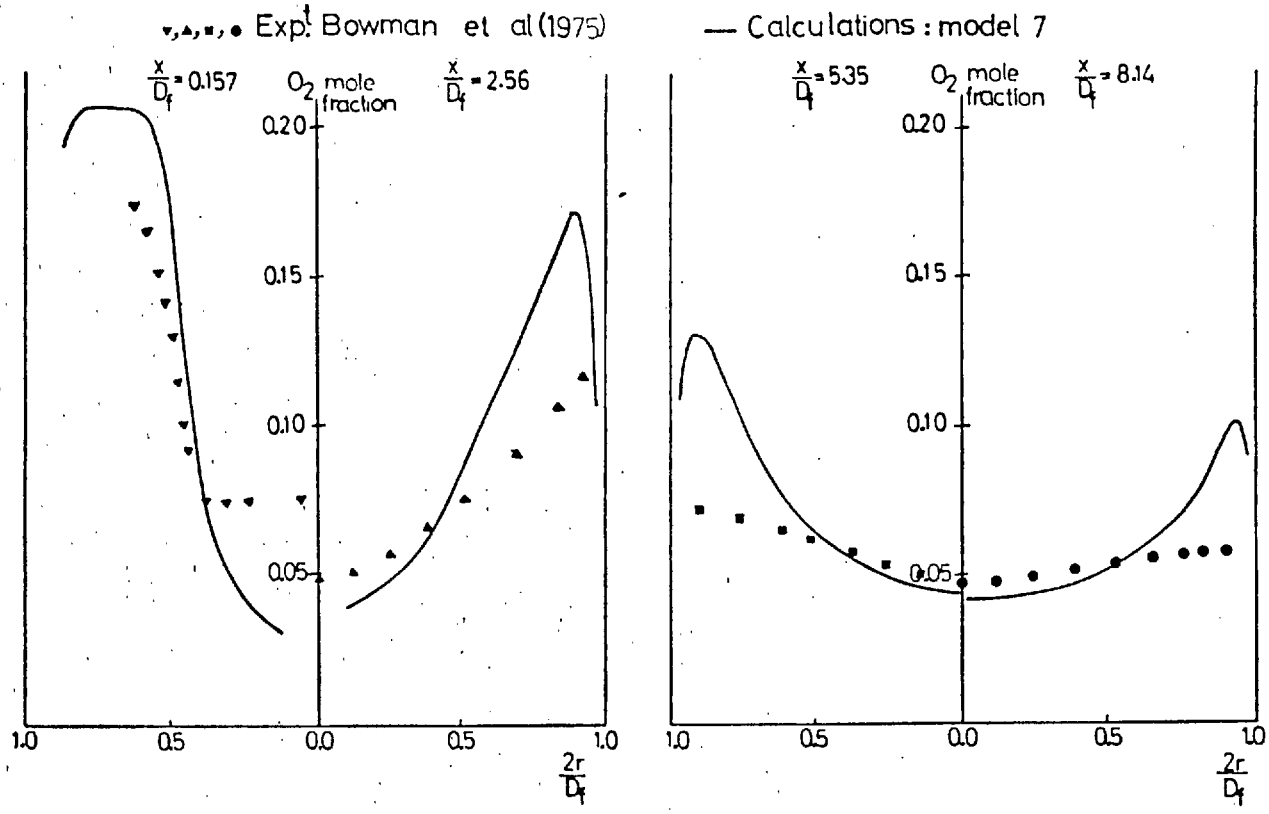

Figure 5.1.27:Measured and calculated profiles of oxygen mole fraction in the furnace of Bowman et al (1975).

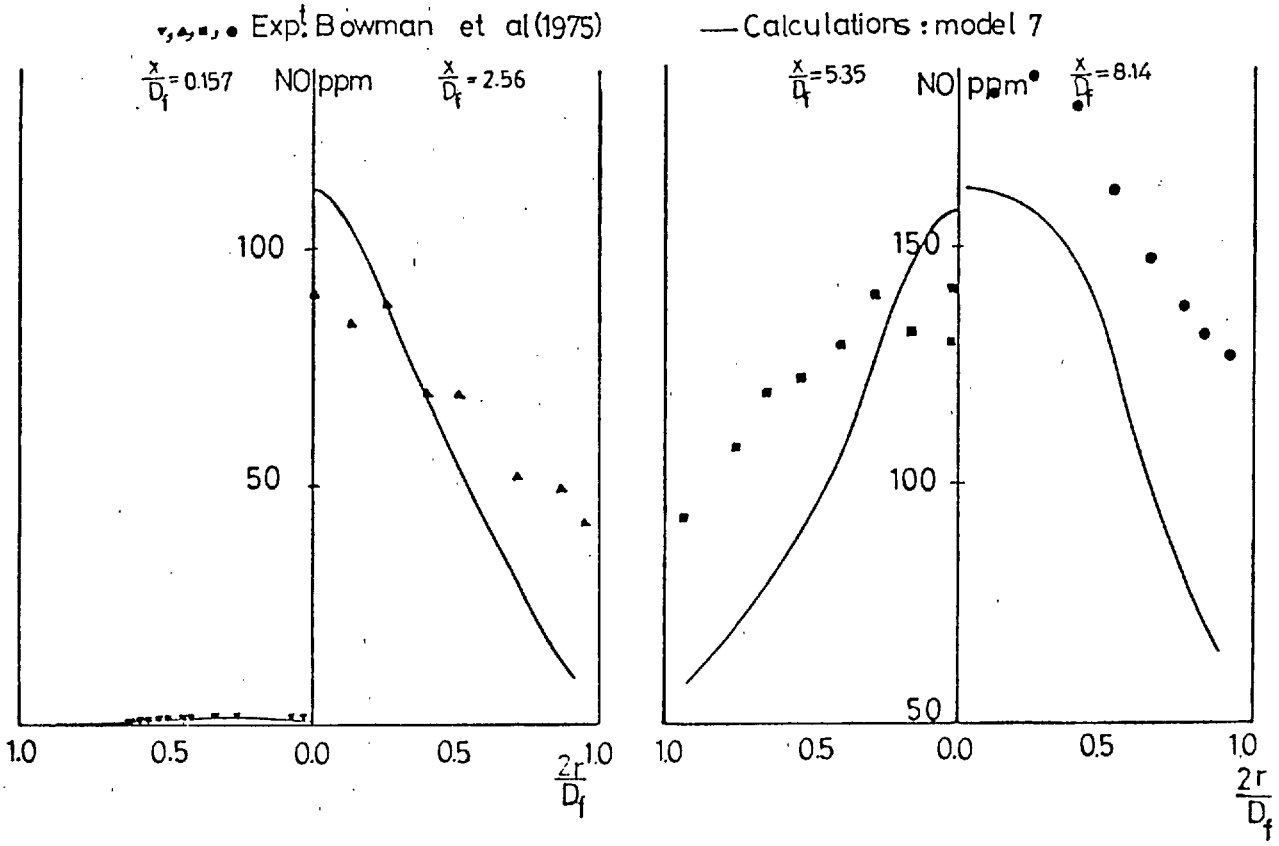

Figure 5.1.28:Measured and calculated profiles of nitric oxide concentrations in the furnace of Bowman et al (1975).

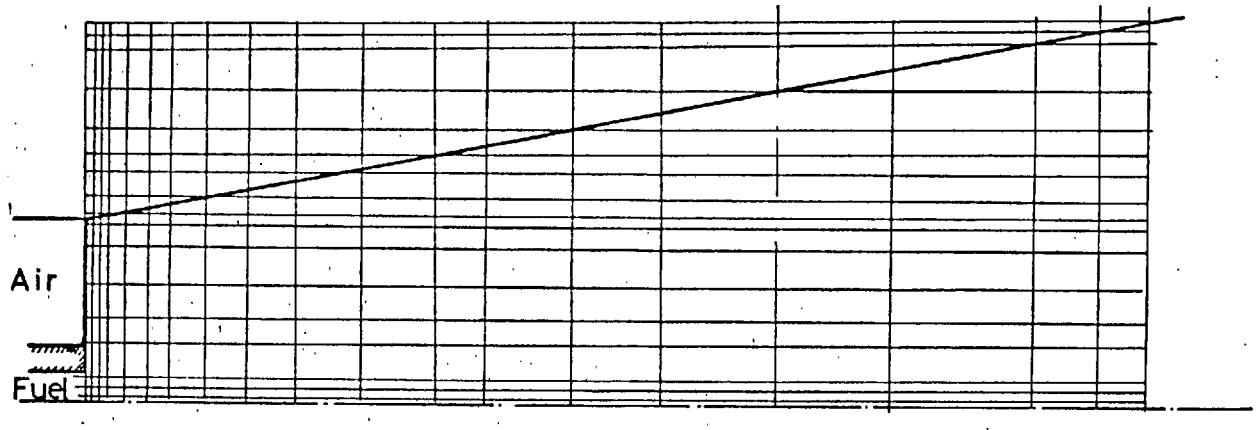

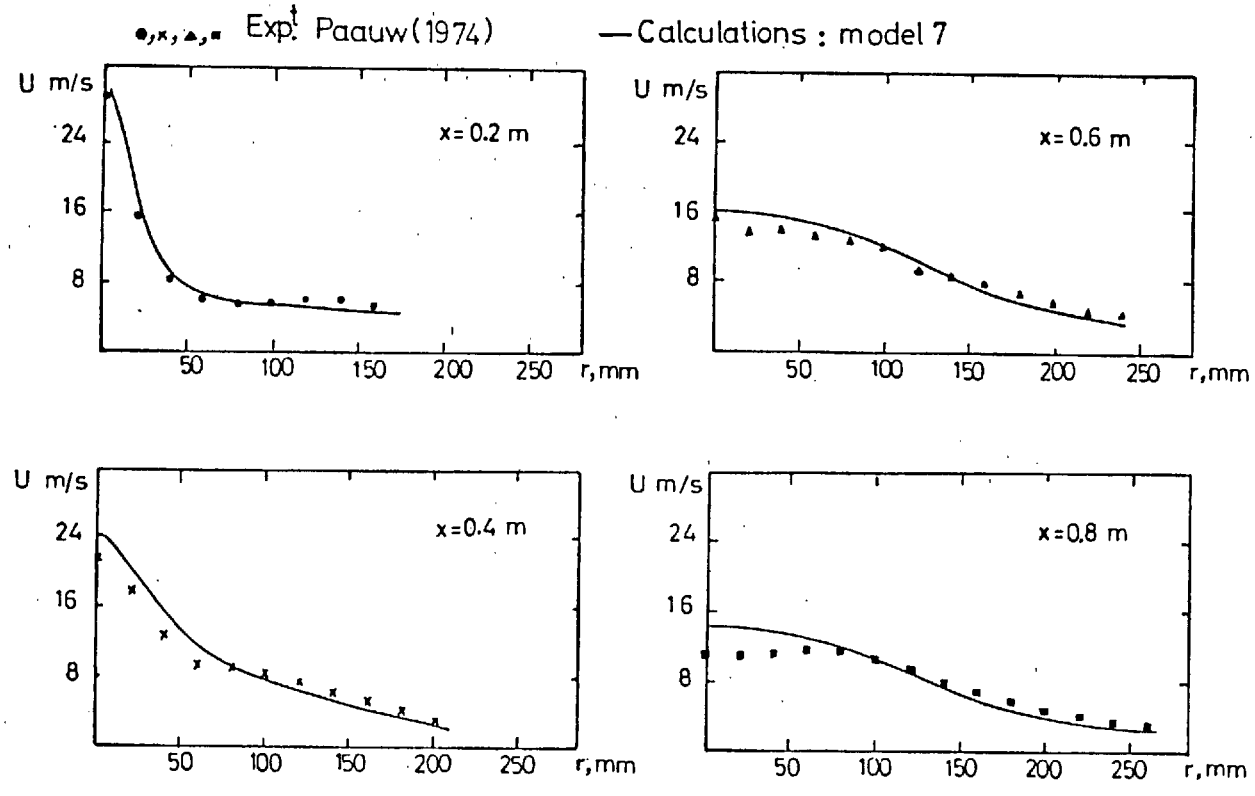

Figure 5.1.29:Measured and calculated profiles of mean axial velocity in the conical furnace of Paauw(1974).

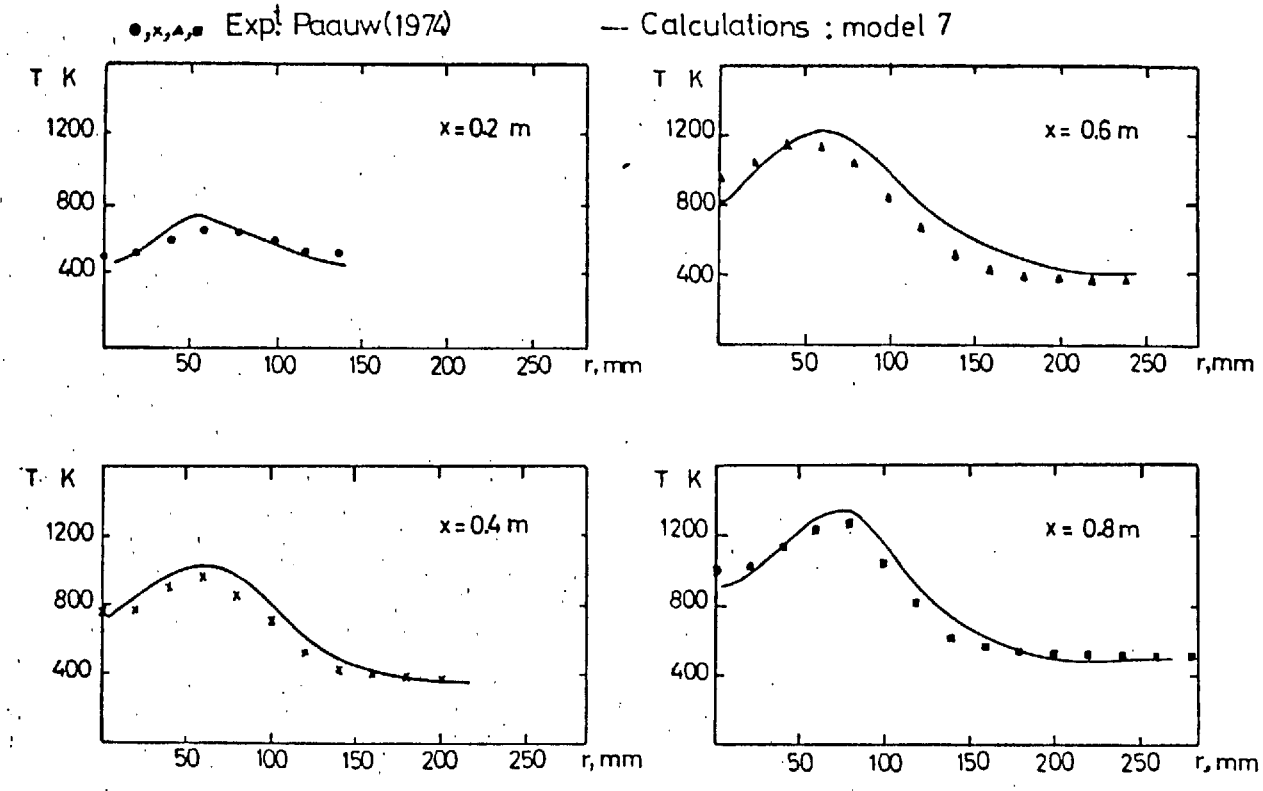

Figure 5.1.30:Measured and calculated profiles of mean temperature in the conical furnace of Paauw(1974).

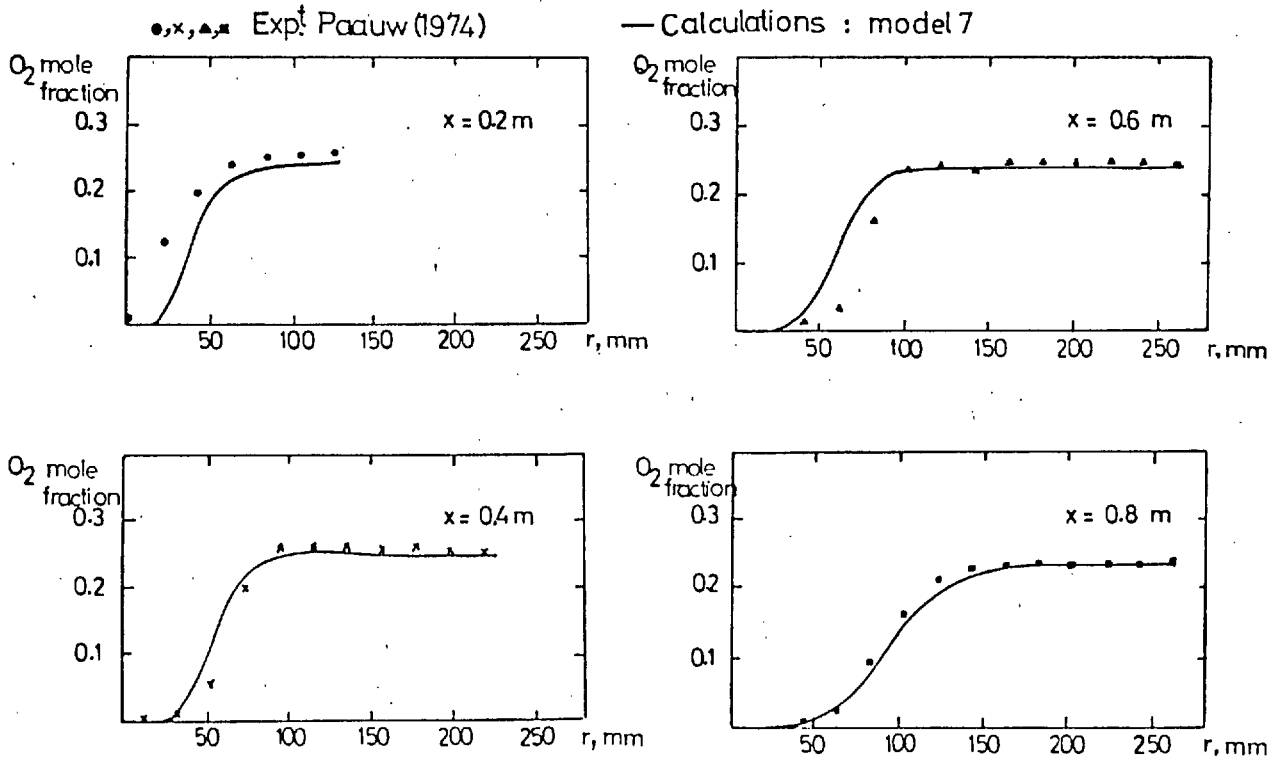

Figure 5.1.31:Measured and calculated profiles of oxygen mole fraction in the conical furnace of Paauw (1974).

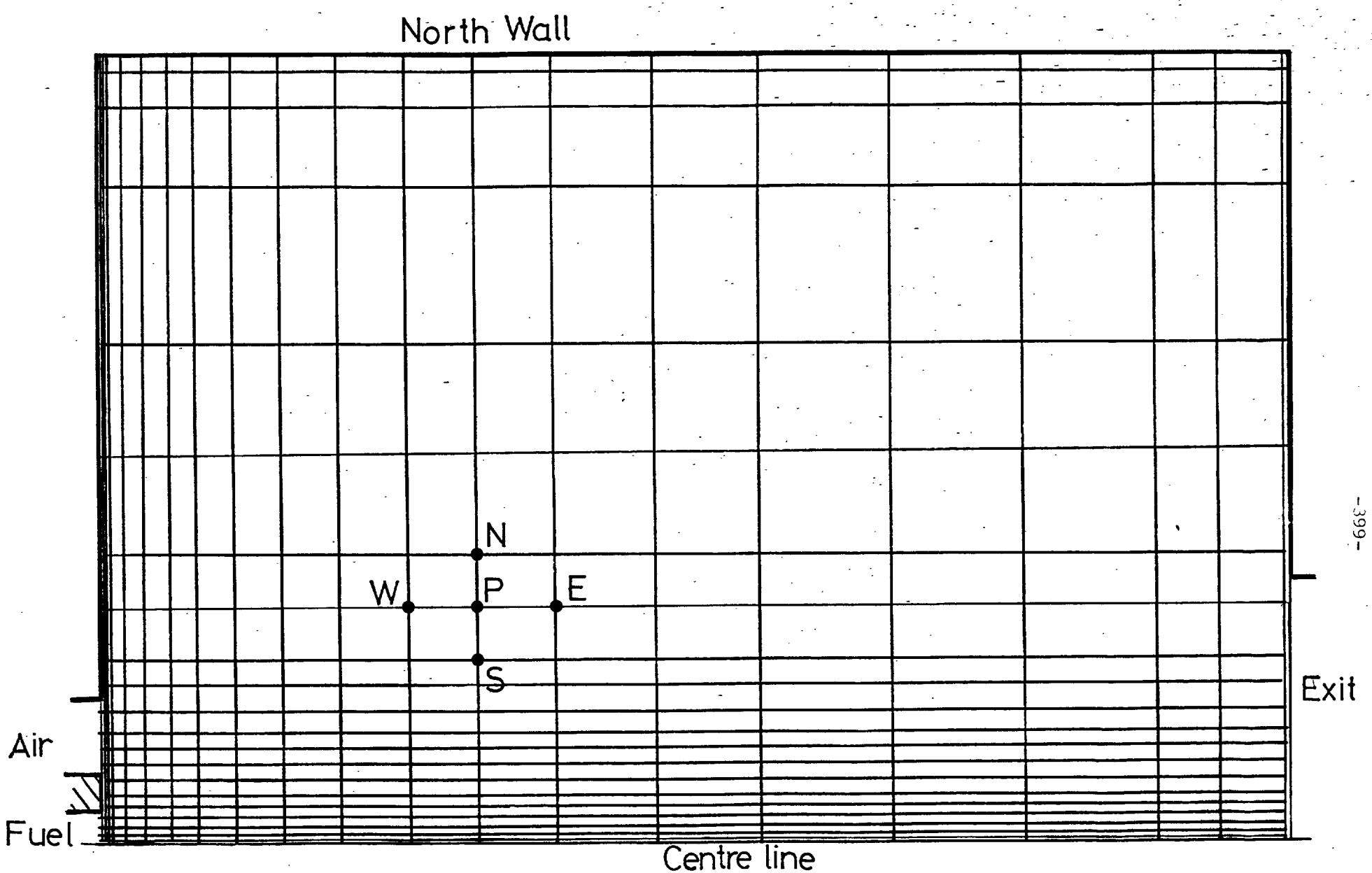

Figure 5.2.1:Grid arrangement for the furnace of the present investigations.

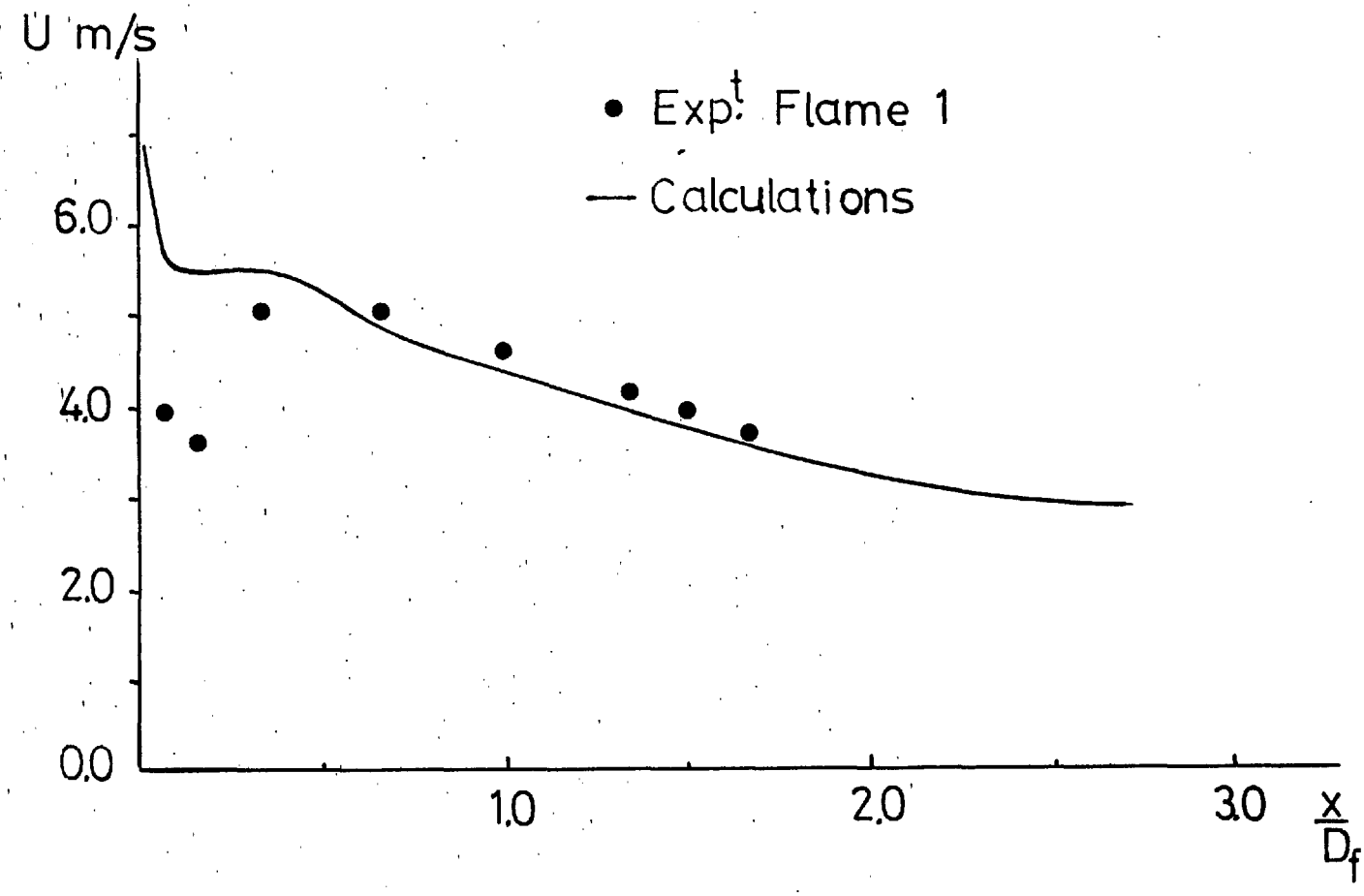

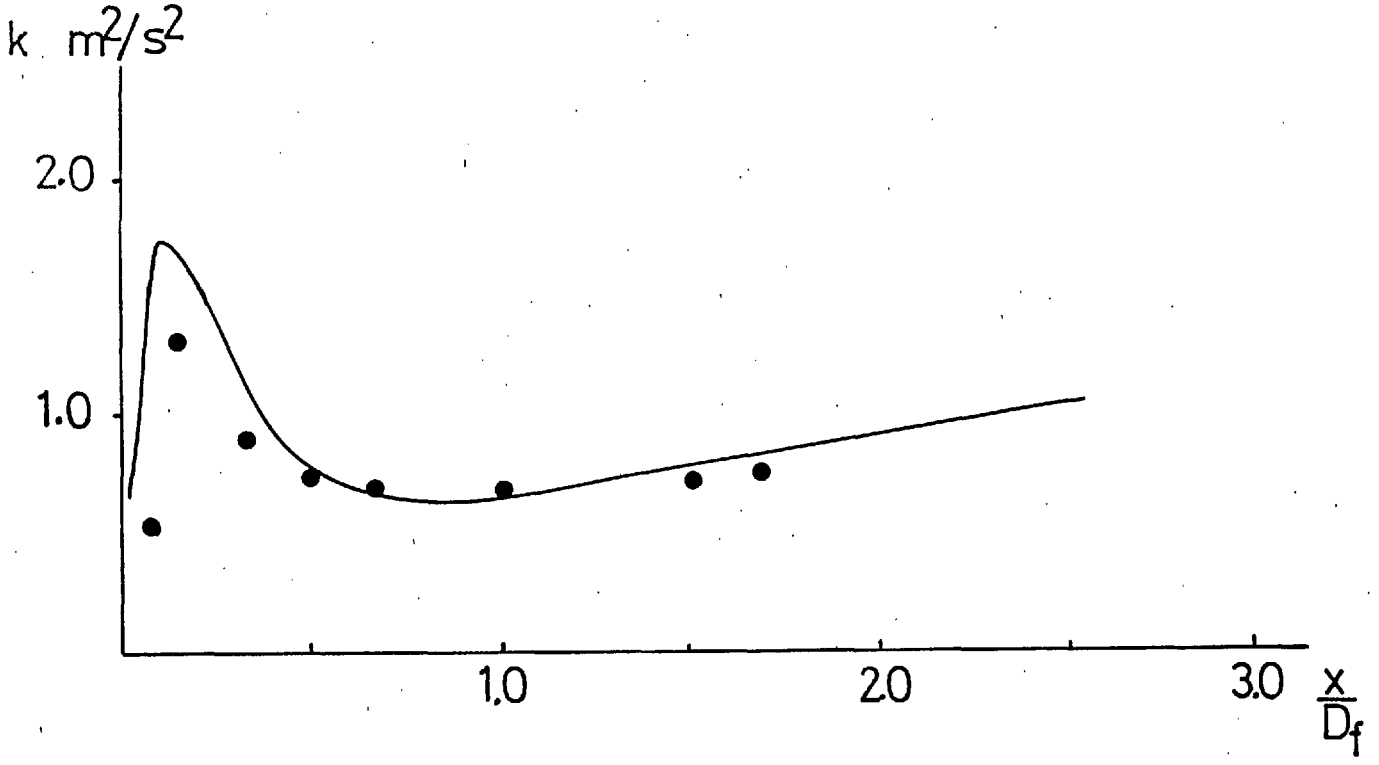

Figure 5.2.2:Measured and calculated centreline distributions of mean axial velocity and kinetic energy of turbulence in flame 1.

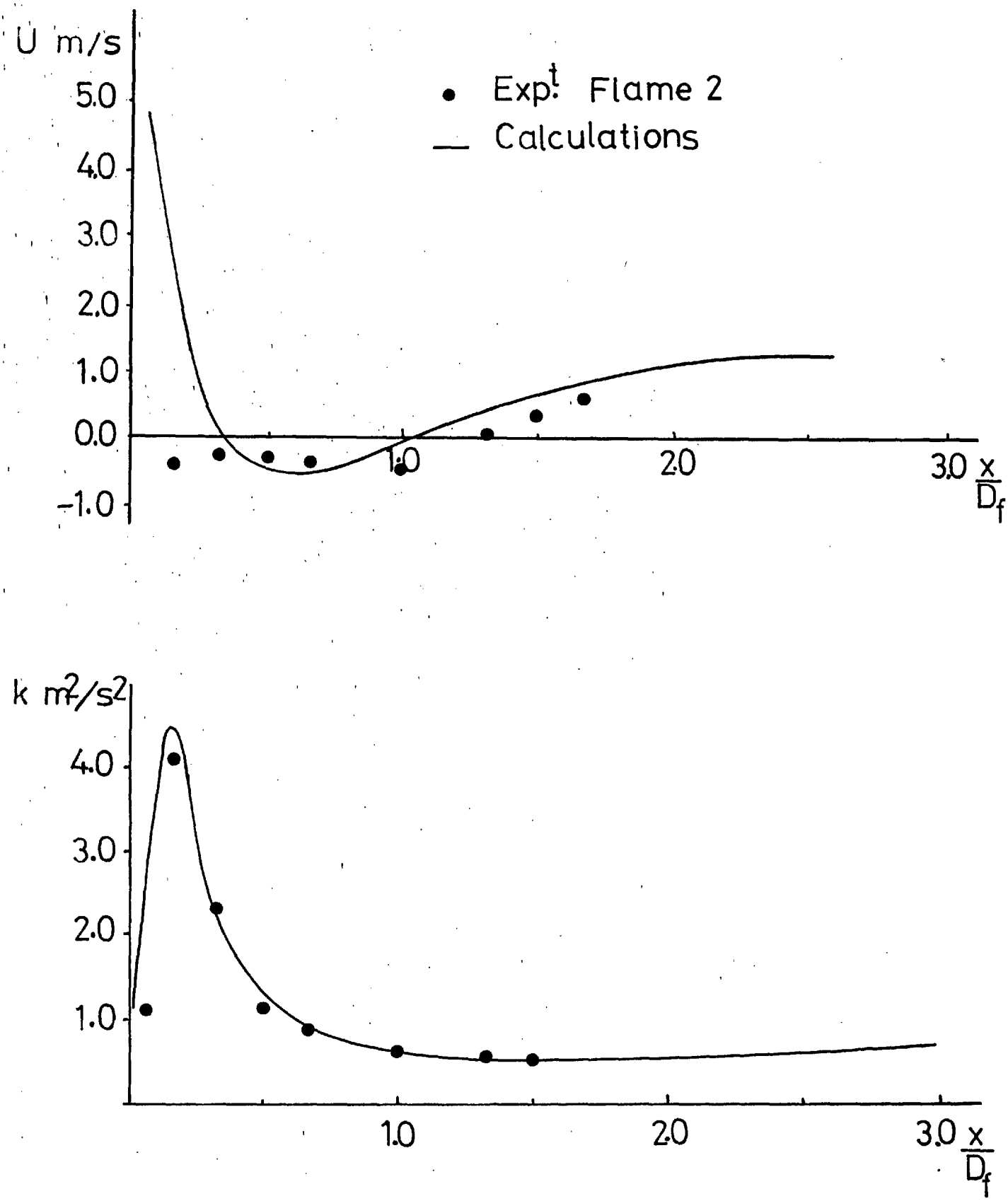

Figure 5.2.3:Measured and calculated centreline distributions of mean axial velocity and kinetic energy of turbulence in flame 2.

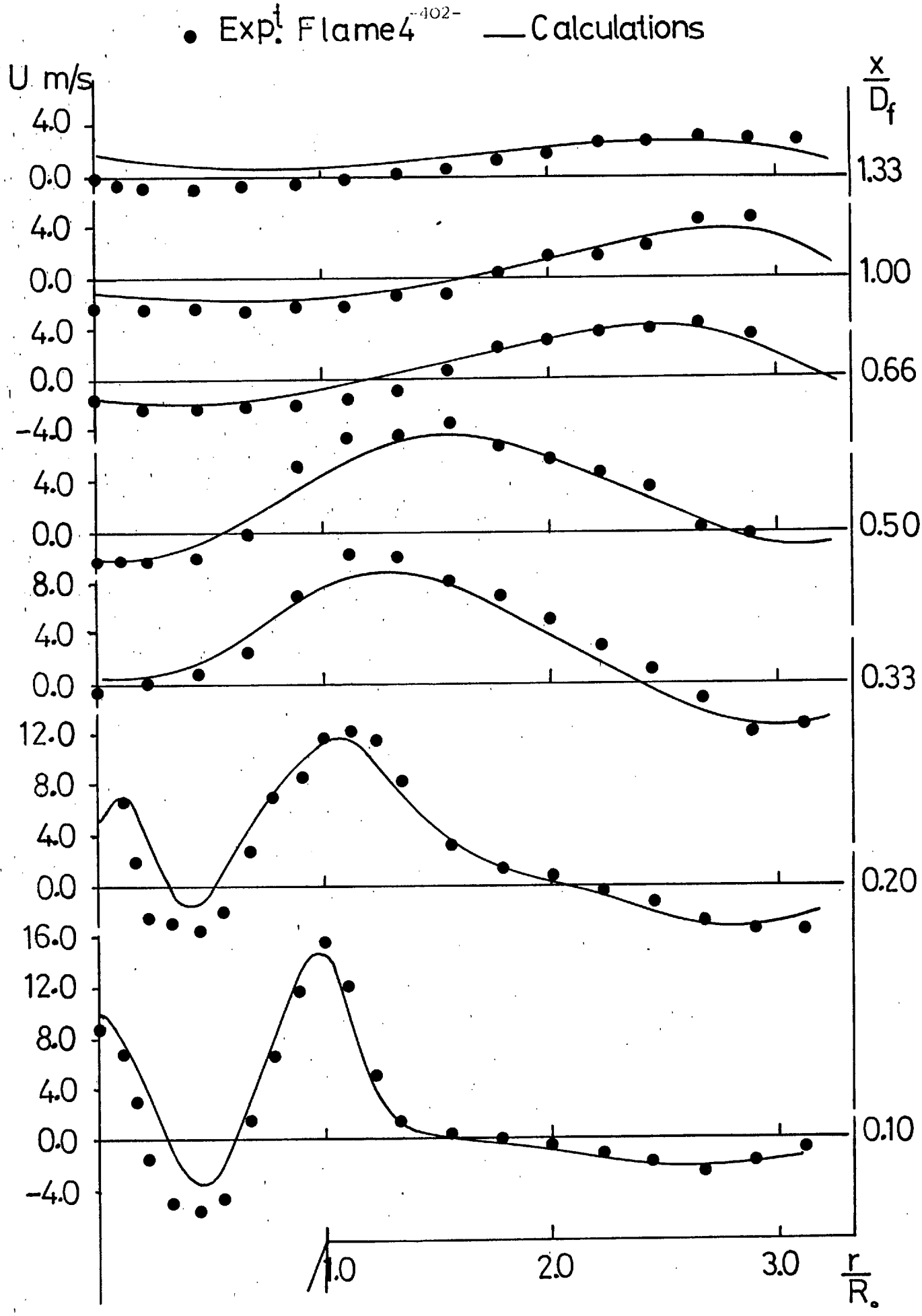

Figure 5.2.4:Measured and calculated mean axial velocity profiles in flame 4.

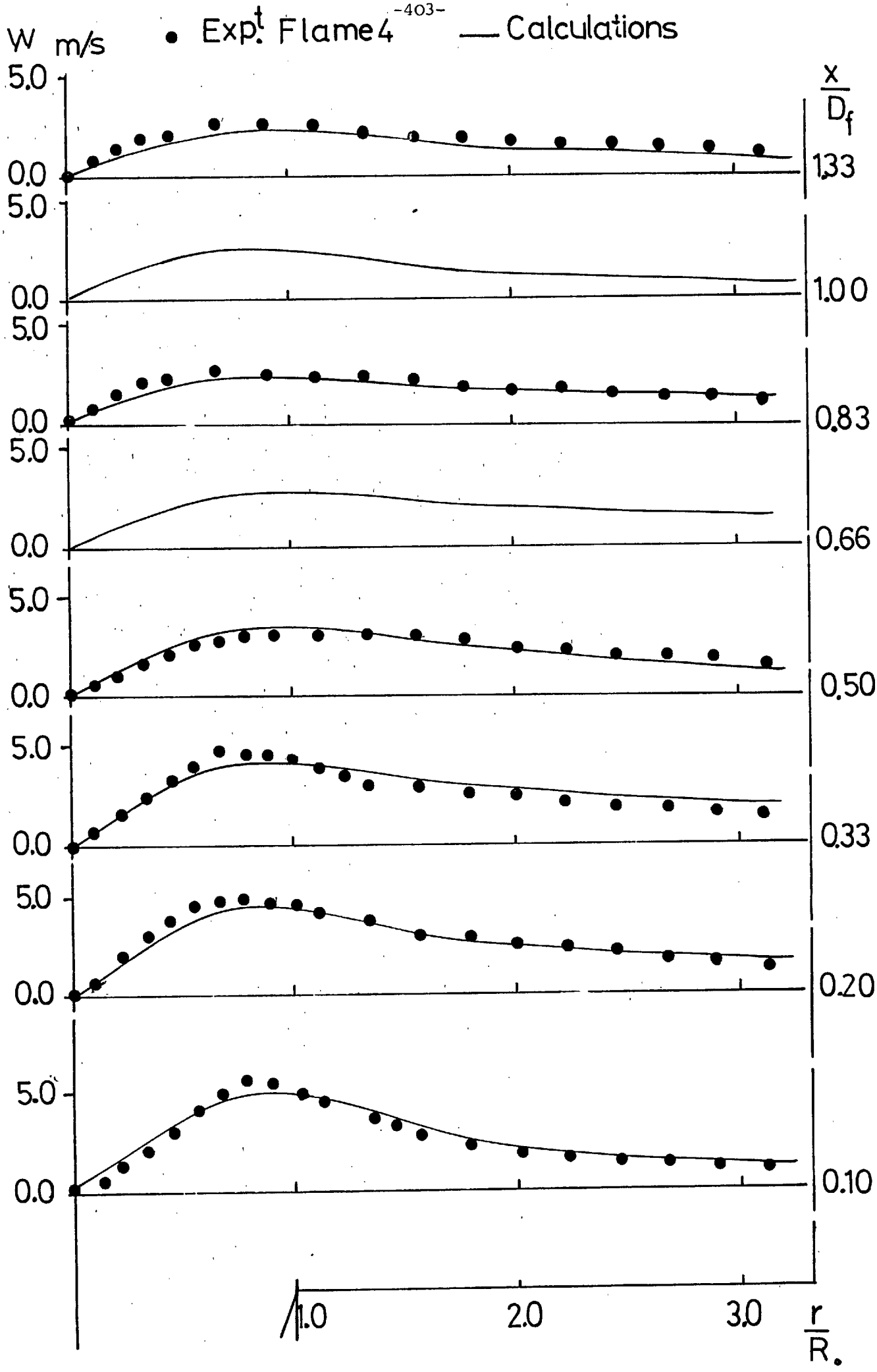

Figure 5.2.5:Measured and calculated tangential velocity profiles in flame 4.

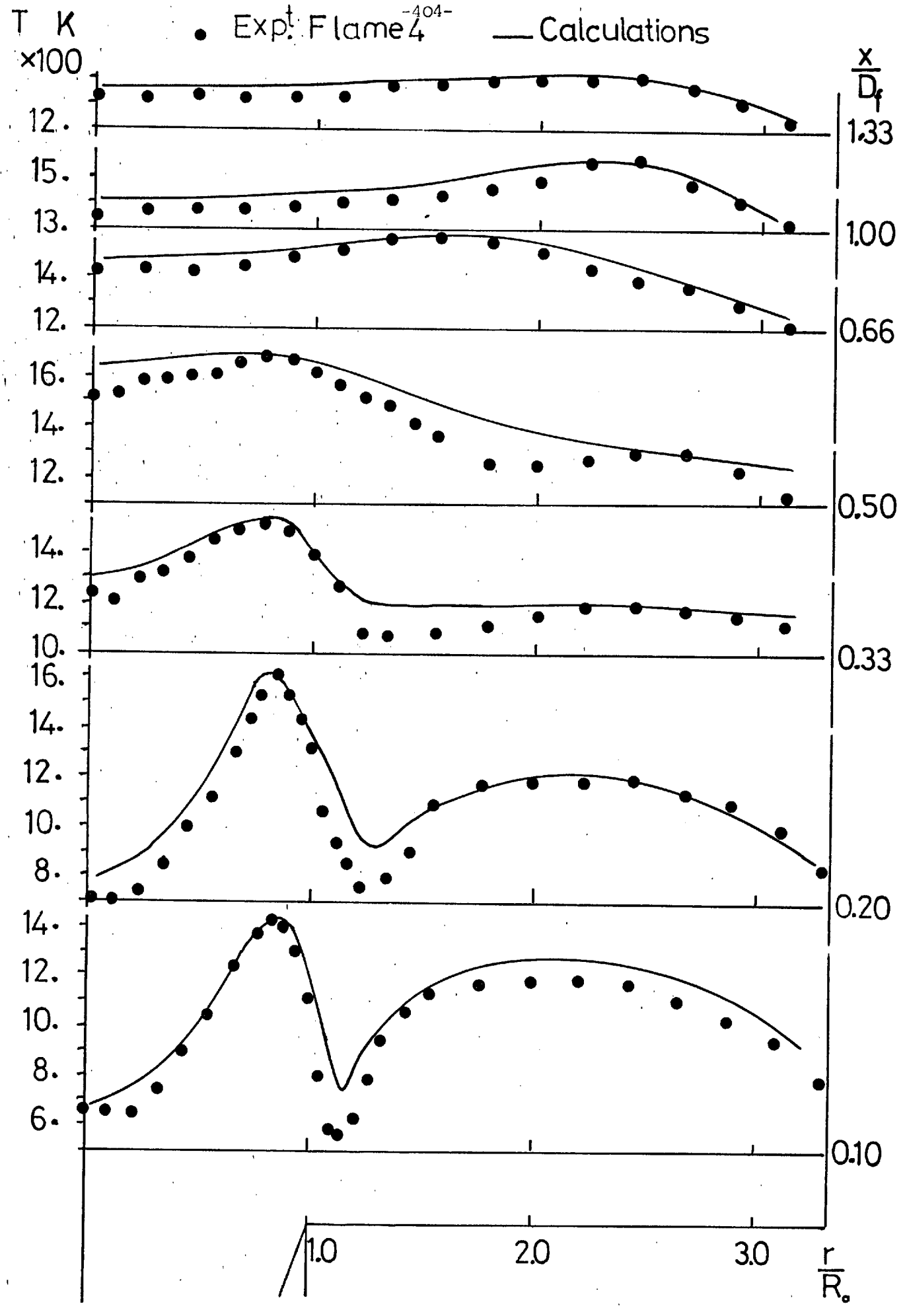

Figure 5.2.6:Measured and calculated mean gas temperature profiles in flame 4.

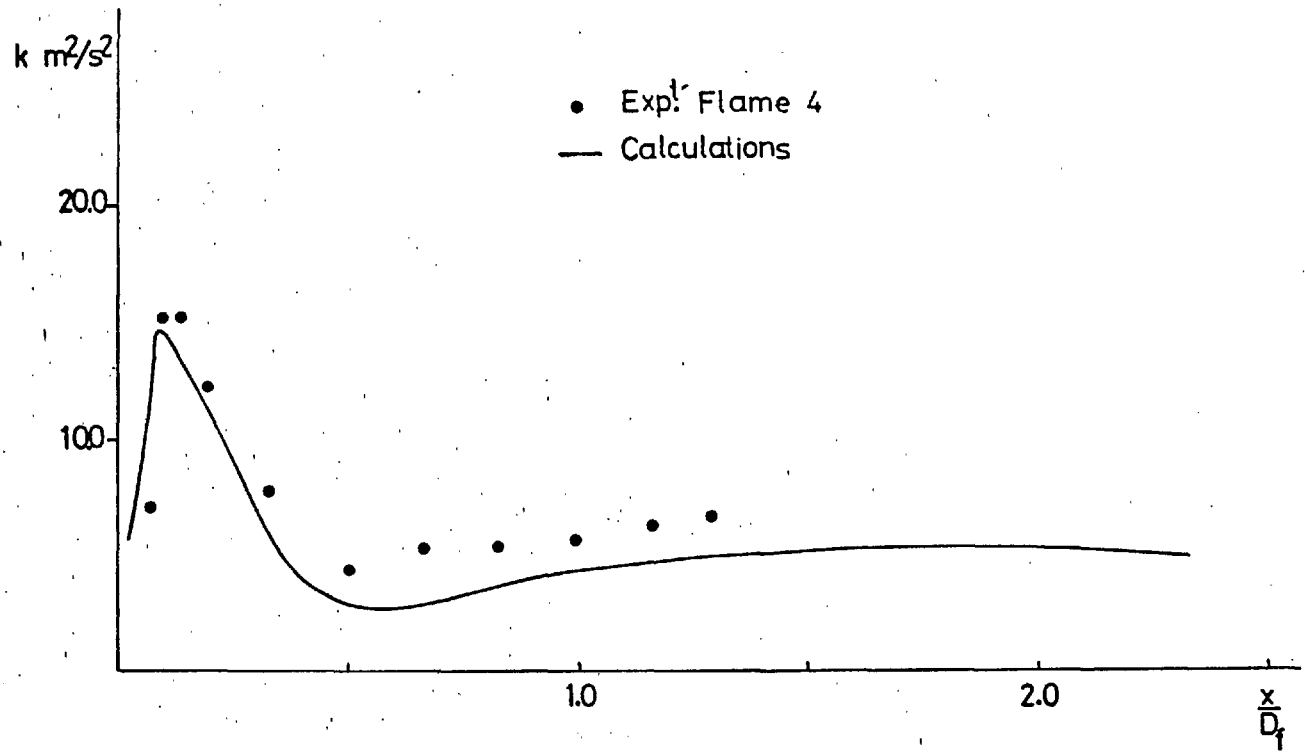

Figure 5.2.7:Measured and calculated centreline distribution of kinetic energy of turbulence in flame 4.

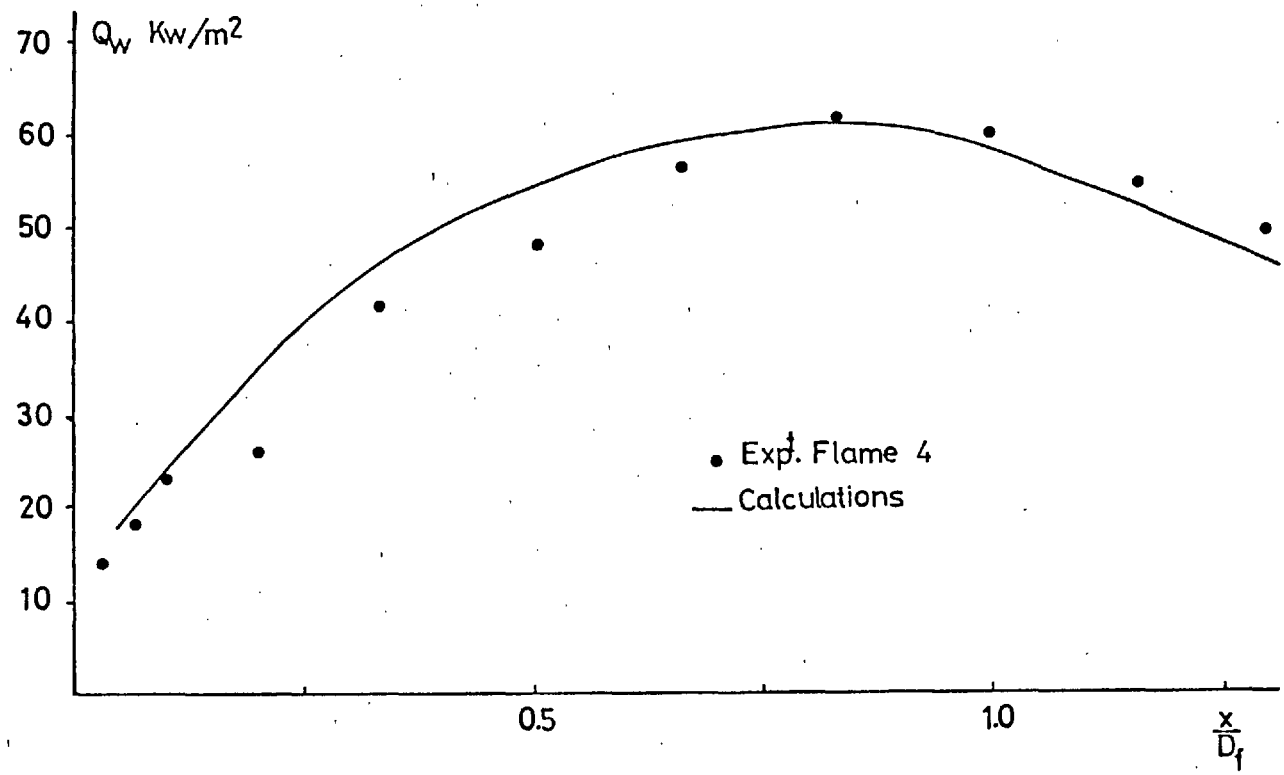

Figure 5.2.8:Measured and calculated total wall heat flux distribution in flame 4.

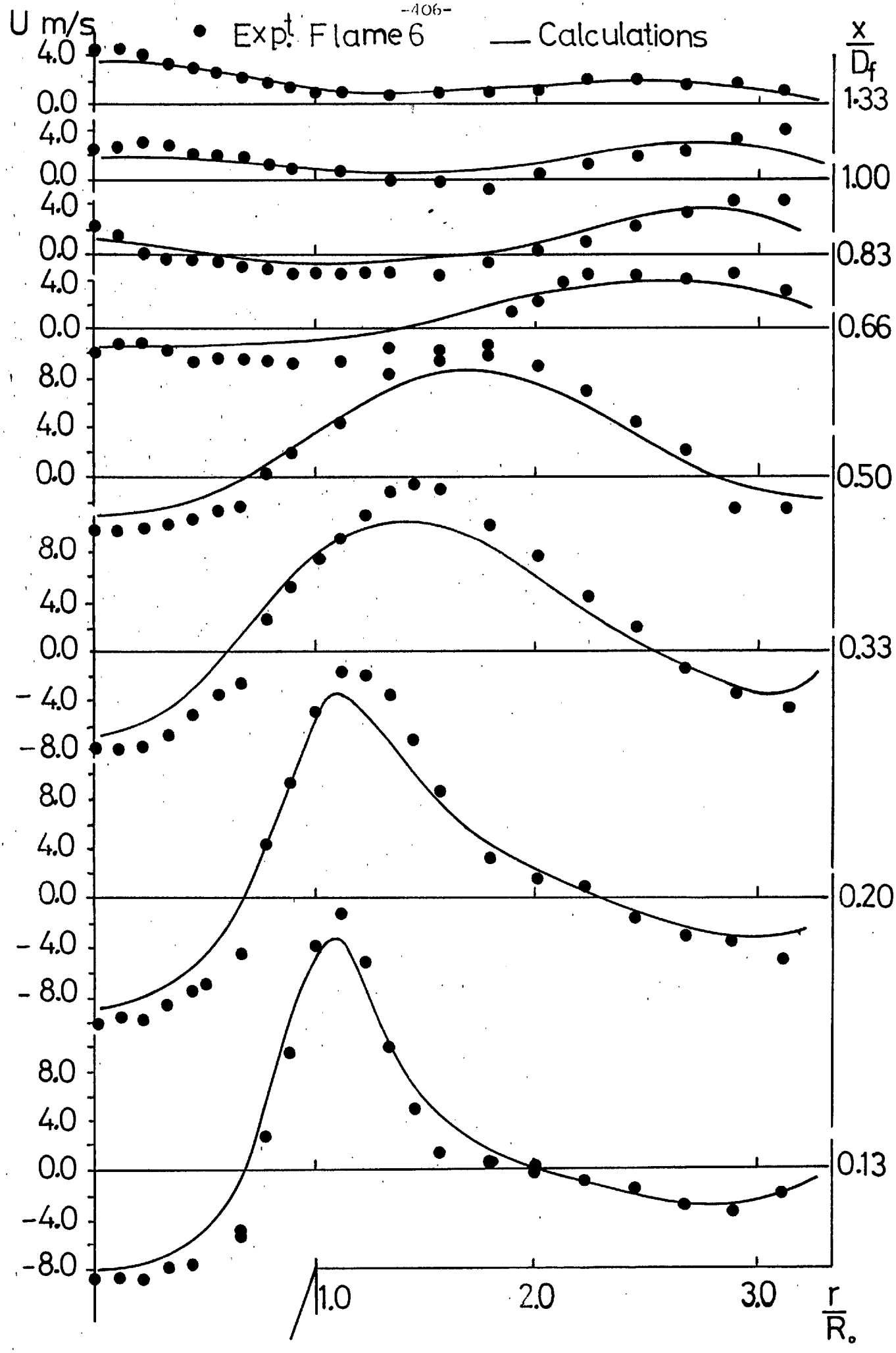

Figure 5.2.9:Measured and calculated mean axial velocity profiles in flame 6.

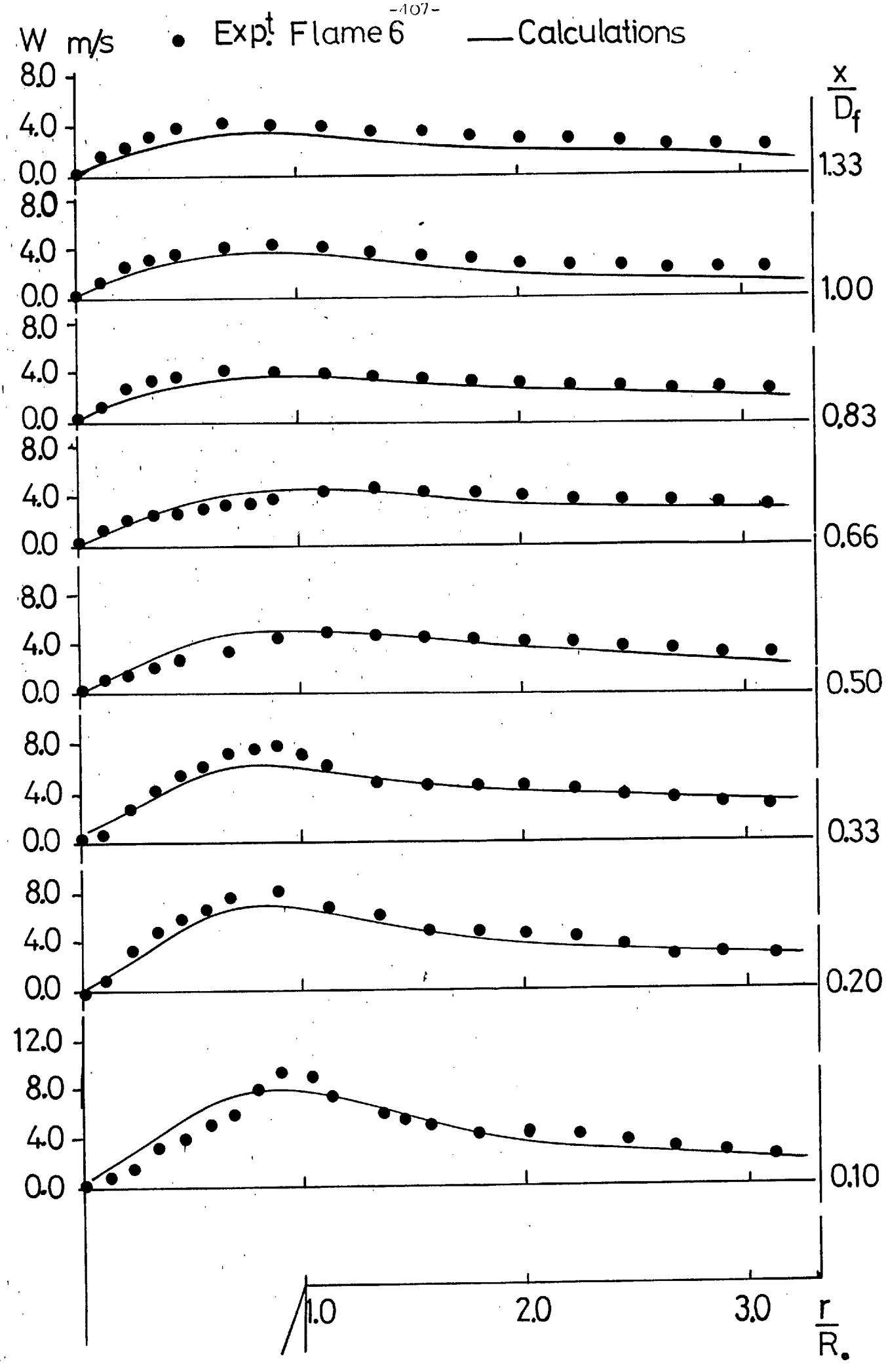

Figure 5.2.10:Measured and calculated tangential velocity profiles in flame 6.

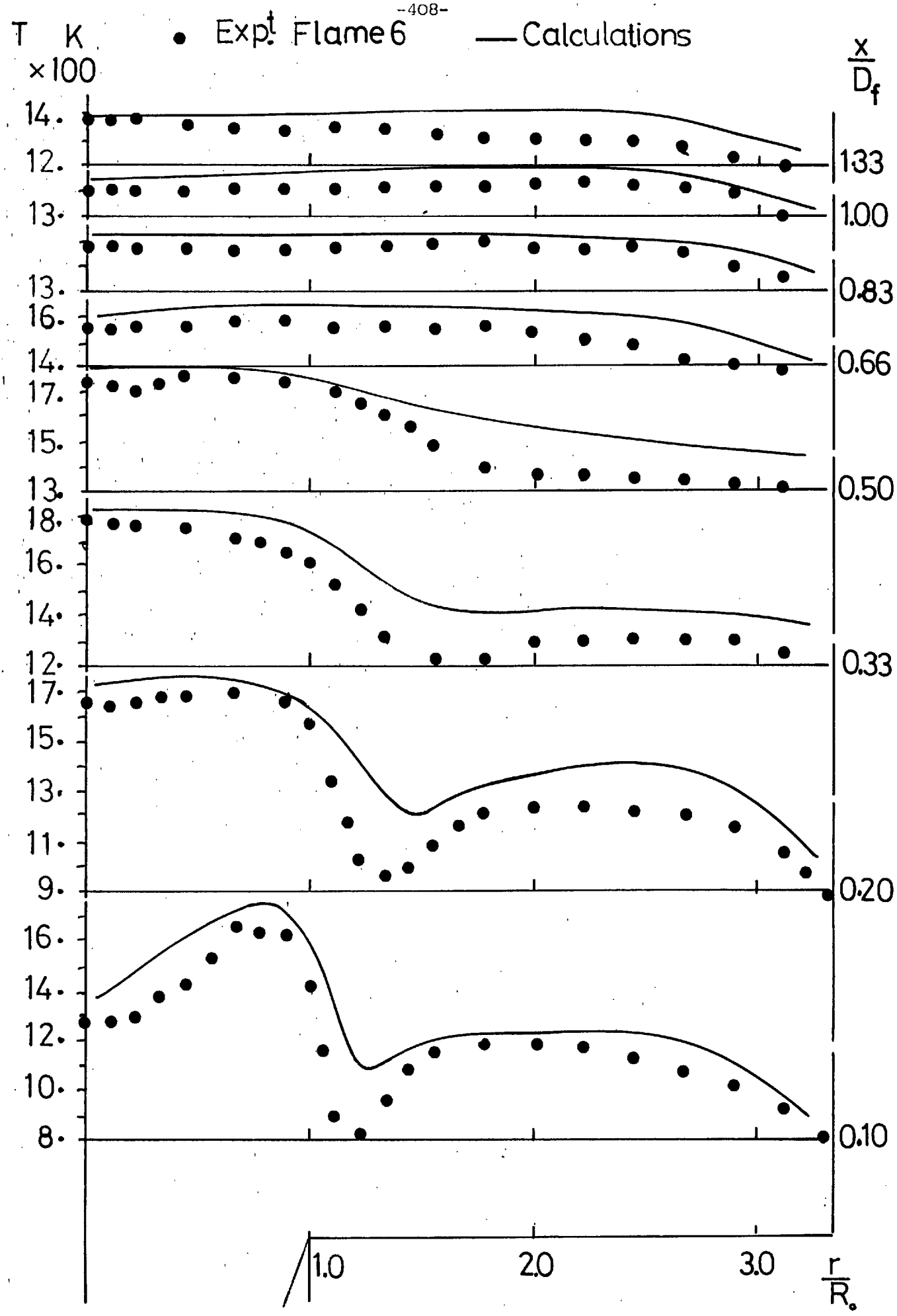

Figure 5.2.11:Measured and calculated mean gas temperature profiles in flame 6.

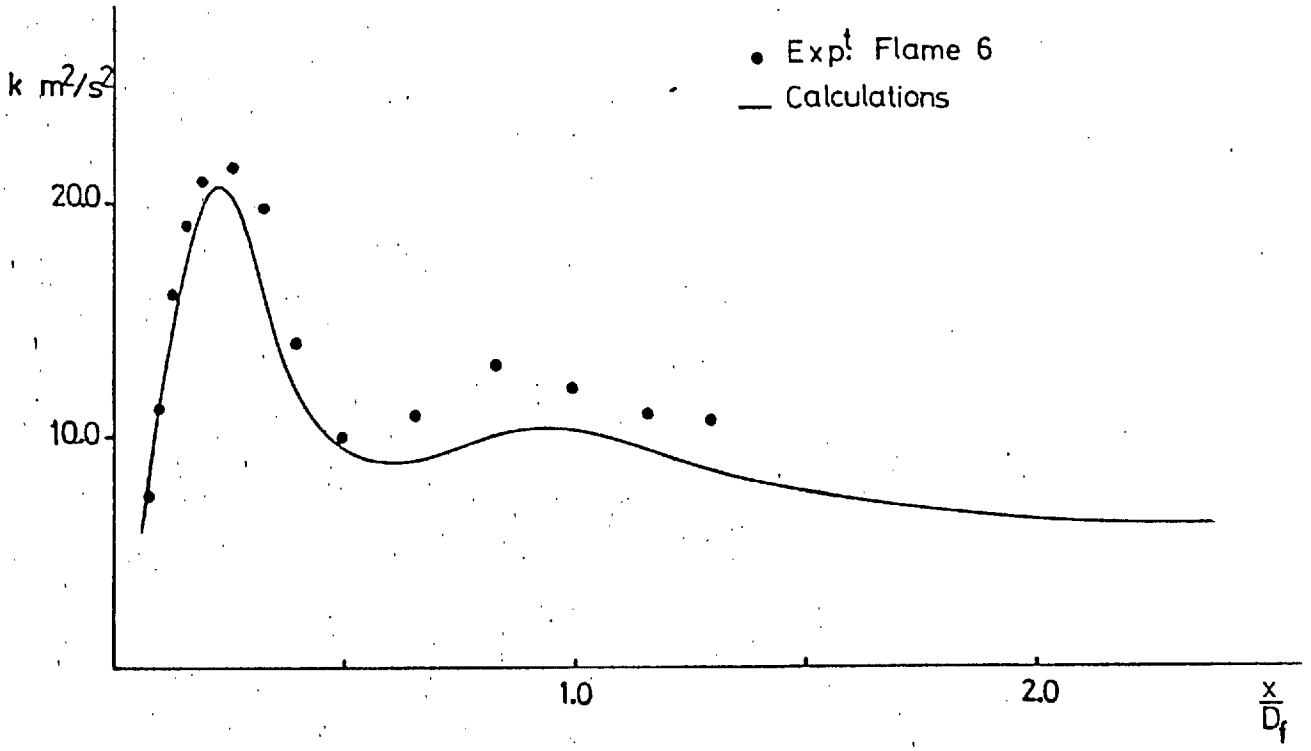

Figure 5.2.12:Measured and calculated centreline distribution of kinetic energy of turbulence in flame 6.

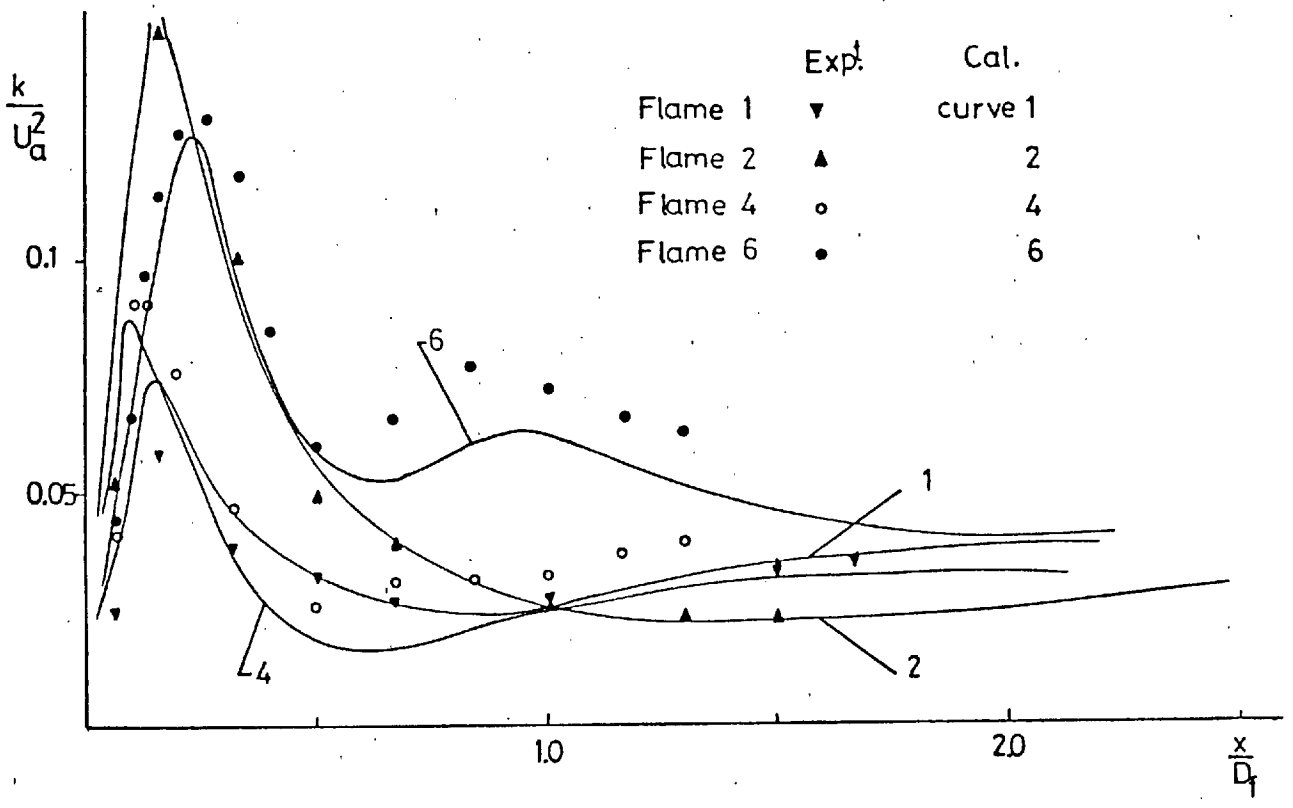

Figure 5.2.13:Measured and calculated centreline distribution of kinetic energy of turbulence for various flames.

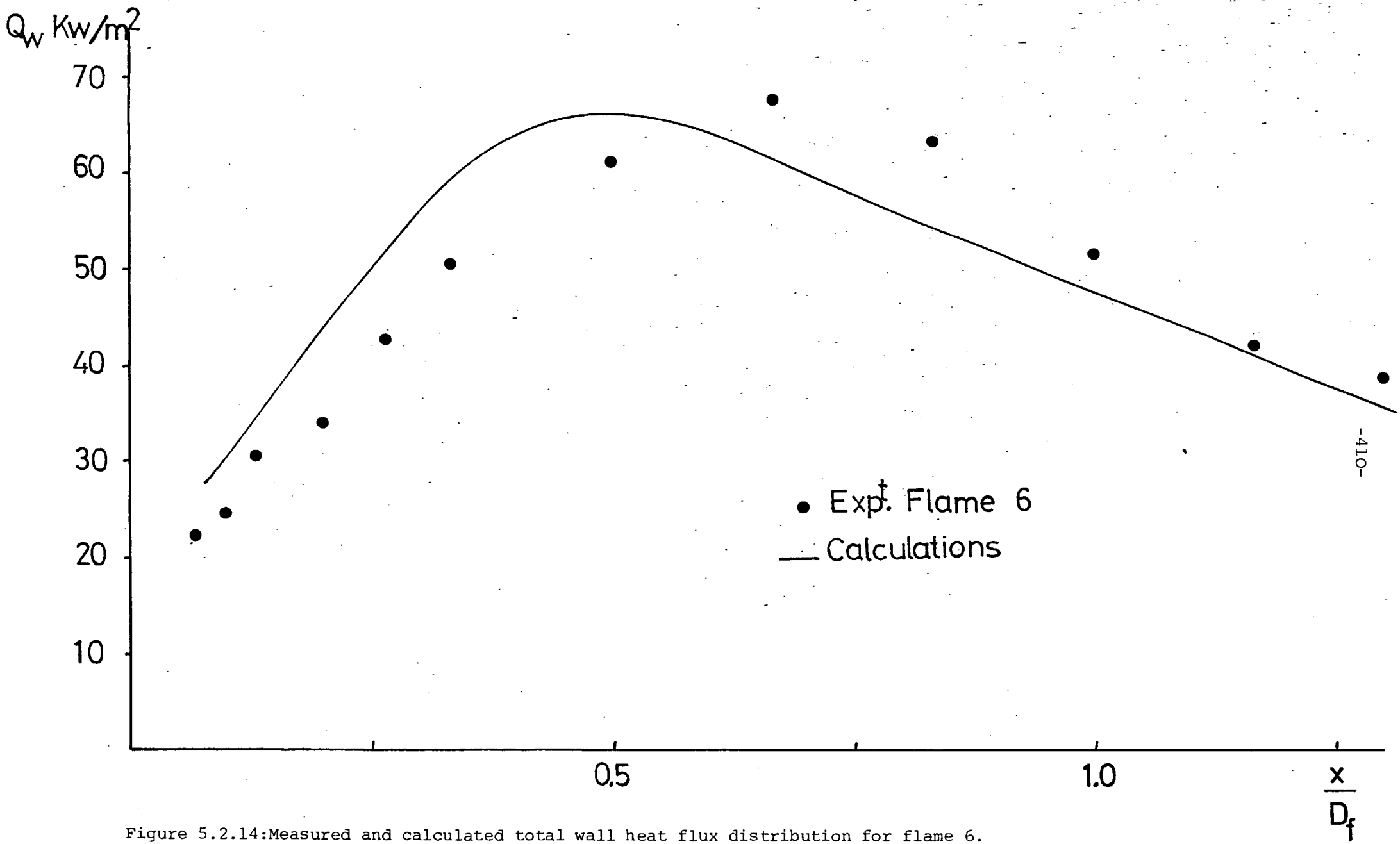

Figure 5.2.14:Measured and calculated total wall heat flux distribution for flame 6.

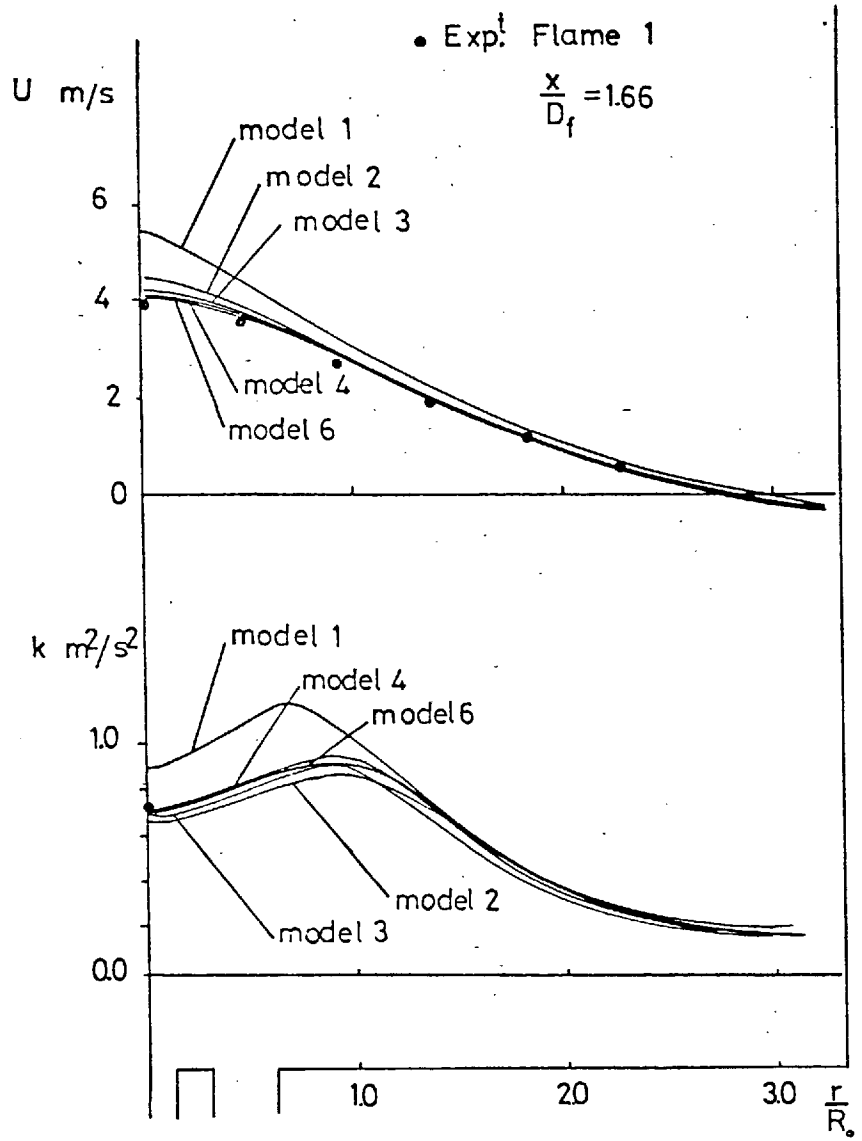

Figure 5.3.1:Radial profiles of mean velocity and kinetic energy in the furnace of section 3.1: a comparison between combustion models.

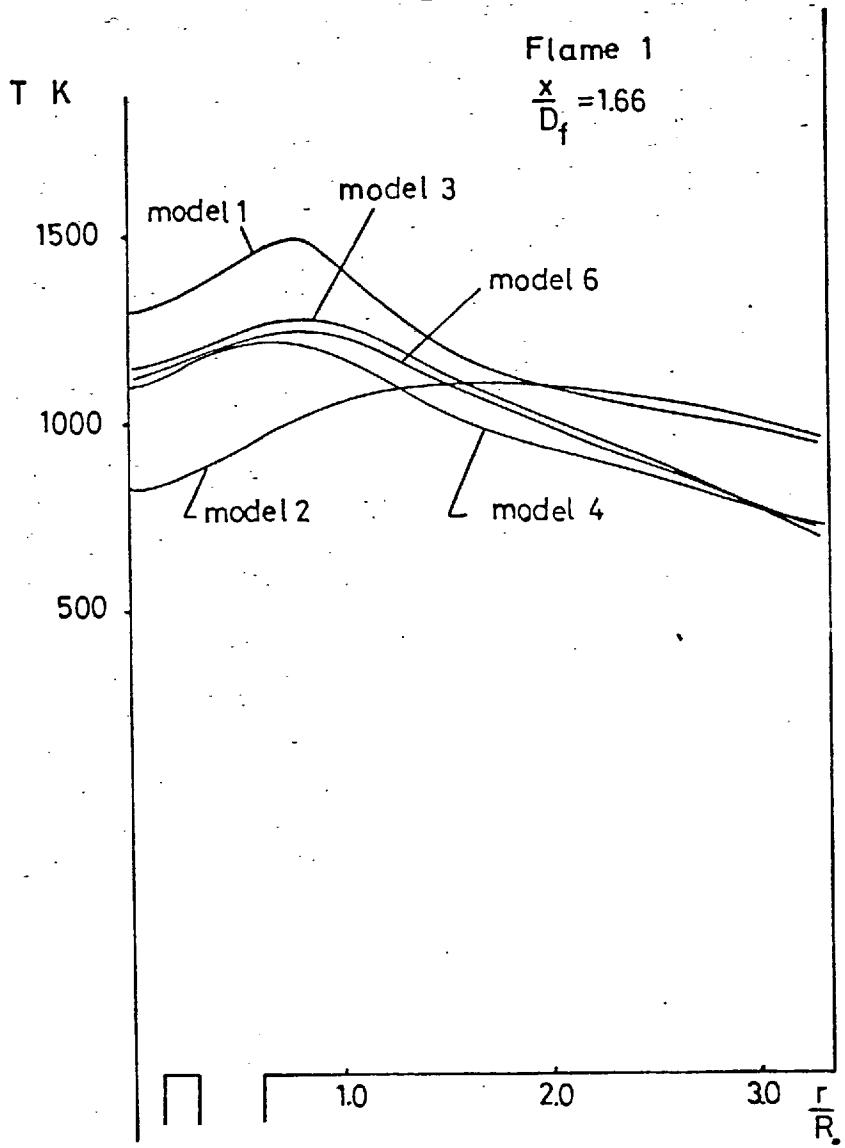

Figure 5.3.2:Radial profiles of mean temperature in the furnace of section 3.1 : a comparison between combustion models.

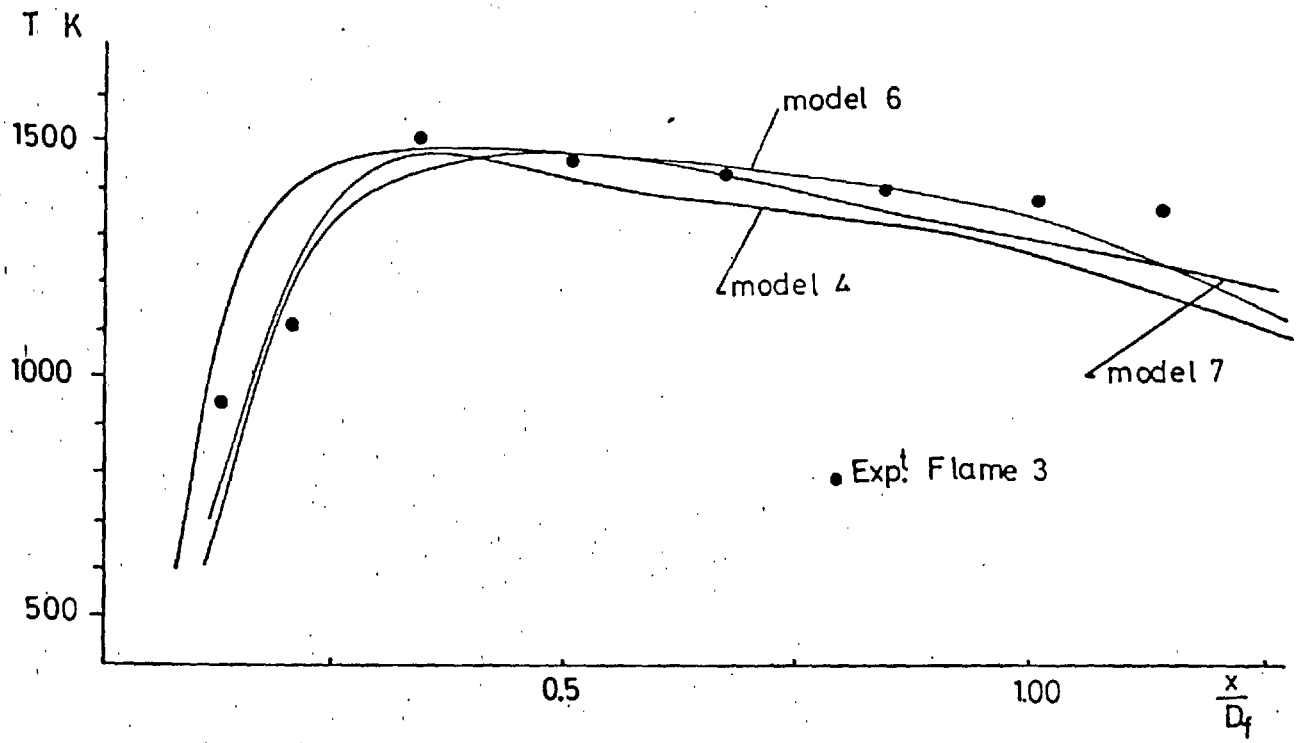

Figure 5.3.3:Centreline temperature distribution in the furnace of section 3.1: a comparison between combustion models.

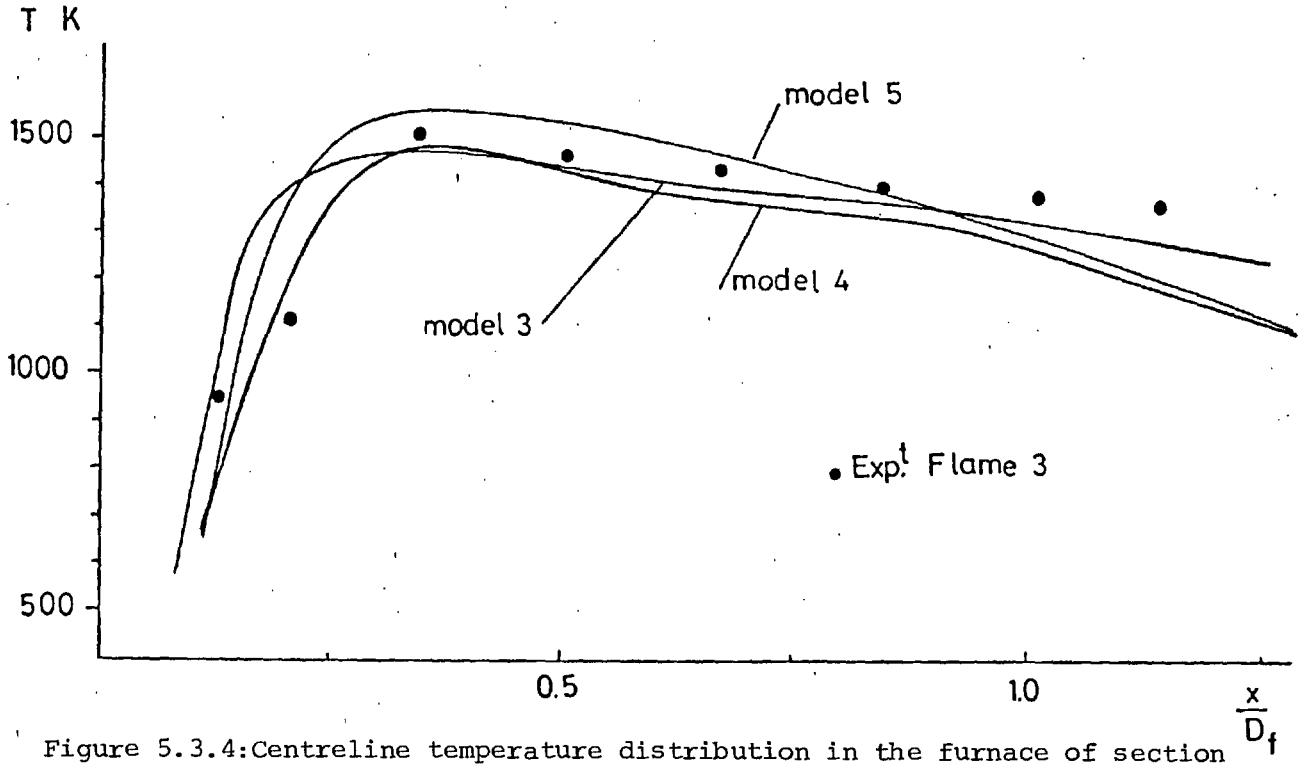

Figure 5.3.4:Centreline temperature distribution in the furnace of section 3.1:a comparison between combustion models.

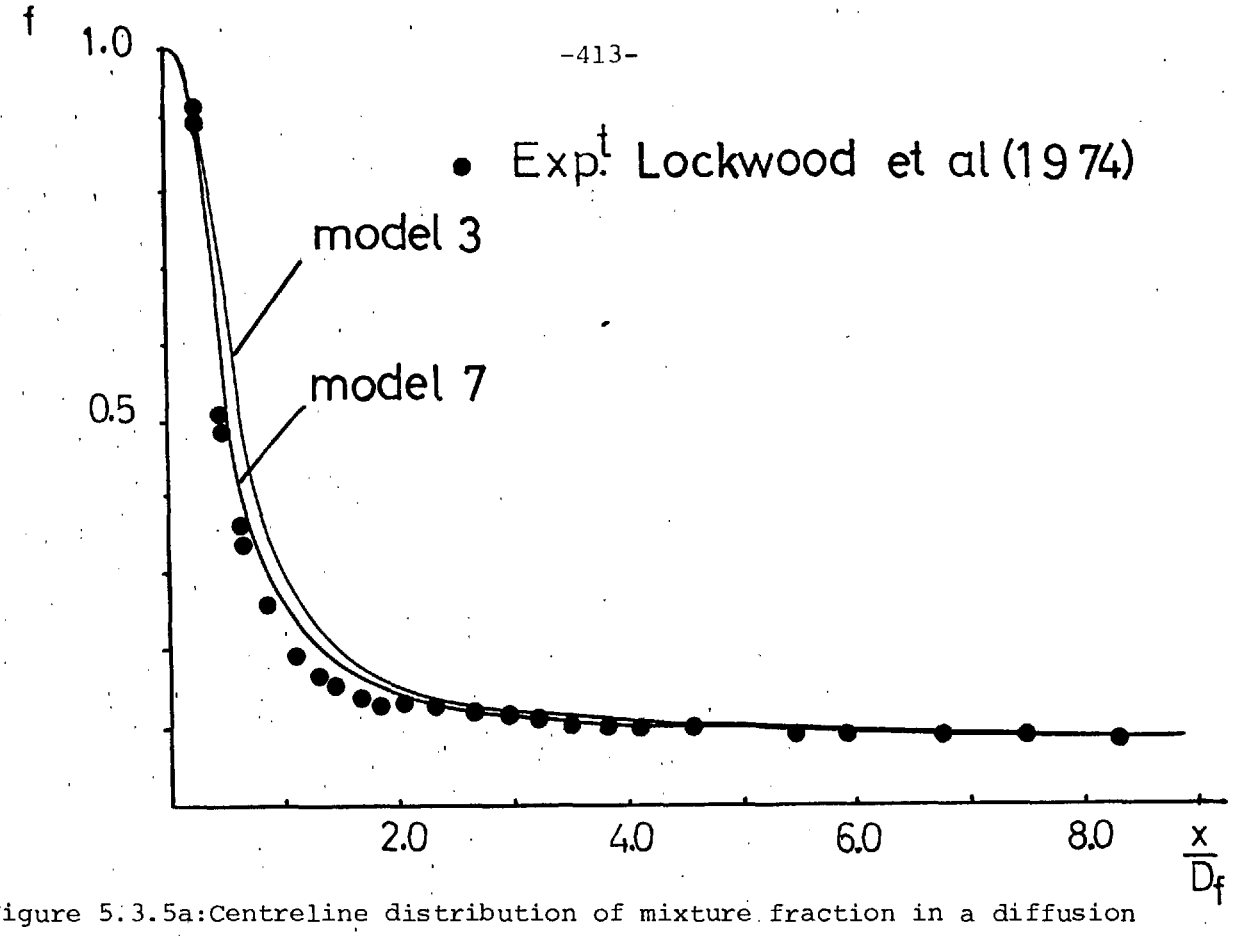

Figure 5.3.5a:Centreline distribution of mixture fraction in a diffusion flame : a comparison between combustion models.

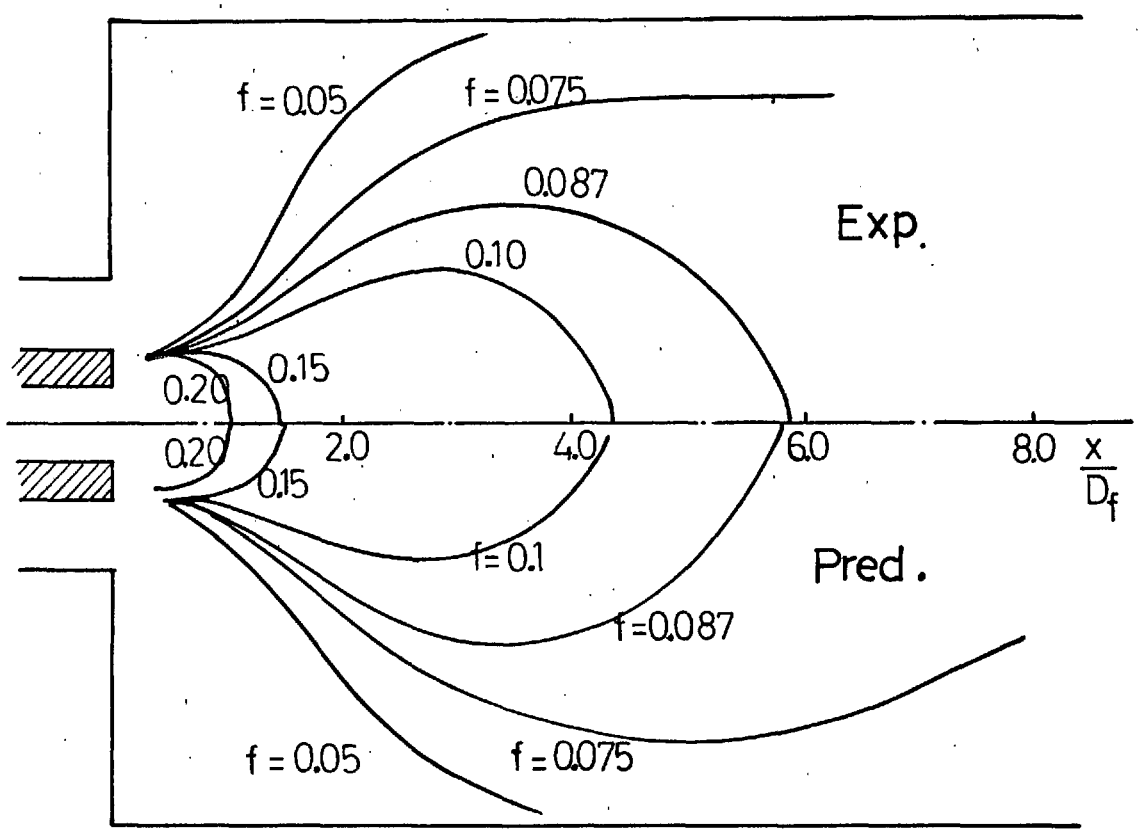

Figure 5.3.5b:Contours of isomixture fraction in a diffusion flame:a comparison between combustion models.

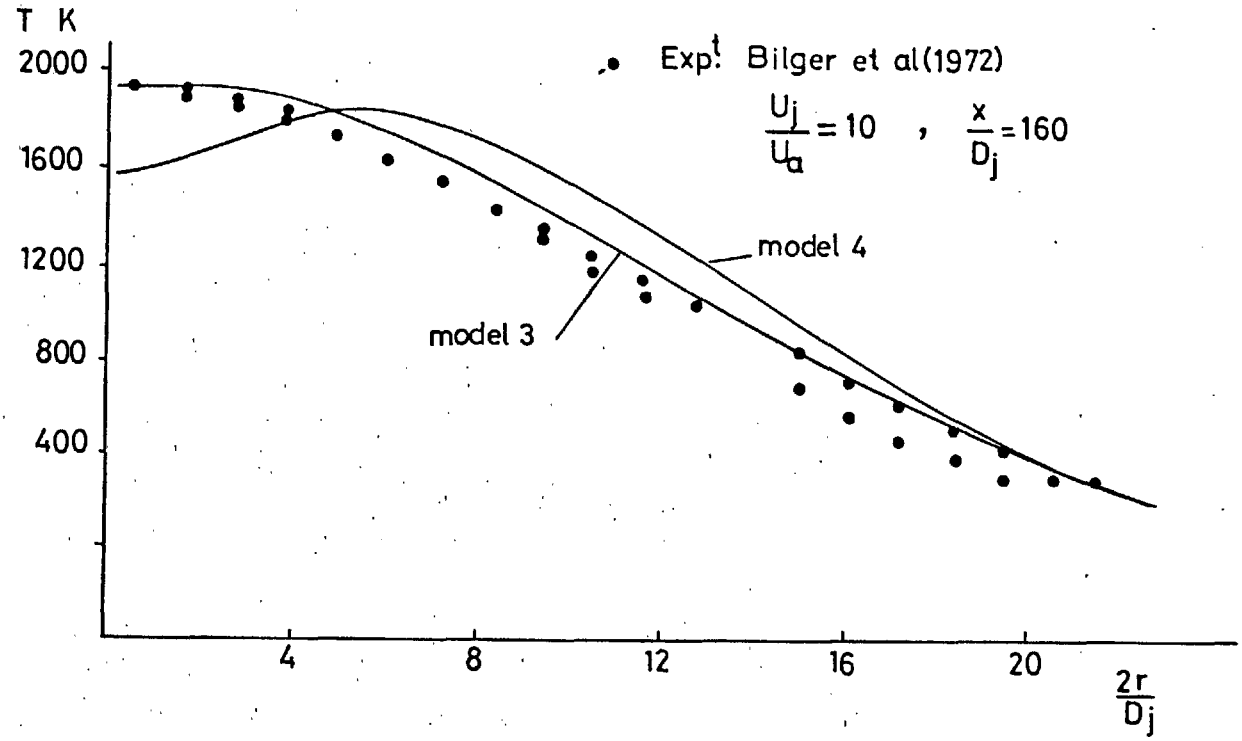

Figure 5.3.6:Radial profiles of mean gas temperature in a hydrogen diffusion flame:a comparison between combustion models.

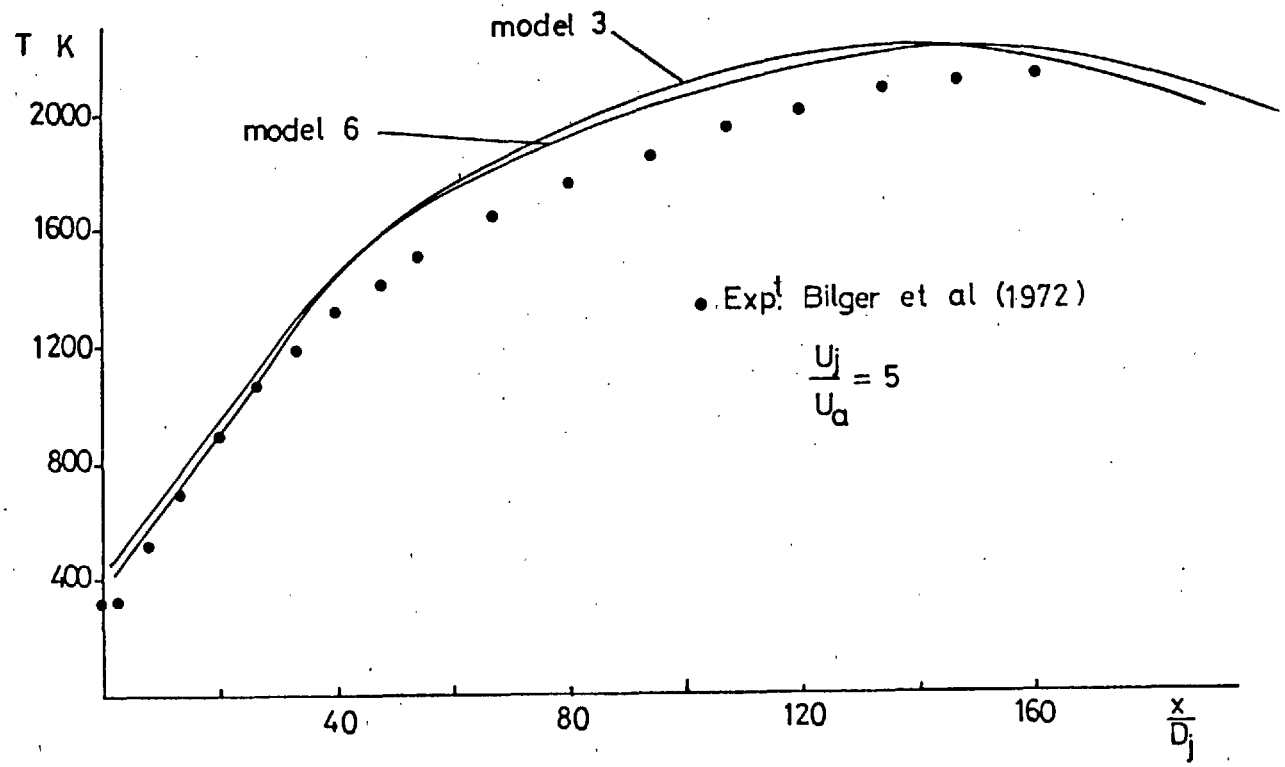

Figure 5.3.7:Centreline distribution of mean gas temperature in a hydrogen diffusion flame: a comparison between combustion models.

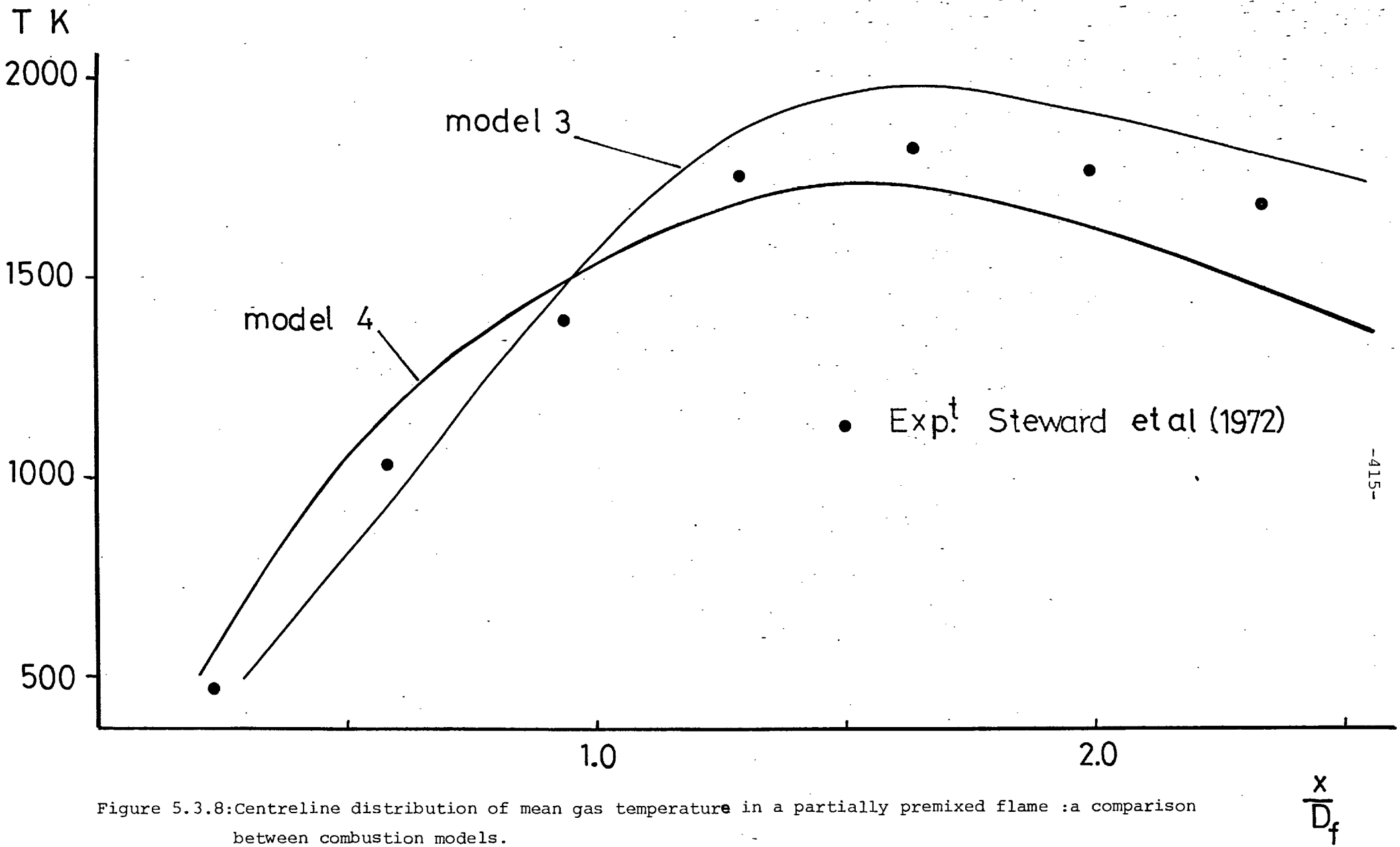

Figure 5.3.8:Centreline distribution of mean gas temperature in a partially premixed flame :a comparison between combustion models.

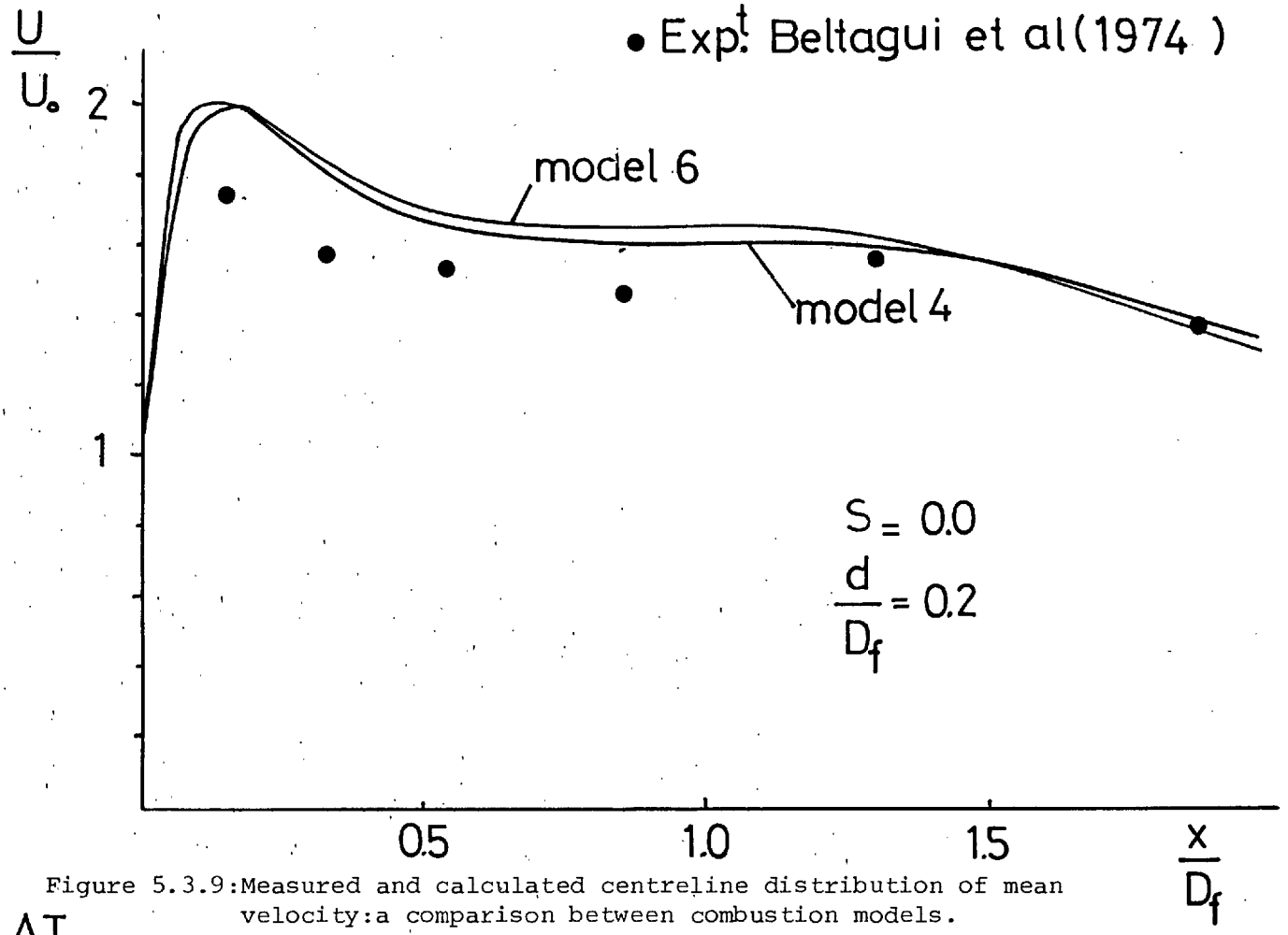

Figure 5.3.9:Measured and calculated centreline distribution of mean velocity:a comparison between combustion models.

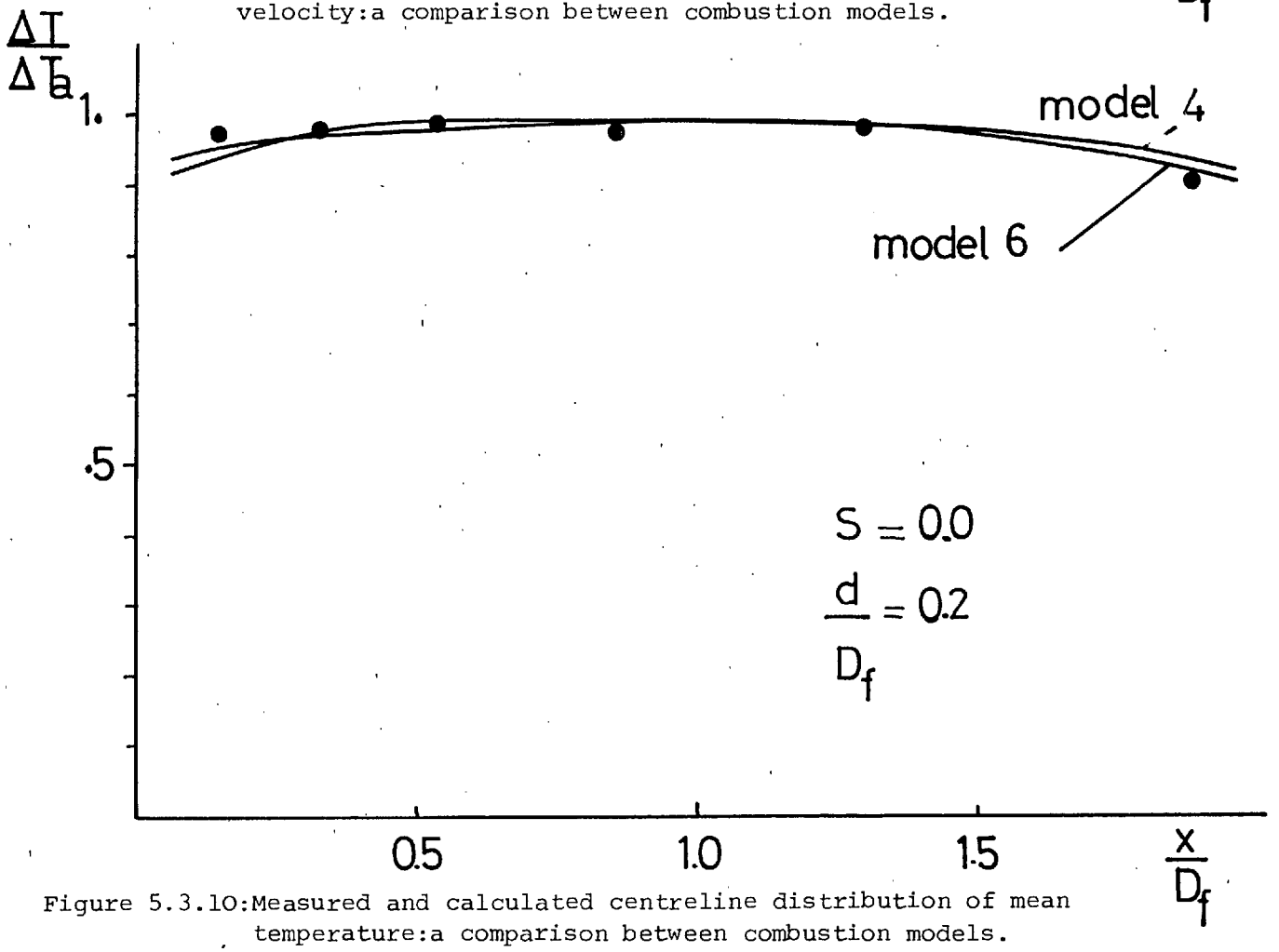

Figure 5.3.10:Measured and calculated centreline distribution of mean temperature:a comparison between combustion models.

Flame 2

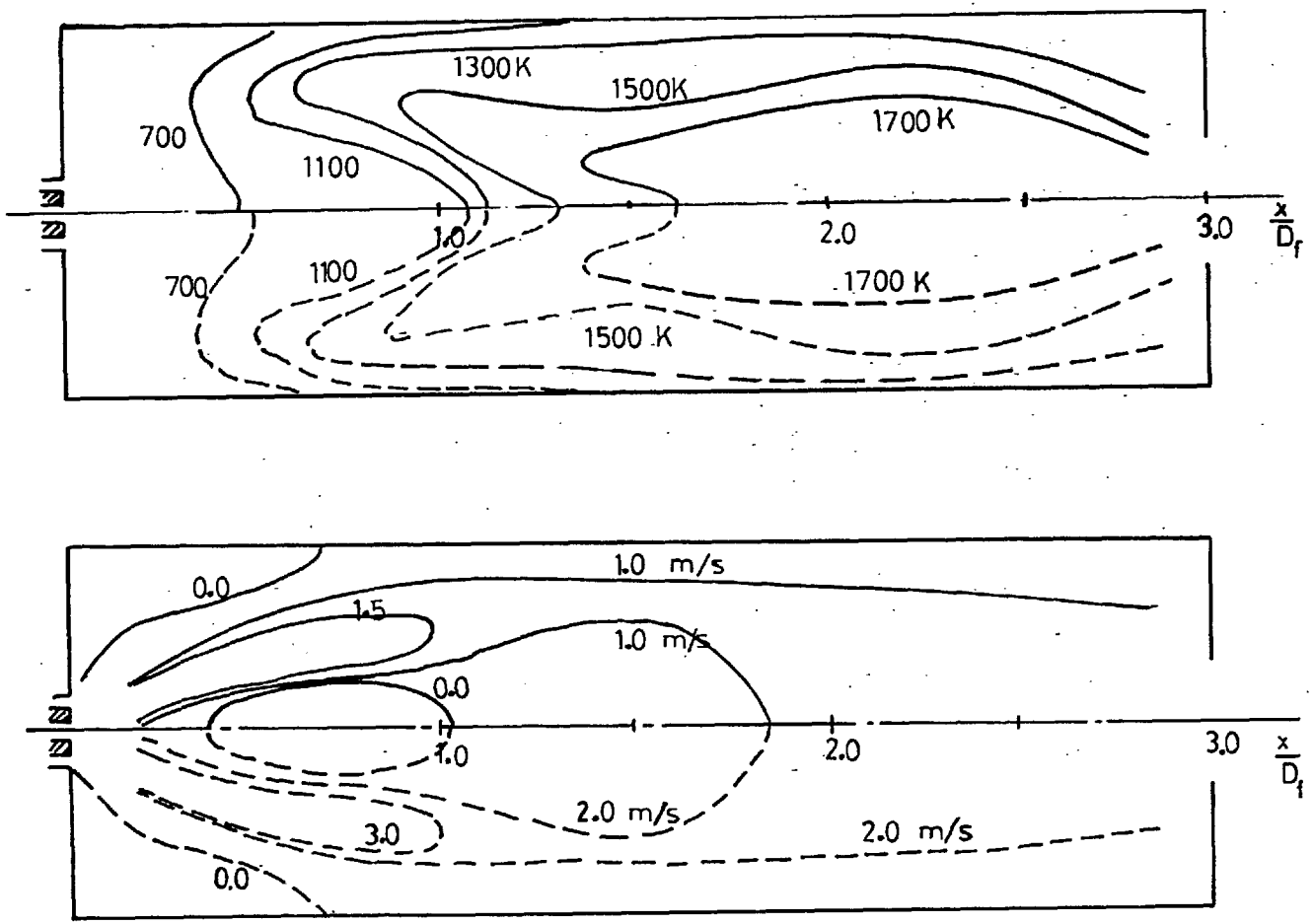

$\dot{M}_a$ = 36.6 Kg/h
a/f = 17.2

$\dot{M}_a$ = 73.2 Kg/h
a/f = 17.2

$\dot{M}_a$ = 36.6 Kg/h
a/f = 17.2

$\dot{M}_a$ = 73.2 Kg/h
a/f = 17.2

Figure 5.4.1:Effect of mass flow rates on mean axial velocity and mean temperature distributions.

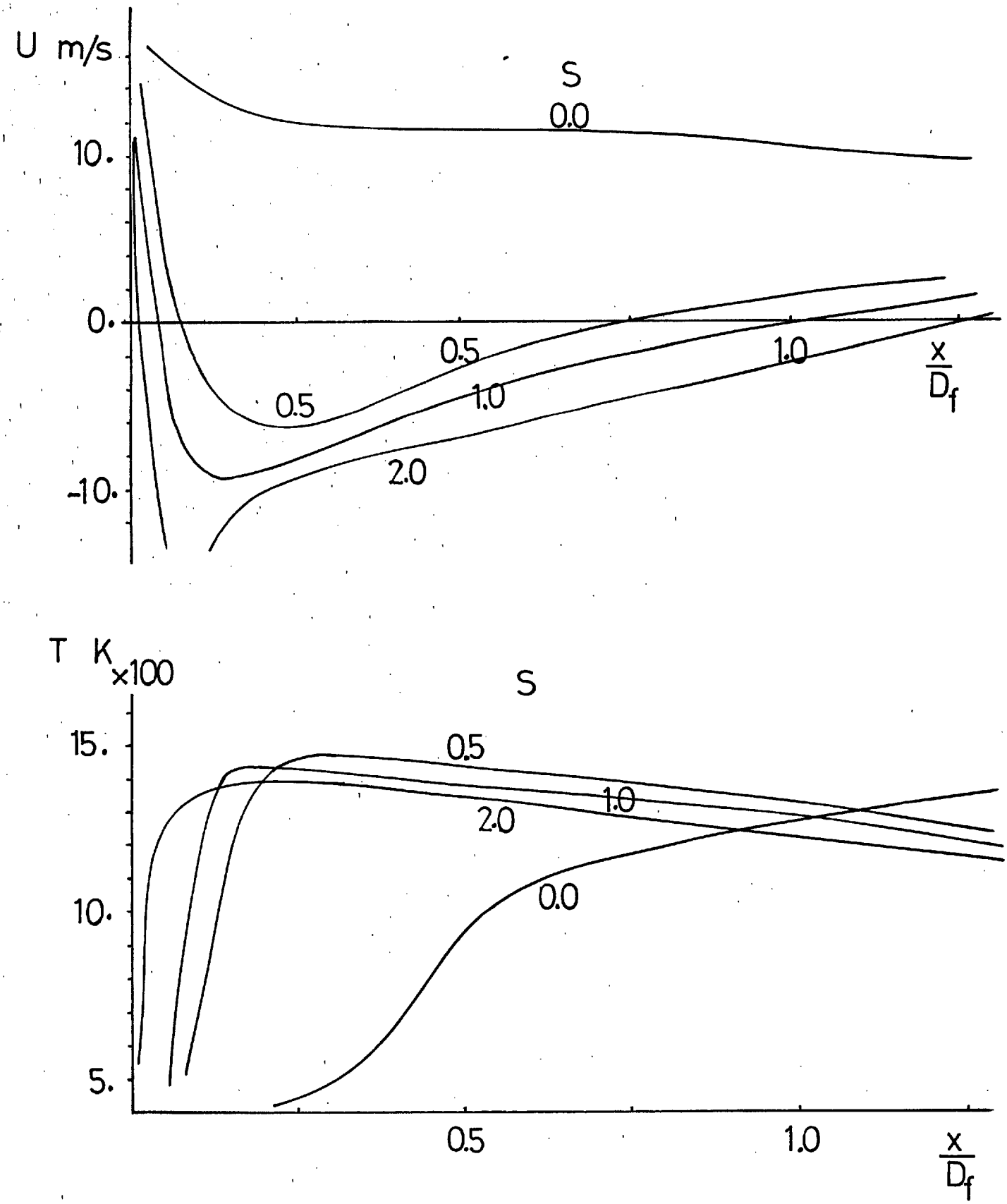

Figure 5.4.2:Effect of swirl number on centreline distributions of mean axial velocity and mean gas temperature for flame 3.

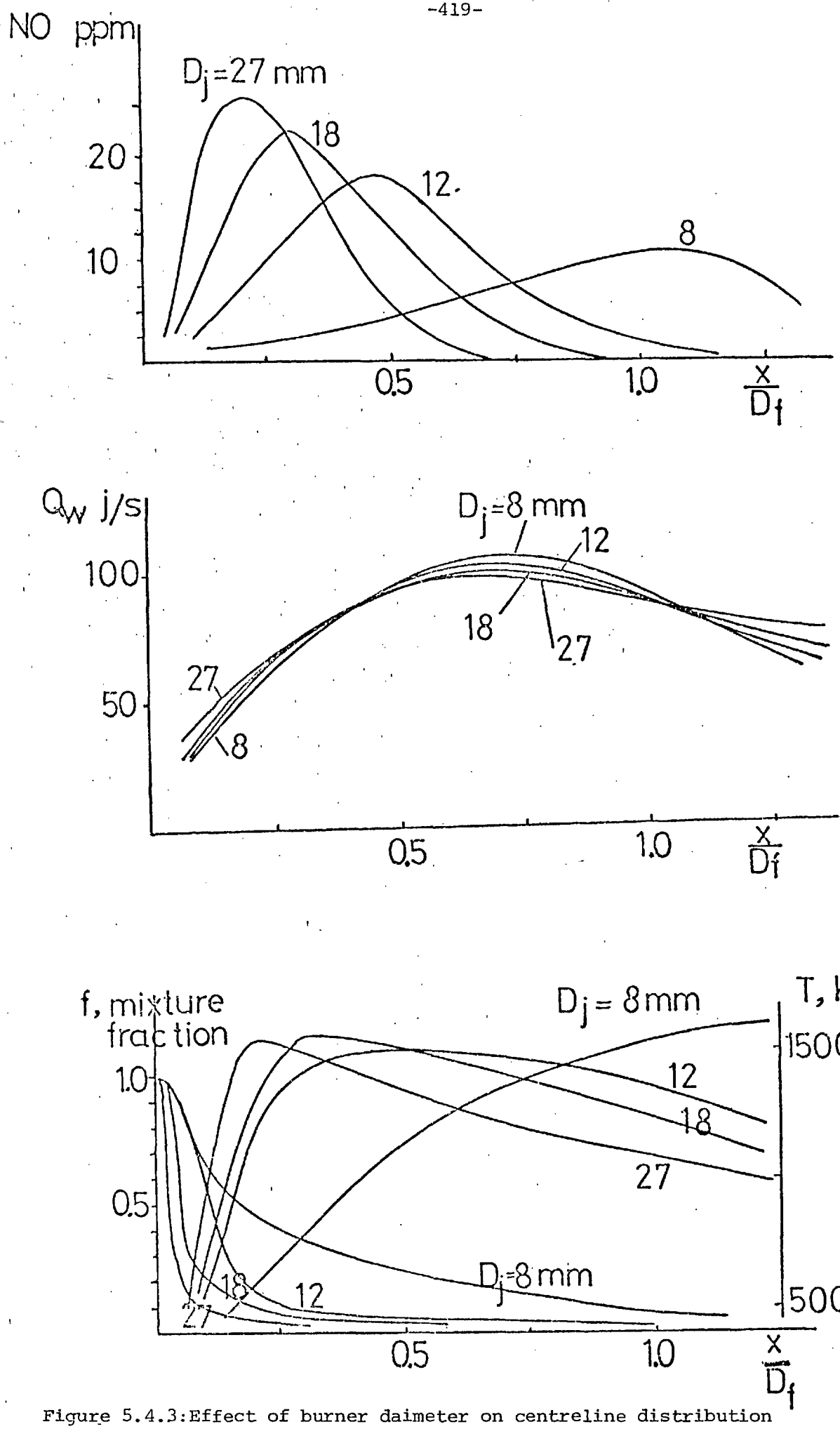

Figure 5.4.3:Effect of burner daimeter on centreline distribution of mixture fraction,mean temperature ,NO and wall

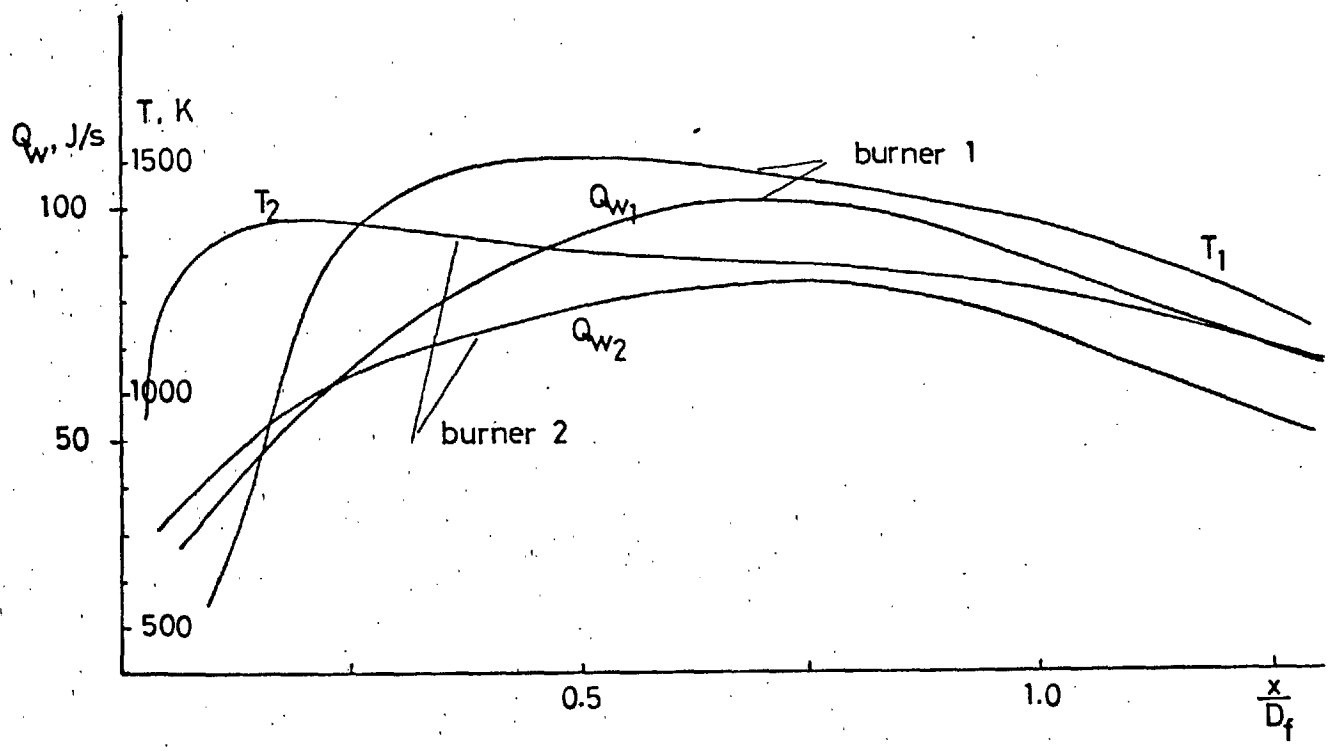

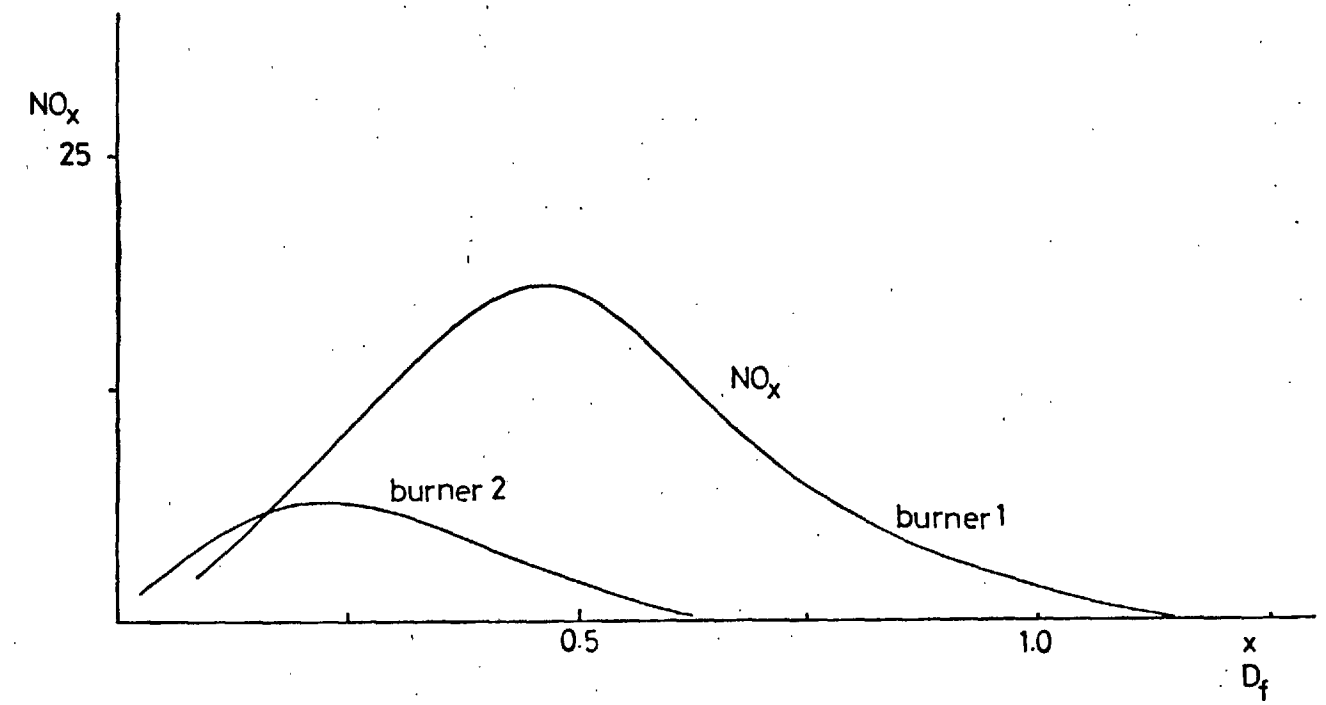

Figure 5.4.4:Effect of fuel nozzle type on centreline distributions of mean temperature,NO and wall heat transfer rates.

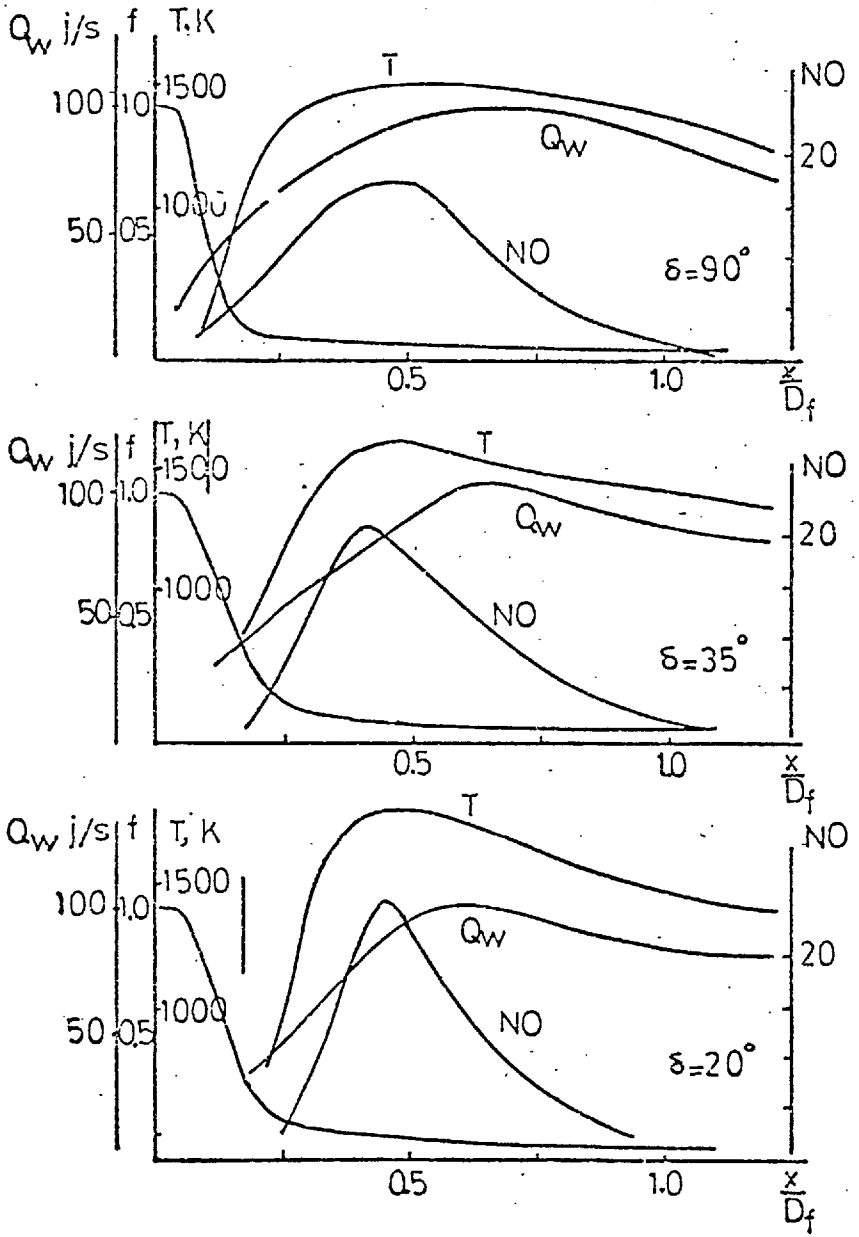

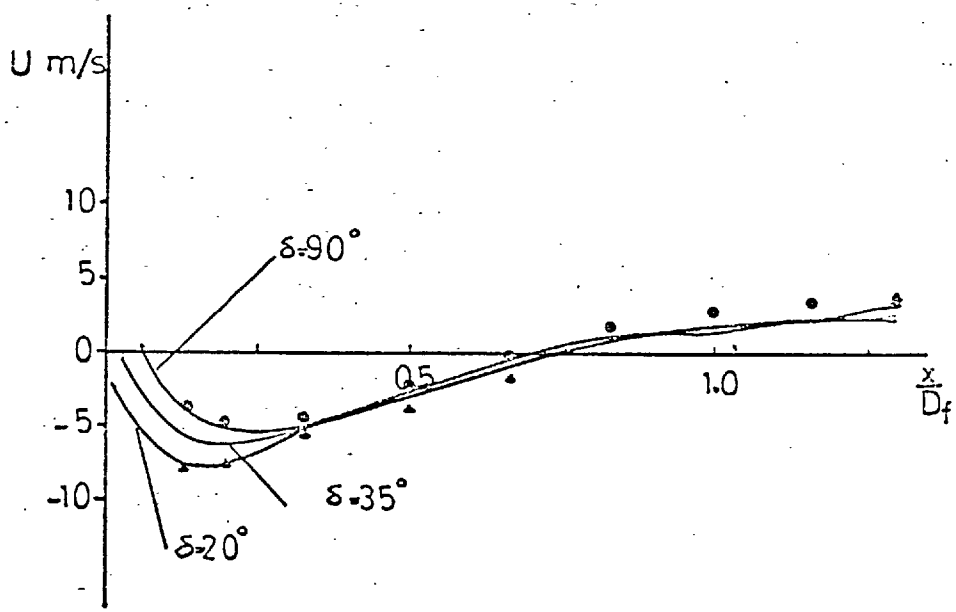

Figure 5.4.5:Effect of quarl angle on centreline distributions of mixture fraction,mean temperature,axial velocity, NO and wall heat transfer rate for the furnace geometry of section 3.1.

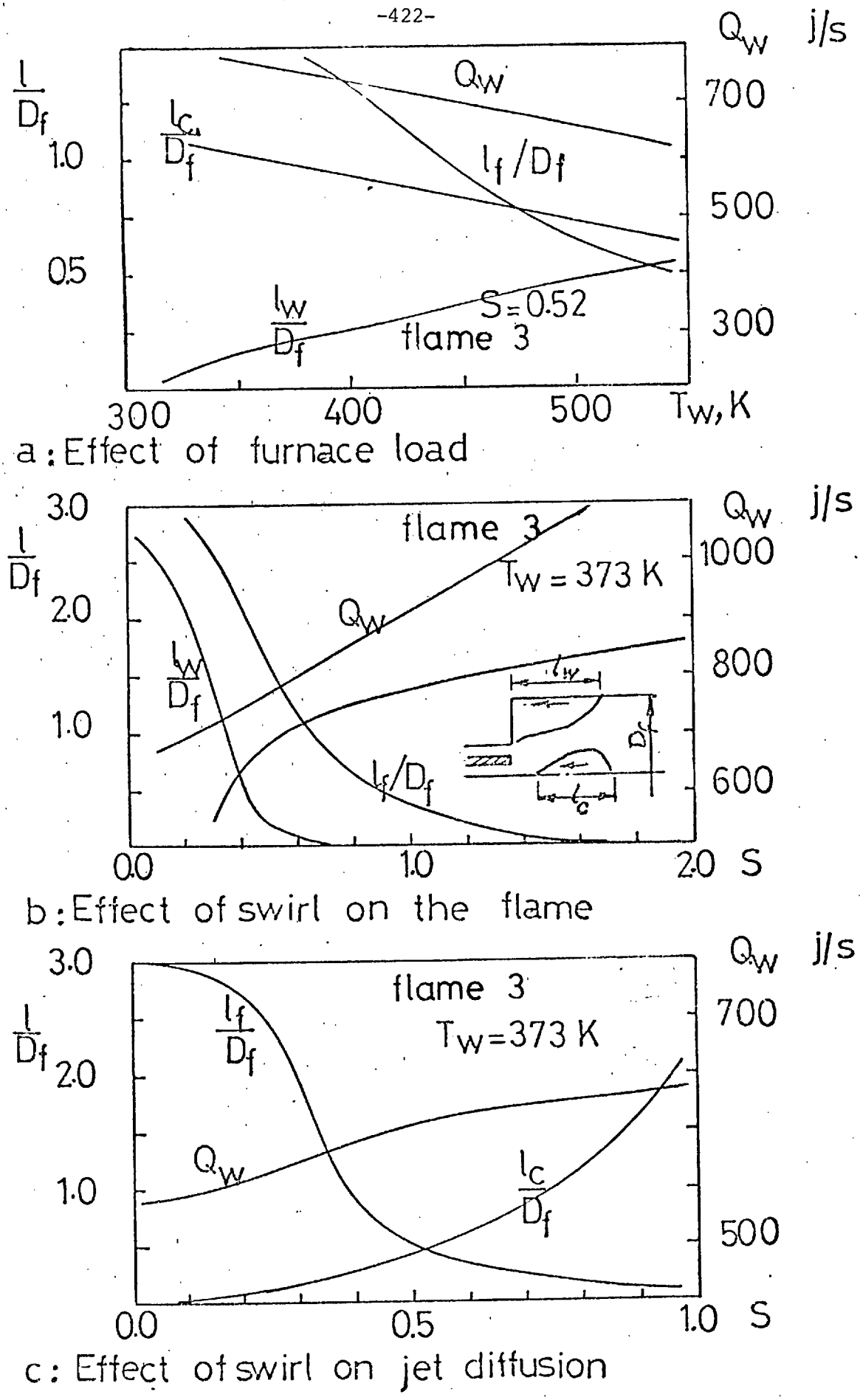

Figure 5.4.6:Effect of wall temperature,swirl number and burner geometry on the flame characteristics.